

AMERICAN UNIVERSITY OF BEIRUT

SYNTHESIS, PHOTOPHYSICAL PROPERTIES
AND APPLICATIONS OF ARYLPYRENE
AND DITHIENOPHENAZINE DERIVATIVES

by
TAREK HOUSSAM EL ASSAAD

A thesis
submitted in partial fulfillment of the requirements
for the degree of Master of Science
to the Department of Chemistry
of the Faculty of Arts and Sciences
at the American University of Beirut

Beirut, Lebanon
February 2016

AMERICAN UNIVERSITY OF BEIRUT

SYNTHESIS, PHOTOPHYSICAL PROPERTIES
AND APPLICATIONS OF ARYLPYRENE
AND DITHIENOPHENAZINE DERIVATIVES

by
TAREK HOUSSAM EL ASSAAD

Approved by:

Dr. Bilal Kaafarani, Associate Professor
Chemistry



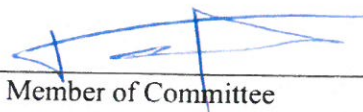
Adviser

Dr. Makhlof Haddadin, Professor
Chemistry



Member of Committee

Dr. Tarek Ghaddar, Associate Professor
Chemistry



Member of Committee

Dr. Digambara Patra, Associate Professor
Chemistry



Member of Committee

Date of thesis defense: February 05, 2016

AMERICAN UNIVERSITY OF BEIRUT

THESIS, DISSERTATION, PROJECT RELEASE FORM

Student Name: El Assaad Tarek Houssam
 Last First Middle

Master’s Thesis Master’s Project Doctoral Dissertation

I authorize the American University of Beirut to: (a) reproduce hard or electronic copies of my thesis, dissertation, or project; (b) include such copies in the archives and digital repositories of the University; and (c) make freely available such copies to third parties for research or educational purposes.

I authorize the American University of Beirut, **three years after the date of submitting my thesis, dissertation, or project,** to: (a) reproduce hard or electronic copies of it; (b) include such copies in the archives and digital repositories of the University; and (c) make freely available such copies to third parties for research or educational purposes.

Signature

Date

ACKNOWLEDGMENTS

I would like to take this opportunity to thank all those who helped and supported me throughout my years of graduate studies at the American University of Beirut. I am very thankful to my adviser, Prof. Bilal R. Kaafarani, for his assistance, guidance and valuable suggestions that have contributed greatly to the completion of this accomplishment along with three publications. I would like to acknowledge my committee members: Prof. Makhlof J. Haddadin, Prof. Digambara Patra and Prof. Tarek H. Ghaddar for their helpful feedback. I would like also to thank Prof. Rabih Sultan for his helpful advising and guidance throughout the graduate program. I present my sincere thanks to past and current research group members: Khaled Al-Kurdi, Christina Haddad, Faten Al-Ghadban, Divina Hasbani, Layal Slika, Karim Ruzz, Kassem Hallal, Rasha Al Moussawi, Abdullah Hilmi, Roy Taoutel, Abbas Matar, Lily Chacra, Sarah Abdul Nabi, Bashir Shaya, Mayssam Najjar and Ghinwa El Hayek for their help and support through my research studies.

I would like to particularly thank our collaborators: Prof. Mohammad H. Al-Sayah from the American University of Sharjah, Prof. Tatiana V. Timofeeva and Dr. Alexander Fonari from New Mexico Highlands University, Prof. Seth R. Marder from Georgia Institute of Technology, Prof. Emil J. W. List-Kratchovil from Graz University of Technology, Prof. Rony S. Khnayzer and Prof. Brigitte Wex from the Lebanese American University.

I highly appreciate the efforts of the Central Research Science Laboratory (CRSL) director and engineers and the staff of the Chemistry Department for providing maintenance of various facilities and equipment.

Furthermore, I want to thank my family for supporting me throughout these tough years that I spent finishing my Masters degree. My father, the man who brought me to life, and always wanted me to reach such big achievements. Unfortunately, due to many health problems, he is not able to recognize what achievement his eldest son has just made. I have to admit that these issues affected me deeply and negatively during the early beginning of my graduate studies; however, they became later on a source of positive energy and motivation for me. This moment when the overall performance increases with no limits, which has been noticed only by the few closest people to me and working with me on a daily basis. I believe that a hard life is the only thing that makes one becoming invincible. My mother, my main source of energy and motivation, took care of the hardest duties and obligations that anyone can imagine, along with my younger brother, just to provide me with the full time-freedom that I needed. I must admit that their tough efforts during the Fall semester allowed me to finish everything up regarding writing my thesis along with finishing the project presented in Chapter 4 of this thesis, auditing a course with Prof. Haddadin, and teaching a new lab for the first time which also required me effort and preparation. I would like to thank my bigger family, the graduate students, those who supported me whenever I needed.

Since the lab I taught and the course I audited were mentioned, I would like to address special thanks to Prof. Haddadin for allowing me to sit for the lectures and exams of the heterocyclic chemistry CHEM 314 course, and for opening the chance for me to give a complete CHEM 225 lecture in class. This very challenging final semester made me confident that I reached the target I always wanted to reach. Thank you so much Prof. Haddadin. I only wish if this semester were the beginning at AUB, but sadly it seems to be the end. However, nothing ends in life, and every end is a new beginning.

AN ABSTRACT OF THE THESIS OF

Tarek Houssam El Assaad for Master of Science
Major: Chemistry

Title: Synthesis, photophysical properties and applications of arylpyrene and dithienophenazine derivatives

The synthesis and full characterization of a series of pyrene-based compounds and their application in organic electronics owing to their blue-emitting properties is reported. The synthesis of these compounds was carried out from pyrene using different procedures including electrophilic aromatic substitution, reduction, oxidation, and Suzuki-Miyaura coupling reaction. The synthesis of a stable fluorescent sensor for anion detection based on a dithienophenazine core is also reported starting from an alpha-diketone and 1,2-benzene diamine. The synthesis involved tosylation, nitration, hydrogenation, keto-amino condensation, and Suzuki-Miyaura coupling reaction.

In Chapter 2, we start by introducing pyrene and its properties. These included its chemical reactivity through electrophilic aromatic substitution, and its photophysical properties. Synthetic routes to reach different arylpyrene categories starting from unsubstituted pyrene are presented along with the photophysical advantages of the 1,3,6,8-tetraarylsubstitution. In this Chapter, the synthesis and full characterization of nine 1,3,6,8-tetraarylpyrene compounds (**2.21-2.29**) is described through three different synthetic procedures. The photophysical properties of these compounds in different environments including solid state will be discussed, in parallel to a discussion of their X-Ray structures and thermal properties. Based on this discussion their potential for being involved in organic electronic devices is evaluated. This is done in comparison to a reference compound (1,3,6,8-tetraphenylpyrene) and to pyrene itself, which illustrates the effect of different substituents on the properties of pyrene from a steric and an electronic point of view.

In Chapter 3, a further step towards other arylpyrene categories (other than the 1,3,6,8-tetraarylpyrenes presented in Chapter 2) is made by the synthesis and characterization of new 2,7-diarylpyrene (**3.1-3.3**) and 2,7-diaryl-4,5,9,10-tetrahydropyrene (**3.4-3.6**) derivatives. The study focuses on their photophysical properties in different solvents of different polarities (acetonitrile, chloroform, cyclohexane, DMF, DMSO, 1,4-dioxane, ethanol, ethyl acetate, and THF) in comparison with reference compounds (2,7-diphenylpyrene for **3.1-3.3**) and (*para*-quaterphenyl and 4,5,9,10-tetrahydropyrene for **3.4** and **3.6**). Deducing the influence of the electronic and steric effect of substituents on the outer benzene ring

connected to positions 2 and 7 on pyrene and 4,5,9,10-tetrahydropyrene cores on these photophysical and thermal properties is done in comparison to similar derivatives previously reported by our research group. Their feasibility for device application will be discussed accordingly.

In Chapter 4, a discussion of carbazole and tercarbazole in terms of their photophysical properties is presented. Their electron-rich character makes of them very useful in compounds having electron-rich and electron-poor moieties. Such compounds are known as the donor-acceptor (D-A) compounds, where the donor is the electron-rich group and the acceptor is the electron-poor group, and can have interesting photophysical properties such as intramolecular charge transfer and extreme sensitivity to polarity variations. The synthesis and characterization of two new D-A-D compounds based on pyrene (**4.5**) and 4,5,9,10-tetrahydropyrene (**4.9**) acceptor cores along with tercarbazole-based donors hanged on positions 2 and 7 of the acceptors will be discussed. The photophysical properties in different solvents of different polarities (acetonitrile, chloroform, cyclohexane, DMF, DMSO, 1,4-dioxane, ethanol, ethyl acetate, and THF) will be presented. The results are compared to D-A model compounds (**4.10** and **4.11**), and other similar compounds previously investigated in the literature (**4.2** and **4.3**), including ones reported by our research group (**4.4**, **4.6-4.8**) in order to reach useful conclusions.

In Chapter 5, we report the synthesis and investigation of three new anion sensors. The different interactions of different anions to a receptor site lying on a chromophore occurs at a different rate, this fact is the basic of the fluorescent sensing that is the main topic in this Chapter. The binding studies of a novel dithienophenazine-based anion sensor (**5.1**) are presented. Determination of the binding affinities to nine different anions through titration experiments using proton NMR, absorption and emission spectroscopy is elaborated. Determination of the binding mechanism by comparison to the response of similar sensors to their guests is also discussed.

CONTENTS

ACKNOWLEDGEMENTS.....	v
ABSTRACT.....	vii
LIST OF ILLUSTRATIONS.....	xiii
LIST OF TABLES AND SCHEMES.....	xxvi
LIST OF ABBREVIATIONS.....	xxx

Chapter

1. GENERAL INTRODUCTION.....	1
1.1. Artificial Lighting: Evolution from Fire to Luminescence.....	1
1.2. Pyrene Derivatives for Organic Light-Emitting Diodes.....	3
1.3. Fluorescence Sensing: Achieving a “Lock to Key” Selectivity on the Molecular Level.....	5
1.4. Aims and Objectives.....	7
2. 1,3,6,8-TETRAARYLPYRENE COMPOUNDS: POTENTIAL BLUE LIGHT-EMITTERS.....	14
2.1. Introduction.....	14
2.1.1. Unsubstituted Pyrene: Forbidden Transition and Excimer Formation.....	14
2.1.2. Electrophilic Aromatic Substitution: Bromination of Pyrene.....	22
2.2. Results and Discussion.....	32
2.2.1. Synthesis.....	32
2.2.2. Molecular Photophysics.....	35

2.2.2.1. Absorption, Emission and the Stokes Shift.....	35
2.2.2.2. Fluorescence Lifetime and Emission Quantum Yield.....	53
2.2.2.3. Substituent Effect: Steric and Electronic Effects	70
2.2.2.4. Solution vs. Solid State.....	91
2.2.2.5. Absence of Excimer Formation in Dilute Solution.	93
2.2.3. Thermal Analysis.....	97
2.2.4. X-ray Structure Analysis: Absence of π - π Stacking.....	102
2.2.5. Application in OLEDs.....	109
2.3. Conclusions and Future Work.....	123
2.4. Experimental.....	124
2.4.1. Synthesis.....	124
2.4.2. Photophysical Studies.....	135
2.4.3. X-ray Diffraction from Single Crystal.....	136

3. ANOTHER CATEGORY OF ARYLPYRENES: 2,7-DIARYLPYRENES AND 2,7-DIARYL-4,5,9,10-TETRAHYDROPYRENES.....	137
3.1. Introduction.....	137
3.2. Results and Discussion.....	139
3.2.1. Synthesis.....	139
3.2.2. Molecular Photophysics.....	141
3.2.2.1. 2,7-Diarylpyrene Derivatives.....	141
3.2.2.2. Lowering of LUMO Energy vs. Substituent Position Effect.....	147
3.2.2.3. The Hydrophobic Cleft and a Reversed Solvatochromism.....	150
3.2.2.4. Emission Quantum Yield: Loose-Bolt Effect vs. Reduction of Non-Radiative Rate Effect.....	152
3.2.2.5. 2,7-Diaryl-4,5,9,10-Tetrahydropyrene Derivatives.....	156
3.2.2.6. Absence of Excimer Formation in Dilute Solution.	166
3.2.3. Thermal Analysis.....	167

3.3. Conclusions and Future Work.....	169
3.4. Experimental.....	170
3.4.1. Synthesis.....	170
3.4.2. Photophysical Studies.....	178
4. TERCARBAZOLE-BASED D-A-D AND D-A COMPOUNDS.....	180
4.1. Introduction.....	180
4.2. Results and Discussion.....	184
4.2.1. Substituent Effect on Positions 3, 6 and 9 of Carbazole.....	184
4.2.2. Intramolecular Charge Transfer (ICT) State vs. Locally Excited (LE) State.....	186
4.2.3. Photophysical Properties of ICT State.....	190
4.2.4. ICT vs. LE in Carbazole and Tercarbazole Derivatives....	190
4.2.4.1. Phenanthroline as Acceptor.....	190
4.2.4.2. Pyrene as Acceptor.....	194
4.2.4.3. Biphenyl, Biphenyl-like and Benzene Acceptors	201
4.2.5. Model D-A Compounds and General Analysis.....	205
4.2.6. Quenching of Fluorescence by Chloroform.....	214
4.2.7. Exclusion of Excimer Formation Possibility.....	224
4.2.8. Synthetic Routes Leading to Compounds 4.5 and 4.9 Starting from Carbazole.....	229
4.3. Conclusions and Future Work.....	234
4.4. Experimental.....	235
4.4.1. Synthesis.....	235
4.4.2. Photophysical Studies.....	236

5. FLUORESCENT ANION SENSORS: DITHIENOPHENAZINE-BASED NOVEL SENSOR FOR ANIONS.....	238
5.1. Introduction.....	238
5.1.1. From Non-Fluorescent Katapinands to Reaction-Induced Fluorescence.....	238
5.1.2. Our Contribution to the Field.....	242
5.2. Results and Discussion.....	248
5.2.1. Synthesis and Stability.....	248
5.2.2. Spectroscopic Titrations of Sensor 5.1	253
5.2.2.1. Absorption and Emission Studies of Sensor 5.1	254
5.2.2.2. Proton NMR Titrations of Sensor 5.1	259
5.2.2.3. Calculation of the Binding Constants.....	269
5.2.3. New Sensor Based on Dibenzophenazine Fluorophore...	272
5.3. Conclusions and Future Work.....	274
5.4. Experimental.....	275
5.4.1. Synthesis.....	275
5.4.2. Spectroscopic Titrations.....	282
5.4.2.1. Absorption and Emission Titrations.....	283
5.4.2.2. Proton NMR titrations.....	284
6. SUPPORTING DATA.....	286
Appendix	
A. ABSORPTION TITRATION OF SENSOR 5.1	287
B. EMISSION TITRATIONS OF SENSOR 5.1	296
C. PROTON NMR TITATIONS OF SENSOR 5.1	305
D. PROTON NMR SPECTRA.....	308
E. CARBON-13 NMR SPECTRA.....	332
REFERENCES.....	353

ILLUSTRATIONS

Figure	Page
1.1. Photoluminescence: absorbed light ($h\nu_A$) of specific properties (violet or blue) excites electrons from S_0 (ground state) to S_1 and S_2 (excited states), leading to new light ($h\nu_F$ and $h\nu_P$) of different properties (green or red).....	3
1.2. Excited states of pyrene vs. 1,3,6,8-tetraphenylpyrene	5
1.3. Structures of the nine 1,3,6,8-tetraarylpyrene derivatives depicting the careful choice of different substituents: electron-releasing (2.21-2.24), electron-withdrawing (2.25-2.28), and thiophene instead of benzene in 2.29 reported in Chapter 2.....	9
1.4. Structures of novel 2,7-diarylpyrene and 2,7-diaryl-4,5,9,10-tetrahydropyrene derivatives (3.1-3.6) reported in Chapter 3.....	10
1.5. Structures of the two new D-A-D compounds (4.5 and 4.9) based on a tercarbazole donor reported in Chapter 4.....	12
1.6. Structures of the two new D-A model compounds (4.10 and 4.11).....	12
1.7. Structure of compound 5.1 : the most stable anion sensor with the most interesting characteristics among the ones reported in Chapter 5.....	13
2.1. Structure of polyaromatic hydrocarbons reported to have blue fluorescence.....	15
2.2. Pyrene: atom numbers, edge letters and Frontier orbitals.....	16
2.3. The principle Cartesian coordinate system used for pyrene.....	17
2.4. Absorption spectrum of unsubstituted pyrene in cyclohexane solution...	19
2.5. Illustration of allowed and forbidden transitions for organic compounds by the analysis of their molar absorptivity and oscillator strength.....	20
2.6. The forbidden transition in cofacial dimers responsible for the quenching of their fluorescence.....	21

2.7.	Solutions to fluorescence quenching induced by the formation of cofacial dimer	22
2.8.	Structures of the compounds that were mentioned as abbreviations below Schemes 2.4 and 2.5.....	31
2.9.	Jablonski diagram illustrating the different photophysical processes with their corresponding duration; illustration of solvent relaxation as a redistribution of solvent molecules around the fluorophore.....	36
2.10.	The vibrational structure in the $S_0 \rightarrow S_1$ transition of anthracene as observed in both absorption and emission spectra.....	37
2.11.	The absorption spectra of <i>sym</i> -tetrazine in vapor phase, in cyclohexane, and in water.....	38
2.12.	Mirror-image rule applies for the full spectra of perylene, and for part of the spectra of quinine sulfate.....	40
2.13.	Structures of the polarity probes used to define the empirical solvent polarity scale.....	44
2.14.	The normalized empirical solvent polarity scale displaying values for some common solvents.....	45
2.15.	Normalized absorption and emission spectra of compound 2.21 in five different solvents.....	49
2.16.	Normalized absorption and emission spectra of compound 2.22 in six different solvents	49
2.17.	Normalized absorption and emission spectra of compound 2.23 in six different solvents.....	50
2.18.	Normalized absorption and emission spectra of compound 2.24 in six different solvents.....	50
2.19.	Normalized absorption and emission spectra of compound 2.25 in six different solvents.....	50
2.20.	Normalized absorption and emission spectra of compound 2.26 in six different solvents.....	51
2.21.	Normalized absorption and emission spectra of compound 2.27 in six different solvents.....	51
2.22.	Normalized absorption and emission spectra of compound 2.28 in five different solvents.....	51

2.23.	Normalized absorption and emission spectra of compound 2.29 in six different solvents.....	52
2.24.	Stokes shifts vs. orientation polarizability for compounds 2.21-2.29 with linear fitting in the six selected solvents.....	52
2.25.	Stokes shifts vs. empirical solvent polarity parameter for compounds 2.21-2.29 with linear fitting in the six selected solvents.....	53
2.26.	Another form of Jablonski diagram illustrating the intersystem crossing and phosphorescence processes.....	55
2.27.	Fluorescence lifetime decays of compound 2.21 in six different solvents under oxygen-free atmosphere with the single-exponential fitting curves and residuals.....	61
2.28.	Fluorescence lifetime decays of compound 2.22 in six different solvents under oxygen-free atmosphere with the single-exponential fitting curves and residuals.....	62
2.29.	Fluorescence lifetime decays of compound 2.23 in six different solvents along with the single-exponential fitting curves and residuals.....	63
2.30.	Fluorescence lifetime decays of compound 2.24 in six different solvents under oxygen-free atmosphere with the single-exponential fitting curves and residuals.....	64
2.31.	Fluorescence lifetime decays of compound 2.25 in six different solvents under oxygen-free atmosphere with the single-exponential fitting curves and residuals.....	65
2.32.	Fluorescence lifetime decays of compound 2.26 in six different solvents under oxygen-free atmosphere with the single-exponential fitting curves and residuals.....	66
2.33.	Fluorescence lifetime decays of compound 2.27 in six different solvents under oxygen-free atmosphere with the single-exponential fitting curves and residuals.....	67
2.34.	Fluorescence lifetime decays of compound 2.28 in six different solvents under oxygen-free atmosphere with the single-exponential fitting curves and residuals.....	68
2.35.	Fluorescence lifetime decays of compound 2.29 in six different solvents under oxygen-free atmosphere with the single-exponential fitting curves and residuals.....	69

2.36.	The effect of adding different saturated substituents on pyrene in positions 1, 3, 6 and 8 on its fluorescence quantum yield in oxygen-free dichloromethane solutions.....	70
2.37.	Simple illustration of allowed and forbidden transitions in pyrene and 1,3,6,8-tetraphenylpyrene to explain fluorescence enhancement in the latter.....	72
2.38.	One of the three sterically hindered 1,3,6,8-tetraarylpyrene derivatives reported in 2007 by Moorthy <i>et al.</i> , and a representation of the dihedral angles between the plane containing the outer phenyl rings and the one having the pyrene core for this derivative.....	73
2.39.	Overlay of pyrene (Py) absorption, excitation and emission spectra in THF solution.....	75
2.40.	Overlay of TPPy absorption, excitation and emission spectra in THF solution.....	76
2.41.	Comparison of the lifetime decay curves of TPPy and Py in oxygen-free THF solutions.....	79
2.42.	Overlay of absorption, excitation and emission spectra of compound 2.21 in chloroform solution.....	84
2.43.	Overlay of absorption, excitation and emission spectra of compound 2.22 in chloroform solution.....	84
2.44.	Overlay of absorption, excitation and emission spectra of compound 2.23 in chloroform solution.....	85
2.45.	Overlay of absorption, excitation and emission spectra of compound 2.24 in chloroform solution.....	85
2.46.	Overlay of absorption, excitation and emission spectra of compound 2.25 in chloroform solution.....	86
2.47.	Overlay of absorption, excitation and emission spectra of compound 2.26 in chloroform solution.....	86
2.48.	Overlay of absorption, excitation and emission spectra of compound 2.27 in chloroform solution.....	87
2.49.	Overlay of absorption, excitation and emission spectra of compound 2.28 in chloroform solution.....	87

2.50.	Overlay of absorption, excitation and emission spectra of compound 2.29 in chloroform solution.....	88
2.51.	Normalized absorption spectra of compounds 2.21-2.29 in chloroform.	88
2.52.	Normalized emission spectra of compounds 2.21-2.29 in chloroform....	89
2.53.	Molar absorptivity spectra of compounds 2.21-2.29 in chloroform.....	89
2.54.	Overlay of fluorescence lifetime decay curves of compound 2.21-2.29 in chloroform solution along with the fitting and residuals.....	90
2.55.	Normalized emission spectra of compounds 2.21-2.29 in the solid state: thin films vs. crystalline solids.....	92
2.56.	Blue light emission upon shining long-wave UV light on compounds 2.24, 2.27, and 2.29 in chloroform solutions in glass vials.....	92
2.57.	Excitation and emission spectra of compound 2.21 collected at different wavelengths in chloroform.....	94
2.58.	Excitation and emission spectra of compound 2.22 collected at different wavelengths in chloroform.....	94
2.59.	Excitation and emission spectra of compound 2.24 collected at different wavelengths in chloroform.....	95
2.60.	Excitation and emission spectra of compound 2.25 collected at different wavelengths in chloroform.....	95
2.61.	Excitation and emission spectra of compound 2.27 collected at different wavelengths in chloroform.....	96
2.62.	Excitation and emission spectra of compound 2.28 collected at different wavelengths in chloroform.....	96
2.63.	Excitation and emission spectra of compound 2.29 collected at different wavelengths in chloroform.....	97
2.64.	TGA results showing the thermal decomposition process of compounds 2.21-2.29 , TPPy and Py.....	99
2.65.	DSC results for compound 2.22	100
2.66.	DSC results for compound 2.25	101
2.67.	DSC results for compound 2.29	101

2.68.	DSC results for compound 2.23 suggesting that sublimation occurs at the melting point of the first heating cycle.....	102
2.69.	Molecular structures of the six compounds studied by X-ray diffraction from single crystal; due to the inversion center only half of the molecule is in the asymmetric unit which is the part numbered and labeled in the structures with 50% probability displacement ellipsoids.....	107
2.70.	Crystal packing of the six compounds studied: a) 2.21 , b) 2.22 , c) 2.24 , d) 2.25 , e) 2.27 , f) 2.29	108
2.71.	The simplest model of electroluminescence from an emitting material...	109
2.72.	The corrected CIE luminous efficacy and eye sensitivity curves for photopic vision (CIE 1978).....	112
2.73.	CIE eye sensitivity function curves for photopic and scotopic vision....	112
2.74.	CIE 1931 chromaticity diagram.....	113
2.75.	Energetic representation of a single layer diode.....	114
2.76.	Energetic representation of a bilayer diode.....	115
2.77.	Different architectures for designing a multilayer diode, and the mechanism of functioning of p-type emitter device.....	116
2.78.	The mode of functioning of multilayer devices.....	116
2.79.	Band energy diagram of the four devices involving compounds 2.22 , 2.23 , 2.24 and 2.27 as emitters.....	120
2.80.	Possible interpretation of the poor device performance of compound 2.27	121
2.81.	<i>J-V-L</i> characteristics of devices 2.22 , 2.23 and 2.24 and their electroluminescence emission spectra monitored over 300 seconds.....	122
2.82.	<i>J-V-L</i> characteristics of device 2.27 in addition to its electroluminescence emission spectrum monitored over 300 seconds....	122
3.1.	2,7-Diarylpyrene derivatives previously reported by Qiao <i>et al.</i> in 2011.....	137
3.2.	The six 2,7-diarylpyrene and 2,7-diaryl-4,5,9,10-tetrahydropyrene derivatives previously reported by our research group.....	139

3.3.	Structures of the new compounds 3.1-3.6 reported in this Chapter.....	139
3.4.	DPPy absorption spectra in dichloromethane solution and in the solid state.....	142
3.5.	General trend of emission maxima vs. substituent effect according to a previous study by our research group on 2,7-diarylpyrenes in 2013.....	143
3.6.	Emission maxima of (Py and DPPy) vs. compounds (3.7-3.9) in dichloromethane.....	144
3.7.	Structures of the three 2,7-diarylpyrene new derivatives 3.1-3.3	145
3.8.	Absorption spectra of compounds 3.1-3.3 in cyclohexane and in DMSO.....	146
3.9.	Emission spectra of compounds 3.1-3.3 in cyclohexane and in DMSO...	147
3.10.	Bathochromic shift in the emission wavelength of some fluorophores attributed to a trifluoromethyl substituent.....	147
3.11.	Switching the position of a trifluoromethyl substituent changes the nature of the shift from hypsochromic to bathochromic in some D-A compounds.....	148
3.12.	Suggested model compounds to be synthesized in order to investigate further regarding the bathochromic shift of the trifluoromethyl derivative 3.1	149
3.13.	Normalized emission spectra of compound 3.1 in nine different solvents.....	151
3.14.	Normalized emission spectra of compound 3.2 in nine different solvents.....	151
3.15.	Normalized emission spectra of compound 3.3 in nine different solvents.....	152
3.16.	Loose-Bolt effect: stretching of sigma bond in the excited state leading to non-radiative relaxation from the excited state.....	153
3.17.	Isoelectronic structures: (a) biphenyl and THP, (b) <i>p</i> -quaterphenyl and 2,7-diaryl-THP.....	157
3.18.	Structures of compounds 3.12-3.14 previously reported by our group....	158
3.19.	Structures of the two 2,7-diaryl-THP new derivatives 3.4 and 3.6	160

3.20.	Normalized absorption spectra of 3.4 and 3.6 in cyclohexane and in DMSO solutions: both showing one single broad bell-like band.....	161
3.21.	Normalized emission spectra of compound 3.4 in nine different solvents.....	162
3.22.	Normalized emission spectra of compound 3.6 in nine different solvents.....	162
3.23.	Molar absorptivity of compounds 3.1 , 3.2 , 3.3 , 3.4 and 3.6 in chloroform.....	164
3.24.	Stokes shifts vs. orientation polarizability for compounds 3.4 and 3.6 with linear fitting in the nine selected solvents.....	165
3.25.	Stokes shifts vs. empirical solvent polarity for compounds 3.4 and 3.6 with linear fitting in the nine selected solvents.....	165
3.26.	The excitation and emission spectra of 3.2 in cyclohexane collected at different wavelengths.....	166
3.27.	The excitation and emission spectra of 3.2 in DMSO collected at different wavelengths.....	167
3.28.	2,7-Diaryl-THP vs. 2,7-diarylpyrene.....	168
3.29.	TGA results illustrating the thermal decomposition upon heating for all the compounds reported in this Chapter.....	168
4.1.	Carbazole numbering of atoms and labeling of edges.....	180
4.2.	Structures of D-A compounds previously reported by Retting and Zander in 1982.....	181
4.3.	Structures of D-A-D compounds previously reported by our research group.....	182
4.4.	Structure of tercarbazole.....	182
4.5.	Tercarbazole applications in D-A systems reported by Zhao <i>et al.</i> in 2007: molecular switches from opened to closed rings leading to dual emission.....	183
4.6.	Structure of ttCBP and CBP with their T_g and T_d (the glass transition and decomposition temperatures, respectively).....	185

4.7.	ICT from a steric perspective: tetraphenylethylene (TPE) – separation of charges leads to free rotation (twisting), and relieves the strain in the excited state.....	186
4.8.	ICT state from kinetic perspective: k_a vs. k_d	187
4.9.	ICT from an electronic perspective: Lippert’s approach – inversion of states in more polar solvents.....	188
4.10.	Structures of compounds 4.1-4.3 reported by McClenaghan <i>et al.</i> in 2003.....	191
4.11.	Molar absorptivity and normalized emission spectra of 4.1, 4.2 and 4.3 in oxygen-free acetonitrile solutions.....	192
4.12.	Normalized emission spectra of compound 4.2 in five different solvents illustrating the large bathochromic shift in emission wavelength with increasing solvent polarity.....	192
4.13.	D-A-D compounds 4.4 and 4.5 having pyrene as acceptor.....	194
4.14.	Absorption and emission spectra of compound 4.4 in different solvents reported by our research group in 2013.....	195
4.15.	Absorption spectra of compound 4.5 in nine different solvents.....	196
4.16.	Excitation spectra of compound 4.5 in nine different solvents.....	196
4.17.	Normalized emission spectra of compound 4.5 in nine different solvents.....	197
4.18.	Scheme of LE vs. ICT in compound 4.5	199
4.19.	D-A compound having an initial photoexcitation localized on the acceptor with a PET blocking of radiative decay.....	200
4.20.	D-A-D compounds previously reported by our group in 2013: (D) carbazole; (A) benzene (4.6), biphenyl (4.7) and THP (4.8).....	201
4.21.	D-A-D compound 4.9 : (D) tercarbazole, (A) THP	202
4.22.	Absorption spectra of compound 4.9 in nine different solvents.....	203
4.23.	Excitation spectra of compound 4.9 in nine different solvents	204
4.24.	Normalized emission spectra of compound 4.9 in nine different solvents	204

4.25.	Absorption and emission spectra of compound 4.8 reported by our group in 2013.....	205
4.26.	Model D-A compounds 4.10 and 4.11	205
4.27.	Absorption spectra of compound 4.10 in nine different solvents	209
4.28.	Excitation spectra of compound 4.10 in nine different solvents.....	209
4.29.	Normalized emission spectra of compound 4.10 in nine different solvents.....	210
4.30.	Absorption spectra of compound 4.11 in nine different solvents.....	210
4.31.	Excitation spectra of compound 4.11 in nine different solvents.....	211
4.32.	Normalized emission spectra of compound 4.11 in nine different solvents.....	211
4.33.	Molar absorptivity of compounds 4.5 , 4.9 , 4.10 and 4.11 in chloroform	212
4.34	Stokes shifts vs. orientation polarizability for compounds 4.5 , 4.9 , 4.10 and 4.11 with linear fitting in the nine selected solvents.....	212
4.35	Stokes shifts vs. empirical solvent polarity for compounds 4.5 , 4.9 , 4.10 and 4.11 with linear fitting in the nine selected solvents.....	213
4.36.	Lifetime decay curves of compound 4.5 in nine different solvents with the fitting and residuals.....	216
4.37.	Lifetime decay curves of compound 4.5 in chloroform and ethanol at different emission wavelengths with the fitting and residuals.....	217
4.38.	Lifetime decay curves of compound 4.9 in nine different solvents with the fitting and residuals.....	218
4.39.	Lifetime decay curves of compound 4.9 in chloroform and ethanol at different emission wavelengths with the fitting and residuals.....	219
4.40.	Lifetime decay curves of compound 4.10 in nine different solvents with the fitting and residuals.....	220
4.41.	Lifetime decay curves of compound 4.10 in chloroform and ethanol at different emission wavelengths with the fitting and residuals.....	221
4.42.	Lifetime decay curves of compound 4.11 in nine different solvents with the fitting and residuals.....	222

4.43.	Lifetime decay curves of compound 4.11 in chloroform and ethanol at different emission wavelengths with the fitting and residuals.....	223
4.44.	Excitation and emission spectra of compound 4.5 in a non-polar solvent (LE state) collected at different wavelengths.....	224
4.45.	Excitation and emission spectra of compound 4.5 in a polar solvent (ICT state) collected at different wavelengths.....	225
4.46.	Excitation and emission spectra of compound 4.9 in a non-polar solvent collected at different wavelengths.....	225
4.47.	Excitation and emission spectra of compound 4.9 in a polar solvent collected at different wavelengths.....	226
4.48.	Excitation and emission spectra of compound 4.10 in a non-polar solvent collected at different wavelengths.....	226
4.49.	Excitation and emission spectra of compound 4.10 in a polar solvent collected at different wavelengths.....	227
4.50.	Excitation and emission spectra of compound 4.11 in a non-polar solvent collected at different wavelengths.....	227
4.51.	Excitation and emission spectra of compound 4.11 in a polar solvent collected at different wavelengths.....	228
4.52.	Absorption spectra of compounds 4.5 , 4.9 , 4.10 and 4.11 in chloroform solutions of different concentrations.....	228
5.1.	The encapsulation of halides in the katapinands cavity.....	238
5.2.	Binding process between the arylurea host (hydrogen bond donor) and the tetrabutylammonium tosylate guest (hydrogen bond acceptor).....	239
5.3.	Deprotection-induced fluorescence selectively used for fluoride detection.....	241
5.4.	Reaction-based sequential relay recognition of fluoride followed by cyanide using a triple output mode.....	242
5.5.	PET signaling that induces a “switch-on” of fluorescence.....	245
5.6.	(a) Excimer to monomer; (b) monomer to excimer.....	246
5.7.	Structures of novel dithienophenazine sensors 5.1 and 5.2 ; and the previously investigated dibenzophenazine sensor 5.7 and quinoxalinophenanthrophenazine sensor 5.8 by our research group.....	250

5.8.	Emission and absorption changes of 10 μM solution of sensor 5.1 in chloroform over 48 hours (kept in dark at 0 $^{\circ}\text{C}$) without the addition of anion.....	251
5.9.	Emission and absorption changes of 5 μM solution of sensor 5.2 in DMSO over 48 hours (kept in dark at 0 $^{\circ}\text{C}$) without the addition of anion	252
5.10.	Emission and absorption changes of 5 μM solution of sensor 5.2 in 5% DMSO in chloroform over 24 hours (kept in dark at 0 $^{\circ}\text{C}$) without the addition of anion.....	252
5.11.	Emission and absorption changes of 5 μM solution of sensor 5.2 in 5% DMSO in acetonitrile over 24 hours (kept in dark at 0 $^{\circ}\text{C}$) without the addition of anion.....	252
5.12.	Emission spectra of sensor 5.1 at different concentrations in chloroform collected at different excitation wavelengths.....	254
5.13.	Absorption and emission spectra of sensor 5.1 (10 μM) upon titration with tetrabutylammonium benzoate in chloroform at 25 $^{\circ}\text{C}$	255
5.14.	Absorption and emission spectra of sensor 5.1 (10 μM) upon titration with tetrabutylammonium cyanide in chloroform at 25 $^{\circ}\text{C}$	256
5.15.	Absorption and emission spectra of sensor 5.1 (10 μM) upon titration with tetrabutylammonium phosphate monobasic in chloroform at 25 $^{\circ}\text{C}$	256
5.16.	Relative change in emission intensity of 5.1 (10 μM) at 560 nm upon titration with different anions in chloroform at 25 $^{\circ}\text{C}$	257
5.17.	Solution of 5.1 (10 μM) turning from orange to yellow upon addition of one equivalent of tetrabutylammonium benzoate in chloroform at 25 $^{\circ}\text{C}$	257
5.18.	Labeling of hydrogens and rings of sensor 5.1	261
5.19.	Changes in chemical shifts of aromatic protons of sensor 5.1 (2.0 mM) upon titration with tetrabutylammonium acetate in CDCl_3	262
5.20.	Illustration of the suggested binding mechanism of tetrabutylammonium acetate to sensor 5.1 and the interactions of H_c and H_g with the guest ions.....	263
5.21.	Change in chemical shifts of H_a upon titration of sensor 5.1 (2.0 mM) with tetrabutylammonium salts of fluoride and dihydrogen phosphate in CDCl_3	265

5.22.	Change in chemical shifts of aliphatic protons upon titration of sensor 5.1 (2.0 mM) with tetrabutylammonium acetate in CDCl ₃	266
5.23.	Change in chemical shifts of H _g upon titration of sensor 5.1 (2.0 mM) with tetrabutylammonium salts of strong and weak binding anions in CDCl ₃	267
5.24.	Change in chemical shifts of H _g upon titration of sensor 5.1 (2.0 mM) with tetrabutylammonium bromide (TBABr) and tetraethylammonium bromide (TEABr) in CDCl ₃	267
5.25.	Structure of the first reported dithienophenazine anion sensor studied by Aboubakr <i>et al.</i>	268
5.26.	Binding isotherms generated from proton NMR titrations of sensor 5.1	270
5.27.	Experimental vs. calculated from model absorption spectra for the titration of sensor 5.1 with tetrabutylammonium acetate in chloroform at 25 °C.....	271
5.28.	Experimental vs. calculated from model absorption spectra for titration of sensor 5.1 with tetrabutylammonium benzoate in chloroform at 25 °C.....	271
5.29.	Experimental vs. calculated from model absorption spectra for titration of sensor 5.1 with tetrabutylammonium cyanide in chloroform at 25 °C.....	272
5.30.	Structure of sensor 5.11 synthesized through condensation of diketone 5.10 with intermediate 5.5	273
5.31.	Stability of emission over 48 hours for sensor 5.11 in chloroform and DMSO (1 μM solutions stored at 0 °C in dark).....	273

TABLES AND SCHEMES

Table	Page
1.1. The difference in molecular geometry among anions and their application.....	7
2.1. The four electronic transitions of pyrene in cyclohexane solution as reported by Crawford <i>et al.</i>	18
2.2. Summary of useful solvent characteristics to be used in our solvatochromic studies.....	45
2.3. Absorption and emission studies in different solvents for compounds 2.21-2.29 displaying the maxima of the $S_0 \rightarrow S_1$ transitions and the corresponding Stokes shifts, in addition to the molar absorptivity in chloroform.....	48
2.4. Summary of the photophysical processes relevant to fluorescent emitters such as compounds 2.21-2.29	55
2.5. Fluorescence lifetimes and emission quantum yields in different solvents with the calculated values of radiative and non-radiative constants and natural lifetimes.....	59
2.6. Experimental photophysical results for Py and TPPy in THF solutions	77
2.7. Absorption maxima of the experimental lowest energy transitions for compounds 2.21-2.29 and shifts with respect to TPPy in THF solutions.....	83
2.8. Emission maxima of the experimental lowest energy transitions for compounds 2.21-2.29 and shifts with respect to TPPy in THF solutions.....	83
2.9. Stokes shift values in nm, eV, and cm^{-1} for Py, TPPy, and compounds 2.21-2.29 in THF solutions.....	83
2.10. Comparison of the emission quantum yields for TPPy and compounds 2.21-2.29 in both solution and solid state.....	92
2.11. Thermal properties of Py, TPPy, and compounds 2.21-2.29	98
2.12. DSC results for compounds 2.22, 2.23, 2.25 and 2.29	100

2.13.	Crystallographic data of compounds 2.21 , 2.22 , 2.24 , 2.25 , 2.27 and 2.29	104
2.14.	Properties of compounds 2.21-2.29 that help to discuss their usefulness in OLED application.....	118
2.15.	Electroluminescent characteristics of compounds 2.22 , 2.23 , 2.24 and 2.27 in a single-layer geometry.....	121
2.16.	Useful literature coupling constant values for C-F coupling in aromatic compounds and H-H coupling in substituted thiophenes relevant to the NMR spectra of compounds 2.25 , 2.27 and 2.29	125
3.1.	Main photophysical properties of 2,7-diarylpyrene derivatives.....	154
3.2.	Main photophysical properties of 2,7-diaryl-THP derivatives.....	163
3.3.	Thermal properties of the novel compounds studied as compared to DPPy.....	168
4.1.	Absorption and emission maxima of compounds 4.1-4.3 as reported by McClenaghan <i>et al.</i> in 2003 in oxygen-free acetonitrile solutions.....	191
4.2.	Emission maxima of 4.4 and 4.5 in non-polar vs. polar solvent.....	197
4.3.	Fluorescence lifetime and emission quantum yield values in different solvents, in addition to the calculated radiative and non-radiative decay rate constants of compound 4.4 reported by our research group in 2013 and the natural lifetimes.....	198
4.4.	Fluorescence lifetime and emission quantum yield values in different solvents, in addition to the calculated radiative and non-radiative decay rate constants and natural lifetimes of compound 4.5	198
4.5.	Emission maxima in non-polar vs. polar solvent for 4.8 and 4.9	203
4.6.	Fluorescence lifetime and emission quantum yield values in different solvents, in addition to the calculated radiative and non-radiative decay rate constants of compound 4.8 reported by our research group in 2013 and the natural lifetimes.....	206
4.7.	Fluorescence lifetime and emission quantum yield values in different solvents, in addition to the calculated radiative and non-radiative decay rate constants and the natural lifetimes of compound 4.9	207
4.8.	Fluorescence lifetime and emission quantum yield values in different solvents, in addition to the calculated radiative and non-radiative decay rate constants and the natural lifetimes of the two D-A model compounds 4.10 and 4.11	207

4.9.	Absorption, emission maxima and Stokes shifts in nine solvents, in addition to the molar absorptivity in chloroform for compounds 4.5 , 4.9 , 4.10 and 4.11	208
4.10.	Theoretical studies useful information for compounds 4.4 , 4.6 , 4.7 and 4.8 reported by our group.....	214
5.1.	Reported pK _a values in DMSO at 25 °C of some neutral receptors.....	247
5.2.	Reported pK _a values in DMSO at 25 °C of some anions.....	247
5.3.	Some properties of the sulfonamide-based anion sensors 5.1 , 5.2 , 5.7 and 5.8	248
5.4.	Affinity constants to weak binding anions determined from the change in chemical shift of H _a in proton NMR titration experiments of 2 mM 5.1 in CDCl ₃ at 25 °C.....	270
5.5.	Affinity constants to strong binding anions determined from absorption titration experiments of 10 μM 5.1 in chloroform at 25 °C.....	271
5.6.	Absorption and emission titration chart for sensor 5.1	284
5.7.	Proton NMR titration chart of sensor 5.1	285
Scheme		Page
2.1.	Direct bromination of pyrene. (a) BnMe ₃ N-Br ₃ (1 eqv), ZnCl ₂ anhydrous (1.1 eqv), AcOH, 25 °C, 12 hrs, or HBr (1.1 eqv), H ₂ O ₂ (1 eqv), MeOH-Et ₂ O (1:1) 15→25 °C, 12 hrs; (b) same conditions as (a) with double equivalents and reaction time; (c) Br ₂ (4.4 eqv), nitrobenzene, 160 °C, 3 hrs.....	25
2.2.	Bromination following mono- <i>tert</i> -butylation of pyrene. (a) <i>t</i> -BuCl (1.2 eqv), AlCl ₃ anhydrous (1.1 eqv), CH ₂ Cl ₂ , 0→25 °C, 3 hrs (b) Br ₂ (1 eqv), CH ₂ Cl ₂ , -78→25 °C, inert atmosphere, 24 hrs (c) same conditions as (b), but with (2 eqv) Br ₂ ; (d) Br ₂ (6 eqv), Fe-powder (5 eqv), CH ₂ Cl ₂ , 25 °C, 4 hrs.....	26
2.3.	Bromination following di- <i>tert</i> -butylation of pyrene. (a) <i>t</i> -BuCl (> 3 eqv), AlCl ₃ anhydrous (1.5 eqv), 0→25 °C, 3 hrs; (b) Br ₂ (1.1 eqv), CCl ₄ , 0→25 °C, 1 hr; (c) CCl ₄ , 25 °C, 3 hrs; (d) Br ₂ (6 eqv), Fe-powder (3 eqv), CH ₂ Cl ₂ , 0→25 °C.....	27
2.4.	Bromination of pyrene in the 2 and/or 7 positions. (a) 1) Raney Ni, EtOAc, 25 °C, 48 hrs; 2) Pd/C, EtOAc, H ₂ (40 – 45 psi), 25 °C, 78 hrs; (b) Br ₂ (2.2 eqv), NaOH (2.2 eqv), AcOH/H ₂ O (1:1), 25 °C, 24 hrs; (c)	

	Br ₂ (2.2 eqv), CS ₂ , 25 °C, 4 hrs; (d) B ₂ pin ₂ (2.2 eqv), [Ir(μ-OMe)cod] ₂ (0.01 eqv), dtbpy (0.02 eqv), THF, 80 °C, inert anhydrous atmosphere, 16 hrs; (e) CuBr ₂ (6 eqv), MeOH/H ₂ O/THF (3:3:1), 90 °C, 16 hrs; (f) B ₂ pin ₂ (1.1 eqv), [Ir(μ-OMe)cod] ₂ (0.01 eqv), dtbpy (0.02 eqv), hexane, 80 °C, inert anhydrous atmosphere, 16 hrs; (g) CuBr ₂ (3 eqv), MeOH/H ₂ O (1:1).....	28
2.5.	Preparation of 4,10-diarylphenylpyrene from four separate benzene rings. (a) K ₂ CO ₃ (3.6 eqv), PEPPSI-IPr (0.05 eqv), 1,4-dioxane, inert anhydrous atmosphere, reflux, 36 hrs; (b) PdCl ₂ (PPh ₃) ₂ (0.15 eqv), THF, inert anhydrous atmosphere, reflux, 48 hrs; (c) HCCMgBr (1 eqv), PhCCH (6 eqv), -40 °C, inert anhydrous atmosphere; (d) PtCl ₂ (1 eqv), toluene, inert anhydrous atmosphere, reflux, 20 hrs.....	30
2.6.	Different synthetic procedures used to synthesize the nine blue emitters 2.21-2.29 and TPPy.....	34
3.1.	Synthesis of compounds 3.1-3.6	140
4.1.	Fridel-Crafts alkylation of carbazole. (a) AlCl ₃ (1 eqv) <i>t</i> -BuCl (6 eqv), 25 °C, 24 hrs; (b) dry ZnCl ₂ (3 eqv), <i>t</i> -BuCl (3 eqv), nitromethane, inert atmosphere, 25 °C, 5 hrs; (c) H ₂ SO ₄ , 25 °C, 24 hrs.....	229
4.2.	From carbazole to tercarbazole: the copper catalyzed Ullman cross-coupling: (a) dry ZnCl ₂ (3 eqv), <i>t</i> -BuCl (3 eqv), nitromethane, inert atmosphere, 25 °C, 5 hrs; (b) KI (1.31 eqv), KIO ₃ (0.78 eqv), CH ₃ COOH, reflux, 24 hrs; (c) TsCl (4.4 eqv), KOH (4.4 eqv), acetone, inert atmosphere, reflux, 15 mins; (d) 4.1 (2.2 eqv), CuI (0.5 eqv), (±)- <i>trans</i> -1,2-diaminocyclohexane (0.52 eqv), K ₂ CO ₃ (2.5 eqv), toluene, inert atmosphere, reflux, 24 hrs; (e) KOH (2 eqv), DMSO:THF:water (3:6:1), inert atmosphere, reflux, 25 mins.....	231
4.3.	The Buchwald-Hartwig palladium-catalyzed cross coupling. (a) tris(dibenzylideneacetone)dipalladium(0), tri- <i>tert</i> -butylphosphine, sodium <i>tert</i> -butoxide, dry toluene, inert anhydrous atmosphere, microwave oven (power: 180 W; max temp: 125 °C; run time: 2 mins; hold time: 60 mins; pressure: 120 psi).....	233
5.1.	Synthetic scheme of sensors 5.1 and 5.2	249

ABBREVIATIONS

[]: Concentration

abs: Absorption

ACN or CH₃CN: Acetonitrile

AcOH or CH₃COOH: Acetic acid

AlCl₃: Aluminum(III) chloride

Anal. Calcd.: Analytically calculated

Ar: Aryl substituent

Blue shift: Hypsochromic shift

BnMe₃N-Br₃: Benzyltrimethylammonium tribromide

Br₂: Bromine

°C: Degree Celsius

C1N: Carbazole donor – naphthalene (from position 1) acceptor

C9P: Carbazole donor – phenanthrene (from position 9) acceptor

CB: Carbazole donor – benzene acceptor

CBN: Carbazole donor – benzonitrile acceptor

CBP: Carbazole donor – biphenyl acceptor (4,4'-*N,N'*-dicarbazole-biphenyl)

CCDC: Cambridge Crystallographic Database Centre

CCl₄: Carbon tetrachloride

cd: Candela

CDCl₃ or chloroform-d: Deuterated chloroform

CHCl₃: Chloroform

CIE: Committee Internationale de l'éclairage (International Commission on Illumination)

CIF: Crystallographic Information File

cm: centimeter

CS₂: Carbon disulfide

CT: Charge Transfer
CuBr₂: Copper(II) bromide
CuI: Copper(I) iodide
Cyclohex: Cyclohexane
d: doublet
dd: doublet of doublets
D-A: Donor-Acceptor
D-A-D: Donor-Acceptor-Donor
DCM or CH₂Cl₂: Dichloromethane
DFT: Density Functional Theory
Diox: 1,4-Dioxane
DMF: *N,N'*-Dimethylformamide
DMSO: Dimethylsulfoxide
DMSO-d₆: Deuterated dimethylsulfoxide
DSC: Differential Scanning Calorimetry
DTA: Differential Thermal Analysis
DPP: Phenanthrophenazine
DPPy: 2,7-Diphenylpyrene
DPV: Differential Pulse Voltammetry
EA: Electron Affinity
E_g: Energy bandgap
EL: Electroluminescence
em: Emission
EQE: External Quantum Efficiency
eqv: Molar equivalent
e.s.d.: Estimated standard deviation
ESIPT: Excited state intramolecular proton transfer
et al.: and others
Et₂O: Diethyl ether

ETHB: Electron-Transporting Hole-Blocking
ETL: Electron-Transporting Layer
ETM: Electron-Transporting Moiety/Material
EtOAc: Ethyl acetate
EtOH or C₂H₅OH: Ethanol
eV: electron Volt
ex: Excitation
Fe-powder: Iron powder
FET: Field Effect Transistor
g: Gram
GOF: Goodness-Of-Fit (X-ray)
H₂: Hydrogen gas
H₂O: Water
H₂O₂: Hydrogen peroxide
H₂SO₄: Sulfuric acid
H-bond: Hydrogen bond
HBr: Hydrogen bromide
HCl: Hydrogen chloride
Hex: Hexane
HNO₃: Nitric acid
HOMO: Highest Occupied Molecular Orbital
hr(s): Hour(s)
HTEB: Hole-Transporting Electron-Blocking
HTL: Hole-Transporting Layer
HTM: Hole-Transporting Moiety/Material
Hz: Hertz
I: Intensity of current (OLED) or Intensity of light (X-ray and absorption)
IC: Internal Conversion
ICT: Intramolecular Charge Transfer

i.e.: illustrative example

IP: Ionization Potential

IQE: Internal Quantum Efficiency

ISC: Intersystem crossing

ITC: Isothermal calorimeter

ITO: Indium Tin Oxide

IUCr: International Union of Crystallography

IUPAC: International Union of Pure and Applied Chemistry

J: Coupling constant (NMR) or current density parameter (OLED)

J/g: Joule per gram

kJ/mol: kilojoule per mole

K: Kelvin

k_{IC} : rate of internal conversion

k_{ISC} : rate of intersystem crossing

k_{nr} : non-radiative decay rate constant

k_r : radiative decay rate constant

k_{tot} : total decay rate constant

K₂CO₃: Potassium carbonate

KI: Potassium iodide

KIO₃: Potassium iodate

L: Liter

L: Luminance parameter (OLED)

LED: Light-Emitting Diode

LE: Locally Excited

Lit.: Literature value

lm: Lumen

LUMO: Lowest Unoccupied Molecular Orbital

M: mol/Liter

m: Meter

m: multiplet

m: Mass

m-: *meta*- (positions 1 and 3 on aromatic ring)

MALDI: Matrix-Assisted Laser Desorption Ionization used in mass spectroscopy

MeOH or CH₃OH: Methanol

mg: milligram

mL: milliliter

mM: mmol/Liter

mmol: millimol

MgSO₄: Magnesium(II) sulfate anhydrous (drying agent)

MHz: Megahertz

min(s): minute(s)

MLCT: Metal-to-Ligand Charge Transfer

MO: Molecular Orbital

mp or *T*_m: Melting temperature

MW or mol wt: molecular weight

n-C₃H₇OH: *n*-propanol

NaOH: Sodium hydroxide

Ni: Nickel

NMR: Nuclear Magnetic Resonance

o-: *ortho*- (positions 1 and 2 on aromatic ring)

OFET: Organic Field Effect Transistor

OLED: Organic Light-Emitting Diode

p-: *para*- (positions 1 and 4 on aromatic ring)

PAH: Polycyclic Aromatic Hydrocarbon

Pd/C: Palladium over carbon catalyst

PdCl₂: Palladium(II) chloride

Pd(OAc)₂ or Pd(CH₃CO₂)₂: Palladium(II) acetate

Pd(PPh₃)₄: Tetrakis(triphenylphosphine)palladium(0)

PEDOT: Poly(3,4-ethylenedioxythiophene)

PET: Photoinduced Electron Transfer

PHOLED: Organic Light-Emitting Diode based on a Phosphorescent emitter

PL: Photoluminescence (fluorescence or phosphorescence)

PLED: Polymer-based Organic Light-Emitting Diode

PPh₃: Triphenylphosphine

ppm: part per million

psi: pounds per square inch

PSS: Poly-styrenesulfonic acid

PtCl₂: Platinum(II) chloride

Py: Pyrene

q: quartet

Red shift: Bathochromic shift

RT: Room temperature (25 °C)

s: singlet (NMR) or second (time)

SMOLED: Small-molecule-based organic light-emitting diode

std: Standard

t: triplet

TADF: Thermally-Activated Delayed Fluorescence

t-butyl or *tert*-butyl: Tertiary butyl

TCSPC: Time-Correlated Single Photon Counting

T_d : Decomposition temperature

T_g : Glass transition temperature

TBA: Tetrabutylammonium

TBABr: Tetrabutylammonium bromide

TBACl: Tetrabutylammonium chloride

TBACN: Tetrabutylammonium cyanide

TBAF: Tetrabutylammonium fluoride

TBAI: Tetrabutylammonium iodide

TBAOAc: Tetrabutylammonium acetate
TBAOBz: Tetrabutylammonium benzoate
TBANO₃: Tetrabutylammonium nitrate
TBAH₂PO₄: Tetrabutylammonium phosphate monobasic (same as dihydrogen phosphate)
TEA: Tetraethylammonium
TGA: Thermogravimetric analysis
THF: Tetrahydrofuran
THP: 4,5,9,10-Tetrahydropyrene
TICT: Twisted intramolecular charge transfer
TLC: Thin-layer chromatography
TMS: Tetramethylsilane
Tol: Toluene
TPPy: 1,3,6,8-Tetraphenylpyrene
TQPP: Quinoxalinophenanthrophenazine
TsCl: 4-Toluenesulfonyl chloride
TTA: Triplet-Triplet Annihilation
ttb...: Tetrakis(*t*-butyl...)
UC: Upconversion
UV: Ultraviolet
UV-vis: Ultraviolet-visible absorption spectroscopy
V: Volt
V_{on}: Turn-on voltage (threshold voltage)
W: Watt
WOLED: White Organic Light-Emitting Diode
% wt: Weight percent
XRD: X-ray diffraction
ZnCl₂: Zinc(II) Chloride
 δ : chemical shift
 Δf : orientation polarizability

ΔH : enthalpy of transition

ϵ : dielectric constant of solvent or molar absorptivity of compound

λ : wavelength

μ : absorption coefficient (X-ray)

μ : charge carrier mobility (OLED)

μ : dipole moment (photophysical studies)

μ -(as prefix): indicates a bridging ligand connected to more than one metal in coordination complexes (synthetic schemes and reagents)

μM : micromole/Liter

π : pi bonding orbital

π^* : pi antibonding orbital

π -acceptor: withdrawing group by mesomeric effect

π -donor: donating group by mesomeric effect

π^* -scale: a polarity scale reported to rank solvents by assigning them π^* -values

π -electrons: electrons in the pi orbitals

ρ : density

σ : standard deviation (X-ray)

σ : sigma bonding orbital

σ^* : sigma antibonding orbital

σ -acceptor: withdrawing group by inductive effect

σ -donor: donating group by inductive effect

τ : lifetime of the excited state

τ_n : natural lifetime (calculated)

ϕ : fluorescence quantum yield (photophysical studies)

ϕ_{pl} : photoluminescent quantum yield (fluorescence or phosphorescence depending on the emitter)

ϕ_{el} : electroluminescent quantum yield (from OLED device)

ϕ_a : anode work function (OLED)

ϕ_c : cathode work function (OLED)

χ^2 : goodness-of-fit parameter for fluorescence lifetime (photophysical studies)

CHAPTER 1

GENERAL INTRODUCTION

1.1. Artificial Lighting: Evolution from Fire to Luminescence

Producing artificial light primarily requires an excitation source able to excite electrons from their ground state to an excited state.¹ Light is generated as photons upon relaxation of electrons from the excited state to the ground state. This process is known as radiative relaxation. Other pathways that lead to the relaxation of the excited electrons without the generation of light as photons are known as non-radiative relaxation processes.¹ The need of artificial lighting is one of the basic needs in daily life activities. Early humans used fire as only source of artificial light.² Later on, the invention of incandescent light bulb (i.e. a lamp having wire filament that glows and emits light upon being heated) in 1860 was a result of the combined effort of Joseph Swan and Thomas Edison.³ However, an incandescent light bulb converts only 5% of the electrical input to visible light, and 95% is wasted as heat.⁴ Fluorescent tube was introduced later on by Peter Cooper Hewitt in 1901.⁵ The main difference between incandescence and fluorescence is the excitation source.⁶ Whereas strong heating triggers a thermal excitation of electrons in incandescence, fluorescence has a major favoring advantage of being a “cold light” referring to the fact that excitation of electrons does not require any heat or flame.⁷ However, fluorescent tubes show major toxicological drawbacks upon breakage or disposal since their toxic mercury content is up to 5 mg per tube.³ Fluorescence is one sub-category of a bigger one known luminescence. There are different types of luminescence that differ by their source of

excitation. These include photoluminescence (fluorescence and phosphorescence),^{8,9} where light is the source of excitation.^{8,9} Mechanoluminescence,¹⁰ where mechanic excitation sources are used to excite electrons. Different mechanic sources include pressure (piezoluminescence¹¹), sound waves (sonoluminescence¹²), or fractures and bond breaking (triboluminescence¹³). Chemiluminescence, in which a chemical reaction induces excitation of electrons.^{9,10} Electroluminescence, in which the flow of electrons between two electrodes induce the excitation.^{10,14} Along with many other types of luminescence were discovered and investigated by researchers.⁸⁻¹⁴ Recently, electroluminescence in combination with photoluminescence (fluorescence and phosphorescence), enabled the development of different electronic devices, such as light-emitting diodes (LEDs) introduced by Nick Holonyak in 1962. These are known as highly efficient environment-friendly lighting techniques that started to develop late in the 20th century commonly referred to as solid-state lighting.³

The main interest of research fields working on luminescence is to design new materials that show efficient fluorescence (i.e. fluorescent materials), and to study their properties (i.e. photophysical studies). Based on which, their efficiency in electroluminescence (i.e. efficiency in LEDs) can be predicted. This imposes different challenges including the design step itself (i.e. synthesis), finding suitable fluorescent materials (i.e. good photophysical properties), and selecting the right material for application in the field of electroluminescence (i.e. electrochemical properties, thermal properties and quantum yield in the solid state).

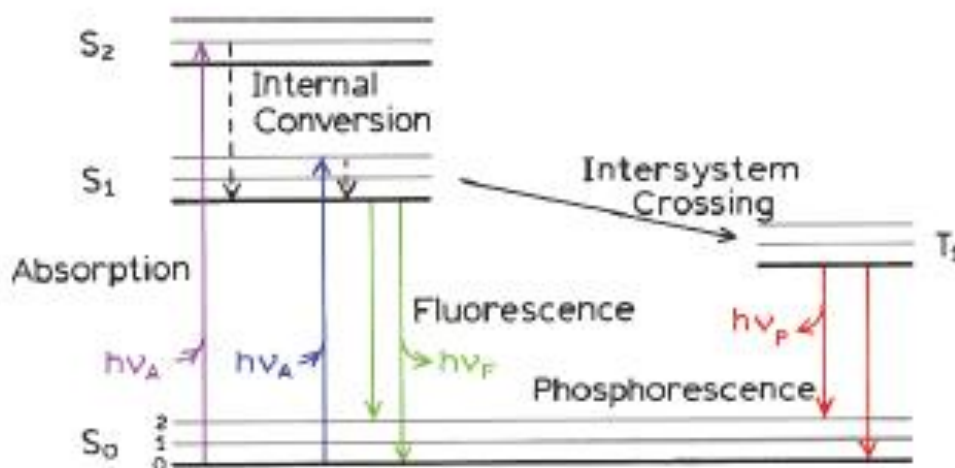


Figure 1.1. Photoluminescence: absorbed light ($h\nu_A$) of specific properties (violet or blue) excites electrons from S₀ (ground state) to S₁ and S₂ (excited states), leading to new light ($h\nu_F$ and $h\nu_P$) of different properties (green or red).¹⁵

1.2. Pyrene Derivatives for Organic Light-Emitting Diodes

Optimizing the performance of Organic Light-Emitting Diodes (OLEDs) is primarily achieved through the inclusion of a strong organic emitting material in the device.^{16,17} Pyrene is a polycyclic aromatic fluorescent hydrocarbon that emits in the blue spectrum with characteristic photophysical properties.¹⁸ However, pyrene by itself has a low efficiency in organic electronic devices due to many factors. Among these, three factors are very important and have to be overridden. First, the interactions between adjacent pyrene molecules in the excited state lead to an excited dimer,¹⁹ also known as excimer, which emits in the green spectrum,²⁰ and results in significant quenching of fluorescence usually occurring in concentrated solution and solid-state.¹⁹ Second, the fact that the S₀→S₁ transition (a transition directly related to fluorescence as can be seen in Figure 1.1),¹⁵ is forbidden in pyrene.²¹ Third, unsubstituted pyrene has a low thermal stability, and this may lead to poor device longevity and resistance.²²

These obstacles can be efficiently overridden through functionalization of pyrene using different substituents at different positions. An investigation of different substituents and their different effects usually focuses on their role regarding the following factors:

- Favoring the forbidden lowest energy transition of pyrene.
- Preventing the formation of excimer through spacing the pyrene cores and decreasing the interactions between adjacent molecules.
- Enhancing the thermal stability with respect to unsubstituted pyrene.

Different substituents lead to different results, and the same substituent in different positions on the pyrene core also leads to different results. In general, aryl substituents (i.e. arylpyrenes) lead to good results. However, there is no single-reaction pathway to reach the arylpyrene derivatives directly from pyrene.¹⁸ The predominant strategy reported in the literature is to achieve the synthesis through electrophilic aromatic substitutions followed by cross coupling reactions.^{18,23,24}

1,3,6,8-Tetraarylpyrene derivatives rank among the most promising for application in organic light-emitting diodes due to the fact that the $S_0 \rightarrow S_1$ transition in these derivatives usually becomes allowed and favored, Figure 1.2;²¹ however, they are only one out of many other arylpyrene categories.¹⁸

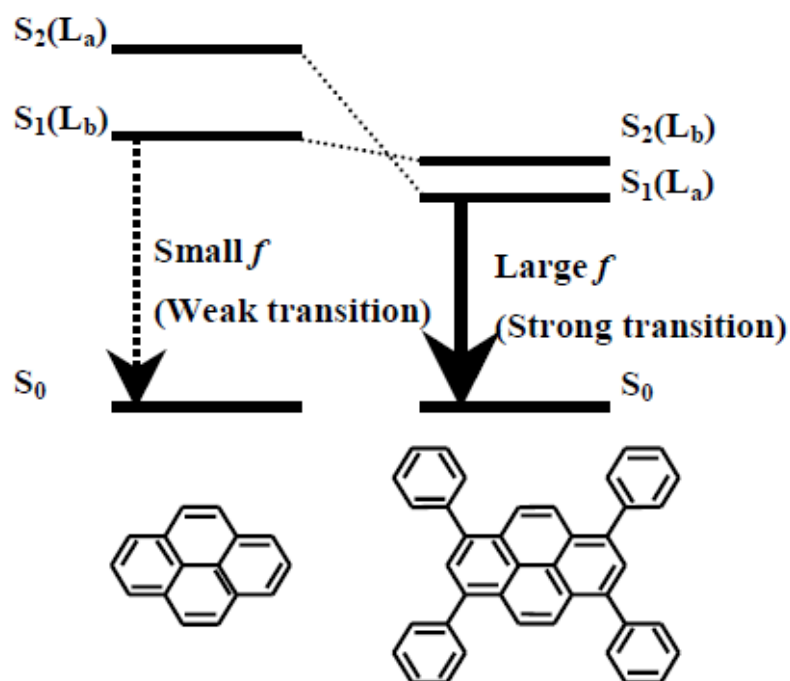


Figure 1.2. Excited states of pyrene (left) vs 1,3,6,8-tetraphenylpyrene (right): L_a denotes the allowed transition (favored only in the latter), L_b denotes the forbidden transition, and f stands for the oscillator strength (probability of the transition). This is more elaborated in Chapter 2.²¹ Sotoyama, W.; Sato, H.; Kinoshita, M.; Takahashi, T.; Matsuura, A.; Kodama, J.; Sawatari, N.; Inoue, H. “Tetra-Substituted Pyrenes: New Class of Blue Emitter for Organic Light-Emitting Diodes”, *Dig. Tech. Pap. - Soc. Inf. Disp. Int. Symp.* **2003**, *34*, 1294-1297. Copyright Wiley-VCH Verlag GmbH & Co. KGaA, Weinheim. Reproduced with permission.

1.3. Fluorescence Sensing: Achieving a “Lock to Key” Selectivity on the Molecular Level

Fluorescence sensing has been a common interest in many research fields.²⁵

Due to high sensitivity and high selectivity,²⁶ fluorescent sensors are becoming more studied and more investigated.²⁷ Fluorescent sensors are sensitive enough to detect their corresponding ligands at significantly low concentrations, even at the picogram level.²⁸ Their molecular geometry can specifically orient their spectrum of detection towards a certain ligand or a family of ligands. These may include: anions²⁹ (i.e. detecting cyanide

toxic anions²⁷), cations²⁶ (i.e. detecting mercury in water³⁰), and some neutral organic molecules possessing specific functional groups (i.e. detecting nitroaromatics explosives²⁸). These “host-guest interactions” resemble a “key-lock interaction” in their high selectivity. The traditional design of a fluorescent sensor consists of a fluorophore and a host. The fluorophore is usually a polyaromatic fluorescent core, and the host is a binding site for the coming guest or ligand.³¹ The fluorophore and the host are either directly connected together or indirectly by the intermediate of a non-conjugated spacer.^{31,32}

Both cation and anion sensors must possess a specific receptor site able to achieve successful binding to specific guests.³³ However, designing selective sensors for anions is usually more challenging.³³ As compared to the corresponding isoelectronic cations, anions are larger in size, and have more diversity in molecular geometry and shape,³⁴ Table 1.1. Hence, they might require more complicated geometries in the host site to achieve the aforementioned specific binding.³³ Furthermore, as compared to similar sized cations, anions show less electrostatic but more dispersion interactions with their environment.³⁵ Anions have more pronounced charge delocalization,³⁶ higher sensitivity to pH variations,³⁴ and exhibit stronger hydration.^{34,36} As a result, the binding of anions in a selective manner to the host site is a more complicated and challenging process.³⁵ Designing fluorescent sensors that can bind selectively to specific anions is a growing research field. Such sensors might be useful in many biomedical, environmental and industrial applications, Table 1.1.

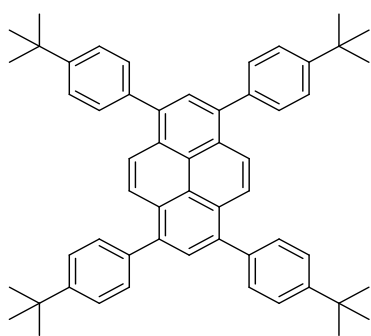
Table 1.1. The difference in molecular geometry among anions and their application.

Anion	Shape	Application
Fluoride	Spherical ³⁵	Biomedical: dental care and treatment of osteoporosis ³⁷
Chloride	Spherical ³⁴	Environmental: tracer of pollution and main tool to detect presence of salt in drinking water ³⁴
Bromide	Spherical ³⁵	Biomedical: diagnosis and treatment of epilepsy ³⁸
Iodide	Spherical ³⁵	Biomedical: treatment of thyroid problems ^{39,40} and protecting thyroid gland against many diseases including cancer ⁴¹
Nitrate	Trigonal planar ³⁴	Environmental: monitoring pollution in agriculture ³⁴
Phosphate	Tetrahedral ³⁵	Environmental: monitoring the increasing phosphate leaching into lakes and rivers ⁴² Biomedical: phosphate is a main component of nucleotides in DNA ⁴³
Cyanide	Linear ³⁴	Biomedical: potentially fatal anion, binds to heme groups in active sites of cytochrome <i>a</i> ₃ inhibiting cellular respiration within only few seconds ²⁷
Carboxylate	Y-shaped ⁴⁴	Industrial: nylon, plastics and paint manufacture ⁴⁵ Biomedical: carboxylate and dicarboxylate (oxalate) presence in some industrially processed food is related to some kidney and intestinal disorders ⁴⁶ and a probable tracer of prostate cancer (acetate) ⁴⁷

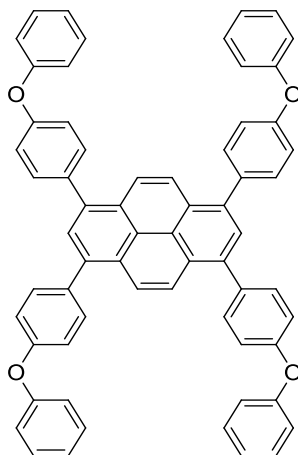
1.4. Aims and Objectives

Different pathways of functionalizing pyrene are presented and discussed in details in Chapter 2, leading to different categories of arylpyrene derivatives. The synthesis of nine derivatives of the 1,3,6,8-tetraarylpyrene (**2.21-2.29**), Figure 1.3, bearing different substituents on the outer benzene ring that were varied from slightly donating to strongly donating (from **2.21** to **2.24**), from slightly withdrawing to strongly withdrawing (from **2.25** to **2.28**), and from a benzene to a heterocyclic thiophene substituent (**2.29**). Synthetic challenges and subsequent procedure modifications are discussed. Complete characterization of these compounds included proton and carbon NMR spectra, elemental analyses, thermal analyses, X-ray of single crystals (when

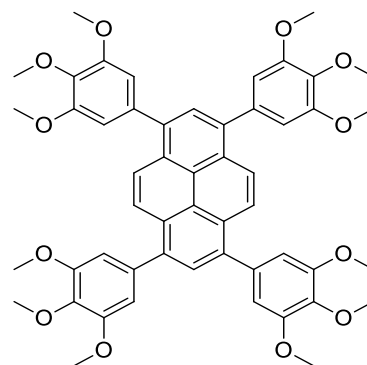
possible), absorption and emission spectra in different solvents having a wide polarity range. A comparison of the absorption, excitation and emission spectra to those of reference compounds (i.e. unsubstituted pyrene Py and 1,3,6,8-tetraphenylpyrene TPPy) is also discussed. Fluorescence lifetimes, natural lifetimes, emission quantum yields (in solution and in solid state), Stokes shifts, radiative and non-radiative decay constants are determined in different solvents, and presented in comparison with those of the two reference compounds. Brief explanation of these concepts is provided along with the discussion, when needed. Part of this work is published in the *Journal of Material Chemistry C*.⁴⁸



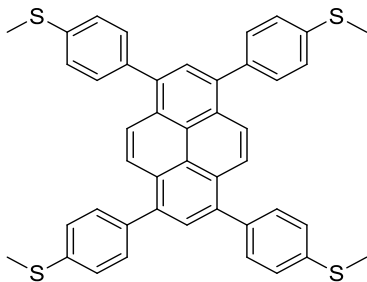
2.21



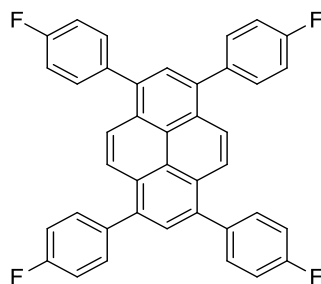
2.22



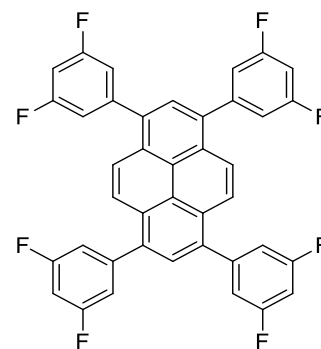
2.23



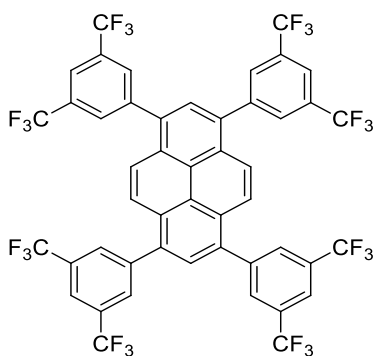
2.24



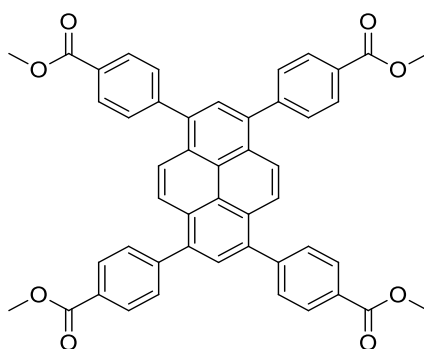
2.25



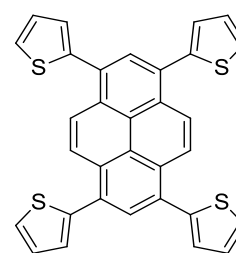
2.26



2.27



2.28



2.29

Figure 1.3. Structures of the nine 1,3,6,8-tetraarylpirene derivatives depicting the choice of different substituents: electron-releasing (2.21-2.24), electron-withdrawing (2.25-2.28), and thiophene instead of benzene (2.29) reported in Chapter 2.

In Chapter 3, the synthesis of 2,7-diarylpyrene (**3.1-3.3**) and 2,7-diaryl-4,5,9,10-tetrahydropyrene (2,7-diaryl-THP, **3.4-3.6**) derivatives with different electron-releasing and electron-withdrawing substituents, Figure 1.4, is reported. The study is similar to the one reported in Chapter 2, but more limited to a photophysical approach. The efficiency of substituting pyrene with different aryl substituents in different positions on enhancing its fluorescence is concluded. This is done through a comparison of the photophysical properties observed for the diaryl derivatives of Chapter 3 with the 1,3,6,8-tetraarylpyrene derivatives of Chapter 2 and the corresponding reference compounds. The effects of 2,7-diaryl and 1,3,6,8-tetraaryl substituents on the forbidden lowest energy transition and on the excimer formation (the two factors that affect the emission quantum yield of pyrene), are also discussed.

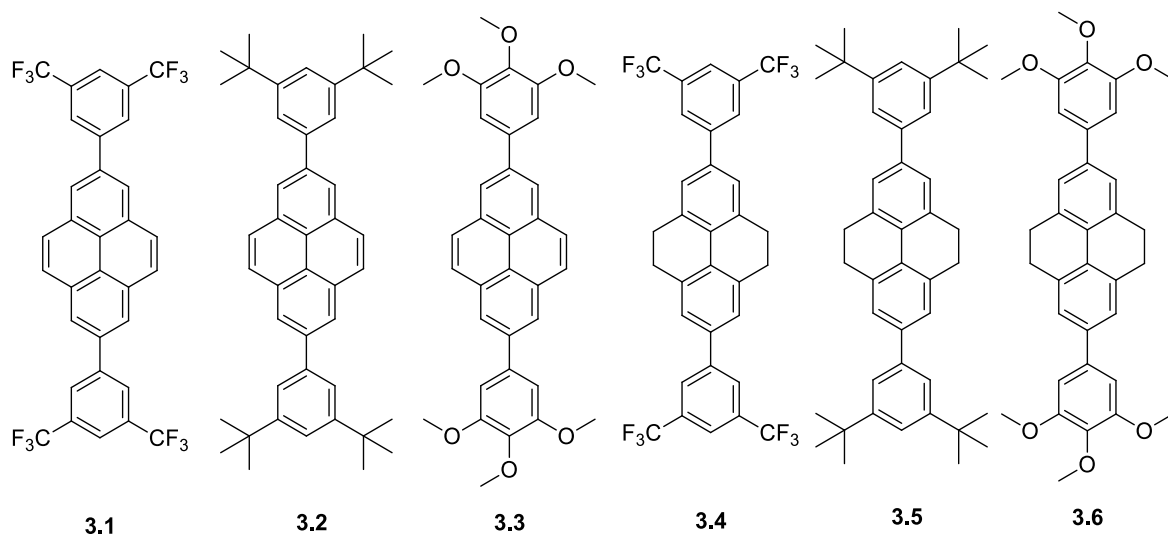


Figure 1.4. Structures of novel 2,7-diarylpyrene and 2,7-diaryl-4,5,9,10-tetrahydropyrene derivatives (**3.1-3.6**) reported in Chapter 3.

In Chapter 4, the photophysical properties of D-A-D (donor-acceptor-donor) (**4.5** and **4.9**) and D-A (donor-acceptor) (**4.10** and **4.11**) compounds are discussed. The use of tercarbazole as donor with pyrene or 4,5,9,10-tetrahydropyrene as acceptor in D-A-D compounds is reported for the first time. D-A-D and D-A systems are compounds made of two different fluorophores (D and A). The donor (D) is electron-rich, and the acceptor (A) is electron-poor with a decent electron affinity. Interesting photophysical results suggest the occurrence of intramolecular charge transfer (ICT) in the excited state from the tercarbazole donor to the acceptor, mainly when the latter is pyrene (**4.5**). Our research group previously investigated compounds having similar structures where the donor is carbazole instead of tercarbazole. Comparison of results obtained upon shifting from carbazole to tercarbazole is described in terms of the photophysical properties of these derivatives. These include absorption, excitation and emission spectra in different solvents having different polarities. Fluorescence lifetimes, natural lifetimes, emission quantum yields, Stokes shifts, radiative and non-radiative decay constants are determined and presented in comparison with those of the carbazole-based compounds.

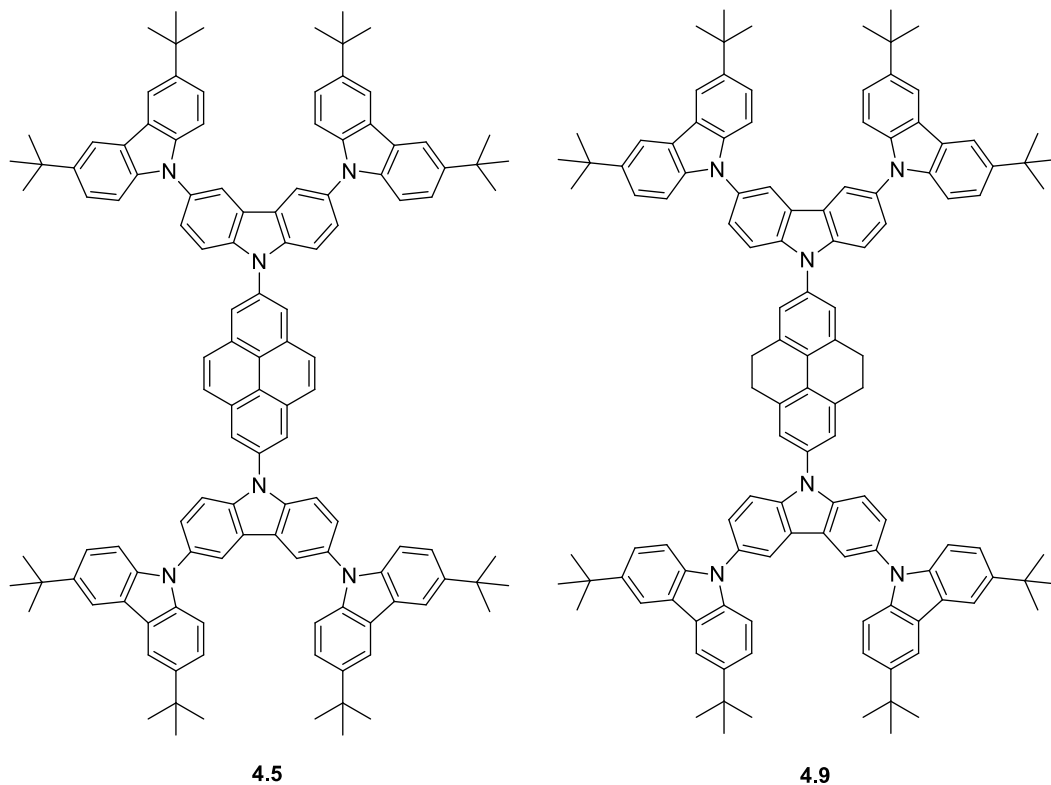


Figure 1.5. Structures of the two new D-A-D compounds (**4.5** and **4.9**) based on a tercarbazole donor reported in Chapter 4.

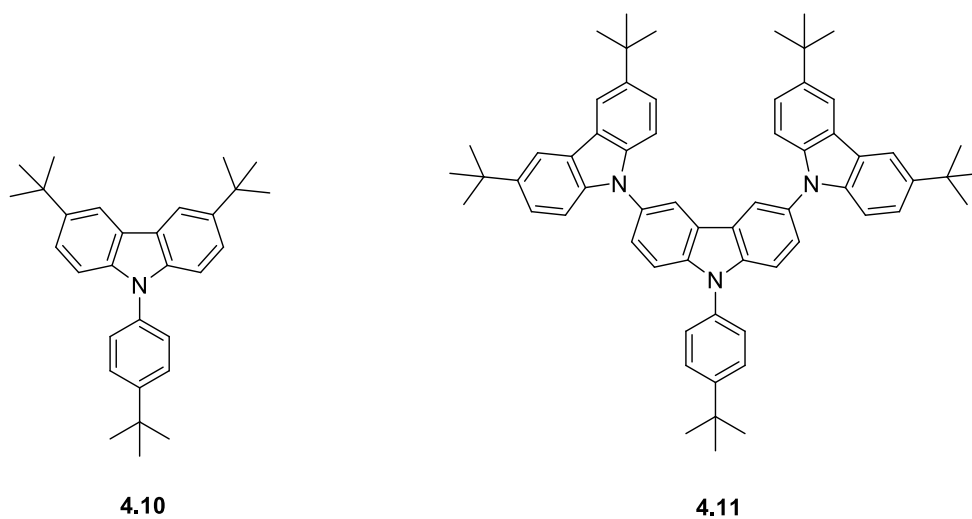


Figure 1.6. Structures of the two new D-A model compounds (**4.10** and **4.11**).

Chapter 5 presents a different concept from the ones discussed in the previous ones. It is about fluorescent sensing of anions. The mechanism is a host-guest interaction between a fluorescent compound known as the sensor, and different guests (i.e. different anions). The interactions take place through a specific site in the sensor molecule known as the binding site (i.e. the N-H of sulfonamide in this Chapter). Dithienophenazine is among the least investigated cores in anion sensors. Our studies suggest a better stability of the sensor induced by the inclusion of the benzene rings bearing bulky *tert*-butyl groups on the dithienophenazine core (as in sensor **5.1**, Figure 1.7). A new binding mechanism, involving a double-recognition of both anions and cations, is suggested through comparing the spectroscopic titration results of sensor **5.1** to other sulfonamide-based sensors reported previously. Two other sensors were also synthesized and investigated in this Chapter. However, these were found to be unstable in solution, and they do not satisfy the criteria for an efficient fluorescent sensor. Conclusions about stability, mechanism of binding, and synthetic routes are presented. Part of this work is published in *RSC Advances*.⁴⁹

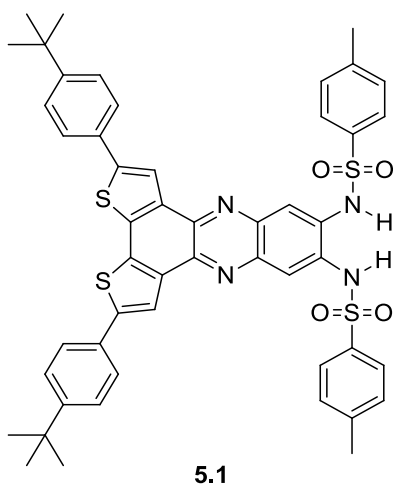


Figure 1.7. Structure of compound **5.1**: the most stable anion sensor with the most interesting characteristics among the ones reported in Chapter 5.

CHAPTER 2⁴⁸

1,3,6,8-TETRAARYLPYRENE COMPOUNDS: POTENTIAL BLUE LIGHT-EMITTERS

2.1. Introduction

2.1.1. Unsubstituted Pyrene: Forbidden Transition and Excimer Formation

Among organic polycyclic aromatic hydrocarbons (PAH) blue emitters, Figure 2.1, anthracene is the first discovered and is the most investigated.⁵⁰ However, others including biphenyl,⁵¹ fluorene,⁵² perylene,⁷ pyrene,⁵²⁻⁵⁴ triphenylene,⁵⁵ truxene,⁵⁶ and their derivatives, Figure 2.1, were also reported to have blue fluorescence properties. Pyrene was discovered in 1837, by the French chemist Auguste Laurent,⁵⁷ through the distillation of coal tar.⁵⁸ Pyrene has particular photophysical^{18,59,60} and chemical¹⁸ properties. These include a very high fluorescence lifetime,⁶¹ a high oxygen sensitivity on the excited state,⁶² and pronounced solvatochromic effects by which pyrene differs from other blue emitting PAHs.⁶⁰ This is why pyrene is known as “the fruit fly of photochemists”.¹⁸

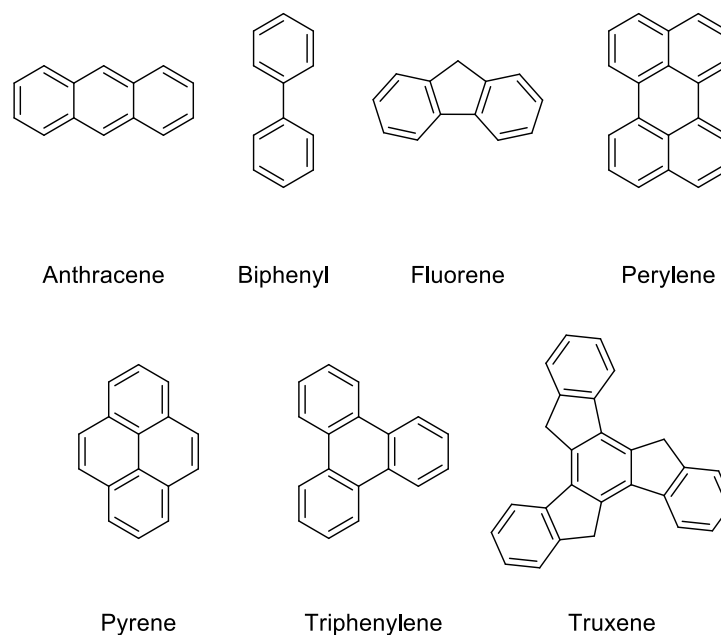


Figure 2.1. Structure of polycyclic aromatic hydrocarbons reported to have blue fluorescence.

Pyrene has been of interest to biomedical and environmental researchers due to its carcinogenic properties.⁶³ Positions 4-5, and 9-10, Figure 2.2, are commonly labeled as the two K-regions of pyrene, and this is due to their direct relation to the carcinogenic properties of pyrene. The term “K-region” originates from rules suggested by Pullman about the carcinogenic effects of polycyclic aromatic hydrocarbons in relation to their geometry and molecular structure.⁶³

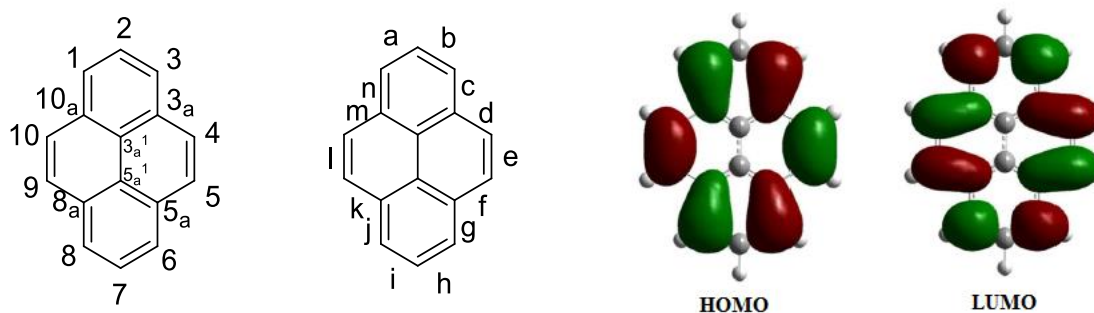


Figure 2.2. Pyrene: (from left to right) atom numbers, edge letters and Frontier orbitals. Numbers and letters were assigned following the IUPAC recommendations on nomenclature of fused and bridged fused ring systems.⁶⁴ Frontier molecular orbital depiction involving $S_0 \rightarrow S_2$ vertical transition of pyrene as calculated at the ω B97/6-31G(d,p) level of theory.⁴⁸

Pyrene is a planar PAH of D_{2h} symmetry.⁶⁵ This implies that the pyrene molecule is bisected by two axes throughout its plane, in addition to a third axis perpendicular to the plane of the molecule. The long axis across positions 2, 3_a¹, 5_a¹, and 7, Figure 2.2, is labeled as z -axis.⁶⁶ The short axis between positions 4, 5, 3_a¹, 5_a¹, 9, and 10, Figure 2.2, is labeled as y -axis, and finally the third axis, which is perpendicular to the other two and to the plane of the molecule (D_{2h} symmetry), is labeled as x -axis.⁶⁶ The three axes together form the principle Cartesian coordinate system used for pyrene as presented in Figure 2.3.

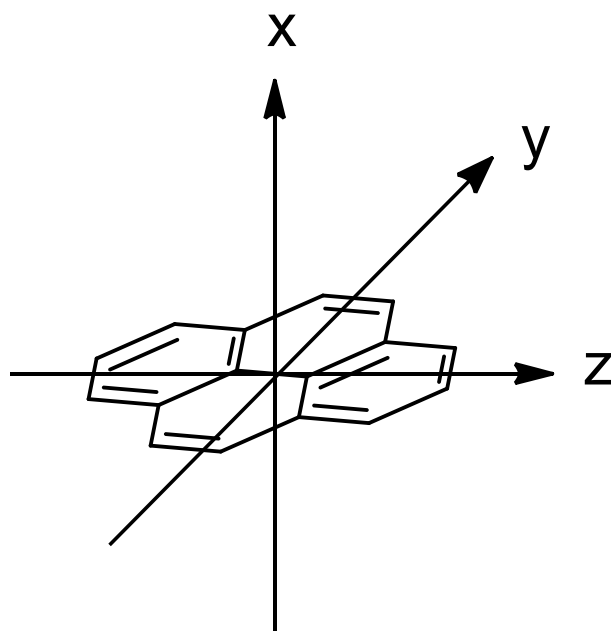


Figure 2.3. The principle Cartesian coordinate system used for pyrene.

According to a review by Ham and Ruedenberg, electronic transitions of aromatic hydrocarbons were studied throughout the 20th century by Clar, Jones, Klevens, Platt, Sponer, Nordheim, McClure, and Sidman.⁶⁷ However, the most commonly used in the literature until this day, are the rules and findings of Clar, Klevens and Platt.^{21,66-68} In fact, a spectral resemblance between aromatic hydrocarbons has been noted, and three main transitions were observed in many of these compounds.⁶⁷ The first is very weak, and is labeled as α according to Clar, and 1L_b according to Klevens and Platt. The second is weak to normal, and is labeled as p according to Clar, and 1L_a according to Klevens and Platt.⁶⁷ The third is strong, and is labeled as β according to Clar, and 1B_b according to Klevens and Platt. Platt suggested that in molecules of lower symmetry than benzene and triphenylene (such as pyrene), a fourth transition labeled as 1B_a exists.^{66,67}

If the lowest energy state (i.e. the S_1 level) corresponds to 1L_a (weak to normal transition), then $S_0 \rightarrow S_1$ is allowed and the aromatic hydrocarbon has good emission properties. However, if the lowest energy state corresponds to the very weak 1L_b transition, the aromatic hydrocarbon is not expected to be a good emitter. Pyrene has four electronic transitions.⁶⁸ $S_0 \rightarrow S_1$ and $S_0 \rightarrow S_3$ are polarized along the short y -axis; however, $S_0 \rightarrow S_2$ and $S_0 \rightarrow S_4$ are polarized along the long z -axis.⁶⁶ The four electronic transitions of pyrene are shown in the absorption spectrum in cyclohexane solution, Figure 2.4, and summarized in Table 2.1.

Table 2.1. The four electronic transitions of pyrene in cyclohexane solution as reported by Crawford *et al.*⁶⁶

$S_0 \rightarrow S_n$	λ (nm)	ϵ ($\times 10^4$ L.mol ⁻¹ .cm ⁻¹)	Clar	Platt	Axis
$S_0 \rightarrow S_1$	372	0.051	α	L_b	y
$S_0 \rightarrow S_2$	334	5.5	p	L_a	z
$S_0 \rightarrow S_3$	272	5.4	β	B_b	y
$S_0 \rightarrow S_4$	243	8.8	β'	B_a	z

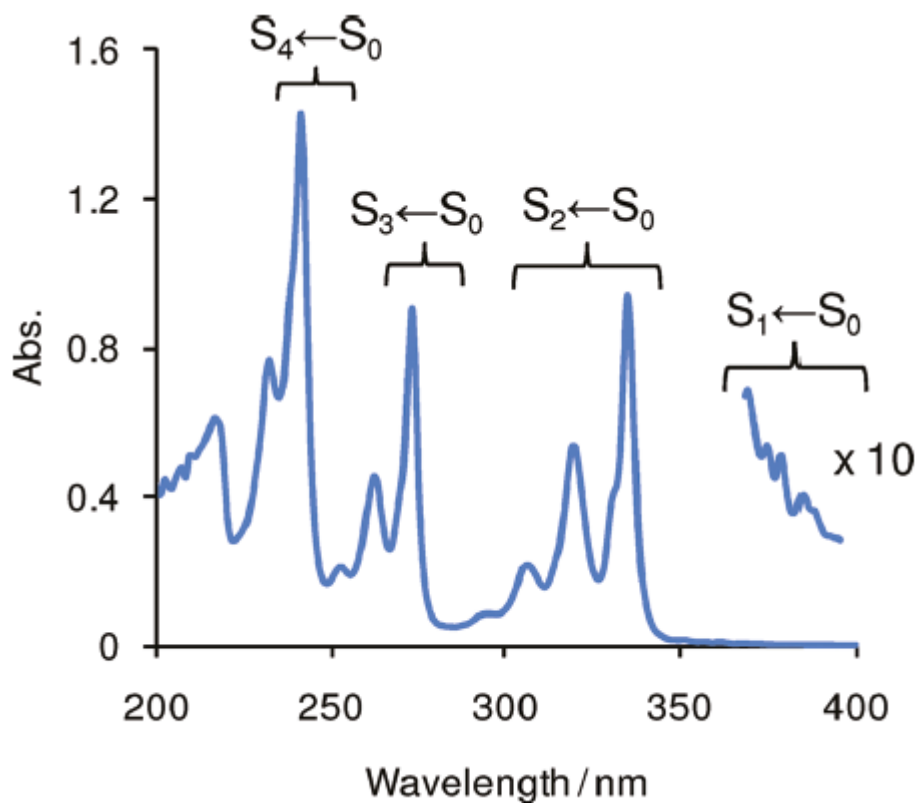


Figure 2.4. Absorption spectrum of unsubstituted pyrene in cyclohexane solution.⁶⁶ Reprinted with permission from (Crawford, A. G.; Dwyer, A. D.; Liu, Z.; Steffen, A.; Beeby, A.; Palsson, L.-O.; Tozer, D. J.; Marder, T. B. *J. Am. Chem. Soc.* **2011**, *133*, 13349). Copyright (2011) American Chemical Society.

The $S_0 \rightarrow S_1$ transition of pyrene corresponds to 1L_b and is forbidden.^{66,69}

The forbidden symmetry of the $S_0 \rightarrow S_1$ transition was also noted for other aromatic hydrocarbons including benzene, biphenyl and naphthalene.⁶⁹ A forbidden transition for organic molecules can be experimentally observed as a transition having $\epsilon < 1$ or $f < 10^{-4}$ (ϵ is the molar absorptivity expressed in $\text{L}\cdot\text{mol}^{-1}\cdot\text{cm}^{-1}$ and f is the oscillator strength of the electronic transition, which is a dimensionless quantity expressing the probability of occurrence of the transition by comparing the strength of the involved transition to a completely allowed transition).⁶⁹

Partially forbidden transitions correspond to ones falling in the range of $1 < \log \epsilon < 3$ or $10^{-4} < f < 10^{-2}$, as illustrated in Figure 2.5.⁶⁹ This implies that pyrene by itself is of limited usefulness as a blue light-emitter in electronic devices, due to the forbidden $S_0 \rightarrow S_1$ transition (i.e. the transition responsible for radiative emission).²¹ This explains the modest emission quantum yield observed for the unsubstituted pyrene molecule.

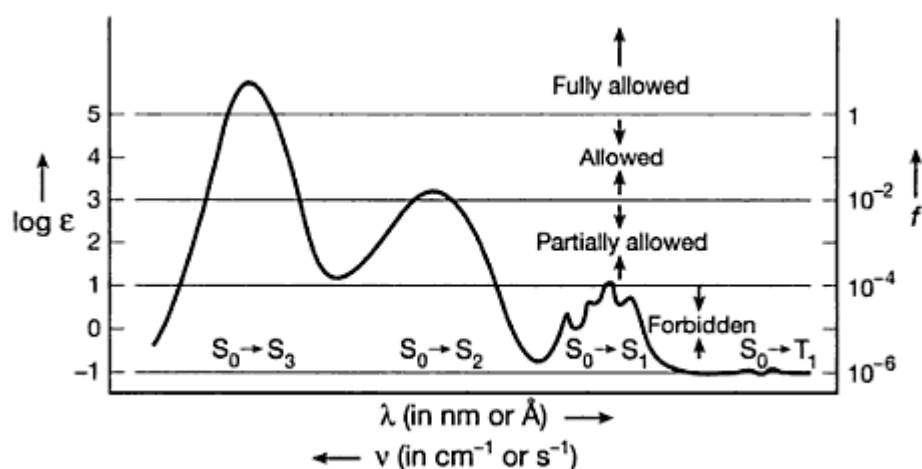


Figure 2.5. Illustration of allowed and forbidden transitions for organic compounds by the analysis of their molar absorptivity and oscillator strength.⁶⁹

Furthermore, pyrene tends to form excimer (i.e. excited dimer),⁶² leading to a significant quenching of fluorescence.²⁴ De Halleux *et al.* explained that adjacent unsubstituted pyrene molecules, being planar hydrocarbons of low polarity, are able to undergo short intermolecular interactions, such as π - π stacking in the solid state. These unwanted interactions might lead to the cofacial dimer, which is known to be non-fluorescent with a forbidden lowest energy transition, Figure 2.6.¹⁹

Therefore, excimer formation is another factor that limits the usefulness of pyrene in electronic devices as a blue emitter.

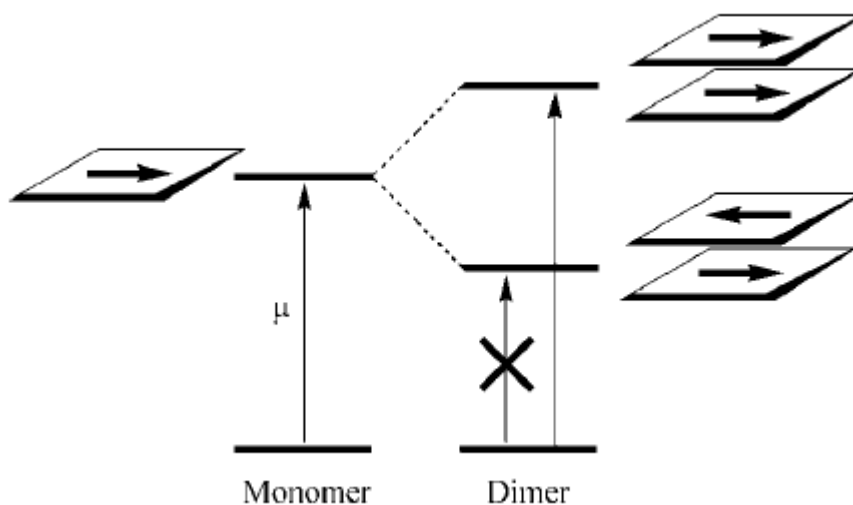


Figure 2.6 The forbidden transition in cofacial dimers responsible for the quenching of their fluorescence.¹⁹ De Halleux, V.; Calbert, J.-P.; Brocorens, P.; Cornil, J.; Declercq, J.-P.; Bredas, J.-L.; Geerts, Y. “1,3,6,8-Tetraphenylpyrene derivatives: Towards fluorescent liquid-crystalline columns”, *Adv. Funct. Mater.* **2004**, *14*, 649-659. Copyright Wiley-VCH Verlag GmbH & Co. KGaA, Weinheim. Reproduced with permission.

Cornil *et al.* reviewed some solutions to the fluorescence quenching induced by the formation of cofacial dimer.⁷⁰ These included a translation along the short or the long axis of one of one of the monomers, or a move from cofacial to perpendicular dimer, or the insertion of substituents that induce changes in the dihedral angle between the two monomers (i.e. substituents that can lie perpendicularly to the plane of the pyrene molecule are the best in spacing adjacent pyrene monomers).⁷⁰ These are illustrated in Figure 2.7.

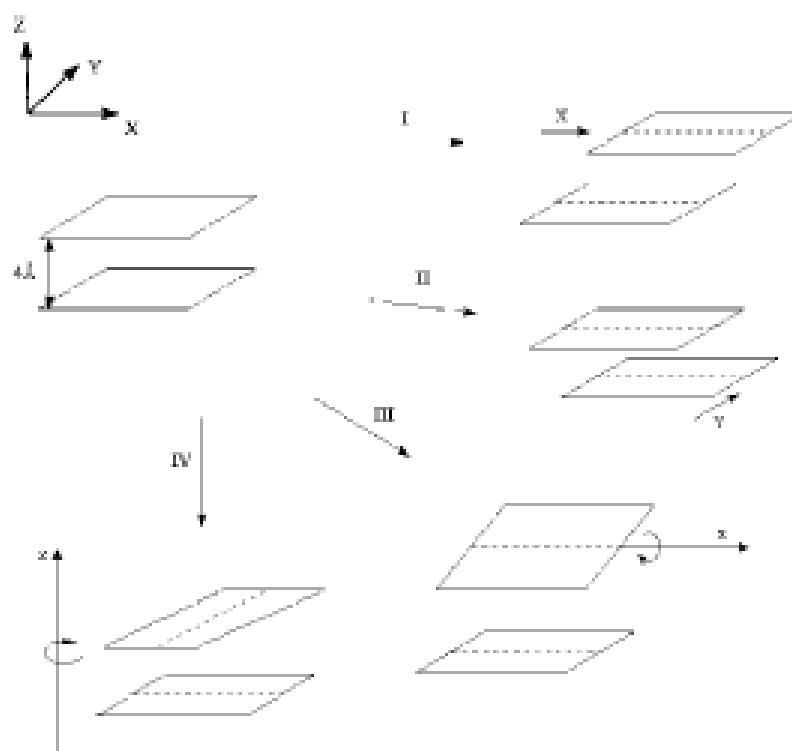


Figure 2.7. Solutions to fluorescence quenching induced by the formation of cofacial dimer: (I) translation along long axis; (II) translation along short axis; (III) change in dihedral angle; (IV) rotation to form a perpendicular dimer.⁷⁰ Cornil, J.; Beljonne, D.; Calbert, J.-P.; Bredas, J.-L. “Interchain Interactions in Organic π -Conjugated Materials: Impact on Electronic Structure, Optical Response, and Charge Transport”, *Adv. Mater.* **2001**, *13*, 1053-1067. Copyright Wiley-VCH Verlag GmbH & Co. KGaA, Weinheim. Reproduced with permission.

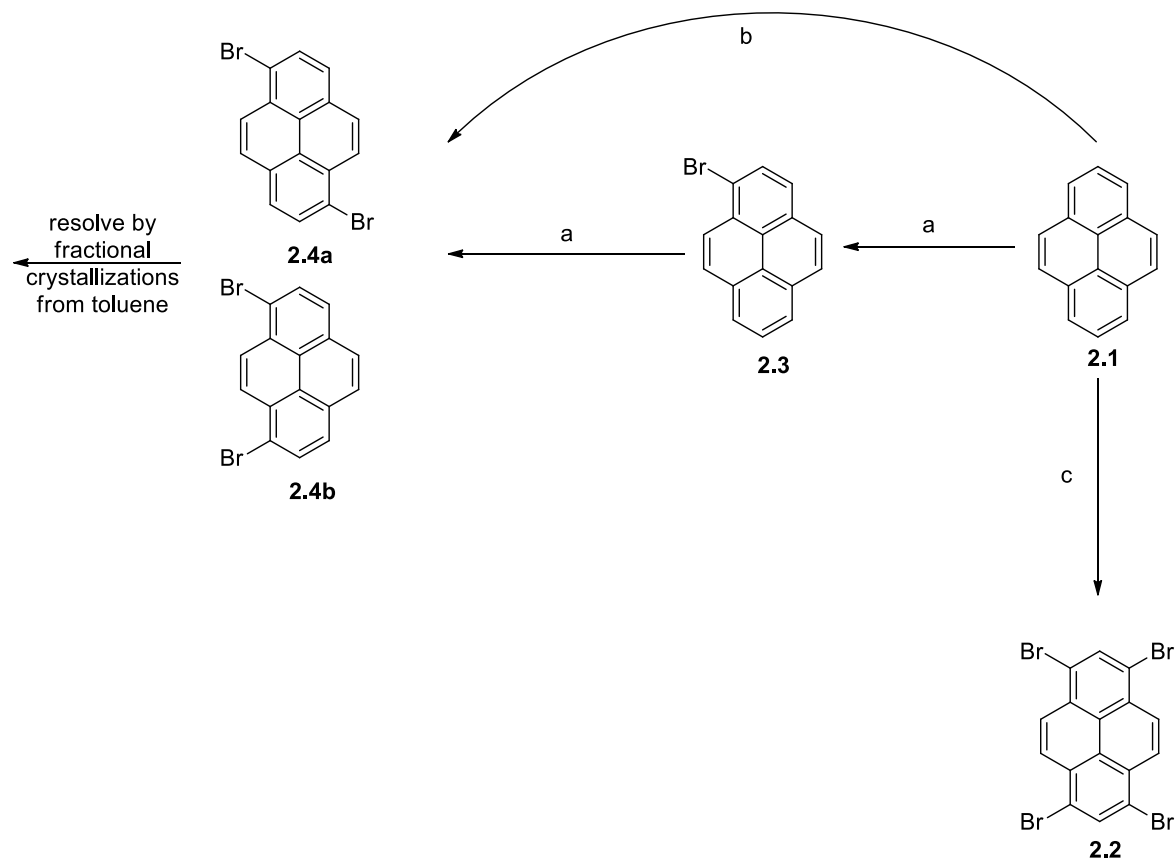
2.1.2. Electrophilic Aromatic Substitution: Bromination of Pyrene

Functionalizing pyrene through the addition of conjugated aromatic branches leading to “arylpyrenes” is one of the most efficient ways to improve its fluorescence quantum yield and subsequently its device usefulness.^{18,19,24} However, starting from unsubstituted pyrene, there is no single-step reaction that can lead to arylpyrene derivatives.¹⁸ This must be done through “building blocks”. Brominated pyrene are the most common building blocks that can undergo cross-coupling reactions leading to arylpyrenes.¹⁸ Schemes 2.1, 2.2, 2.3 and 2.4 summarize the synthesis of different building blocks reported in the literature.

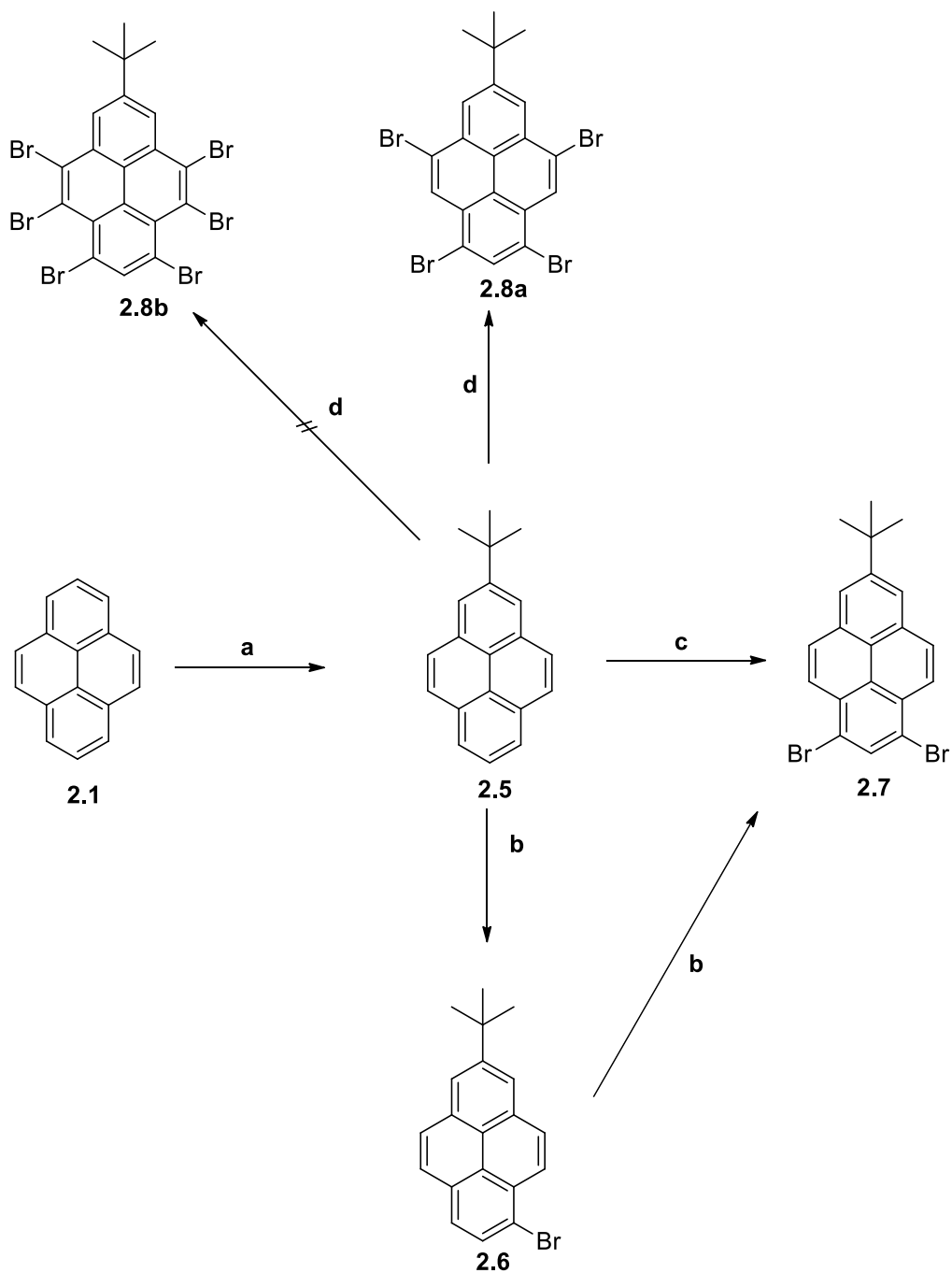
Direct bromination of pyrene occurs in positions 1, 3, 6 and 8, Scheme 2.1.⁷¹ This is because these are the electron-rich sites according to Frontier Molecular Orbital theory, Figure 2.2.⁷² The presence of a nodal plane, bisecting pyrene through positions 2, 3_a¹, 5_a¹ and 7, Figure 2.2, renders positions 2 and 7 electron-deficient. Therefore, the reactivity of these positions is significantly smaller than the electron-rich sites (i.e. positions 1, 3, 6 and 8) in electrophilic aromatic substitution reactions.⁷² An exception is the Friedel-Crafts alkylation where the alkyl is a bulky *tert*-butyl group.⁷³ The steric factor overcomes the electronic factor in this case, favoring the addition of the bulky substituent in the electron-poor positions (**2.5**, Scheme 2.2; **2.9**, Scheme 2.3).⁷³ Following a mono-*tert*-butylation on position 2 (**2.5**, Scheme 2.2),⁷⁴ the most reactive sites of pyrene would be positions 6 and 8, due to both steric and electronic effects.⁷⁴ The addition of excess bromine in the presence of powder iron to 2-*tert*-butylpyrene would result in the tetrabromination at positions 4, 6, 8, and 10 (**2.8a**, Scheme 2.2). This novel resulting building block was reported in 2013 by Feng *et al.*, and was used for the preparation of butterfly-shape 1,3,5,9-tetraaryl-7-*tert*-butylpyrene compounds for OLED applications as blue emitters, due to their excellent photophysical and electrochemical properties and high thermal stability.⁷⁴ The role of iron as catalyst is to enhance the bromination probability in the K-region of pyrene through a sterically-favored Lewis acid-catalyzed rearrangement of the bromine atom from the electron-rich positions to the K-region carbons.^{18,74-76} In the case of mono-*tert*-butylated pyrene, such rearrangement involves the two carbons of the K-region that are on the side of the *tert*-butyl bulky substituent exclusively (**2.8a**, Scheme 2.2).⁷⁴ Such rearrangement does not involve the two carbons of the K-region on the opposite side from the bulky group, and no bromination is observed on these carbons, (**2.8b**, Scheme 2.2).

However, in the di-*tert*-butylated pyrene the rearrangement occurs in both sides achieving a complete bromination of the K-region of the di-*tert*-butylated pyrene (**2.13**, Scheme 2.3).^{75,76} Lewis acid must be FeBr₃ in this acid-catalyzed rearrangement.^{75,76} TiCl₄, FeCl₃, and AlCl₃ were tried and found to be not successful according to Yamamoto *et al.* (**2.12**, Scheme 2.3).⁷⁶ Interestingly, according to Hu *et al.*, doubling the reaction time without changing any other reaction condition, leads to the pentabromo derivative (**2.14**, Scheme 2.3).⁷⁵ This *detert*-butylation could be closely related to what the review of Figueira-Duarte and Müllen mentioned regarding a removal of the *tert*-butyl from positions 2 and 7 positions of pyrene through reflux with a Lewis acid and an activated aromatic acceptor like toluene.¹⁸ The removal of *tert*-butyl groups (i.e. *detert*-butylation) is further elaborated in Chapter 4, Paragraph 4.2.8.

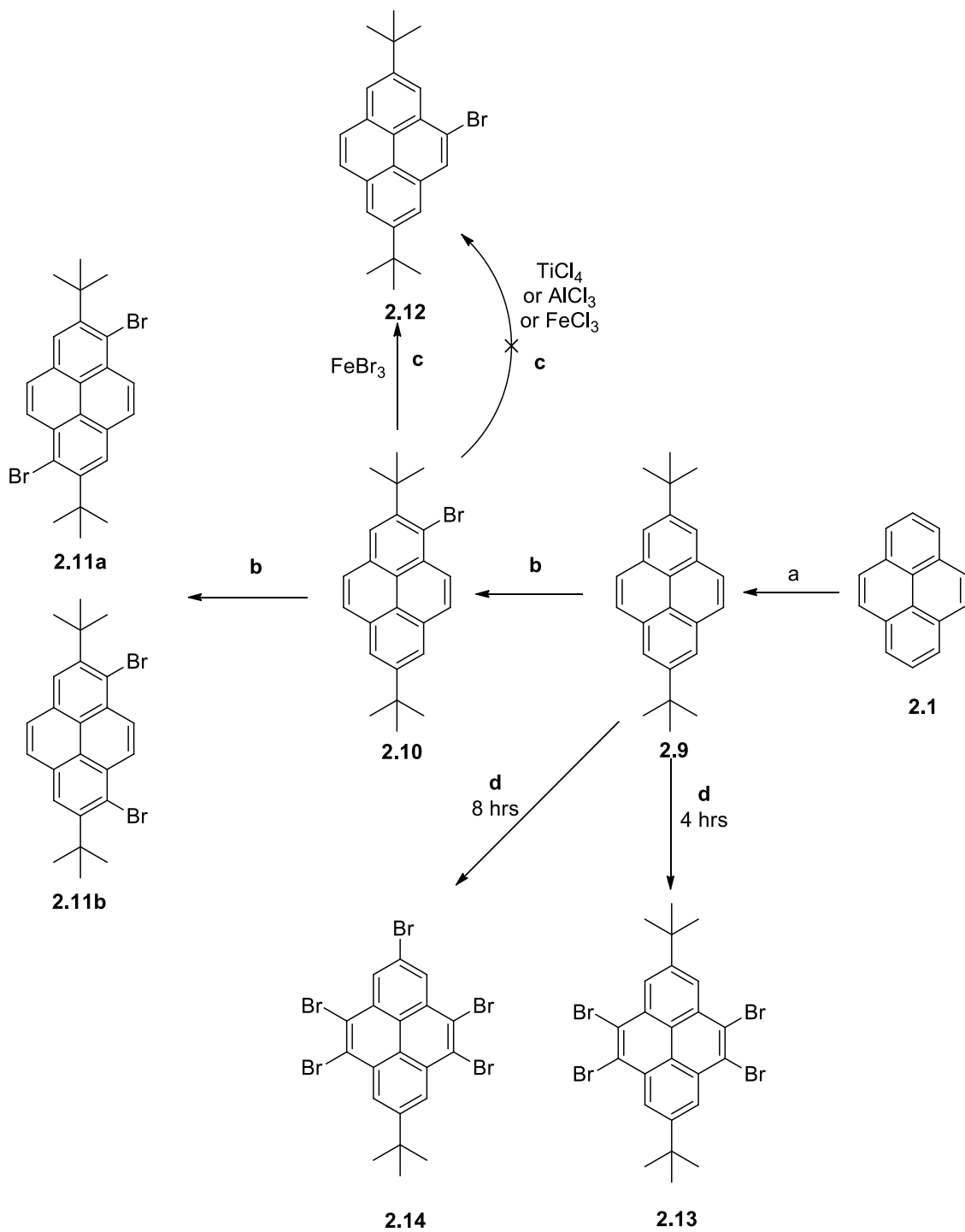
Indirect bromination can occur in positions 2 and 7, Scheme 2.4. This can be achieved by the removal of the nodal plane through a hydrogenation reaction (**2.15**, Scheme 2.4)⁷⁷ to enhance the reactivity of these positions,⁷² followed by the bromination (**2.16**, Scheme 2.4),⁷⁸ and an oxidation step to restore the nodal plane (**2.17**, Scheme 2.4).⁷⁹ The selective C-H borylation to form a five membered ring boronic ester (**2.18** and **2.19**, Scheme 2.4),⁷² is mainly favored in the 2 and 7 positions of pyrene, due to steric effect.^{72,80} The latter offers an alternate pathway to achieve bromination of pyrene on positions 2 and 7.



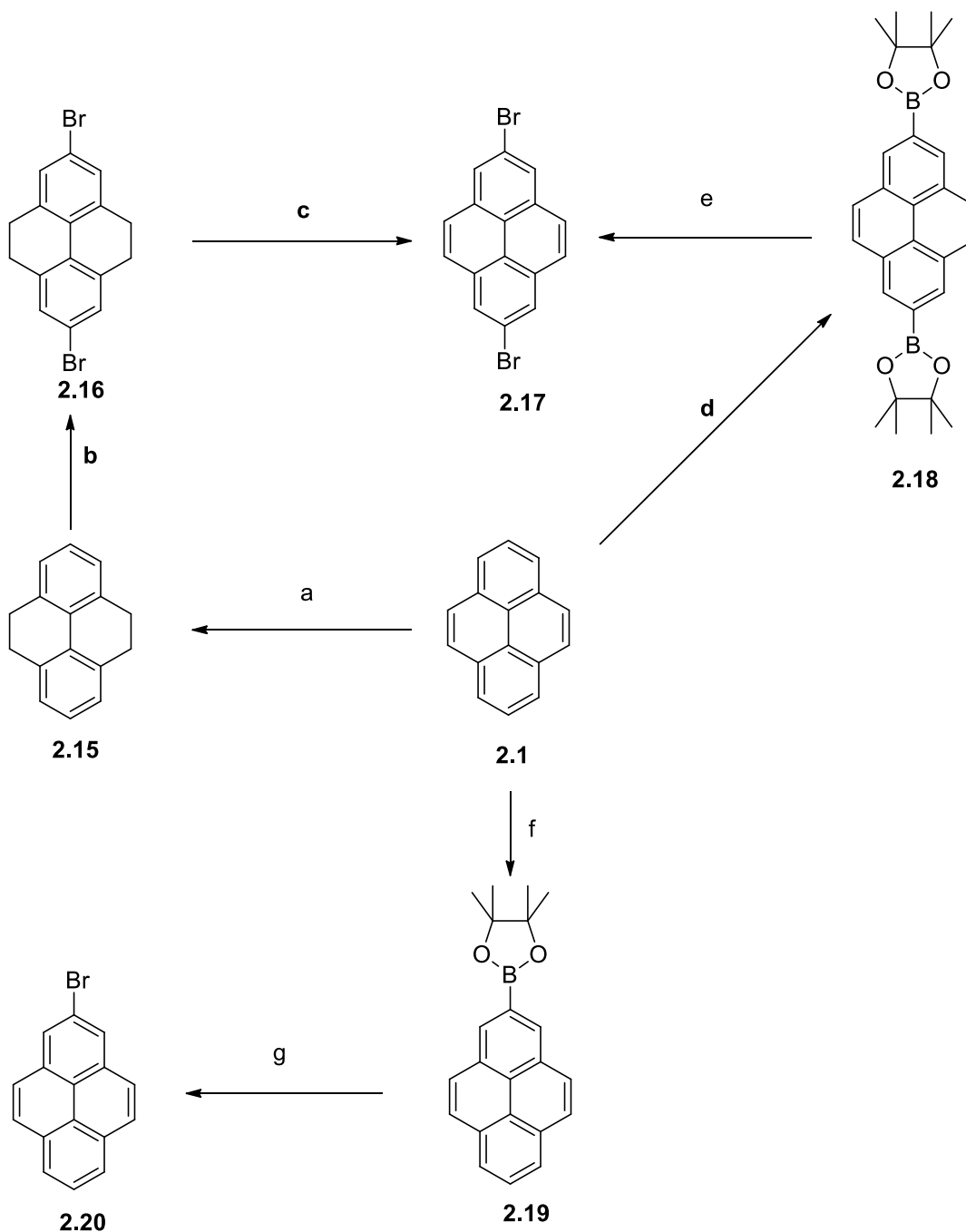
Scheme 2.1. Direct bromination of pyrene. (a) $\text{BnMe}_3\text{N-Br}_3$ (1 eqv), ZnCl_2 anhydrous (1.1 eqv), AcOH, 25 °C, 12 hrs⁸¹ or HBr (1.1 eqv), H_2O_2 (1 eqv), MeOH-Et₂O (1:1) 15→25 °C, 12 hrs;⁸² (b) same conditions as (a) with double equivalents and reaction time;^{81,82} (c) Br_2 (4.4 eqv), nitrobenzene, 160 °C, 3 hrs.⁷¹



Scheme 2.2. Bromination following mono-*tert*-butylation of pyrene. (a) *t*-BuCl (1.2 eqv), AlCl₃ anhydrous (1.1 eqv), CH₂Cl₂, 0→25 °C, 3 hrs;⁷³ (b) Br₂ (1 eqv), CH₂Cl₂, (-78→25 °C), inert atmosphere, 24 hrs;⁸³ (c) same conditions as (b), but with (2 eqv) Br₂;⁸³ (d) Br₂ (6 eqv), Fe-powder (5 eqv), CH₂Cl₂, 25 °C, 4 hrs.⁷⁴

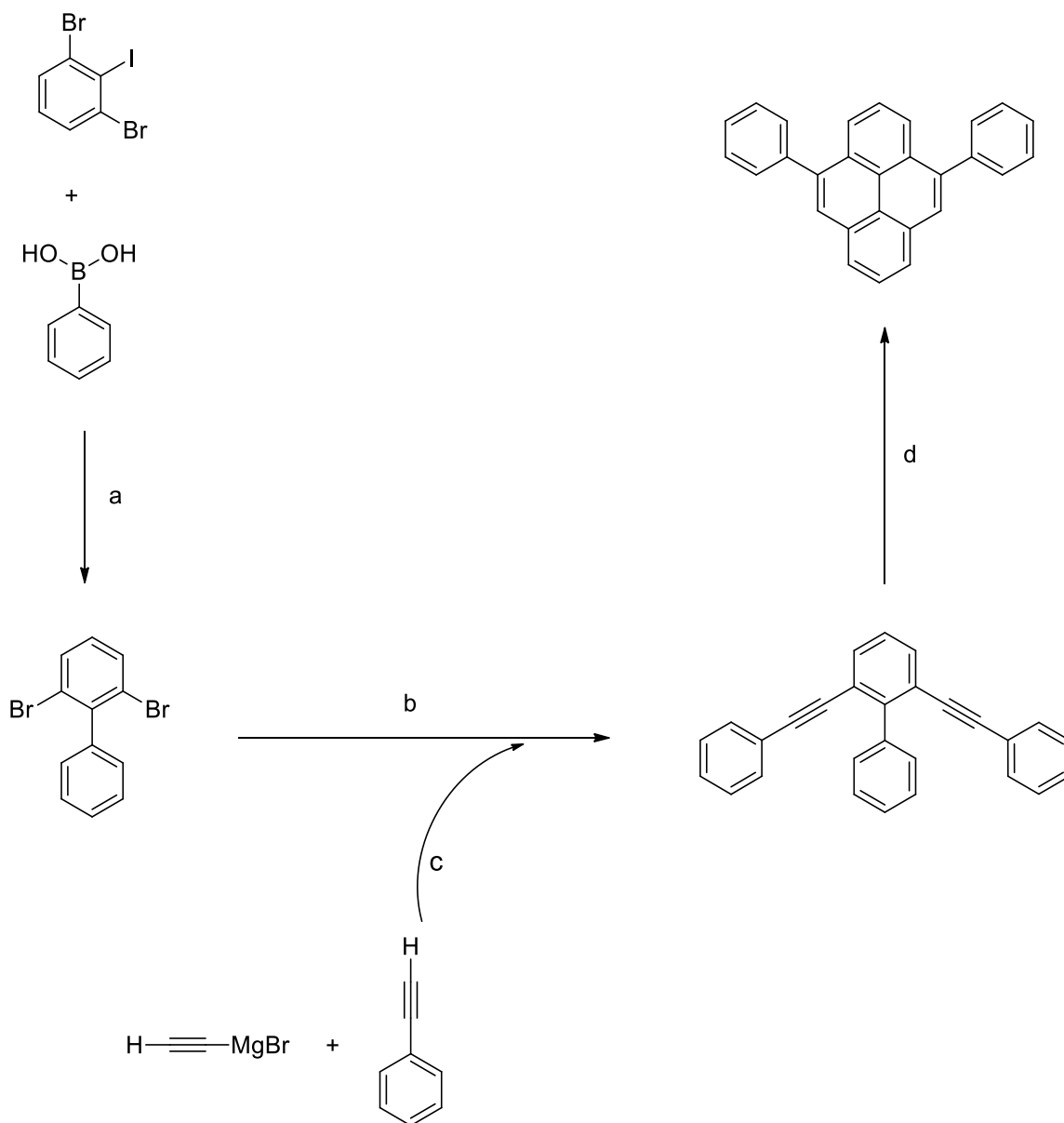


Scheme 2.3. Bromination following di-*tert*-butylation of pyrene. (a) *t*-BuCl (> 3 eqv), AlCl₃ anhydrous (1.5 eqv), 0→25 °C, 3 hrs;^{73,84} (b) Br₂ (1.1 eqv), CCl₄, 0→25 °C, 1 hr;⁷⁶ (c) CCl₄, 25 °C, 3 hrs;⁷⁶ (d) Br₂ (6 eqv), Fe-powder (3 eqv), CH₂Cl₂, 0→25 °C.⁷⁵



Scheme 2.4. Bromination of pyrene in the 2 and/or 7 positions. (a) (1) Raney Ni, EtOAc, 25 °C, 48 hrs;⁷⁷ (2) Pd/C, EtOAc, H₂ (40 – 45 psi), 25 °C, 78 hrs;⁷⁷ (b) Br₂ (2.2 eqv), NaOH (2.2 eqv), AcOH/H₂O (1:1), 25 °C, 24 hrs;⁷⁸ (c) Br₂ (2.2 eqv), CS₂, 25 °C, 4 hrs; (d) B₂pin₂ (2.2 eqv), [Ir(μ-OMe)cod]₂ (0.01 eqv), dtbpy (0.02 eqv), THF, 80 °C, inert anhydrous atmosphere, 16 hrs;⁷² (e) CuBr₂ (6 eqv), MeOH/H₂O/THF (3:3:1), 90 °C, 16 hrs;⁷² (f) B₂pin₂ (1.1 eqv), [Ir(μ-OMe)cod]₂ (0.01 eqv), dtbpy (0.02 eqv), hexane, 80 °C, inert anhydrous atmosphere, 16 hrs;⁷² (g) CuBr₂ (3 eqv), MeOH/H₂O (1:1), 90 °C, 16 hrs.⁷²

Once the synthesis of the brominated building blocks is achieved, a cross-coupling reaction is the following step.^{18,24,54,72} Cross-coupling reactions, a type of organometallic reactions, are known to be useful strategies in creating new carbon-carbon bonds, especially when one of these is an aryl group.⁸⁵ Many interesting applications of cross-coupling reactions were recently reported.^{85,86} Beside their application in organic synthesis to achieve extended π -conjugated systems; recently, important biomedical achievements using these reactions were reported.⁸⁶ It is worth showing a very recent achievement that illustrates the importance of these coupling reactions in organic synthesis. In which a new protocol, involving a three-step synthesis including Suzuki-Miyaura coupling and Kumada coupling reactions, was described by Machuy *et al.* in 2012 to achieve the synthesis of 4,10-diarylpyrene compounds starting from four separate benzene rings, Scheme 2.5.⁸⁷ 4,10-Diarylpyrene is a very uncommon and non-investigated category of arylpyrene derivatives.⁸⁷ This is well-understood by the fact that there are no corresponding building blocks for this category of arylpyrene in Schemes 2.1-2.4 (i.e. a building block having bromine atoms on positions 4 and 10 exclusively).



Scheme 2.5. Preparation of 4,10-diarylsilylphenylpyrene from four separate benzene rings. (a) K_2CO_3 (3.6 eqv), PEPPSI-IPr (0.05 eqv), 1,4-dioxane, inert anhydrous atmosphere, reflux, 36hrs;⁸⁷ (b) $\text{PdCl}_2(\text{PPh}_3)_2$ (0.15 eqv), THF, inert anhydrous atmosphere, reflux, 48 hrs;⁸⁷ (c) HCCMgBr (1 eqv), PhCCH (6 eqv), -40°C , inert anhydrous atmosphere;⁸⁷ (d) PtCl_2 (1 eqv), toluene, inert anhydrous atmosphere, reflux, 20 hrs.⁸⁷

The first step is the Suzuki-Miyaura coupling reaction, Scheme 2.5 (a).⁸⁷ The second step appears as similar to a regular Grignard reaction; however, involving arylhalides requires the reaction to be palladium-catalyzed, and this is known as the Kumada coupling reaction, Scheme 2.5 (b).⁸⁷ A transmetalation step at (-40°C) is required, and is achieved separately, Scheme 2.5 (c). The product of the latter is used, in excess, as a reactant for the Kumada coupling step. The last step is an electrophilic cyclization, Scheme 2.5 (d).⁸⁷ All these four reactions show a particular sensitivity to oxygen and water, and require inert and dry conditions.⁸⁷ The inclusion of substituents on the outer benzene rings on positions 4 and 10 of pyrene is possible through starting by a substituted ethynylbenzene derivative in the transmetalation step. The inclusion of substituents on the pyrene core is also achievable by using substituted arylboronic acids in the Suzuki reaction.⁸⁷ This strategy might be promising towards the synthesis of relatively obscure 4,10-diarylpyrenes derivatives bearing different substituents on different positions.

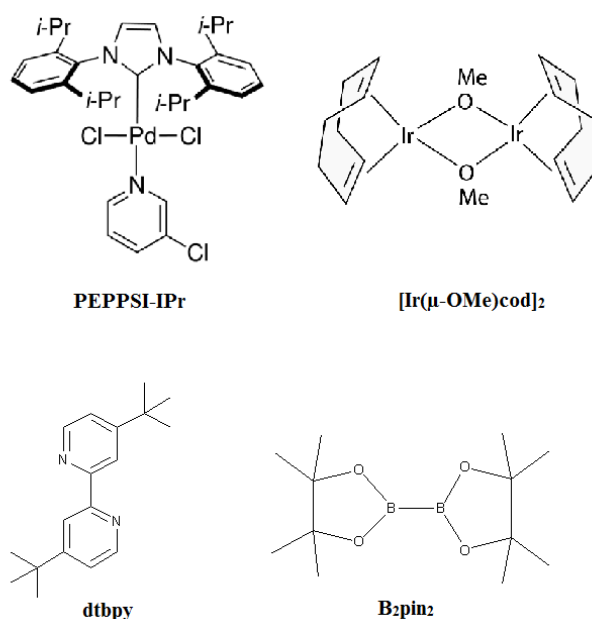


Figure 2.8. Structures of the compounds that were mentioned as abbreviations below Schemes 2.4 and 2.5.

In this Chapter, the synthesis of functionalized pyrene blue emitters is reported. Functionalization was achieved through the direct tetrabromination pathway (**2.2**, Scheme 2.1), followed by a Suzuki-Miyaura coupling reaction to reach blue light-emitting 1,3,6,8-tetraarylpyrene compounds.

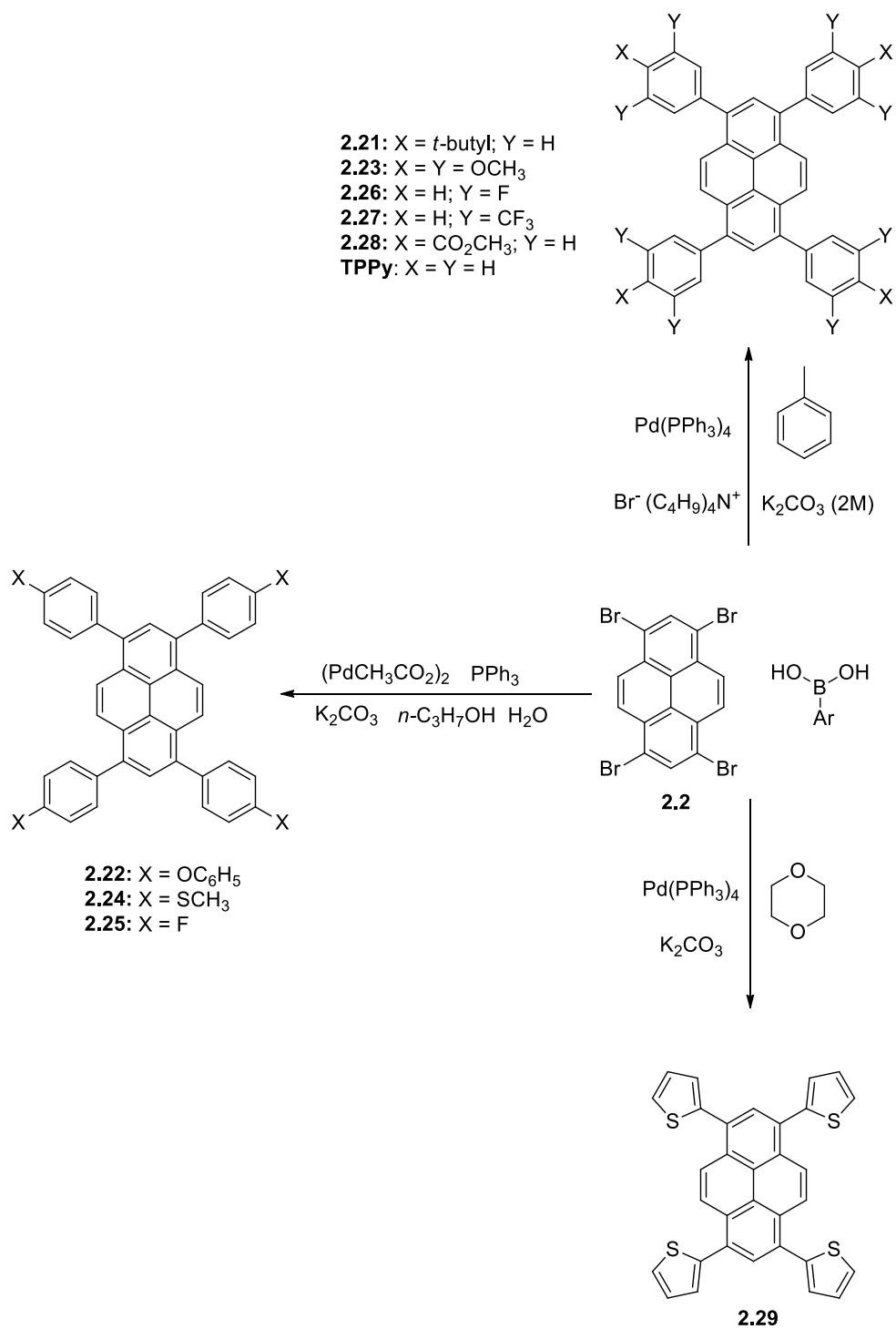
2.2. Results and Discussion

2.2.1. Synthesis

The low solubility of 1,3,6,8-tetrabromopyrene (**2.2**, Scheme 2.6), in most organic solvents, made the Suzuki-Miyaura procedure difficult. Therefore, many synthetic procedures had to be investigated. A total of ten different compounds were synthesized using three different literature procedures for the Suzuki reaction, involving 1,4-dioxane,¹⁹ *n*-propanol,⁸⁸ and toluene²³ as solvents, Scheme 2.6. The procedure with the toluene solvent was found to be the most suitable for running a Suzuki reaction starting from 1,3,6,8-tetrabromopyrene **2.2**. This is illustrated by the fact that the synthesis and purification of compounds **2.21** and **2.26** could be achieved through this specific procedure exclusively. After earlier attempts using the two remaining procedures have failed. This might be explained by a heat-induced very low solubility of 1,3,6,8-tetrabromopyrene in boiling toluene, which is not the case for 1,4-dioxane and *n*-propanol. Longer reaction time was required when the boronic acid had an electron-withdrawing group (**2.25**, **2.26**, **2.27**, **2.28** Scheme 2.6). This is due to the fact that the organoboron carbon is less electron-rich, and is subsequently less reactive.⁸⁵

The instability of the palladium zero catalyst, Pd(PPh₃)₄, is due to a high sensitivity to oxygen, heat and light.⁸⁹ This prevents the storage of large amounts of the catalyst for long periods of time, even at low temperature and under inert atmosphere.

Therefore, in an attempt to improve the outcome of the Suzuki reaction, the *n*-propanol procedure involved in-situ generation of this catalyst out of palladium acetate and triphenyl phosphine.⁸⁸ However, the best choice was found to be the synthesis and purification of the catalyst starting from palladium chloride and triphenyl phosphine in a separate small-scale reaction shortly before running the Suzuki reaction. The freshly synthesized catalyst lead to better outcome in the Suzuki reaction using the procedure involving toluene as a solvent.



Scheme 2.6. Different synthetic procedures used to synthesize the nine blue emitters and TPPy.

2.2.2. *Molecular Photophysics*

2.2.2.1. Absorption, Emission and the Stokes Shift

The ground state and the excited state have different dipole moments.¹⁵ In general, fluorophores have larger dipole moments in their excited state than in their ground state. An excitation from the ground state S_0 to an excited state (S_1 or S_2 or any higher energy levels S_n), Figure 2.9 (left), occurs by the absorption of a photon of a specific wavelength. This absorption occurs within a relatively short duration, on the order of femtoseconds (10^{-15} s).¹⁵ In the excited states, internal conversions and vibrational relaxations occur to allow the relaxation of the excited electron to the lowest vibrational level of the first excited state. These relaxations are non-radiative (i.e. do not release photons/light), and they occur within few picoseconds (10^{-12} s). If the excited molecule has no interactions with its environment (i.e. in gas phase), the emission occurs at this stage.¹⁵ A photon of a longer wavelength than that of the absorption is emitted. This difference in wavelengths is due to the relaxations taking place before the emission. The relaxations in the excited state lower the energy of the emitted photon with respect to the one absorbed. Emission occurs within few nanoseconds, and it is a radiative relaxation (i.e. does release photons/light).¹⁵ However, in the presence of interactions between the molecule and its environment (i.e. in solution), additional relaxations take place before the emission. These are known as solvent relaxations, and occur within less than 100 picoseconds at room temperature (10^{-10} s). Solvent relaxations are described as a redistribution of solvent molecules around the excited state of the fluorophore accompanied by a redistribution of electrons in the solvent molecules, Figure 2.9 (right).¹⁵ All non-radiative relaxation phenomena, including the solvent relaxations, are faster than the emission, but slower than the absorption.

Thus, these relaxations are more likely to affect the wavelength of the emitted photon rather than the absorbed one. Furthermore, the excited state, in general, has a larger dipole moment than that of the ground state. As a result, a more polar solvent is able to offer more solvent relaxation to the excited state than a less polar one, Figure 2.9 (left).¹⁵ This leads to a bathochromic shift in the emission wavelength upon changing from a non-polar to a polar solvent. The bathochromic shift induced by an increasing solvent polarity is referred to as a solvatochromic shift. Subsequently, the more polar the fluorophore is, the more pronounced its solvatochromic shift will be (i.e. more affected than non-polar fluorophores by solvent relaxation processes in polar solvents).¹⁵ At very low temperature, the solvent relaxation becomes slower than the emission process, especially in solvents that tend to become too viscous upon cooling. Thus, emission at very low temperatures occurs from the non-solvent-relaxed state and the solvent polarity factor tends to be less contributing.¹⁵

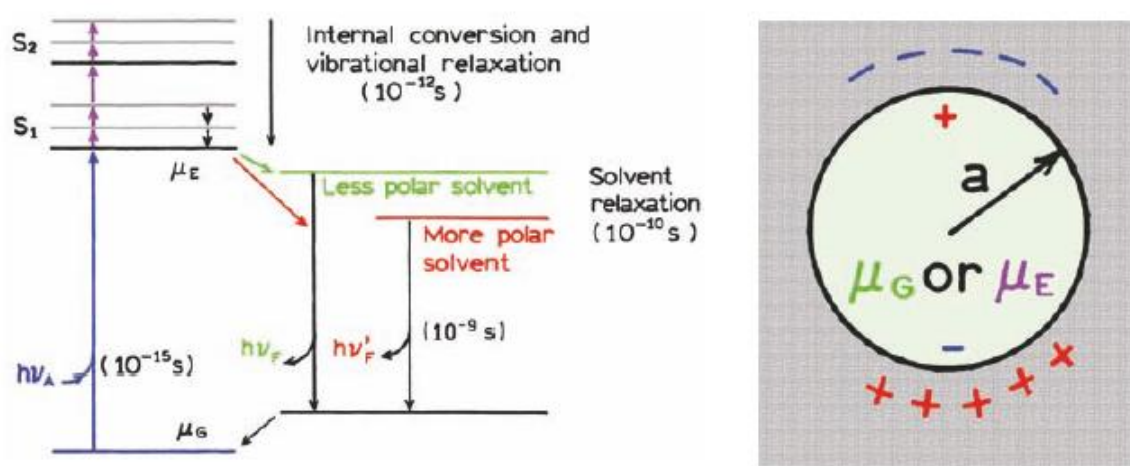


Figure 2.9. Jablonski diagram illustrating the different photophysical processes with their corresponding duration (left); illustration of solvent relaxation as a redistribution of solvent molecules around the fluorophore (right).¹⁵

The fact that many vibrational levels exist within the ground state and the excited states creates a vibrational structure in the absorption or/and emission spectra.¹⁵ The absorption and emission spectra of anthracene are a good example. Whereas both absorption and emission show a single transition ($S_0 \rightarrow S_1$), many peaks can be observed in these spectra (i.e. vibrational structure in the spectra). This is due to the existence of many vibrational levels within both S_0 and S_1 as shown in Figure 2.10.¹⁵

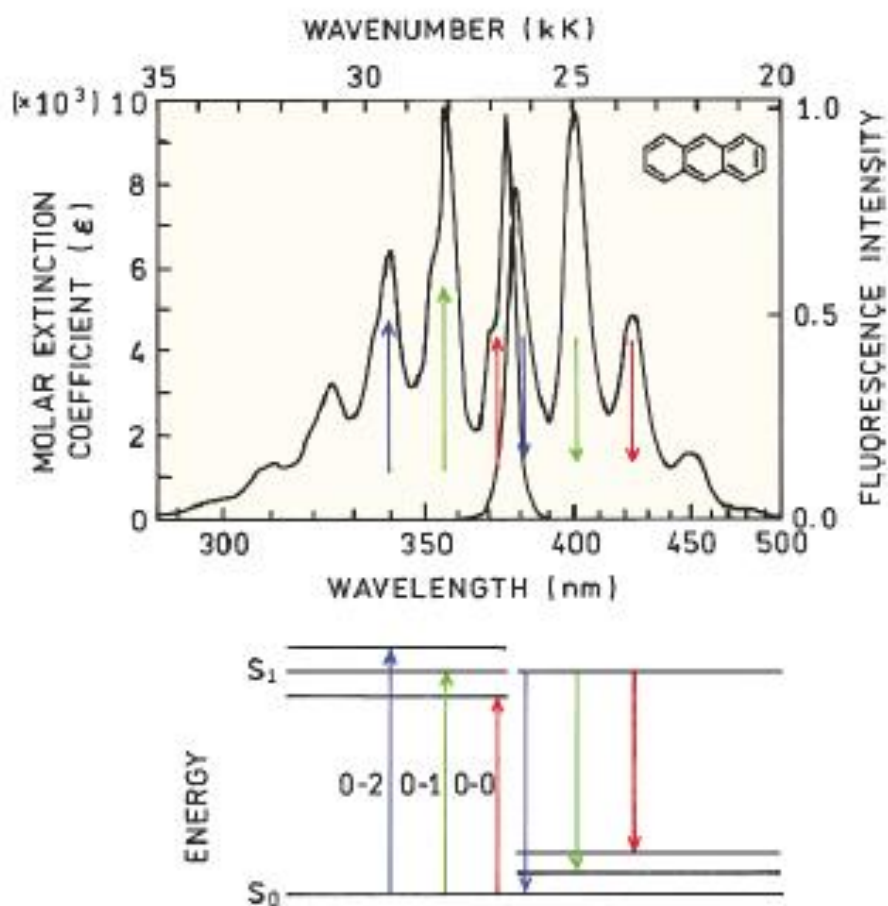


Figure 2.10. The vibrational structure in the $S_0 \rightarrow S_1$ transition of anthracene as observed in both absorption and emission spectra.¹⁵

The vibrational structure is observed in the experimental spectra usually under conditions where less interaction between the compound and its surrounding environment exists.¹⁵ This is explained by the example of 1,2,4,5-tetrazine (*sym*-tetrazine), reported by Mason in 1959. The compound has a very sensitive fine vibrational structure that decreases upon moving from gas phase to non-polar solution (i.e. in cyclohexane), and turns into one single broad band in aqueous solution, Figure 2.11.⁹⁰ A decrease in temperature inhibits the solvent-solute interactions,¹⁵ and subsequently leads to more vibrational structure in the spectra.⁹⁰

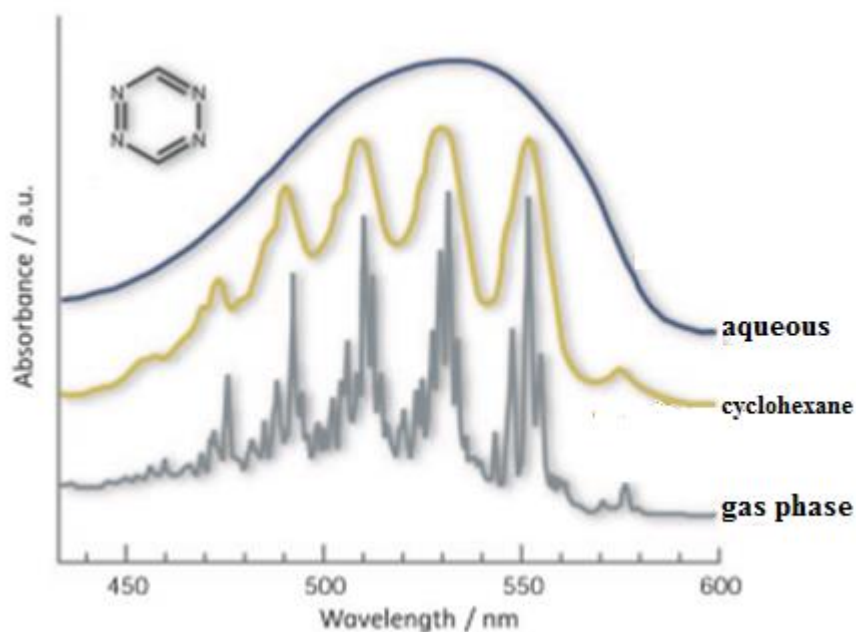


Figure 2.11. The absorption spectra of *sym*-tetrazine in vapor phase, in cyclohexane, and in water (from bottom upwards).⁹¹ Oh, M. H. J.; Salvador, M. R.; Wong, C. Y.; Scholes, G. D. “Three-Pulse Photon-Echo Peak Shift Spectroscopy and its Application for the Study of Solvation and Nanoscale Excitons”, *ChemPhysChem* **2011**, *12*, 88-100. Copyright Wiley-VCH Verlag GmbH & Co. KGaA, Weinheim. Reproduced with permission.

Unsubstituted aromatic hydrocarbons are usually of little sensitivity towards the polarity of the environment, due to their low polarity.¹⁵ However, unsubstituted pyrene displays a decent sensitivity of the vibrational structure to polarity variations,⁶⁰ to an extent that a special polarity scale known as *Py*-scale of solvent polarity has been established. The *Py*-scale uses pyrene as a probe for polarity by measuring the intensity ratio of the first to the third emission band in its emission spectrum in a specific medium.⁶⁰ This ratio is known to be vulnerable to any polarity change in the medium. A linear relation has been established between the ratio of intensity of the first to the third emission band of pyrene and the polarity of different solvents.⁶⁰ This change in emission intensity ratio of the vibrational structure bands for pyrene with respect to solvent polarity depends on the dipole moment and the dielectric constant of the solvent, and it is known as the Ham effect.²⁴ In any pyrene-based emitter, it is important to discuss the conservation or loss of the vibrational structure and the Ham effect of the unsubstituted pyrene.²⁴

The excitation process does not usually induce any changes in the energy difference separating different vibrational energy levels, and subsequently it is expected that the absorption and emission spectra will always be mirror images of each other as is the case for anthracene in Figure 2.10.¹⁵ This is known as the mirror-image rule for absorption and emission spectra. However, this is not always the case. The emission is the relaxation from lowest excited S_1 to ground S_0 state. Therefore, the mirror-image rule applies for the $S_0 \rightarrow S_1$ part of the absorption spectrum and not the full spectrum.¹⁵ Figure 2.12 shows the absorption and emission spectra of perylene, in which, like anthracene, the mirror-image rule applies for the full spectrum. On the opposite side, for quinine sulfate, a shoulder is observed at 320 nm in the absorption spectrum.

This extra shoulder is not detected in the emission spectrum, and it has been attributed to the $S_0 \rightarrow S_2$ transition. This explains why this specific part of the absorption spectrum does not obey the mirror-image rule.¹⁵ Most organic fluorophores mimic quinine sulfate, and only few mimic perylene or anthracene in this regard. In fact, the absorption spectra of most organic fluorophores usually show many electronic transitions, and only few show one single $S_0 \rightarrow S_1$ transition.¹⁵ The same applies for excitation and emission spectra, the mirror-image rule is applicable only for the $S_0 \rightarrow S_1$ transition, other higher energy transitions might show in the excitation spectrum if they end up with a radiative emission from the S_1 level, as in the case of perylene.

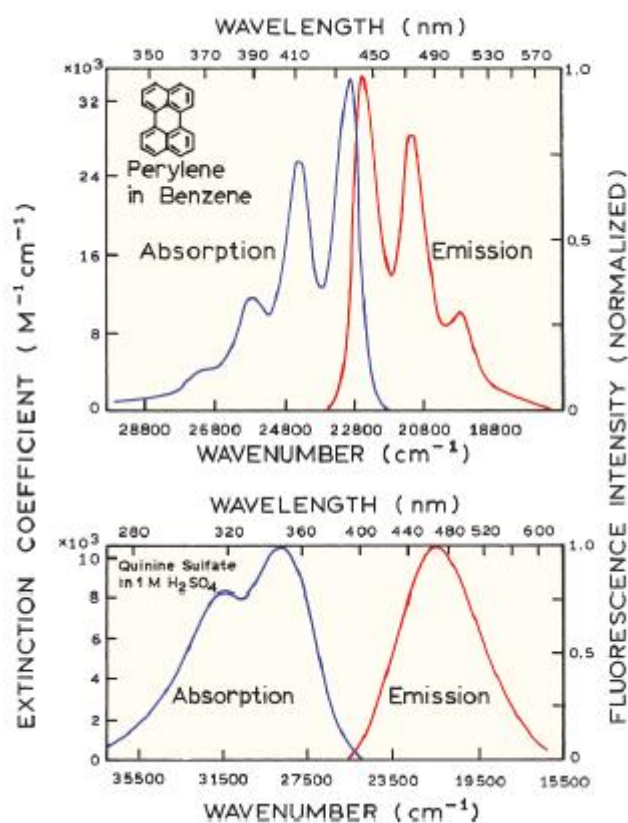


Figure 2.12. Mirror-image rule applies for the full spectra of perylene (up), and for part of the spectra of quinine sulfate (down).¹⁵

The pre-emission relaxations that take place in the excited state (internal conversions, vibrational relaxations, solvent relaxations), leading to a bathochromic shift in emission as compared to absorption, are the origin of the Stokes shift. The Stokes shift is defined as the difference in energy between the absorbed and the emitted photons.¹⁵ Experimental determination of Stokes shift is done through measuring the difference between the emission maximum and the absorption maximum of the lower energy transition.

Different solvents exhibit different interactions with different solutes (i.e. hydrogen bonding, Van Der Waals forces...). Solvent relaxations usually affect the emission wavelength more than the absorption due to the fact that the latter occurs too fast and does not allow any relaxation from the solvent molecules to affect the experimental wavelength.¹⁵ Hence, the solvatochromic shifts in the absorption wavelengths are usually attributed to solvation of the ground state. A hypsochromic shift occurs in the $n \rightarrow \pi^*$ transition upon increasing the polarity of the solvent due to the fact that the non-bonding electrons become more solvated and of lower energy in more polar solvents in its ground state (i.e. a photon of higher energy/shorter wavelength is required for excitation in more polar solvents). Similarly but for opposite reason, a bathochromic shift occurs in the $\pi \rightarrow \pi^*$ transition upon increasing solvent polarity. This is due to the increased hydrophobicity of the ground state as compared to the excited state, which renders the ground state less solvated and of higher energy in more polar solvents (i.e. a photon of lower energy/longer wavelength is required for excitation in more polar solvents).

In order to describe the solvatochromic shifts in both absorption and emission, a useful approximation known as the Lippert-Mataga equation can be used.

The equation, suggested in 1957, takes into consideration two basic solvents parameters: the dielectric constant ϵ of the solvent and its refractive index n .¹⁵

The equation relates the difference in energy Δv between the absorbed and emitted photons (the Stokes shift in cm^{-1}) to the two solvent parameters as follows:¹⁵

$$\Delta v = \frac{2}{hc} \left(\frac{\epsilon - 1}{2\epsilon + 1} - \frac{n^2 - 1}{2n^2 + 1} \right) \frac{(\mu_E - \mu_G)^2}{a^3} + \text{constant}$$

Where h is the Planck constant, c is the velocity of light in vacuum, a is the radius of the cavity in which the fluorophore resides, Figure 2.9 (right), and μ is the dipole moment of the fluorophore, and subscripts E and G denote the excited state and the ground state, respectively, Figure 2.9.¹⁵

According to this equation, using a solvent of a higher dielectric constant ϵ leads to more relaxation and larger Stokes shift value. On the other side, a solvent with a higher refractive index n leads to less relaxation and smaller Stokes shift value. Solvent relaxation is a redistribution of solvent molecules around the excited state of the fluorophore, along with a redistribution of electrons in the solvent molecules, Figure 2.9 (right).¹⁵ The dielectric constant of a solvent describes both redistributions of molecules and electrons; however, the refractive index describes the redistribution of electrons only. To simplify the equation above, the use of one single parameter known as the orientation polarizability Δf that accounts for both dielectric constant and refractive index together is suggested as follows:¹⁵

$$\Delta f = \left(\frac{\epsilon - 1}{2\epsilon + 1} - \frac{n^2 - 1}{2n^2 + 1} \right)$$

Combining the two equations together leads to the following simplified equation:

$$\Delta v = \frac{2\Delta f (\mu_E - \mu_G)^2}{hc a^3} + \text{constant}$$

Based on this simplified equation, the Lippert-Mataga plots are defined as the plots of Stokes shift values against the orientation polarizability in different solvents of different polarities.¹⁵ The slope of this plot is expected to be linear, and illustrates the response of the compound to a change in solvent polarity. A non-linear slope means that the Lippert-Mataga approximation is not valid for the system under study. Solvents that exhibit particular interactions such as hydrogen bonding with the fluorophore do not usually fall on the linear plot generated for other solvents that do not exhibit such interactions. This is known to be one of the limitations of this equation.¹⁵

Another solvent polarity scale used to evaluate solvatochromic shifts in fluorophores is the one established by Dimroth *et al.* in 1963.⁹² In this scale, a dye known as pyridinium *N*-phenoxide betaine, Figure 2.13 with R = H, commonly known as the $E_T(30)$ molecule,⁹³ was used to probe the polarity of different solvents. The empirical solvent polarity scale was established based on the great sensitivity of this dye to solvent polarity variations.^{92,94} The dye exhibits solvatochromic shifts along the visible spectrum detectable by naked eyes. This sensitivity made of the dye a good polarity indicator.⁹² The scale was established by simply measuring the molar transition energy (ν_{max}) of the dye in the investigated solvent at 25 °C under atmospheric pressure, and assigning it as the $E_T(30)$ value (in kcal/mol or kj/mol) of this specific solvent according to the following equation:⁹⁴

$$E_T(30) = h \cdot c \cdot \nu_{max} \cdot N_A$$

Which can be further written as follows:

$$E_T(30)(kcal.mol^{-1}) = \frac{28591}{\lambda_{max}(nm)}$$

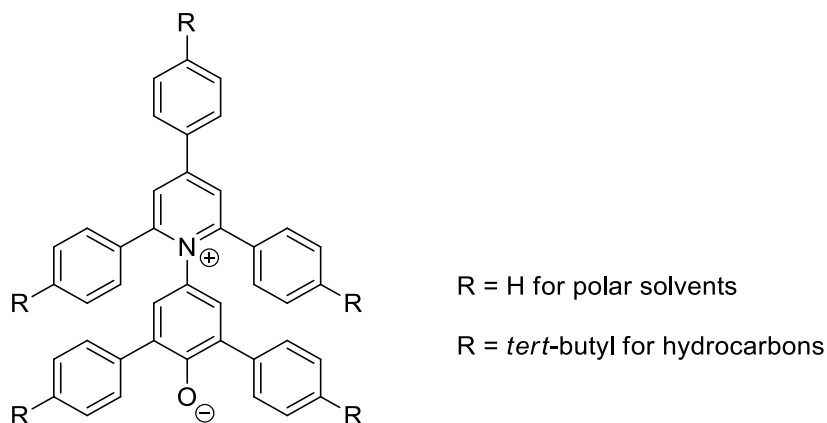


Figure 2.13. Structures of the polarity probes used to define the empirical solvent polarity scale.⁹⁴

For non-polar solvents such as hydrocarbons, the dye shown in Figure 2.13 was used with R = *tert*-butyl due to better solubility. The authors indicated that replacing the hydrogens with *tert*-butyl groups has no effect on the linearity of the established scale.⁹⁴

In order to avoid recalculations from kcal/mol to kJ/mol (and vice-versa), a dimensionless scale was established in 1983 known as the normalized E_T scale, by considering TMS and water as polarity extremes with normalized E_T values of 0 and 1 respectively.⁹⁴ Other solvents could be assigned according to the following equation:⁹⁴

$$E_T^N \text{ solvent} = \frac{E_T(30) \text{ solvent} - E_T(30) \text{ TMS}}{E_T(30) \text{ water} - E_T(30) \text{ TMS}} = \frac{E_T(30) \text{ solvent} - 30.7}{32.4}$$

Values of the normalized scale of common solvents are shown in Figure 2.14. Another strategy to analyze the solvent-solute interactions is achieved by plotting the values of Stokes shift in cm^{-1} against $E_T(30)$ or the normalized E_T values (E_T^N) in different solvents, similar to Lippert-Mataga plots, but using a different polarity scale.

Table 2.2 summarizes the main solvent characteristics (refractive index, orientation polarizability, empirical solvent polarity constant and the normalized value) of different solvents used for photophysical studies in all Chapters of this thesis.

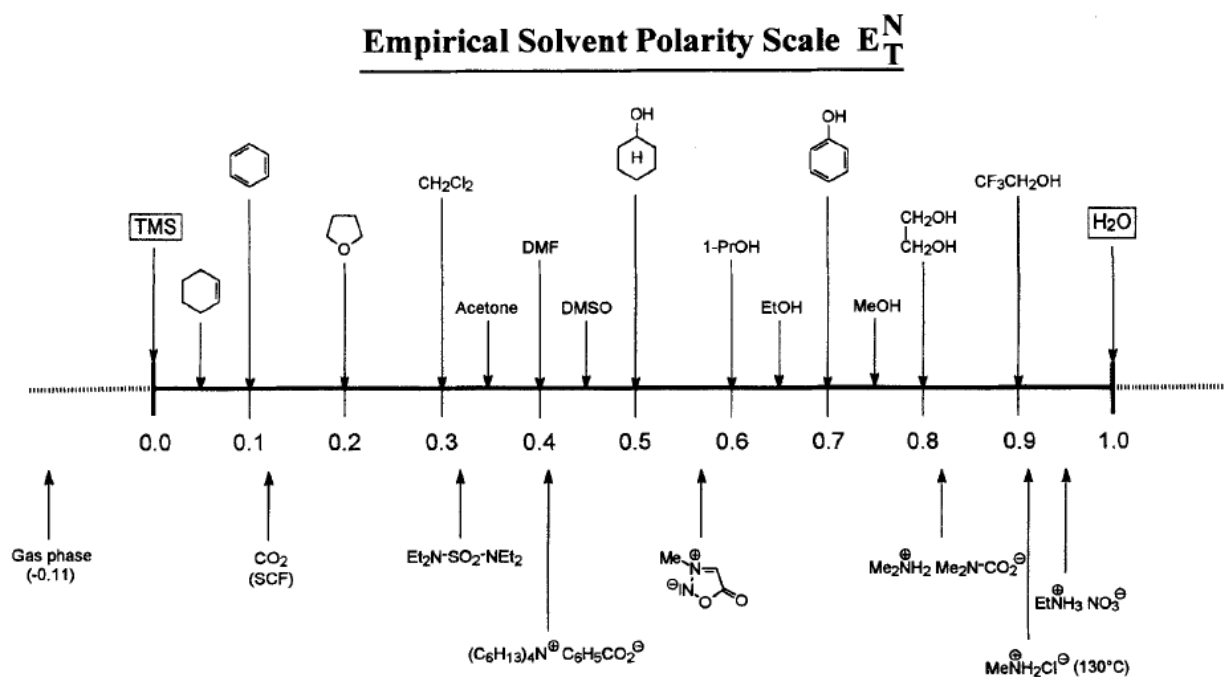


Figure 2.14. The normalized empirical solvent polarity scale displaying values for some common solvents.⁹⁴

Table 2.2. Summary of useful solvent characteristics to be used in our solvatochromic studies.

Solvent (Abbreviation)	n	E_T (30) kcal.mol ⁻¹	E_T^N	Δf
Acetonitrile (ACN)	1.3415	45.6	0.46	0.33
Chloroform (CHCl ₃)	1.4458	39.1	0.26	0.15
Cyclohexane (Cyclohex)	1.4262	30.9	0.01	0.00
Dichloromethane (DCM)	1.4241	40.7	0.31	0.23
<i>N,N</i> -Dimethylformamide (DMF)	1.4305	43.2	0.39	0.30
Dimethylsulfoxide (DMSO)	1.4793	45.1	0.44	0.29
1,4-Dioxane (Diox)	1.4224	36.0	0.16	0.02
Ethanol (EtOH)	1.3614	51.9	0.65	0.31
Ethyl acetate (EtOAc)	1.3724	38.1	0.23	0.20
Hexane (Hex)	1.3749	31.0	0.01	0.01
Methanol (MeOH)	1.3284	55.4	0.76	0.33
Tetrahydrofuran (THF)	1.4072	37.4	0.21	0.22
Toluene (Tol)	1.4969	33.9	0.10	0.02

In addition to the Lippert-Mataga equation and the empirical solvent polarity scale, other scales were reported throughout the literature; however, they are still less common. One of which is the *Py*-scale, it uses the ratio of emission intensity of the first to the third band in pyrene's vibrational structure for determining the polarity of the medium.⁶⁰ A fourth useful scale is the π^* scale established in 1977 by Kamlet *et al.*⁹⁵ It is named as such due to its high ability in correlating the spectral shifts of $\pi \rightarrow \pi^*$ and $n \rightarrow \pi^*$ transitions together in a single polarity scale.⁹⁵ The scale attributes a π^* value for every solvent, cyclohexane and DMSO are selected as references with π^* values of 0 and 1, respectively.^{95,96} This scale works by simple comparison of experimental solvent relaxations observed for a specific polarity probe to the relaxations observed in the two reference solvents as follows:

$$\pi^* = \frac{\nu_s - \nu_{cyclohexane}}{\nu_{DMSO} - \nu_{cyclohexane}}$$

Where ν is the frequency corresponding to the maximum absorption/emission of the band on which the solvatochromic effect is being investigated.⁹⁶ The subscript *s* stands for the solvent for which the π^* value is being calculated. π^* values below 0 and above 1 do exist, and thus the scale does not assume the reference solvents, cyclohexane and DMSO, as being the least and the polar most polar, respectively.⁹⁵ However, the reliability of this scale has been attributed to the evaluation of solvatochromic shifts with respect to these two specific reference solvents, in addition to some specific probes used to establish the scale and compute the π^* values for different solvents (i.e. *para*-disubstituted benzene ring compounds, where one substituent is electron-releasing and the other one is electron-withdrawing).⁹⁶

Compounds that show pronounced solvatochromic shifts upon variation of solvent polarity, and the ones that do not exhibit linearity against the polarity constant in

the considered scale, are usually studied according to more than one of the four scales described above. For compounds having negligible responses to polarity variations the use of one or two scales is enough.

Photophysical data in solution were collected in six different solvents covering a wide range of polarity. Namely, eight spectroscopic grade solvents were selected: acetonitrile, chloroform, cyclohexane, DMF, DMSO, 1,4-dioxane, ethanol and THF. However, due to the poor solubility of the majority of the compounds in acetonitrile and ethanol, the photophysical studies were limited to the six remaining solvents. The change of solvent polarity seemed to affect the absorption and emission wavelengths mainly through a clear bathochromic shift upon increasing the solvent polarity. This is an expected behavior for the $\pi \rightarrow \pi^*$ transition; however, the spectral features were maintained similar in all the six solvents. Stokes shift were almost independent of the solvent polarity. This is consistent with the bathochromic shifts occurring simultaneously in both absorption and emission spectra upon the increase of solvent polarity. Plots of Stokes shift versus Δf (orientation polarizability) and E_T30 (empirical solvent polarity scale) were generated for each compound in all solvents, Figures 2.24 and 2.25. The slopes were too small for the nine compounds, which indicates the absence of major solvatochromic effects. Bathochromic shifts described in this paragraph are the ones due to solvent polarity variations, and not the ones due to the change of substituent (i.e. same compound in different solvents). Compounds **2.21** and **2.27** showed low solubility in DMSO. Similar poor solubility occurred for compound **2.28** in cyclohexane. Due to this, incomplete photophysical data in these two solvents was collected. The results of the absorption and emission experiments with the Stokes shifts in different solvents are summarized in Table 2.3 and Figures 2.15-2.23.

Table 2.3. Absorption and emission studies in different solvents for compounds **2.21-2.29** displaying the maxima of the $S_0 \rightarrow S_1$ transitions and the corresponding Stokes shifts, in addition to the molar absorptivity in chloroform.

Compound	Solvent	λ_{max}^{em} , nm	λ_{max}^{abs} , nm (ϵ , L.mol ⁻¹ .cm ⁻¹)	$\Delta\lambda$ (cm ⁻¹)	$\Delta\lambda$ (eV)
2.21	Chloroform	426	391 (43062)	2101	0.26
	DMF	428	393	2081	0.26
	THF	424	390	2056	0.25
	DMSO	--	--	--	--
	1,4-Dioxane	425	389	2178	0.27
	Cyclohexane	423	387	2199	0.27
2.22	Chloroform	430	388 (43960)	2517	0.31
	DMF	432	391	2427	0.30
	THF	429	389	2397	0.30
	DMSO	434	387	2798	0.35
	1,4-Dioxane	429	389	2397	0.30
	Cyclohexane	425	384	2512	0.31
2.23	Chloroform	434	387 (39103)	2798	0.35
	DMF	438	392	2679	0.33
	THF	434	389	2665	0.33
	DMSO	440	395	2589	0.32
	1,4-Dioxane	432	388	2625	0.33
	Cyclohexane	432	384	2894	0.36
2.24	Chloroform	444	396 (49461)	2730	0.34
	DMF	447	400	2629	0.33
	THF	442	396	2628	0.33
	DMSO	450	403	2592	0.31
	1,4-Dioxane	441	396	2577	0.32
	Cyclohexane	437	396	2369	0.29
2.25	Chloroform	416	382 (38925)	2140	0.27
	DMF	417	384	2061	0.26
	THF	415	383	2013	0.25
	DMSO	421	387	2087	0.26
	1,4-Dioxane	415	383	2013	0.25
	Cyclohexane	413	381	2034	0.25
2.26	Chloroform	419	380 (28777)	2449	0.30
	DMF	425	381	2717	0.34
	THF	422	383	2413	0.30
	DMSO	427	386	2488	0.31
	1,4-Dioxane	419	382	2312	0.29
	Cyclohexane	415	379	2289	0.28
2.27	Chloroform	416	382 (37713)	2140	0.27
	DMF	427	386	2488	0.31
	THF	420	383	2300	0.29
	DMSO	427	387	2421	0.30
	1,4-Dioxane	419	382	2312	0.29
	Cyclohexane	413	382	1965	0.24

2.28	Chloroform	443	391 (42022)	3002	0.37
	DMF	446	393	3024	0.37
	THF	440	390	2914	0.36
	DMSO	448	398	2804	0.35
	1,4-Dioxane	441	390	2965	0.37
	Cyclohexane	--	--	--	--
2.29	Chloroform	467	407 (30523)	3157	0.39
	DMF	470	413	2936	0.36
	THF	464	408	2958	0.37
	DMSO	474	416	2941	0.36
	1,4-Dioxane	466	407	3111	0.39
	Cyclohexane	460	403	3075	0.38

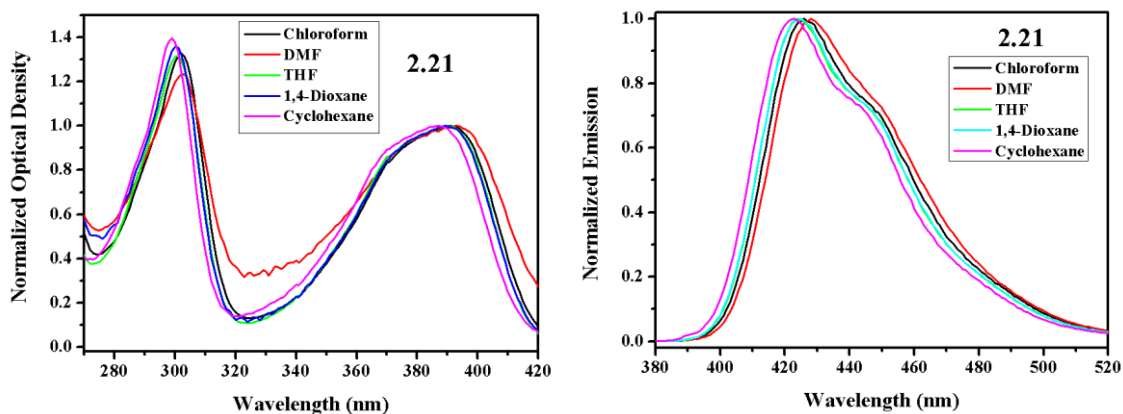


Figure 2.15. Normalized absorption (left) and emission (right) spectra of compound 2.21 in five different solvents.

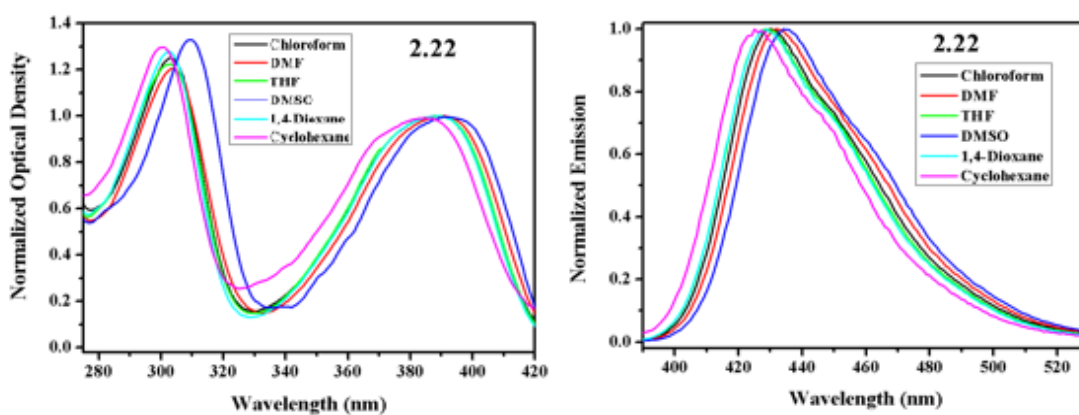


Figure 2.16. Normalized absorption (left) and emission (right) spectra of compound 2.22 in six different solvents.

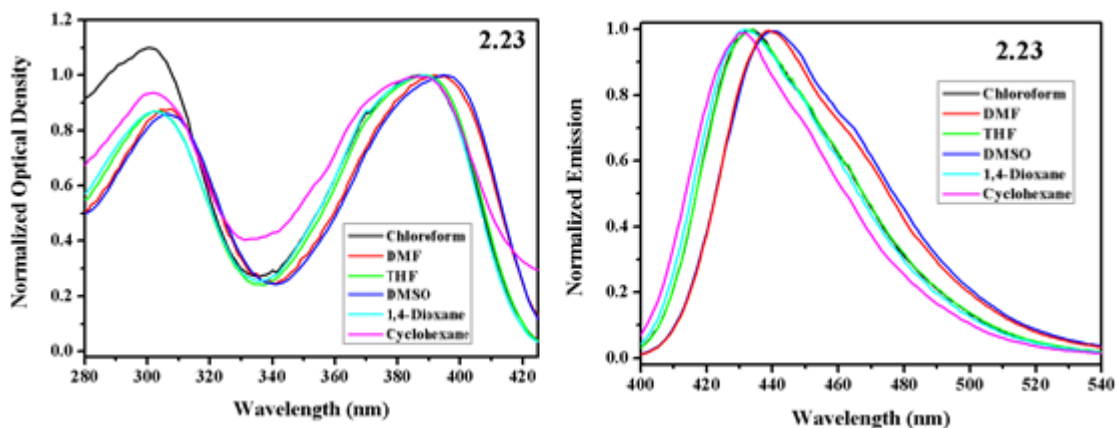


Figure 2.17. Normalized absorption (left) and emission (right) spectra of compound **2.23** in six different solvents.

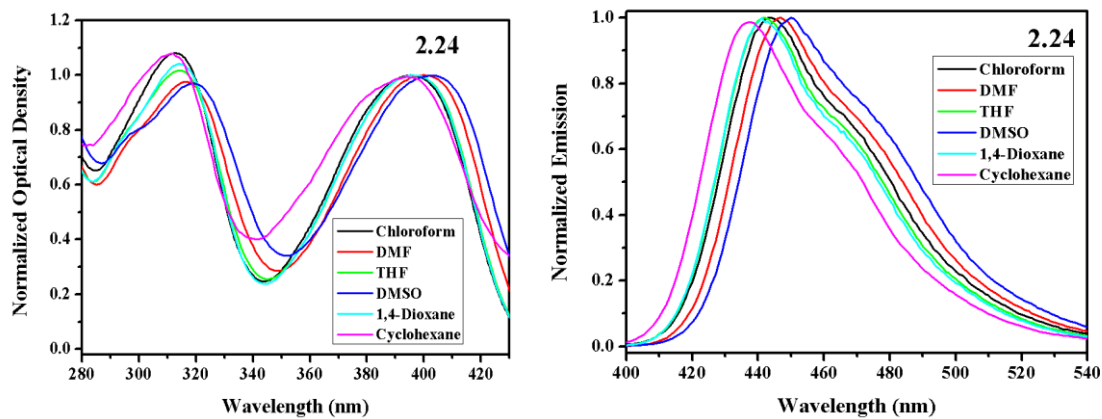


Figure 2.18. Normalized absorption (left) and emission (right) spectra of compound **2.24** in six different solvents.

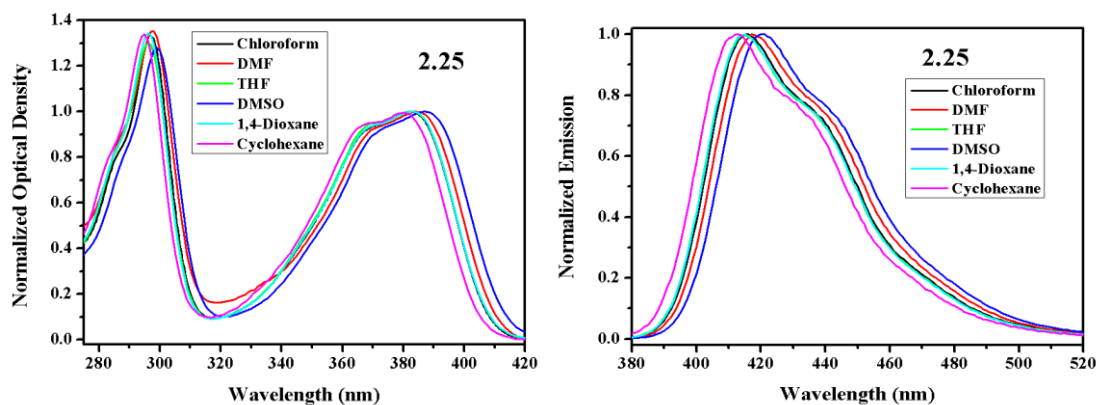


Figure 2.19. Normalized absorption (left) and emission (right) spectra of compound **2.25** in six different solvents.

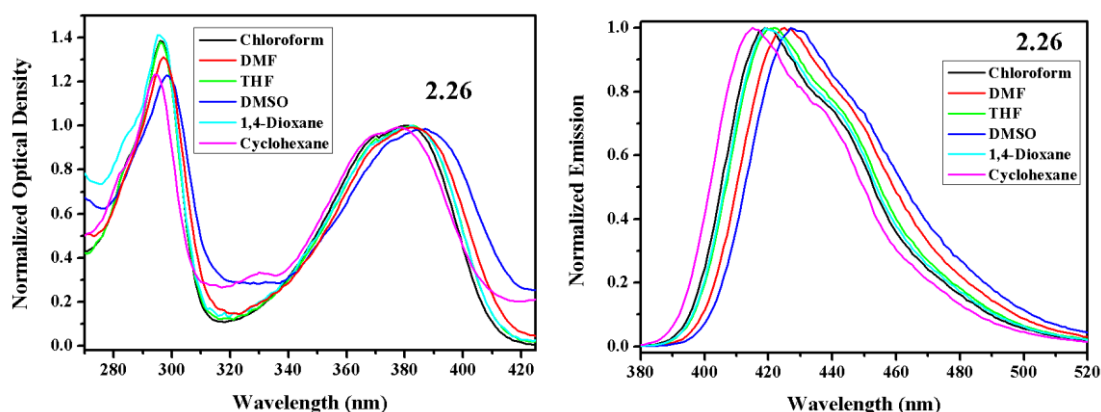


Figure 2.20. Normalized absorption (left) and emission (right) spectra of compound 2.26 in six different solvents.

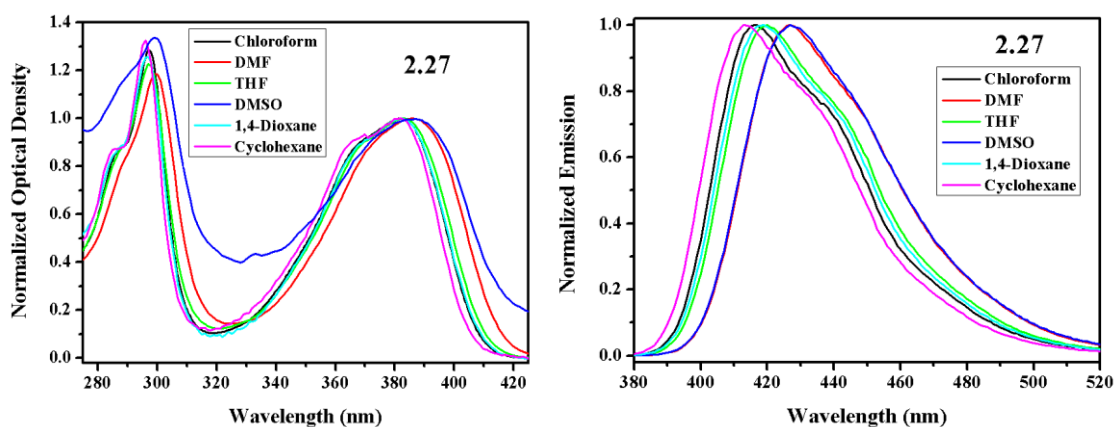


Figure 2.21. Normalized absorption (left) and emission (right) spectra of compound 2.27 in six different solvents.

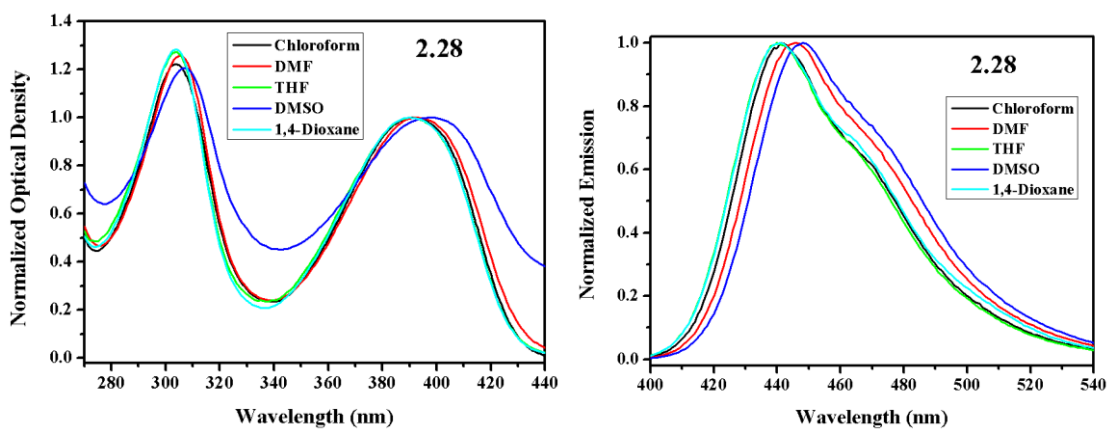


Figure 2.22. Normalized absorption (left) and emission (right) spectra of compound 2.28 in five different solvents.

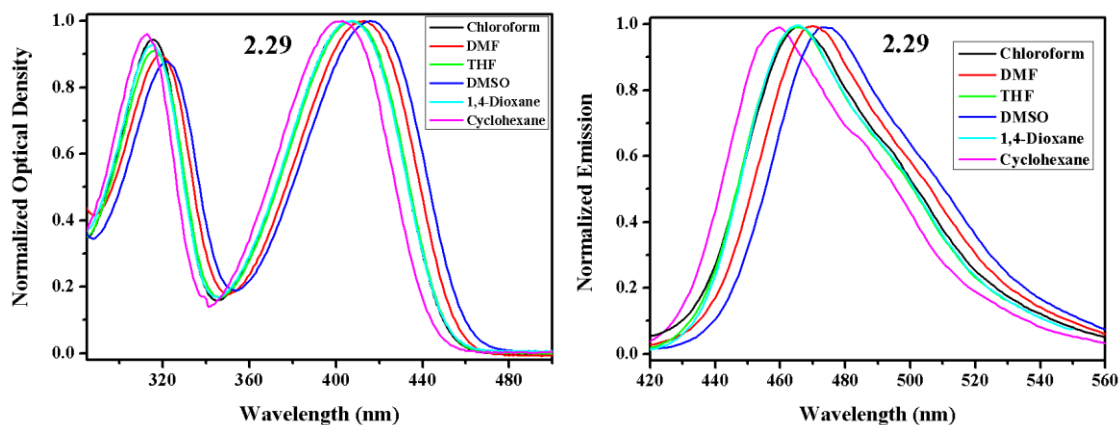


Figure 2.23. Normalized absorption (left) and emission (right) spectra of compound **2.29** in six different solvents.

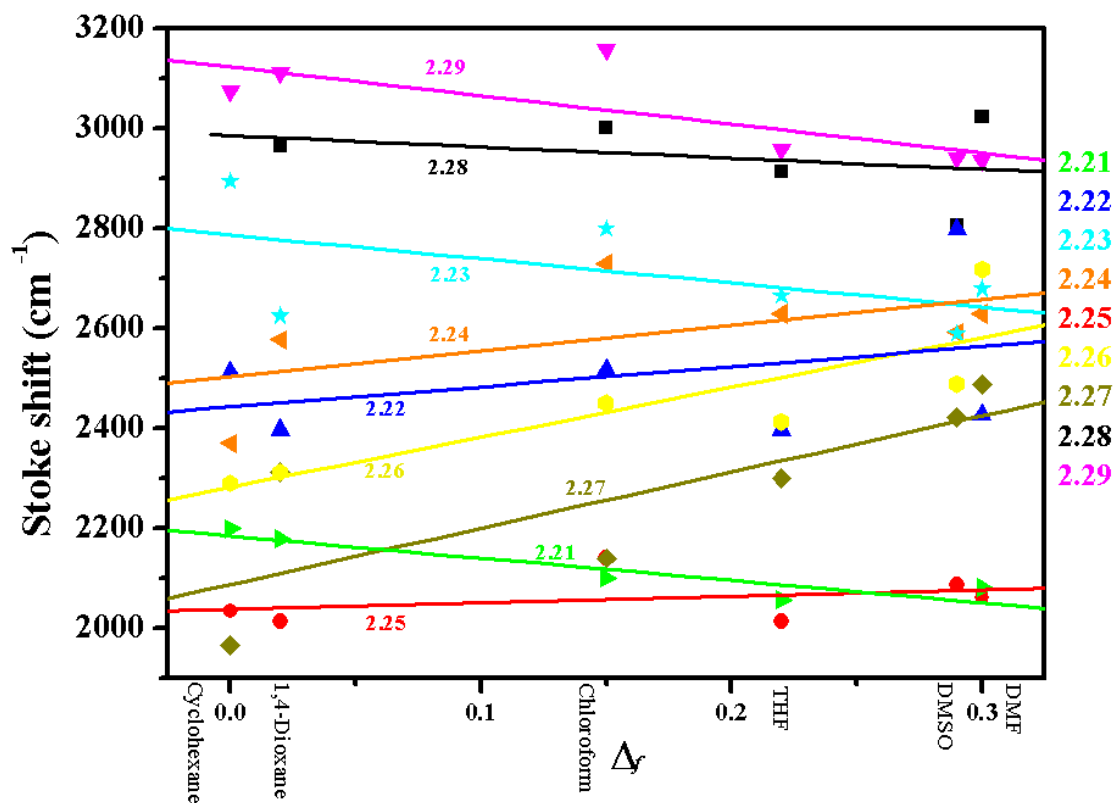


Figure 2.24. Stokes shifts vs. orientation polarizability for compounds **2.21-2.29** with linear fitting in the six selected solvents.

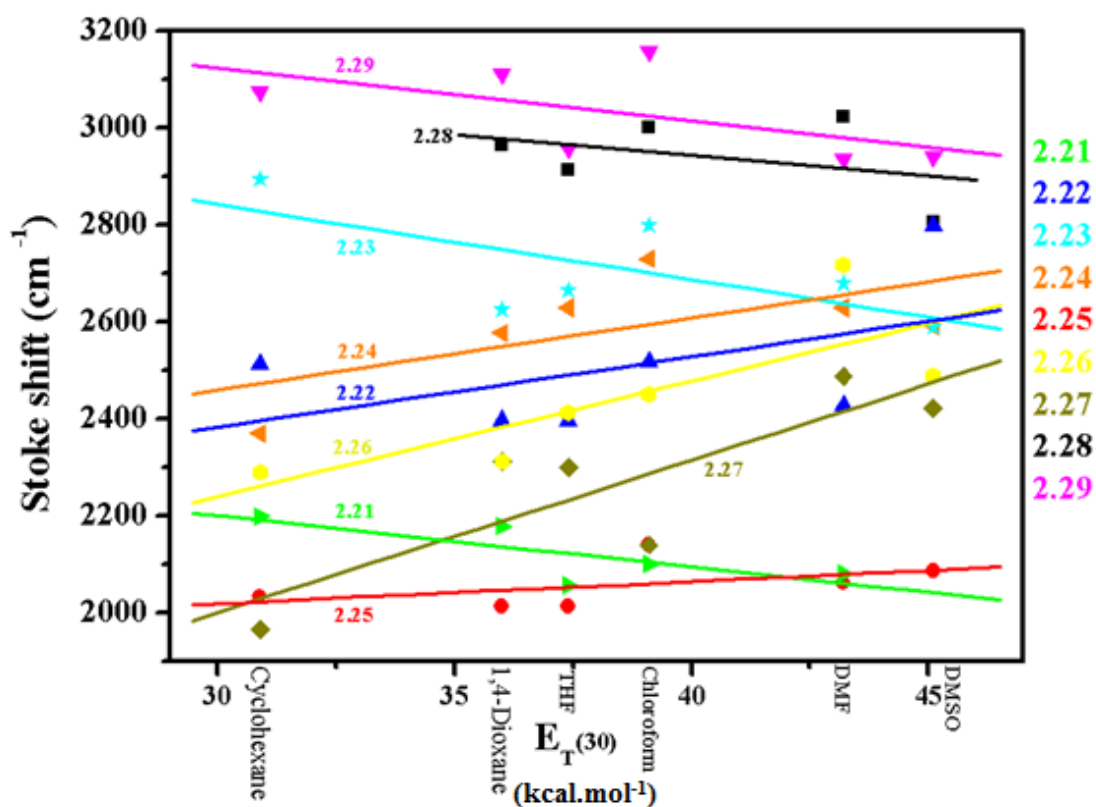


Figure 2.25. Stokes shifts vs. empirical solvent polarity parameter for compounds 2.21-2.29 with linear fitting in the six selected solvents.

2.2.2.2. Fluorescence Lifetime and Emission Quantum Yield

Photophysical processes are classified into radiative and non-radiative processes. For a fluorescent compound, the emission occurs from the lowest vibrational level of the lowest singlet excited state S_1 . Emission from the lowest triplet excited state T_1 , which is lower in energy than the singlet excited state, occurs following an intersystem crossing from S_1 to T_1 .¹⁵ Relaxation from T_1 is considered as non-radiative in fluorescent emitters.⁹⁷ However, for a phosphorescent emitter, it is a radiative process, and is known as phosphorescence, Figure 2.26.¹⁵ An emitter might be phosphorescent at room temperature rather than fluorescent usually when it possesses heavy atoms (i.e. bromine,¹⁵ iodine¹⁵ and some heavy metals⁹⁷). Since it has been shown

that their presence leads to facilitating the spin-forbidden intersystem crossing process and radiative emission from the lowest triplet excited state T_1 .¹⁵ The fact behind this is that different molecules do not behave similarly upon excitation and relaxation. Many molecules do not emit light at all, and they have no emission spectra. However, these molecules do have absorption spectra. Electrons in these compounds can get excited from the S_0 ground state to higher energy levels similar to the case of an emitter, and this is why these non-emitters have absorption spectra.¹⁵ The excited electron relaxes back to the ground state as well. However, the $S_1 \rightarrow S_0$ relaxation for a non-emitter compound is a non-radiative photophysical process (i.e. by emitting heat instead of light).¹⁵ Here comes the main difference between the excitation and absorption spectra. Whereas the absorption spectrum shows all transitions from the ground state to any excited state, an excitation spectrum displays the transitions that will end up by radiative relaxation processes of the excited state exclusively.¹⁵ Thus, a non-emitter compound has no excitation spectrum as well. In the present study, we are mainly interested in fluorescent emitters rather than phosphorescent ones. Hence, radiative and non-radiative photophysical processes are summarized in Table 2.4 according to the interest of the study.

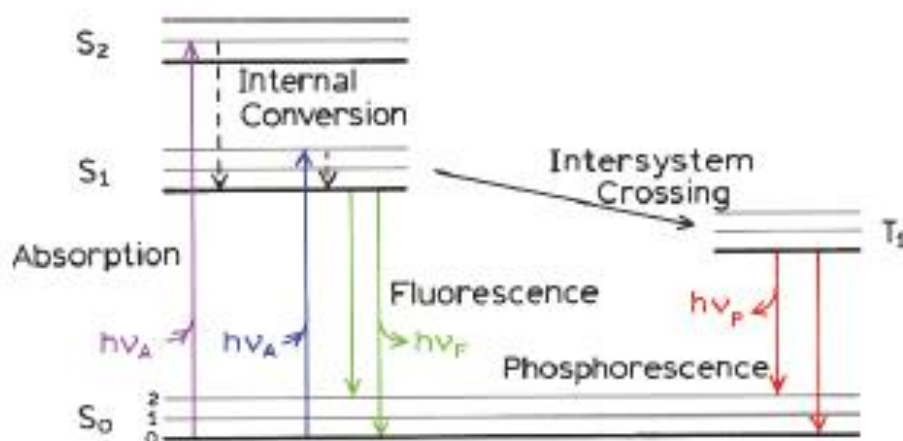


Figure 2.26. Another form of Jablonski diagram illustrating the intersystem crossing and phosphorescence processes.¹⁵

Table 2.4. Summary of the photophysical processes relevant to fluorescent emitters such as compounds 2.21-2.29.

Photophysical process	Nature
Internal conversion	Non-radiative
Vibrational relaxation	Non-radiative
Solvent relaxation	Non-radiative
Intersystem crossing	Non-radiative (fluorescent compound)
Excitation	Radiative ($S_0 + h\nu \rightarrow S_1$)
Fluorescence	Radiative ($S_1 \rightarrow S_0 + h\nu$)

Fluorescence lifetime τ is the average time an electron spends in the excited states before the emission occurs.¹⁵ Hence, it depends on both radiative and non-radiative processes (i.e. the faster the rate of these processes is, the smaller the lifetime will be). This can be defined by the following equation:

$$\tau = \frac{1}{k_r + k_{nr}} = \frac{1}{k_{tot}}$$

Where τ is the fluorescence lifetime, k_r and k_{nr} are rate constants of the radiative and non-radiative decays respectively, and k_{tot} is the sum of k_r and k_{nr} and is the rate constant of all photophysical processes.¹⁵

Furthermore, given a population of n identical fluorophores being excited to their excited state at a reference time $t = 0$, the fluorescence lifetime can be defined by a single-exponential decay, as the time needed to achieve a relaxation down to $1/e$ of the initially excited population (i.e. the duration needed to relax from n to $\sim 0.37n$ excited fluorophores).⁹⁸ The intensity of light emission from the excited population can be described at any time t by the single-exponential decay equation as follows:

$$I_t = I_0 \cdot e^{(-t/\tau)} \quad \text{Or} \quad \tau = \frac{t}{\ln(I_0/I_t)}$$

Where I_0 and I_t are defined respectively as the intensities of emission emerging from the fluorophore population at $t = 0$ (i.e. the moment of the excitation when n fluorophores are excited), and at a certain time t after the excitation source is removed and the n excited fluorophores start to relax progressively.⁹⁸

A fitting of the decay curve to the exponential decay equation is then performed. Deviations between the measured data and the fitted data at a specific time t are labeled as the residuals. The goodness-of-fit parameter χ^2 reveals the overall deviation of the measured decay to the fitted one at any time t . This parameter is an important indicative about errors in the fitting itself. In many instances, the experimental decay does not fit a single-exponential equation, and a multi-exponential fitting is then required.¹⁵ Experimental lifetime decays and the fitting are reported along with a separate graph showing the residuals at each specific time t . In some cases, the fact of fitting to single or multi-exponential decay, with a small χ^2 value, might indicate the presence of one or more emitting species, respectively. Such case is discussed in Chapter 4 of this thesis (compound **4.5**).

The duration spent at the excited state through radiative processes, exclusively, is referred to as natural lifetime τ_n , and it is inversely related to k_r exclusively by neglecting any relaxation through non-radiative processes. Since it refers to the largest reachable lifetime in case all non-radiative processes were inhibited, the natural lifetime cannot be measured experimentally. Instead, it is calculated according to the following equation:⁹⁸

$$\tau_n = \frac{1}{k_r}$$

Interestingly, experimental lifetime values that tend to be closer to the natural lifetime indicate smaller impact for the non-radiative processes and subsequently higher emission quantum yield.

The fluorescence quantum yield ϕ is defined as the ratio of emitted to absorbed photons. It can also be considered as the ratio of the rate constants for radiative processes to all photophysical processes (radiative and non-radiative) as in the following equation:¹⁵

$$\phi = \frac{k_r}{k_r + k_{nr}} = k_r \cdot \tau = \frac{\tau}{\tau_n}$$

Determination of the emission quantum yield is done by integrating the area under the intensity curve in the emission spectrum of a solution having known optical density, and comparing it to a reference compound for which the emission quantum yield is previously reported. Many reference compounds are listed in the literature. These are known as fluorescence quantum yield standards. The quantum yield of a standard compound in a specific solvent is usually independent of the excitation wavelength. Thus, the experimental excitation wavelength for quantum yield experiments is chosen to be in the range where the excitation spectra of both the studied

fluorophore and the standard compound overlap.¹⁵ In our studies, the standard used was 9,10-diphenylanthracene, with a quantum yield value of 1.00 in cyclohexane.⁹⁹

Dilute solutions of optical density values below 0.05 at the chosen wavelength are used. This is to make sure that the intensity changes in absorption and emission are proportional to each other.¹⁵ Another factor affecting the quantum yield determination is the refractive index of the solvent used (i.e. in case different solvents are used for the compound being studied and the standard compound). Upon switching to a higher refractive index solvent, the light intensity increases proportionally to the square of the ratio of refractive indices of the two solvents.¹⁵ This leads to an equation by which the quantum yield of the compound investigated can be related to the quantum yield of the standard compound as follows:¹⁵

$$\phi = \phi_{std} \frac{F}{F_{std}} \frac{A_{std}}{A} \frac{n^2}{n_{std}^2}$$

Where ϕ is the fluorescence quantum yield, F is the integrated intensity of the emission spectrum, A is the optical density (< 0.05), and n is the refractive index of the solvent used. The subscript “*std*” indicates that the corresponding parameter is that of the standard compound.

An experimental determination of the fluorescence lifetime and the emission quantum yield enables the calculation of k_r and k_{nr} as follows:¹⁵

$$k_r = \frac{\phi}{\tau}$$

$$k_{nr} = k_{tot} - k_r = \frac{1}{\tau} - k_r$$

The non-radiative rate constant can be further split into different components, where each component refers to a single non-radiative transition as follows:

$$k_{nr} = k_{IC} + k_{ISC} + k'$$

Where k_{IC} and k_{ISC} are the rate constants of the internal conversions and intersystem crossing processes respectively, and k' is the rate constant of any other possible non-radiative relaxation process.¹⁰⁰

The results obtained are summarized in Table 2.5 and Figures 2.27-2.35.

Table 2.5. Fluorescence lifetimes and emission quantum yields in different solvents under oxygen-free atmosphere, with the calculated values of radiative and non-radiative constants and natural lifetimes.

Compound	Solvent	τ , ns (χ^2)	ϕ_F	k_r (10^8) s ⁻¹	k_{nr} (10^8) s ⁻¹	τ_n , ns
2.21	Chloroform	1.83 (1.10)	0.97	5.30	0.16	1.89
	DMF	1.92 (1.33)	0.89	4.64	0.57	2.16
	THF	1.94 (1.57)	0.90	4.64	0.52	2.16
	DMSO	--	--	--	--	--
	1,4-Dioxane	1.89 (1.38)	0.82	4.34	0.95	2.30
	Cyclohexane	1.89 (1.56)	0.81	4.29	1.01	2.33
2.22	Chloroform	1.86 (1.97)	0.98	5.27	0.11	1.90
	DMF	1.94 (1.71)	0.91	4.69	0.46	2.13
	THF	1.91 (1.63)	0.998	5.23	0.01	1.91
	DMSO	1.84 (1.88)	0.69	3.75	1.68	2.67
	1,4-Dioxane	1.86 (1.78)	0.85	4.57	0.81	2.19
	Cyclohexane	1.85 (1.77)	0.79	4.27	1.14	2.34
2.23	Chloroform	1.75 (1.77)	0.85	4.86	0.86	2.06
	DMF	1.99 (1.46)	0.83	4.17	0.85	2.40
	THF	1.88 (1.63)	0.75	3.99	1.33	2.51
	DMSO	1.95 (1.90)	0.78	4.00	1.13	2.50
	1,4-Dioxane	1.83 (1.94)	0.75	4.10	1.37	2.44
	Cyclohexane	1.75 (1.63)	0.93	5.31	0.40	1.88
2.24	Chloroform	1.66 (1.81)	0.80	4.82	1.20	2.08
	DMF	1.73 (1.78)	0.73	4.22	1.56	2.37
	THF	1.63 (1.57)	0.72	4.42	1.72	2.26
	DMSO	1.71 (2.31)	0.68	3.98	1.87	2.51
	1,4-Dioxane	1.58 (1.53)	0.72	4.56	1.77	2.19
	Cyclohexane	1.47 (1.99)	0.47	3.20	3.61	3.13
2.25	Chloroform	2.27 (2.24)	0.84	3.70	0.70	2.70
	DMF	2.34 (1.54)	0.87	3.72	0.56	2.70
	THF	2.51 (1.81)	0.81	3.23	0.76	3.10
	DMSO	2.13 (2.01)	0.84	3.94	0.75	2.54
	1,4-Dioxane	2.44 (1.96)	0.82	3.36	0.74	2.98
	Cyclohexane	2.74 (2.92)	0.83	3.03	0.62	3.30

2.26	Chloroform	1.93 (1.59)	0.75	3.89	1.30	2.57
	DMF	2.11 (1.14)	0.80	3.79	0.95	2.64
	THF	2.09 (2.35)	0.81	3.88	0.91	2.58
	DMSO	1.93 (1.50)	0.68	3.52	1.66	2.84
	1,4-Dioxane	2.03 (1.62)	0.80	3.94	0.99	2.54
	Cyclohexane	2.12 (1.31)	0.72	3.40	1.32	2.94
2.27	Chloroform	2.02 (1.57)	0.88	4.36	0.59	2.30
	DMF	2.13 (1.91)	0.91	4.27	0.42	2.34
	THF	2.14 (1.66)	0.85	3.97	0.70	2.52
	DMSO	2.07 (2.44)	--	--	--	--
	1,4-Dioxane	2.08 (1.51)	0.80	3.85	0.96	2.60
	Cyclohexane	2.18 (1.68)	0.93	4.27	0.32	2.34
2.28	Chloroform	1.93 (2.07)	0.89	4.61	0.57	2.17
	DMF	1.97 (1.95)	0.78	3.96	1.12	2.53
	THF	1.88 (1.87)	0.75	3.99	1.33	2.51
	DMSO	1.95 (2.51)	0.57	2.92	2.21	3.42
	1,4-Dioxane	1.87 (1.84)	0.75	4.01	1.34	2.49
	Cyclohexane	1.78 (1.78)	--	--	--	--
2.29	Chloroform	0.54 (2.26)	0.17	3.15	15.4	3.18
	DMF	0.56 (2.17)	0.15	2.68	15.2	3.73
	THF	0.50 (2.65)	0.14	2.80	17.2	3.57
	DMSO	0.63 (2.83)	0.16	2.54	13.3	3.94
	1,4-Dioxane	0.47 (1.70)	0.14	2.98	18.3	3.36
	Cyclohexane	0.47 (1.91)	0.11	2.34	18.9	4.27

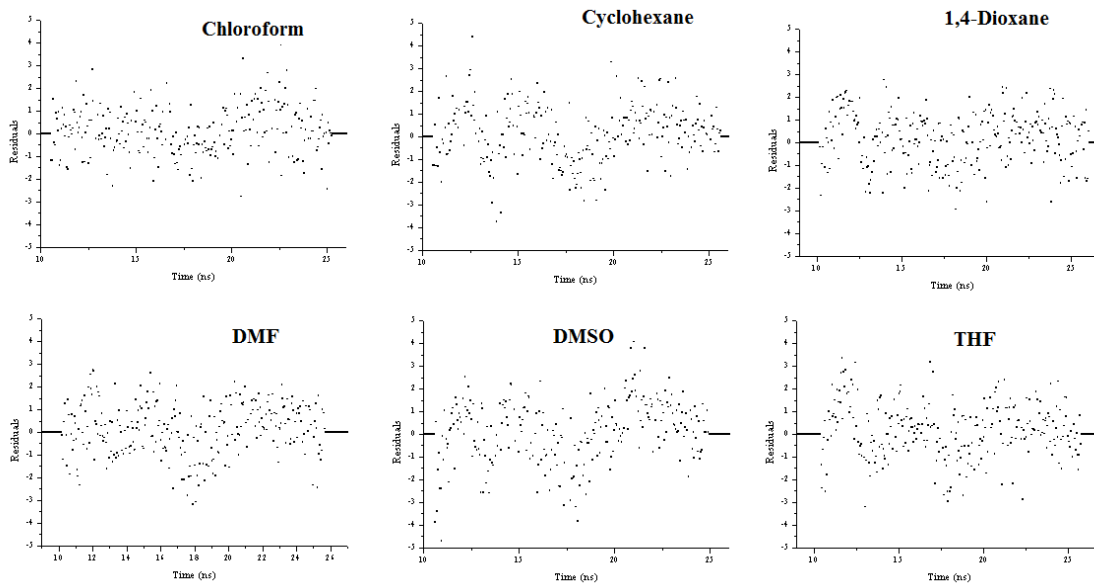
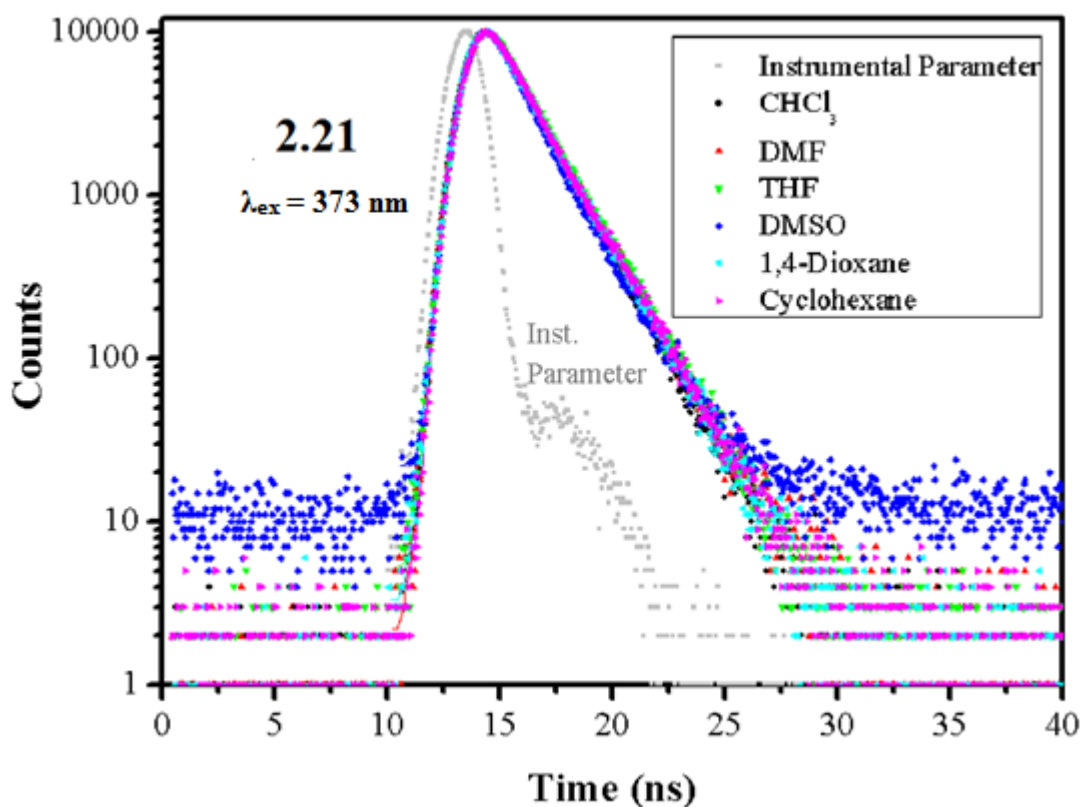


Figure 2.27. Fluorescence lifetime decays of compound **2.21** in six different solvents under oxygen-free atmosphere with single-exponential fitting and residuals.

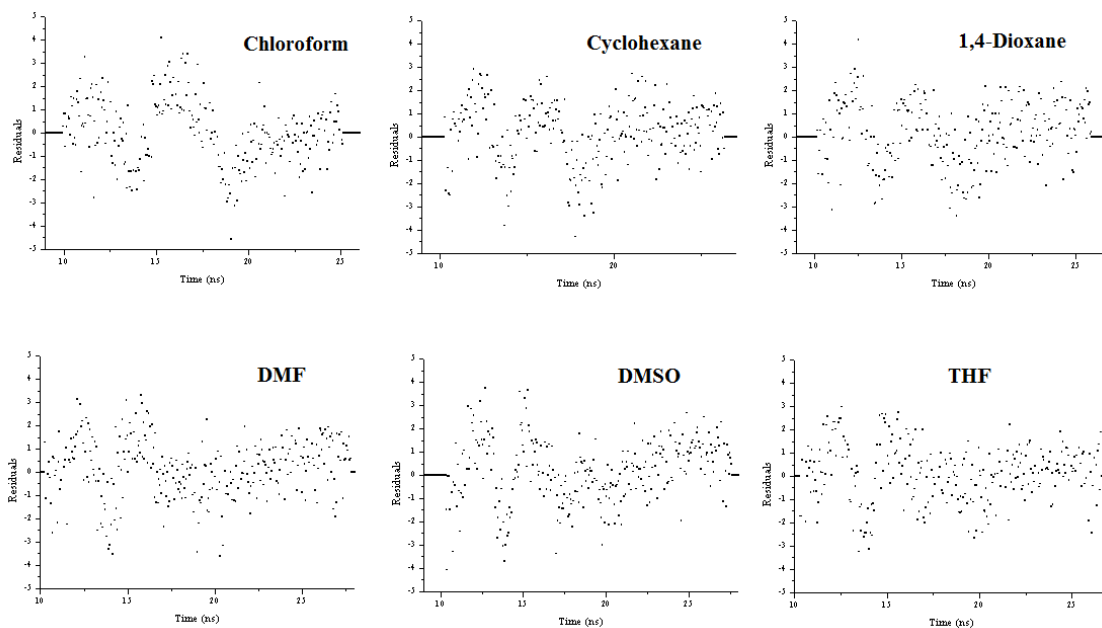
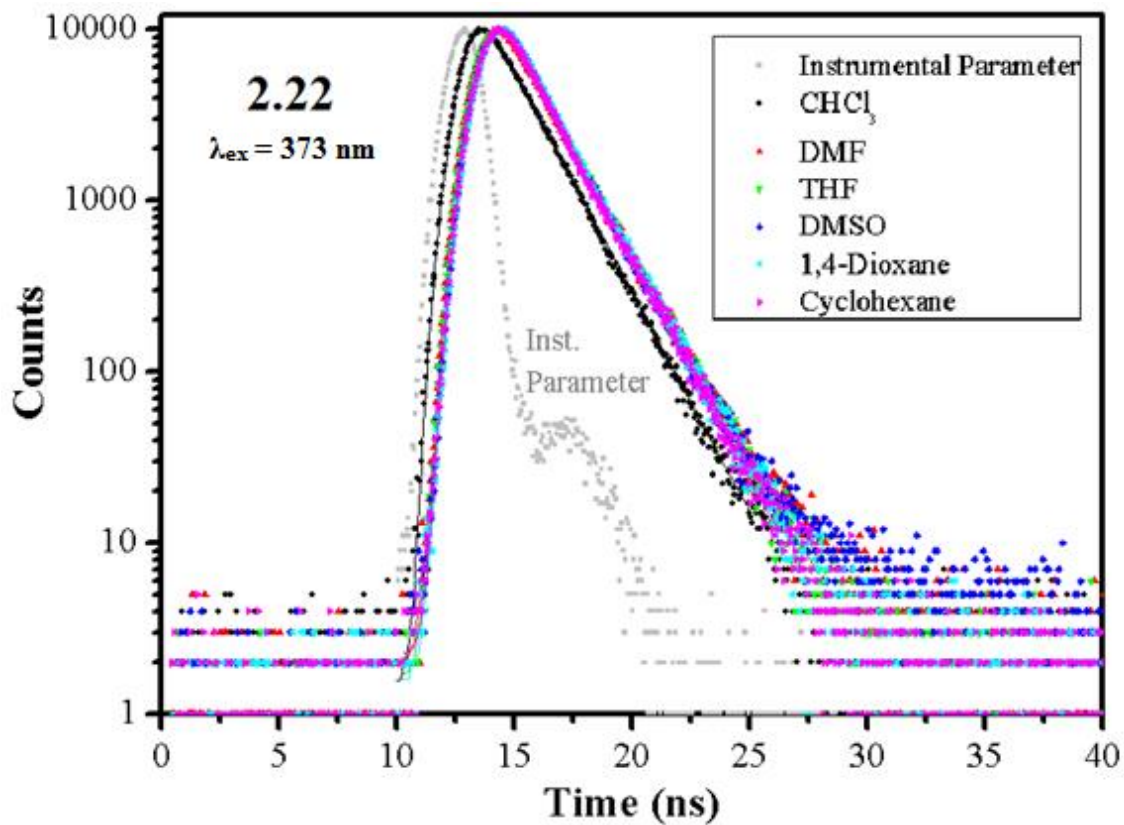


Figure 2.28. Fluorescence lifetime decays of compound **2.22** in six different solvents under oxygen-free atmosphere with single-exponential fitting and residuals.

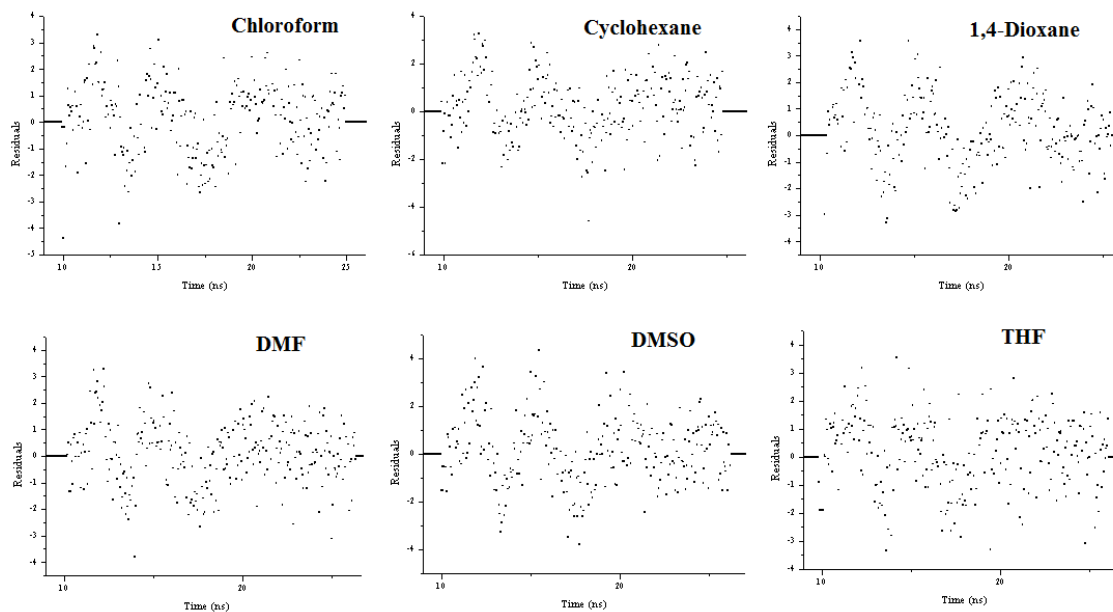
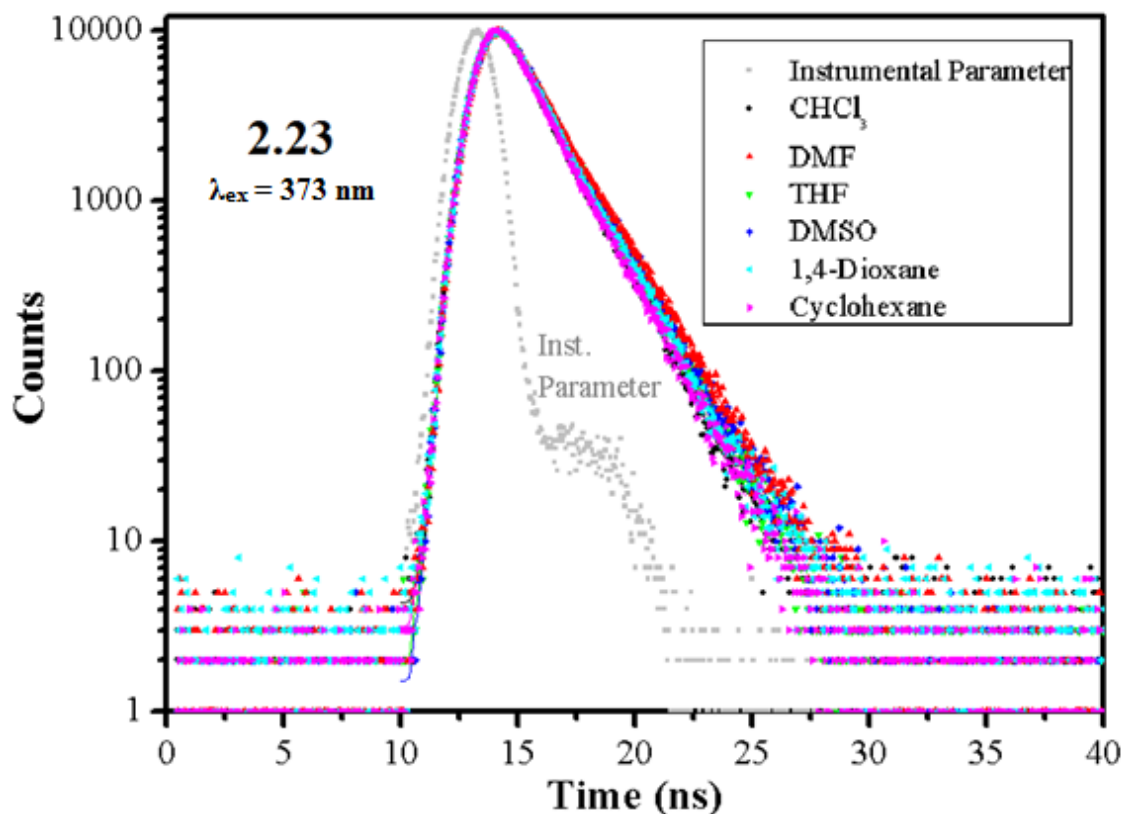


Figure 2.29. Fluorescence lifetime decays of compound **2.23** in six different solvents under oxygen-free atmosphere with single-exponential fitting and residuals.

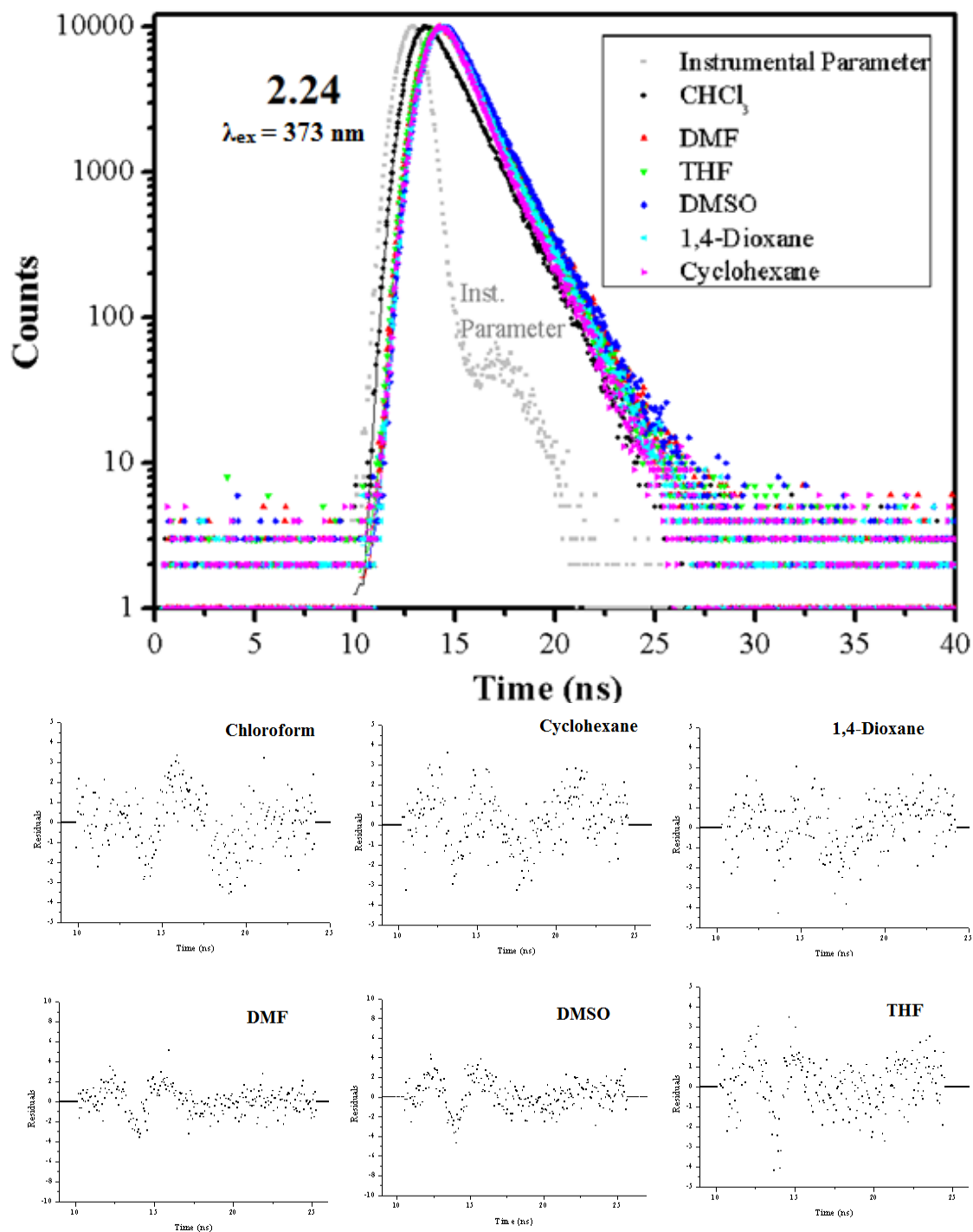


Figure 2.30. Fluorescence lifetime decays of compound **2.24** in six different solvents under oxygen-free atmosphere with single-exponential fitting and residuals.

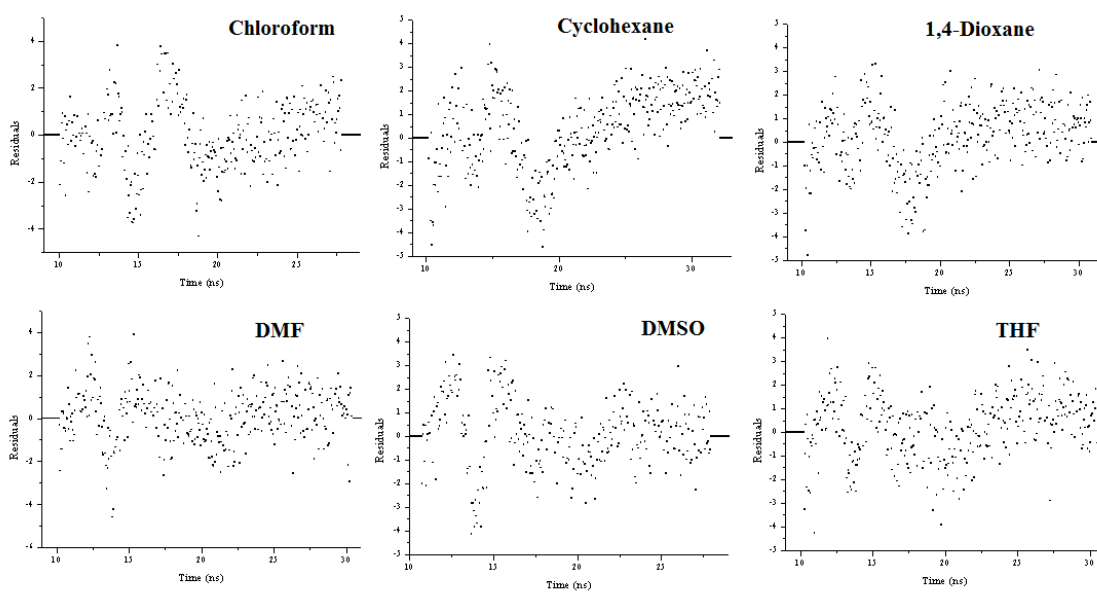
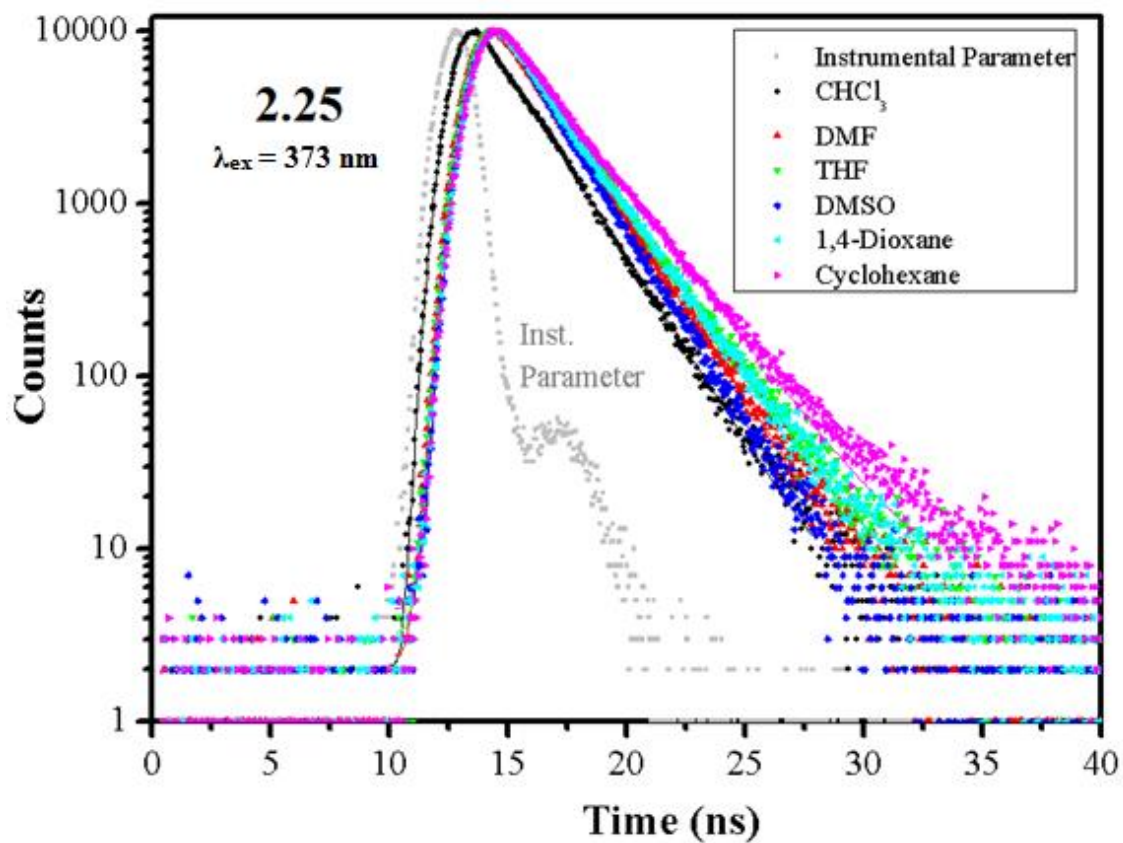


Figure 2.31. Fluorescence lifetime decays of compound **2.25** in six different solvents under oxygen-free atmosphere with single-exponential fitting and residuals.

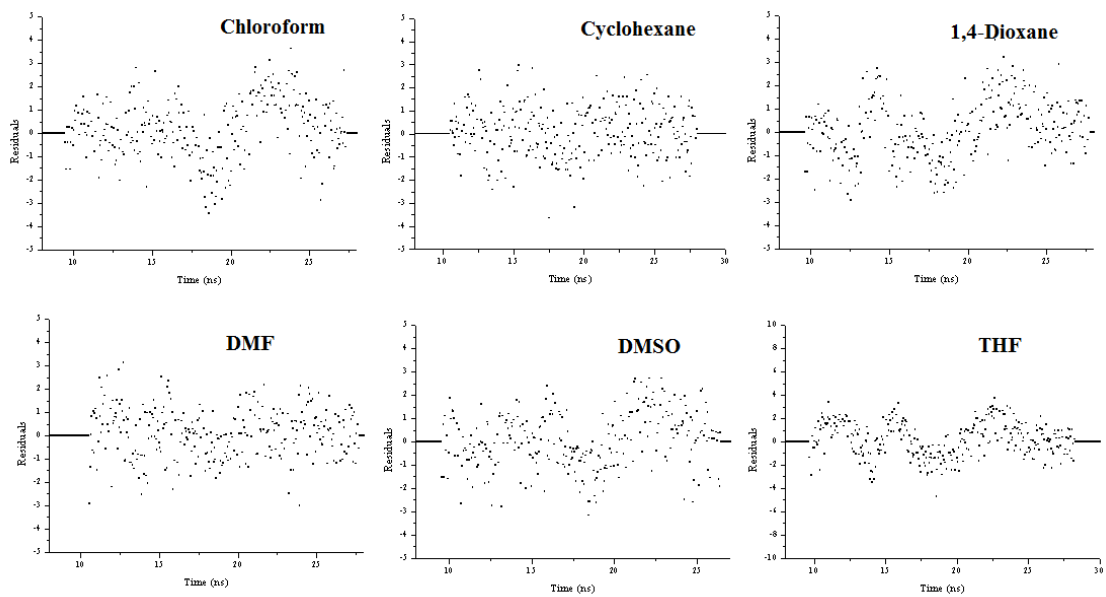
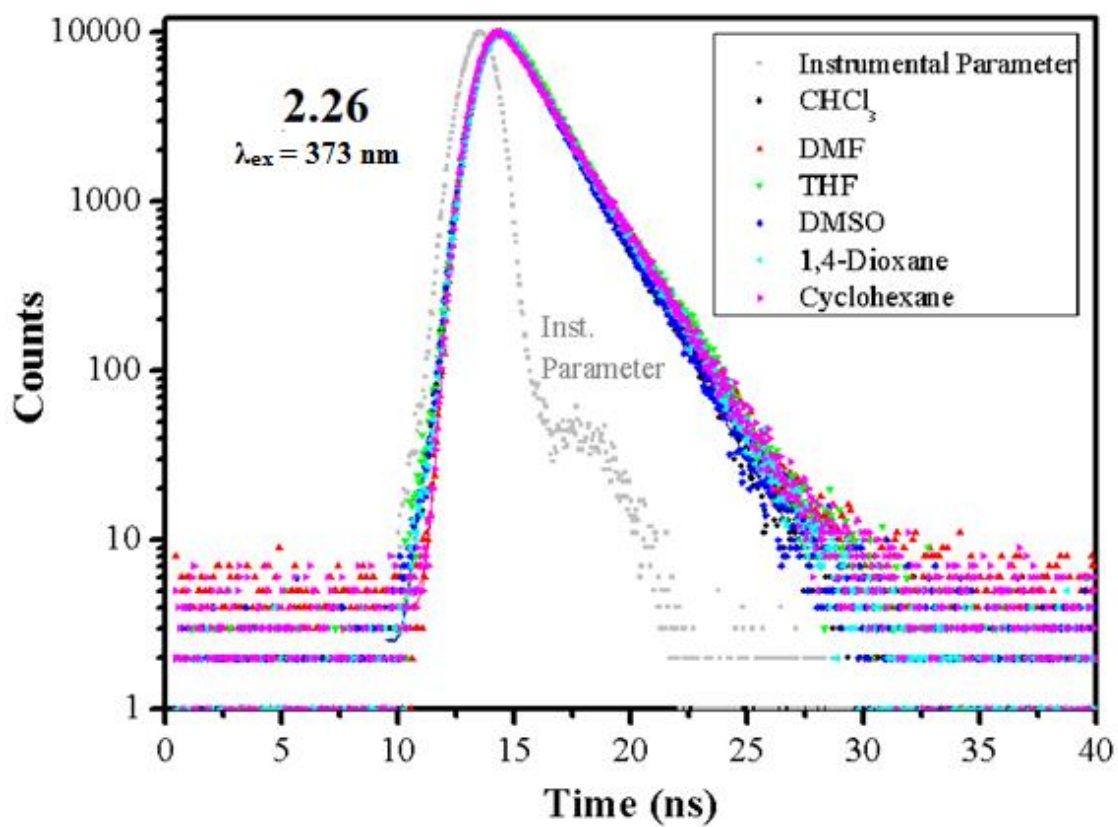


Figure 2.32. Fluorescence lifetime decays of compound **2.26** in six different solvents under oxygen-free atmosphere with single-exponential fitting and residuals.

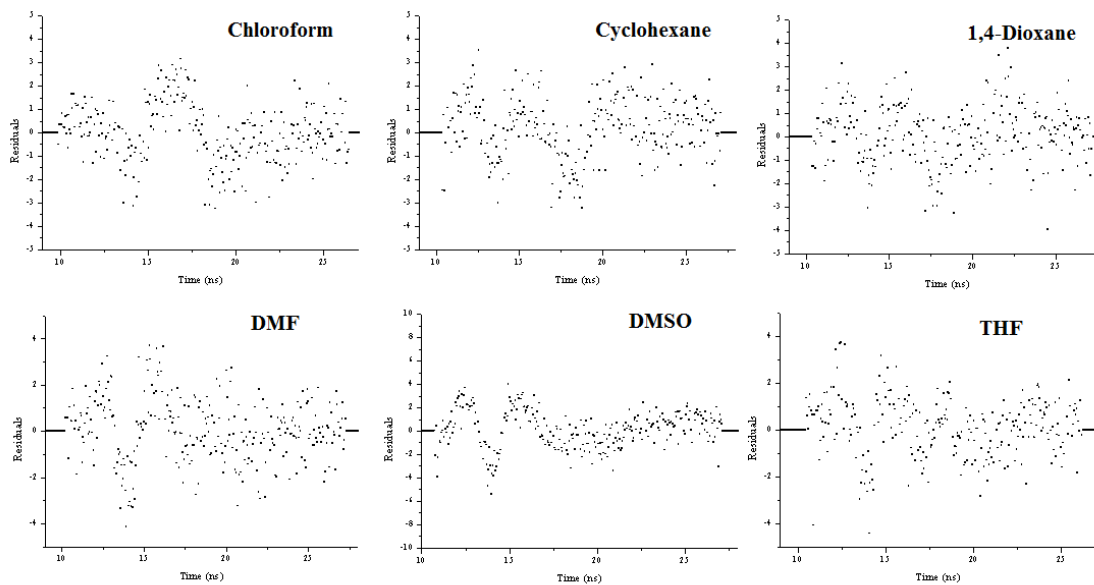
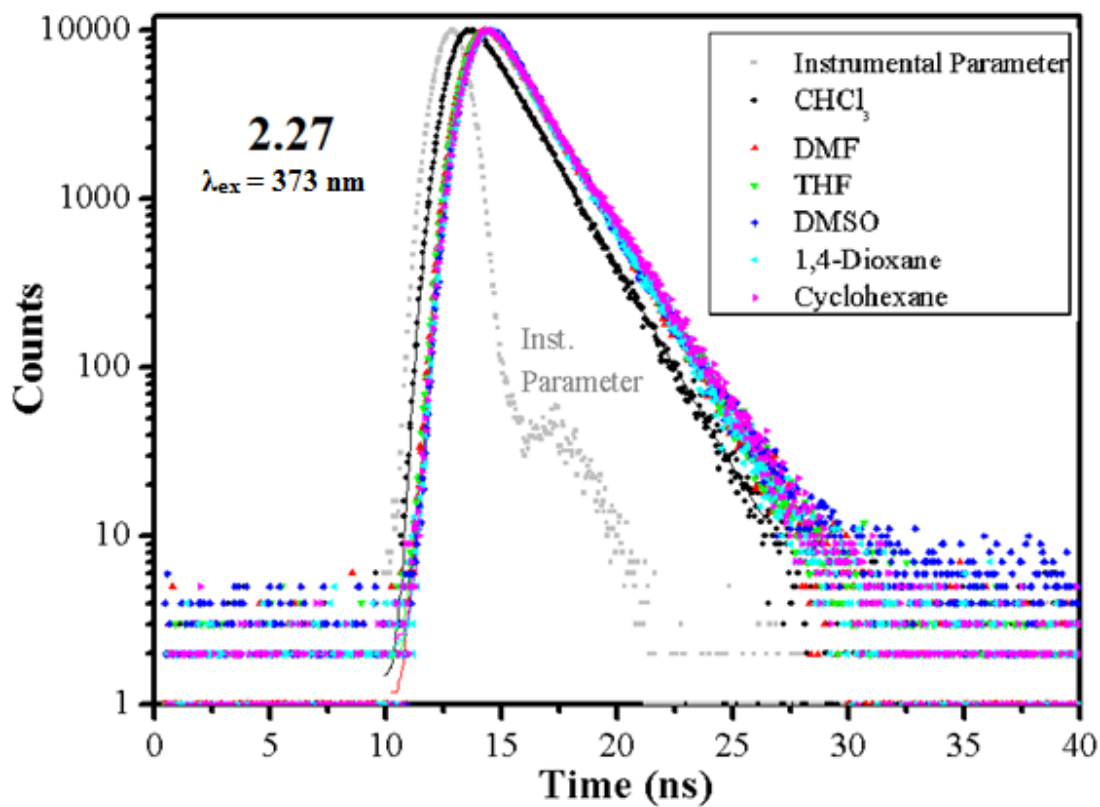


Figure 2.33. Fluorescence lifetime decays of compound **2.27** in six different solvents under oxygen-free atmosphere with single-exponential fitting and residuals.

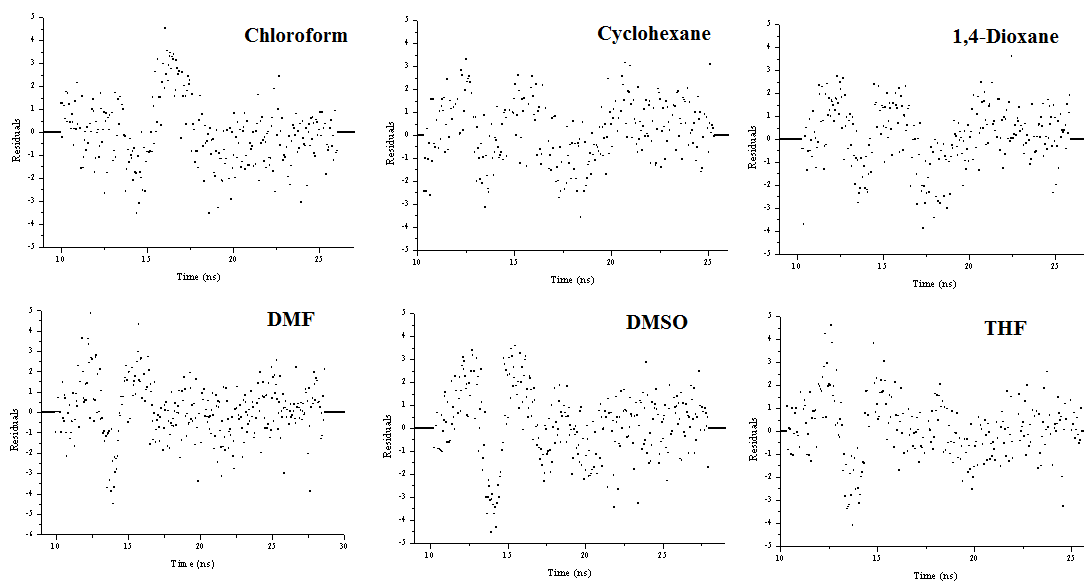
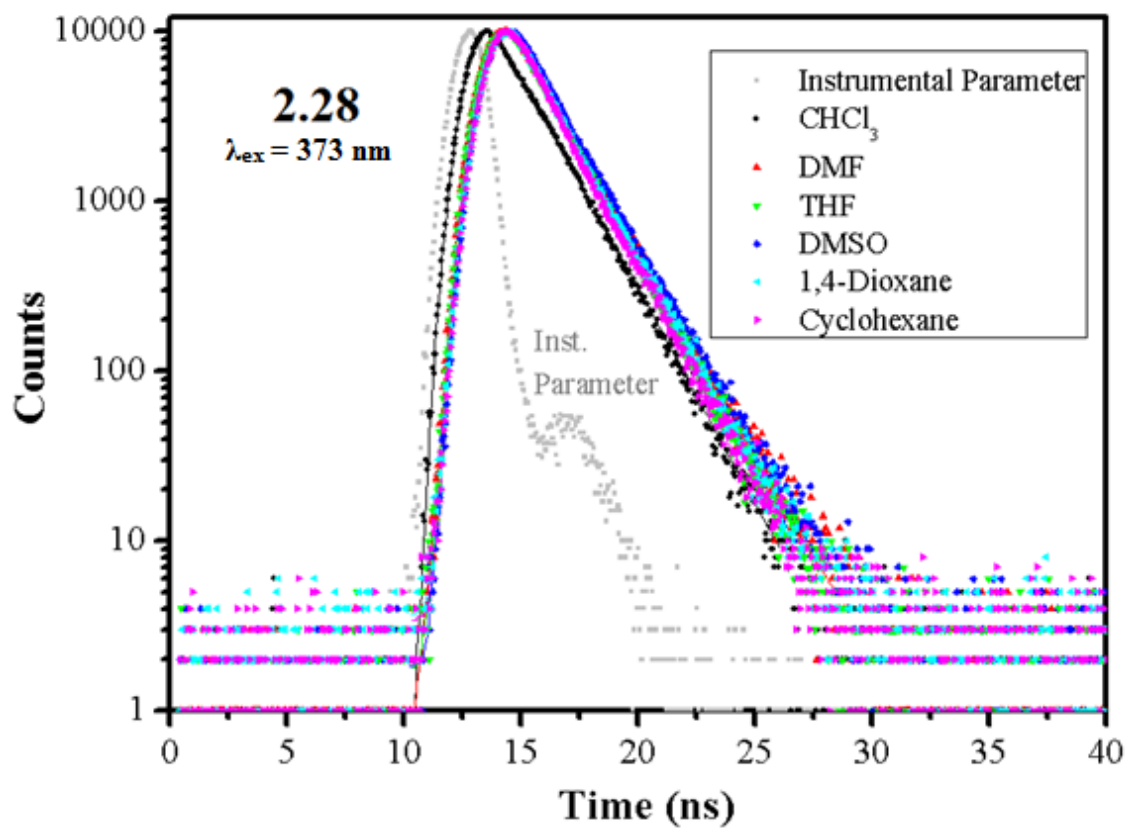


Figure 2.34. Fluorescence lifetime decays of compound **2.28** in six different solvents under oxygen-free atmosphere with single-exponential fitting and residuals.

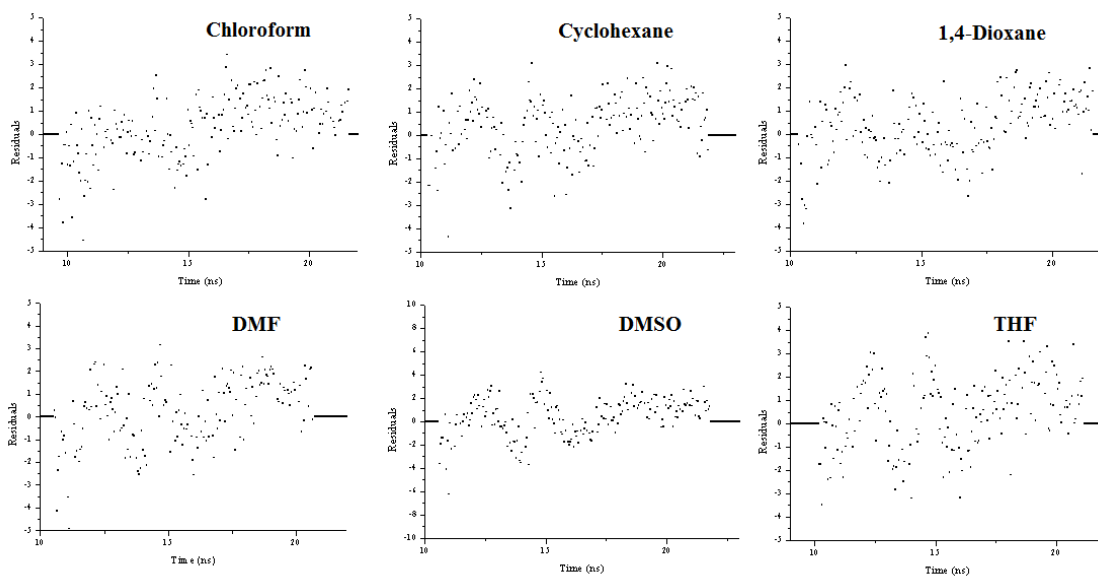
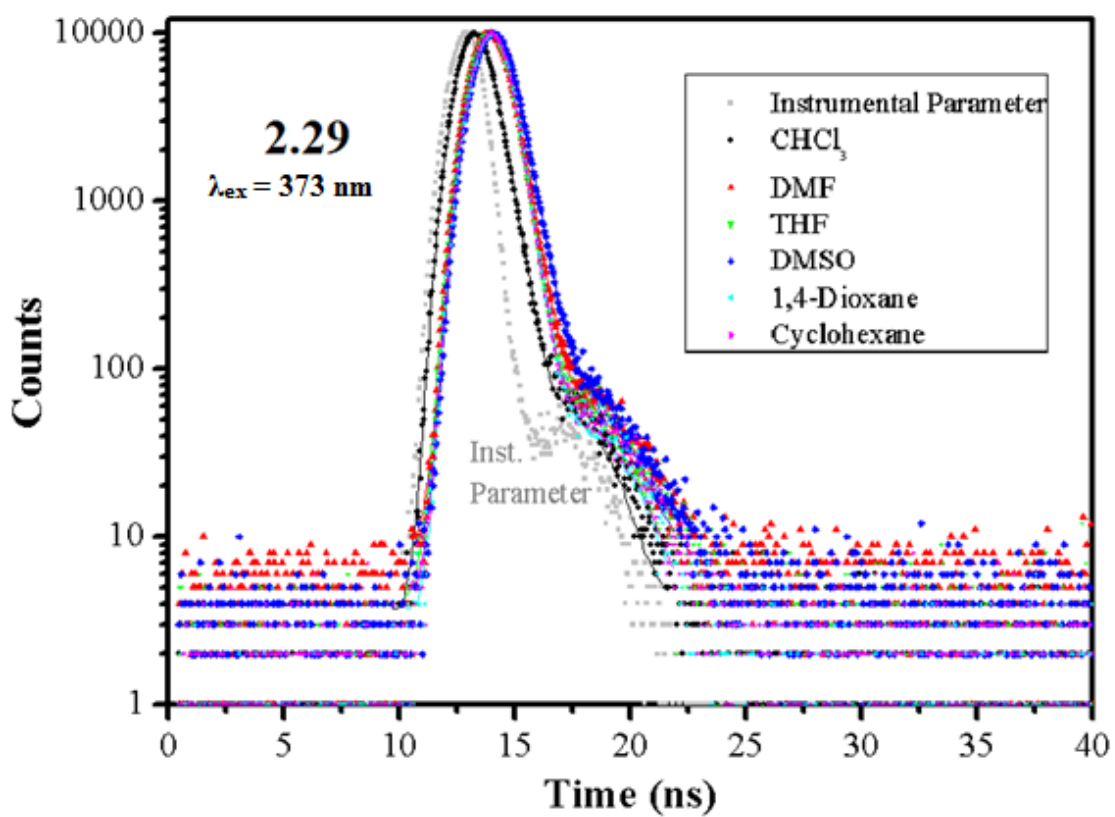


Figure 2.35. Fluorescence lifetime decays of compound **2.29** in six different solvents under oxygen-free atmosphere with single-exponential fitting and residuals.

2.2.2.3. Substituent Effect: Steric and Electronic Effects

Substituting pyrene in positions 1, 3, 6 and 8, even with saturated alkyl groups, was directly related to an enhancement of its emission quantum yield.^{101,102} In 2013, Niko *et al.* studied the effect of inserting saturated alkyl chains in these positions,¹⁰² and noted significant increase in quantum yields due to σ - π conjugation, and prevention of aggregation, and therefore inhibition of excimer formation. The fluorescence quantum yield increased from 0.28 to 0.61 in oxygen-free dichloromethane solution upon 1,3,6,8-tetraalkylsubstitution, Figure 2.36.¹⁰²

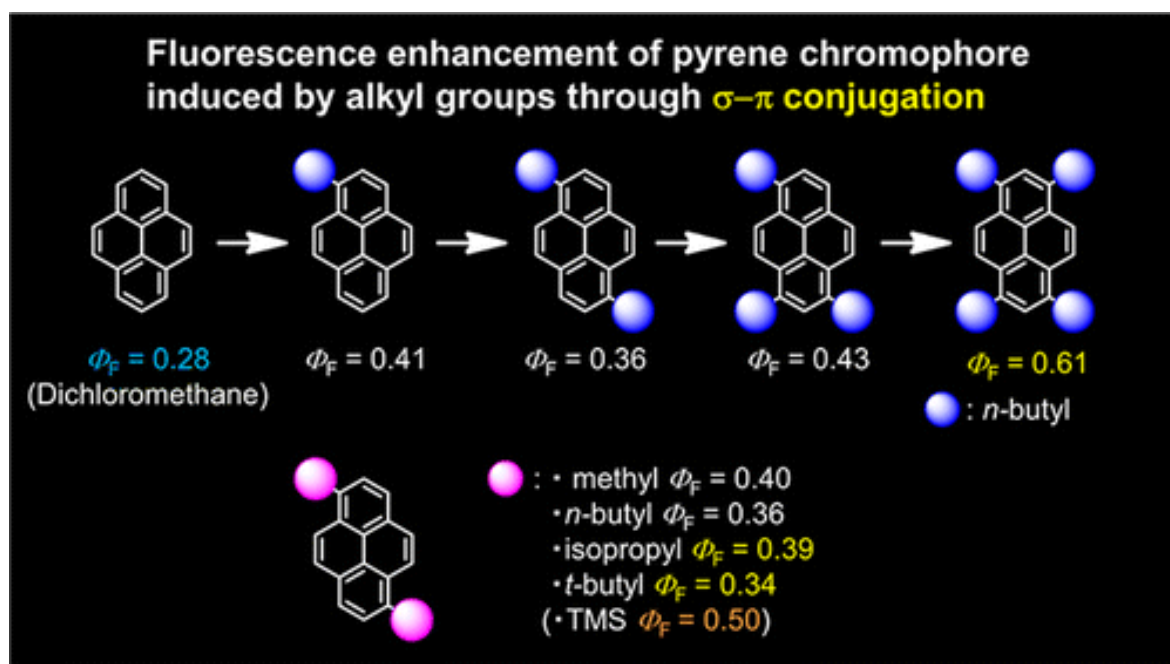


Figure 2.36. The effect of adding different saturated substituents on pyrene in positions 1, 3, 6 and 8 on its fluorescence quantum yield in oxygen-free dichloromethane solutions.¹⁰² Reprinted with permission from (Niko, Y.; Kawauchi, S.; Otsu, S.; Tokumaru, K.; Konishi, G.-i. *J. Org. Chem.* **2013**, 78, 3196). Copyright (2013) American Chemical Society.

Furthermore, the π - π conjugation seems to enhance fluorescence quantum yield beyond the limit of 0.61.¹⁰² Sotoyama *et al.* reported a dramatic increase in fluorescence quantum yield up to 0.90 upon 1,3,6,8-tetraphenyl substitution in oxygen-free cyclohexane solution.²¹ This has been attributed to an extension of the conjugation space of the system, which in turns creates a partial double bond character between the pyrene rings and the outer phenyl rings at the 1,3,6,8 positions of pyrene, leading to the inhibition of the rotation of the outer rings with respect to the single bond connecting them to the pyrene core due to this partial double bond character, leading to more efficient inhibition of aggregation and thus the formation of excimer.²¹ However, a much more important factor, is that the forbidden $S_0 \rightarrow S_1$ transition in pyrene becomes favored in 1,3,6,8-tetraphenylpyrene, Figure 2.37.²¹ This is explained by the higher oscillator strength of the lowest energy transition (L_a) in 1,3,6,8-tetraphenylpyrene, as compared to pyrene (L_b), Figure 2.37.²¹ The forbidden $S_0 \rightarrow S_1$ transition in pyrene implies a forbidden $S_1 \rightarrow S_0$ emission as well. This explains the longer-lived excited state in pyrene, in addition to the dramatic decrease in fluorescence lifetime upon moving from pyrene to 1,3,6,8-tetraarylpyrene compounds. The $S_1 \rightarrow S_0$ transition is favored in the latter, and the excited state is subsequently shorter-lived.⁶⁹

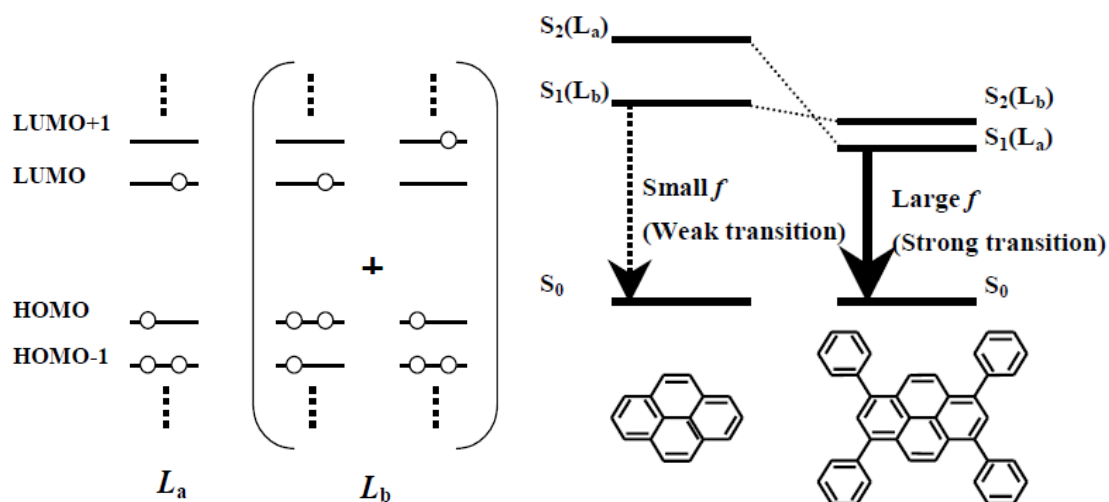


Figure 2.37. Simple illustration of allowed and forbidden transitions in pyrene and 1,3,6,8-tetraphenylpyrene to explain fluorescence enhancement in the latter.²¹ Sotoyama, W.; Sato, H.; Kinoshita, M.; Takahashi, T.; Matsuura, A.; Kodama, J.; Sawatari, N.; Inoue, H. “Tetra-Substituted Pyrenes: New Class of Blue Emitter for Organic Light-Emitting Diodes”, *Dig. Tech. Pap. - Soc. Inf. Disp. Int. Symp.* **2003**, *34*, 1294-1297. Copyright Wiley-VCH Verlag GmbH & Co. KGaA, Weinheim. Reproduced with permission.

The increase in fluorescence quantum yield is more difficult to achieve in solid state than solution due to increased aggregation and π - π stacking that may lead to fluorescence quenching by excimer formation.²¹ In 2007, Moorthy *et al.* reported the synthesis of three sterically hindered 1,3,6,8-tetraphenylpyrene derivatives with *ortho* substituents (methyl groups) on all the outer phenyl rings, Figure 2.38.¹⁰³ Keeping both methyl groups on *ortho* positions, the change from one derivative to the other was on the *meta* and *para* positions, and the results obtained were all similar. These derivatives showed similar fluorescence quantum yields in solid state and in cyclohexane solution, which indicates the absence of fluorescence quenching due to π - π stacking in the solid state.¹⁰³ This has been explained by a steric inhibition of the rotation of the outer phenyl rings around the single bond connecting it to the pyrene core in a perfect angle that makes them very close from being perpendicular to each other, Figure 2.38.¹⁰³

Thus, the outer phenyl rings, being blocked by the steric hindrance at a dihedral angle approaching 90° from the plane of the pyrene core, act as efficient spacers by preventing any possible unwanted aggregation or π - π stacking of pyrene cores from adjacent molecules in solution and in solid state, respectively. However, the three sterically hindered derivatives showed fluorescence quantum yields below 0.44 in both solid state and solution.¹⁰³ This keeps them far from being the best candidates in OLED device application.

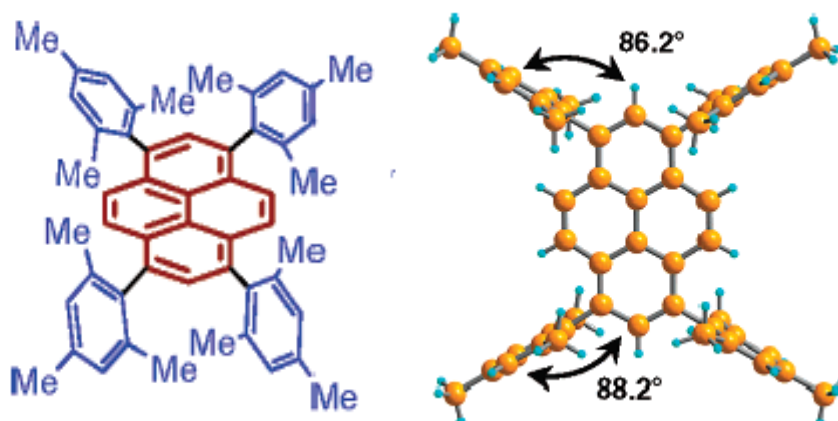


Figure 2.38. One of the three sterically hindered 1,3,6,8-tetraarylpyrene derivatives reported in 2007 by Moorthy *et al.* (left), and a representation of the dihedral angles between the plane containing the outer phenyl rings and the one having the pyrene core for this derivative (right).¹⁰³ Reprinted with permission from (Moorthy, J. N.; Natarajan, P.; Venkatakrishnan, P.; Huang, D.-F.; Chow, T. *J. Org. Lett.* **2007**, *9*, 5215). Copyright (2007) American Chemical Society.

In summary, playing on the substituents residing on the outer phenyl rings of 1,3,6,8-tetraarylpyrene derivatives leads to different effects that are worth investigation. In our novel substituted 1,3,6,8-tetraarylpyrene compounds, the inclusion of substituents having a variety of electronic and steric properties (i.e. electron-releasing **2.21-2.24** vs. electron-withdrawing **2.25-2.28**, bulky **2.21** vs. non-bulky **2.25**), on the

outer benzene rings, may lead to different photophysical properties. Significant increase in fluorescence quantum yield, up to 0.91 in solid state for compound **2.27**, is observed. This renders the novel 1,3,6,8-tetraarylpyrene compounds potential candidates for OLED device applications.

Absorption, excitation and emission spectra were collected for unsubstituted pyrene (Py) and 1,3,6,8-tetraphenylpyrene (TPPy) were collected in THF for comparison purpose, Figures 2.39 and 2.40, respectively.

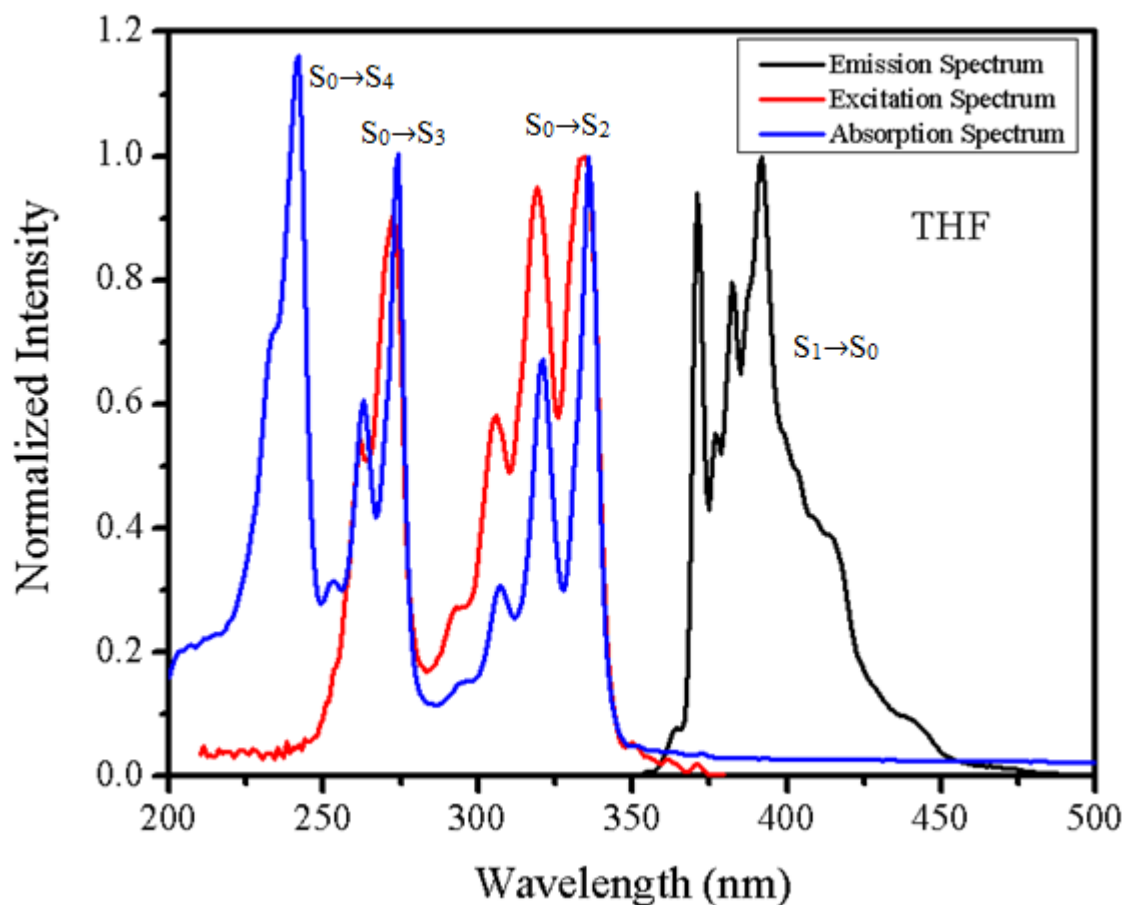


Figure 2.39. Overlay of pyrene (Py) absorption, excitation and emission spectra in THF solution.

The absorption spectrum of pyrene, Figure 2.39, shows four electronic transitions occur around 245 (strongest), 270, 335, and 375 (weakest/forbidden) nm, Table 2.1. As compared to the excitation spectrum, Figure 2.39, the difference is in the absence of the transition around 245 nm in the latter (the $S_0 \rightarrow S_4$ transition). This means that this transition leads to a non-radiative relaxation from the excited state of pyrene. Otherwise, the remaining transitions are almost matched for both the absorption and excitation spectra. The transition around 375 nm is not detectable experimentally, and this is consistent with the forbidden character of this transition. The vibrational structure

is characteristic of both the absorption and emission spectra as previously mentioned. The ratio of the first to the third emission peaks is found to be in the range of 1.18-1.20 (from different solutions having different concentrations), which is consistent with the values reported by Dong and Winnik in the *Py*-scale of solvent polarity where this ratio is supposed to be around 1.22.⁶⁰

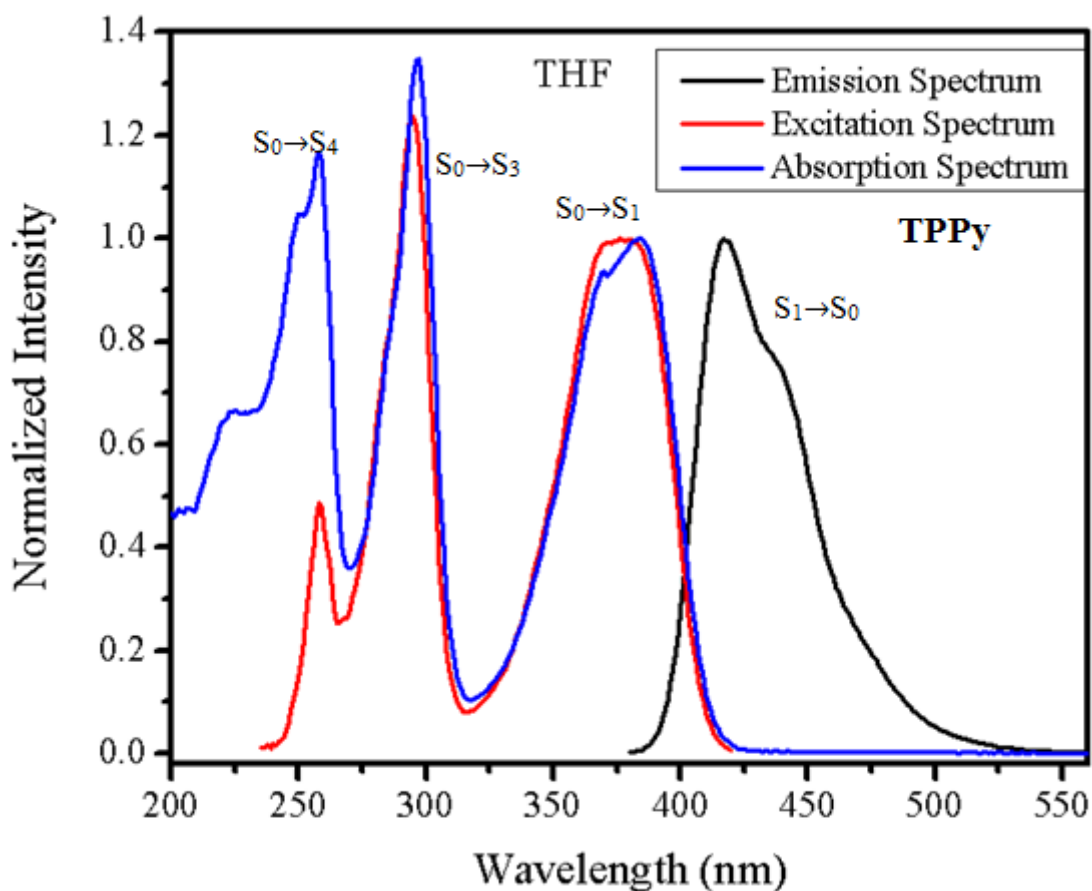


Figure 2.40. Overlay of TPPy absorption, excitation and emission spectra in THF solution.

Moving from Py to TPPy, a large bathochromic shift in the emission spectrum occurs, along with a loss of the vibrational structure of pyrene, Figure 2.40. The bathochromic shift is explained by increased conjugation and the loss of vibrational

structure is explained by the fact that TPPy is non-planar with a D_2 symmetry. Non-planar polyaromatic emitters, unlike the planar ones, usually do not display vibrational structure in their absorption and emission spectra. The transition centered around 375 nm ($S_0 \rightarrow S_1$) in pyrene, is bathochromically-shifted (384 nm) and becomes significantly stronger. This explains the significant increase in emission quantum yield for TPPy (0.73) as compared to Py (0.29). Whereas the transition centered around 335 nm in pyrene ($S_0 \rightarrow S_2$) becomes forbidden in TPPy, and it is not observed experimentally. This is consistent with the inversion of the L_a and L_b states upon moving from Py to TPPy, as previously explained. The $S_0 \rightarrow S_1$ transition clearly obeys the mirror-image rule. The two observed lowest energy transitions ($S_0 \rightarrow S_1$ and $S_0 \rightarrow S_3$) in the excitation spectrum of TPPy are overlapping with their correspondings in the absorption spectrum. However, similarly to pyrene, the highest energy transition ($S_0 \rightarrow S_4$) appear of much lower intensity in the excitation spectrum of TPPy, Figure 2.40, which suggests that this transition favors non-radiative relaxation pathways from the excited state. Our interest in the study of compounds **2.21-2.29** was focused on the two lowest energy transitions, due to the fact that they are the only transitions directly affected by the substituents. In addition to their influence on radiative and non-radiative photophysical processes (i.e. whenever $S_0 \rightarrow S_1$ corresponds to L_a instead of L_b may suggest a higher emission quantum yield). The results of the Py and TPPy comparison are summarized in Table 2.6.

Table 2.6. Experimental photophysical results for Py and TPPy in THF solutions.

	λ_{max}^{em} , nm	λ_{max}^{abs} , nm	$\Delta\lambda$, eV	$\Delta\lambda$, cm ⁻¹	Py value (I/III) for THF	τ , ns (χ^2)	ϕ_F	k_r (10 ⁷) s ⁻¹	k_{nr} (10 ⁷) s ⁻¹	τ_n , ns
TPPy	417	384	0.26	2061	---	2.24 (1.31)	0.73	32.6	12.1	3.07
Py	392	373	0.16	1299	1.18-1.20 (Lit. ⁶⁰ 1.22)	322.30 (2.89)	0.29	0.09	0.22	1111.38

An expected increase in radiative decay constant k_r in TPPy occurs in parallel to the increase in emission quantum yield, Table 2.6. However, the non-radiative constant k_{nr} also increased in TPPy as compared to Py. This is inconsistent with the higher quantum yield of TPPy. The ratio of increase in k_r (362-fold: 32.6×10^7 in TPPy vs. 0.09×10^7 in Py) in comparison with that of k_{nr} (55-fold: 12.1×10^7 in TPPy vs. 0.22×10^7 in Py), Table 2.6, indicates that all photophysical processes occur faster in TPPy than in Py, including the non-radiative processes listed in Table 2.4 (i.e. intersystem crossing, vibrational relaxation and internal conversion). However, the radiative processes occur 362 times faster in TPPy than in Py, whereas the non-radiative ones occur only 55 times faster. This explains the increase in emission quantum yield in TPPy despite the larger non-radiative decay rate k_{nr} , Table 2.6. This is also consistent with the short-lived excited state in TPPy, Figure 2.41, where all the photophysical processes (radiative and non-radiative) occur at a faster rate than Py. These results may be explained by the work of Nijegorodov *et al.*, where a higher intersystem crossing rate constant k_{ISC} , a sub-component of k_{nr} , was reported. This has been related to the non-planarity of TPPy as compared to a planar pyrene molecule.¹⁰⁰

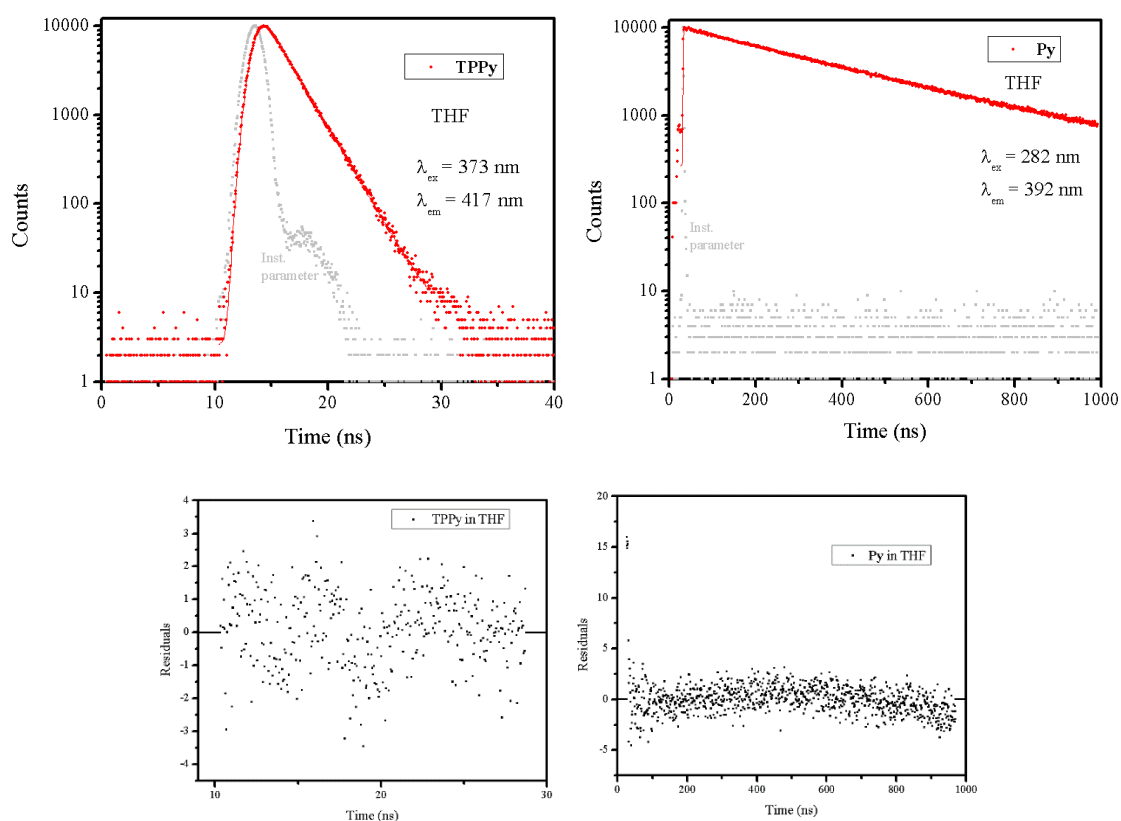


Figure 2.41. Comparison of the lifetime decay curves of TPPy (left) and Py (right) in oxygen-free THF solutions with single exponential fitting and residuals.

The $S_0 \rightarrow S_1$ transition was shown to be affected by the inclusion of electron releasing groups. This is clearly observed by the significant bathochromic shifts up to 0.10 eV for compound **2.24**. This suggests that the introduction of such groups on the outer benzene ring of the compound leads to an enhancement of the conjugation between the outer benzene and the pyrene core leading to such bathochromic shifts in absorption wavelengths. Negligible shifts were observed for electron withdrawing groups except for compound **2.28**, where a bathochromic shift of 0.05 eV was observed, which is comparable to the shifts occurring in the case of electron-releasing substituents. This can be explained by a “push-pull” interaction taking place between the substituents on the outer benzene rings and the pyrene core. In other words,

introducing any effective electronic effect (releasing or withdrawing) might contribute to increased conjugation between the outer benzene ring and the inner pyrene core. The difference will be in the direction of the electron delocalization, which is from the outer ring towards the inner core in case the substituent is electron-releasing (i.e. pyrene pulls and the outer benzene pushes electrons), and the opposite in case the substituent is electron withdrawing (i.e. the outer ring pulls and pyrene pushes). This is confirmed by the fact that the largest bathochromic shifts were observed for substituents having strong mesomeric effects rather than inductive ones (0.10 eV for the methylthio (**2.24**) substituent due to its high π -donor effect among electron-releasing substituents, and 0.05 eV for the methoxycarbonyl (**2.28**) substituent due to its high π -acceptor effect among electron-withdrawing substituents). Smaller shifts occurred in compounds bearing substituents that are σ -donors/acceptors, such as alkyl groups and halogens, respectively (**2.21**, **2.25**, **2.26** and **2.27**). Similarly, switching from a benzene ring to an outer thiophene ring induces pronounced bathochromic shift of 0.20 eV, which is higher than the ones observed in both electron-releasing and electron-withdrawing substituents in the case of benzene. This is due to increased effective conjugation of the thiophene with the pyrene core as compared to a benzene substituent. This might be explained by the more electron-rich carbon atoms in thiophene than in benzene. The six aromatic π -electrons are distributed over five p-orbitals (in thiophene) instead of six (in benzene). The larger bathochromic shifts in both absorption and emission spectra upon switching from an outer benzene to an outer thiophene substituent has been previously reported by Qiao *et al.*¹⁰⁴ However, in that study, thiophene and benzene substituents were investigated on positions 2 and 7 of pyrene. The 2,7-diarylpirene derivatives are further discussed in Chapter 3 of this thesis.

The switch from inductive to mesomeric effect is clearly observed in the changes in emission wavelengths. In compounds **2.22**, **2.23**, **2.24**, **2.28** and **2.29** bathochromic shifts larger than 0.05 eV compared to the reference compound TPPy were observed. Bathochromic shifts were smaller than 0.05 eV in compounds **2.21**, **2.26**, **2.27** (for which the substituents exhibit inductive effects), and negligible hypsochromic in the case of a single fluorine substituent (**2.25**). Significant bathochromic shifts (larger than 0.15 eV) occurred in compounds **2.24**, **2.28** and **2.29**, which is expected due to the large π -donor/acceptor effect observed in these compounds as previously discussed. Shifts in absorption and emission maxima as compared to TPPy are summarized in Tables 2.7 and 2.8, respectively. Bathochromic shifts discussed in this paragraph are the ones related to the substituent effect, and not the ones due to solvatochromic effects and solvent polarity variations (i.e. comparison of different compounds in the same solvent).

Similar trend was observed for the Stokes shifts as well. Largest Stokes shift occurred in π -donor/acceptor compounds **2.23**, **2.24**, **2.28** and **2.29**, compared to much smaller Stokes shift values for σ -donor/acceptor compounds **2.21**, **2.25**, **2.26** and **2.27**. Stokes shift values for Py, TPPy and the nine compounds are presented in Table 2.9. Absorption, excitation and emission spectra for each compound are shown in Figures 2.42-2.50 and overlaid in Figures 2.51 and 2.52. Figures 2.53 and 2.54 present the molar absorptivity and fluorescence lifetime, respectively, for all compounds in chloroform. All compounds showed lifetimes similar to that of TPPy. The short-lived excited state further confirms the occurrence of the inversion of L_a and L_b transitions, leading to an allowed lowest energy transition for all nine compounds. It is interesting to note that the smallest lifetime values occurred in sulfur-containing compounds (**2.29** then **2.24**), and

the largest ones occurred in fluorinated compounds on the *para*-position of the outer benzene (**2.25**) followed by the *meta*-position (compounds **2.26** and **2.27**). We recall that the largest bathochromic shifts in emission spectra with respect to TPPy occurred in the sulfur-containing compounds (**2.29** followed by **2.24**), whereas the smallest ones occurred in the fluorine-containing compounds. An interesting hypothesis could be as follows: when comparing 1,3,6,8-tetraarylpyrene derivatives, the one showing a larger bathochromic shift in the emission wavelength (with respect to TPPy) is expected to have a smaller fluorescence lifetime.

Table 2.7. Absorption maxima of the experimental lowest energy transitions for compounds **2.21-2.29** and shifts with respect to TPPy in THF solutions.

Compound	λ_{max}^{abs} , nm	$\Delta\lambda_{max}^{abs}$, nm (eV) vs. TPPy	Shift vs. TPPy
TPPy	384	0 (0.00)	---
2.21	390	6 (0.05)	Bathochromic
2.22	389	5 (0.04)	Bathochromic
2.23	389	5 (0.04)	Bathochromic
2.24	396	12 (0.10)	Bathochromic
2.25	383	1 (< 0.01)	Hypsochromic
2.26	383	1 (< 0.01)	Hypsochromic
2.27	383	1 (< 0.01)	Hypsochromic
2.28	390	6 (0.05)	Bathochromic
2.29	408	24 (0.20)	Bathochromic

Table 2.8. Emission maxima of the experimental lowest energy transitions for compounds **2.21-2.29** and shifts with respect to TPPy in THF solutions.

Compound	λ_{max}^{em} , nm	$\Delta\lambda_{max}^{em}$, nm (eV) vs. TPPy	Shift vs. TPPy
TPPy	417	0 (0.00)	---
2.21	424	7 (0.05)	Bathochromic
2.22	429	12 (0.08)	Bathochromic
2.23	434	17 (0.12)	Bathochromic
2.24	442	25 (0.17)	Bathochromic
2.25	415	2 (0.01)	Hypsochromic
2.26	422	5 (0.04)	Bathochromic
2.27	420	3 (0.02)	Bathochromic
2.28	440	23 (0.16)	Bathochromic
2.29	464	47 (0.30)	Bathochromic

Table 2.9. Stokes shift values in nm, eV, and cm^{-1} for Py, TPPy, and compounds **2.21-2.29** in THF solutions.

Compound	λ_{max}^{em} , nm	λ_{max}^{abs} , nm	$\Delta\lambda$ (nm)	$\Delta\lambda$ (eV)	$\Delta\lambda$ (cm^{-1})
Py	392	373	19	0.16	1299
TPPy	417	384	33	0.26	2061
2.21	424	390	34	0.25	2056
2.22	429	389	40	0.30	2397
2.23	434	389	45	0.33	2665
2.24	442	396	46	0.33	2628
2.25	415	383	32	0.25	2013
2.26	422	383	39	0.30	2413
2.27	420	383	37	0.29	2300
2.28	440	390	50	0.36	2914
2.29	464	408	56	0.37	2958

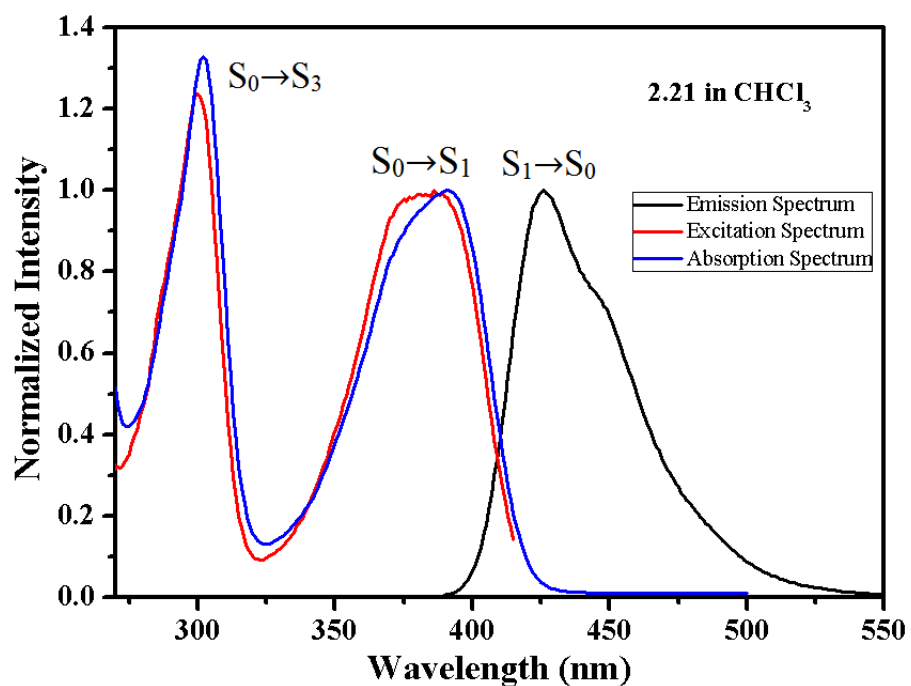


Figure 2.42. Overlay of absorption, excitation and emission spectra of compound 2.21 in chloroform solution.

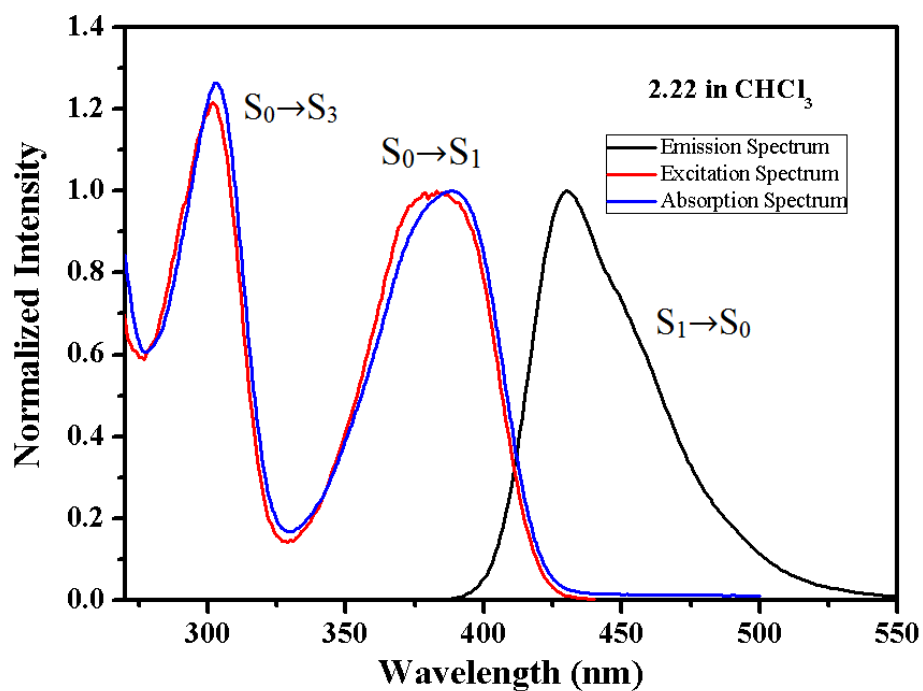


Figure 2.43. Overlay of absorption, excitation and emission spectra of compound 2.22 in chloroform solution.

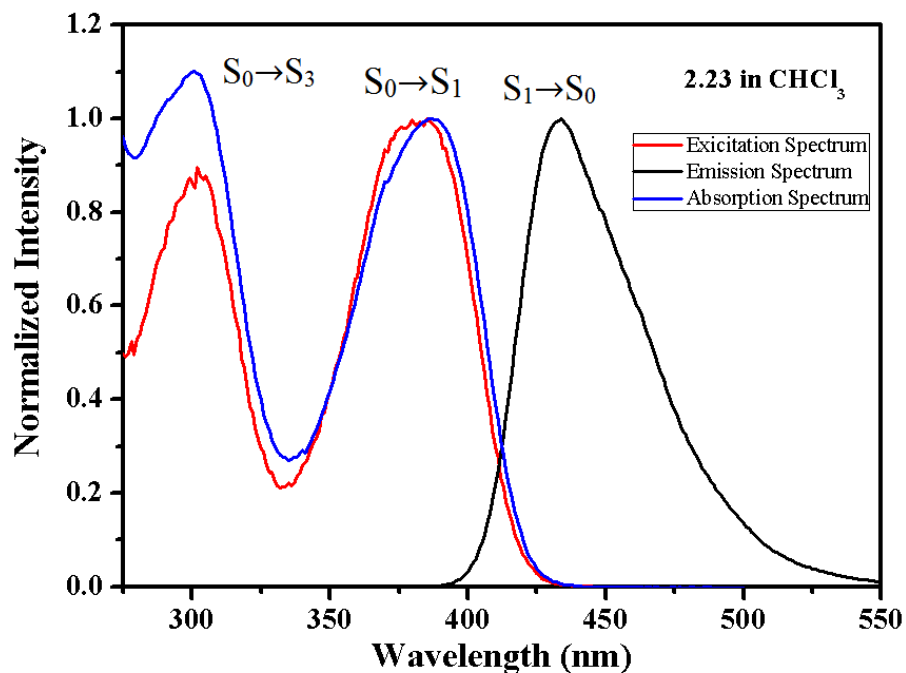


Figure 2.44. Overlay of absorption, excitation and emission spectra of compound 2.23 in chloroform solution.

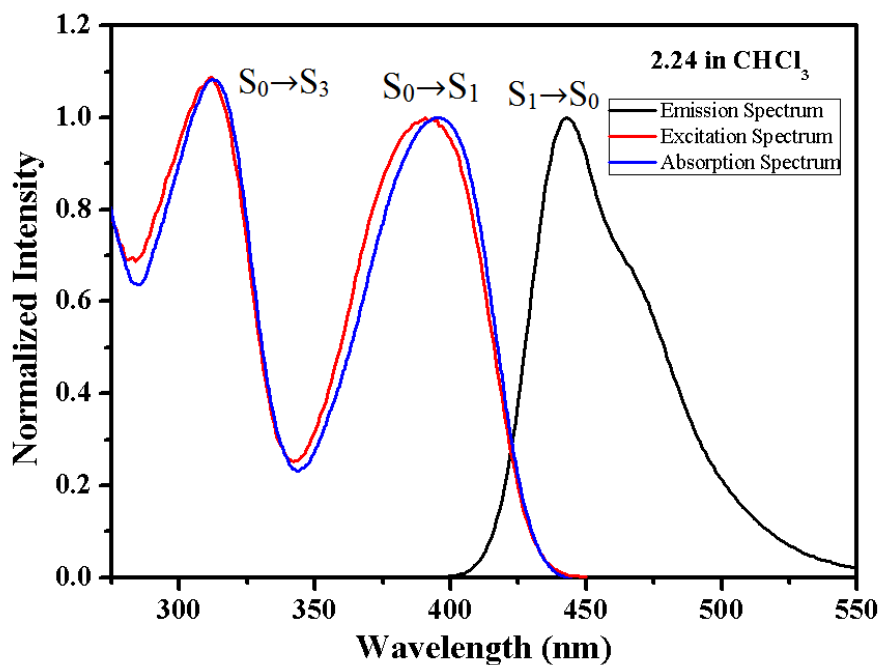


Figure 2.45. Overlay of absorption, excitation and emission spectra of compound 2.24 in chloroform solution.

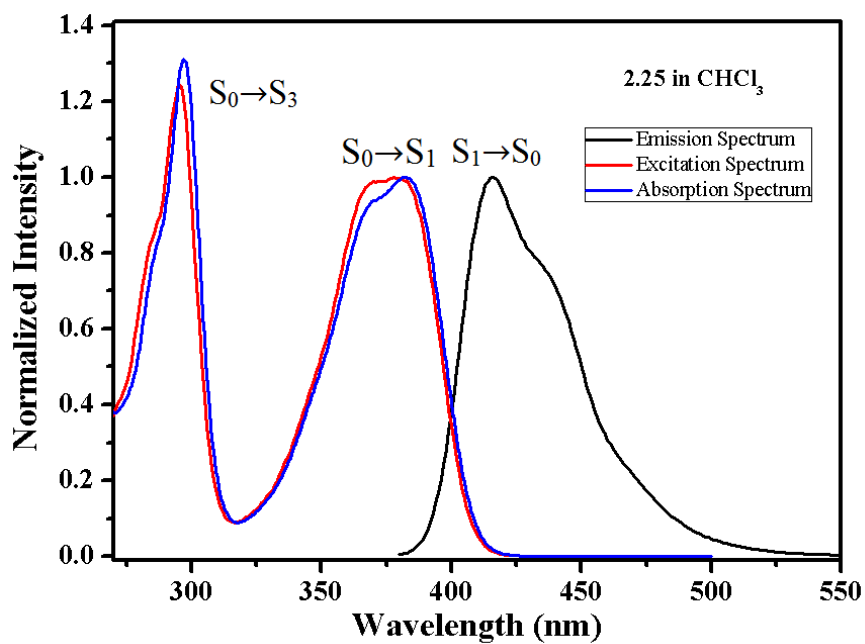


Figure 2.46. Overlay of absorption, excitation and emission spectra of compound 2.25 in chloroform solution.

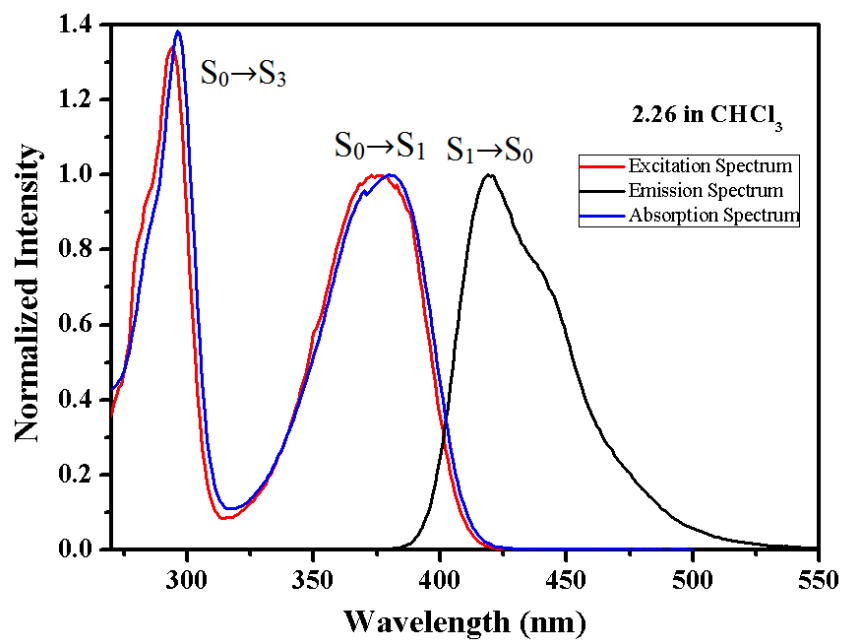


Figure 2.47. Overlay of absorption, excitation and emission spectra of compound 2.26 in chloroform solution.

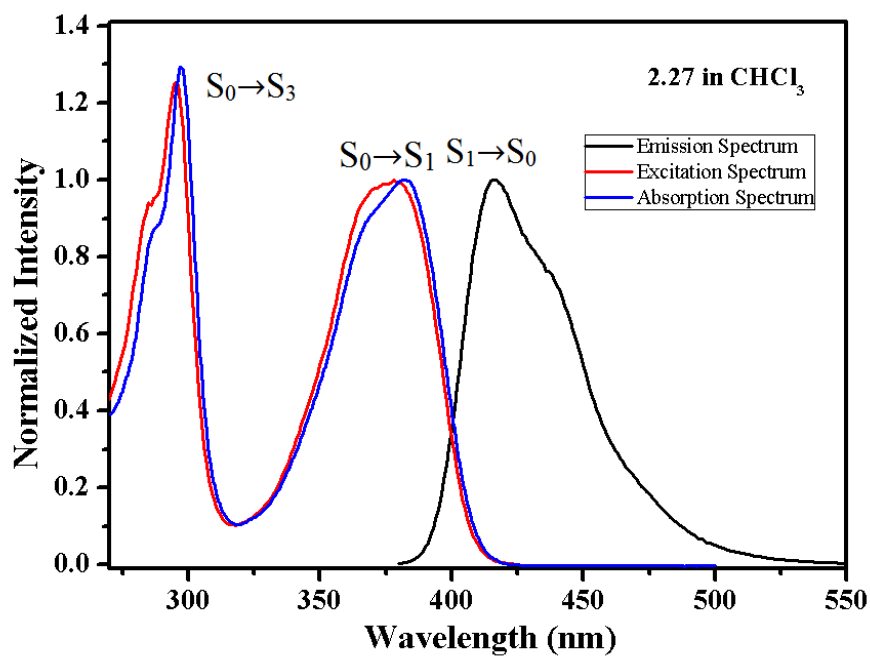


Figure 2.48. Overlay of absorption, excitation and emission spectra of compound 2.27 in chloroform solution.

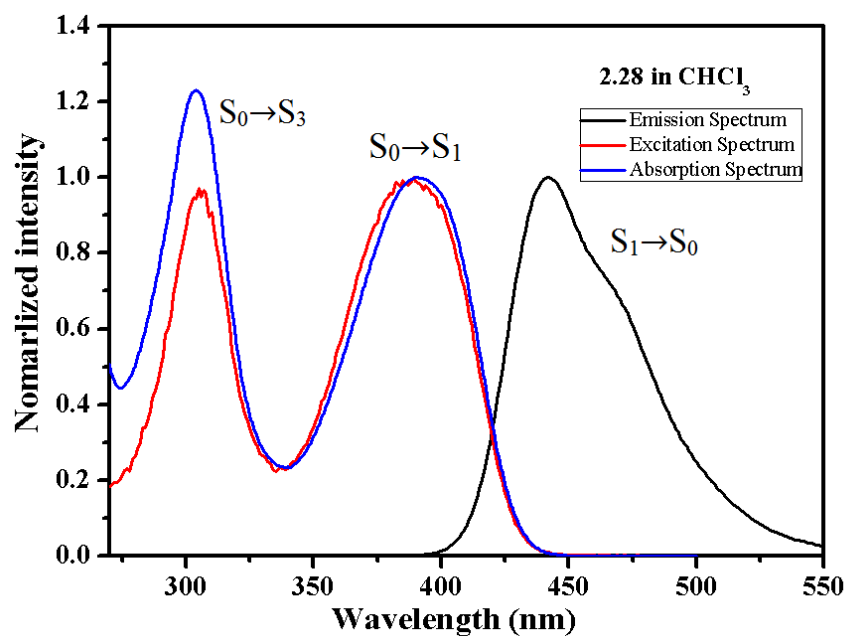


Figure 2.49. Overlay of absorption, excitation and emission spectra of compound 2.28 in chloroform solution.

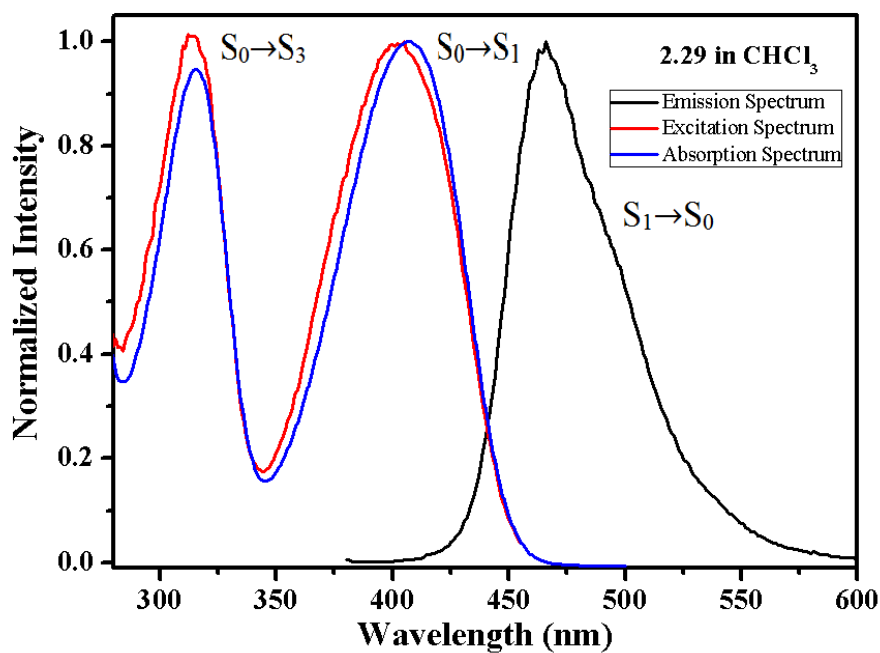


Figure 2.50. Overlay of absorption, excitation and emission spectra of compound 2.29 in chloroform solution.

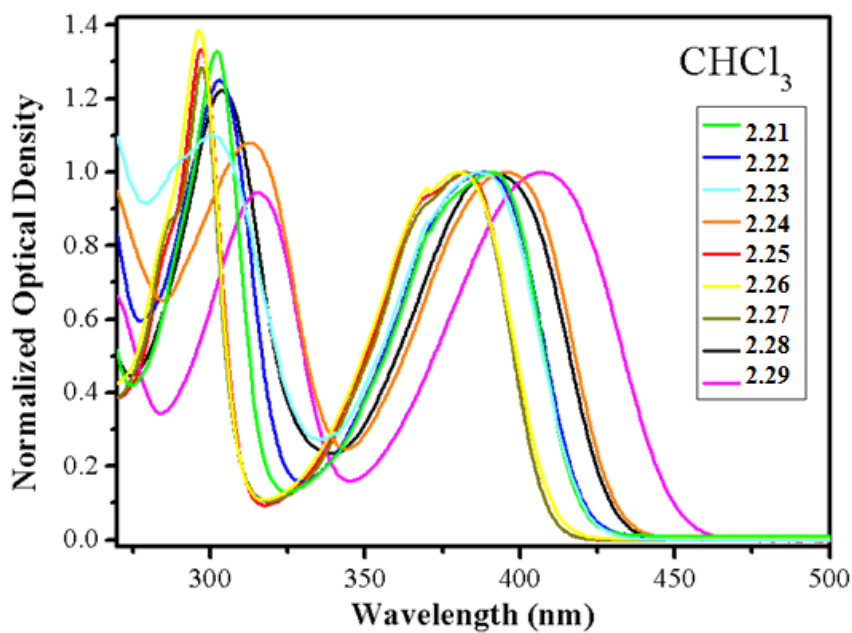


Figure 2.51. Normalized absorption spectra of compounds 2.21-2.29 in chloroform.

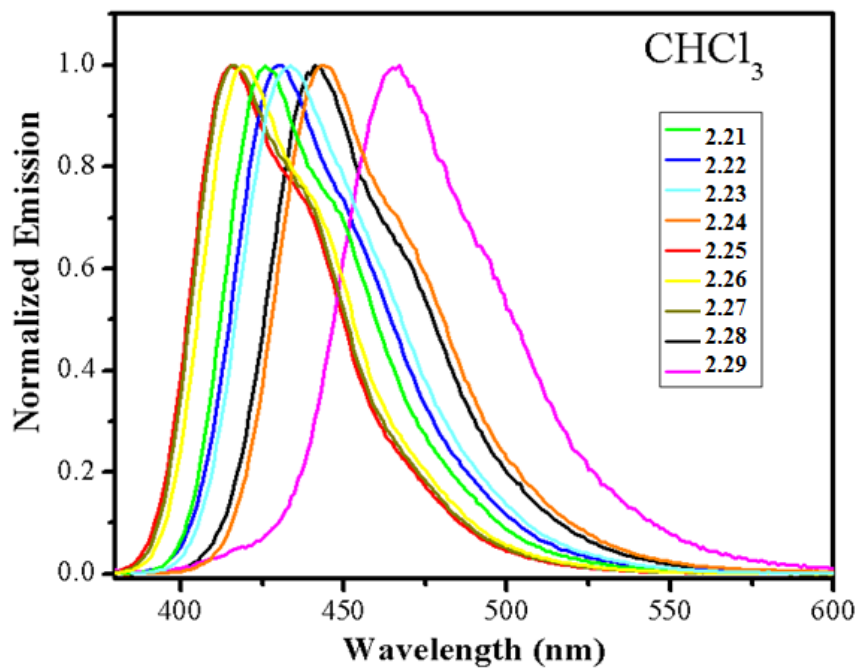


Figure 2.52. Normalized emission spectra of compounds **2.21-2.29** in chloroform.

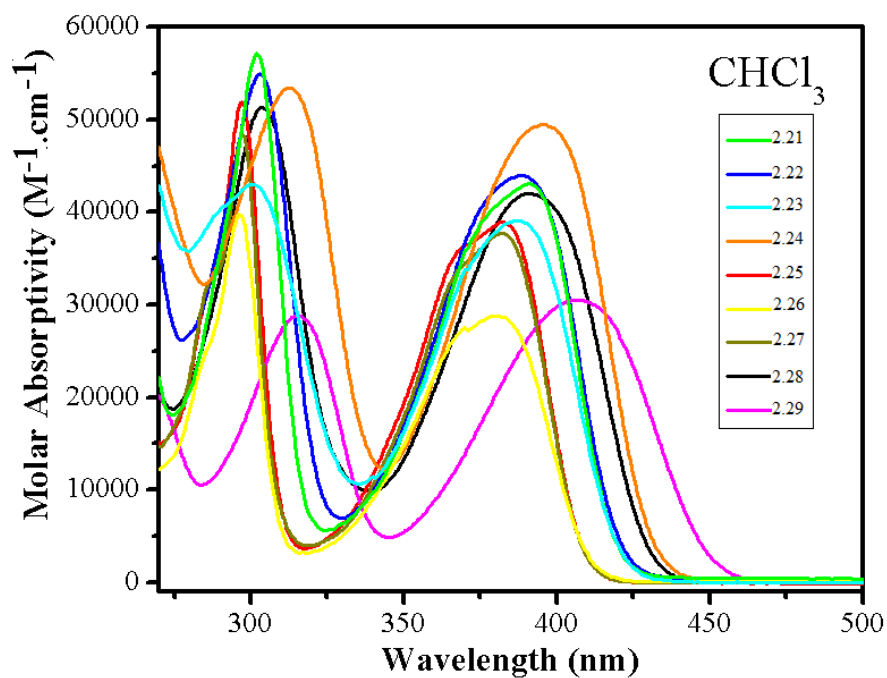


Figure 2.53. Molar absorptivity in chloroform for compounds **2.21-2.29**.

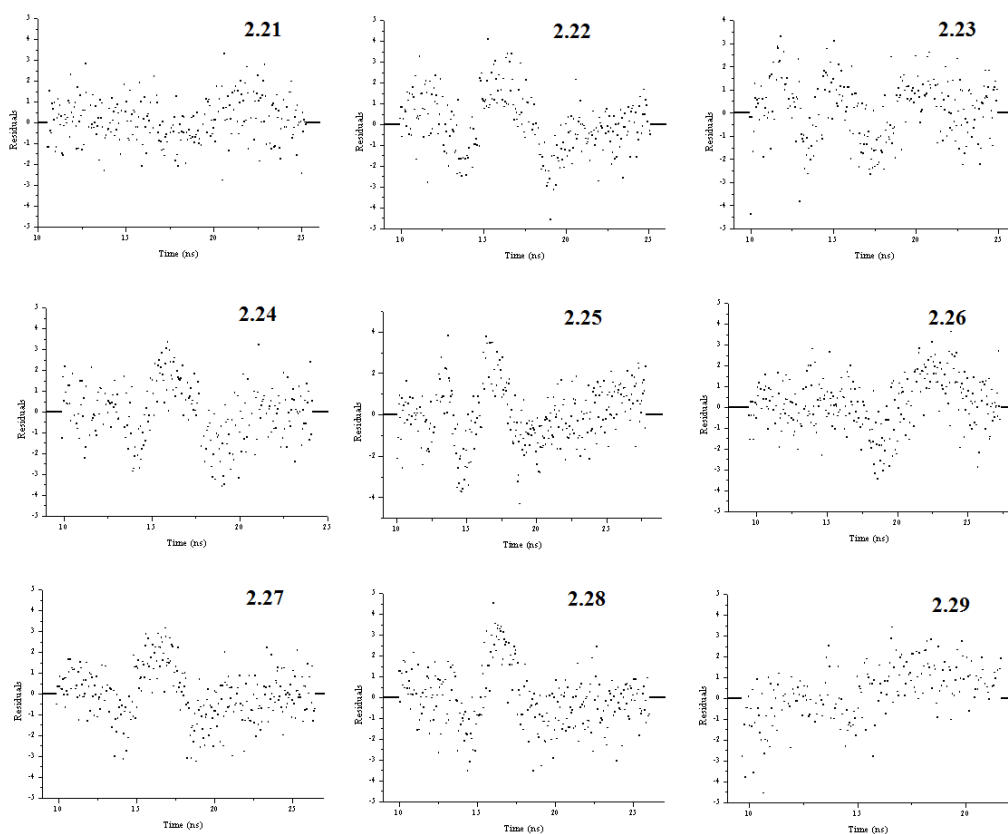
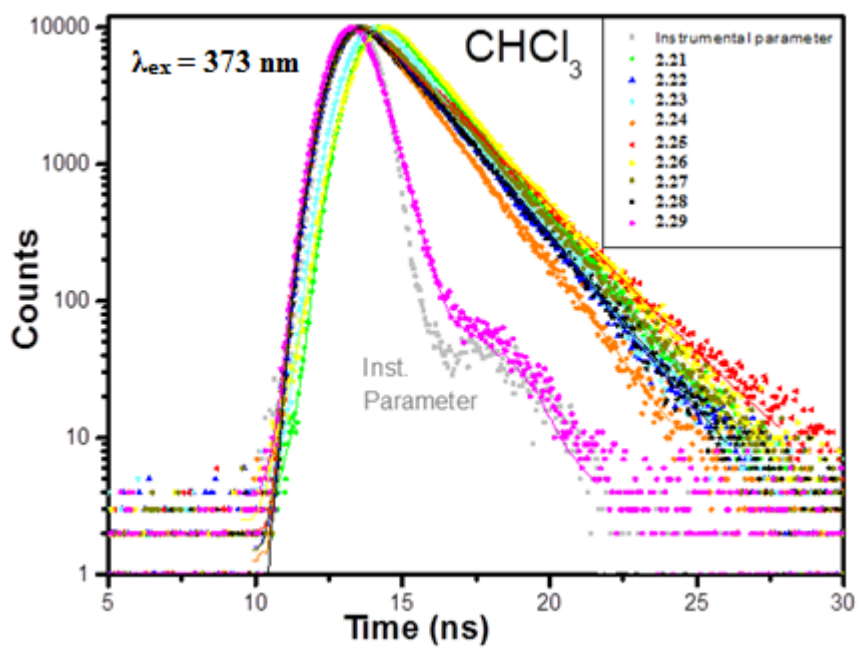


Figure 2.54. Overlay of fluorescence lifetime decay curves of compound 2.21-2.29 in oxygen-free chloroform solution with single-exponential fitting and residuals.

2.2.2.4. Solution vs. Solid State

A bathochromic shift in the emission wavelength was observed upon moving from solution to thin film to crystalline solid. This is attributed to the parallel increase in crystallinity, and therefore increased intermolecular interactions that lead to longer emission wavelengths. This effect is pronounced for compound **2.29**, where the emission maximum shifted from 464 nm in solution, to 540 nm in thin film, and furthermore to 585 nm in crystalline powder. Due to the same crystallinity increase effect, the emission quantum yield trend was in generally decreasing as moving from solution to thin film to crystalline solid. However, this trend was not applicable for compounds **2.21**, **2.26** and **2.28**, where the lowest emission was in thin films, possibly due to the crystal packing of the molecules in thin films as compared to the crystalline state. In general, moving from solution to thin film then to crystalline solid lead to an increase in the intermolecular interactions due to increased crystallinity. The least emissive compound was **2.29** in both solution and solid state; however, compound **2.22** was the most emissive in solution whereas compound **2.27** was the most emissive in solid state. The fluorescence quantum yield values were not affected by the change of solvent polarity. All compounds showed similar quantum yield values that might be considered to fall within the error margin upon changing solvent polarity. The low fluorescence quantum yield of compound **2.29** is consistent with the findings of Henssler *et al.* who reported that a thiophene ring connected to a fluorescent core leads to a decrease in its emission; however a thiophene fused to a fluorescent core leads to an enhancement of fluorescence.¹⁰⁵ The results are shown in Table 2.10.

Table 2.10. Comparison of the emission quantum yields for TPPy and compounds **2.21-2.29** in both solution and solid state.

Compound	THF	Chloroform	Thin film ± 0.004	Crystalline solid ± 0.004
TPPy	0.73	--	0.680 (± 0.020) ¹⁰⁶	0.450 (± 0.020) ¹⁰⁶
2.21	0.90	0.97	0.540	0.735
2.22	0.998	0.98	0.747	0.539
2.23	0.75	0.85	0.881	0.124
2.24	0.72	0.80	0.506	0.464
2.25	0.81	0.84	0.306	0.183
2.26	0.81	0.75	0.485	0.776
2.27	0.85	0.88	0.911	0.918
2.28	0.75	0.89	0.222	0.626
2.29	0.14	0.17	0.077	0.048

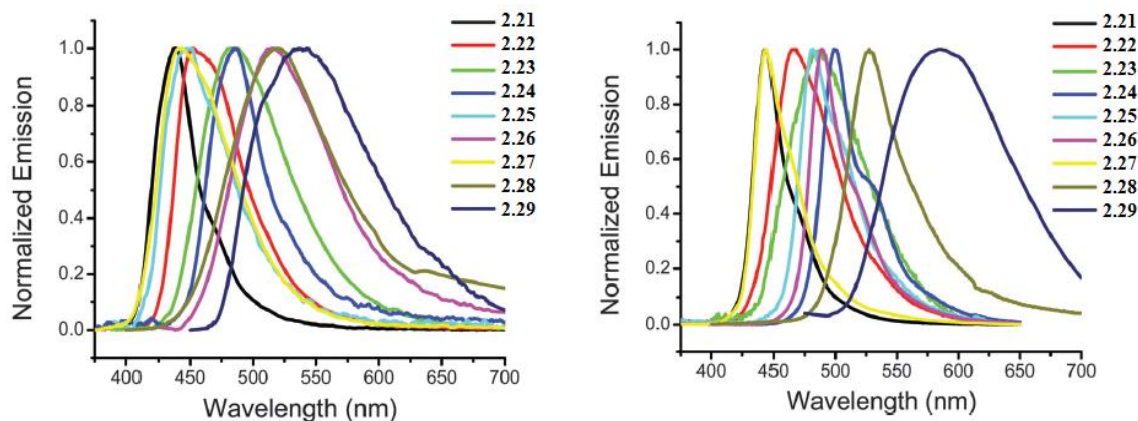


Figure 2.55. Normalized emission spectra of compounds **2.21-2.29** in the solid state: thin films (left), crystalline solids (right).⁴⁸



Figure 2.56. Blue light emission upon shining long-wave UV light on compounds **2.24** (right), **2.27** (middle), and **2.29** (left) in chloroform solutions in glass vials.

2.2.2.5. Absence of Excimer Formation in Dilute Solution

The presence of pyrene excimer (i.e. excited dimer) can be easily detected due to a pronounced bathochromic shift in the emission reaching the green light spectrum wavelengths (since the excimer emits at longer wavelength than the monomer). In our studies, the emission spectra at different excitation wavelengths were collected for compounds **2.21-2.29** and TPPy in different solvents. No changes were observed in the emission maxima. In other words, for every single compound in every single solvent, the emission maximum remains unchanged, despite the excitation at different wavelengths. Similarly, the excitation spectra collected at different emission wavelengths did not show any change, Figures 2.57-2.63. Given that the monomer and the excimer absorb and emit at different wavelengths, the overlap of the obtained spectra suggests that the presence of a single emitting species, and rules out the possibility of excimer formation in dilute solution. Therefore, all the nine compounds and TPPy obey the Kasha's rule, which states that the emission of a fluorophore is independent of the excitation wavelength, if due to a single emitting species.¹⁵ The absence of excimer formation may be attributed to both steric and electronic effects of the substituents previously discussed (i.e. inhibiting unwanted aggregation and/or cofacial stacking between adjacent pyrene cores). This is consistent with the very high fluorescence quantum yield of all compounds (except **2.29**) recorded in solution. The lifetime decays obtained at different emission wavelengths also showed no difference and were all fit to a single-exponential decay equation. This supports the same conclusion about the presence of one single emitting species in solution within the concentration range used for the photophysical experiments.

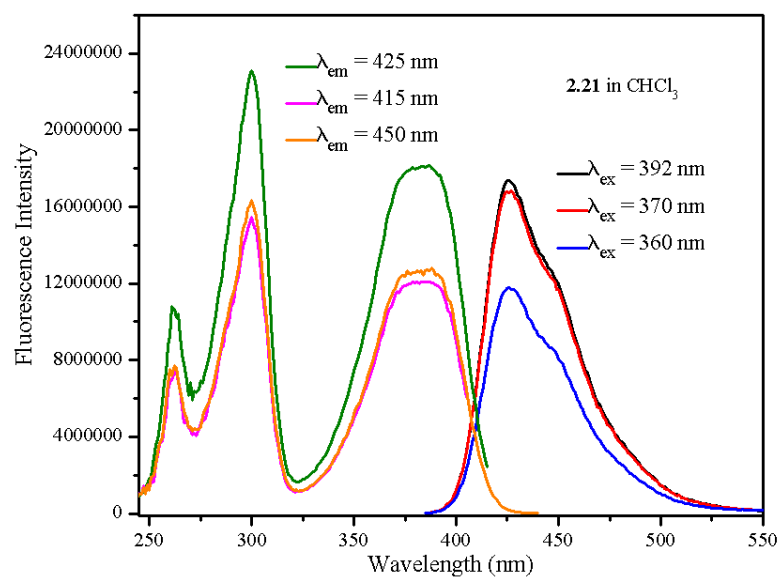


Figure 2.57. Excitation and emission spectra of compound **2.21** collected at different wavelengths in chloroform.

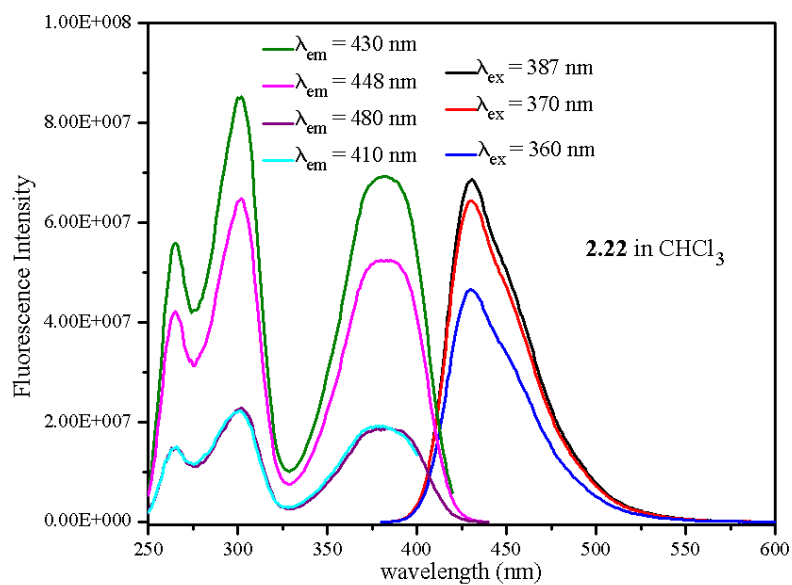


Figure 2.58. Excitation and emission spectra of compound **2.22** collected at different wavelengths in chloroform.

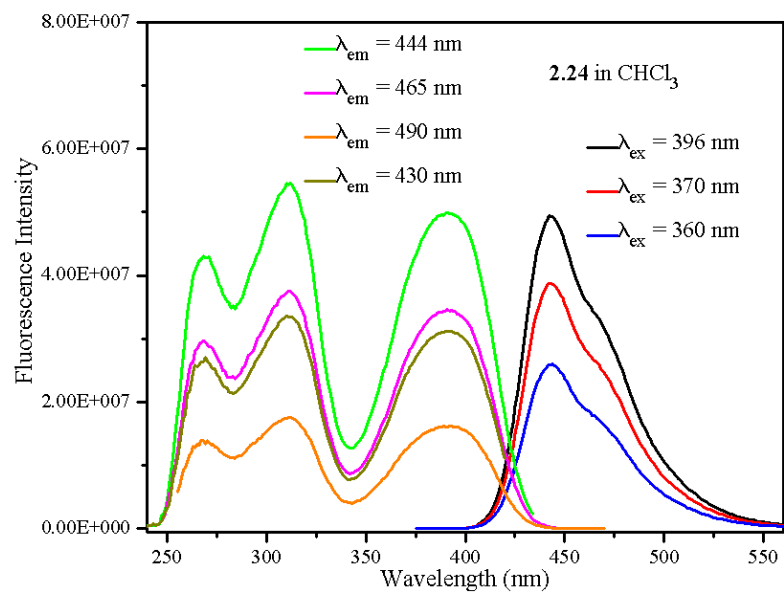


Figure 2.59. Excitation and emission spectra of compound **2.24** collected at different wavelengths in chloroform.

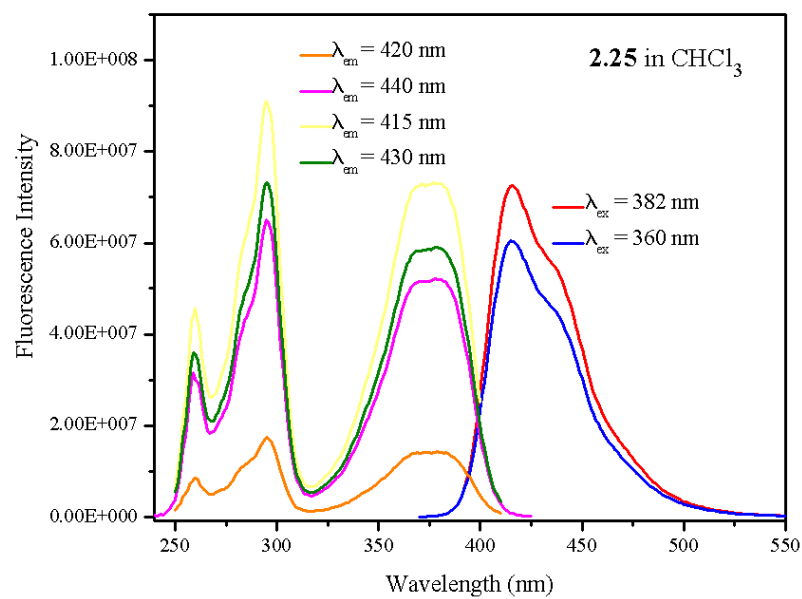


Figure 2.60. Excitation and emission spectra of compound **2.25** collected at different wavelengths in chloroform.

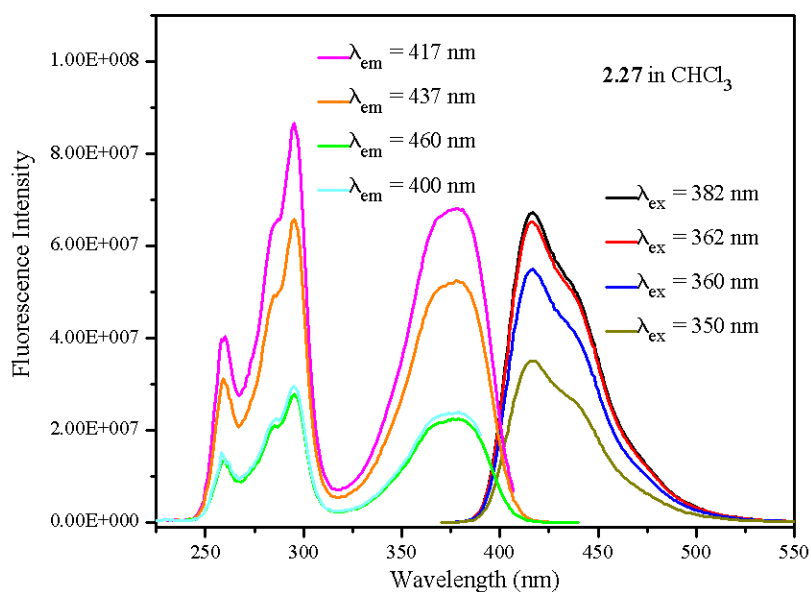


Figure 2.61. Excitation and emission spectra of compound **2.27** collected at different wavelengths in chloroform.

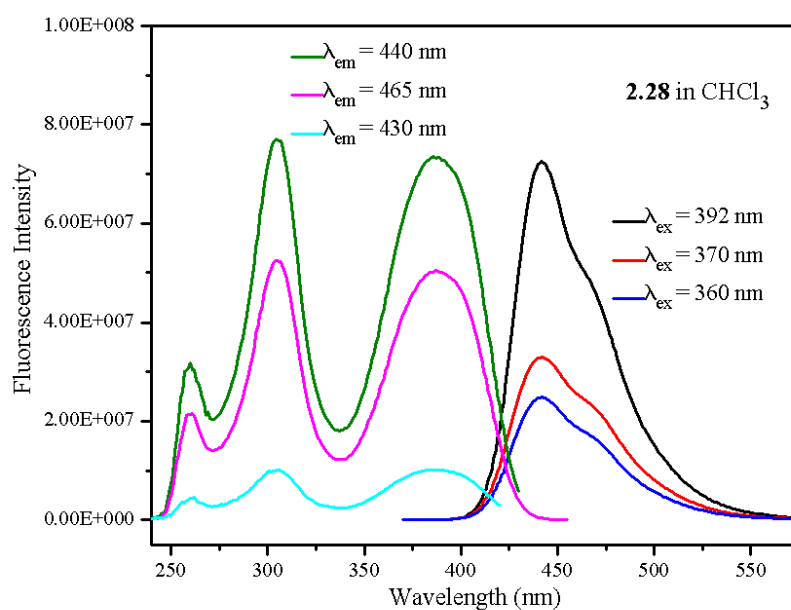


Figure 2.62. Excitation and emission spectra of compound **2.28** collected at different wavelengths in chloroform.

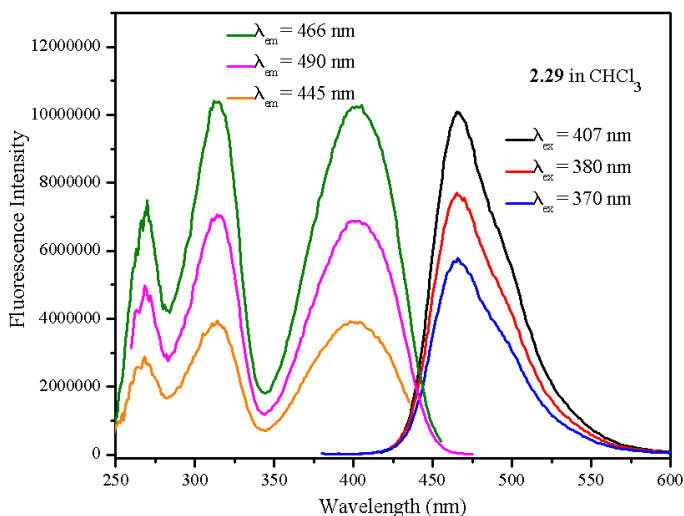


Figure 2.63. Excitation and emission spectra of compound **2.29** collected at different wavelengths in chloroform.

2.2.3. Thermal Analysis

It has been reported that polycyclic aromatic hydrocarbons (PAHs) made of four aromatic rings such as pyrene undergo charring and thermal degradation at high temperature to form smaller-size PAHs.¹⁰⁷ Compounds **2.21-2.29**, pyrene and 1,3,6,8-tetraphenylpyrene (TPPy) were all studied by TGA to reveal their decomposition temperatures. The results revealed increased thermal stability for all nine compounds and TPPy as compared to unsubstituted pyrene. This appears logical due to the increased molecular weight due to the substitution. In general, compounds **2.21-2.29** have higher decomposition temperatures than that of TPPy, except for the fluorinated compounds, where a decreasing trend in decomposition temperature was observed upon increasing the number of fluorine atoms in the molecule. It is also interesting that in these fluorine containing compounds the melting point was either above the decomposition temperature (**2.26**) or very close to it (**2.27**). It is also interesting that these fluorinated compounds were the most stable upon heating till 300 °C, where they did not show any weight loss and performed better than other compounds, Figure 2.64.

However, after exceeding 300 °C, they quickly lose their thermal stability, and the decomposition takes place at a very fast rate. The highest decomposition temperature was recorded for the most carbon-containing compound (**2.22**), whereas the lowest for the most fluorine-containing compound (**2.27**), despite having the highest molecular weight among all the studied compounds. This might be related to the observations reported by Johns *et al.* in 1962, where it has been noted that partial fluorination is a source of thermal instability, whereas perfluorination increases thermal stability.¹⁰⁸ This has been explained by the easy elimination of H-F upon heating in molecules containing both C-F and C-H bonds. Due to this fact, fluorobenzene is less thermally stable than benzene, whereas perfluorobenzene is more thermally stable than both.¹⁰⁸ This conclusion is supported by similar trends observed for the fluorinated derivatives studied in Chapter 3, Paragraph 3.2.3. No specific trend was observed in the oxygen and sulfur-containing compounds that leads to any clear conclusion regarding their thermal stability. The results are presented in Table 2.11 and Figure 2.64.

Table 2.11. Thermal properties of Py, TPPy, and compounds **2.21-2.29**.

Compound	Empirical Formula	Molecular weight, g.mol ⁻¹	%wt Fluorine	T_m (°C) ± 0.5	T_d (°C)
Py	C ₁₆ H ₁₀	202.25	--	150.4 (Lit. ¹⁰⁹ 151)	211.3
TPPy	C ₄₀ H ₂₆	506.63	--	299.4	372.0
2.21	C ₅₆ H ₅₈	731.06	--	> 410.0	439.1
2.22	C ₆₄ H ₄₂ O ₄	875.02	--	276.1	503.6
2.23	C ₅₂ H ₅₀ O ₁₂	866.95	--	325.0	408.7
2.24	C ₄₄ H ₃₄ S ₄	691.00	--	318.5	392.4
2.25	C ₄₀ H ₂₂ F ₄	578.60	13.13	309.0	381.8
2.26	C ₄₀ H ₁₈ F ₈	650.56	23.36	> T_d	368.2
2.27	C ₄₈ H ₁₈ F ₂₄	1050.62	43.40	314.7	318.4
2.28	C ₄₈ H ₃₄ O ₈	738.78	--	345.8	410.0
2.29	C ₃₂ H ₁₈ S ₄	530.75	--	306.4 (Lit. ¹¹⁰ 308)	400.1 (Lit. ¹¹⁰ 428)

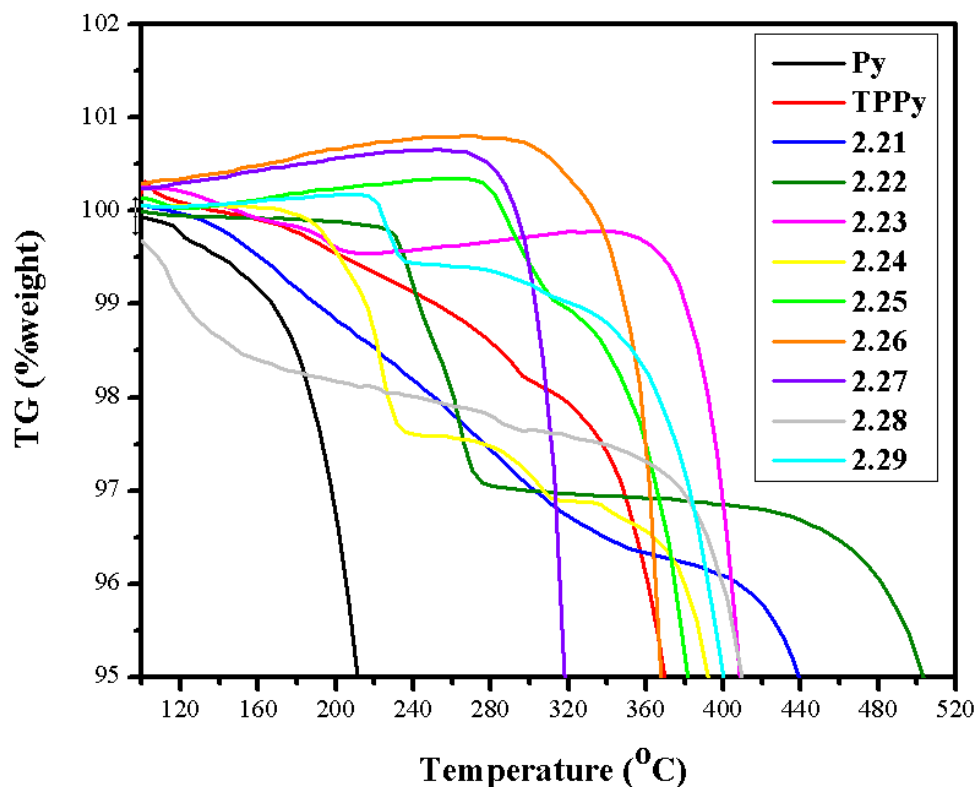


Figure 2.64. TGA results showing the thermal decomposition process of compounds 2.21-2.29, TPPy and Py.

DSC experiments for compounds 2.21-2.29 were performed. Heating cycles were set till around 30 degrees below the corresponding decomposition temperatures determined by TGA. DSC results could be obtained for compounds 2.22, 2.23, 2.25, and 2.29. Whereas no peaks could be observed for the other compounds within the scanning temperature range. The melting points obtained by DSC matched with the ones obtained experimentally. The absence of peaks in the scanning temperature range for the fluorine compounds (2.26 and 2.27) could be explained by the melting points obtained experimentally, which were around or above their decomposition temperatures (i.e. outside the scanning range). Interestingly, the first and second heating cycles for compound 2.23 were not similar. The first cycle showed a melting point close to the one

obtained experimentally. However, no peaks at all were obtained neither in the first cooling cycle nor in the second heating cycle. This might suggest that this compound sublimates at its melting point. Thus, the endothermic transition observed in the first heating cycle for this compound might be indicating sublimation instead of melting. The results are summarized in Table 2.12 and Figures 2.65-2.68.

Table 2.12. DSC results for compounds **2.22**, **2.23**, **2.25** and **2.29**.

	Mol wt, g.mol ⁻¹	Transition	Onset temp (°C)	Maximum temp (°C)	Area, J.g ⁻¹	Molar enthalpy kJ.mol ⁻¹
2.22	875.02	crystallization	183.75	170.47	35.99	31.49
		melting	271.07	275.10	73.62	64.42
2.23	866.95	crystallization	---	---	---	---
		melting	319.92	323.61	59.02	51.17
2.25	578.60	crystallization	245.40	244.62	8.244	4.77
		melting	305.30	310.35	80.76	46.73
2.29	530.75	crystallization	225.07	224.47	34.08	18.09
		melting	302.27	307.52	76.45	40.58

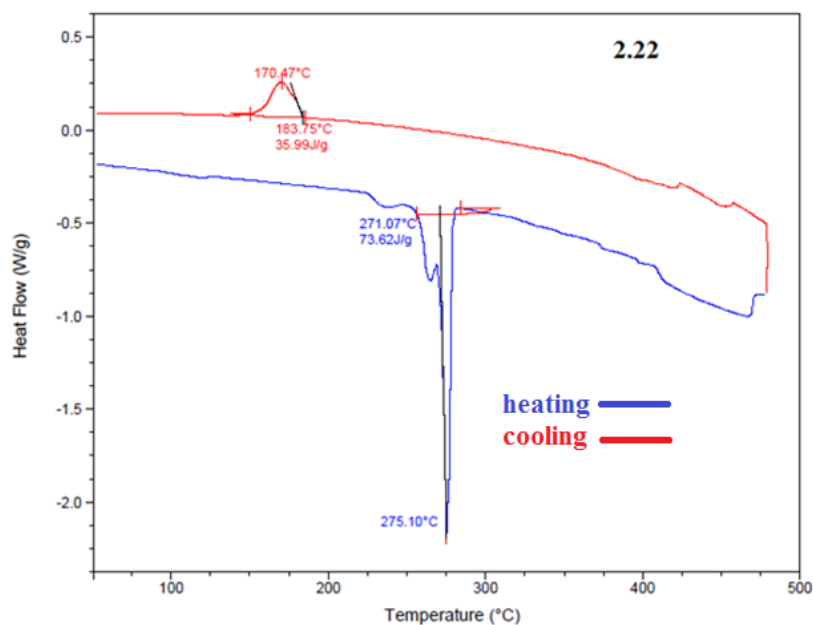


Figure 2.65. DSC results for compound **2.22**.

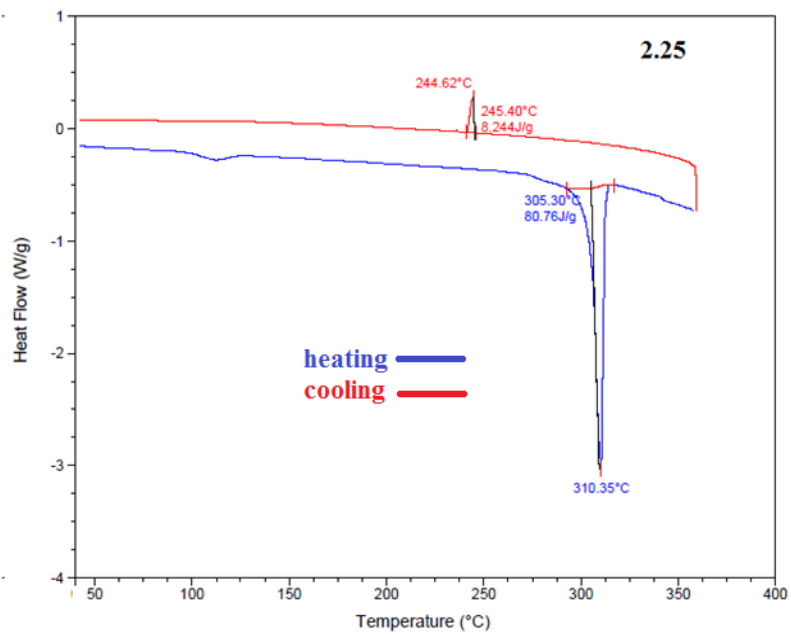


Figure 2.66. DSC results for compound 2.25.

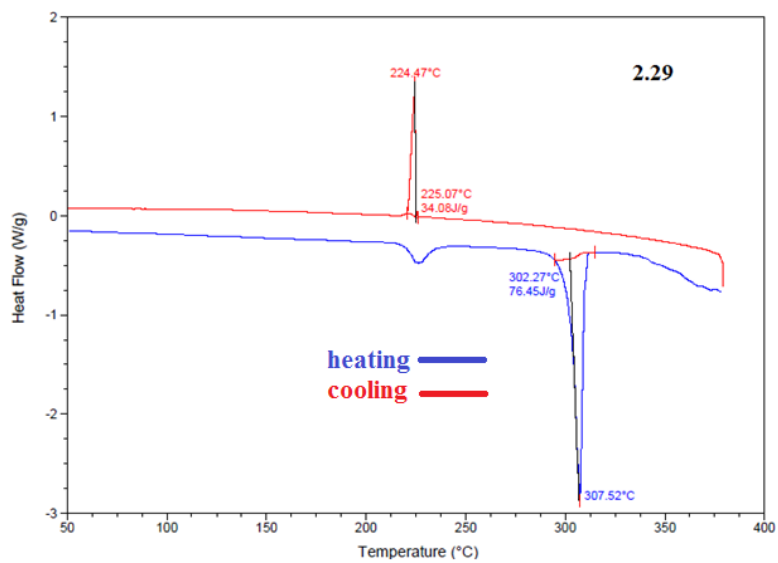


Figure 2.67. DSC results for compound 2.29.

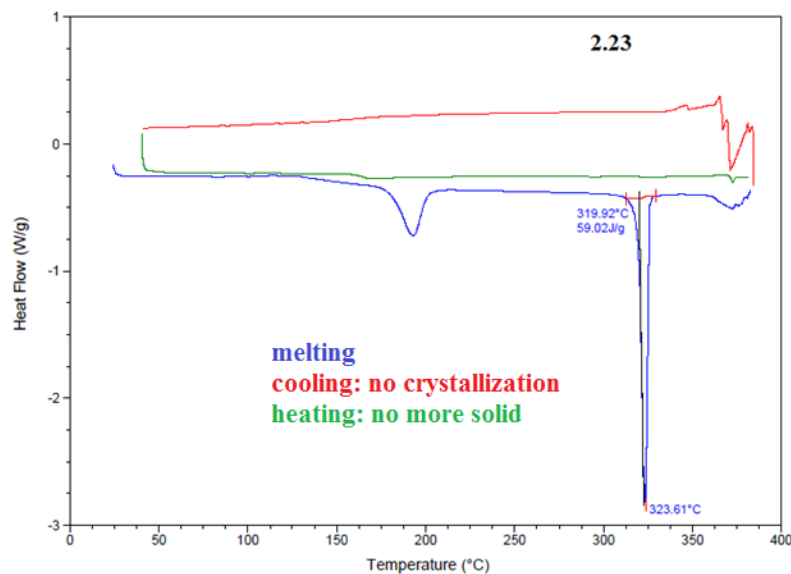


Figure 2.68. DSC results for compound **2.23** suggesting that sublimation occurs at the melting point of the first heating cycle (blue).

2.2.4. X-ray Structure Analysis: Absence of π - π Stacking

Crystals of compounds **2.21**, **2.22**, **2.24**, **2.25**, **2.27** and **2.29** were grown using the slow vapor diffusion technique. Dichloromethane and chlorobenzene were used as solvents. No suitable crystals could be obtained from the remaining compounds. Crystals were sent to Prof. Tatiana Timofeeva, at New Mexico Highlands University. The analysis of the crystal packing showed that compound **2.21** crystallizes in the orthorhombic space group No. 61 (*Pbca*): $\alpha = \beta = \gamma = 90^\circ$. Whereas the other compounds crystallize in the monoclinic space group No. 14: $\alpha = \gamma = 90^\circ$, $\beta > 90^\circ$; (*P2₁/c*) for **2.22**, **2.24** and **2.29**, and (*P2₁/n*) for **2.25** and **2.27**. The different aryl substituents were found to be not coplanar with the pyrene core for all compounds as previously discussed.

Dihedral angles of the plane containing the aryl substituent on position 1 and on position 3 relative to the plane of the pyrene core were determined. Since all molecules reside on inversion centers, what applies to position 1 is applicable to position 6, and the same goes for positions 3 and 8 of the pyrene core. Dihedral angles were found to fall in the range of 41.7° (for compound **2.24**) and 67.2° (for compound **2.22**). The dihedral angles did not approach perfect orthogonal ones, as in the case of the mesitylene substituents, reported by Moorthy *et al.*, Figure 2.38. In the latter case, the steric hindrance offered by the methyl groups branched on the *ortho*-positions of the outer phenyl rings lead to almost perpendicular angles between the plane containing the mesityl groups and the one containing the pyrene core, as previously mentioned, Figure 2.38.¹⁰³ For our compounds, non-perpendicular dihedral angles offer an explanation to the generally decreasing trend in fluorescence quantum yields as moving from solution to solid state, due to an increased interaction between the pyrene cores of adjacent molecules in the solid state. The crystal packing showed no evidence for short intermolecular contacts between the molecules responsible for specific interactions such as π - π stacking. Compound **2.29** was previously reported by Zhang *et al.* in 2006 (CCDC number 287258) in a study about 1,3,6,8-tetraarylpyrene derivatives for organic semiconductor field effect transistors (OFETs).¹¹⁰ Dihedral angles and crystal properties found were similar to the ones that we obtained. Results of the crystallographic analysis are shown in Table 2.13 and Figures 2.69-2.70.

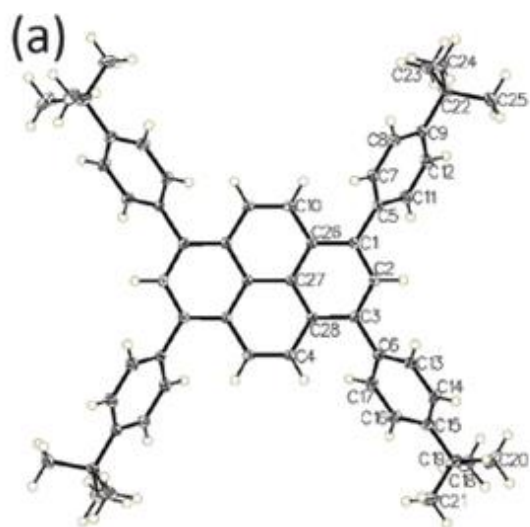
Table 2.13. Crystallographic data of compounds **2.21**, **2.22**, **2.24**, **2.25**, **2.27** and **2.29**.⁴⁸

Compound	2.21	2.22	2.24	2.25	2.27	2.29
Empirical formula	C ₅₆ H ₅₈	C ₆₄ H ₄₂ O ₄	C ₄₄ H ₃₄ S ₄	C ₄₀ H ₂₂ F ₄	C ₄₈ H ₁₈ F ₂₄	C ₃₂ H ₁₈ S ₄
Formula weight	731.02	875.04	690.95	578.61	1050.64	530.70
Temperature, K	100	100	297	100	100	100
Crystal system	orthorhombic	monoclinic	monoclinic	monoclinic	monoclinic	monoclinic
Space group	<i>Pbca</i>	<i>P2₁/c</i>	<i>P2₁/c</i>	<i>P2₁/n</i>	<i>P2₁/n</i>	<i>P2₁/c</i>
<i>a</i> , Å	14.829(6)	15.87(3)	16.4099(17)	3.914(3)	4.795(5)	13.688(3)
<i>b</i> , Å	12.324(5)	7.203(12)	6.9907(7)	11.932(10)	14.347(14)	8.4634(16)
<i>c</i> , Å	23.182(9)	19.66(3)	16.3466(17)	27.87(2)	28.88(3)	10.987(2)
α , °	90	90	90	90	90	90
β , °	90	106.884(17)	114.8800(10)	90.739(12)	92.154(14)	111.999(3)
γ , °	90	90	90	90	90	90
<i>V</i> , Å ³	4236(3)	2151(6)	1701.2(3)	1301.6(18)	1985(3)	1180.2(4)
<i>Z</i>	4	2	2	2	2	2
$\rho_{\text{calculated}}$, g.cm ⁻³	1.146	1.351	1.349	1.476	1.7576	1.493
<i>F</i> (000)	1576	916	724	596	1044	548
μ , mm ⁻¹	0.064	0.083	0.312	0.104	0.181	0.425
Independent reflections	2913	1736	5209	2336	3678	5209
<i>R</i> ₁ ; w <i>R</i> ₂ (<i>I</i> > 2 σ (<i>I</i>))	0.0467, 0.0968	0.0552, 0.1115	0.0576, 0.1351	0.1071, 0.2833	0.0700, 0.1493	0.0335, 0.0891
GOF on <i>F</i> ²	1.050	1.090	1.018	1.064	1.029	1.060
Dihedral angles	53.9° 57.3°	44.4° 67.2°	41.7° 53.0°	44.8° 44.8°	53.6° 53.8°	54.6° 59.4° (Lit. ¹¹⁰ 55.1° 57.8°)

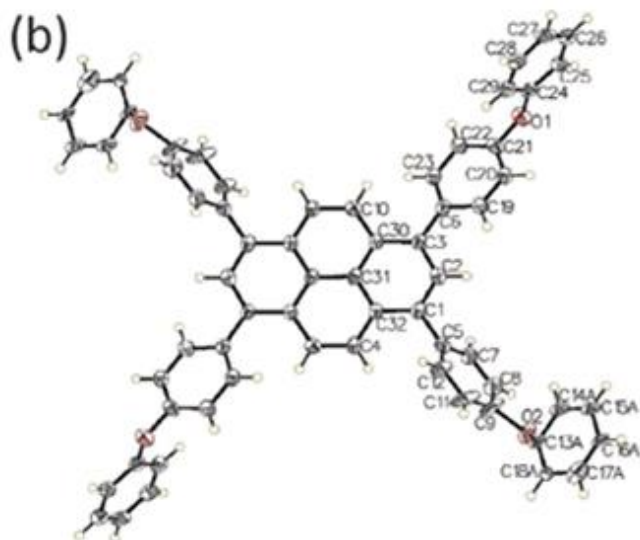
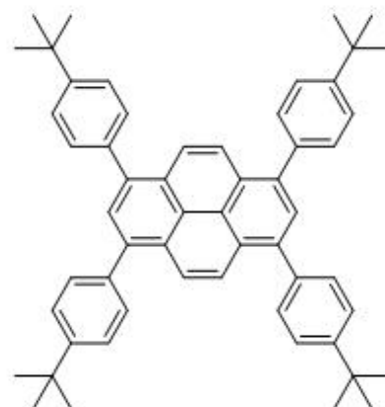
According to Table 2.13, compound **2.21** has an edge *a* = 14.829(6) Å.

This refers to a length of 14.829 Å with an estimated standard deviation of 0.006 Å on this length, and the same applies for other compounds. Otherwise the X-ray density can be calculated for compound **2.21** (and other compounds) as follows:

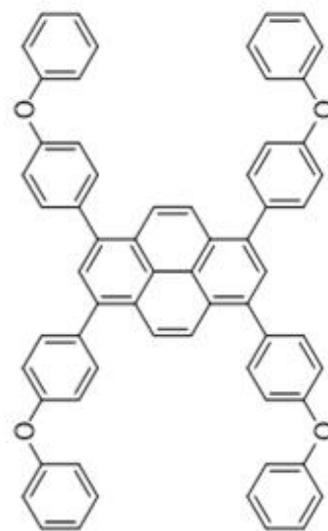
$$\rho = \frac{M \cdot Z}{V \cdot N_A} = \frac{(731.02) \cdot (4)}{(4236 \times 10^{-24}) \cdot (6.023 \times 10^{23})} = \frac{29240.8}{25513.4} = 1.146 \text{ g.cm}^{-3}$$



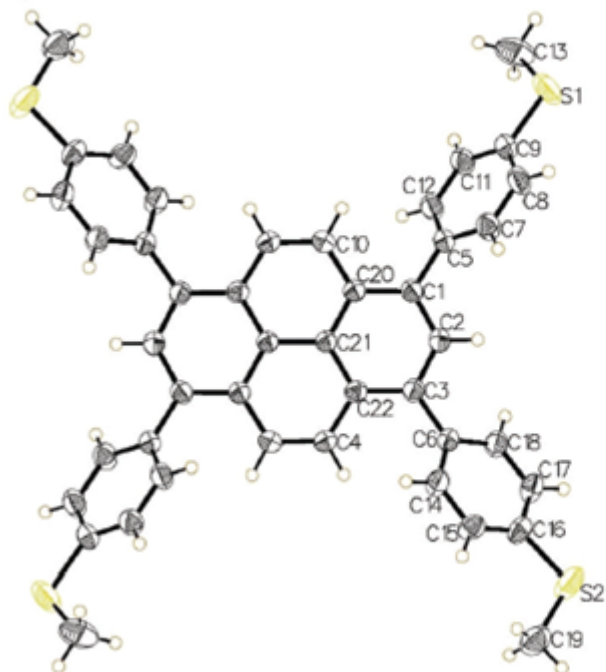
2.21



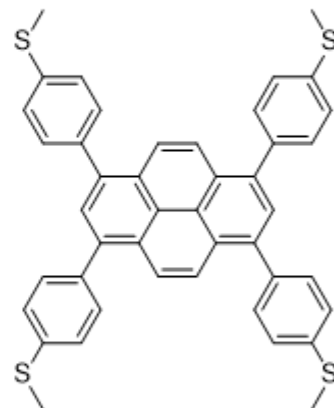
2.22



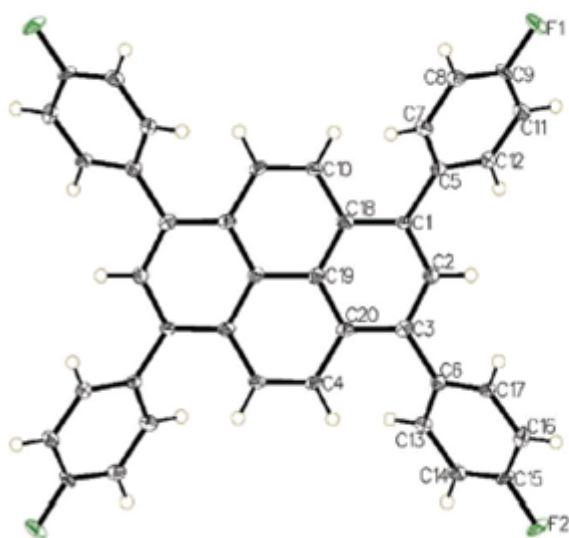
(c)



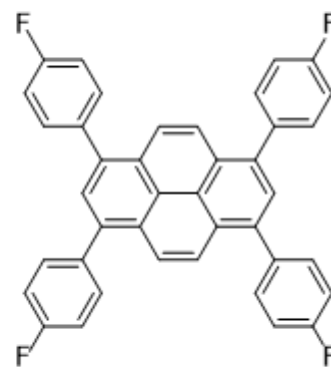
2.24

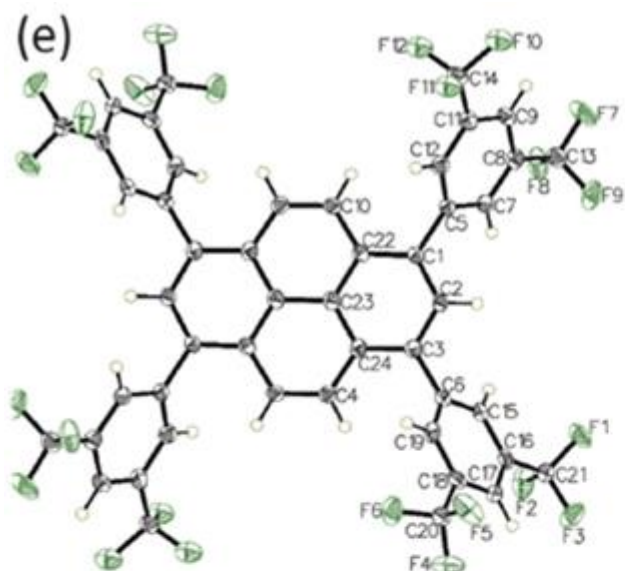


(d)

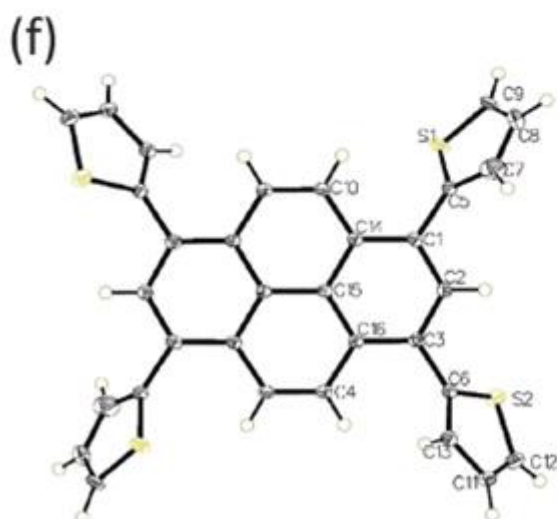
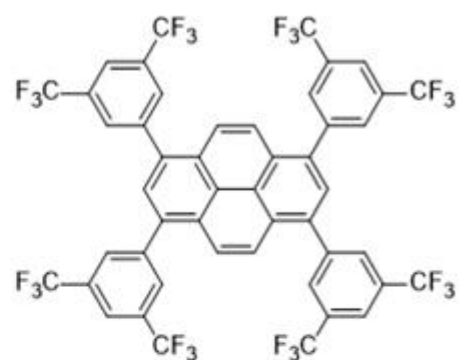


2.25





2.27



2.29

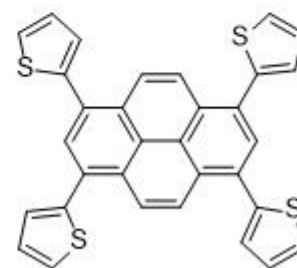


Figure 2.69. Molecular structures of the six compounds studied by X-ray diffraction from single crystal; due to the inversion center only half of the molecule is in the asymmetric unit which is the part numbered and labeled in the structures with 50% probability displacement ellipsoids.⁴⁸

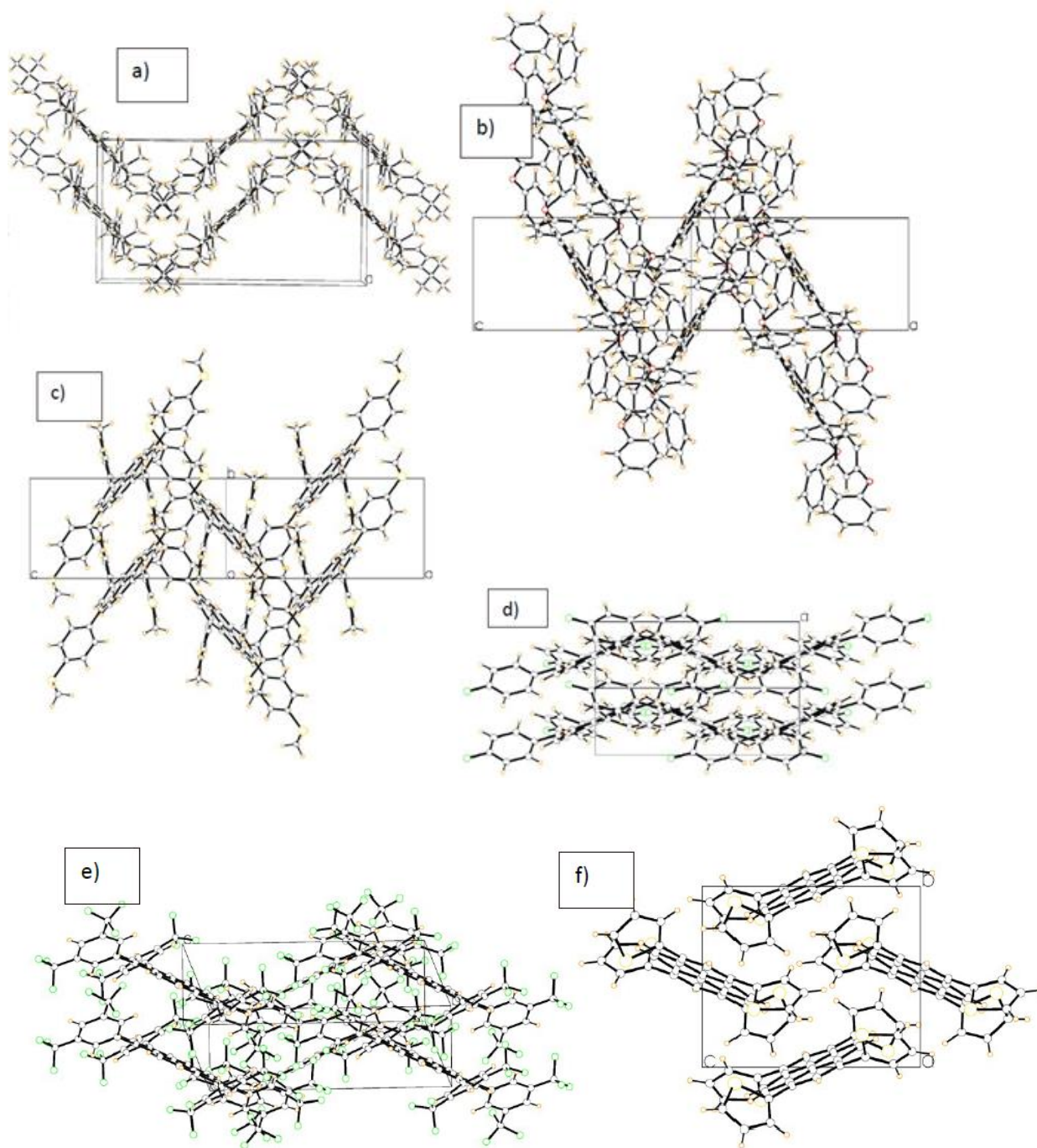


Figure 2.70. Crystal packing of the six compounds studied: a) **2.21**, b) **2.22**, c) **2.24**, d) **2.25**, e) **2.27**, f) **2.29**.⁴⁸

2.2.5. Application in OLEDs

The simplest model to achieve light emission from a semiconductor emitting material by the effect of an external electric current is illustrated in Figure 2.71.⁹⁷ Organic light-emitting diodes are devices of that model, based on an organic emitting material. In these devices, electrons and holes flow into the emissive organic material from the cathode and anode respectively, where they recombine together to form excitons. The relaxation of the exciton leads to emission of light. This is referred to as electroluminescence, where electric charges (i.e. electrons and holes) are behind the excited state that lead to the emission of light.^{1,97}

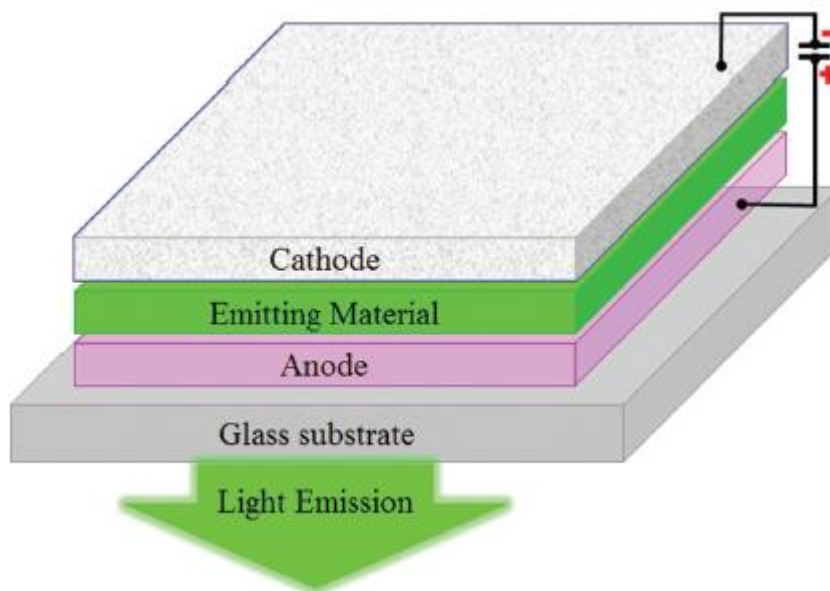


Figure 2.71. The simplest model of electroluminescence from an emitting material.⁹⁷ Reproduced from Jou, J.-H.; Kumar, S.; Agrawal, A.; Li, T.-H.; Sahoo, S. *J. Mater. Chem. C* **2015**, *3*, 2974, with permission of The Royal Society of Chemistry.

Among the earliest reports about electroluminescence in organic material was that of Pope *et al.* in 1963, where a light emission from anthracene has been observed following the application of an external voltage of 400 Volts.¹⁴ Another report by Bernanose *et al.* in 1953, suggested that some organic dyes such as Gonacrine and Acridine Brilliant Orange E, could emit light when adsorbed on Cellophane under an external electric field of 400-800 Volts.¹¹¹ The minimum voltage required to achieve light emission from the semiconductor material is known as turn-on voltage V . The current I measured in Ampere, stands for the number of electrons flowing in the device per second. The current density is the number of electrons flowing in one meter square of the device's lateral surface per second in A/m^2 . It is known as the J parameter.¹ The emissive material generates light as photons upon the relaxation of excitons. A fraction of the total number of generated photons is able to exit the device as light. The number of emitted photons by the device per second is the light output (in Watt) of the device (equally known as flux).¹ The light emitted is received by a luminance meter to measure the luminance of the device noted as L parameter in cd/m^2 . This tells about the brightness of the light generated by the device.¹ The threshold voltage, current density and luminance together are known as J - V - L characteristics of the device. Subsequently, the luminous current efficiency H can be defined as the variation of the luminance L (in cd/m^2) with respect to the current density J (in A/m^2) is known as the luminous current efficiency and is one of the three efficiency parameters commonly reported for devices and is expressed in cd/A .¹¹²

The brightness of light should be reported with respect to the human-eye detectors (i.e. cones and rods), not only to an artificial detector. Under well-lit conditions (i.e. a luminance of 3 cd/m^2 or greater), cones are the actual detectors of a

human eye. This is known as white vision or photopic vision.¹⁷ Under non-lit conditions (i.e. a luminance of 0.003 cd/m² or less), the rods are the detectors. This is known as black vision or scotopic vision.¹⁷ In between is the mesotopic vision, where both cones and rods work simultaneously. Cones and rods are primarily sensitive to green and cyan light respectively.¹⁷ This implies that 100 Watts of green light appears brighter to a human eye than 100 Watts of red or blue light; therefore, a new photometric unit system considering human eye sensitivities along visible spectrum was introduced using Lumen as unit to visualize brightness. One Lumen for a human eye is equivalent to one Watt for a physical detector.¹⁷ The relation between the two unit systems is defined as luminous efficacy in Lumen per Watt (lm/W). The International Commission on Illumination (CIE) assigned standard values for luminous efficacy based on an average human eye sensitivity in 1931 for photopic vision, and in 1951 for scotopic vision, Figure 2.73.¹⁷ A correction for the blue-violet human eye sensitivity in photopic vision was made later in 1978, Figure 2.72.¹⁷ CIE defined the maximum luminous efficacy under photopic vision to be 683 lm/W at 555 nm (green light), Figure 2.72.¹⁷

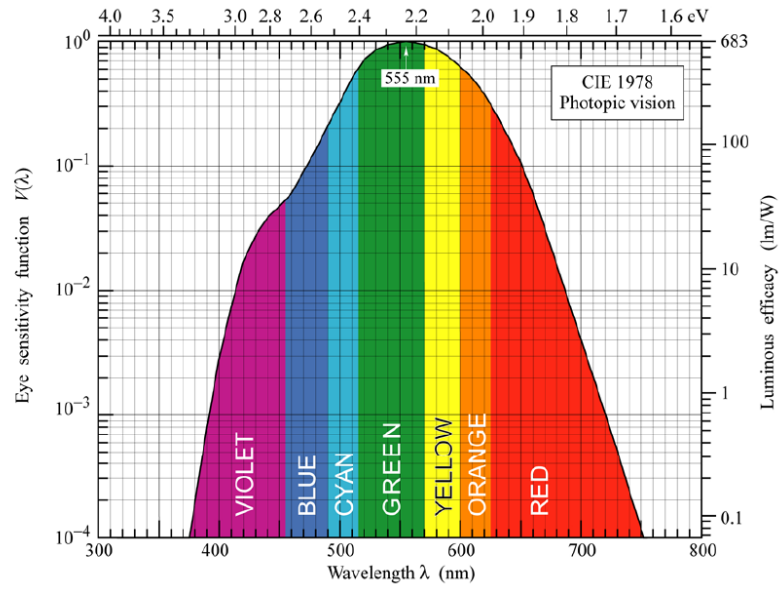


Figure 2.72. The corrected CIE luminous efficacy and eye sensitivity curves for photopic vision (CIE 1978).¹⁷

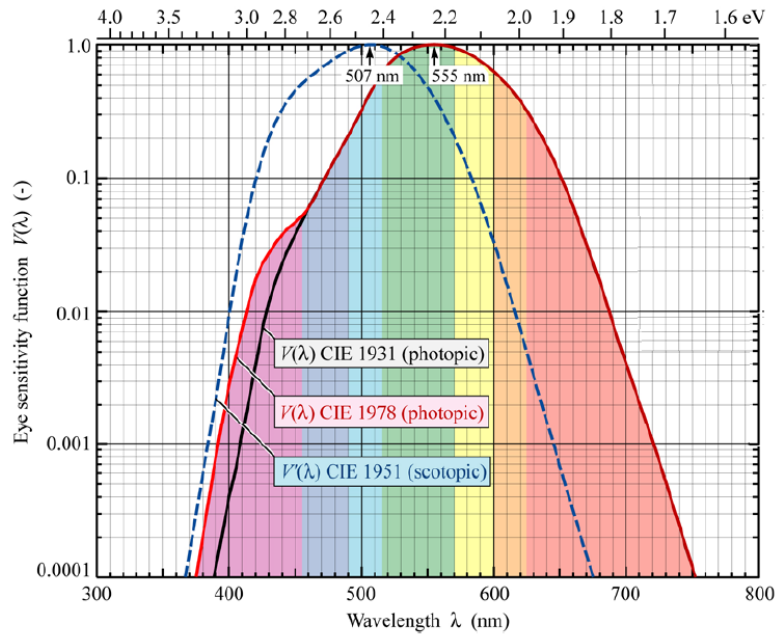


Figure 2.73. CIE eye sensitivity function curves for photopic and scotopic vision.¹⁷

CIE also defined a triangle-like color space known as the CIE chromaticity diagram, and contains all possible variety along the visible spectrum wavelengths, Figure 2.74 (permission from CIE was granted to reprint Figures 2.72-2.74 from literature in this thesis). The color of the light emitted by the devices reported in the literature is evaluated by assigning specific x and y chromaticity coordinates.¹⁷

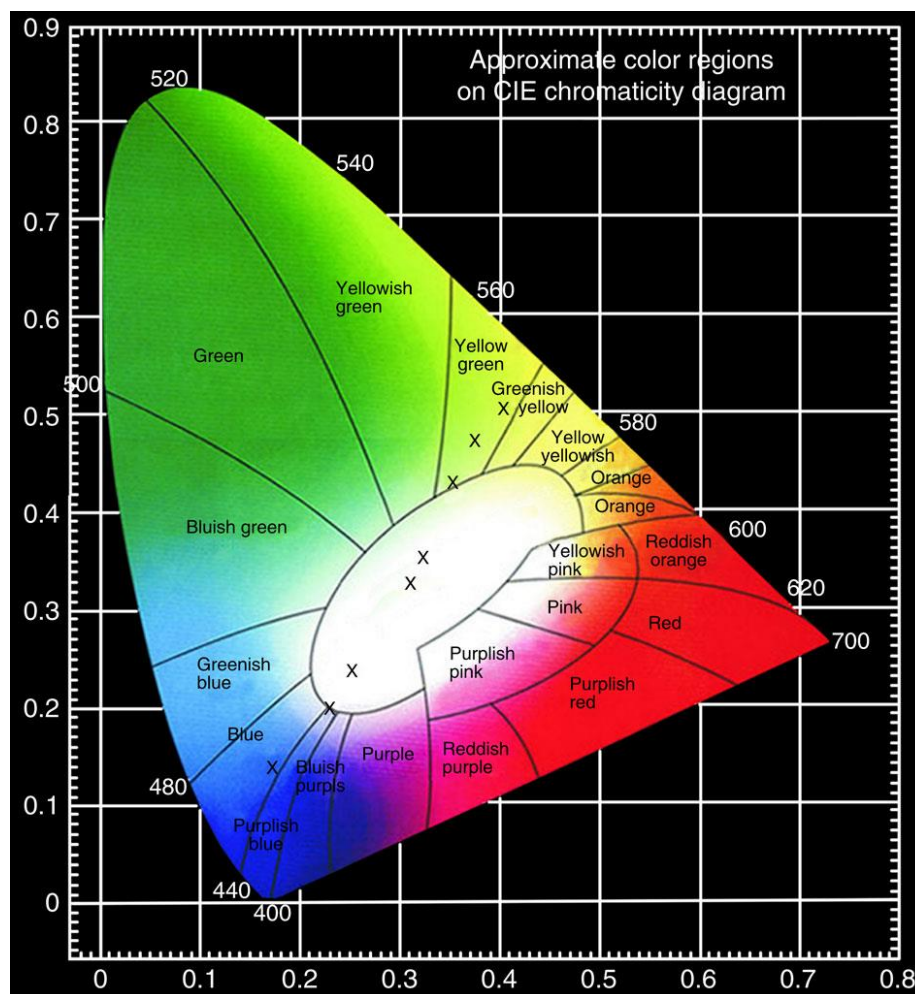


Figure 2.74. CIE 1931 chromaticity diagram.¹¹³ Sun, C.-Y.; Wang, X.-L.; Zhang, X.; Qin, C.; Li, P.; Su, Z.-M.; Zhu, D.-X.; Shan, G.-G.; Shao, K.-Z.; Wu, H.; Li, J. *Nat Commun* **2013**, *4*, 2717. Copyright (2013) Nature Publishing Group. Reproduced with permission.

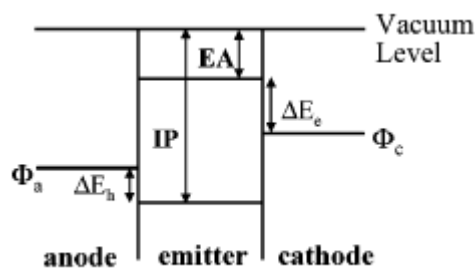


Figure 2.75. Energetic representation of a single layer diode.¹¹⁴ Reprinted with permission from (Kulkarni, A. P.; Tonzola, C. J.; Babel, A.; Jenekhe, S. A. *Chem. Mater.* **2004**, *16*, 4556). Copyright (2004) American Chemical Society.

Sandwiching the organic emitter between the electrodes creates two energy barriers at the electrode-organic interfaces (electron injection barrier at the cathode ΔE_e and hole injection barrier ΔE_h at the anode), Figure 2.75.^{114,115} These barriers must be reduced to a minimum in order to achieve a better charge injection from the electrodes into the emissive layer. Low work-function metals such as calcium or magnesium offer the best electron injection rates, and are the most suitable to be used as cathode.¹¹⁵ However, their high tendency of losing electrons makes them more susceptible to atmospheric oxidation and corrosion.^{115,116} Decreased sensitivity to atmospheric oxidation is achieved by combining these low work-function metals to a protective layer of higher work-function such as silver or aluminum in a 10:1 ratio.^{115,116} High work-function electrodes such as ITO is commonly used as anode.^{115,116} In summary, achieving a better device performance requires lower work-function cathode (ϕ_c), higher work-function anode (ϕ_a), higher electron affinity and lower ionization potential of the emitting material.¹¹⁷ However, high fluorescence quantum yield, high electron affinity, low ionization potential are usually hard to be satisfied by a single organic material. Therefore, in order to optimize the device performance, it is possible to use many layers in the device of different organic materials, where every layer has a specific role.¹¹⁴

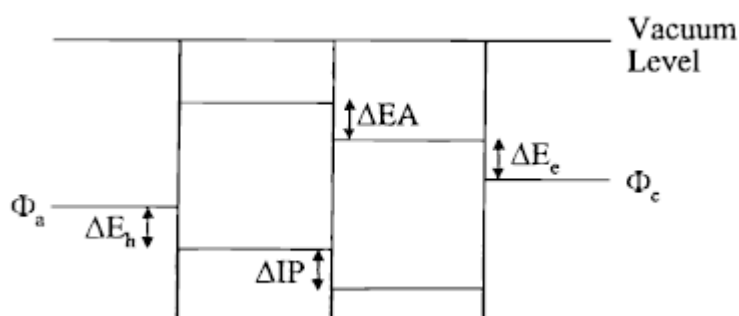


Figure 2.76. Energetic representation of a bilayer diode.¹¹⁸ Reprinted with permission from (Zhang, X.; Jenekhe, S. A. *Macromolecules* **2000**, *33*, 2069.). Copyright (2000) American Chemical Society.

The use of multilayer design in OLEDs was pioneered in 1987 by Tang and Van Slyke.¹¹⁶ An emitter that is good in hole transport, but has high barrier for electron injection (i.e. has a low electron affinity), it is called a p-type emitter.¹¹⁴ The ETM (electron-transport material) layer is placed between the p-type emitter and the cathode, and performs the transport of electrons from the cathode to the p-type emitter, where the recombination with holes and light emission occurs. The role of this layer is to facilitate the transport of electrons from cathode to the emissive layer in a way the electron-hole recombination occurring far from any organic-inorganic interface in order to avoid a Förster Resonance Energy Transfer between the exciton and the metallic electrode as a non-radiative relaxation pathway, and subsequently achieving higher emission efficiency.¹¹⁴ Emitter with high electron affinity (good in transporting electrons) is known as n-type emitter. It is used along with a HTM (hole-transport material) layer.¹¹⁴

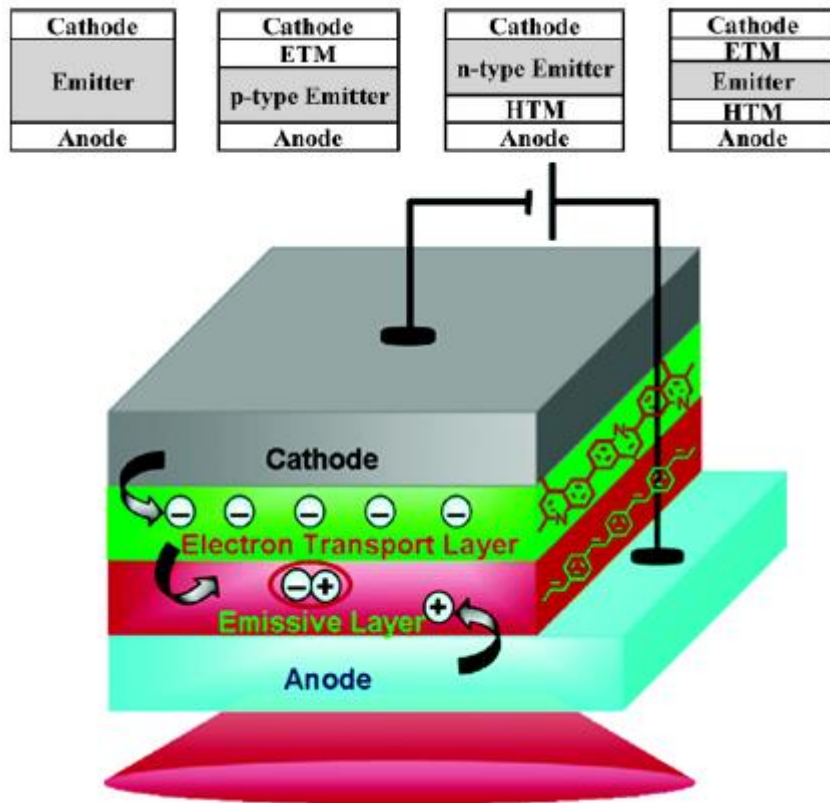


Figure 2.77. Different architectures for designing a multilayer diode (up), and the mechanism of functioning of p-type emitter device (down).¹¹⁴ Reprinted with permission from (Kulkarni, A. P.; Tonzola, C. J.; Babel, A.; Jenekhe, S. A. *Chem. Mater.* **2004**, *16*, 4556). Copyright (2004) American Chemical Society.

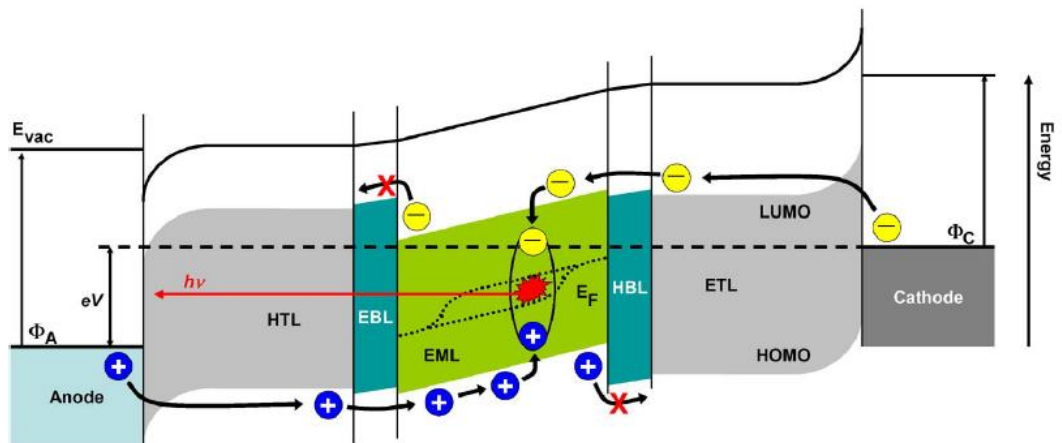


Figure 2.78. The mode of functioning of multilayer devices.¹¹² 2009 IEEE. Reprinted, with permission, from Meerheim, R.; Luessem, B.; Leo, K. *Proc. IEEE*, Efficiency and Stability of p-i-n Type Organic Light Emitting Diodes for Display and Lighting Applications, **2009**, *97*, 1606.

Blue light devices are still to date the most challenging to design because they require an emitter having a HOMO-LUMO bandgap of 2.6 eV at least.¹¹⁹ This in turns makes it harder for a blue emitter to fit the energy levels of the adjacent layers in the device, and therefore creates high energy barriers for charge injection.¹¹⁴ This wide energy gap also facilitates the non-radiative transfer of the exciton energy from the emissive layer to any adjacent material. This leads to higher turn-on voltage, and lower external quantum efficiency for the device as compared to green or red counterparts.¹¹² This imposes the continuous challenge of finding stable and efficient blue emitting material for OLEDs as a door for highly efficient white OLEDs (WOLEDs), which are traditionally designed by stacking red, green, and blue monochromatic OLEDs altogether.¹¹²

In the following, the interest is the OLED device applications of the 1,3,6,8-tetraarylpyrene compounds that were synthesized and characterized. We note that the first report about the introduction of 1,3,6,8-tetraarylpyrene derivatives as blue emitters in OLEDs is attributed to Sotoyama *et al.* and dates back to 2003.²¹

As explained above, from device application perspective, the most important electrochemical properties are the ionization potential IP, electron affinity EA and HOMO-LUMO bandgap E_g . A relatively narrow bandgap was observed in the thiophene derivative **2.29**, which was as small as 2.76 eV. This puts compound **2.29** on the limit of a blue-green light-emitter. On the opposite side, the largest bandgap was for the trifluoromethyl derivative, compound **2.27**, and was as high as 3.04 eV, approaching deep-blue emitter properties. The general trend observed for compounds **2.21-2.28** was that the presence of electron-withdrawing groups increases both the electron affinity and the ionization potential together, and subsequently increases the HOMO-LUMO

bandgap. The presence of electron-releasing groups had the opposite effect. This might suggest that in device application, the hole injection is easier in compounds bearing electron-releasing groups due to their electron-rich character. On the opposite side, the electron injection is easier in compounds bearing electron-withdrawing groups due to their electron-poor character. Table 2.14 summarizes these electrochemical properties for all nine compounds, in addition to the emission quantum yield values in thin films.

Table 2.14. Properties of compounds **2.21-2.29** that help to discuss their usefulness in OLED application.⁴⁸

Compound	IP (V)	EA (V)	E_g (V)	ϕ (+/- 0.004)
2.21	5.4	2.44	2.96	0.540
2.22	5.4	2.45	2.95	0.747
2.23	5.4	2.45	2.95	0.881
2.24	5.4	2.52	2.88	0.506
2.25	5.5	2.47	3.03	0.306
2.26	--	--	3.02	0.485
2.27	5.9	2.86	3.04	0.911
2.28	5.7	2.82	2.88	0.222
2.29	5.4	2.64	2.76	0.077

Among the nine compounds, the most promising were compounds **2.21**, **2.22**, **2.23**, **2.24** and **2.27** due to their very high fluorescence quantum yield in thin-film solid state emission (i.e. > 0.50), Table 2.14. Compound **2.21** was previously reported by Sotoyama *et al.*, in 2003, in an optimized multilayer device.²¹ Therefore, these five compounds, except **2.21**, were investigated in device application by the research group of Prof. Emil. J. W. List-Kratchovil in Graz University.

Electroluminescence characteristics of the new compounds were investigated in devices featuring them as the active layer in a standard sandwich geometry: indium tin oxide (ITO)/poly(3,4-ethylenedioxythiophene)-poly-styrenesulfonic acid (Baytron P

VPAI 4083) (PEDOT:PSS)/**2.22**, **2.23**, **2.24** and **2.27**/Ca/Al. ITO-covered glass substrates were first carefully rinsed with deionized water, acetone and isopropyl alcohol. Afterwards the substrates were subjected to various ultrasonic treatments in detergent, deionized water, acetone, and isopropanol. A dry cleaning step in oxygen plasma finished the cleaning procedure while at the same time providing an enhancement of the surface wettability of PEDOT:PSS. Consecutively, a layer of PEDOT:PSS was applied via spin-coating under ambient conditions and dried under ambient conditions at 200 °C for 5 minutes. The active layers were evaporated at a rate of $0.6 \text{ \AA}\cdot\text{s}^{-1}$ from a resistively heated crucible under dynamic vacuum at an initial base pressure lower than 1.0×10^{-6} mbar. The layer thicknesses were controlled by a quartz-crystal microbalance and verified by a Veeco Dimension V atomic force microscope equipped with a Nanoscope V controller in tapping mode at several positions. The resulting layer thickness amounted to 80 nm. The cathode materials (Ca, Al) were deposited onto the substrate with thicknesses of 10 nm and 100 nm for Ca and Al respectively without breaking the vacuum through a shadow mask. Consequently multiple devices with a device-area of 10 mm^2 were formed on a single substrate. Electroluminescence (EL) spectra were acquired using an ORIEL spectrometer with an attached calibrated charge-coupled device (CCD) camera. Current–luminance–voltage (I–L–V) characteristics were recorded in a customized setup using a Keithley 2612A source measure unit for recording the I–V characteristics while the luminance was measured by a Keithley 6517 Electrometer using a photodiode calibrated by a Konica-Minolta LS-100 Luminancemeter. The results are shown in Table 2.15 and Figures 2.79-2.82.

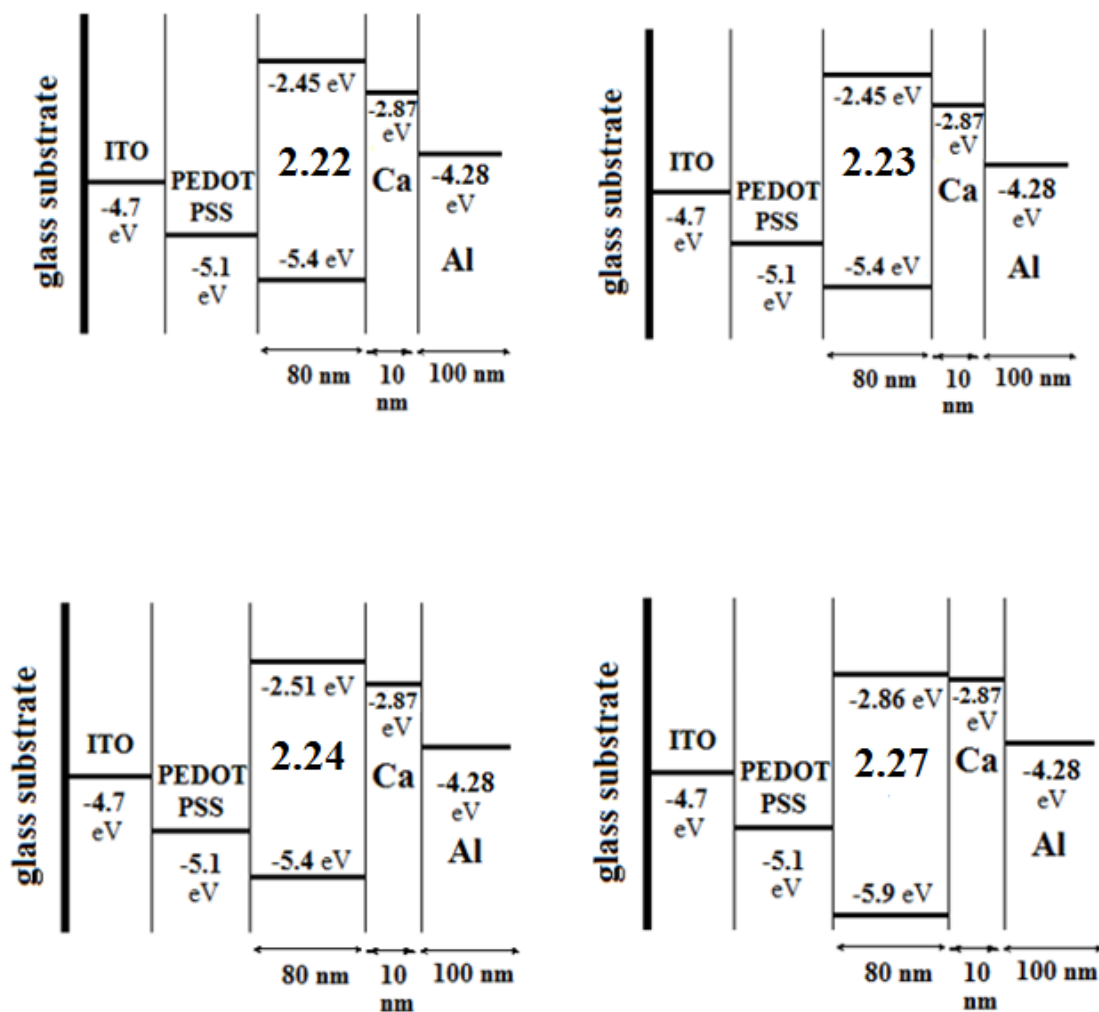


Figure 2.79. Band energy diagram of the four devices involving compounds **2.22**, **2.23**, **2.24** and **2.27** as emitters. The work-function values of metals were taken from a review by Michaelson in which the work function of many elements of the periodic table are mentioned.¹¹⁷ Those of ITO and PEDOT:PSS are taken from a specific study about these materials.¹²⁰

The device made of compound **2.22** showed the highest luminance maximum and lowest turn-on voltage of 13543 cd/m² and 2.8 V, respectively, Table 2.15.

Whereas, unexpectedly, the device made of the most promising compound and having a fluorescent quantum yield close to the unity in the solid state (**2.27**) showed the poorest performance. A relatively high turn-on voltage of 8.6 V was observed with a maximum luminance of only 7 cd/m². In addition to a very low maximum luminous current

efficiency of 0.0039 cd/A. This could be due to the very high ionization potential of 5.9 eV, which increases the energy barrier of hole injection from the PEDOT/PSS layer; compared to a very low energy barrier for electron injection from the cathode. This might lead to an unequal charge injection in the emissive layer, and therefore will decrease the recombination and exciton formation significantly, Figure 2.80.

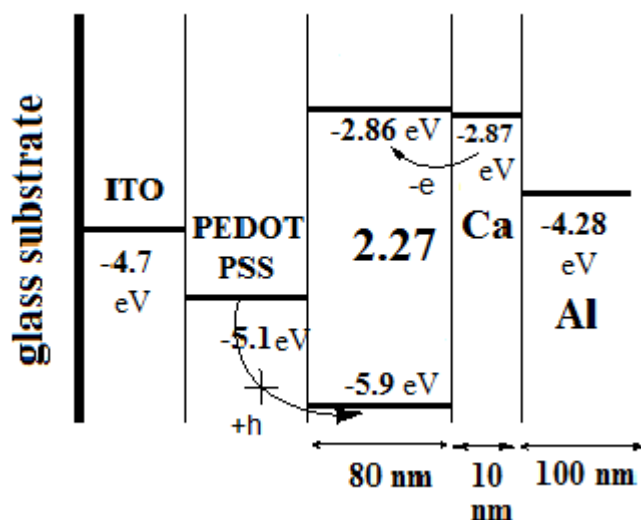


Figure 2.80. Possible interpretation of the poor device performance of compound **2.27**.

Table 2.15. Electroluminescent characteristics of compounds **2.22**, **2.23**, **2.24** and **2.27** in a single-layer geometry.⁴⁸

Blue emitter	V_{on} (Volts)	L_{max} (cd/m ²)	H_{max} (cd/A)	CIE 1931 [x, y]
2.22	2.8	13542	2.0000	0.163, 0.200
2.23	2.9	6902	2.6000	0.148, 0.243
2.24	2.9	85	0.0050	0.148, 0.244
2.27	8.6	7	0.0039	0.153, 0.124

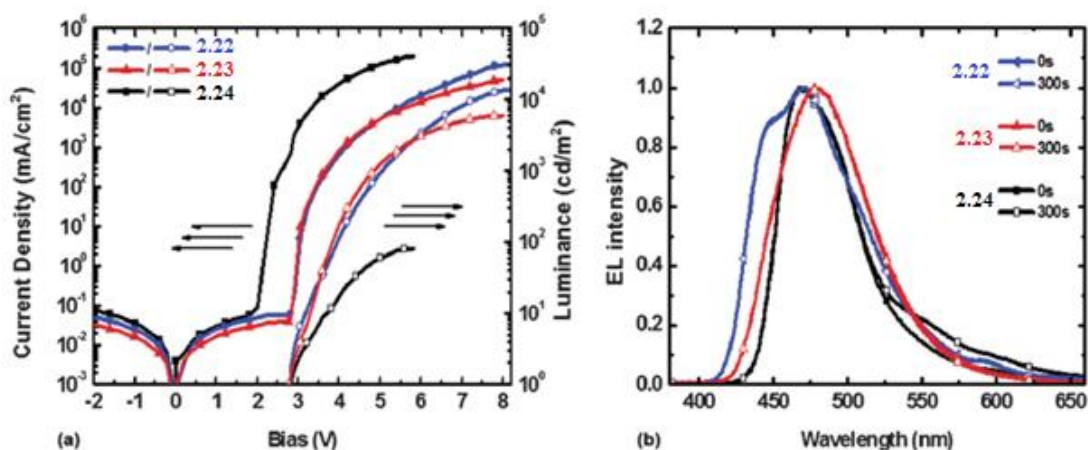


Figure 2.81. (a) J - V - L characteristics of devices **2.22**, **2.23** and **2.24**; (b) their electroluminescence emission spectra monitored over 300 seconds.⁴⁸ Reproduced from El-Assaad, T. H. *et al.*, *J. Mater. Chem. C*, DOI: 10.1039/C5TC02849C - by permission of The Royal Society of Chemistry.

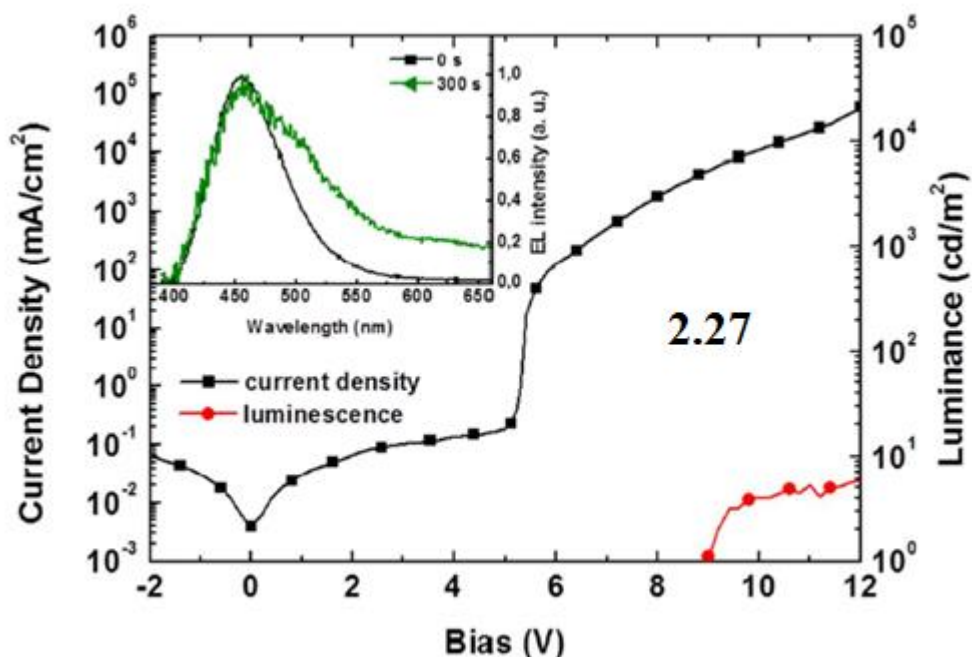


Figure 2.82. J - V - L characteristics of device **2.27** in addition to its electroluminescence emission spectrum monitored over 300 seconds.⁴⁸ Reproduced from El-Assaad, T. H. *et al.*, *J. Mater. Chem. C*, DOI: 10.1039/C5TC02849C - by permission of The Royal Society of Chemistry.

2.3. Conclusions and Future Work

A review of several reported pathways to functionalize pyrene into arylpyrenes through brominated building blocks (**2.1-2.20**) was presented; along with the advantage of the 1,3,6,8-tetraarylsubstitution on the fluorescence quantum yield of pyrene. Based on that, nine compounds were synthesized (**2.21-2.29**), through Suzuki-Miyaura coupling, from 1,3,6,8-tetrabromopyrene (**2.2**). The synthetic pathway was discussed and three different literature procedures were compared. The analysis of their photophysical properties in solution and in the solid state suggested that five of them (the ones with electron-releasing substituents **2.21-2.24**, in addition to the trifluoromethyl derivative **2.27**) are highly promising for application in OLEDs. Mainly, improved fluorescence quantum yield as compared to pyrene and unsubstituted 1,3,6,8-tetraphenylpyrene in both solid state and solution was achieved. Decreased unwanted molecular interactions such as excimer formation was proven and discussed. The electronic effect of substituents on the outer benzene ring and its impact on the photophysical properties of pyrene was discussed in details. Full characterization of all compounds including absorption spectra, emission spectra, fluorescence lifetimes, emission quantum yields, calculation of Stokes shift values, natural lifetimes, radiative and non-radiative rate constants was done in six solvents of different polarities. In addition to this, proton and carbon NMR spectra, elemental analyses, X-ray structures, melting and decomposition temperatures were reported.

Future work related to 1,3,6,8-tetraarylpyrene may include the synthesis of new derivatives using different electron-releasing and electron-withdrawing substituents from the ones reported in this Chapter. This may be helpful in supporting the observed trends for photophysical and thermal properties that were reported in this Chapter.

More challenging work may include the use of synthetic routes presented in Schemes 2.1-2.5, in order to achieve the synthesis of new compounds belonging to different arylpyrene categories. Comparing their properties with those of 1,3,6,8-tetraarylpyrenes presented in this Chapter can be done in order to check about their usefulness for OLED application.

Compounds **2.22** and **2.23** showed the highest device performance and stability over time. Compound **2.27** has a fluorescence quantum yield close to unity in solid state and in solution. However, this compound showed the poorest performance in a single layer device, probably due to its electrochemical properties. Future work may include finding a suitable multilayer device structure for compound **2.27**, in order to benefit from its high fluorescence quantum yield for application in electroluminescence.

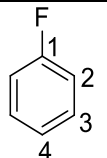
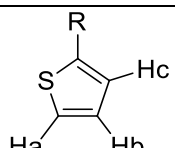
2.4. Experimental

2.4.1. Synthesis

All reactions were run using clean and oven dried glassware. Melting points (mp) were determined using a digital automatic melting point meter (Krüss M5000) that can detect melting points up to 410 °C with an error margin of 0.5 °C. Decomposition temperatures (T_d) were determined using a NETZSCH thermogravimetric analyzer and were defined to be as a loss of 5% of the initial sample mass upon heating at a 10 °C/min rate; under continuous flow of nitrogen gas in order to ensure a completely inert atmosphere inside the heating chamber during measurements. All NMR experiments were performed in chloroform-d as solvent, using TMS as internal standard. NMR spectra were acquired using a 500 MHz Bruker NMR machine. Elemental analyses were performed at Atlantic Microlab, Inc., Norcross, USA.

The ^{13}C NMR spectra of compounds **2.25** and **2.27** showed long-range C-F coupling. Inconsistent coupling constants were observed in the ^1H NMR of compound **2.29** between adjacent protons of the thiophene rings. Table 2.16 summarizes useful literature values for coupling constants of C-F coupling in fluorinated aromatic compounds,¹²¹ and H-H coupling in 2-substituted thiophene rings.¹²² These values are useful for the interpretation of ^{13}C NMR spectra of compounds **2.25** and **2.27**, and to assign the protons of compound **2.29** to the corresponding peaks in the ^1H NMR spectrum. The C-F coupling values in Table 2.16 were also used to interpret the ^{13}C NMR spectrum of compound **3.4** discussed in Chapter 3.

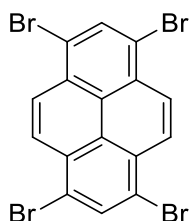
Table 2.16. Useful literature coupling constant values for C-F coupling in aromatic compounds,¹²¹ and H-H coupling in substituted thiophenes,¹²² reported in cycles per second (cps) (same as Hertz (Hz)) relevant to the NMR spectra of compounds **2.25**, **2.27** and **2.29**.

	$J_{\text{C1-F}}$	$J_{\text{C2-F}}$	$J_{\text{C3-F}}$	$J_{\text{C4-F}}$
	245.3	21.0	7.7	3.3
	$J_{\text{Ha-Hb}}$	$J_{\text{Ha-Hc}}$	$J_{\text{Hb-Hc}}$	
	4.7 – 6.0	1.4 – 1.8	3.5 – 3.9	

1,3,6,8-Tetrabromopyrene (2.2)

The title compound was synthesized according to a literature procedure.⁷¹ To a solution of pyrene **2.1** (5.00 g, 24.72 mmols) in 150 mL nitrobenzene, bromine (17.38 g, 108.77 mmols, 4.4 eqv) was added dropwise under vigorous stirring. The mixture was stirred overnight at 160 °C. The reaction was quenched with water/acetone mixture. The precipitate was collected by vacuum filtration, and recrystallized from

1,2-dichlorobenzene. 1,3,6,8-Tetrabromopyrene **2.2** (12.16 g, 23.48 mmol, 95%) was obtained as yellow solid, mp 405.1 °C (Lit.¹²³ mp 403 °C). No NMR data could be collected due to low solubility in most organic solvents.



2.2

Tetrakis(triphenylphosphine)palladium(0)

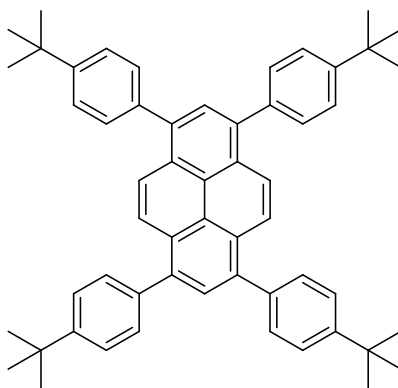
The title compound was synthesized according to a literature procedure.⁸⁹ To a stirred solution of palladium(II) chloride (0.50 g, 2.82 mmol) in 30 mL DMSO, triphenylphosphine (3.70 g, 14.10 mmols, 5 eqv) was added. The mixture was purged with argon for 20 minutes, and stirred at 165 °C for 30 minutes under argon atmosphere. The reaction mixture turns from turbid to clear orange solution. Hydrazine monohydrate (550 µL) was then added dropwise, and the reaction was allowed to cool down gradually to room temperature over one hour under argon atmosphere and in the dark. Vacuum filtration was performed, a shiny yellow solid was obtained. The solid was washed with ethanol (3 x 10 mL), then with diethyl ether (3 x 10 mL), and dried under reduced pressure, in the dark, for 48 hrs. Tetrakis(triphenylphosphine)palladium(0) (3.00 g, 2.60 mmols, 92%) was immediately used for the next step without any further purification.

General procedure,²³ involving toluene as solvent, was used for the synthesis of compounds **2.21**, **2.23**, **2.26**, **2.27**, **2.28** and **TPPy**:

1,3,6,8-Tetrabromopyrene **2.2** (0.50 g, 0.97 mmol) and the corresponding boronic acid (5.82 mmol, 6 eqv) were added to 30 mL of toluene followed by 3 mL of 2 M aqueous K₂CO₃, and a catalytic amount (~ 10 mg) of tetrabutylammonium bromide. The mixture was purged with argon for 20 min, before the freshly synthesized tetrakis(triphenylphosphine)-palladium(0) (67 mg, 0.057 mmol) was added and the mixture was refluxed under argon atmosphere and in the dark at 110 °C, for 48 hrs for compounds **2.21** and **2.23**, while for 72 hrs for compounds **2.26**, **2.27** and **2.28**. After evaporation of the solvent under reduced pressure, the obtained solid was triturated with chloroform using a Soxhlet extraction apparatus. The chloroform extract was then washed with 5% K₂CO₃ aqueous solution (2 x 50 mL) followed by brine (2 x 50 mL). Due to poor solubility, compound **2.26** was directly filtered and obtained at this level. The organic phase was dried over MgSO₄ and filtered, and the solvent was removed under reduced pressure.

1,3,6,8-Tetrakis(4-(*tert*-butyl)phenyl)pyrene (2.21)

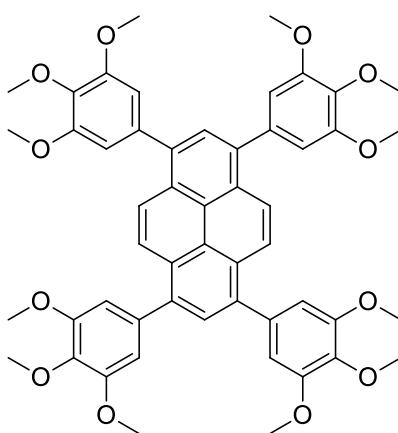
The obtained beige solid was then purified by column chromatography using hexanes to 5% dichloromethane in hexanes as eluent, to obtain the desired product, which was then recrystallized from toluene first, then from chloroform to yield 1,3,6,8-tetrakis(4-(*tert*-butyl)phenyl)pyrene **2.21** (0.50 g, 70%) as a shiny white solid, mp > 410 °C. *T_d* = 439.1 °C. ¹H NMR (500 MHz, CDCl₃): δ 8.14 (s, 4H), 7.97 (s, 2H), 7.55 (d, *J* = 8.5 Hz, 8H), 7.49 (d, *J* = 8.5 Hz, 8H), 1.35 (s, 36H). ¹³C NMR (125 MHz, CDCl₃): δ 150.1, 138.1, 136.9, 130.3, 129.5, 129.0, 128.0, 126.0, 125.2, 34.6, 31.4. Anal. calcd for C₅₆H₅₈: C, 92.00; H, 8.00. Found: C, 91.97; H, 8.06.



2.21

1,3,6,8-Tetrakis(3,4,5-trimethoxyphenyl)pyrene (2.23)

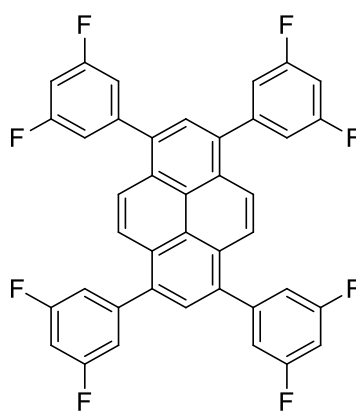
The obtained orange solid was recrystallized from toluene to yield 1,3,6,8-tetrakis(3,4,5-trimethoxyphenyl)pyrene **2.23** (0.40 g, 48%) as yellow crystals, mp 325.0 °C, $T_d = 408.7$ °C. ^1H NMR (500 MHz, CDCl_3): δ 8.18 (s, 4H), 7.97 (s, 2H), 6.80 (s, 8H), 3.90 (s, 12H), 3.84 (s, 24H). ^{13}C NMR (125 MHz, CDCl_3): δ 153.1, 137.4, 137.2, 136.4, 128.9, 128.1, 125.8, 125.3, 107.8, 61.0, 56.3. Anal. calcd for $\text{C}_{52}\text{H}_{50}\text{O}_{12}$: C, 72.04; H, 5.81. Found: C, 71.85; H, 5.84.



2.23

1,3,6,8-Tetrakis(3,5-difluorophenyl)pyrene (2.26)

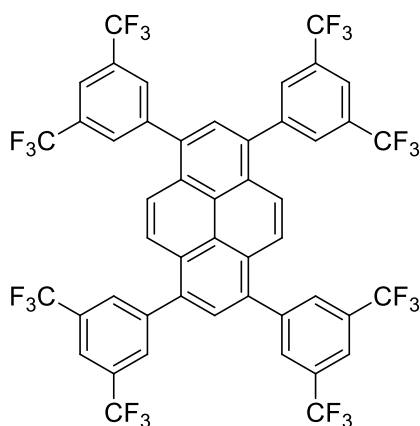
The obtained dark green insoluble solid was recrystallized from 1,2-dichlorobenzene to yield 1,3,6,8-tetrakis(3,5-difluorophenyl)pyrene **2.26** (0.25 g, 40%) as shiny yellow greenish needle-like crystals, mp > $T_d = 368.2$ °C. No NMR data could be collected due to low solubility in most organic solvents. Anal. calcd for $C_{40}H_{18}F_8$: C, 73.85; H, 2.79. Found: C, 73.67; H, 2.69.



2.26

1,3,6,8-Tetrakis(3,5-bis(trifluoromethyl)phenyl)pyrene (2.27)

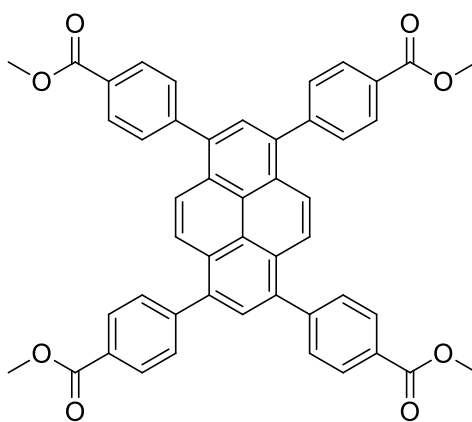
The obtained solid was recrystallized from chlorobenzene to yield 1,3,6,8-tetrakis(3,5-bis(trifluoromethyl)phenyl)pyrene **2.27** (0.68 g, 67%) as a shiny white solid, mp 314.7 °C, $T_d = 318.4$ °C. 1H NMR (500 MHz, $CDCl_3$): δ 8.05 (bs, 8H), 8.03 (s, 4H), 7.99 (bs, 4H), 7.95 (s, 2H); ^{13}C NMR (125 MHz, $CDCl_3$): δ 142.1, 135.1, 132.6 (q, $^2J_{C-F} = 32.5$ Hz), 130.5, 129.5, 128.8, 126.5 (q, $^1J_{C-F} = 271.3$ Hz), 125.8, 125.5, 121.9. Anal. calcd for $C_{48}H_{18}F_{24}$: C, 54.87; H, 1.73. Found: C, 54.90; H, 1.61.



2.27

Tetramethyl 4,4',4'',4'''-(pyrene-1,3,6,8-tetrayl)tetrabenzoate (2.28)

The orange solid was recrystallized from chlorobenzene, and tetramethyl 4,4',4'',4'''-(pyrene-1,3,6,8-tetrayl)tetrabenzoate **2.28** (0.43 g, 60%) was obtained as a yellow solid, mp 345.8 °C, $T_d = 410.0$ °C. ^1H NMR (500 MHz, CDCl_3): δ 8.15 (d, $J = 8.0$ Hz, 8H), 8.07 (s, 4H), 7.92 (s, 2H), 7.67 (d, $J = 8.0$ Hz, 8H), 3.91 (s, 12H). ^{13}C NMR (125 MHz, CDCl_3): δ 166.9, 145.35, 136.5, 130.6, 129.7, 129.2, 129.2, 128.3, 125.7, 125.5, 52.3. Anal. calcd for $\text{C}_{48}\text{H}_{34}\text{O}_8$: C, 78.04; H, 4.64. Found: C, 78.31; H, 4.77.



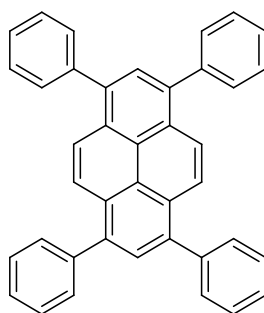
2.28

1,3,6,8-Tetraphenylpyrene (TPPy)

The crude brown solid was recrystallized from chlorobenzene and purified by column chromatography using hexane to 5% chloroform in hexane as mobile phase.

TPPy (0.35 g, 71%) was isolated as a shiny yellow solid, mp 299.4 °C, $T_d = 372.0$ °C.

^1H NMR (CDCl_3 , 500 MHz): δ 8.18 (s, 4H), 8.01 (s, 2H), 7.68 (d, $J = 7.5$ Hz, 8H), 7.56 (t, $J = 7.5$ Hz, 8H), 7.48 (t, $J = 7.5$ Hz, 4H). ^{13}C NMR (CDCl_3 , 125 MHz): δ 141.05, 137.23, 130.65, 129.54, 128.35, 128.10, 127.30, 125.92, 125.31.



TPPy

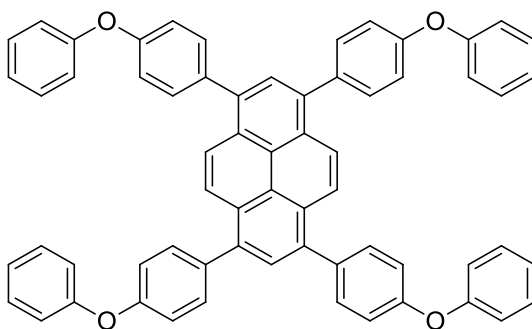
General procedure,⁸⁸ involving *n*-propanol as solvent, was used for the synthesis of compounds **2.22**, **2.24**, **2.25**:

1,3,6,8-Tetrabromopyrene **2.2** (0.50 g, 0.97 mmol) was added to 20 mL of *n*-propanol, then the corresponding boronic acid (4.27 mmol, 4.4 eqv) was added. The mixture was purged with argon for 20 min, after which palladium(II) acetate (0.70 mg, 3.12 mmol), triphenylphosphine (2.47 mg, 9.42 mmol), and 0.56 mL of 2 M aqueous K_2CO_3 solution were added, followed by 0.34 mL of deionized water. The mixture was refluxed for 36 hrs for compounds **2.22** and **2.24**, while for 48 hrs for compound **2.25**, under argon atmosphere and in the dark. The reaction was cooled to room temperature, quenched with water and extracted with ethyl acetate. The combined organic layer was

washed with a 5% aqueous K_2CO_3 solution and a brine solution, dried over $MgSO_4$, filtered, and solvent was removed under reduced pressure.

1,3,6,8-Tetrakis(4-phenoxyphenyl)pyrene (2.22)

The obtained yellow needle-like crystals were purified by column chromatography starting with hexanes as the mobile phase, and then increasing the polarity to 5% dichloromethane in hexanes to obtain 1,3,6,8-tetrakis(4-phenoxyphenyl)pyrene **2.22** (0.42 g, 49%) as a white solid, mp 276.1 °C, $T_d = 503.6$ °C. 1H NMR (500 MHz, $CDCl_3$): δ 8.14 (s, 4H), 7.94 (s, 2H), 7.57 (d, $J = 8.5$ Hz, 8H), 7.34 (t, $J = 8.0$ Hz, 8H), 7.12 (d, $J = 8.5$ Hz, 8H), 7.08–7.06 (m overlapping, 12H). ^{13}C NMR (125 MHz, $CDCl_3$): δ 157.1, 156.8, 136.6, 135.9, 131.9, 129.8, 129.0, 128.1, 126.0, 125.2, 123.5, 119.1, 118.6. Anal. calcd for $C_{64}H_{42}O_4$: C, 87.85; H, 4.84. Found: C, 87.91; H, 4.96.

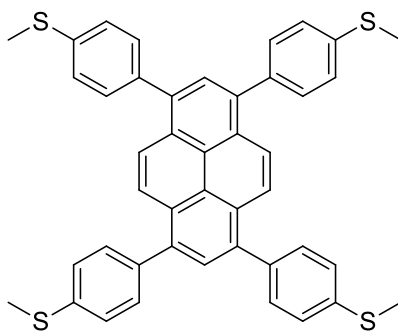


2.22

1,3,6,8-Tetrakis(4-(methylthio)phenyl)pyrene (2.24)

The obtained yellow greenish solid was recrystallized from toluene to yield 1,3,6,8-tetrakis(4-(methylthio)phenyl)pyrene **2.24** as a shiny yellow solid (1.00 g, 29%), mp 318.5 °C, $T_d = 392.4$ °C. 1H NMR (500 MHz, $CDCl_3$): δ 8.09 (s, 4H), 7.89 (s, 2H),

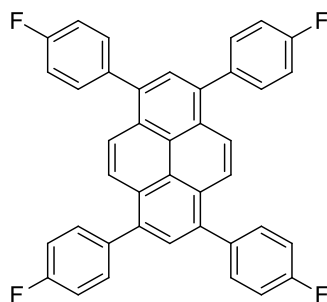
7.53 (d, $J = 8.0$ Hz, 8H), 7.37 (d, $J = 8.0$ Hz, 8H), 2.52 (s, 12H). ^{13}C NMR (125 MHz, CDCl_3): δ 137.7, 136.6, 131.0, 129.4, 129.05, 128.1, 126.4, 126.0, 125.2, 15.85. Anal. calcd for $\text{C}_{44}\text{H}_{34}\text{S}_4$: C, 76.48; H, 4.96; S, 18.56. Found: C, 76.60; H, 5.09; S, 18.41.



2.24

1,3,6,8-Tetrakis(4-fluorophenyl)pyrene (2.25)

The obtained greenish solid was recrystallized from toluene and then from chlorobenzene to yield 1,3,6,8-tetrakis(4-fluorophenyl)pyrene **2.25** (0.70 g, 24%) as yellow crystals, mp 309.0 °C, $T_d = 381.8$ °C. ^1H NMR (500 MHz, CDCl_3): δ 8.05 (s, 4H), 7.87 (s, 2H), 7.56 (dd, $^3J_{\text{H-H}} = 8.5$ Hz, $^3J_{\text{H-F}} = 5.5$ Hz, 8H), 7.17 (d, $J = 8.5$ Hz, 8H). ^{13}C NMR (125 MHz, CDCl_3): δ 163.4 (d, $^1J_{\text{C-F}} = 245$ Hz), 136.7 (d, $^4J_{\text{C-F}} = 2.5$ Hz), 136.3, 132.1 (d, $^3J_{\text{C-F}} = 7.5$ Hz), 129.6, 128.2, 125.8, 125.3, 115.5 (d, $^2J_{\text{C-F}} = 20$ Hz). Anal. calcd for $\text{C}_{40}\text{H}_{22}\text{F}_4$: C, 83.03; H, 3.83. Found: C, 82.92; H, 4.01.

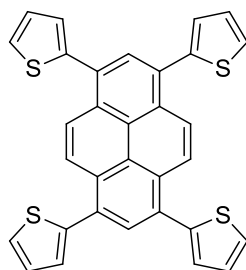


2.25

General procedure¹⁹ involving 1,4-dioxane as solvent was used for the synthesis of compound **2.29**.

1,3,6,8-Tetra(thiophen-2-yl)pyrene (2.29)

1,3,6,8-Tetrabromopyrene **2.2** (4.50 g, 8.69 mmol) and the corresponding boronic acid (52.14 mmol, 6 eqv) were added to 100 mL of 1,4-dioxane followed by 3 g of anhydrous K₂CO₃. The mixture was purged with argon for 20 min, tetrakis(triphenylphosphine)-palladium(0) (100 mg, 0.087 mmol) was added and the mixture was stirred at 80 °C for 48 hrs under argon atmosphere and in the dark. The reaction was quenched with water, and poured over ice/HCl solution. Extraction with dichloromethane was performed (3 x 50 mL). The combined organic extract was then washed with 5% K₂CO₃ aqueous solution (2 x 50 mL) followed by brine (2 x 50 mL). The organic phase was then dried over MgSO₄ and filtered, and the solvent was removed under reduced pressure. Recrystallization from toluene yielded light orange solid 1,3,6,8-tetra(thiophen-2-yl)pyrene **2.29** (0.78 g, 17%), mp 306.4 °C (Lit.¹¹⁰ 308 °C), *T_d* = 400.1 °C (Lit.¹¹⁰ 428 °C), ¹H NMR (500 MHz, CDCl₃): δ 8.45 (s, 4H), 8.17 (s, 2H), 7.46 (dd, *J* = 5.0, 1.0 Hz, 4H), 7.34 (dd, *J* = 3.5, 1.0 Hz, 4H), 7.20 (dd, *J* = 5.0, 3.5 Hz, 4H). ¹³C NMR (125 MHz, CDCl₃): δ 141.8, 131.2, 129.7, 129.1, 128.4, 127.5, 126.5, 125.8, 125.7. Anal. calcd for C₃₂H₁₈S₄: C, 72.42; H, 3.42; S, 24.17. Found: C, 72.33; H, 3.28; S, 24.06.



2.29

2.4.2. *Photophysical Studies*

Absorption spectra were measured using a double-beam JASCO V-570 UV-vis-NIR spectrophotometer, and the fluorescence measurements were done using a Jobin-Yvon-Horiba Fluorolog III spectrofluorometer. The excitation source was a 100 W xenon lamp, and the detector used was R-928 operating at a voltage of 950 V. Right angle mode detection was used. Slit widths were fixed at 5 nm for both entrance and exit slits during both emission and excitation experiments. Corrected emission spectra S_1/R_1 were collected to account for any fluctuation in the xenon lamp over different wavelengths. In parallel to that, S_1 spectra were collected to make sure that the intensity of emission is below 2×10^6 counts per second in order to avoid saturation of the detector. A blank measurement with no sample in the sample holder was subtracted from all actual spectra to account for any error possible due to the sample holder.

Stock solutions of concentration ranging from 0.5-5 mM of each compound were prepared in chloroform depending on the solubility limit of each compound. Around 0.1 mL of each stock solution was transferred into six dry glass vials and chloroform was left to evaporate. Then the corresponding solvent was added and diluted to 100 μ M for absorption measurements and to 1-2 μ M for fluorescence studies. Stock solutions were kept in the freezer and used discarded if not used within two days. Molar absorptivity was determined in chloroform due to a decent solubility of all compounds in this solvent. Quantum yield measurements were done using 9,10-diphenylanthracene in cyclohexane as standard with an attributed quantum yield of 1.00.⁹⁹ Excitation wavelength was set to 370 nm for all compounds and the standard. Lifetime and quantum yield measurements were performed on nitrogen-purged solutions, and optical density was maintained below 0.05 for all samples. UV-transparent quartz cuvette

(1 x 1 cm) was used for all experiments. Lifetime decays were all collected at emission maxima using the same spectrofluorometer with a nanoLED for excitation at 373 nm, and were all fit to single-exponential decays with χ^2 values below 3. Three runs were performed for all molar absorptivity, quantum yield and lifetime experiments. The average value resulting from the three runs was reported in this Chapter. A fourth run was performed in the case where inconsistent results were obtained in the first three runs.

2.4.3. *X-ray Diffraction from Single Crystals*

X-ray diffraction experiments from single crystal of each compound were performed using a Bruker SMART APEX II diffractometer with monochromated Mo K α radiations ($\lambda = 0.71073 \text{ \AA}$) at 100 K for compounds **2.21**, **2.22**, **2.25**, **2.27**, **2.29**; whereas for compound **2.24**, the experiment was carried at 297 K. The raw data was integrated with the SAINT+ program using a narrow-frame algorithm.¹²⁴ Absorption corrections were applied using the semi-empirical method of the SADABS program.¹²⁵ Structures were solved by direct methods and refined using Olex2,¹²⁶ by full-matrix least-square methods on F^2 using SHELXL-97 in anisotropic approximation for all non-hydrogen atoms.¹²⁷ CIF files (Crystallographic Information File, a standard format for the transmission and storage of crystallographic data defined by the IUCr) for the studied compounds were deposited in the Cambridge Crystallographic Data Centre (CCDC, a database repository having all crystal structures for molecules that do contain C-H bonds reported in the literature), and were given the numbers 1044326, 1015953, 1011328, 1011330, 1015949 and 1039264, respectively for compounds **2.21**, **2.22**, **2.24**, **2.25**, **2.27** and **2.29**.

CHAPTER 3

ANOTHER CATEGORY OF ARYLPYRENES: 2,7-DIARYLPYRENES AND 2,7-DIARYL-4,5,9,10-TETRAHYDROPYRENES

3.1. Introduction

In this Chapter, our attempt is to investigate more arylpyrene derivatives as blue light-emitters. The photophysical and thermal properties of 2,7-diarylpyrenes and 2,7-diaryl-4,5,9,10-tetrahydropyrenes are discussed in comparison with 1,3,6,8-tetraarylpyrene derivatives of Chapter 2. Positions 2 and 7 of pyrene are electron-poor and less reactive. Hence, functionalizing pyrene at these positions is more challenging and less investigated in the literature than 1,3,6,8-tetraarylpyrenes.¹⁰⁴ In 2011, the synthesis and photophysical studies of 2,7-diphenylpyrene (DPPy) in solution and in the solid state has been accomplished for the first time by Qiao *et al.* Their study has also investigated the effect of involving heterocyclic substituents in these positions on the photophysical properties of pyrene, Figure 3.1.¹⁰⁴

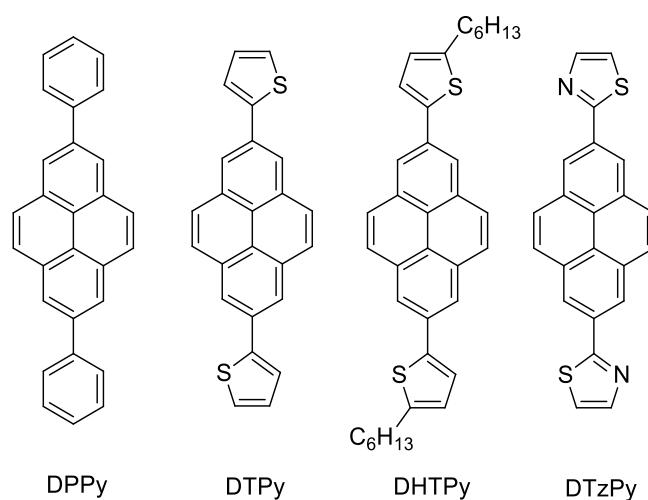


Figure 3.1. 2,7-Diarylpyrene derivatives previously reported by Qiao *et al.* in 2011.¹⁰⁴

In 2013, our research group reported the synthesis and characterization of such derivatives and their application. 2,7-Diaryl-4,5,9,10-tetrahydropyrene derivatives were found to have interesting applications. This is due to their high fluorescence quantum yield in both solution and solid state, and their long-lived triplet state. Hence, they can be used in triplet-triplet annihilation upconversion (TTA-UC) photochemistry.²⁴ UC processes lead to a light emission at a shorter wavelength than the absorbed one. This is achieved through an absorption of two small-energy photons by two molecules of an emitter (the small-energy photon cannot excite them all the way to the singlet excited state S_1). Instead, it can excite them to their triplet excited state T_1 (which is lower in energy than the singlet excited state S_1). After that, the TTA process is achieved through an energy transfer between the two triplet excited states T_1 , the first releases energy and falls down to the ground state S_0 , and the second receives energy and goes up to the singlet excited state S_1 . Subsequently, the latter leads to a radiative $S_1 \rightarrow S_0$ emission from the singlet excited state, releasing a higher energy photon (i.e. lower wavelength) than the small-energy photon used for the excitation. The process involves anti-Stokes shift (i.e. emission at a shorter wavelength than the absorption). The small-energy photons provider is known as sensitizer, and is a molecule having a heavy atom, such as iridium, in order to favor the transitions leading to the triplet excited state.²⁴ The derivatives explored by our research group in that study consisted of substituted outer phenyl rings in the 2,7-diphenyl-4,5,9,10-tetrahydropyrene and 2,7-diphenylpyrene cores. Substituents were chosen to sit on the *para*-position, and were either electron-withdrawing (i.e. *para*-fluoro), or electron-releasing (i.e. *para*-*tert*-butyl), or strongly electron-releasing (i.e. *para*-methoxy), Figure 3.2.²⁴ The photophysical properties were investigated in solution and in the solid state.

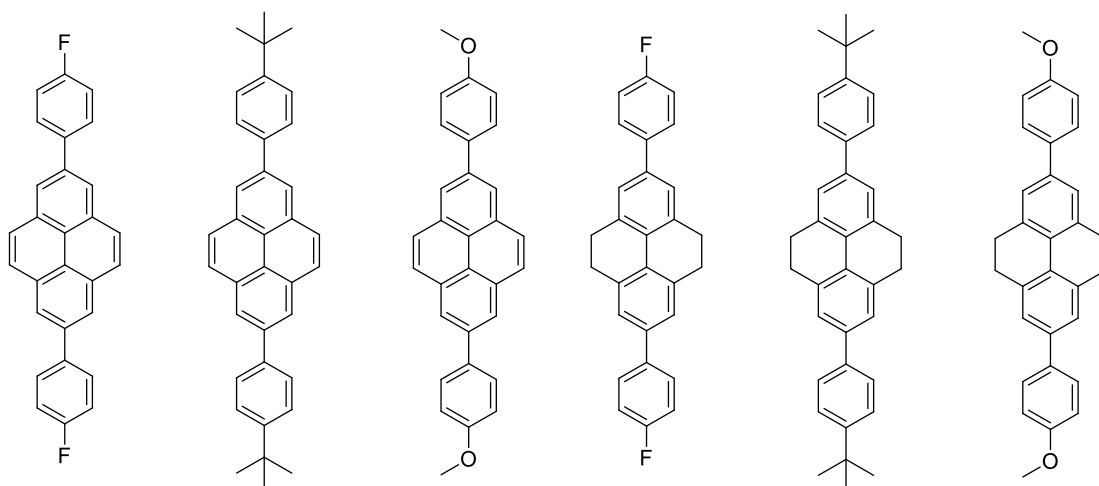


Figure 3.2. The six 2,7-diarylpyrene and 2,7-diaryl-4,5,9,10-tetrahydropyrene derivatives previously reported by our research group.²⁴

3.2. Results and Discussion

3.2.1. Synthesis

Synthesis of compounds **3.1-3.6**, Figure 3.3, was achieved according to the three-step pathway to functionalize pyrene in position 2 and 7, previously introduced in Chapter 2 (Scheme 2.4), through intermediate **2.15**, and building blocks **2.16** and **2.17**, via the Suzuki-Miyaura coupling reaction, using toluene as a solvent, Scheme 3.1.

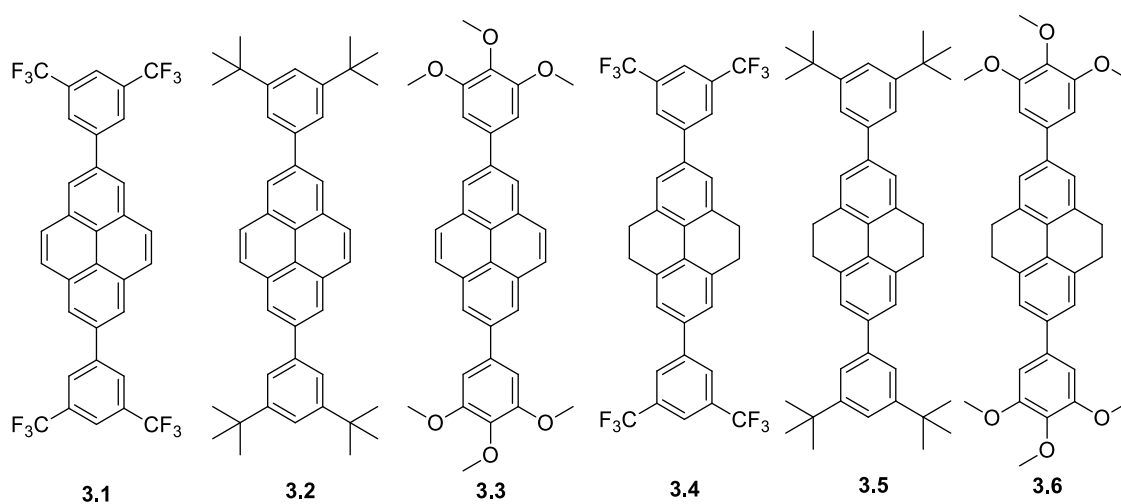
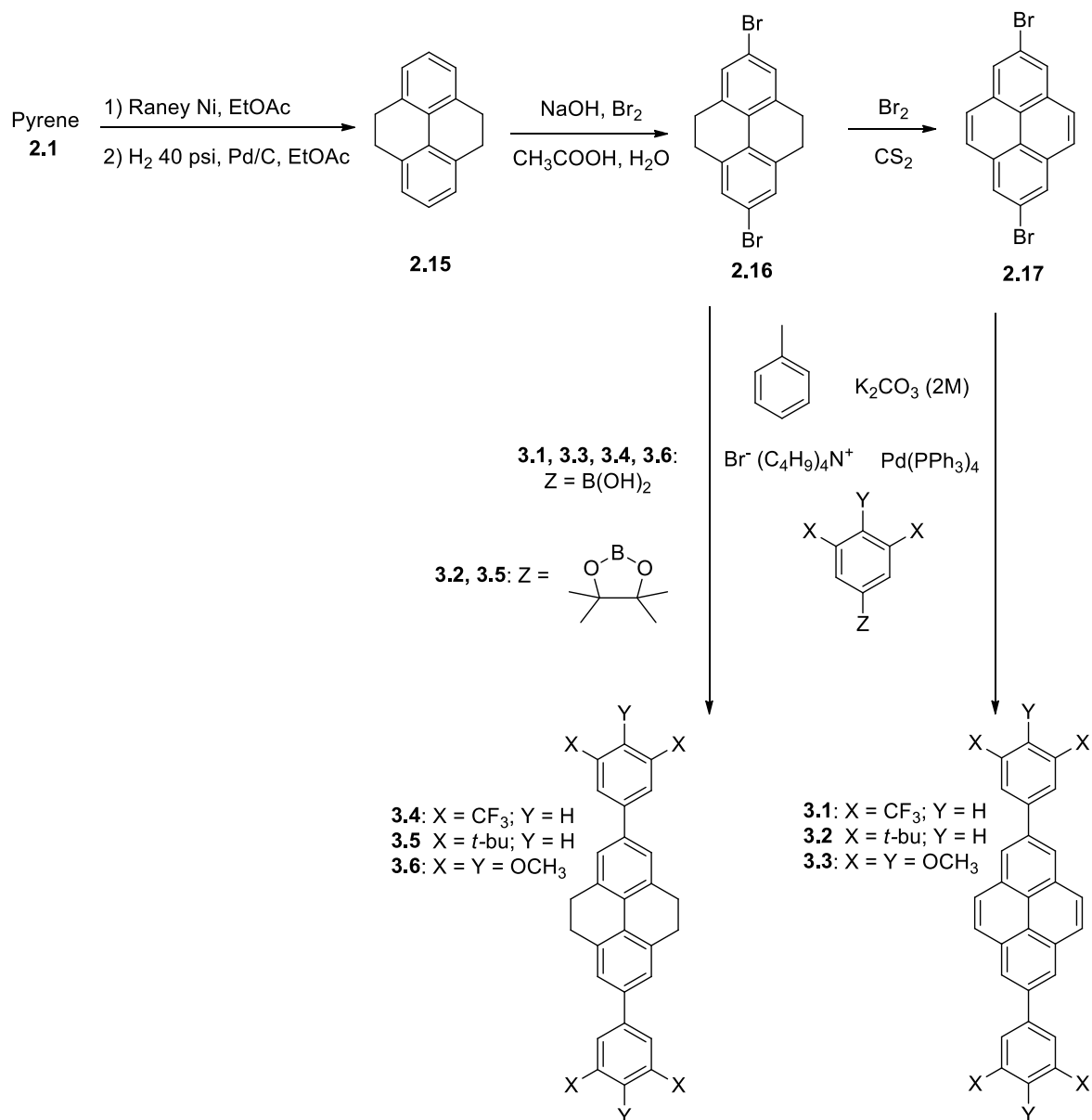


Figure 3.3. Structures of the new compounds **3.1-3.6** reported in this Chapter.



Scheme 3.1. Synthesis of compounds **3.1-3.6**.

3.2.2. Molecular Photophysics

3.2.2.1. 2,7-Diarylpyrene Derivatives

Comparing the absorption spectra of pyrene and DPPy, the vibrational structure of pyrene, that was lost upon 1,3,6,8-tetraaryl substitution (compounds **2.21-2.29** and TPPy from Chapter 2), remains unaffected in DPPy.¹⁰⁴ The forbidden lowest energy transition in pyrene at around 370-375 nm remains very weak in DPPy, and not detected in the experimental absorption spectrum, Figure 3.4.¹⁰⁴ This suggests that the $L_a - L_b$ inversion observed in the case of 1,3,6,8-tetraarylsubstitution does not occur in the case of the 2,7-diarylsubstitution. This is consistent with the theoretical modeling performed on DPPy by Qiao *et al.* The results showed that the lowest energy transition ($S_0 \rightarrow S_1$) corresponds to the L_b state with a major contributor HOMO-1 \rightarrow LUMO at 361.66 nm and a relatively low oscillator strength (0.0016).¹⁰⁴ Similarly to pyrene, the HOMO \rightarrow LUMO transition is the major contributor to the second lowest energy transition ($S_0 \rightarrow S_2$), at 335.81 nm.¹⁰⁴ This confirms that DPPy, unlike TPPy, shows similarity to pyrene regarding the two lowest energy transitions.

Furthermore, the bathochromic shift induced by the introduction of the benzene ring on the positions 2 and 7 of pyrene was negligible in the observed lowest energy transition of the absorption spectra (i.e. $S_0 \rightarrow S_2$). Thus, for pyrene, the HOMO \rightarrow LUMO transition is not significantly affected by introducing phenyl rings at the electron-poor (i.e. positions 2 and 7, Py 334 nm vs. DPPy 336 nm, and remains forbidden). Whereas it is significantly affected by introducing phenyl rings at the electron-rich sites (i.e. positions 1, 3, 6 and 8, TPPy 384 nm, and becomes allowed). A very strong absorption band appeared at 291 nm. This band has been attributed to the absorption of the benzene substituents enhanced by some contribution from the parent pyrene, Figure 3.4.¹⁰⁴

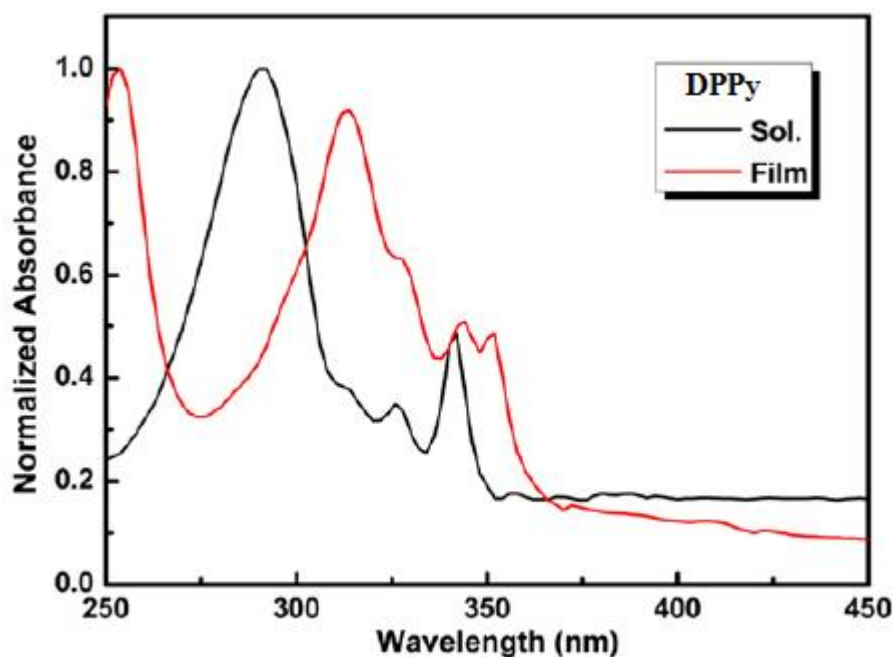


Figure 3.4. DPPy absorption spectra in dichloromethane solution and in the solid state.¹⁰⁴ Reprinted from “Novel 2,7substitutedpyrene derivatives: syntheses, solid-state structures, and properties”, 67, Qiao, Y.; Zhang, J.; Xu, W.; Zhu, D., 3395, Copyright (2011) with permission from Elsevier.

On the other side, a significant bathochromic shift (0.21 eV) occurs in the emission, from 388 to 415 nm, for Py and DPPy, respectively, in dichloromethane.¹⁰⁴ The bathochromic shifts were more pronounced (up to 437 nm) in the derivatives having five-membered heterocyclic substituents on positions 2 and 7 of pyrene, Figure 3.1. This has been attributed to an enhanced effective conjugation in the case of the heterocyclic substituents.¹⁰⁴ This larger bathochromic shift for a heterocyclic ring mimics the one observed for the thiophene derivative **2.29** of 1,3,6,8-tetraarylpyrenes discussed in Chapter 2. Another study by Crawford *et al.* in 2011, investigated the effects of different aromatic and aliphatic substituents were investigated. The $S_0 \rightarrow S_1$ transition has been found to be influenced by the introduced substituents, and was described as a “substituent-influenced” transition.⁶⁶

The substituent effect on the $S_0 \rightarrow S_1$ transition can be tracked by monitoring the change in emission. The $S_0 \rightarrow S_2$ transition has been described as a “pyrene-like” transition, and is almost not affected by the introduction of substituents at positions 2 and 7.⁶⁶

The substituent effect on the $S_0 \rightarrow S_2$ transition can be tracked by monitoring the change in absorption.

A previous investigation of some substituted 2,7-diphenylpyrene derivatives by our research group has been done. Substituents were placed at the *para*-position of the outer benzene ring. An increasing trend in the emission wavelength, upon moving from an electron-withdrawing fluorine (**3.7**) to an electron-releasing methoxy substituent (**3.9**), has been observed, Figure 3.5.²⁴

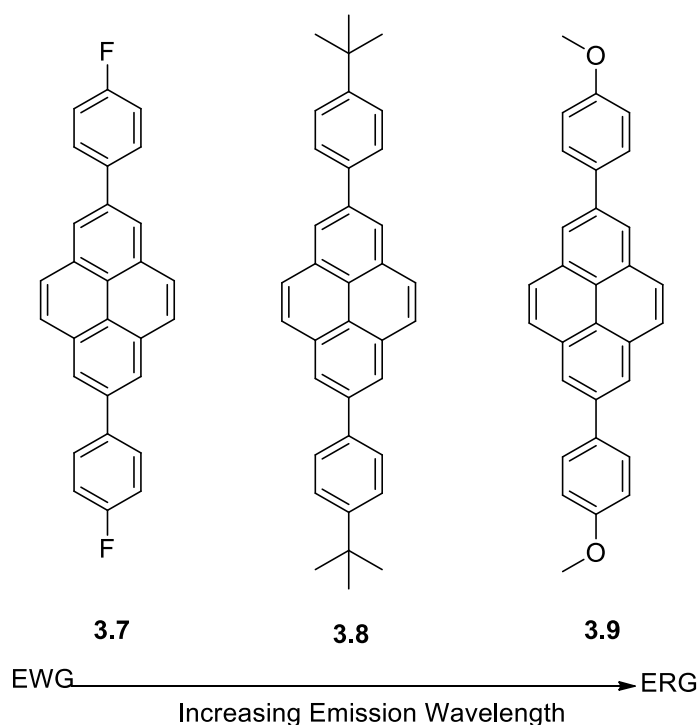


Figure 3.5. General trend for emission maxima vs. substituent effect according to a previous study by our research group on 2,7-diarylpyrenes in 2013.²⁴

Figure 3.6 represents a ranking of compounds **3.7-3.9**, DPPy and Py, in increasing order of emission wavelength in dichloromethane solution.

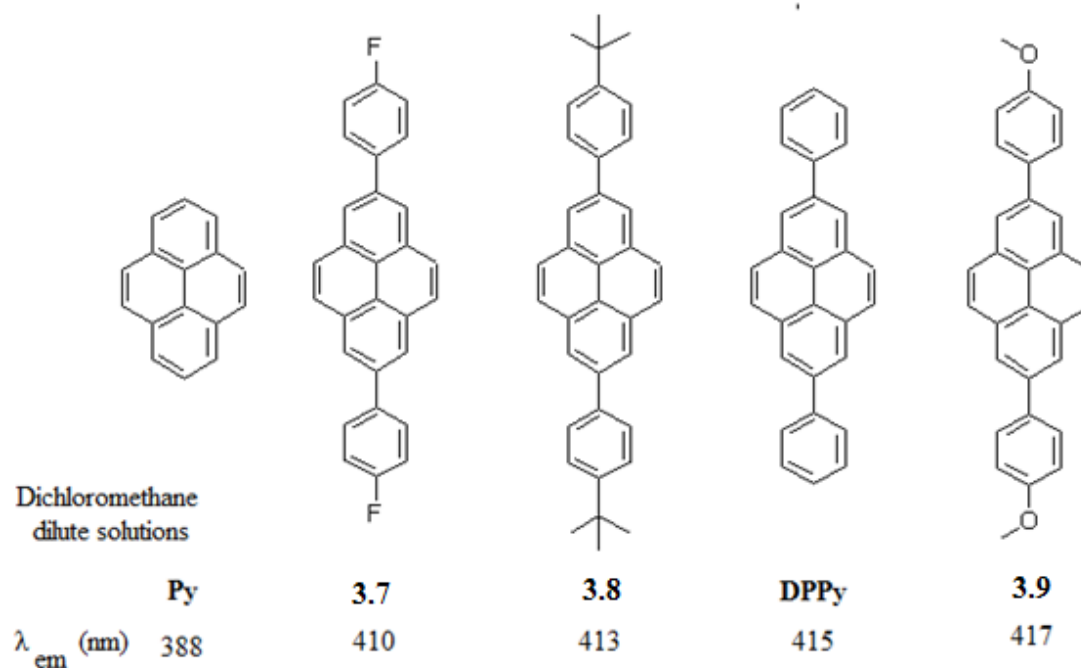


Figure 3.6. Emission maxima of (Py and DPPy)¹⁰⁴ vs. compounds (**3.7-3.9**)²⁴ in dichloromethane (increasing order from left to right).

Interestingly, the absorption band centered around 291 nm (i.e. $S_0 \rightarrow S_3$) has been found to follow a similar trend in response to substituent effect, as the $S_0 \rightarrow S_1$ trend observed in the emission spectra, Figure 3.5 (i.e. hypsochromic for the *para*-fluoro derivative **3.7** and bathochromic for the *para*-methoxy derivative **3.9**).²⁴

In the new derivatives investigated in this Chapter, the electronic effect of substituents at the *meta*-position at the outer phenyl ring of DPPy is explored for the first time. In addition to this, substituents of more pronounced electronic effects are used (i.e. trifluoromethyl in **3.1** is more withdrawing than fluorine in **3.7**; *tert*-butyl in **3.2** was used as twice per phenyl ring substituent; methoxy was used as thrice per phenyl ring in **3.3**). This was done in order to optimize the electronic effects exerted by the outer substituents on the inner pyrene core that may lead to clearer conclusions.

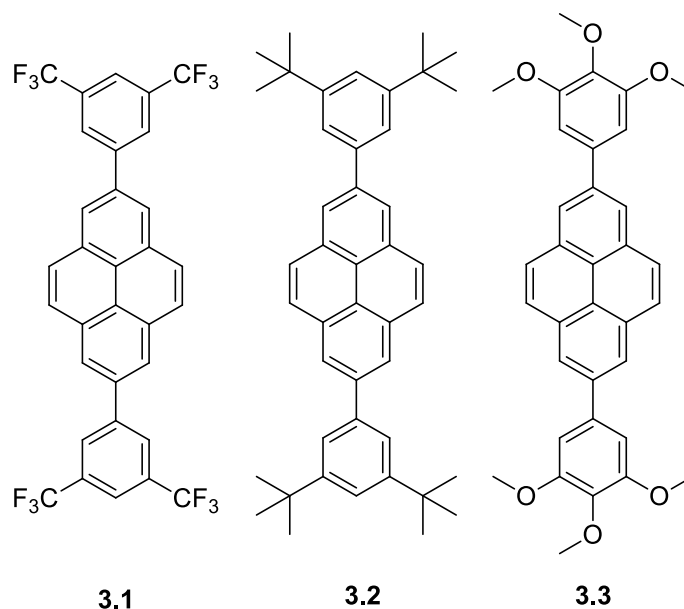


Figure 3.7. Structures of the three 2,7-diarylpirene new derivatives **3.1-3.3**.

The overall spectral features in absorption spectra of compounds **3.1-3.3** are similar to those of DPPy and compounds **3.7-3.9** in both polar and non-polar media. The observed lowest energy transition ($S_0 \rightarrow S_2$) for compounds **3.1-3.3** in the normalized absorption spectra of compounds are clearly overlapping despite the change of substituent, Figure 3.8.

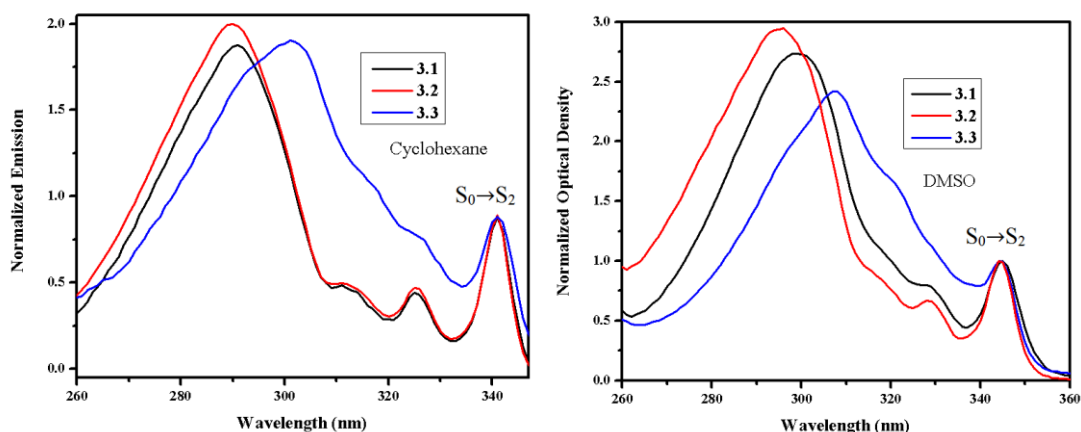


Figure 3.8. Absorption spectra of compounds **3.1-3.3** in cyclohexane (left) and in DMSO (right).

However, unexpected substituent-induced shifts were observed in the emission spectra of the trifluoromethyl derivative **3.1**. Given the highly pronounced electron-withdrawing effect of the trifluoromethyl substituent, and following the trend presented in Figures 3.5 and 3.6, compound **3.1** is expected to emit at shorter wavelength with respect to all other 2,7-diarylpirene derivatives investigated in this Chapter (**3.1-3.3**, **3.7-3.9** and DPPy). However, the experimental emission spectra showed that, in any solvent (except in cyclohexane and chloroform), this derivative tends to emit at higher wavelength as compared to all these compounds (up to 424 nm in DMSO), Figure 3.9 (right). Another interesting observation is that the trifluoromethyl derivative **3.1** displays the most structured emission spectrum. On the opposite side, the electron-releasing derivatives **3.2** and **3.3** display a single broad emission peak in the non-polar solvents, Figure 3.9 (left).

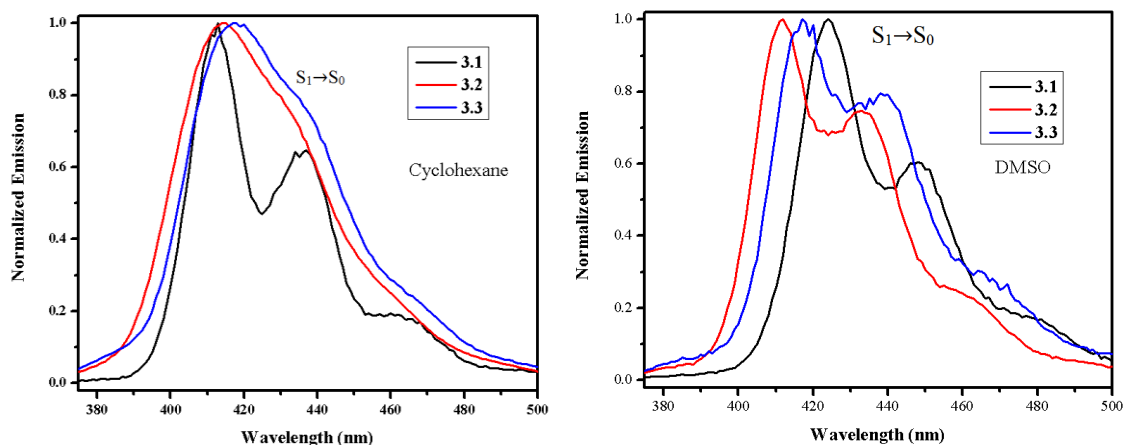


Figure 3.9. Emission spectra of compounds **3.1-3.3** in cyclohexane (left) and in DMSO (right).

3.2.2.2. Lowering of LUMO Energy vs Substituent Position Effect

The unexpected bathochromic shift of compound **3.1** can be explained in comparison to similar cases from the literature, Figure 3.10, where similar bathochromic shifts occurred in emission upon introducing a trifluoromethyl substituent. These shifts have been attributed to a lower energy of the LUMO orbitals in these compounds.¹²⁸⁻¹³⁰ This might explain the bathochromic shift occurring in the emission of **3.1** with respect to DPPy and the remaining 2,7-diarylpyrene derivatives (**3.2**, **3.3**, and **3.7-3.9**).

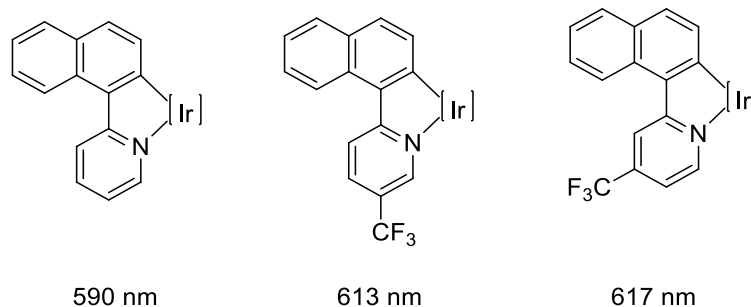


Figure 3.10. Bathochromic shift in the emission wavelength of some fluorophores attributed to a trifluoromethyl substituent.¹²⁹

Another possible explanation is that changing from the *para*-position (**3.7**) to the *meta*-position (**3.1**) switches the shift from hypsochromic to bathochromic. Such cases in the literature have been related to a substituent-induced stabilization vs. destabilization of partial charges or charges that may occur in the excited state, Figure 3.11.¹³¹

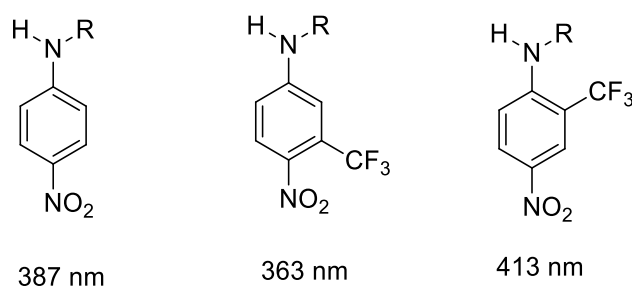


Figure 3.11. Switching the position of a trifluoromethyl substituent changes the nature of the shift from hypsochromic to bathochromic in some D-A compounds.¹³¹

One photophysical approach to check if the unusual trend observed in compound **3.1** is related to the change of substituent (from fluorine in **3.7** to trifluoromethyl in **3.1**) or to the change of position (from *para* in **3.7** to *meta* in **3.1**), consists of synthesizing two new model compounds **3.10** (trifluoromethyl on *para*-position) and **3.11** (fluorine on *meta*-positions), Figure 3.12, and comparing their photophysical properties (i.e. emission in different solvents) to those of compound **3.1** (trifluoromethyl on *meta*-positions), and **3.7** (fluorine on *para*-position) discussed in the present Chapter.

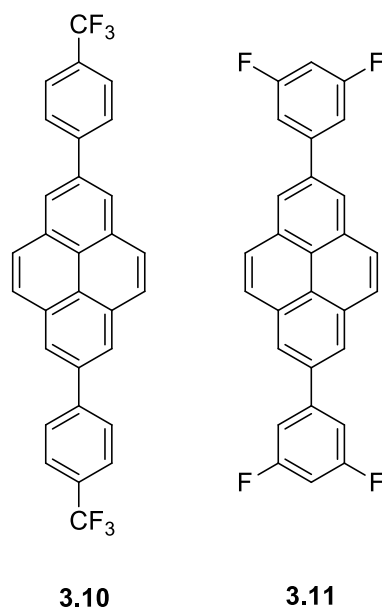


Figure 3.12. Suggested model compounds to be synthesized in order to investigate further regarding the bathochromic shift of the trifluoromethyl derivative **3.1**.

If model compound **3.11**, having the withdrawing fluorine substituent in the *meta*-position, exhibits similar bathochromic shift as **3.1**, the hypothesis of substituent position can be validated. Subsequently, the bathochromic shift can be attributed to the change from *para* (in **3.7**) to *meta*-position (in **3.1**). However, if compound **3.10** is the one to exhibit similar bathochromic shift to that of **3.1**, the shift can be attributed to the trifluoromethyl substituent by itself (i.e. probably due to lowering the energy of the LUMO orbital). In this case, further electrochemical and theoretical studies might be needed. This falls in the category of future work related to this project.

3.2.2.3. The Hydrophobic Cleft and a Reversed Solvatochromism

Another interesting observation is that the *tert*-butyl derivative **3.2** (*meta*-positions) exhibited a reversal in solvatochromic behavior, showing a hypsochromic shift in its emission wavelength upon increasing the solvent polarity. This contradicts the regular solvatochromism, which is usually seen as a bathochromic shift with increasing solvent polarity, due to increased polarity of the excited state over the ground state. Compound **3.2** emits at 414 nm in cyclohexane, whereas it shifts to 409 nm in acetonitrile. This behavior mimics that of compound **3.8**, the other *tert*-butyl derivative (*para*-position), where the emission maximum shifted from 416 nm in hexane to 411 nm in acetonitrile.²⁴ Furthermore, the single broad emission band of compound **3.2** in cyclohexane becomes resolved, with a vibrational structure consisting of three clear bands in DMSO, Figures 3.9 and 3.14. This suggests that solvent-solute interactions (solvent relaxation) in the excited state are stronger in non-polar solvents than in polar ones. This reversal in solvatochromism is probably related to the hydrophobic character of the *tert*-butyl substituent, where a more polar solvent fails to exert solvent relaxation process on the excited state, and the emission occurs from the non-relaxed state (i.e. higher energy/shorter wavelength). Although this was not observed in the 1,3,6,8-tetraarylpyrene *tert*-butyl derivative **2.21**, Chapter 2, Table 2.3.

In 2007, Panigrahi *et al.* investigated a series of *N*-hexadecylstyrylpyridinium derivatives exhibiting a reversed solvatochromic behavior (despite the presence of a polar pyridinium group expected to facilitate the interaction with more polar solvents). However, the reversal has been attributed to their “hydrophobic cleft”, which refers to the hydrophobic hexadecyl chain.¹³² This might be comparable to the *tert*-butyl substituents (i.e. hydrophobic cleft) in compounds **3.2** and **3.8**.

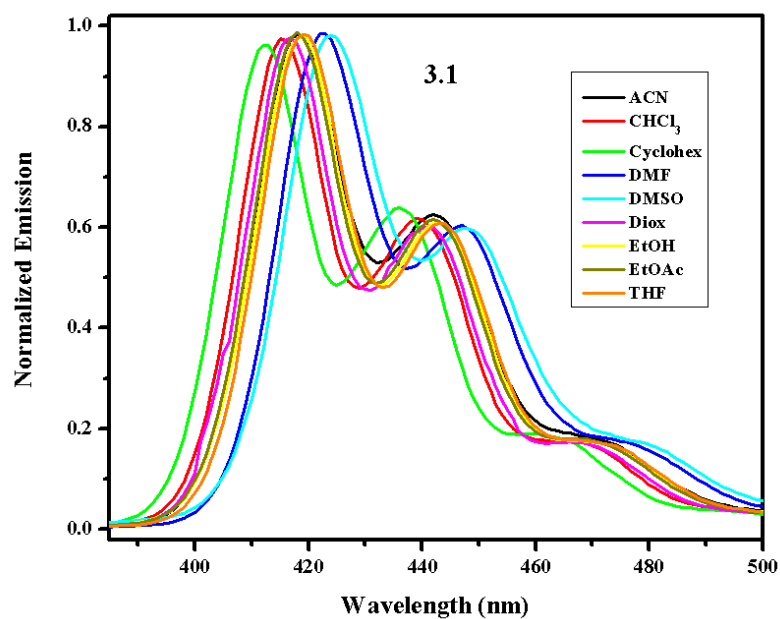


Figure 3.13. Normalized emission spectra of compound **3.1** in nine different solvents.

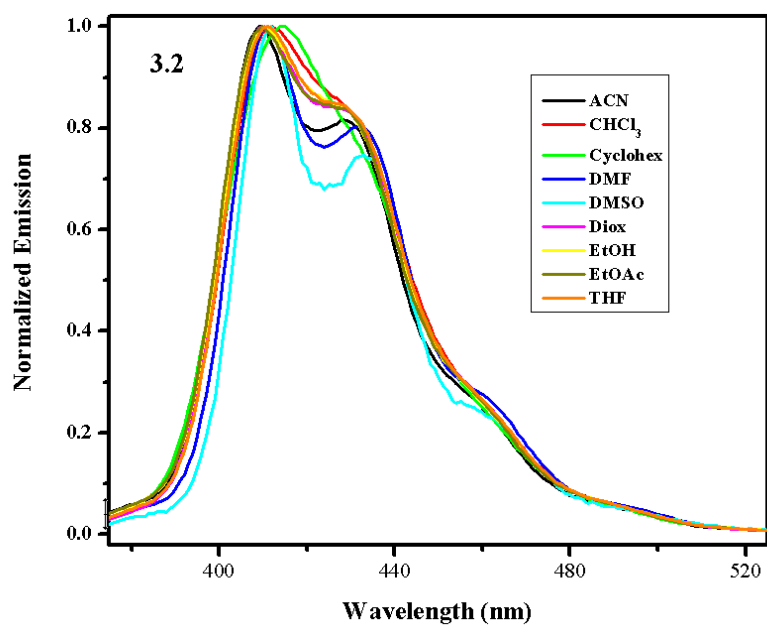


Figure 3.14. Normalized emission spectra of compound **3.2** in nine different solvents.

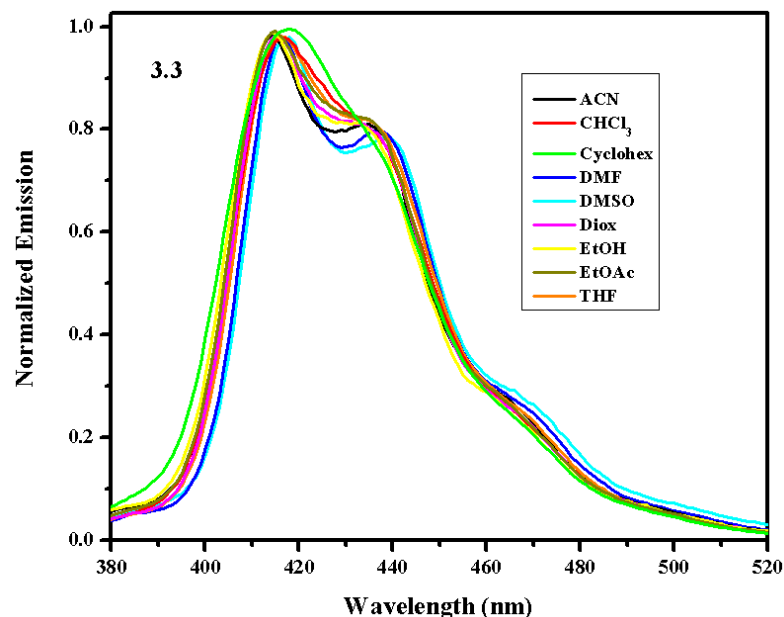


Figure 3.15. Normalized emission spectra of compound **3.3** in nine different solvents.

3.2.2.4. Emission Quantum Yield: Loose-Bolt Effect vs. Reduction of Non-Radiative Rate Effect

Quaternary alkyl substituents, such as *tert*-butyl groups, are related to a higher rate of internal conversion k_{IC} (a non-radiative relaxation). A comparison between the internal conversion rate constant of toluene ($\sim 10^7 \text{ s}^{-1}$) to that of *tert*-butylbenzene ($\sim 10^8 \text{ s}^{-1}$) shows that the latter undergo non-radiative internal conversions 10 times faster than the former.¹³³ This has been attributed to a stretching of the sigma bond connecting *tert*-butyl to benzene in the excited state. The bond becomes partially broken due to the stability of a resulting charge or radical on the *tert*-butyl group. The energetics of both the excited state and the ground state lead to easy non-radiative internal conversion from the excited state to the ground state, Figure 3.16.¹³³ The substituent is described as a bolt attached loosely to a core (loose-bolt), which is the reason behind the occurrence of this effect. The non-radiative relaxation offered by the loose-bolt effect contributes to lower emission quantum yield.

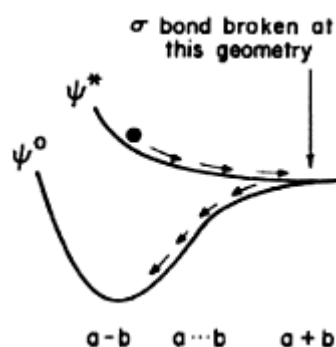


Figure 3.16. Loose-Bolt effect: stretching of sigma bond in the excited state leading to non-radiative relaxation from the excited state ($a = \textit{tert}$ -butyl, $b = \text{benzene ring}$).¹³³

On the other side, the presence of a carbon-fluorine bond has been related to an increase in fluorescence quantum yield in many instances, mainly in compounds having many C-F bonds, such as trifluoromethyl substituents. The C-F bond has a low vibrational frequency as compared to a C-H bond. From this perspective, a C-H bond is regarded as a promoter of radiationless decay (lower quantum yield), whereas a C-F bond is an inhibitor of radiationless processes (higher quantum yield).^{134,135} In addition to this, an efficient inhibition of π - π stacking can be attributed to the steric effect provided by the trifluoromethyl group (which also occurs in the case of a more bulky *tert*-butyl substituent).^{134,135} The positive influence of the C-F bond is supported by previous findings in Chapter 2, for the 1,3,6,8-tetraarylpyrene trifluoromethyl derivative **2.27**, where the emission quantum yield, in both solid state and solution, was approaching unity.

Unsubstituted DPPy has a low quantum yield of 0.006 in dichloromethane.¹⁰⁴ This is even lower than that of unsubstituted pyrene (0.28 in dichloromethane).^{102,104} Among compounds **3.7-3.9**, which all possess higher quantum yields than DPPy, the lowest quantum yield values were attributed to the *para*-fluoro derivative (**3.7**) in both

solution and solid state. Hence, there is no evidence for the occurrence of loose-bolt effect in the *para-tert*-butyl derivative **3.8** since its emission was found to be better than the *para*-fluoro derivative **3.7**.²⁴ However, for *meta-tert*-butyl derivative **3.2**, the fluorescence quantum yield in different solvents may suggest that this derivative is affected by the loose-bolt effect in solvents of low polarity. This is explained by smaller quantum yield values than those of compounds **3.1** and **3.3** in the four least polar solvents (i.e. chloroform, cyclohexane, 1,4-dioxane, and tetrahydrofuran), Table 3.1. Due to the forbidden $S_0 \rightarrow S_1$ transition, which cannot be experimentally detected in the absorption spectra, Stokes shifts for compounds **3.1-3.3** could not be calculated from the experimental results. Stokes shift reported in the literature by considering the absorption of the second lowest energy transition ($S_0 \rightarrow S_2$) were not shown in Table 3.1.

Table 3.1. Main photophysical properties of 2,7-diarylpirene derivatives.

Compound	Solvent	λ_{max}^{em} , nm	λ_{max}^{abs} , nm ($S_0 \rightarrow S_2$)	λ_{max}^{abs} , nm ($S_0 \rightarrow S_3$)	ϕ_F
DPPy ¹⁰⁴	Dichloromethane	415	342	291	0.006
	Thin film	--	352	313	--
3.1	Acetonitrile	418	341	292	0.24
	Chloroform	415	343	293	0.09
	Cyclohexane	413	341	291	0.14
	DMF	423	343	297	0.33
	DMSO	424	345	299	0.55
	1,4-Dioxane	417	342	293	0.22
	Ethanol	419	341	293	0.33
	Ethyl Acetate	418	340	293	0.29
	THF	420	342	294	0.36
	3.2	Acetonitrile	409	340	292
Chloroform		412	343	293	0.06
Cyclohexane		414	341	290	0.07
DMF		411	343	294	0.23
DMSO		412	344	296	0.25
1,4-Dioxane		410	342	291	0.17
Ethanol		410	340	277	0.14
Ethyl Acetate		410	340	290	0.23
THF		411	342	292	0.18

3.3	Acetonitrile	415	341	302	0.11
	Chloroform	417	344	303	0.08
	Cyclohexane	417	342	303	0.15
	DMF	416	343	306	0.21
	DMSO	417	344	307	0.22
	1,4-Dioxane	416	342	304	0.24
	Ethanol	416	341	302	0.25
	Ethyl Acetate	416	341	303	0.20
	THF	416	342	304	0.23
3.7²⁴	Acetonitrile	408	340	--	0.08
	Cyclohexane	412	341	--	0.04
	Dichloromethane	410	342	--	0.08
	DMF	410	343	--	0.09
	Ethanol	409	340	--	0.05
	Hexane	412	339	--	0.02
	Methanol	408	339	--	0.05
	THF	410	340	--	0.07
	Toluene	411	343	--	0.07
	Thin film	440	353	--	0.08
3.8²⁴	Acetonitrile	411	341	--	0.07
	Cyclohexane	415	341	--	0.11
	Dichloromethane	413	342	--	0.04
	DMF	412	343	--	0.38
	Ethanol	413	340	--	0.13
	Hexane	416	341	--	0.04
	Methanol	414	341	--	0.12
	THF	412	342	--	0.08
	Toluene	414	343	--	0.09
	Thin film	428	353	--	0.17
3.9²⁴	Acetonitrile	415	340	--	0.13
	Cyclohexane	419	341	--	0.08
	Dichloromethane	417	343	--	0.19
	DMF	417	343	--	0.34
	Ethanol	416	341	--	0.12
	Hexane	419	340	--	0.04
	Methanol	418	340	--	0.09
	THF	417	342	--	0.17
	Toluene	417	344	--	0.09
	Thin film	443	354	--	0.12

3.2.2.5. 2,7-Diaryl-4,5,9,10-Tetrahydropyrene Derivatives

Understanding the photophysical properties of 4,5,9,10-tetrahydropyrene (THP) derivatives starts by understanding the similarities and differences between THP and biphenyl. These isoelectronic structures only differ by two methylene bridges connecting the two benzene rings present in THP.⁶⁸ However, the impact of the two methylene bridges on the photophysical properties is not negligible. This is due to their impact on the geometry of the molecule.¹⁰⁰ The $S_0 \rightarrow S_1$ transition in biphenyl is symmetry-forbidden, similarly to pyrene. Biphenyl is mainly excited through the $S_0 \rightarrow S_3$ transition, which is the only favored transition (i.e. $S_0 \rightarrow S_2$ is also forbidden). This excitation is followed by internal conversions to the S_1 level, from which the emission occurs upon relaxation to any vibrational energy level of the ground state, leading to a vibrational structure in the emission spectrum.¹⁰⁰ Biphenyl's emission is sensitive to changes in concentration. Similar to unsubstituted pyrene, biphenyl tends to aggregate when unsubstituted. Due to this, a quenching of fluorescence is mainly induced in more concentrated solution, where aggregation occurs easily. 4,5,9,10-Tetrahydropyrene (THP) is reported to have three transitions at 307 (forbidden), 295, 217-221 nm, red-shifted as compared to their biphenyl correspondings, with a forbidden $S_0 \rightarrow S_1$ transition, similarly to biphenyl.

Upon moving from biphenyl to *para*-quaterphenyl, the $S_0 \rightarrow S_1$ transition becomes symmetry-allowed and favored.¹⁰⁰ Hence, the effect of moving from biphenyl to *para*-quaterphenyl on the lowest energy transition is similar to that of moving from pyrene to TPPy, as discussed in Chapter 2. This is enough to explain the increase in emission quantum yield from 0.25 for biphenyl to 0.82 for *para*-quaterphenyl, in oxygen-free cyclohexane solutions.¹⁰⁰ The energy level of the allowed transition

($S_0 \rightarrow S_3$ in biphenyl) is lowered following the inclusion of the two extra benzene rings (*para*-quaterphenyl). However, the energy levels of forbidden transitions ($S_0 \rightarrow S_1$ and $S_0 \rightarrow S_2$ in biphenyl) are less affected by the substituents. This leads to a reversal of the allowed and forbidden transition in *para*-quaterphenyl with respect to biphenyl.

2,7-Diarylsubstituted-THP derivatives are similar to *para*-quaterphenyl (i.e. isoelectronic structures, Figure 3.17).¹⁰⁰ This explains the higher fluorescence quantum yield of 2,7-diaryl-THP derivatives (i.e. *para*-quaterphenyl emitting core, $S_0 \rightarrow S_1$ transition is allowed), as compared to the corresponding 2,7-diarylpyrene derivatives (i.e. pyrene emitting core, $S_0 \rightarrow S_1$ transition is forbidden).

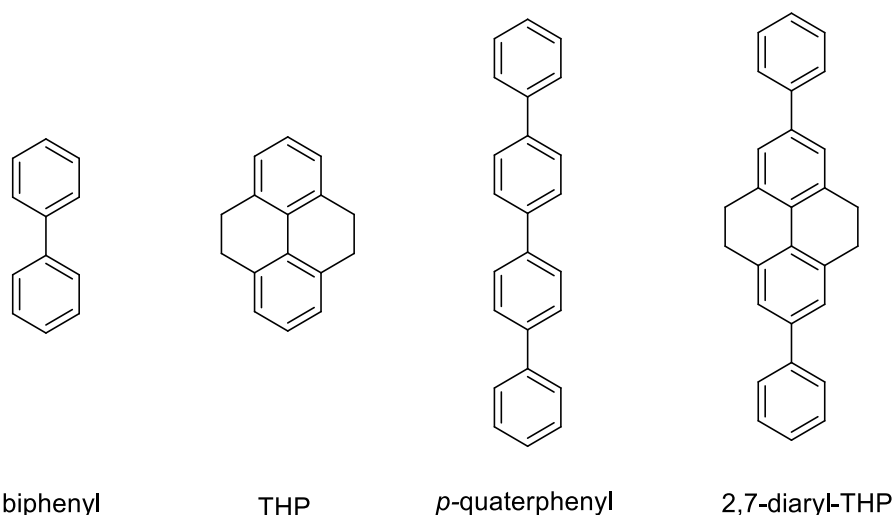


Figure 3.17. Isoelectronic structures: (a) biphenyl and THP, (b) *p*-quaterphenyl and 2,7-diaryl-THP.

We recall from Chapter 2 that non-planar fluorophores (i.e. TPPy and 1,3,6,8-tetraarylpyrene derivatives **2.21-2.29**) tend to lose the vibrational structure that exists in the corresponding planar ones (i.e. pyrene). *Para*-quaterphenyl is characterized by one broad structureless absorption band described as a “bell-like band” centered around 276 nm.¹⁰⁰ On the opposite side, it has a structured emission with a vibrational

structure. This has been explained by the fact of being non-planar in the ground state and planar in the excited state. The planarity of the excited state leads to a vibrational structure in the emission spectrum, which is not the case for the absorption spectrum (i.e. non-planar ground state).¹⁰⁰ *Para*-substituted 2,7-diaryl-THP compounds (**3.12-3.14**) have been previously investigated by our research group, Figure 3.18.²⁴

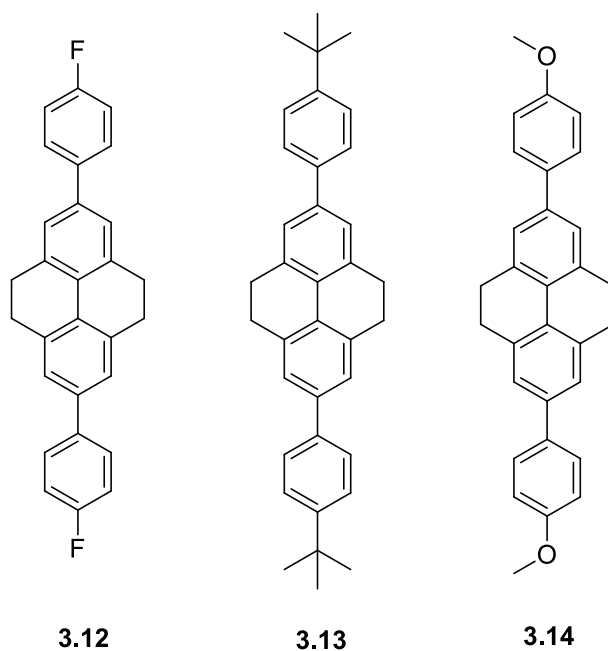


Figure 3.18. Structures of compounds **3.12-3.14** previously reported by our group.²⁴

Structureless bell-like absorption spectra, similar to that of *para*-quaterphenyl, were obtained for all 2,7-diaryl-THP derivatives **3.4**, **3.6** and **3.12-3.14**.²⁴ However, the difference is that these derivatives have significantly red-shifted absorption and emission maxima as compared to both *para*-quaterphenyl and THP. The bell-like absorption band, corresponding to the $S_0 \rightarrow S_1$ transition, confirms that these compounds mimic *para*-quaterphenyl (allowed lowest energy transition) rather than THP (forbidden

lowest energy transition). The $S_0 \rightarrow S_1$ transition is substituent-influenced rather than pyrene-like. Therefore, both absorption and emission wavelengths of 2,7-diaryl-THP derivatives are affected by the effect of substituent.²⁴ Whereas in the case of 2,7-diarylpyrene (**3.1-3.3**) derivatives, it is only the emission wavelength that gets affected, as previously discussed. Similar trend was observed for *para*-substituted 2,7-diarylpyrenes (**3.7-3.9**) and 2,7-diaryl-THP (**3.12-3.14**) regarding the electronic effect of substituents on the emission wavelength. The *para*-fluoro derivative **3.12** is the most blue-shifted and the *para*-methoxy **3.14** is the most red-shifted.²⁴ Lowest emission quantum yield in both solid state and solution was attributed to the *para*-fluoro derivative **3.12**. Furthermore, all the THP derivatives had much higher quantum yields than their pyrene corresponding, due to the allowed vs. forbidden lowest energy transition, respectively.²⁴

In this Chapter, we report on the photophysical properties of two new THP derivatives using trifluoromethyl (**3.4**) and trimethoxy (**3.6**) as electron-withdrawing and electron-releasing substituents, respectively, Figure 3.19. The work-up of the Suzuki coupling reaction to synthesize the *tert*-butyl derivative (**3.5**) did not lead to a pure sample of the compound. Failure of this synthesis might be related to an extreme sensitivity of the boronic ester to water and oxygen. Synthesizing **3.5** on a large scale requires an oxygen-free working space (i.e. glove box or argon bag). This may also require changing the experimental conditions used for the Suzuki coupling step, in order to ensure a water-free reaction mixture. This is considered as possible future work related to the actual study.

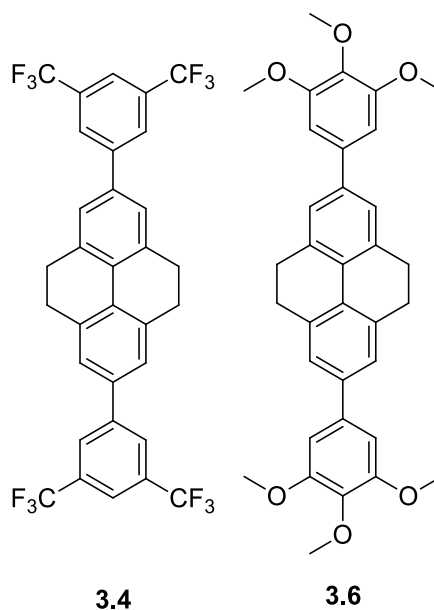


Figure 3.19. Structures of the two 2,7-diaryl-THP new derivatives **3.4** and **3.6**.

Both compounds **3.4** and **3.6** showed the bell-like single broad absorption peak similar to that of *para*-quaterphenyl and the *para*-derivatives (**3.12-3.14**), Figure 3.20, along with a well-structured emission, Figures 3.21 and 3.22. According to the previous trends observed for compounds **3.12-3.14**, emission at longer wavelength is expected for the trimethoxy derivative **3.6** due to the presence of three strong electron-releasing groups, and this was seen experimentally.

However, an unusual trend occurred for the trifluoromethyl derivative **3.4**, where the expected shift is hypsochromic, due to the strong electron-withdrawing substituent. Whereas a bathochromic shift took place experimentally, which is against the trend reported for the *para*-substituted derivatives **3.12-3.14**. The bathochromic shift of the trifluoromethyl derivative **3.4** lead to absorption and emission wavelengths comparable to the derivative having the strongest electron-releasing trimethoxy substituents (**3.6**), in most solvents, Figures 3.20-3.22. This mimics the bathochromic

shift of the trifluoromethyl compound **3.1** of the 2,7-diarylpyrene derivatives discussed earlier in this Chapter.

The emission quantum yields were close to unity for both compounds **3.4** and **3.6** namely in more polar solvents. In both 2,7-diarylpyrene and 2,7-diaryl-THP, an increase in emission quantum yield was observed with increasing number of substituents on the outer benzene ring, regardless the nature of the substituent (i.e. 2,7-diarylpyrene derivative **3.3** and 2,7-diaryl-THP derivative **3.6** both having three methoxy substituents per benzene ring, and they both showed higher emission quantum yield than the corresponding single methoxy derivatives **3.9** and **3.14**, respectively). The results of the photophysical studies for all compounds are summarized in Table 3.2.

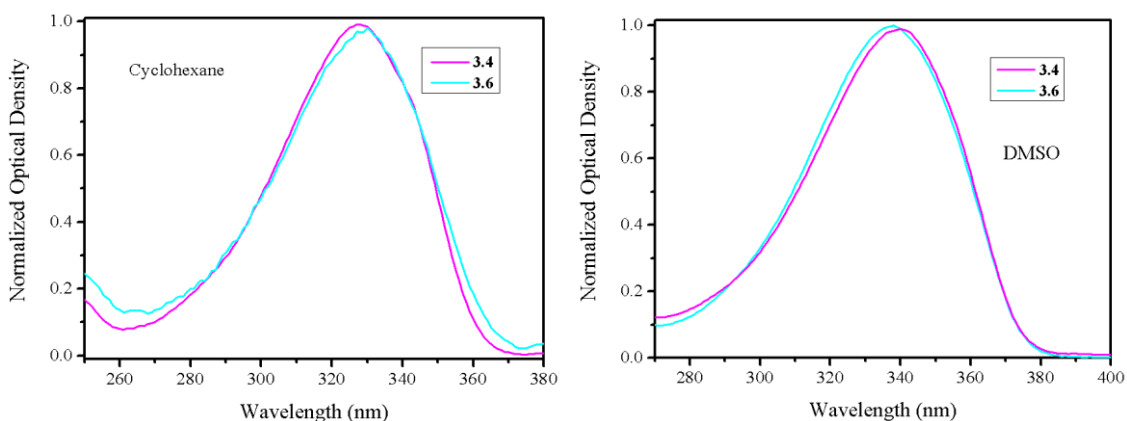


Figure 3.20. Normalized absorption spectra of **3.4** and **3.6** in cyclohexane (left) and in DMSO (right) solutions: both showing one single broad bell-like band.

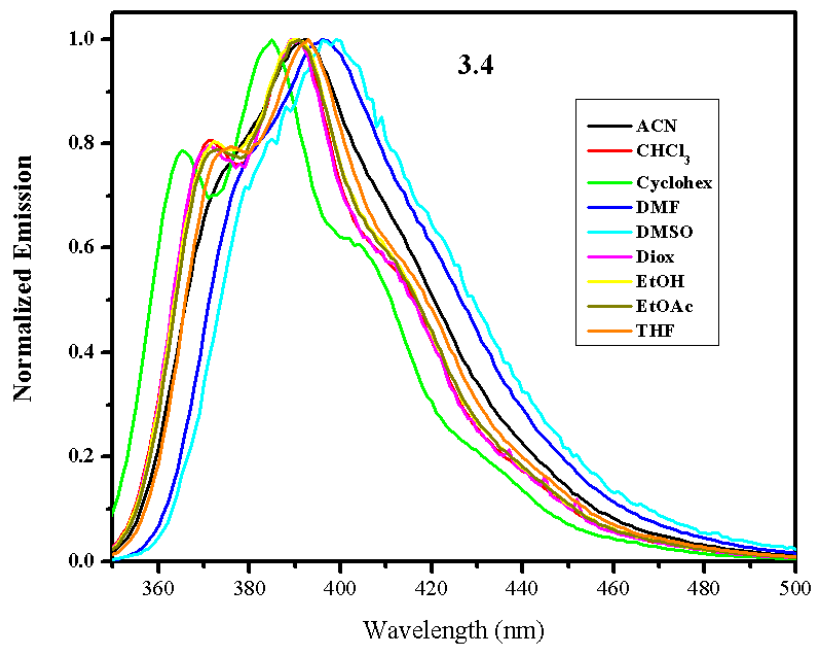


Figure 3.21. Normalized emission spectra of compound **3.4** in nine different solvents.

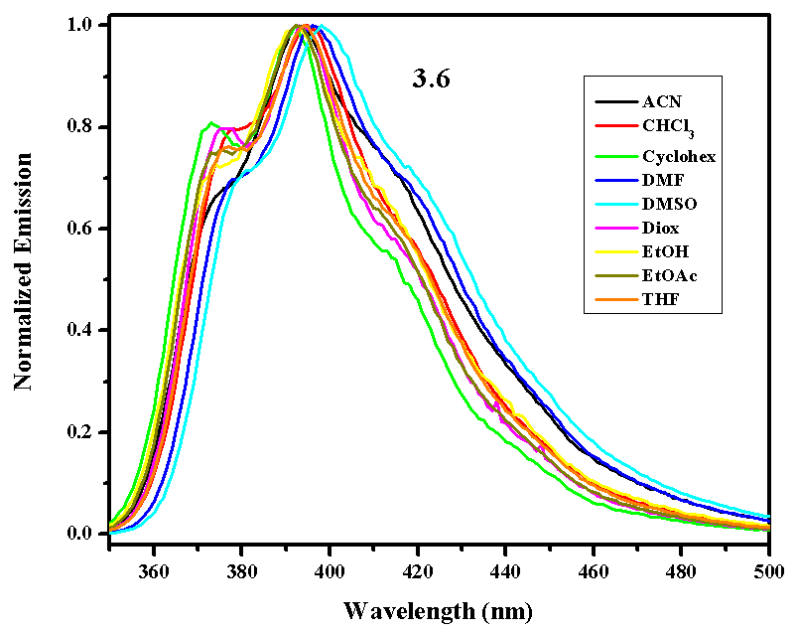


Figure 3.22. Normalized emission spectra of compound **3.6** in nine different solvents.

Table 3.2. Main photophysical properties of 2,7-diaryl-THP derivatives.

Compound	Solvent	λ_{max}^{em} , nm	λ_{max}^{abs} , nm	$\Delta\lambda$ (cm ⁻¹)	$\Delta\lambda$ (eV)	ϕ_F
3.4	Acetonitrile	392	330	4793	0.59	0.83
	Chloroform	390	330	4662	0.58	0.85
	Cyclohexane	385	328	4514	0.56	0.86
	DMF	396	337	4421	0.55	1.00
	DMSO	399	340	4349	0.54	0.99
	1,4-Dioxane	391	331	4636	0.57	0.88
	Ethanol	390	331	4570	0.57	0.81
	Ethyl Acetate	391	332	4545	0.56	0.89
	THF	393	333	4585	0.57	0.99
3.6	Acetonitrile	392	332	4610	0.57	0.94
	Chloroform	394	332	4740	0.59	0.72
	Cyclohexane	392	330	4793	0.59	0.79
	DMF	396	337	4421	0.55	1.00
	DMSO	398	338	4460	0.55	1.00
	1,4-Dioxane	393	331	4766	0.59	0.84
	Ethanol	392	330	4793	0.59	1.00
	Ethyl Acetate	392	332	4610	0.57	0.98
	THF	394	333	4649	0.58	1.00
3.12 ²⁴	Acetonitrile	376	323	4364	0.54	0.19
	Cyclohexane	376	321	4557	0.57	0.48
	Dichloromethane	380	322	4740	0.59	1.00
	DMF	381	326	4428	0.55	0.56
	Ethanol	375	320	4533	0.56	0.18
	Hexane	374	320	4512	0.56	0.55
	Methanol	375	322	4389	0.54	0.24
	THF	378	323	4504	0.56	0.81
	Toluene	381	325	4521	0.56	1.00
	Thin film	425	360	4248	0.53	0.45
	3.13 ²⁴	Acetonitrile	383	328	4378	0.54
Cyclohexane		383	327	4471	0.55	0.61
Dichloromethane		387	329	4555	0.56	1.00
DMF		387	332	4280	0.53	0.66
Ethanol		383	326	4565	0.57	0.48
Hexane		381	327	4334	0.54	0.52
Methanol		382	330	4125	0.51	0.39
THF		385	330	4329	0.54	0.68
Toluene		388	330	4530	0.56	1.00
Thin film		---	311	---	---	0.76

3.14²⁴	Acetonitrile	389	330	4596	0.57	0.60
	Cyclohexane	387	328	4648	0.58	0.81
	Dichloromethane	391	332	4545	0.56	1.00
	DMF	392	334	4430	0.55	0.55
	Ethanol	387	326	4835	0.60	0.53
	Hexane	385	327	4607	0.57	0.92
	Methanol	387	328	4648	0.58	0.45
	THF	390	331	4754	0.59	0.76
	Toluene	392	333	4520	0.56	1.00
	Thin film	431	306	9478	1.18	0.52

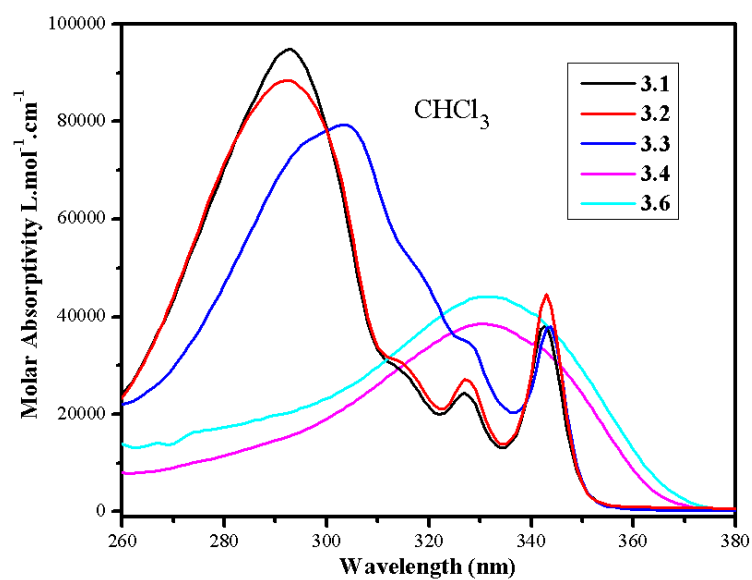


Figure 3.23. Molar absorptivity of compounds **3.1**, **3.2**, **3.3**, **3.4** and **3.6** in chloroform.

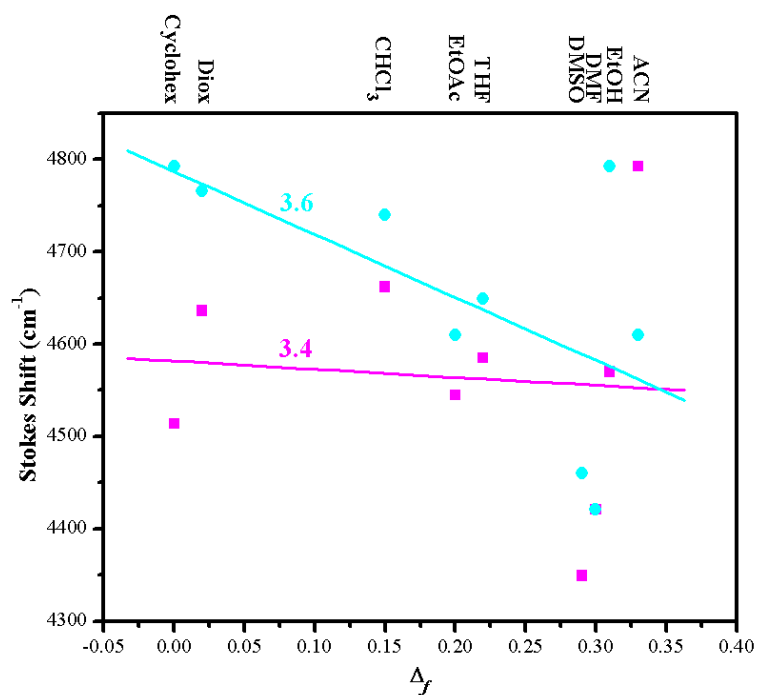


Figure 3.24. Stokes shifts vs. orientation polarizability for compounds **3.4** and **3.6** with linear fitting in the nine selected solvents.

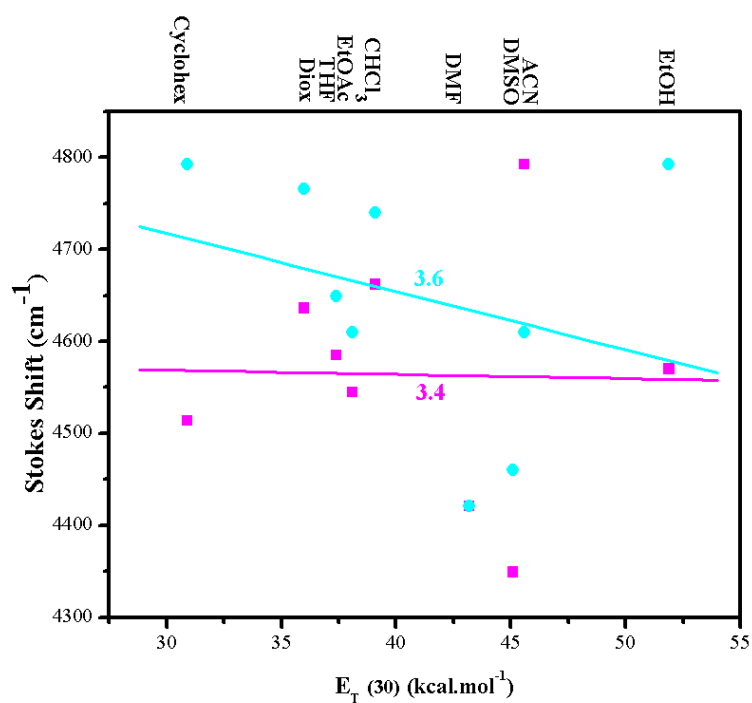


Figure 3.25. Stokes shifts vs. empirical solvent polarity for compounds **3.4** and **3.6** with linear fitting in the nine selected solvents.

3.2.2.6. Absence of Excimer Formation in Dilute Solution

The excitation and emission spectra were collected for compounds **3.1**, **3.2**, **3.3**, **3.4** and **3.6** at different wavelengths in different solvents. These spectra showed complete overlap if normalized. The maximum wavelengths did not change in all these spectra. This rules out the excimer formation for these derivatives in dilute solution. This observation regarding the absence of excimer in the concentration range used for photophysical studies was previously discussed for the 1,3,6,8-tetraarylpyrene derivatives reported in Chapter 2, Paragraph 2.2.2.5. The spectra of compound **3.2** are presented in cyclohexane and DMSO in Figures 3.26 and 3.27, respectively.

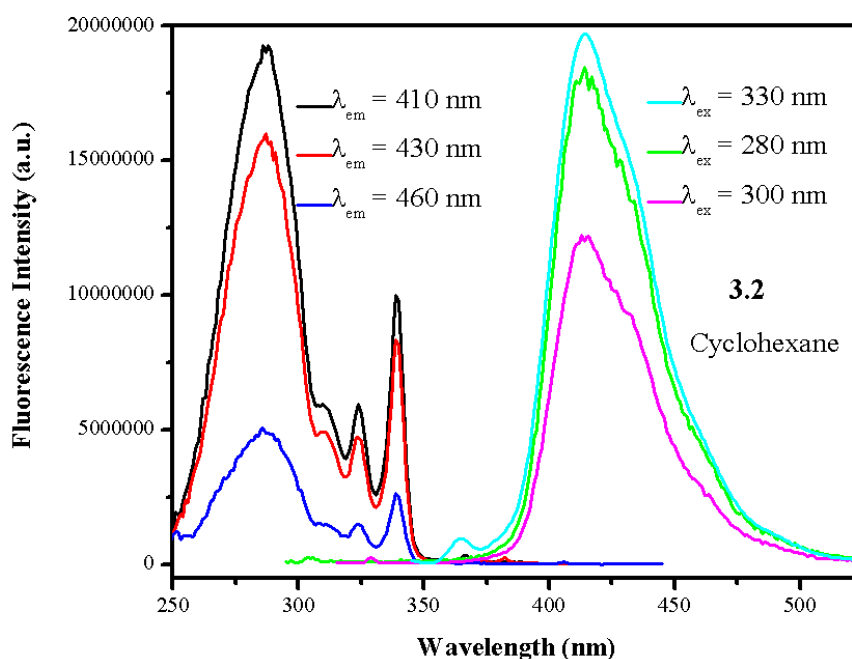


Figure 3.26. The excitation and emission spectra of **3.2** in cyclohexane collected at different wavelengths.

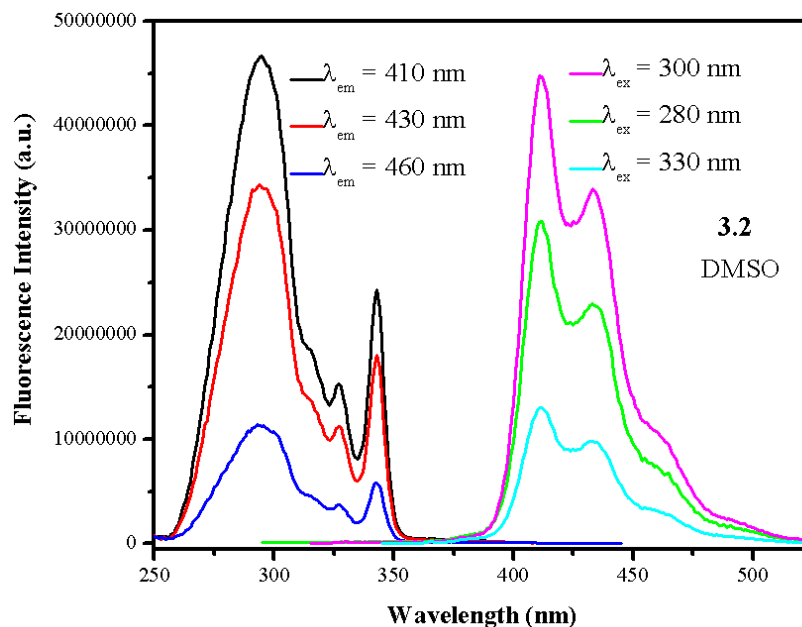


Figure 3.27. The excitation and emission spectra of **3.2** in DMSO collected at different wavelengths.

3.2.3. Thermal Analysis

The fluorinated derivatives **3.1** and **3.4** show the lowest decomposition temperatures, and did not melt before decomposing, Table 3.3. This thermal stability trend mimics the one observed and elaborated in details in Chapter 2, paragraph 2.2.3. 2,7-Diarylpyrene compounds showed higher melting and decomposition temperatures than their corresponding 2,7-diaryl-4,5,9,10-tetrahydropyrene derivatives. This might be explained by the increased planar character in the former, which allows more contact and interactions such as π - π stacking between adjacent molecules, Figure 3.28.

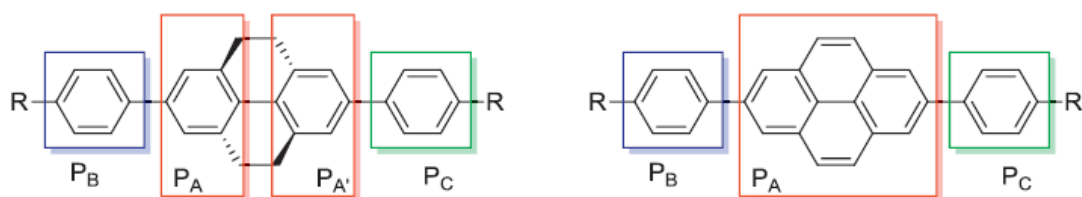


Figure 3.28. 2,7-Diaryl-THP (left) vs. 2,7-diaryropyrene (right).²⁴

Table 3.3. Thermal properties of the novel compounds studied as compared to DPPy.

Compound	Empirical Formula	Molecular weight, g.mol ⁻¹	%wt Fluorine	T_m (°C) ± 0.5	T_d (°C)
DPPy ¹⁰⁴	C ₂₈ H ₁₈	354.44	--	316	338
3.1	C ₃₂ H ₁₄ F ₁₂	626.43	36.39	> T_d	300.0
3.2	C ₄₄ H ₅₀	578.87	--	321.3	342.6
3.3	C ₃₄ H ₃₀ O ₆	534.60	--	253.2	396.0
3.4	C ₃₂ H ₁₈ F ₁₂	630.47	36.16	> T_d	277.4
3.6	C ₃₄ H ₃₄ O ₆	538.63	--	250.6	326.0

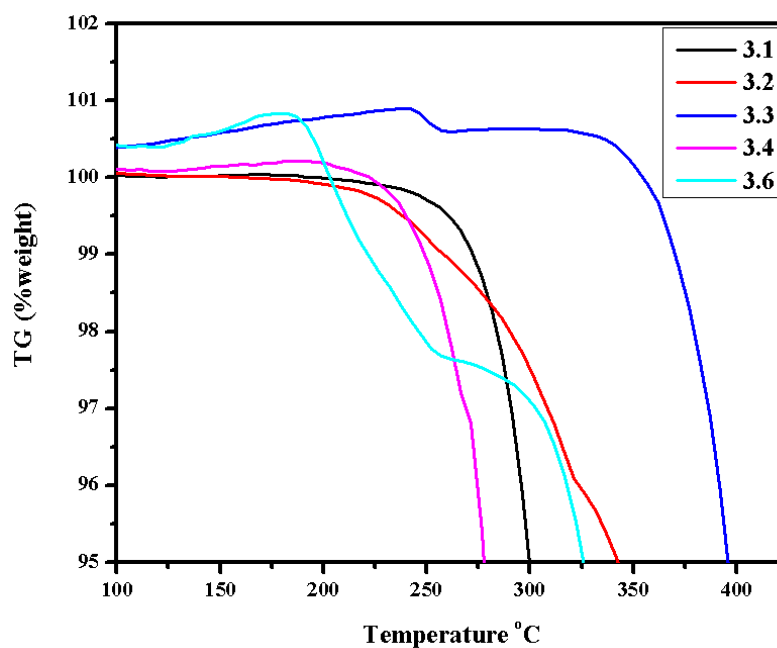


Figure 3.29. TGA results illustrating the thermal decomposition upon heating for all the compounds reported in this Chapter.

3.3. Conclusions and Future Work

Novel 2,7-Diarylpyrene and 2,7-diaryl-THP derivatives were investigated in comparison to selected model compounds from the literature. The study focused on the photophysical properties of these derivatives. An interesting common observation for all these derivatives is that the emission quantum yield increases with increasing number of substituents on the outer phenyl ring. This could be due to both steric inhibition of unwanted interactions between adjacent molecules and the electronic effect of the substituents. Another conclusion, that still needs further investigation, is the one regarding the trifluoromethyl substituent, which despite being the strongest electron-withdrawing among the investigated ones, an interesting observation was a bathochromic shift in both 2,7-diarylpyrene (**3.1**) and 2,7-diaryl-THP (**3.4**) derivatives, comparable to the strongest electron-releasing groups in both cases. This is against the trends reported for the *para*-substituted compounds (**3.7-3.9** and **3.12-3.14**). Further investigations may include the synthesis and characterization of compounds **3.10** and **3.11**, which can serve as model compounds in order to check if the bathochromic shift is related to the introduction of the trifluoromethyl at the *meta*-position instead of *para*, or due to the electronic effect of this substituent itself.

Furthermore, the inversion of allowed L_a and forbidden L_b transitions of pyrene (the main factor that enhances the emission quantum yield), does not occur upon substituting pyrene by benzene rings on positions 2 and 7. In contrast to positions 1, 3, 6 and 8, where this inversion does occur, and leads to high emission quantum yields, as discussed in Chapter 2. The inversion also occurs also upon moving from biphenyl to *para*-quaterphenyl and 2,7-diaryl-THP compounds. This explains their high emission quantum yields, approaching unity.

3.4. Experimental

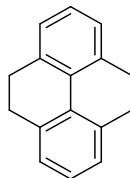
3.4.1. Synthesis

All reactions were run using clean and oven dried glassware. Melting points (mp) were determined using a digital automatic melting point meter (Krüss M5000) that can detect melting points up to 410 °C with an error margin of 0.5 °C. Decomposition temperatures (T_d) were determined using a NETZSCH thermogravimetric analyzer and were defined to be as a loss of 5% of the initial sample mass upon heating at a 10 °C/min rate; under continuous flow of nitrogen gas in order to ensure a completely inert atmosphere inside the heating chamber during measurements. All NMR experiments were performed in chloroform-d as solvent, using TMS as internal standard. NMR spectra were acquired using 300 MHz and 500 MHz Bruker NMR machines. Elemental analyses were performed at Atlantic Microlab, Inc., Norcross, USA. The C-F coupling constants values reported in Chapter 2, Table 2.16,¹²¹ were used to interpret the ¹³C NMR spectrum of compound **3.4**, in which long-range C-F coupling was observed.

4,5,9,10-Tetrahydropyrene (2.15)

The title compound was synthesized according to a modified literature procedure.¹³⁶ Pyrene **2.1** (10.00 g, 49.44 mmols) was dissolved in 100 mL ethyl acetate. A suspension of activated Raney Nickel in 100 mL ethyl acetate was then added, and the mixture was kept stirring for 3 days at room temperature. Raney Nickel was filtered off, and 1.40 g of Pd/C (10% Pd) was added. The mixture was shaken in a Parr hydrogenator for 5 days at 40 psi H. Pd/C was then filtered off, and solvent was removed under reduced pressure. 4,5,9,10-Tetrahydropyrene **2.15** (9.70 g, 95%) was

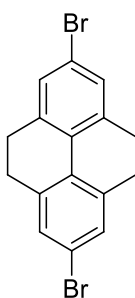
obtained as a white solid, and was used directly for the next step without any further purification. ^1H NMR (300 MHz, CDCl_3): δ 7.05-7.15 (m, 6H), 2.87 (s, 8H).



2.15

2,7-Dibromo-4,5,9,10-tetrahydropyrene (2.16)

The title compound was synthesized according to a modified literature procedure.⁷⁸ 4,5,9,10-Tetrahydropyrene **2.15** (5.00 g, 24.24 mmols) was dissolved in 160 mL of acetic acid, to which a stirred solution of Br_2 (8.52 g, 2.75 mL, 53.33 mmols, 2.2 eqv) and NaOH (2.13 g, 53.33 mmols, 2.2 eqv) in 160 mL of distilled water was added dropwise over one hour while stirring in an ice bath. The mixture was then stirred vigorously overnight at room temperature. The obtained yellow precipitate was then isolated by vacuum filtration and recrystallized from ethanol. This yielded pure 2,7-Dibromo-4,5,9,10-tetrahydropyrene **2.16** (7.94 g, 90%), mp 219.7 °C (Lit.⁷⁸ 218-219 °C). ^1H NMR (500 MHz, CDCl_3): δ 7.21 (s, 4H), 2.81 (s, 8H). ^{13}C NMR (125 MHz, CDCl_3): δ 137.09, 128.90, 128.40, 120.82, 27.82.



2.16

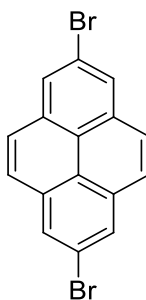
2,7-Dibromopyrene (2.17)

The title compound was synthesized according to a modified literature procedure.⁷⁹ 2,7-Dibromo-4,5,9,10-tetrahydropyrene **2.16** (5.00 g, 13.73 mmols) was dissolved in 120 mL CS₂, to which a stirred solution of Br₂ (11.00 g, 3.55 mL, 30.21 mmols, 2.2 eqv) in 120 mL CS₂ was added dropwise over one hour. The mixture was then stirred for 4 hours at room temperature. Solvent was removed under reduced pressure.

It is of high importance to consider the following three experimental remarks:

- Not to run the reaction for more or less than 4 hours.
- To avoid using more or less than 2.2 eqv of bromine.
- To avoid excessive heating during the removal of the solvent under reduced pressure.

These errors were found to increase the amount of side products including partial oxidation or further bromination after oxidation. The crude brown solid was recrystallized from 1,2-dichlorobenzene to yield pure 2,7-dibromopyrene **2.17** (2.48 g, 50%), mp 324.2 °C (Lit.⁷⁹ > 230 °C) as beige brownish solid. ¹H NMR (500 MHz, CDCl₃): δ 8.31 (s, 4H), 8.02 (s, 4H). ¹³C NMR (125 MHz, CDCl₃): δ 132.36, 127.88, 127.55, 122.89, 120.29.



2.17

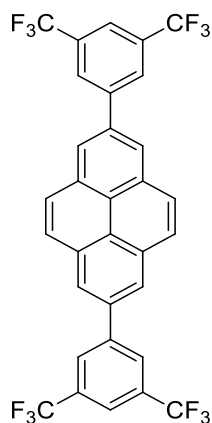
General procedure²³ used for the synthesis of 2,7-diarylpyrene derivatives

3.1-3.3:

2,7-Dibromopyrene **2.17** (0.35 g, 0.97 mmols) and the corresponding boronic acid (for **3.1** and **3.3**) or boronic ester (for **3.2**) (2.91 mmol, 3 eqv) were added to 30 mL of toluene followed by 3 mL of 2 M aqueous K₂CO₃, and a catalytic amount (~ 10 mg) of tetrabutylammonium bromide. The mixture was purged with argon for 20 min, before the freshly synthesized tetrakis(triphenylphosphine)-palladium(0) (67 mg, 0.057 mmol) was added and the mixture was refluxed under argon atmosphere and in the dark at 110 °C, for 48 hrs for compounds **3.2** and **3.3**, while for 72 hrs for compounds **3.1**. After evaporation of the solvent under reduced pressure, the obtained solid was triturated with chloroform using a Soxhlet extraction apparatus. The chloroform extract was then washed with 5% K₂CO₃ aqueous solution (2 x 50 mL) followed by brine (2 x 50 mL). The organic phase was dried over MgSO₄ and filtered, and the solvent was removed under reduced pressure.

2,7-Bis(3,5-bis(trifluoromethyl)phenyl)pyrene (3.1)

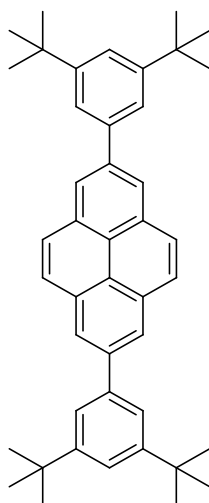
The obtained orange solid has a moderate solubility in chloroform, this allows recrystallization from this solvent. 2,7-Bis(3,5-bis(trifluoromethyl)phenyl)pyrene **3.1** (0.14 g, 23 %) mp > T_d was obtained as shiny yellow solid. T_d = 300.0 °C. ¹H NMR (300 MHz, CDCl₃): δ 8.45 (s, 4H), 8.33 (s, 4H), 8.25 (s, 4H), 7.97 (s, 2H). No ¹³C NMR data could be collected due to low solubility. Anal. Calcd: C, 61.35; H, 2.25. Found: C, 61.26; H, 2.42.



3.1

2,7-Bis(3,5-di-*tert*-butylphenyl)pyrene (3.2)

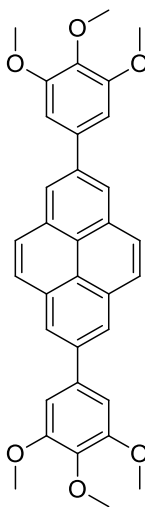
The obtained grey solid was recrystallized from heptane, and 2,7-bis(3,5-di-*tert*-butylphenyl)pyrene **3.2** (0.05 g, 9%), mp 321.3 °C, was isolated as shiny white crystals. $T_d = 342.6$ °C. $^1\text{H NMR}$ (500 MHz, CDCl_3): δ 8.32 (s, 4H), 8.11 (s, 4H), 7.64 (d, $J = 2$ Hz, 4H), 7.47 (t, $J = 2$ Hz, 2H), 1.40 (s, 36H). $^{13}\text{C NMR}$ (125 MHz, CDCl_3): δ 151.38, 141.00, 140.19, 131.42, 127.88, 124.17, 123.70, 122.64, 122.02, 35.11, 31.63. Anal. Calcd: C, 91.29; H, 8.71. Found: C, 91.32; H, 8.83.



3.2

2,7-Bis(3,4,5-trimethoxyphenyl)pyrene (3.3)

The obtained dark brown solid was recrystallized from chlorobenzene, and 2,7-bis(3,4,5-trimethoxyphenyl)pyrene **3.3** (0.06 g, 12%) mp 253.2 °C, was isolated as shiny yellow solid. $T_d = 396.0$ °C. $^1\text{H NMR}$ (300 MHz, CDCl_3): δ 8.37 (s, 4H), 8.17 (s, 4H), 7.07 (s, 4H), 4.03 (s, 12H), 3.96 (s, 6H). No $^{13}\text{C NMR}$ data could be collected due to low solubility. Anal. Calcd: C, 76.39; H, 5.66. Found: C, 76.24; H, 5.76.



3.3

General procedure²³ used for the synthesis of 2,7-diaryl-4,5,9,10-tetrahydropyrene compounds **3.4-3.6**:

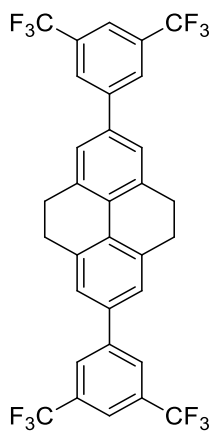
2,7-Dibromo-4,5,9,10-tetrahydropyrene **2.16** (0.35 g, 0.96 mmols) and the corresponding boronic acid (for **3.4** and **3.6**) or boronic ester (for **3.5**) (2.88 mmol, 3 eqv) were added to 30 mL of toluene followed by 3 mL of 2 M aqueous K_2CO_3 , and a catalytic amount (~ 10 mg) of tetrabutylammonium bromide. The mixture was purged with argon for 20 min, before the freshly synthesized tetrakis(triphenylphosphine)-palladium(0) (67 mg, 0.057 mmol) was added and the mixture was refluxed under argon atmosphere and in the dark at 110 °C, for 48 hrs for compounds **3.5** and **3.6**, while for

72 hrs for compounds **3.4**. After evaporating the solvent under reduced pressure, the obtained residue was triturated with chloroform using a Soxhlet extraction apparatus. The chloroform extract was then washed with 5% K_2CO_3 aqueous solution (2 x 50 mL) followed by brine (2 x 50 mL). The organic phase was dried over $MgSO_4$ and filtered, and the solvent was removed under reduced pressure.

2,7-Bis(3,5-bis(trifluoromethyl)phenyl)-4,5,9,10-tetrahydropyrene (3.4)

The obtained grey solid was recrystallized from toluene was performed to yield a light grey solid. The recrystallized solid, showing impurities on TLC using hexane as mobile phase, was purified by column chromatography using hexane to 5% chloroform in hexane as mobile phase.

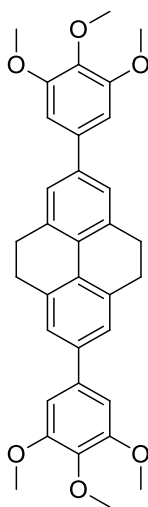
Pure 2,7-bis(3,5-bis(trifluoromethyl)phenyl)-4,5,9,10-tetrahydropyrene **3.4** (0.15 g, 25%), mp > T_d , was isolated as white needles. $T_d = 277.4$ °C. 1H NMR (300 MHz, $CDCl_3$): δ 7.99 (s, 4H), 7.79 (s, 2H), 7.30 (s, 4H), 2.97 (s, 8H). ^{13}C NMR (75 MHz, $CDCl_3$): δ 142.29, 136.39, 135.59, 131.89 (q, $^2J_{C-F} = 33$ Hz), 129.71, 127.90 (q, $^1J_{C-F} = 271$ Hz), 126.03 (q, $^3J_{C-F} = 2.86$ Hz), 124.03, 119.86 (q, $^3J_{C-F} = 3.77$ Hz), 27.33. Anal. Calcd: C, 60.96; H, 2.88. Found: C, 60.69; H, 2.77.



3.4

2,7-Bis(3,4,5-trimethoxyphenyl)-4,5,9,10-tetrahydropyrene (3.6)

The obtained dark brown solid was recrystallized from heptane to yield an orange brownish solid that showed impurities on TLC using hexane as mobile phase. Column chromatography using hexane to 5% chloroform in hexane as eluent was performed, and pure 2,7-bis(3,4,5-trimethoxyphenyl)-4,5,9,10-tetrahydropyrene **3.6** (0.10 g, 19%), mp 250.6 °C, was obtained as light orange solid. $T_d = 326.0$ °C. $^1\text{H NMR}$ (300 MHz, CDCl_3): δ 7.22 (s, 4H), 6.75 (s, 4H), 3.88 (s, 12H), 3.84 (s, 6H), 2.93 (s, 8H). $^{13}\text{C NMR}$ (75 MHz, CDCl_3): δ 153.42, 140.19, 137.47, 137.27, 135.79, 129.65, 124.77, 104.19, 61.02, 56.22, 28.48. Anal. Calcd: C, 75.82; H, 6.36. Found: C, 76.10; H, 6.48.



3.6

3.4.2. *Photophysical Studies*

Absorption spectra were measured using a double-beam JASCO V-570 UV-vis-NIR spectrophotometer, and the fluorescence measurements were done using a Jobin-Yvon-Horiba Fluorolog III spectrofluorometer. The excitation source was a 100 W xenon lamp, and the detector used was R-928 operating at a voltage of 950 V. Right angle mode detection was used. Slit widths were fixed at 5 nm for both entrance and exit slits during both emission and excitation experiments. Corrected emission spectra S_1/R_1 were collected to account for any fluctuation in the xenon lamp over different wavelengths. In parallel to that, S_1 spectra were collected to make sure that the intensity of emission is below 2×10^6 counts per second in order to avoid saturation of the detector. A blank measurement with no sample in the sample holder was subtracted from all actual spectra to account for any error possible due to the sample holder.

Stock solutions of concentration ranging from 0.5-5 mM of each compound were prepared in chloroform depending on the solubility limit of each compound. Around 0.1 mL of each stock solution was transferred into nine dry glass vials and chloroform was left to evaporate. Then the corresponding solvent was added and diluted to 100 μ M for absorption measurements and to 1-2 μ M for fluorescence studies. Stock solutions were kept in the freezer and used discarded if not used within two days. Molar absorptivity was determined in chloroform due to a decent solubility of all compounds in this solvent. Quantum yield measurements were done using 9,10-diphenylanthracene in cyclohexane as standard with an attributed quantum yield of 1.00.⁹⁹ Excitation wavelength was set to 330 nm for all compounds and the standard. Quantum yield measurements were performed on nitrogen-purged solutions, and optical density was maintained below 0.05 for all samples. UV-transparent quartz cuvette (1 x 1 cm) was

used for all experiments. Molar absorptivity and quantum yield were performed as three runs for each compound in every single solvent, and the average value of the three runs was reported. A fourth run was performed in case non-consistent results were obtained in one of the first three runs.

CHAPTER 4

TERCARBAZOLE-BASED D-A-D AND D-A COMPOUNDS

4.1. Introduction

Carbazole is a blue emitter heterocyclic aromatic compound having excellent hole-transport properties for OLED application.¹³⁷ This is due to its electron-rich character (i.e. good electron-donor and hole-acceptor). The structure of carbazole is shown in Figure 4.1. In addition to this, carbazole derivatives have a high energy triplet state, which allows it to be an excellent host for triplet-emitting guests in phosphorescent OLEDs (PHOLEDs),¹³⁸ and for thermally-activated delayed fluorescence (TADF).¹³⁹ Due to its excellent emission properties, it was reported as a core in fluorescent sensors for anions and cations,¹⁴⁰ the main topic of Chapter 5.

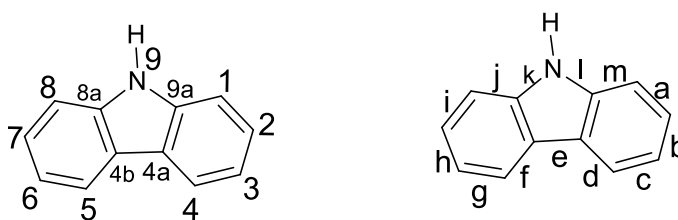


Figure 4.1. Numbering of atoms of carbazole (left), and labeling of edges (right). Numbers and letters were assigned following the IUPAC recommendations on nomenclature of fused and bridged fused ring systems.⁶⁴

The electron-rich character of carbazole makes it suitable to be a donor in D-A compounds (i.e. compounds having a donor and an acceptor).¹⁴¹ Investigating the properties of compounds with two fluorophores, carbazole as donor and another

aromatic fluorophore as acceptor, is an interesting field of research. Many acceptors were reported in the literature such as benzene, *para*-cyanobenzene, naphthalene and phenanthrene, Figure 4.2. These are known as D-A compounds, where carbazole is the donor D and the other is the acceptor A.¹⁴¹

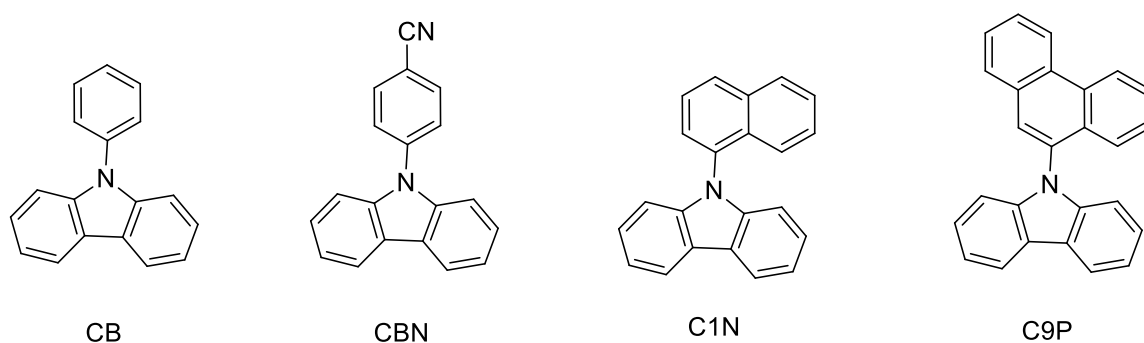


Figure 4.2. Structures of D-A compounds previously reported by Retting and Zander in 1982.¹⁴¹

Our research group previously reported the synthesis and characterization of D-A-D compounds, where two carbazole donors are connected on a single aromatic acceptor. Different acceptors were selected such as benzene, biphenyl, 4,5,9,10-tetrahydropyrene (THP) and pyrene (Py). The carbazole donors were studied with and without *tert*-butyl groups on positions 3 and 6, Figure 4.3.¹³⁷

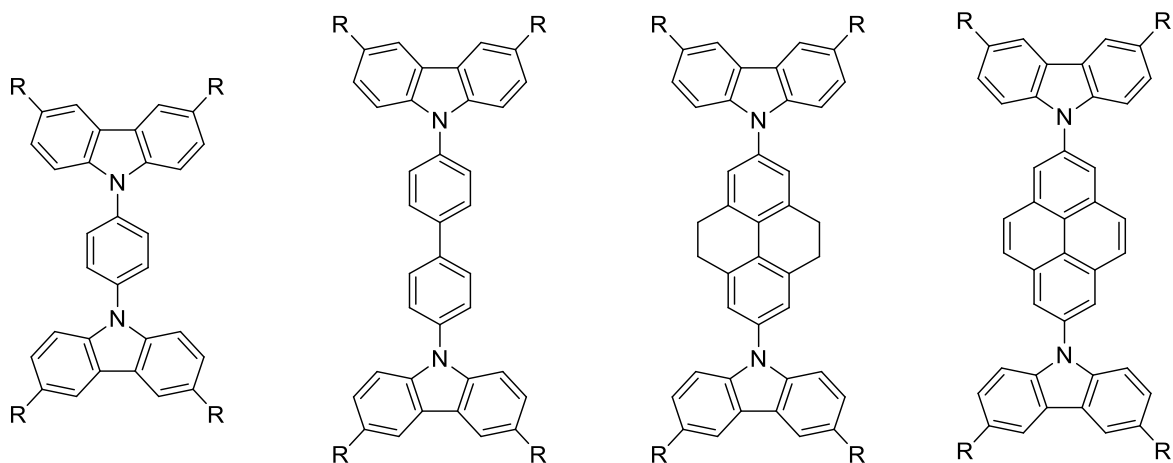


Figure 4.3. Structures of D-A-D compounds previously reported by our research group (R = H or *tert*-butyl).¹³⁷

Tercarbazole, Figure 4.4, has similar donor properties to those of carbazole, and has been suggested for similar applications.¹⁴² However, due to being more electron-rich than carbazole (i.e. a better donor), more interesting applications have been reported for tercarbazole-based derivatives. These included donor-acceptor induced molecular switches and dual emission, Figure 4.5.¹⁴³

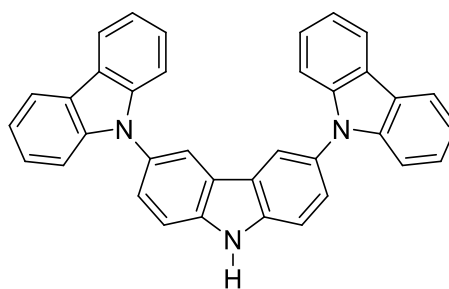


Figure 4.4. Structure of tercarbazole.

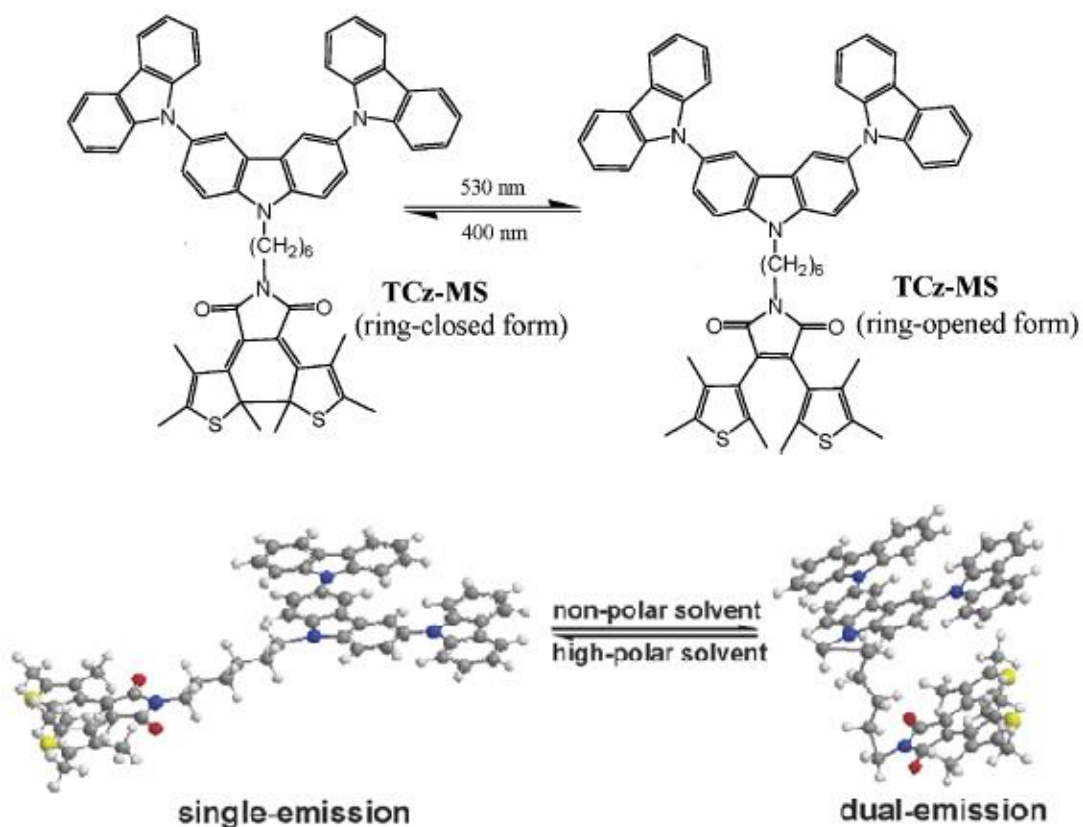


Figure 4.5. Tercarbazole applications in D-A systems reported by Zhao *et al.* in 2007: molecular switches from opened to closed rings leading to dual emission.¹⁴³ Reprinted with permission from (Zhao, Z.; Xing, Y.; Wang, Z.; Lu, P. *Org. Lett.* **2007**, *9*, 547). Copyright (2007) American Chemical Society.

In the present study, we investigate the photophysical properties of new D-A-D compounds using tercarbazole as donor. Pyrene and 4,5,9,10-tetrahydropyrene were selected as acceptors (compounds **4.5** and **4.9**, respectively). The two resulting D-A-D derivatives are not reported in the literature previously. The photophysical properties of these tercarbazole-donor derivatives is compared to that of carbazole-donor ones having the corresponding acceptor (**4.4** and **4.8**), which were reported by our group in 2013. Other D-A-D derivatives from the literature were also found to be excellent references for comparison purpose. These include both carbazole and tercarbazole as donors and phenanthroline as acceptor (**4.2** and **4.3**).

4.2. Results and Discussion

4.2.1. Substituent Effect on Positions 3, 6 and 9 of Carbazole

Substituting position 9 of carbazole with an alkyl group induces a bathochromic shift in its emission spectrum. The red shift has been explained by a selective destabilization of the HOMO orbital of carbazole.¹⁴⁴ More pronounced shift has been observed upon substituting this position with a phenyl group.¹⁴⁴

Furthermore, the substitution of carbazole with strong electron-releasing groups on positions 3 and 6, such as quaternary alkyl groups (*tert*-butyl) or amino groups, induces further bathochromic shifts in both absorption and emission wavelengths.¹⁴⁵ Similar findings were previously reported by our research group regarding the effect of *tert*-butyl substituents on positions 3 and 6 of carbazole, Figure 4.3 (R = H vs. R = *tert*-butyl).¹³⁷ The bulkiness of the *tert*-butyl substituents has been related to increase in thermal stability of the carbazole-containing system. Ho *et al.* reported a higher glass transition (T_g) and decomposition (T_d) temperatures for ttbCBP as compared to CBP, Figure 4.6.¹⁴⁵ The glass transition temperature is known to be one of the most important factors regarding the thermal stability of non-polymer material used in OLEDs (i.e. the higher the glass transition temperature, the more air-resistant the device will be). HTM materials for OLEDs are described as the “weakest link” regarding the thermal stability of the whole device. This makes the increase in thermal stability of carbazole and tercarbazole derivatives used for OLED application, which usually have HTM properties, one of the most essential needs in order to achieve a better device.¹⁴⁵

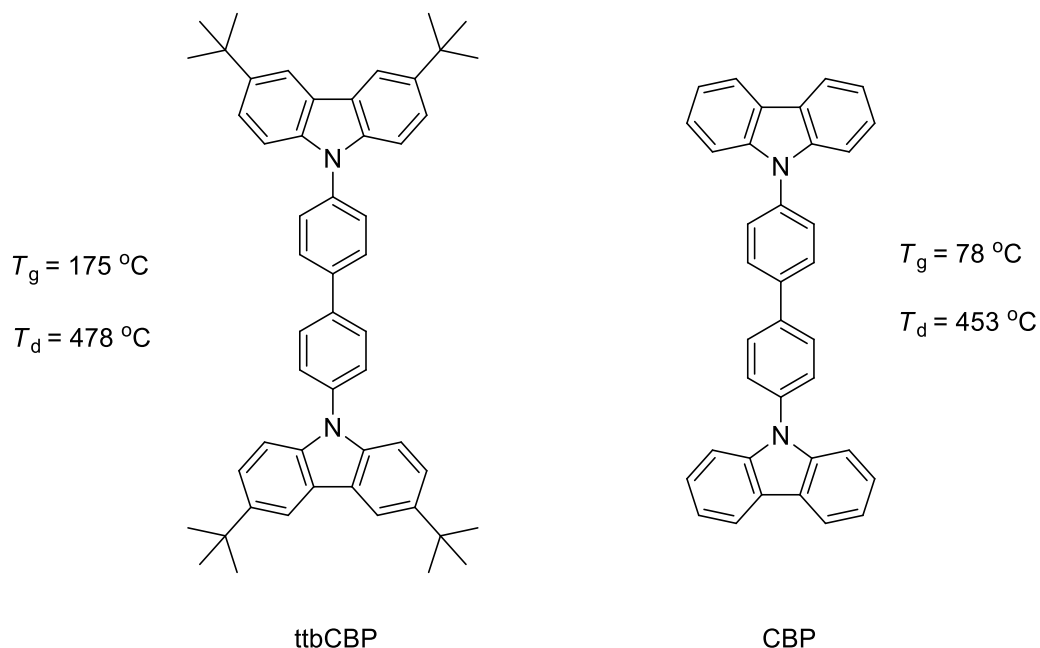


Figure 4.6. Structure of ttbCBP and CBP with their T_g and T_d (the glass transition and decomposition temperatures, respectively).¹⁴⁵

In addition to this, Ambrose *et al.* reported that blocking the C-3, C-6 and N-9 positions, also known as the reactive sites of carbazole, by inert substituents prevents unwanted dimerization or polymerization reactions through cation radicals.¹⁴⁶ The benefits of the 3,6-*tert*-butyl substitution extend also to the electrochemical properties of carbazole. It has been reported that the bulky substituent offers reversible electrochemistry to the system being studied.¹³⁷ Carbazole undergoes irreversible oxidation due to the coupling of carbazole radical through positions 3 and 6, when kept unsubstituted.¹³⁷

Due to the enhanced physical and chemical stability of the *tert*-butyl substituted carbazole at positions 3 and 6, the focus of this study is limited to derivatives having *tert*-butyl substituents on these positions.

4.2.2. Intramolecular Charge Transfer (ICT) State vs. Locally Excited (LE) State

Previous studies of carbazole and tercarbazole with aromatic acceptors show evidence for the existence of intramolecular charge transfer (ICT) states in many cases. An interesting study by Rettig and Zander in 1982 has compared the photophysical properties of CB, CBN, C1N, C9P, Figure 4.2, and concluded that the emission from ICT state takes place in polar solvents for these derivatives, except for CB, where no ICT emission occurs.¹⁴¹ This has been attributed to the weak acceptor character of benzene (in CB) as compared to a *para*-cyano benzene (in CBN) or to polyaromatic hydrocarbons (naphthalene in C1N and phenanthrene in C9P).¹⁴¹

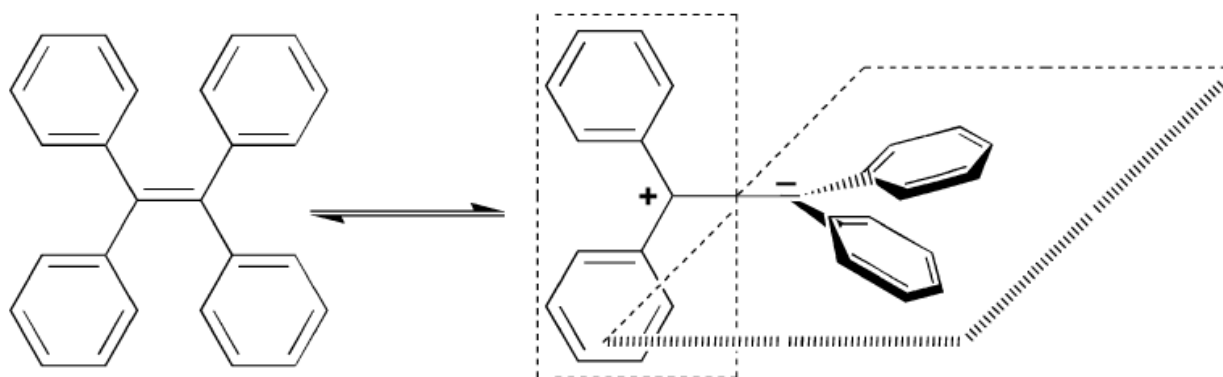


Figure 4.7. ICT from a steric perspective: tetraphenylethylene (TPE) – separation of charges leads to free rotation (twisting), and relieves the strain in the excited state.¹⁴⁷ Reprinted with permission from (Grabowski, Z. R.; Rotkiewicz, K.; Rettig, W. *Chem. Rev.* **2003**, *103*, 3899). Copyright (2003) American Chemical Society.

Intramolecular charge transfer is an excited state in which a complete separation of charges occurs before the emission takes place, Figure 4.7.¹⁴⁷ In this case, the initial excited state (before charge separation) is known as locally excited state (LE). The excited state following the charge separation is known as intramolecular charge transfer state (ICT). The theory behind the occurrence of ICT has been a well-debated one in the literature, and different approaches exist to explain it, Figures 4.7-4.9.¹⁴⁷

From a kinetic approach, if the separation of charges is fast enough ($k_a > k_d$, Figure 4.8), the emission occurs from the ICT state or from both LE and ICT states (dual fluorescence). If the charge separation is too slow ($k_a < k_d$), the emission will occur from LE exclusively.¹⁴⁸ Different factors can affect the rate of charge separation, which might include the polarity of the molecule itself (i.e. the inclusion of stronger donors and stronger acceptors makes the charge separation easier and faster),¹⁵ the polarity of the solvent (i.e. more polar solvents stabilize the separated charges and the larger dipole moment of the ICT state, as compared to non-polar solvents),¹⁴⁷ and the temperature of the medium (i.e. under very low temperature, the reorganization of the system from LE to ICT tends to be slower).¹⁵ This is presented in Figure 4.8, where k_a and k_d are affected by all the aforementioned factors.¹⁴⁸ From Le Chatelier perspective, the LE/ICT equilibrium is favored towards the formation of the shorter-lived state. In other words, a longer-lived ICT and a shorter-lived LE favor the equilibrium towards the formation of LE (vice-versa), and the emission takes place from LE, Figure 4.8.¹⁴⁸

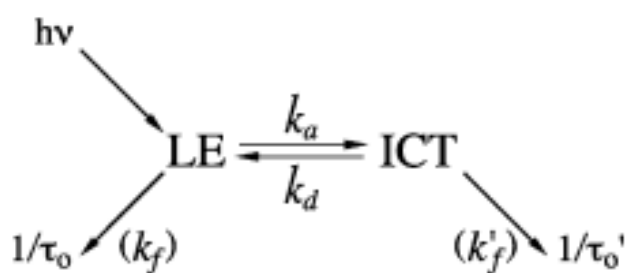


Figure 4.8. ICT state from a kinetic perspective: k_a vs. k_d .¹⁴⁸

Other explanations for ICT relate its occurrence to the pseudo Jan-Taller effect leading to a change in the excited states orbitals energy level. This renders the L_a state (S_1 in CT, S_2 in LE) lower in energy than L_b state (S_2 in CT, S_1 in LE), Figure 4.9. This suggests that the closer the gap between L_b and L_a the more favored the formation of CT will be. In such explanation, L_b can be regarded as responsible for LE emission and L_a for CT emission, Figure 4.9.¹⁴⁷

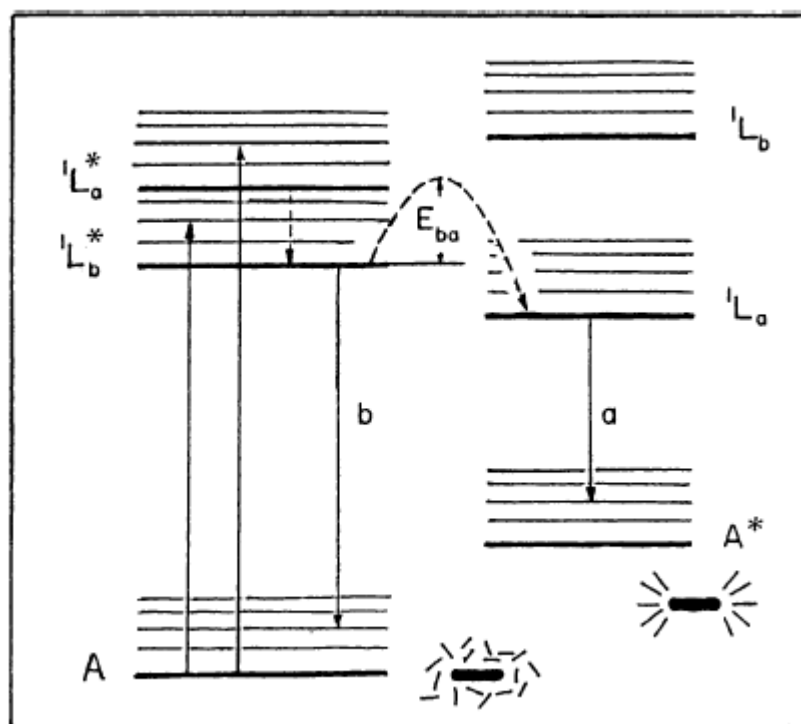


Figure 4.9. ICT from an electronic perspective: Lippert's approach - inversion of states in more polar solvents - the closer L_b and L_a in energy, the more favored is this inversion.¹⁴⁷ Reprinted with permission from (Grabowski, Z. R.; Rotkiewicz, K.; Rettig, W. *Chem. Rev.* **2003**, *103*, 3899). Copyright (2003) American Chemical Society.

Others suggest that twisting of the excited state, in order to become less strained, is the main reason behind the occurrence of CT.¹⁴⁷ In such cases, the twisted intramolecular charge transfer (TICT) state cannot be achieved without separation of charges. To illustrate the twisted ICT (TICT), a good example is tetraphenylethylene (TPE), in which the separation of charges enables the rotation and the subsequent relief of the excited state without the need of breaking the aromaticity of any of the four rings, Figure 4.7.¹⁴⁷

Suggested theories and approaches succeed in explaining the photophysical properties for some ICT systems, and fail in others. This is why in this Chapter, the term “ICT” will be used rather than “TICT” or any other described ICT, in order to avoid such debates which are beyond the scope of this thesis. Although it is good to mention that TICT is accepted for carbazole and tercarbazole D-A-D compounds, in which ICT emission is observed.¹⁴²

4.2.3. *Photophysical Properties of ICT State*

The occurrence of ICT state is usually characterized by different photophysical spectral behaviors including the following:^{15,147}

- Complete loss of vibrational structure in the emission peak attributed to the CT state.
- Significant bathochromic shift emission as compared to the LE state.
- Significant increase in fluorescence halfwidth as compared to the LE emission band.
- High dependence of the bathochromic shift in emission wavelength on the solvent polarity due to the increased dipole moment of the CT state as compared to the LE state.

Hence, the existence of these properties in the experimental spectra may suggest the presence of emission from a charge transfer state.

4.2.4. *ICT vs. LE in Carbazole and Tercarbazole Derivatives*

4.2.4.1. Phenanthroline as Acceptor

The photophysical properties of compounds **4.1**, **4.2** and **4.3**, Figure 4.10, studied by McClenaghan *et al.* in 2003 is presented in Table 4.1 and Figures 4.11-4.12.¹⁴²

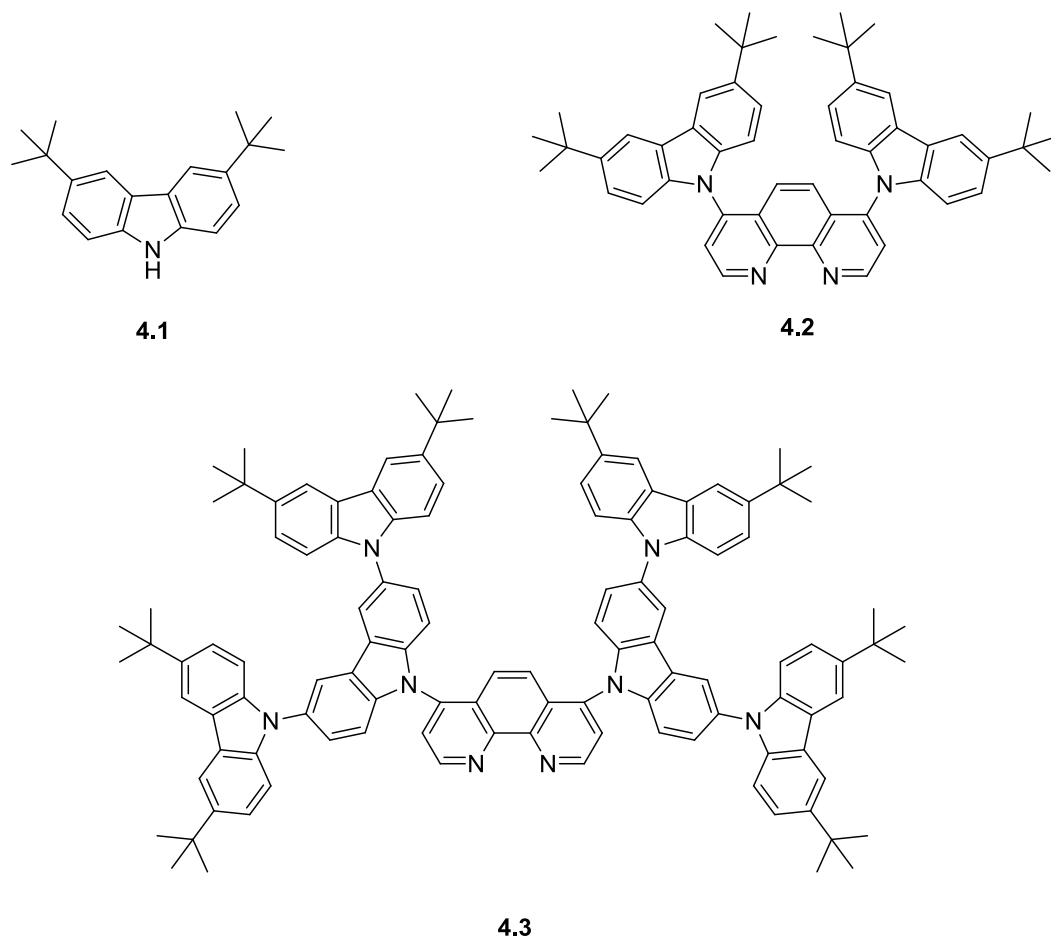


Figure 4.10. Structures of compounds **4.1-4.3** reported by McClenaghan *et al.* in 2003.¹⁴²

Table 4.1. Absorption and emission maxima of compounds **4.1-4.3** as reported by McClenaghan *et al.* in 2003 in oxygen-free acetonitrile solutions.¹⁴²

Compound	Substituent (D)	Bridge/Core (A)	λ_{max}^{abs} , nm, ($\epsilon \cdot 10^4 \text{ M}^{-1} \cdot \text{cm}^{-1}$)	λ_{max}^{em} , nm
4.1	--	--	236 (4.60), 248 (2.72), 260 (2.08), 295 (2.31), 327 (0.35)	352
4.2	Carbazole	Phenanthroline	232 (17.80), 260 (7.03), 289 (4.67), 338 (1.70), 358 (0.73)	486
4.3	Tercarbazole	Phenanthroline	235 (31.50), 266 (15.47), 295 (12.05), 333 (3.50), 346 (3.57)	530

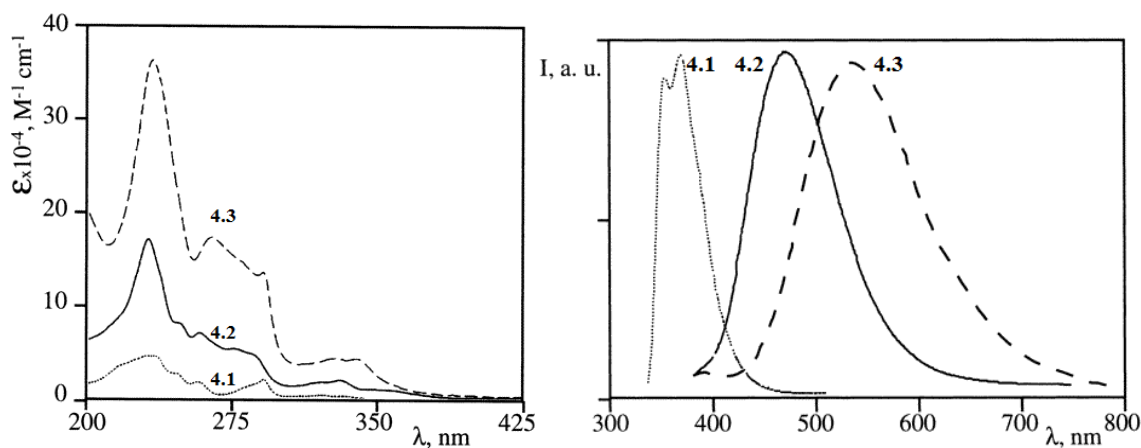


Figure 4.11. Molar absorptivity (left) and normalized emission (right) spectra of **4.1**, **4.2** and **4.3** in oxygen-free acetonitrile solutions.¹⁴² Reprinted with permission from (McClenaghan, N. D.; Passalacqua, R.; Loiseau, F.; Campagna, S.; Verheyde, B.; Hameurlaine, A.; Dehaen, W. *J. Am. Chem. Soc.* **2003**, *125*, 5356). Copyright (2003) American Chemical Society.

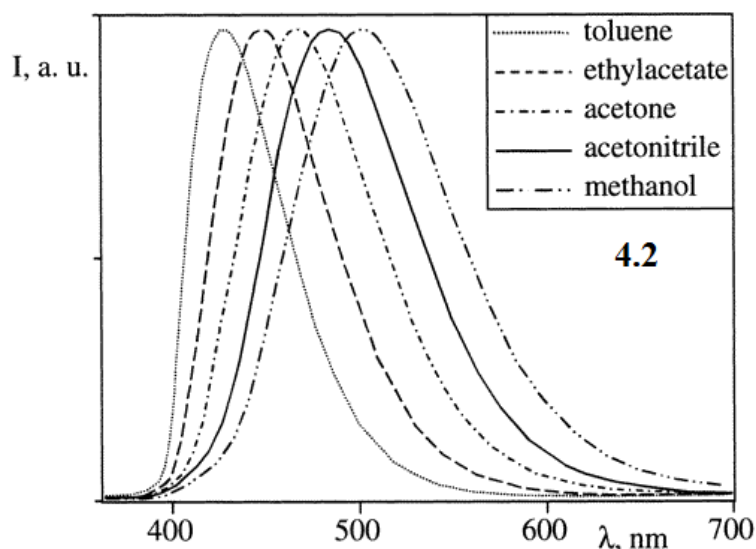


Figure 4.12. Normalized emission spectra of compound **4.2** in five different solvents illustrating the large bathochromic shift in emission wavelength with increasing solvent polarity.¹⁴² Reprinted with permission from (McClenaghan, N. D.; Passalacqua, R.; Loiseau, F.; Campagna, S.; Verheyde, B.; Hameurlaine, A.; Dehaen, W. *J. Am. Chem. Soc.* **2003**, *125*, 5356). Copyright (2003) American Chemical Society.

The absorption bands in **4.2** and **4.3** are assigned as follows: the band in the 230-240 nm region which is present in **4.1** is due to carbazole, and the one around 260 nm is due to contribution from both phenanthroline and carbazole, given the $\pi \rightarrow \pi^*$ transition of phenanthroline falls in this region.¹⁴² Bands falling above 300 nm are attributed to the twisted intramolecular charge transfer state TICT.¹⁴² In order to prove the occurrence of ICT, emission spectra of **4.1**, **4.2** and **4.3** in acetonitrile are overlaid, Figure 4.11 (right), and compared together.¹⁴² This comparison revealed a complete loss of the vibrational structure present in **4.1** for both emission spectra of **4.2** and **4.3**. In addition to this, a single emission peak with a large halfwidth is found for both **4.2** and **4.3**, characteristic of the emission from ICT state. Significant bathochromic shift has been noted upon moving from toluene to methanol was observed in the emission wavelength, Figure 4.12.¹⁴² An increase in the ratio of molar absorptivity of the bands coming from the ICT state (i.e. 330-360 nm) to the band at 260-265 nm for **4.3** as compared to **4.2**, Figure 4.11 (left) is consistent with increased ICT properties for **4.3** as compared to **4.2** in all previously mentioned spectral criteria (i.e. tercarbazole is a better donor than carbazole).¹⁴²

The absence of LE emission is explained by the very strong donor properties of carbazole and very strong acceptor properties of phenanthroline.¹⁴² Moreover, the more favored ICT for tercarbazole derivative (**4.3**) as compared to carbazole derivative (**4.2**) is attributed to the stabilization of the hole formed on carbazole by the two outer electron-rich carbazole subunits (in the case of tercarbazole). Thus, ICT in tercarbazole donor **4.3** is described as being more stable and more favored than in carbazole donor **4.2**.¹⁴² These conclusions are needed for the interpretation of the spectra of our new compounds.

4.2.4.2. Pyrene as Acceptor

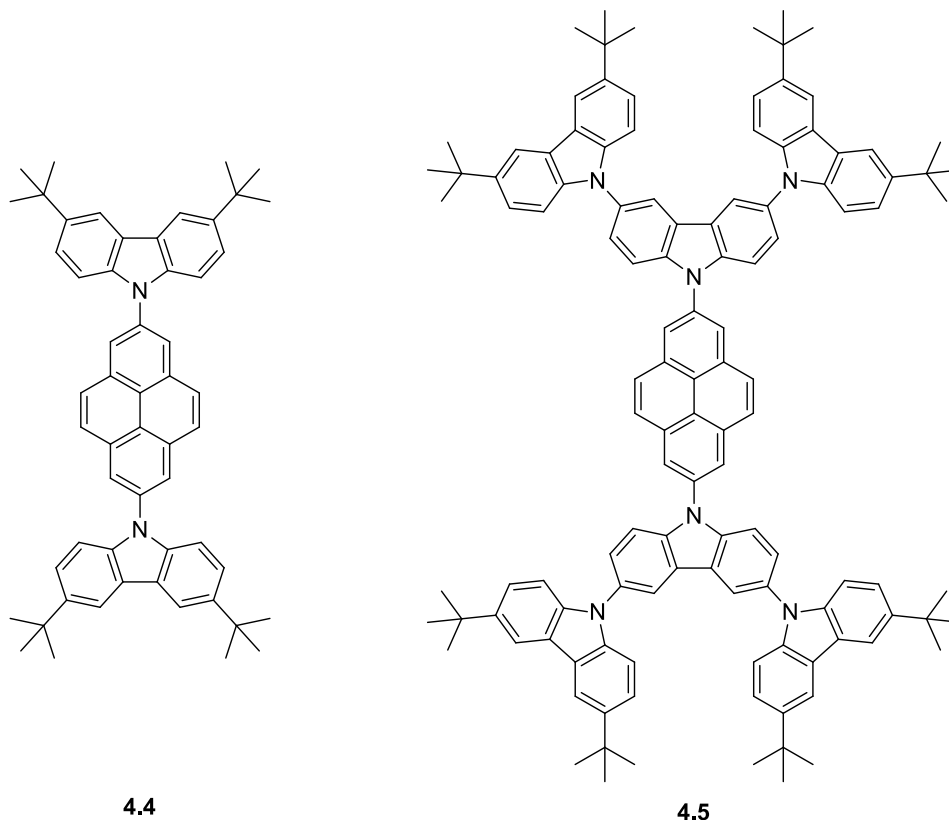


Figure 4.13. D-A-D compounds **4.4** and **4.5** having pyrene as acceptor.

In the absorption spectrum of compound **4.5**, the bands around 240 and 290 nm are attributed to carbazole. This is consistent with an increasing intensity of these bands in the tercarbazole compound **4.5** as compared to the carbazole compound **4.4**.

The absorption bands of lower intensity occurring above 300 nm, are attributed to $\pi \rightarrow \pi^*$ transitions. Interestingly, **4.4** and **4.5** have very similar emission profiles in cyclohexane, both with an emission maximum of 423 nm, Table 4.2. However, with increased solvent polarity, a much larger bathochromic shift was observed for the tercarbazole derivative **4.5**, as compared to the carbazole derivative **4.4**, Table 4.2.

Furthermore, the bathochromic shift of **4.5** is larger than the solvatochromic shifts observed in all other carbazole-based D-A-D compounds shown in Figure 4.3 (i.e. benzene, biphenyl and THP acceptors). This strongly suggests that in the case of **4.5** (with a bathochromic shift even larger than that of **4.4**), something that does not occur in the carbazole-based D-A-D derivatives of Figure 4.3, is taking place. Compound **4.5** has two emission bands. The band centered around 400 nm is barely affected by the solvent polarity variation. It can be attributed to the emission from the LE state. However, the other band exhibits a large bathochromic shift with increasing solvent polarity (i.e. up to around 540 nm in polar solvents). It can be attributed to the emission from the ICT state, Figure 4.17. Therefore, it might be suggested that compound **4.5** emits with dual fluorescence mode (from both LE and ICT) in polar solvents, and from the LE state in non-polar solvents. This is consistent with the findings of McClenaghan *et al.* about a more favored ICT state in tercarbazole derivatives as compared to carbazole. This explains why the tercarbazole derivative **4.5** showed a different behavior from that of the carbazole derivative **4.4** towards polarity variation. Experimental spectra of these compounds are presented in Figures 4.14-4.17.

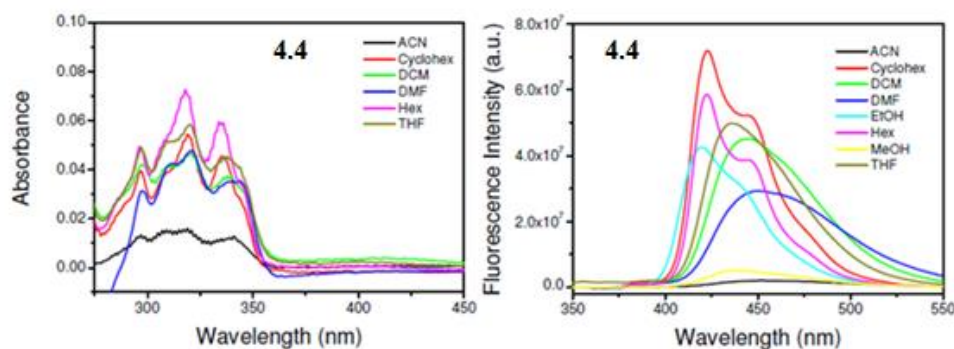


Figure 4.14. Absorption spectra (left) and emission spectra (right) of compound **4.4** in different solvents.¹³⁷ Reprinted from Kaafarani, B. R.; El-Ballouli, A. O.; Trattnig, R.; Fonari, A.; Sax, S.; Wex, B.; Risko, C.; Khnayzer, R. S.; Barlow, S.; Patra, D.; Timofeeva, T. V.; List, E. J. W.; Bredas, J.-L.; Marder, S. R. *J. Mater. Chem. C* **2013**, *1*, 1638. Published by The Royal Society of Chemistry.

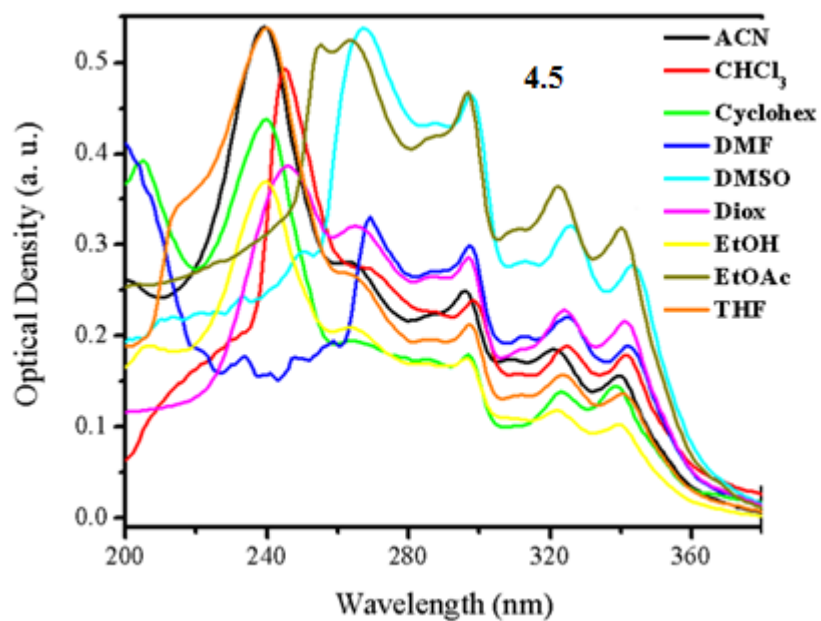


Figure 4.15. Absorption spectra of compound **4.5** in nine different solvents.

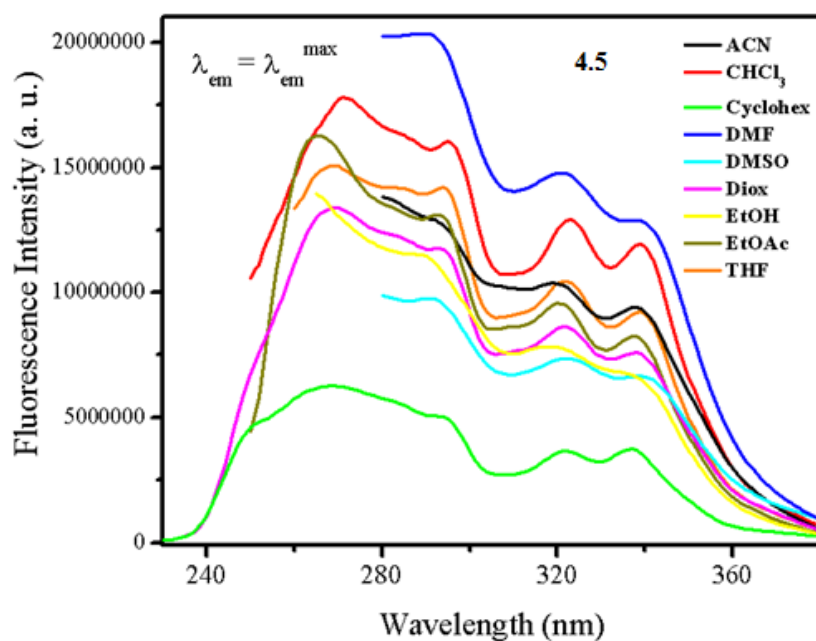


Figure 4.16. Excitation spectra of compound **4.5** in nine different solvents.

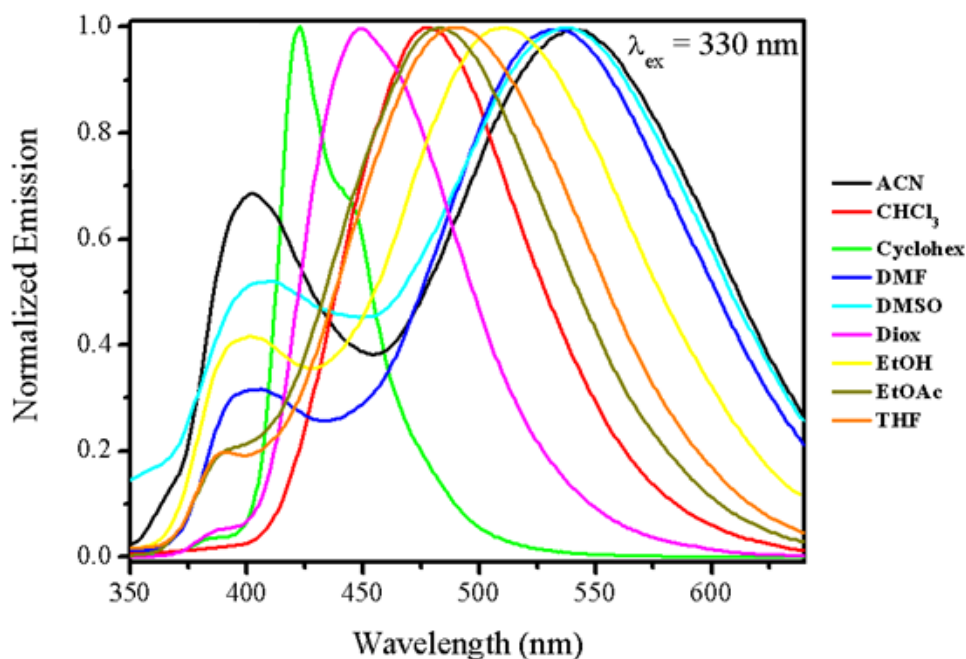


Figure 4.17. Normalized emission spectra of compound **4.5** in nine different solvents.

Table 4.2. Emission maxima of **4.4** and **4.5** in non-polar vs. polar solvent.

Compound	Substituent (D)	Bridge/Core (A)	λ_{max}^{em} , nm, cyclohexane	λ_{max}^{em} , nm, acetonitrile
4.4 ¹³⁷	Carbazole	Pyrene	423	451
4.5	Tercarbazole	Pyrene	423	539

Another observation that supports to a large extent the occurrence of ICT in the tercarbazole derivative **4.5** is noted in the fluorescence lifetime measurement results. The lifetime decays of the carbazole derivative **4.4** are all single-exponential, Table 4.3. Whereas double-exponential decays were observed in the case of **4.5**, Table 4.4, which might suggest the presence of two excited states in this compound. This analysis is further validated by the single-exponential decays observed for **4.5** in solvents that can be considered as polarity extremes exclusively (i.e. the non-polar 1,4-dioxane, and the polar DMF and acetonitrile). A single-exponential decay in the non-polar 1,4-dioxane clearly indicates that the emission takes place from the LE state exclusively in this solvent (i.e. the 100% populated excited state is the LE state).

Similarly, a single-exponential decay in the polar DMF and acetonitrile is an indicator of an emission from the ICT state (i.e. the 100% populated excited state is the ICT state). Interestingly, the lifetime of **4.5** significantly decreases with increasing solvent polarity. A decrease from 43-44 ns in 1,4-dioxane (LE) to 16-17 ns in acetonitrile and DMF (ICT) was noted. This suggests that the longer-lived state corresponds to the LE state.

Table 4.3. Fluorescence lifetime and emission quantum yield values in different solvents, in addition to the calculated radiative and non-radiative decay rate constants of compound **4.4** reported by our research group in 2013 and the natural lifetimes.¹³⁷

Compound	Solvent	τ , ns	χ^2	ϕ	k_r (10^7) s ⁻¹	k_{nr} (10^7) s ⁻¹	τ_n , ns
4.4	Acetonitrile	11.90	1.66	0.14	1.17	7.23	85.00
	Cyclohexane	18.40	2.38	0.49	2.66	2.77	37.55
	DCM	22.60	2.46	0.56	2.48	1.95	40.36
	DMF	18.90	1.87	0.42	2.22	3.07	45.00
	Ethanol	17.20	1.95	0.51	2.97	2.85	33.73
	Hexane	11.20	1.72	0.27	2.41	6.52	41.48
	Methanol	14.20	1.86	0.07	0.49	6.55	202.86
	THF	17.90	2.09	0.40	2.23	3.35	44.75

Table 4.4. Fluorescence lifetime and emission quantum yield values in different solvents, in addition to the calculated radiative and non-radiative decay rate constants and natural lifetimes of compound **4.5**.

Compound	Solvent	τ_1 , ns (%)	τ_2 , ns (%)	τ_{avg} , ns	χ^2	ϕ	k_r (10^7) s ⁻¹	k_{nr} (10^7) s ⁻¹	τ_n , ns
4.5	Acetonitrile	16.26 (100)	--	16.26	2.45	0.03	0.18	5.97	542.00
	Chloroform	22.40 (36)	31.91 (64)	28.45	1.91	0.13	0.46	3.06	218.85
	Cyclohexane	10.10 (8)	21.85 (92)	20.95	1.89	0.26	1.24	3.53	80.58
	DMF	16.61 (100)	--	16.61	1.64	0.08	0.48	5.54	207.63
	DMSO	10.95 (25)	19.45 (75)	17.29	1.56	0.04	0.23	5.55	432.32
	1,4-dioxane	43.86 (100)	--	43.86	2.99	0.34	0.78	1.50	129.00
	Ethanol	10.25 (8)	21.33 (92)	20.49	1.68	0.05	0.24	4.64	409.80
	Ethyl acetate	14.69 (7)	30.70 (93)	29.65	2.13	0.08	0.27	3.10	370.63
	THF	13.96 (5)	29.26 (95)	28.44	1.79	0.13	0.46	3.06	218.87

Applying the kinetic approach from Figure 4.8 for compound **4.5** leads to the scheme presented in Figure 4.18.

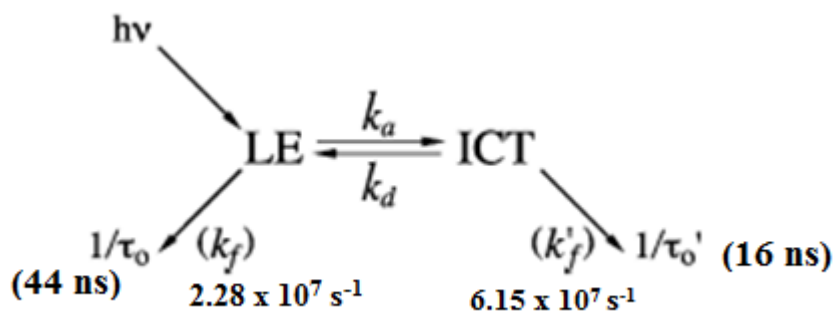


Figure 4.18. Scheme of LE vs ICT in compound **4.5** ($k_a \gg k_d$ in acetonitrile; $k_a \ll k_d$ in 1,4-dioxane); values in the Figure stand for the lifetimes of LE vs ICT, in addition to the total decay rate constant (radiative + non radiative).

The emission quantum yield of **4.5** is also a good indicator of the ICT state occurrence in polar solvents. The quantum yield decreased from 0.34 in 1,4-dioxane (LE) to 0.03 in acetonitrile (ICT). This could be explained by the existence of ICT in acetonitrile in addition to the so-called “photo-induced electron transfer (PET) quenching” of fluorescence. In 2010, Kowalczyk *et al.* investigated some D-A compounds, and explained that in such systems the HOMO of the donor is usually higher in energy than that of the acceptor.¹⁴⁹ If the initial excitation is localized on the acceptor, a subsequent electron transfer takes place from the HOMO of the donor to the vacant position created by the initial excitation on the acceptor. This electron transfer blocks the initially excited electron and keeps it at its excited state, preventing the occurrence of emission, Figure 4.19. This leads to non-radiative relaxation pathways of the blocked electron, and subsequent decrease in the emission quantum yield.¹⁴⁹

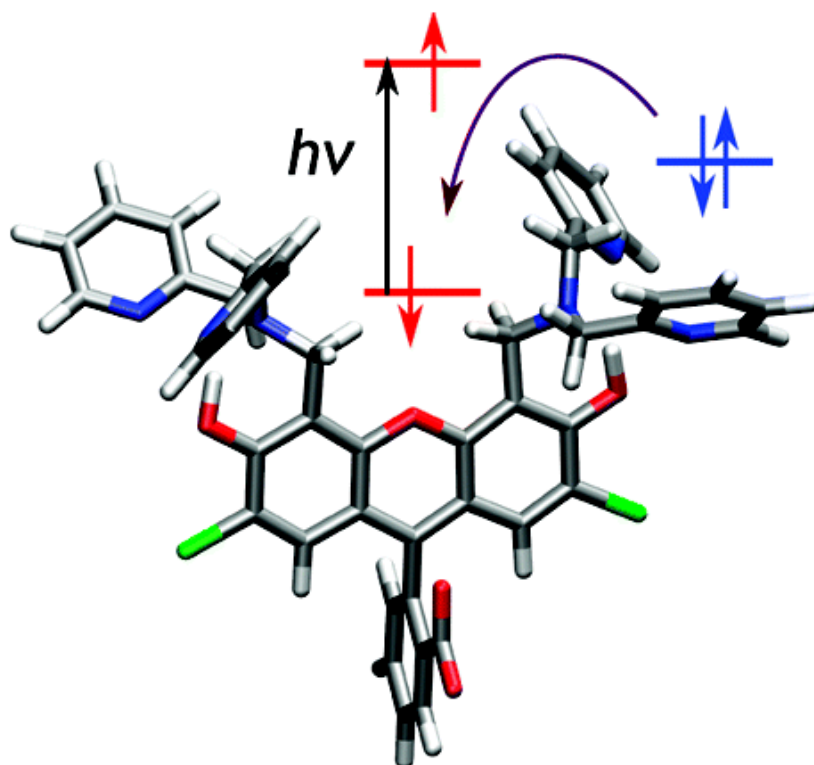


Figure 4.19. D-A compound having an initial photoexcitation localized on the acceptor with a PET blocking of radiative decay (blue: electrons of the donor; red: electrons of the acceptor).¹⁴⁹ Reprinted with permission from (Kowalczyk, T.; Lin, Z.; Van Voorhis, T. *J. Phys. Chem. A* **2010**, *114*, 10427.). Copyright (2010) American Chemical Society.

4.2.4.3. Biphenyl, Biphenyl-like and Benzene Acceptors

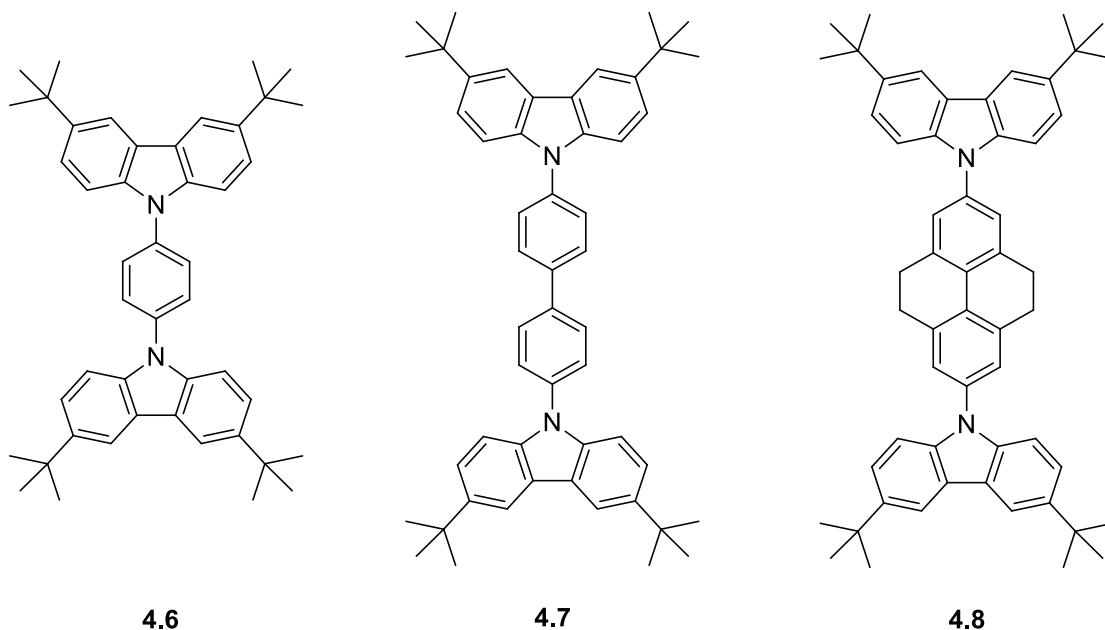


Figure 4.20. D-A-D compounds previously reported by our group in 2013: (D) carbazole; (A) benzene (**4.6**), biphenyl (**4.7**) and THP (**4.8**), reported previously by our group in 2013.¹³⁷

Compounds **4.6-4.8**, Figure 4.20, were previously reported by our research group. Similarity was noted between the absorption and emission spectra of **4.7** and **4.8**, where biphenyl and 4,5,9,10-tetrahydropyrene are the acceptors respectively. This is because 4,5,9,10-tetrahydropyrene (THP) can be regarded as a doubly bridged biphenyl acceptor,¹³⁷ as previously explained in Chapter 3.

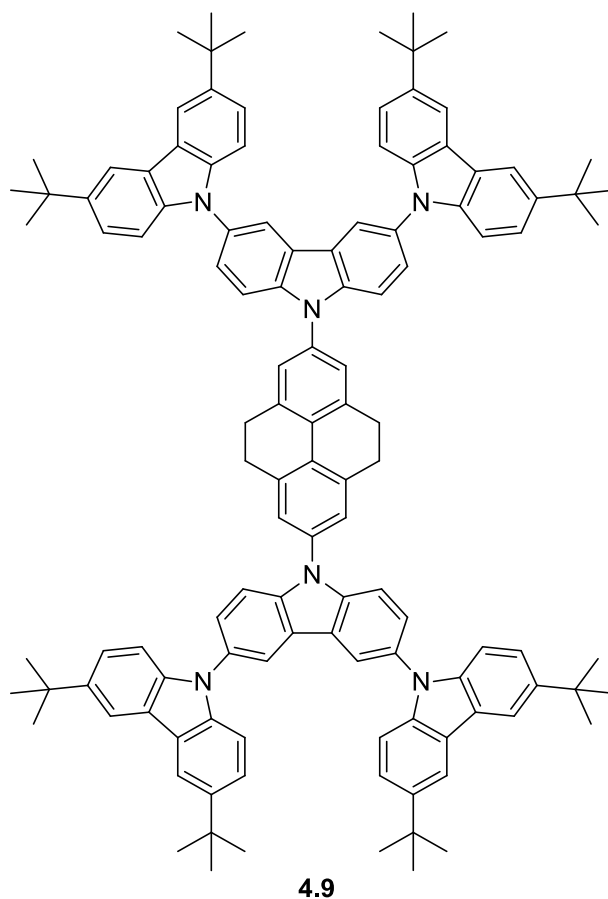


Figure 4.21. D-A-D compound **4.9**: (D) tercarbazole, (A) THP.

The absorption spectrum of **4.9**, similarly to that of **4.7** and **4.8**, shows absorption bands around 290 nm corresponding to carbazole, and above 300 nm attributed to HOMO→LUMO transitions described as $\pi\rightarrow\pi^*$ transitions. However, the bathochromic shift in emission upon increasing solvent polarity is much smaller than that of the pyrene-based derivative **4.5**. Furthermore, the emission of **4.9** is bathochromically shifted as compared to **4.8** in both polar and non-polar solvents, Table 4.5, which is consistent with the previously discussed findings of McClenaghan *et al.* regarding the differences between carbazole and tercarbazole donors.¹⁴²

Table 4.5. Emission maxima in non-polar vs. polar solvent for **4.8** and **4.9**.

Compound	Substituent (D)	Bridge/Core (A)	λ_{max}^{em} , nm, cyclohexane	λ_{max}^{em} , nm, acetonitrile
4.8 ¹³⁷	Carbazole	4,5,9,10-Tetrahydropyrene	365	390
4.9	Tercarbazole	4,5,9,10-Tetrahydropyrene	386	398

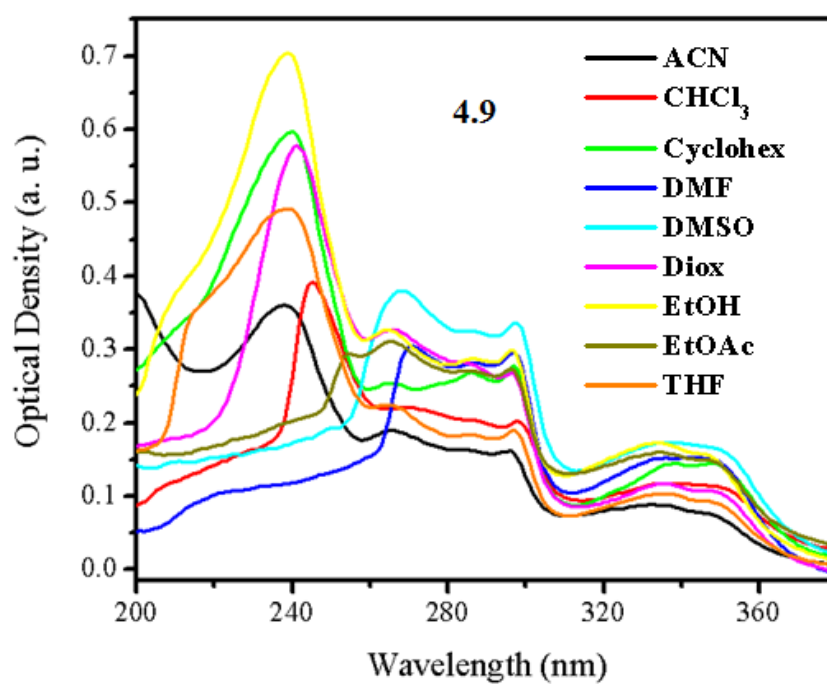


Figure 4.22. Absorption spectra of compound **4.9** in nine different solvents.

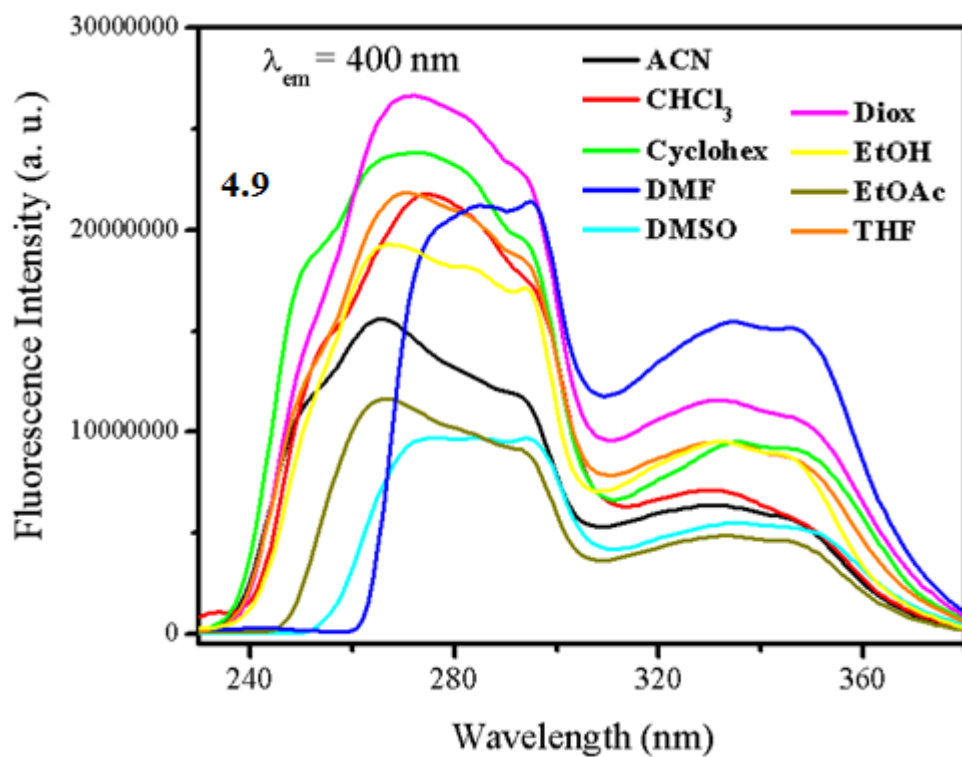


Figure 4.23. Excitation spectra of compound **4.9** in nine different solvents.

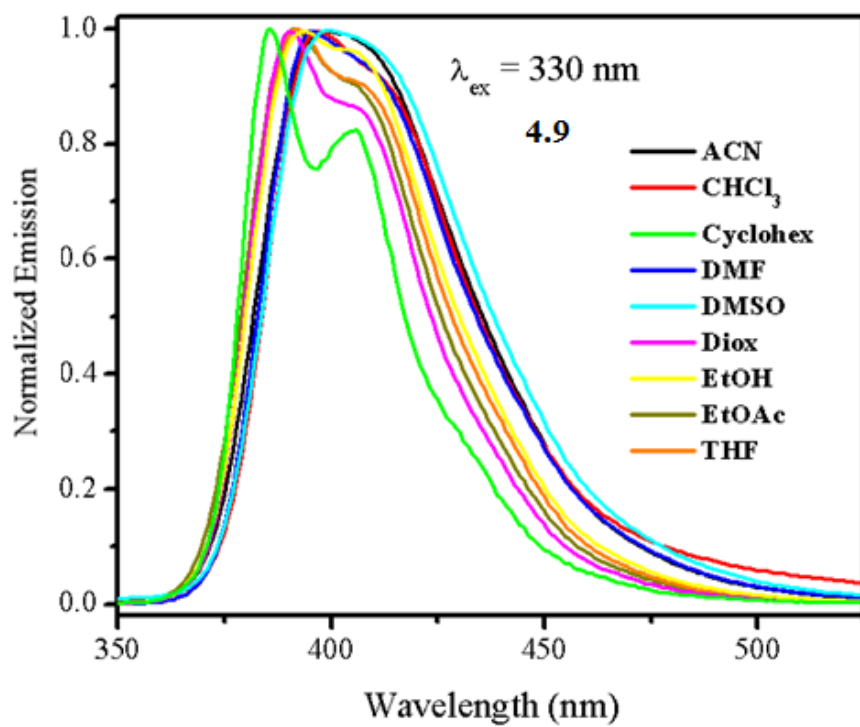


Figure 4.24. Normalized emission spectra of compound **4.9** in nine different solvents.

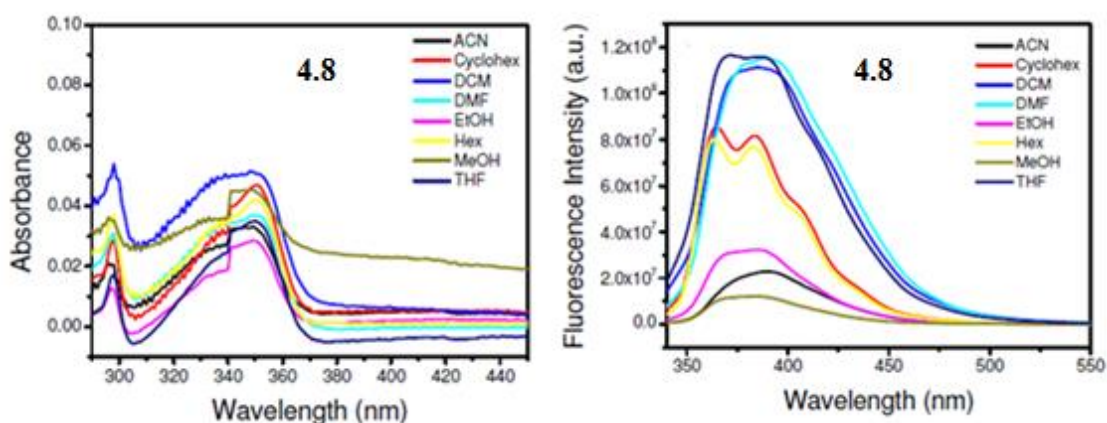


Figure 4.25. Absorption spectra (left) and emission spectra (right) of **4.8** reported by our group in 2013.¹³⁷ Reprinted from Kaafarani, B. R.; El-Ballouli, A. O.; Trattnig, R.; Fonari, A.; Sax, S.; Wex, B.; Risko, C.; Khnayzer, R. S.; Barlow, S.; Patra, D.; Timofeeva, T. V.; List, E. J. W.; Bredas, J.-L.; Marder, S. R. *J. Mater. Chem. C* **2013**, *1*, 1638. Published by The Royal Society of Chemistry.

4.2.5. Model D-A Compounds and General Analysis

In order to have suitable reference compounds, and to compare them with the experimental photophysical results that we obtained, the design of two D-A derivatives was done, with a relatively weak acceptor (4-*tert*-butylphenyl) and a carbazole or tercarbazole donor, Figure 4.26.

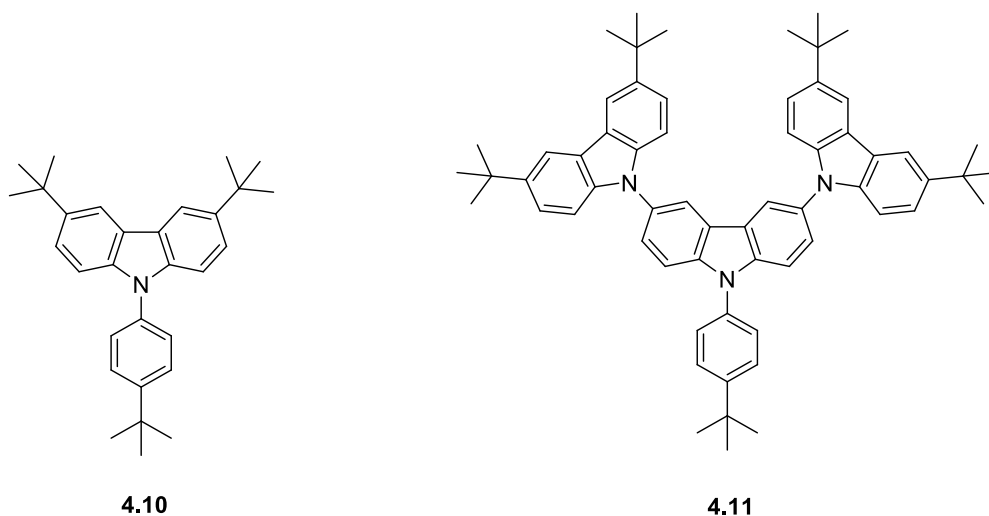


Figure 4.26. Model D-A compounds **4.10** and **4.11**.

Previous studies on carbazole-based D-A compounds indicate that weak acceptors, such as benzene, favor the emission from LE state. In contrast to stronger acceptors such as polycyclic aromatic hydrocarbons or benzene with an electron withdrawing group, in which the emission from ICT state is observed in polar solvents.¹⁴¹

The absorption spectra were quite similar for both D-A compounds **4.10** and **4.11**. However, the emission of **4.11** is red-shifted in both non-polar and polar solvents as compared to **4.10**. Furthermore, unlike tercarbazole D-A derivative **4.11**, compound **4.10** does not show loss in vibrational structure upon increasing the solvent polarity, confirming the absence of emission from ICT state for carbazole D-A derivative **4.10**.

Table 4.6. Fluorescence lifetime and emission quantum yield values in different solvents, in addition to the calculated radiative and non-radiative decay rate constants of compound **4.8** reported by our research group in 2013 and the natural lifetimes.¹³⁷

Compound	Solvent	τ_1 , ns (%)	τ_2 , ns (%)	τ_{avg} , ns	χ^2	ϕ	k_r (10^8) s ⁻¹	k_{nr} (10^8) s ⁻¹	τ_n , ns
4.8 ¹³⁷	Acetonitrile	2.15 (79)	10.10 (20)	3.72	1.15	0.70	1.88	0.81	5.31
	Cyclohexane	1.49 (66)	8.88 (34)	4.00	1.60	0.25	0.63	1.88	16.00
	DCM	1.89 (47)	9.05 (52)	5.59	1.38	0.43	0.77	1.02	13.00
	DMF	2.03 (56)	0.12 (43)	1.19	1.49	0.69	5.80	2.61	1.72
	Ethanol	2.01 (47)	9.56 (53)	6.01	1.62	0.58	0.97	0.70	10.36
	Hexane	1.38 (70)	5.63 (30)	2.66	1.58	0.82	3.08	0.68	3.24
	Methanol	2.69 (25)	9.65 (75)	7.91	1.40	0.31	0.39	0.87	25.52
	THF	1.87 (42)	9.26 (58)	6.16	1.38	0.43	0.70	0.93	14.33

Table 4.7. Fluorescence lifetime and emission quantum yield values in different solvents, in addition to the calculated radiative and non-radiative decay rate constants and the natural lifetimes of compound **4.9**.

Compound	Solvent	τ_1 , ns (%)	τ_2 , ns (%)	τ_{avg} , ns	χ^2	ϕ	k_r (10^8) s ⁻¹	k_{nr} (10^8) s ⁻¹	τ_n , ns
4.9	Acetonitrile	6.96	--	6.96	1.96	0.39	0.56	0.88	17.85
	Chloroform	1.09 (82)	1.85 (18)	1.23	1.33	0.07	0.57	7.56	17.57
	Cyclohexane	4.70	--	4.70	1.67	0.25	0.53	1.60	18.80
	DMF	5.02 (8)	6.47 (92)	6.35	1.93	0.34	0.54	1.04	18.68
	DMSO	4.32 (9)	6.54 (91)	6.34	1.81	0.40	0.63	0.95	15.85
	1,4-dioxane	4.37 (10)	5.43 (90)	5.33	1.64	0.24	0.45	1.43	22.21
	Ethanol	5.92	--	5.92	1.64	0.29	0.49	1.20	20.41
	Ethyl acetate	5.95 (80)	4.90 (20)	5.74	1.75	0.30	0.52	1.22	19.13
THF	3.75 (9)	4.75 (91)	4.66	1.70	0.23	0.49	1.65	20.26	

Table 4.8. Fluorescence lifetime and emission quantum yield values in different solvents, in addition to the calculated radiative and non-radiative decay rate constants and the natural lifetimes of the two D-A model compounds **4.10** and **4.11**.

Compound	Solvent	τ_1 , ns (%)	τ_2 , ns (%)	τ_{avg} , ns	χ^2	ϕ	k_r (10^7) s ⁻¹	k_{nr} (10^7) s ⁻¹	τ_n , ns
4.10	Acetonitrile	10.89	--	10.89	1.52	0.48	4.41	4.78	22.69
	Chloroform	0.49	--	0.49	1.26	0.04	8.16	195.92	12.25
	Cyclohexane	8.98 (82)	10.92 (18)	9.32	1.40	0.20	2.15	8.58	46.60
	DMF	4.72 (5)	8.06 (95)	7.89	1.58	0.37	4.69	7.98	21.32
	DMSO	7.27 (17)	9.31 (83)	8.96	1.46	0.44	4.91	6.25	20.36
	1,4-dioxane	8.35 (41)	10.42 (59)	9.57	1.46	0.58	6.06	4.39	16.50
	Ethanol	6.83 (9)	10.11 (91)	9.81	1.44	0.46	4.69	5.50	21.33
	Ethyl acetate	7.63 (10)	10.42 (90)	10.13	1.40	0.50	4.94	4.94	20.26
THF	9.95	--	9.95	1.43	0.52	5.23	4.82	19.13	
4.11	Acetonitrile	7.61	--	7.61	1.57	0.40	5.26	7.88	19.03
	Chloroform	1.20	--	1.20	2.20	0.06	5.00	78.33	20.00
	Cyclohexane	5.44	--	5.44	1.55	0.18	3.31	15.07	30.22
	DMF	2.61 (17)	6.76 (83)	6.04	1.56	0.32	5.30	11.26	18.88
	DMSO	6.99	--	6.99	1.63	0.32	4.58	9.73	21.84
	1,4-dioxane	4.68 (14)	6.02 (86)	5.83	1.63	0.37	6.35	10.81	15.76
	Ethanol	6.37	--	6.37	1.57	0.32	5.02	10.68	19.91
	Ethyl acetate	6.24	--	6.24	1.55	0.35	5.61	10.42	17.83
THF	6.17	--	6.17	1.73	0.41	6.65	9.56	15.05	

Table 4.9. Absorption, emission maxima and Stokes shifts in nine solvents, in addition to the molar absorptivity in chloroform for compounds **4.5**, **4.9**, **4.10** and **4.11**.

Compound	Solvent	λ_{max}^{em} , nm	λ_{max}^{abs} , nm (ϵ , L.mol ⁻¹ .cm ⁻¹)	$\Delta\lambda$ (cm ⁻¹)	$\Delta\lambda$ (eV)
4.5	Acetonitrile	539	340	10859	1.35
	Chloroform	478	341 (88667)	8405	1.04
	Cyclohexane	423	339	5858	0.73
	DMF	533	343	10392	1.29
	DMSO	537	344	10448	1.30
	1,4-Dioxane	449	341	7054	0.87
	Ethanol	509	340	9765	1.21
	Ethyl acetate	483	341	8622	1.07
	THF	490	340	9004	1.12
4.9	Acetonitrile	398	347	3693	0.46
	Chloroform	397	349 (57703)	3464	0.43
	Cyclohexane	386	349	2747	0.34
	DMF	395	348	3419	0.42
	DMSO	399	348	3673	0.46
	1,4-Dioxane	391	348	3160	0.39
	Ethanol	393	346	3456	0.43
	Ethyl acetate	392	347	3308	0.41
	THF	392	347	3308	0.41
4.10	Acetonitrile	373	347	2009	0.25
	Chloroform	372	349 (3808)	1772	0.22
	Cyclohexane	369	347	1718	0.21
	DMF	373	347	2009	0.25
	DMSO	375	348	2069	0.26
	1,4-Dioxane	372	347	1937	0.24
	Ethanol	371	347	1864	0.23
	Ethyl acetate	371	347	1864	0.23
	THF	372	347	1937	0.24
4.11	Acetonitrile	405	348	4044	0.50
	Chloroform	399	349 (12101)	3591	0.45
	Cyclohexane	385	348	2762	0.34
	DMF	406	349	4023	0.50
	DMSO	406	350	3941	0.49
	1,4-Dioxane	390	349	3012	0.37
	Ethanol	403	347	4005	0.50
	Ethyl acetate	392	348	3225	0.40
	THF	392	348	3225	0.40

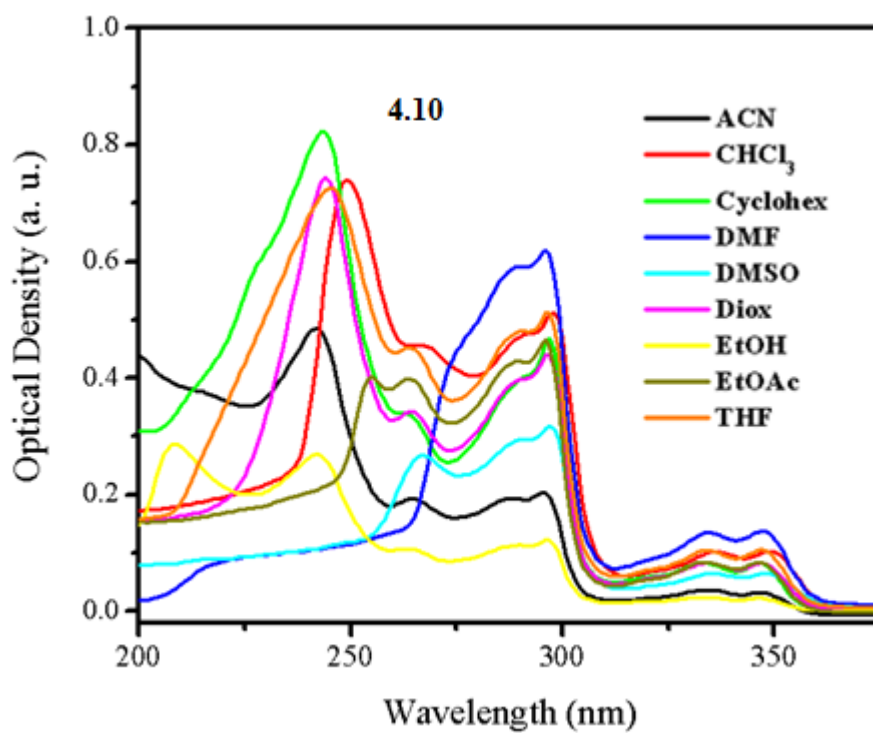


Figure 4.27. Absorption spectra of compound **4.10** in nine different solvents.

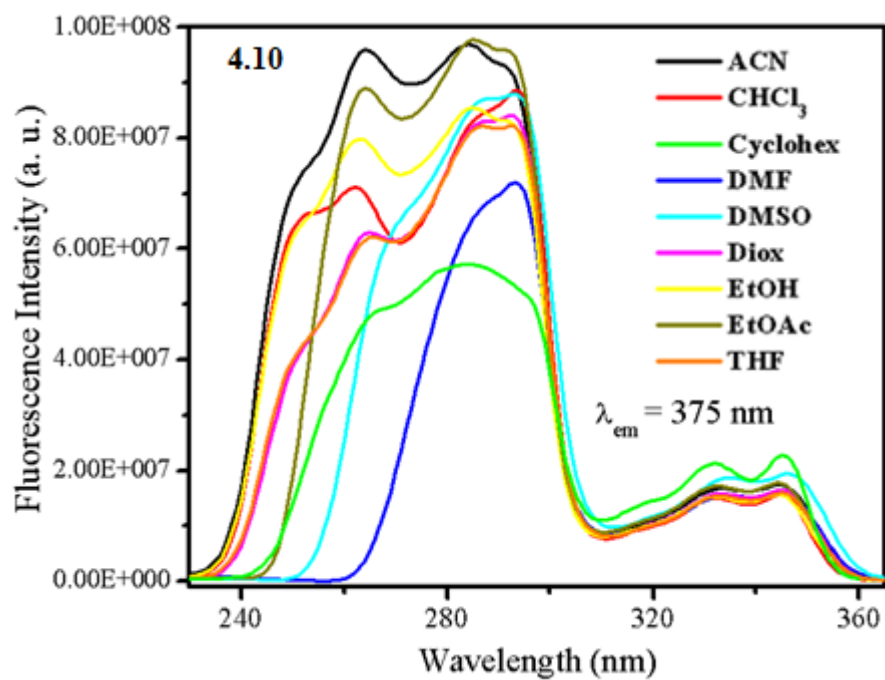


Figure 4.28. Excitation spectra of compound **4.10** in nine different solvents.

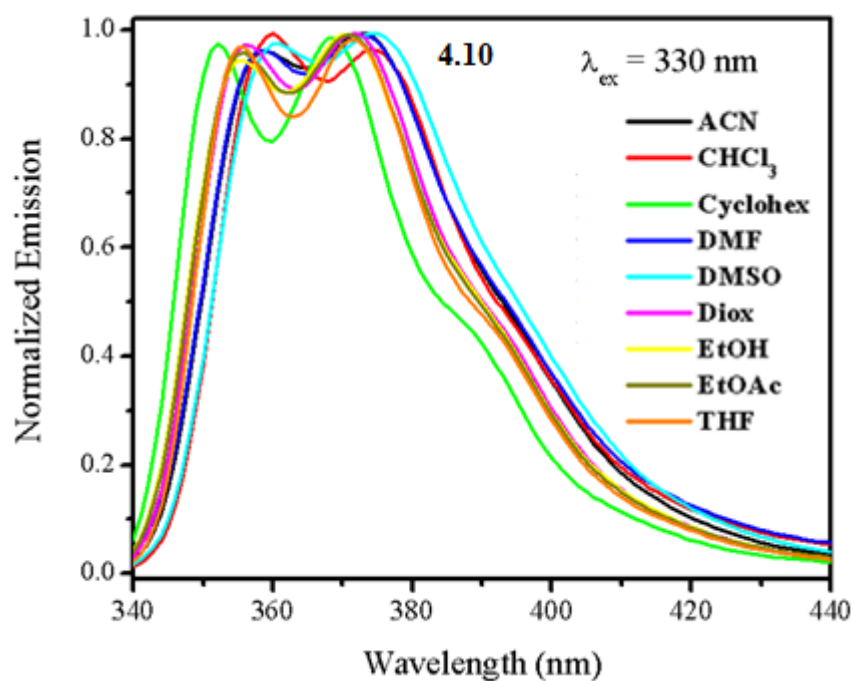


Figure 4.29. Normalized emission spectra of compound **4.10** in nine different solvents.

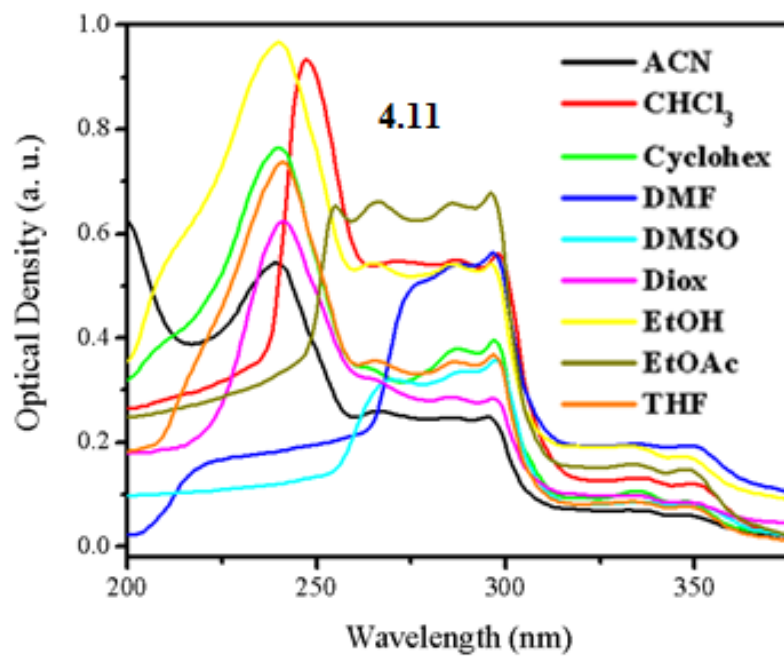


Figure 4.30. Absorption spectra of compound **4.11** in nine different solvents.

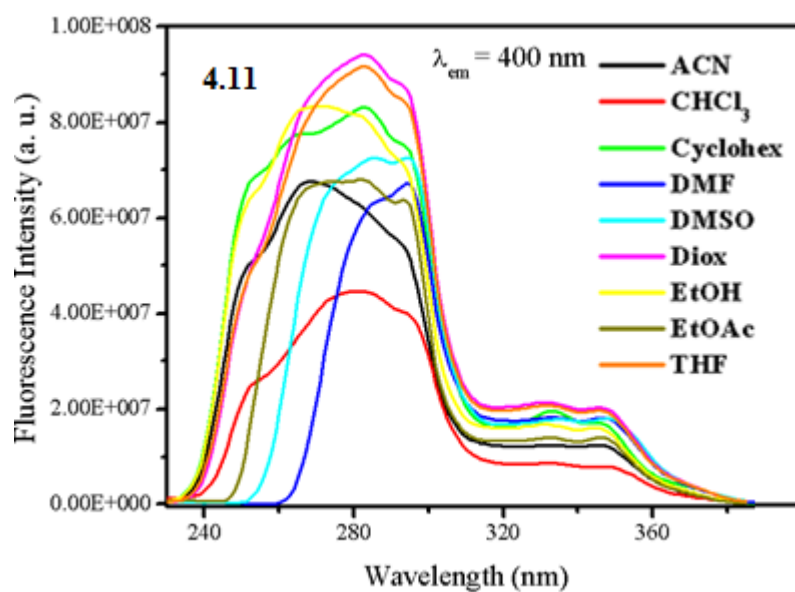


Figure 4.31. Excitation spectra of compound **4.11** in nine different solvents.

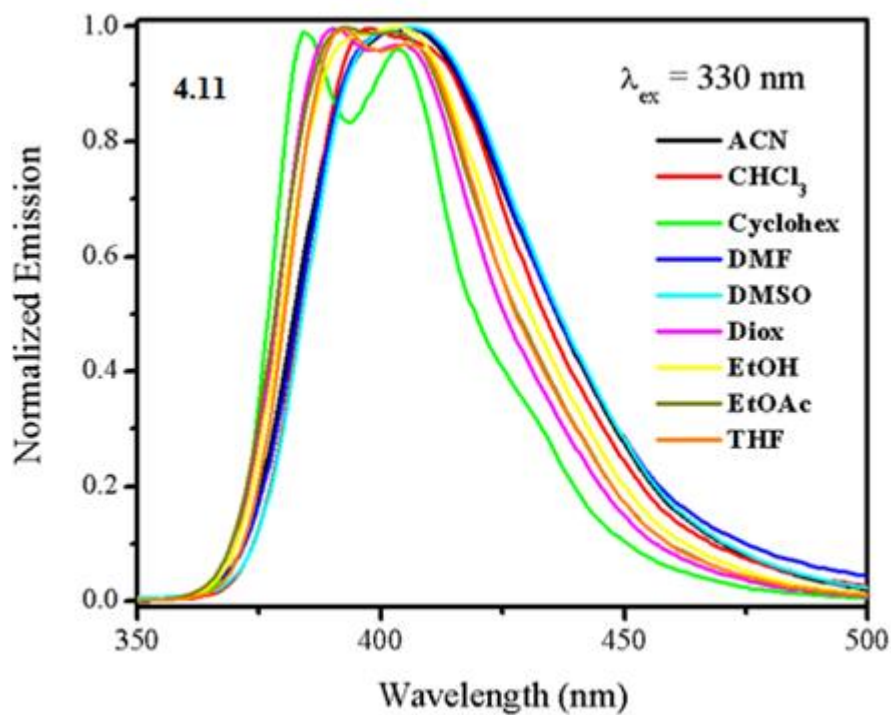


Figure 4.32. Normalized emission spectra of compound **4.11** in nine different solvents.

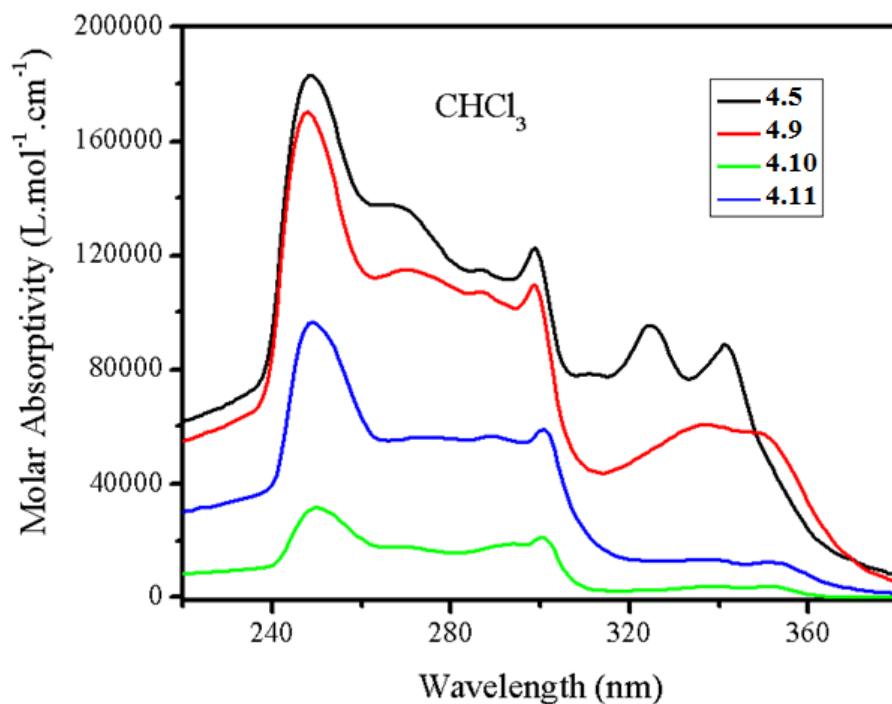


Figure 4.33. Molar absorptivity of compounds 4.5, 4.9, 4.10 and 4.11 in chloroform.

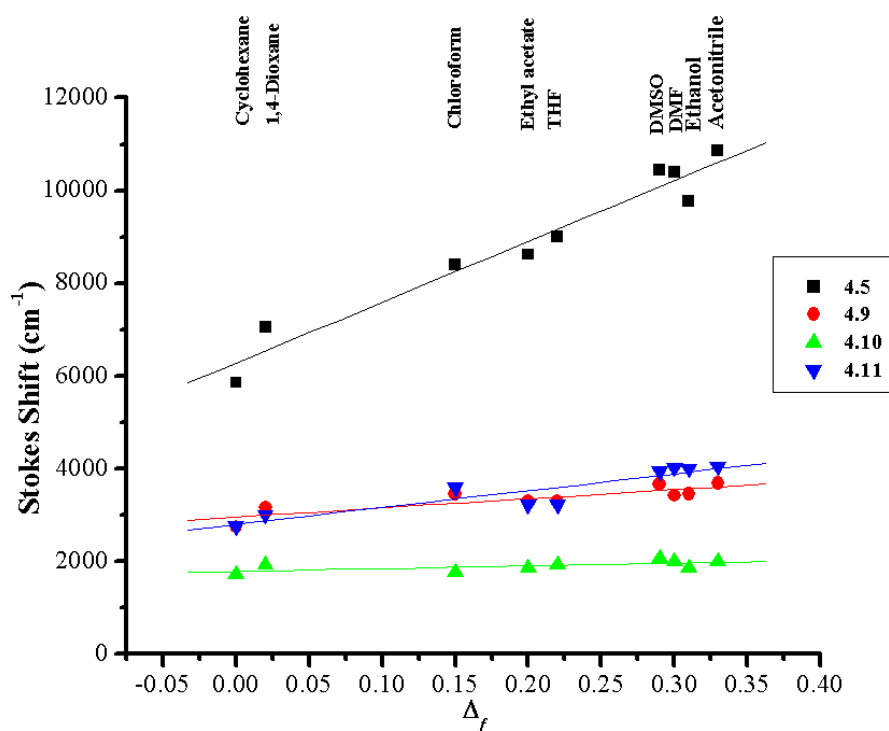


Figure 4.34. Stokes shifts vs. orientation polarizability for compounds 4.5, 4.9, 4.10 and 4.11 with linear fitting in the nine selected solvents.

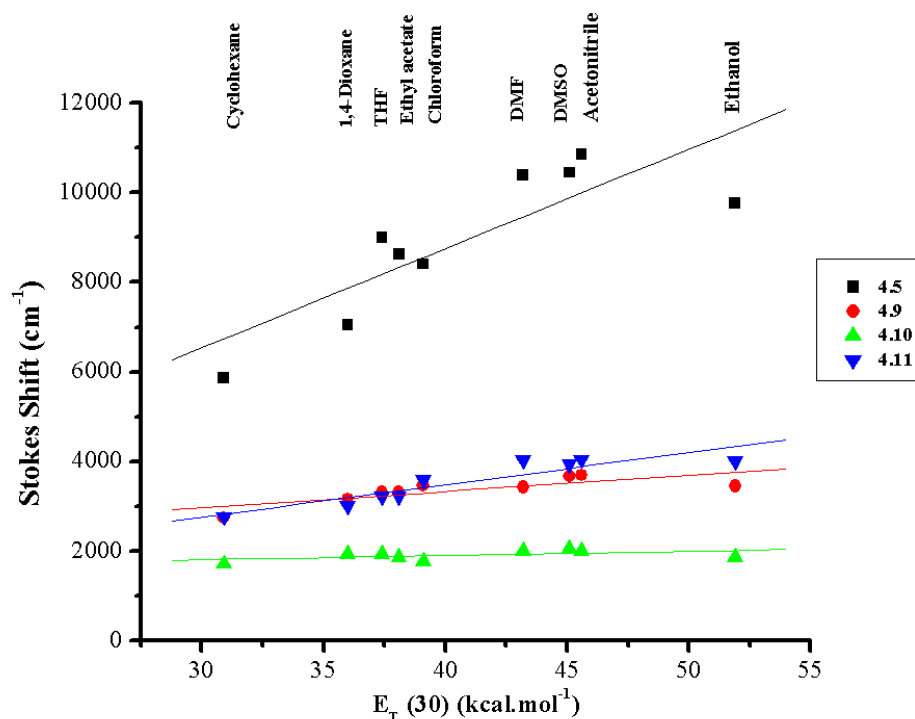


Figure 4.35. Stokes shifts vs. empirical solvent polarity for compounds **4.5**, **4.9**, **4.10** and **4.11** with linear fitting in the nine selected solvents.

The photophysical results obtained for compounds **4.9-4.11** are not much informative, except with respect to the absence of unusually large bathochromic shifts with increasing solvent polarity, such as the ones observed for the tercarbazole-pyrene D-A-D derivative **4.5**. More informative data can be found in the theoretical studies reported by our group on compounds **4.4**, **4.6-4.8**. The comparison of the degree of localization of HOMO and LUMO orbitals between the donor and the acceptor may be more informative, Table 4.10.¹³⁷ The optimized conditions that favor ICT are a localized HOMO on the donor and a localized LUMO on the acceptor. These two conditions were both satisfied for the carbazole-pyrene D-A-D derivative **4.4**, in which the HOMO is localized on carbazole (donor), and the LUMO is localized on pyrene (acceptor). It is expected that for the stronger tercarbazole donor (**4.5**), the localization of HOMO and LUMO would be retained and probably more favored (i.e. tercarbazole is

a stronger donor). Weak acceptors such as benzene showed delocalization in both HOMO and LUMO orbitals which prevents efficient ICT. Better acceptors (biphenyl **4.7** and THP **4.8**) showed a delocalized HOMO, opposed to a localized LUMO.

Table 4.10. Theoretical studies useful information for compounds **4.4**, **4.6**, **4.7** and **4.8**. reported by our group.¹³⁷

Substituent (D)	Bridge/Core (A)	HOMO	LUMO
Carbazole	Benzene (4.6)	Delocalized on both D and A	Delocalized on both D and A
Carbazole	Biphenyl (4.7)	Delocalized on both D and A	Localized on A
Carbazole	4,5,9,10-Tetrahydropyrene (4.8)	Delocalized on both D and A	Localized on A
Carbazole	Pyrene (4.4)	Localized on D	Localized on A

4.2.6. Quenching of Fluorescence by Chloroform

A common interesting observation for compounds **4.9-4.11** is that they showed exceptionally small fluorescence lifetime and emission quantum yield, when studied in chloroform, Figures 4.38-4.43 and Tables 4.7-4.8. Exceptionally high non-radiative rate constant values were also observed in this solvent. In contrast to non-affected radiative decay rate constant values, which remained comparable to the ones calculated in other solvents. Compounds **4.1-4.4**, and **4.6-4.8** were not reported in chloroform in the corresponding literature studies. Compound **4.5** did not show similar trend to the three compounds tested in chloroform. Its lifetime and quantum yield values in chloroform were comparable to the ones measured in other solvents, Figures 4.36-4.37, Table 4.4.

It is reported that carbazole is efficiently quenched by polychlorinated hydrocarbons. Johnson reported in 1980 the quenching of carbazole and its derivatives by different quenchers.¹⁵⁰ One of these quenchers is the trichloromethyl group

preferably (but not necessarily) connected to an electron withdrawing group.¹⁵⁰ For example, carbon tetrachloride (CCl₄), in which the trichloromethyl group is connected to an electron withdrawing chlorine atom, is a better quencher for carbazole and its derivatives than chloroform (CHCl₃), in which the trichloromethyl group is connected to a hydrogen. The mechanism of quenching is described as charge transfer interaction between the excited state of carbazole and the ground state of the quencher.¹⁵⁰ The presence of quencher induces a decrease in fluorescence lifetime. The amount of decrease in lifetime (due to quenching) depends on the concentration of the quencher according to the Stern-Volmer equation as follows:

$$\frac{\tau_0}{\tau} = 1 + k_q \cdot \tau_0 \cdot C_q$$

Where τ_0 is the lifetime of the unquenched carbazole derivative, τ is the lifetime upon the addition of the quencher, C_q is the concentration of the added quencher, k_q is the rate constant of the quenching reaction for a specific quencher under specific conditions, which tells about the sensitivity of the derivative to the quencher.¹⁵⁰

In our photophysical experiments, chloroform was used as a solvent, which means that its quenching effect is pronounced due to the large excess. This explains the abnormally high non-radiative decay constants obtained in this solvent; where the non-radiative pathway could be due to a relaxation of the excited state through a charge transfer from the excited state of **4.9**, **4.10** and **4.11** to the ground state of chloroform. This suggests that D-A and D-A-D systems similar with carbazole or tercarbazole donors are efficiently quenched by chloroform. The fact that the tercarbazole-pyrene D-A-D derivative **4.5** was not quenched might be related to the special photophysical properties observed in this compound, such as effective ICT in polar solvents, an initial excitation localized on pyrene and the subsequent PET quenching, Figure 4.19.

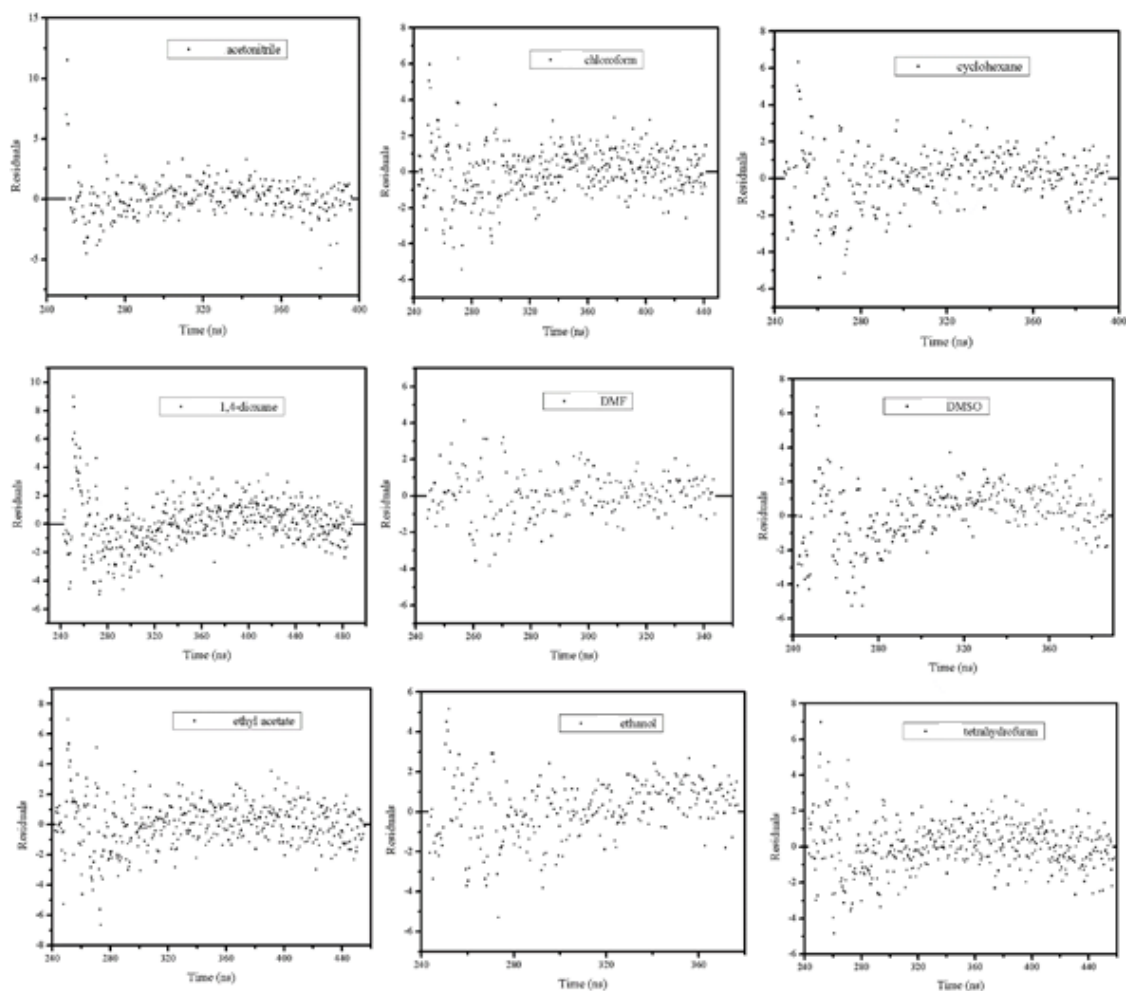
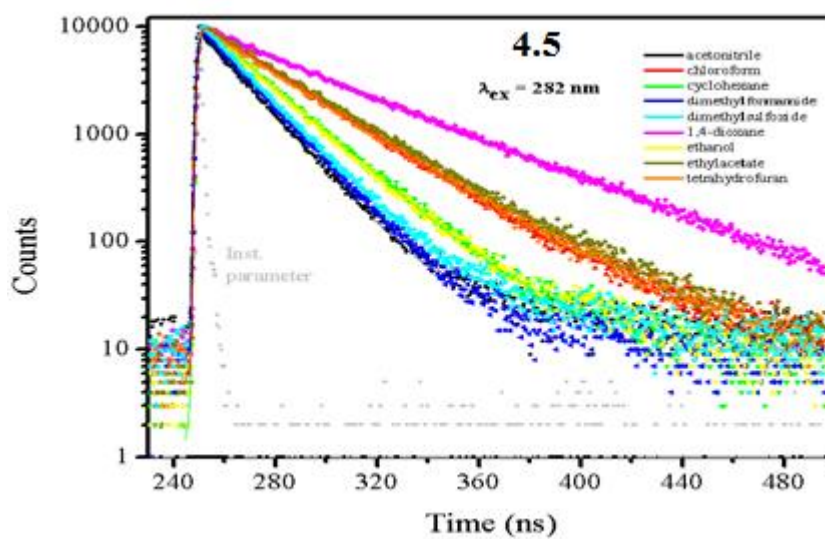


Figure 4.36. Lifetime decay curves of compound **4.5** in nine different solvents with the fitting and residuals.

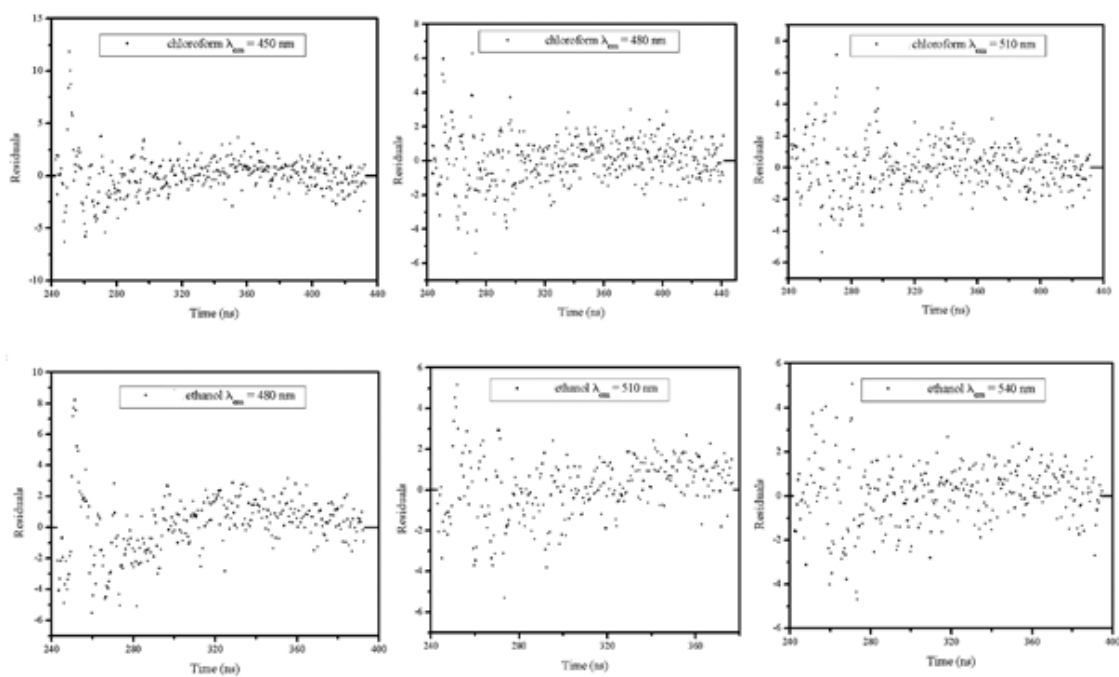
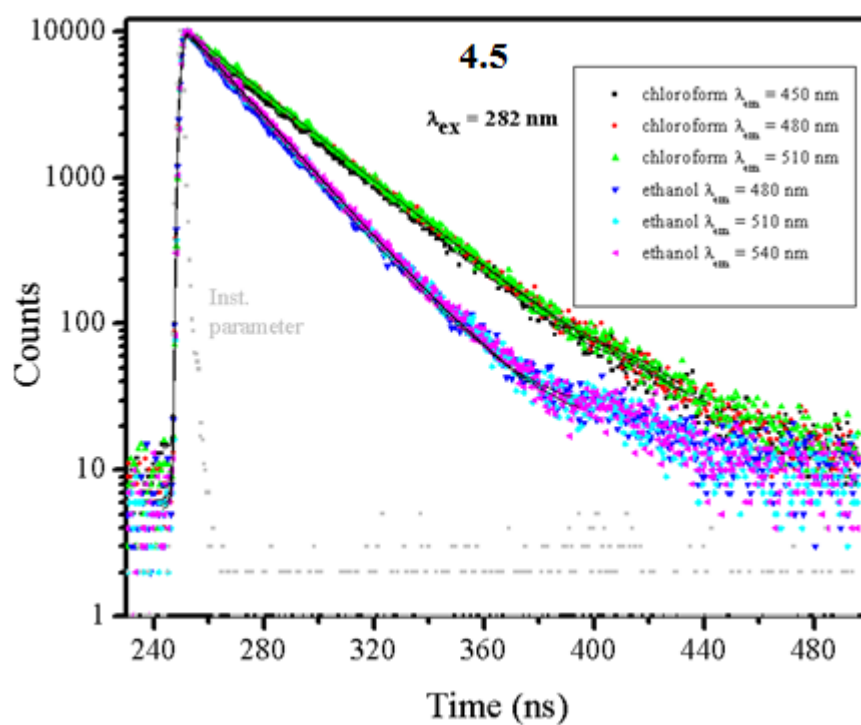


Figure 4.37. Lifetime decay curves of compound **4.5** in chloroform and ethanol at different emission wavelengths with the fitting and residuals.

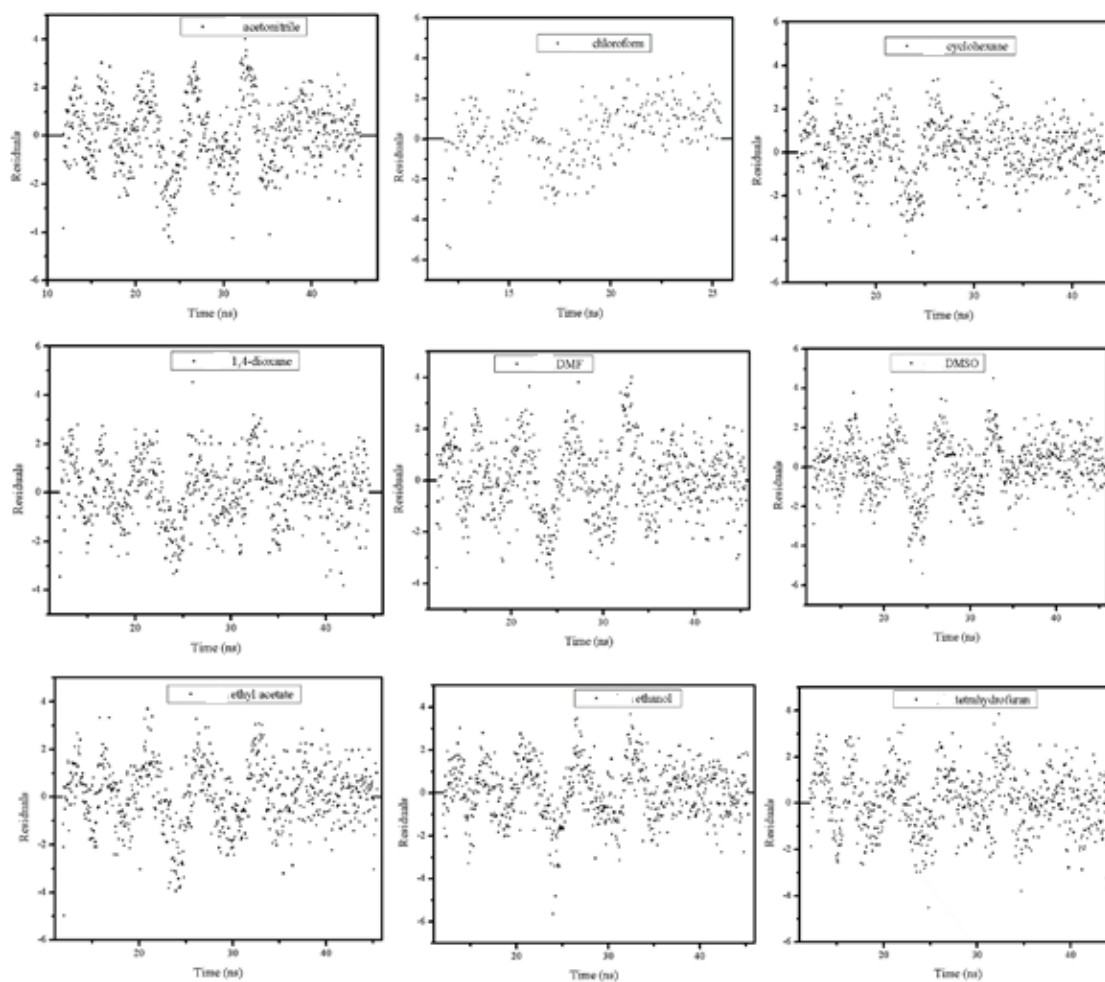
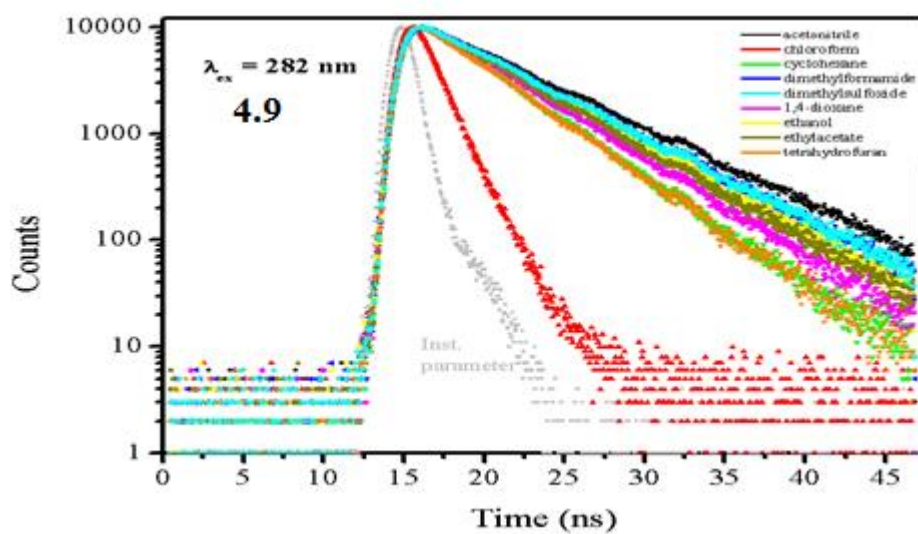


Figure 4.38. Lifetime decay curves of compound **4.9** in nine different solvents with the fitting and residuals.

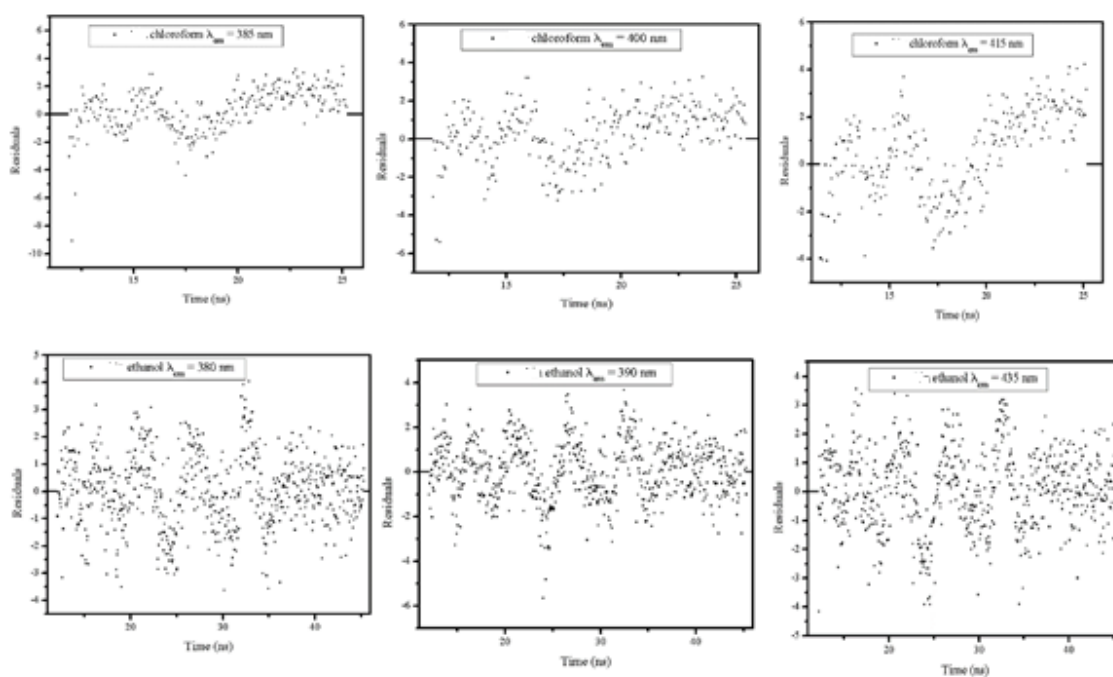
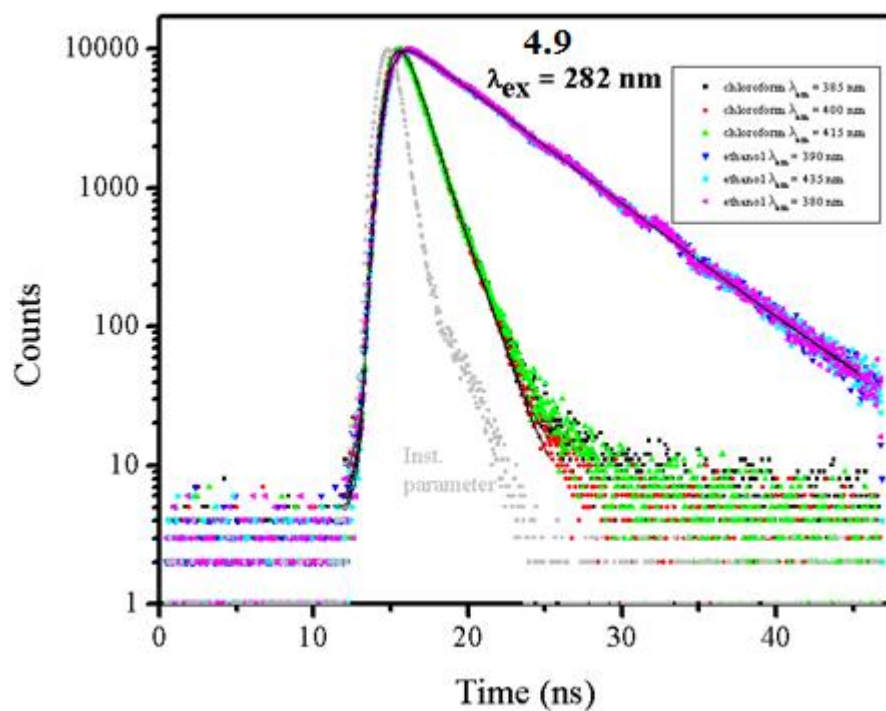


Figure 4.39. Lifetime decay curves of compound **4.9** in chloroform and ethanol at different emission wavelengths with the fitting and residuals.

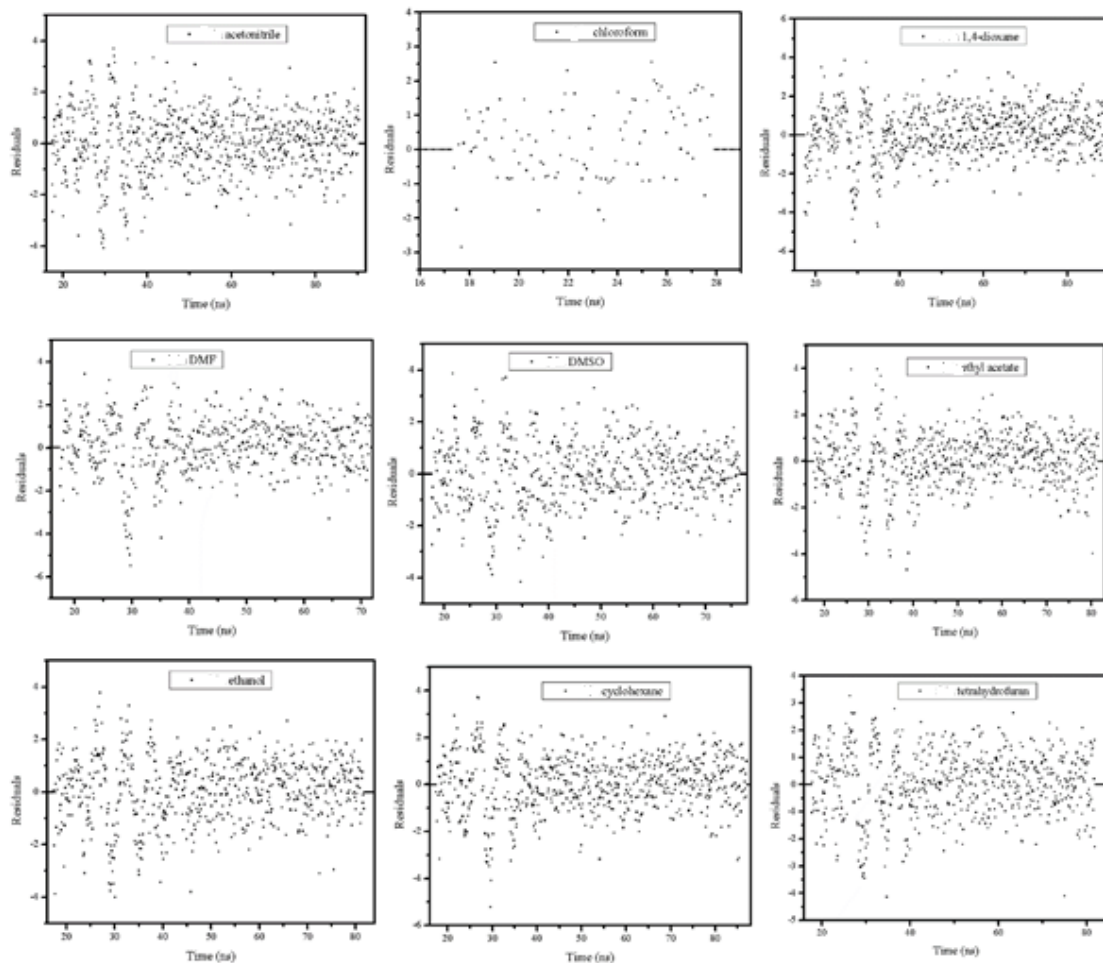
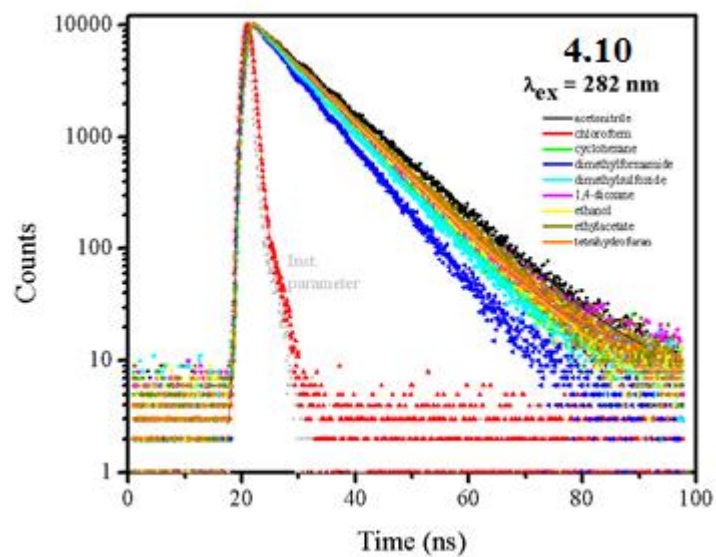


Figure 4.40. Lifetime decay curves of compound **4.10** in nine different solvents with the fitting and residuals.

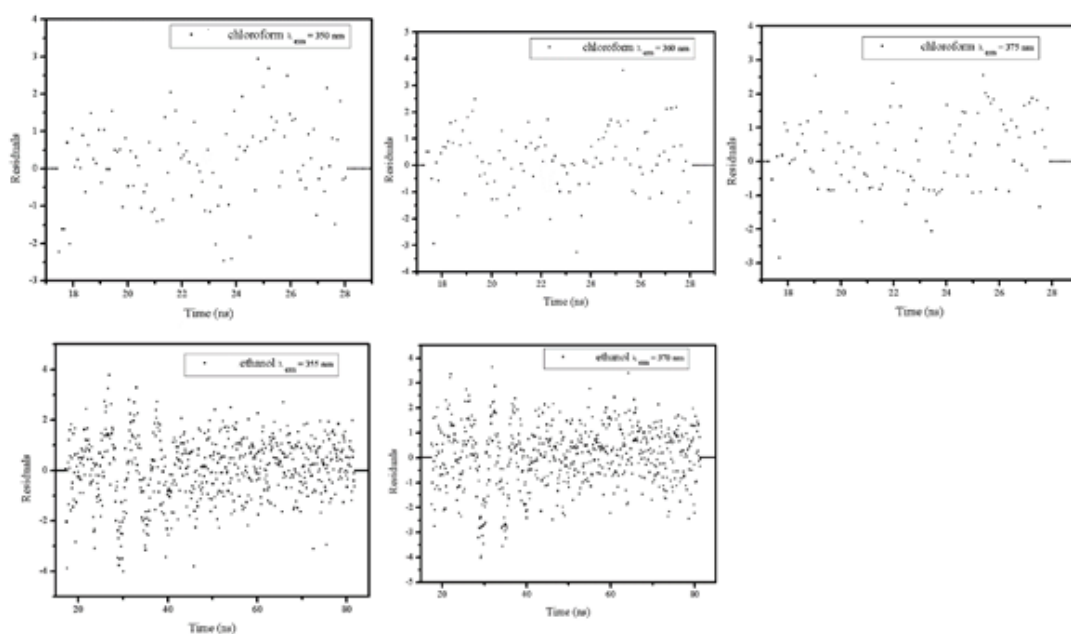
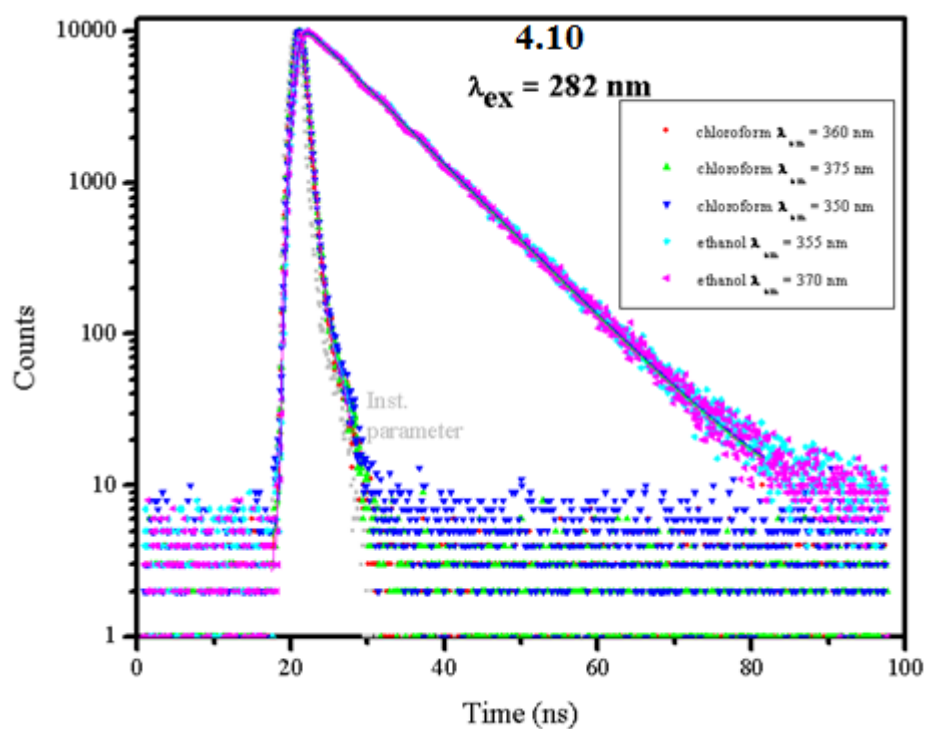


Figure 4.41. Lifetime decay curves of compound **4.10** in chloroform and ethanol at different emission wavelengths with the fitting and residuals.

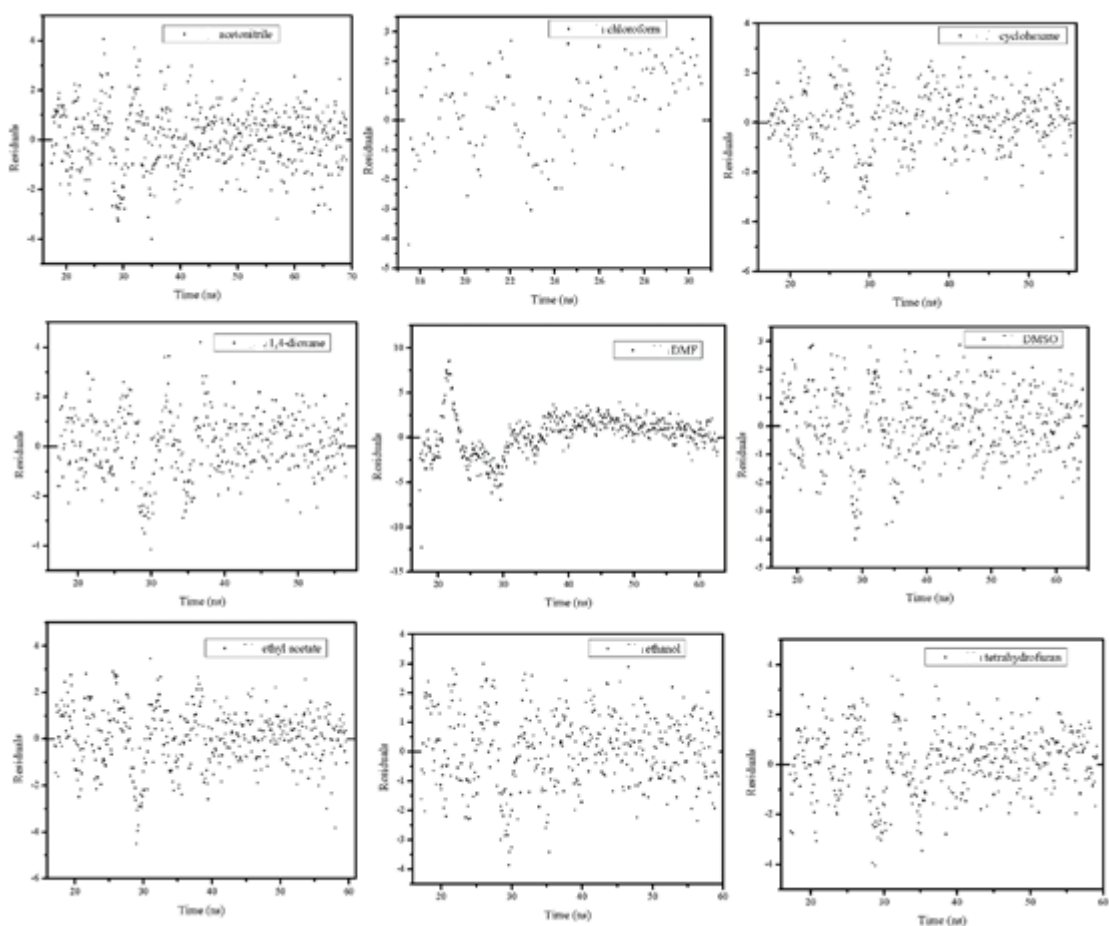
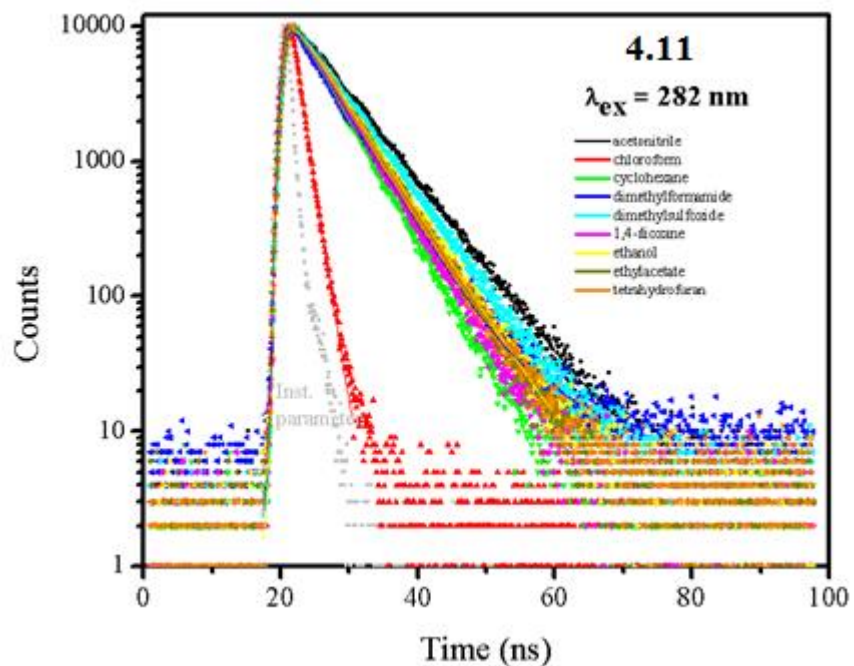


Figure 4.42. Lifetime decay curves of compound **4.11** in nine different solvents with the fitting and residuals.

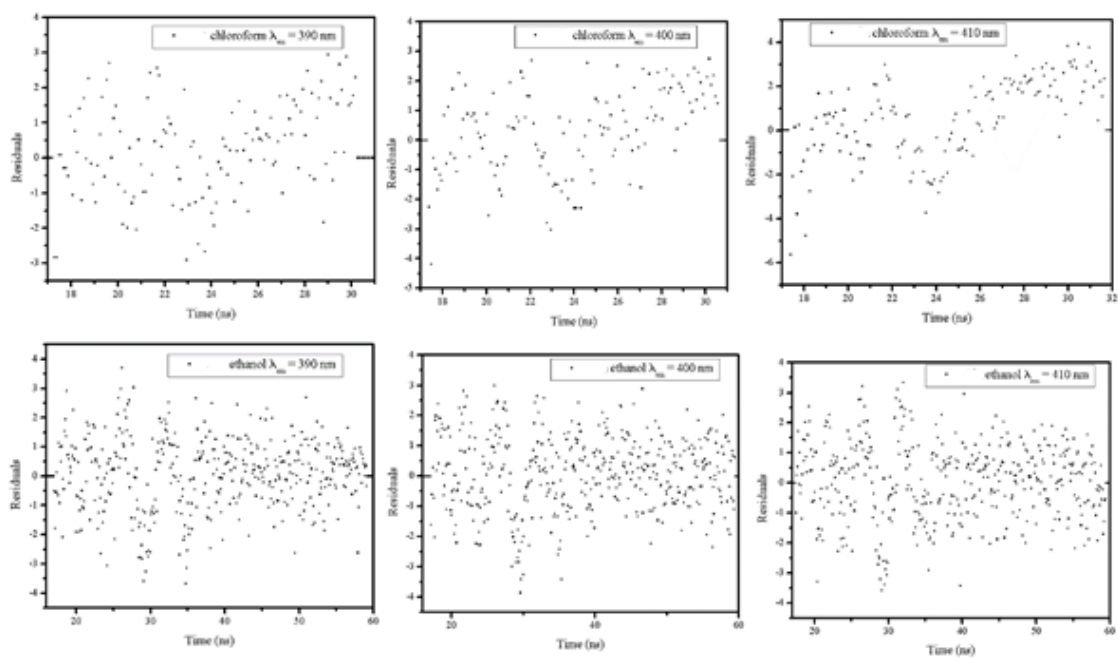
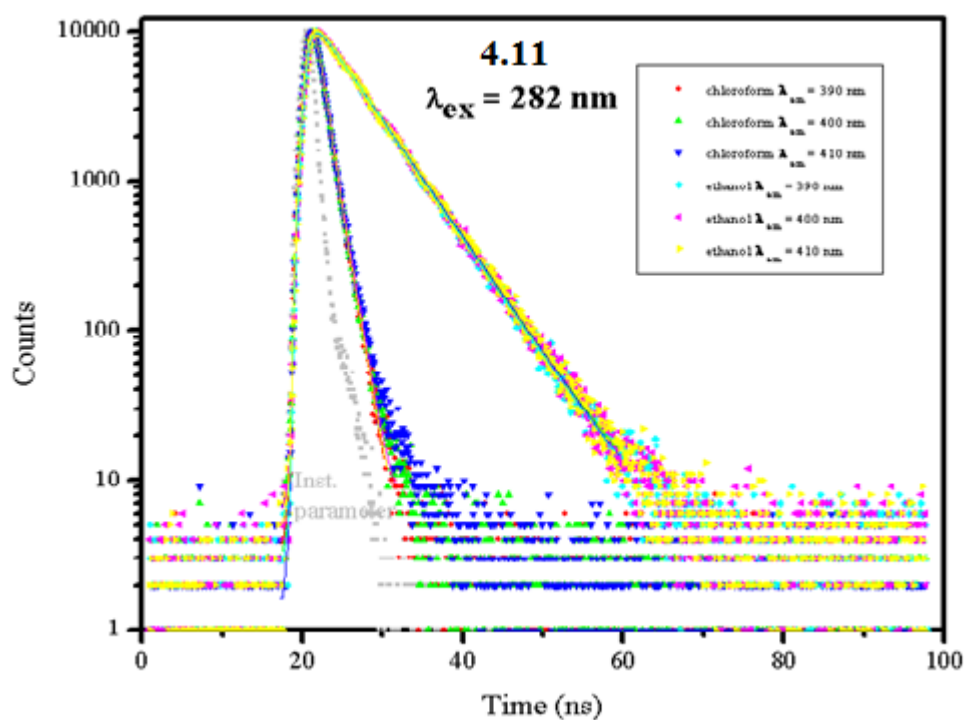


Figure 4.43. Lifetime decay curves of compound **4.11** in chloroform and ethanol at different emission wavelengths with the fitting and residuals.

4.2.7. Exclusion of Excimer Formation Possibility

In order to exclude the probability of the excimer formation leading to the dual emission observed for compound **4.5**, the excitation spectra at different emission wavelengths and the emission spectra at different excitation wavelengths were collected for all studied compounds (**4.5**, **4.9**, **4.10** and **4.11**) in all solvents used. No changes in the emission wavelengths were observed, Figures 4.44-4.51. Similarly, lifetime decays were collected at different emission wavelengths, which showed similar overlapping decay profiles independent of the emission wavelength, Figures 4.37, 4.39, 4.41 and 4.43. The absorption spectra were also collected at different concentrations and no unexpected change was observed, Figure 4.52. Therefore, a single emitting species is present in solution within the concentration range used for our photophysical studies. The excimer formation possibility can be safely excluded.

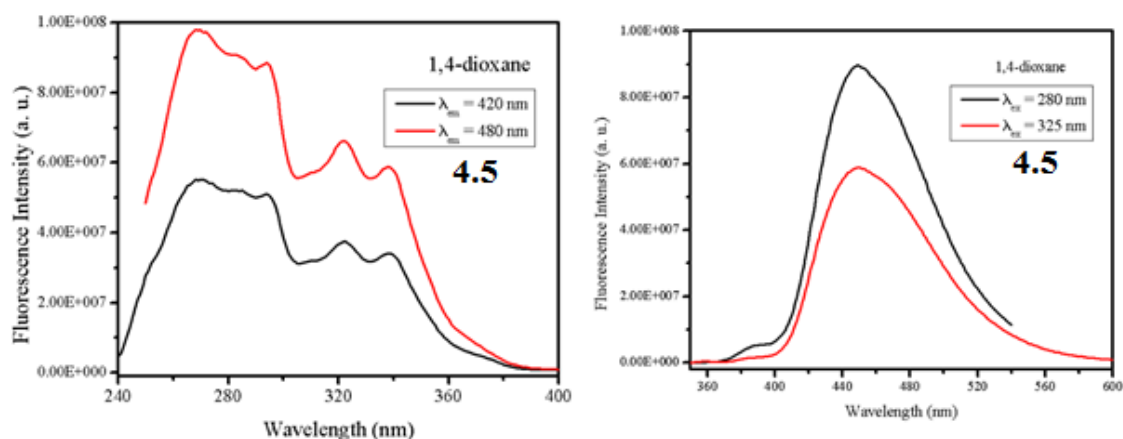


Figure 4.44. Excitation (left) and emission (right) spectra of compound **4.5** in a non-polar solvent (LE state) collected at different wavelengths.

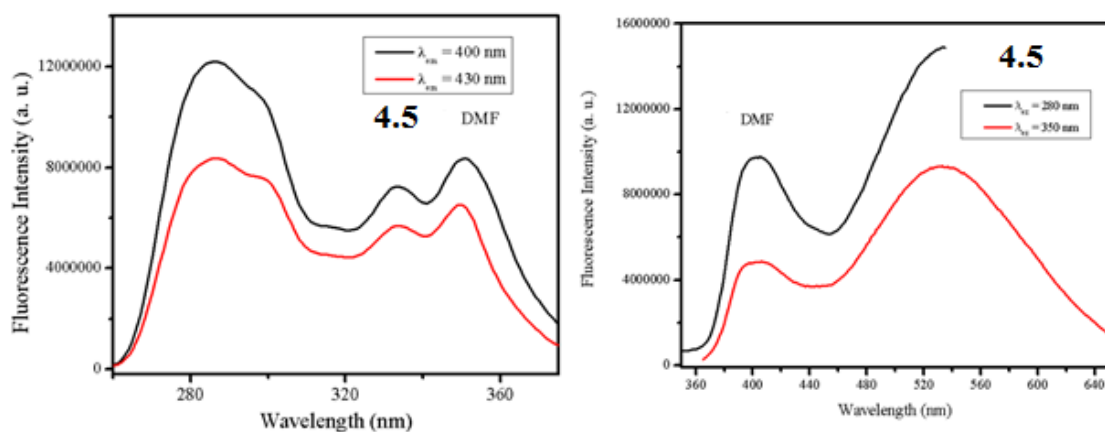


Figure 4.45. Excitation (left) and emission (right) spectra of compound **4.5** in a polar solvent (ICT state) collected at different wavelengths.

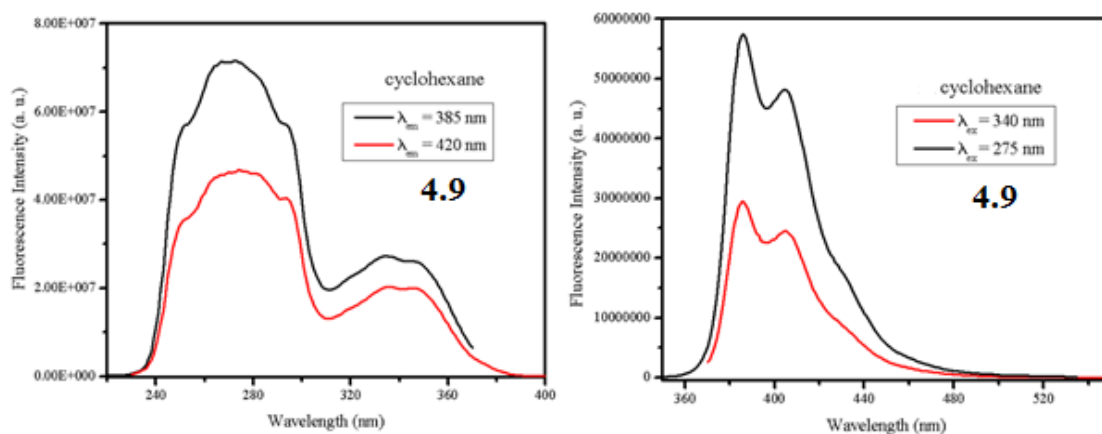


Figure 4.46. Excitation (left) and emission (right) spectra of compound **4.9** in a non-polar solvent collected at different wavelengths.

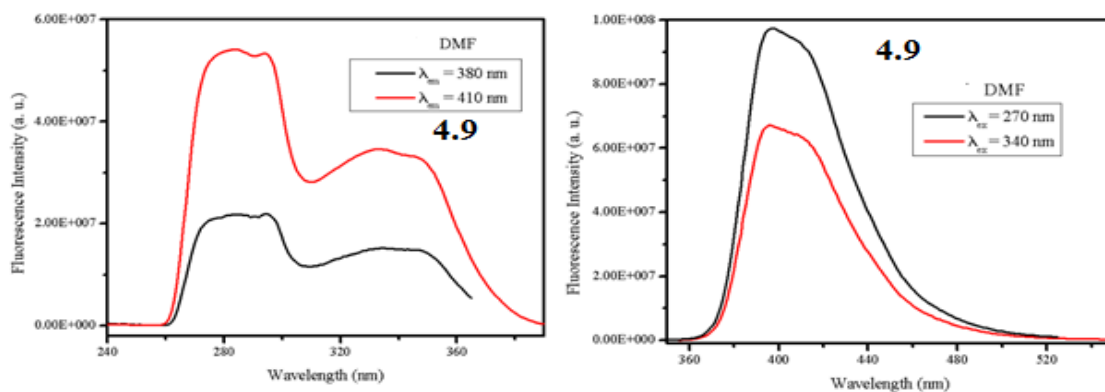


Figure 4.47. Excitation (left) and emission (right) spectra of compound **4.9** in a polar solvent collected at different wavelengths.

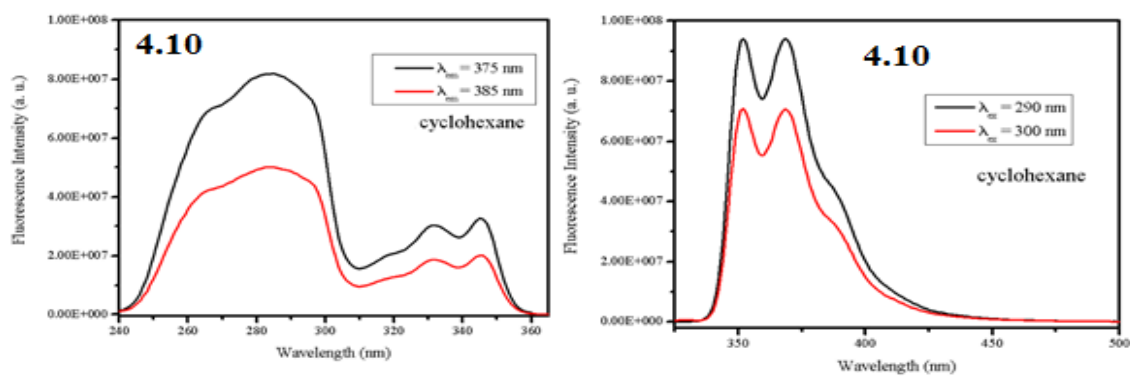


Figure 4.48. Excitation (left) and emission (right) spectra of compound **4.10** in a non-polar solvent collected at different wavelengths.

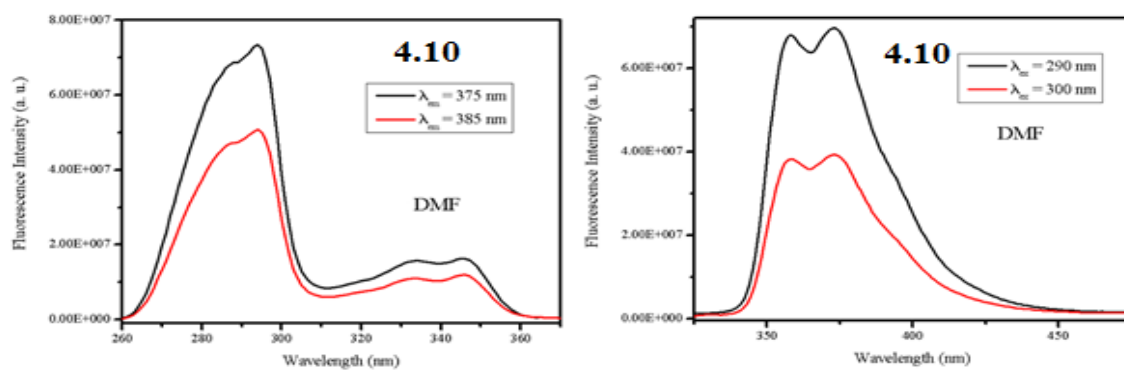


Figure 4.49. Excitation (left) and emission (right) spectra of compound **4.10** in a polar solvent collected at different wavelengths.

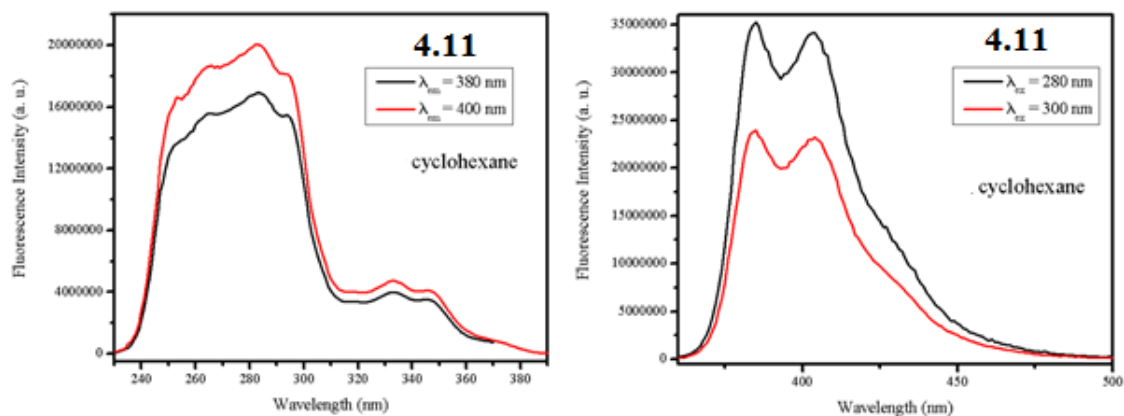


Figure 4.50. Excitation (left) and emission (right) spectra of compound **4.11** in a non-polar solvent collected at different wavelengths.

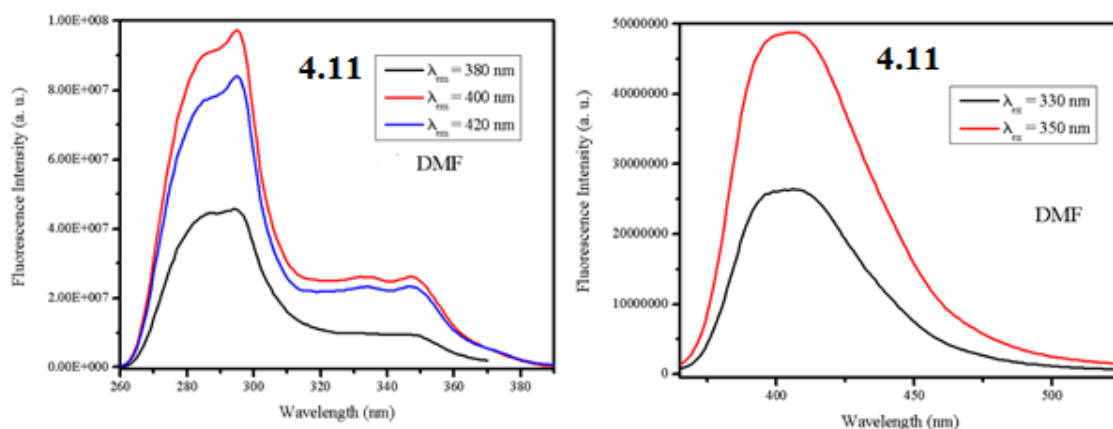


Figure 4.51. Excitation (left) and emission (right) spectra of compound **4.11** in a polar solvent collected at different wavelengths.

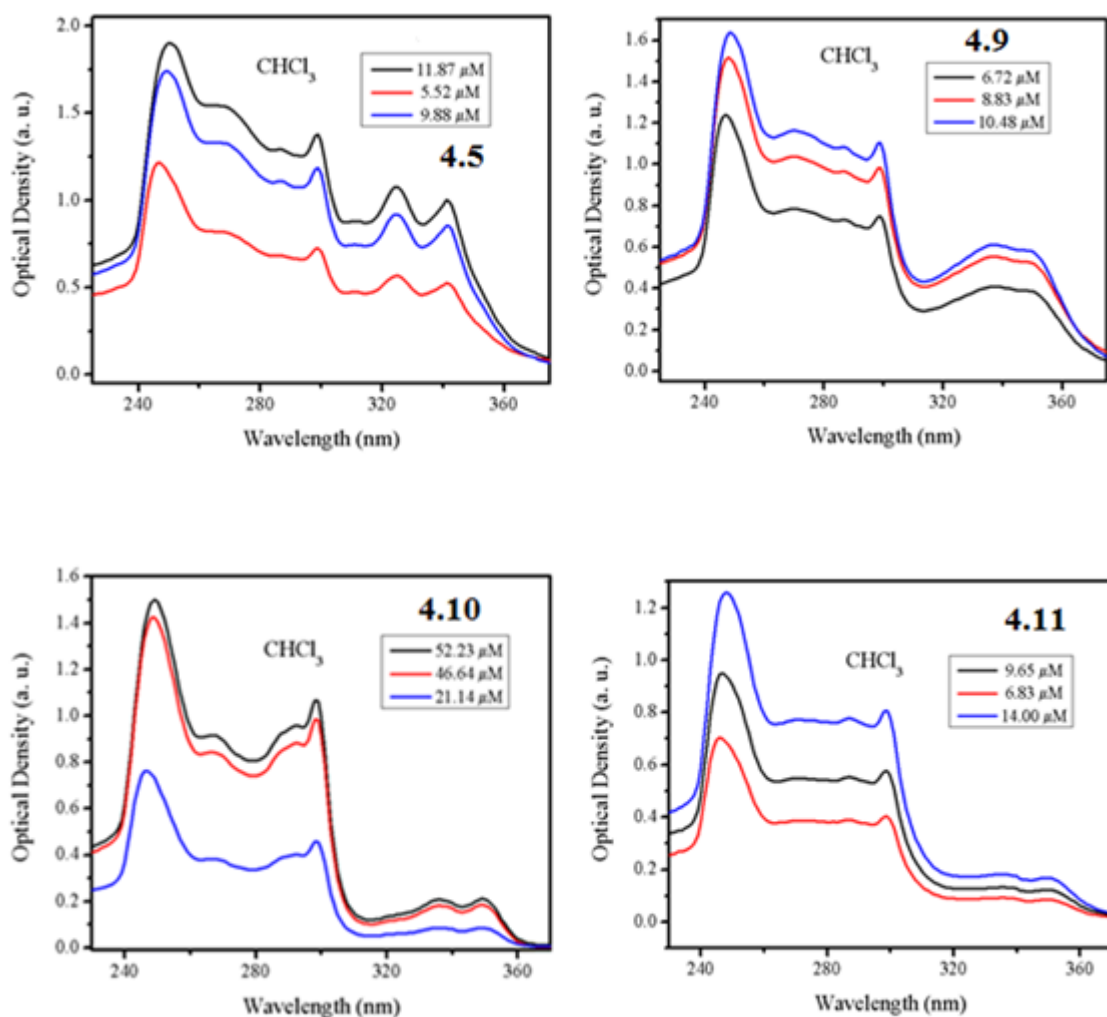
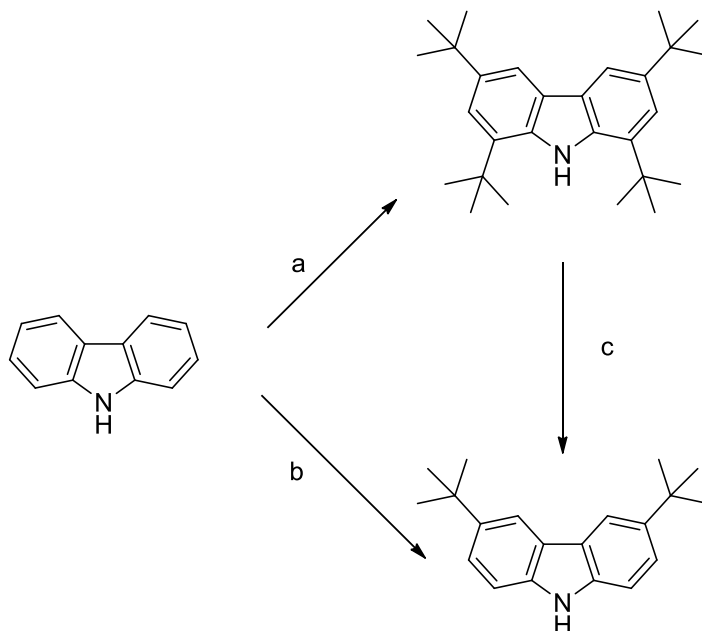


Figure 4.52. Absorption spectra of compounds **4.5**, **4.9**, **4.10** and **4.11** in chloroform solutions of different concentrations.

4.2.8. Synthetic Routes Leading to Compounds 4.5 and 4.9 Starting from Carbazole

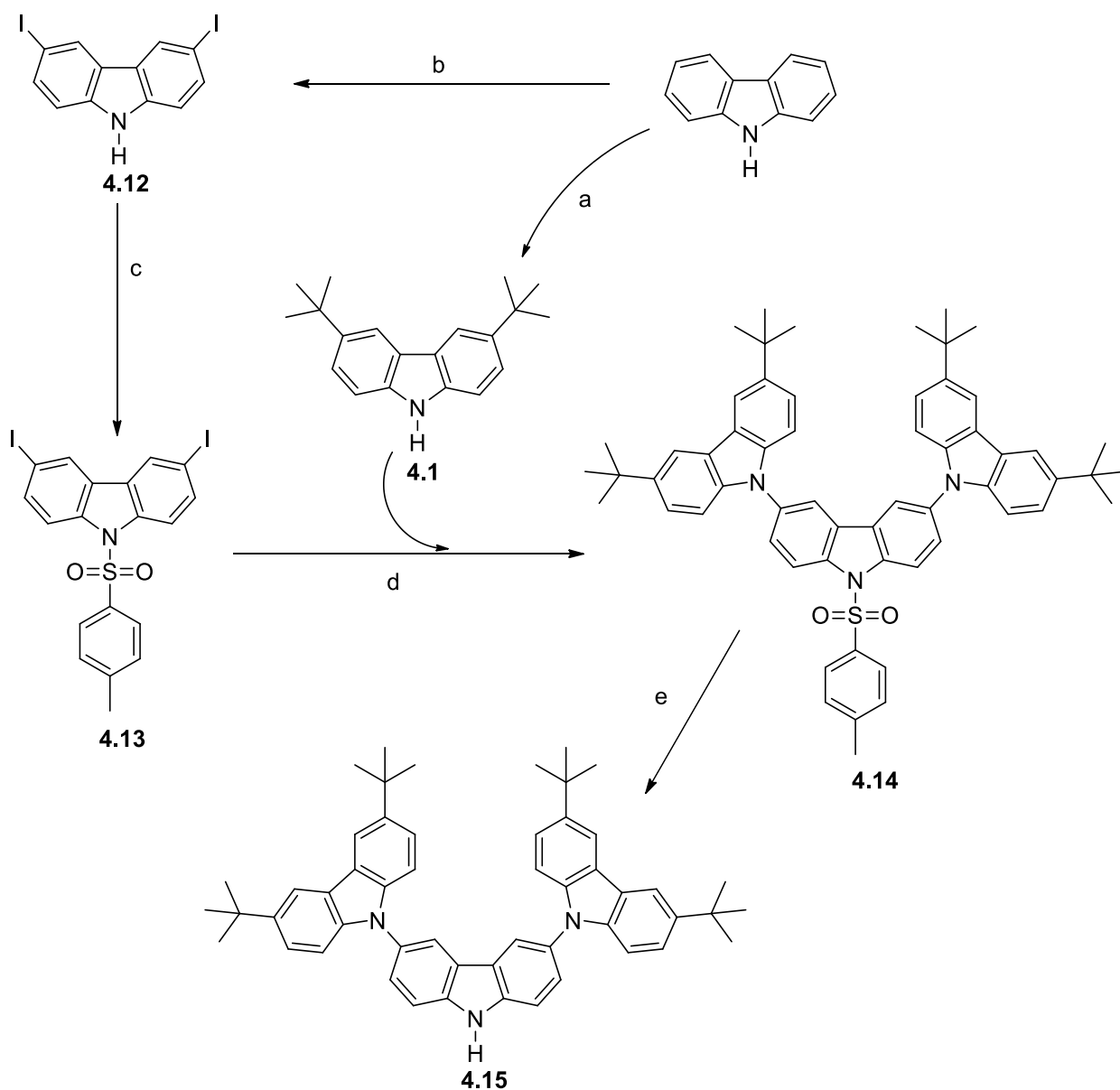


Scheme 4.1. Friedel-Crafts alkylation of carbazole. (a) AlCl_3 (1 eqv) *t*-BuCl (6 eqv), 25 °C, 24 hrs;¹⁵¹ (b) dry ZnCl_2 (3 eqv), *t*-BuCl (3 eqv), nitromethane, inert atmosphere, 25 °C, 5 hrs;¹⁵² (c) H_2SO_4 , 25 °C, 24 hrs.¹⁵¹

As presented in Scheme 4.1, a Friedel-Crafts alkylation of carbazole with *tert*-butyl chloride performed using AlCl_3 , a very strong Lewis acid, leads usually to an over-alkylation problem.¹⁵¹ The reaction leads to a mixture of the di, tri, and tetra-alkylated products. The tetra-alkylated product is the major product when *tert*-butyl chloride is used in excess.¹⁵¹ However, the use of a weaker Lewis acid catalyst such as ZnCl_2 , leads exclusively to the di-alkylated product, even when *tert*-butyl chloride is used in excess.¹⁵² Treatment of the tri and tetra-alkylated derivatives with sulfuric acid leads to a *detert*-butylation and gives the dialkylated product as the major product.¹⁵¹ This can be compared to the *detert*-butylation discussed previously in pyrene, Scheme 2.3. In fact, the two electrophilic aromatic substitution reactions in benzene ring

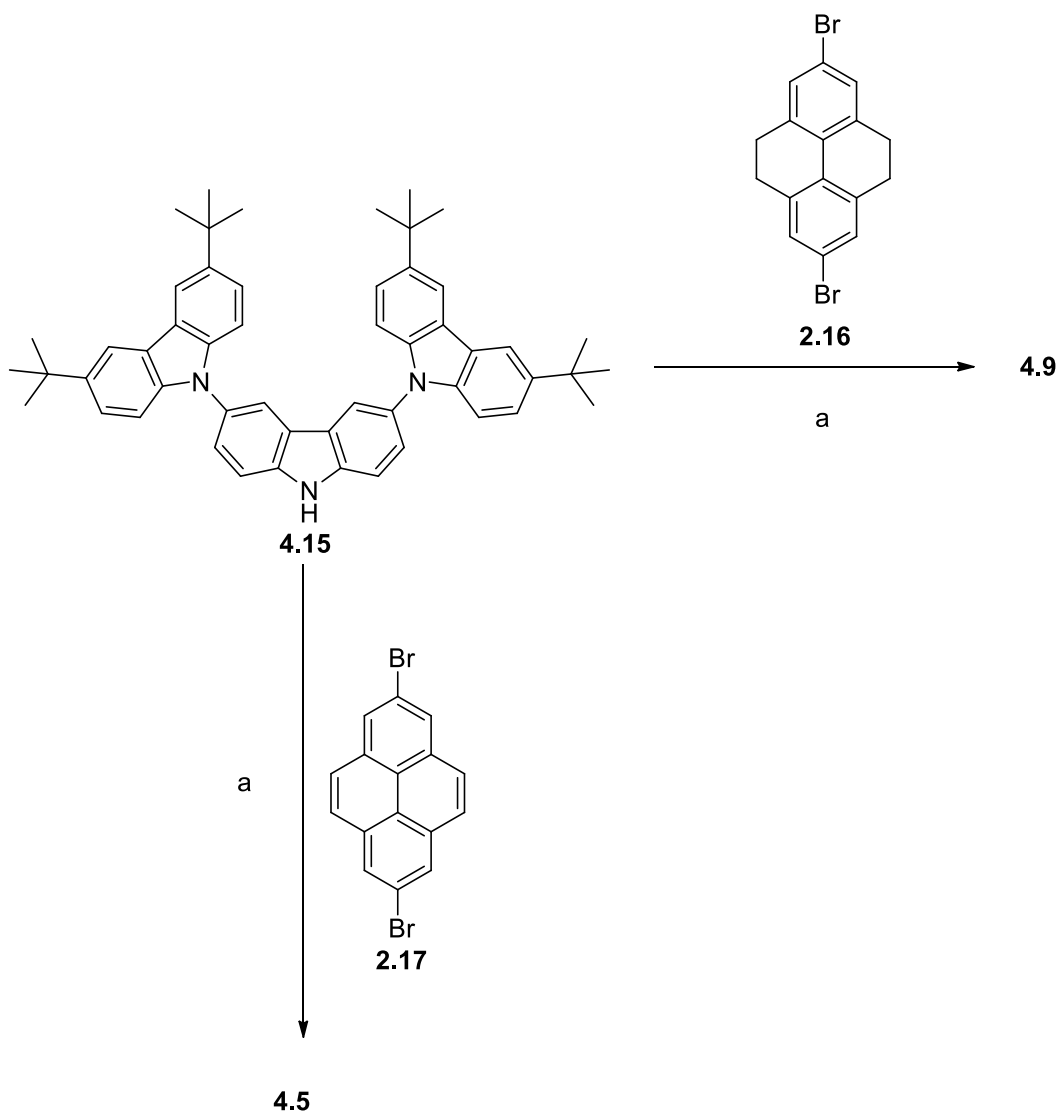
derivatives that are known to be reversible by steric and electronic effects are the Friedel-Crafts alkylation with a bulky alkyl group^{153,154} (i.e. what is being discussed in Scheme 4.1) and the sulfonation reaction.^{153,155} This reversibility explains the unusual *tert*-butylation step discussed in Chapter 2 for some pyrene derivatives as observed by Hu *et al.*,⁷⁵ Scheme 2.3, and similarly for carbazole, Scheme 4.1. It is also known that the detached *tert*-butyl group can either undergo Friedel-Crafts reaction on another aromatic ring (in case an appropriate acceptor is provided, the acceptor can be toluene or a benzene ring more activated than toluene to be able to receive the detached *tert*-butyl group: SN₁-like reaction),¹⁵³ or undergo elimination to form 2-methylpropene which leaves the reaction mixture as a gas (in case an acceptor to receive the *tert*-butyl is not provided i.e. E₁-like reaction).¹⁵³

Many literature reports^{142,156} discussed the synthesis of the disubstituted derivative, exclusively, using AlCl₃ with a limiting amount of *tert*-butyl chloride or limited reaction time. However, to stay on the safe side, our synthesis was carried using the weaker Lewis acid ZnCl₂.



Scheme 4.2. From carbazole to tercarbazole: the copper catalyzed Ullman cross-coupling: (a) dry ZnCl_2 (3 eqv), *t*-BuCl (3 eqv), nitromethane, inert atmosphere, 25 °C, 5 hrs;¹⁵² (b) KI (1.31 eqv), KIO_3 (0.78 eqv), CH_3COOH , reflux, 24 hrs;¹⁵⁷ (c) TsCl (4.4 eqv), KOH (4.4 eqv), acetone, inert atmosphere, reflux, 15 mins;¹⁵⁸ (d) **4.1** (2.2 eqv), CuI (0.5 eqv), (\pm)-*trans*-1,2-diaminocyclohexane (0.52 eqv), K_2CO_3 (2.5 eqv), toluene, inert atmosphere, reflux, 24 hrs;¹⁵⁸ (e) KOH (2 eqv), DMSO:THF:water (3:6:1), inert atmosphere, reflux, 25 mins.¹⁵⁸

The move from carbazole to tercarbazole is achieved through a four-step pathway involving protection of the nitrogen of carbazole following the iodination on positions 3 and 6, Scheme 4.2. The diiodinated nitrogen-protected carbazole (**4.13**) can undergo Ullman cross-coupling (N-C copper-catalyzed coupling) with two other non-nitrogen protected carbazole units previously alkylated with *tert*-butyl groups in positions 3 and 6 (**4.1**).¹⁵⁶ This leads to the nitrogen-protected tercarbazole derivative **4.14**. Finally, a deprotection to get rid of the tosylate introduced in the protection step leads to a tercarbazole unit with four *tert*-butyl substituents blocking all its reactive carbon centers, **4.15** Scheme 4.2.



Scheme 4.3. The Buchwald-Hartwig palladium-catalyzed cross coupling. (a) tris(dibenzylideneacetone)dipalladium(0), tri-*tert*-butylphosphine, sodium *tert*-butoxide, dry toluene, inert anhydrous atmosphere, microwave oven (power: 180 W; max temp: 125 °C; run time: 2 min; hold time: 60 min; pressure: 120 psi).¹³⁷

Reacting compound **4.15** with 2,7-dibromopyrene (**2.17**) or 2,7-dibromo-4,5,9,10-tetrahydropyrene (**2.16**) yields compounds **4.5** and **4.9**, respectively. This is known as the Buchwald-Hartwig coupling (N-C palladium-catalyzed coupling) reaction, and performed in a microwave oven under totally dry and inert conditions, Scheme 4.3.

4.3. Conclusions and Future Work

The investigation of two new tercarbazole-based D-A-D compounds with a pyrene acceptor (**4.5**) and a 4,5,9,10-tetrahydropyrene acceptor (**4.9**) was presented in comparison with previously reported phenanthroline acceptor compound (**4.3**).

Phenanthroline D-A-D derivatives **4.2** (carbazole donor) and **4.3** (tercarbazole donor) emit from their ICT state even in non-polar solvents. Whereas compound **4.5** exhibits a dual emission from both LE and ICT states, where the ICT emission was clearly observed and bathochromically shifted in polar solvents. This conclusion was supported by the double-exponential lifetime decays for this compound except in the most polar (ICT) and the most non-polar (LE) solvents. An increased emission quantum yield for **4.5** in non-polar solvents as compared to polar solvents suggests the occurrence of PET quenching in competition with the radiative decay processes. Whereas for the other compounds, little evidence for ICT was observed in **4.7**, **4.8**, **4.9**, **4.11**, and was limited to a loss of vibrational structure in emission spectra in polar solvent, without any significant bathochromic shift with increasing solvent polarity (unlike compound **4.5**). Absence of ICT evidence was noted for the compounds having weak acceptor (i.e. benzene) and weak donor (i.e. carbazole) (**4.6** and **4.10**).

These results confirm that tercarbazole is a better donor than carbazole. Similarly, phenanthroline is a better acceptor than pyrene, owing to the imine nitrogen present in the former. Pyrene is a better acceptor than 4,5,9,10-tetrahydropyrene and biphenyl, which are both better acceptors than benzene. ICT is more favored with increasing strength of donor and/or acceptor. Chloroform was found to be an excellent quencher for D-A-D and D-A derivatives both based on carbazole (**4.10**) or tercarbazole (**4.9** and **4.11**), possibly through a charge transfer from the donor to chloroform.

Interestingly, quenching by chloroform did not occur in the pyrene derivative **4.5**, this could be related to the PET quenching explained in Figure 4.19.

4.4. Experimental

4.4.1. Synthesis

The syntheses of compounds **2.16** and **2.17** were described earlier in Chapter 3, Paragraph 3.4.1.

The syntheses of compounds **4.5**, **4.9**, **4.10**, **4.11**, **4.12**, **4.13**, **4.14** and **4.15** were performed by Prof. Bilal R. Kaafarani at the laboratories of Prof. Seth R. Marder at Georgia Institute of Technology.

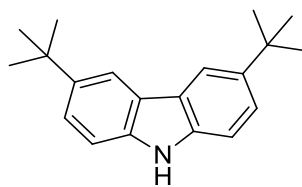
3,6-Di-*tert*-butyl-9*H*-carbazole (4.1)

The title compound was synthesized according to a modified literature procedure.¹⁵² Using a vacuum oven, ZnCl₂ was dried by allowing 20 g of the solid to melt completely and crystallize under reduced pressure (1.5 mmHg).¹⁵⁹ The bulky solid was then ground to fine powder using mortar and pestle, and stored in cryodesiccation freeze-drying apparatus. 9-*H*-carbazole (3.34 g, 20.00 mmols) was dissolved in 100 ml of nitromethane, and the mixture was purged with argon for 20 minutes while stirring at 0 °C. Dry ZnCl₂ (8.18 g, 60.00 mmols, 3 eqv) was then added.

2-Chloro-2-methylpropane (5.55 g, 6.61 mL, 60.00 mmols, 3 eqv) was added to the mixture dropwise over five minutes while stirring at 0 °C. The resulting mixture was allowed to warm-up gradually, and was stirred for 12 hours at room temperature under argon atmosphere. The reaction was quenched with 200 mL water, and extracted with dichloromethane. The combined organic layer was washed with a brine solution (2 x 50 mL), dried over MgSO₄, and filtered. Solvent was removed under reduced

pressure, and the remaining brown solid was recrystallized from heptane.

3,6-Di-*tert*-butyl-9*H*-carbazole **4.1** (5.00 g, 89%), mp 225.6 °C (Lit.¹⁶⁰ 228 °C), was isolated as dark grey needles. ¹H NMR (500 MHz, CDCl₃): δ 8.07 (d, *J* = 2.0 Hz, 2H), 7.57 (bs, 1H), 7.44 (dd, *J* = 8.5, 2.0 Hz, 2H), 7.18 (d, *J* = 8.5 Hz, 2H) 1.44 (s, 18H). ¹³C NMR (125 MHz, CDCl₃): δ 142.13, 137.93, 123.46, 123.16, 116.08, 110.03, 34.65, 32.01.



4.1

4.4.2. *Photophysical Studies*

Absorption spectra were measured using a double-beam JASCO V-570 UV-vis-NIR spectrophotometer, and the fluorescence measurements were done using a Jobin-Yvon-Horiba Fluorolog III spectrofluorometer. The excitation source was a 100 W xenon lamp, and the detector used was R-928 operating at a voltage of 950 V. Right angle mode detection was used. Slit widths were fixed at 5 nm for both entrance and exit slits during both emission and excitation experiments. Corrected emission spectra S_1/R_1 were collected to account for any fluctuation in the xenon lamp over different wavelengths. In parallel to that, S_1 spectra were collected to make sure that the intensity of emission is below 2×10^6 counts per second in order to avoid saturation of

the detector. A blank measurement with no sample in the sample holder was subtracted from all actual spectra to account for any error possible due to the sample holder.

Stock solutions of concentration ranging from 0.5-5 mM of each compound were prepared in chloroform depending on the solubility limit of each compound. Around 0.1 mL of each stock solution was transferred into nine dry glass vials and chloroform was left to evaporate. Then the corresponding solvent was added and diluted to 100 μ M for absorption measurements and to 1-2 μ M for fluorescence studies. Stock solutions were kept in the freezer and used discarded if not used within two days. Molar absorptivity was determined in chloroform due to a decent solubility of all compounds in this solvent. Quantum yield measurements were done using 9,10-diphenylanthracene in cyclohexane as standard with an attributed quantum yield of 1.00.⁹⁹ Excitation wavelength was set to 330 nm for all compounds and the standard. Lifetime and quantum yield measurements were performed on nitrogen-purged solutions, and optical density was maintained below 0.05 for all samples. UV-transparent quartz cuvette (1 x 1 cm) was used for all experiments. Lifetime decays were all collected at emission maxima using the same spectrofluorometer with a nanoLED for excitation at 282 nm, and were all fit to single or double-exponential decays with χ^2 values below 3. Molar absorptivity, quantum yield and fluorescence lifetime were performed as three runs for each compound in every single solvent, and the average value of the three runs was reported. A fourth run was performed in case non-consistent results were obtained in any of the first three runs.

CHAPTER 5⁴⁹

FLUORESCENT ANION SENSORS: DITHIENOPHENAZINE-BASED NOVEL SENSOR FOR ANIONS

5.1. Introduction

5.1.1. From Non-Fluorescent Katapinands to Reaction-Induced Fluorescence

In 1966, Frant and Ross reported for the first time a mechanism of sensing fluoride anions by an electrode.¹⁶¹ It was the beginning of anion sensing, and the electrode used was labeled as electronic sensor (optical sensors were later introduced). In 1968, Park and Simmons reported the selective encapsulation of chloride ions by non-fluorescent diprotonated diazabicyclic compounds, known as katapinands, Figure 5.1.¹⁶² At that time, binding sites for anions were designed as positively charged cations (i.e. the alkyl ammonium cation in Park and Simmons case). The authors suggested that the size and shape of the synthesized bicyclic system played a major role in dictating its selectivity towards spherical halides anions.¹⁶² Their work in 1968 led to the birth of the “anion coordination chemistry”.¹⁶³ Similarly, the older and well-investigated “transition-metal coordination chemistry” was initiated following Alfred Werner’s Nobel Prize in chemistry in 1913.¹⁶³

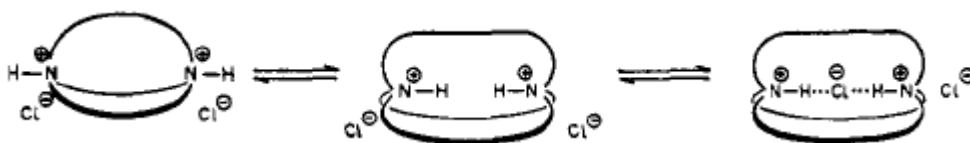


Figure 5.1. The encapsulation of halides in the katapinands cavity.¹⁶²

Positively charged receptors interact with their guest anions via electrostatic binding.²⁹ Whereas neutral binding sites, introduced later on, are able to interact with guests through hydrogen bonding.²⁹ In 1992, Smith *et al.* investigated arylurea used as a non-positively charged receptor, Figure 5.2.¹⁶⁴ Due to the complementary geometry, urea receptor showed enhanced selectivity for Y-shape carboxylate anions through a double hydrogen bonding recognition.^{29,44} Other oxoanions like sulfonates, phosphates, nitrate and nitrite showed similar double hydrogen bonding with the urea receptor, Figure 5.2.^{29,164} The affinity of urea to these oxoanions was found to be linearly proportional to their basicity.^{29,44} Similarly to urea, thiourea receptors showed high affinity for Y-shape carboxylate anion, also due to complementarity, Figure 5.2.⁴⁴

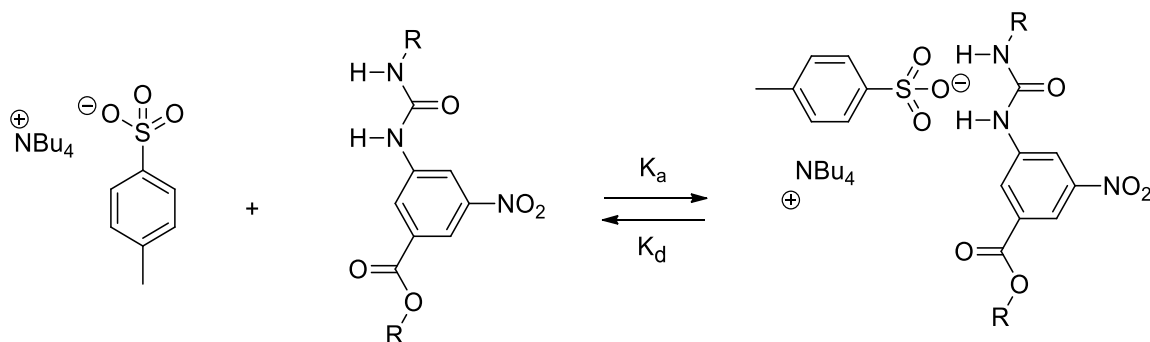


Figure 5.2. Binding process between the arylurea host (hydrogen bond donor) and the tetra-n-butylammonium tosylate guest (hydrogen bond acceptor).¹⁶⁴

After urea and thiourea, different neutral receptors were investigated. These typically included amides,¹⁶⁵ squaramides,^{44,166} thioamides,¹⁶⁵ pyrroles^{37,43} and sulfonamides.^{44,49} Therefore, beside pyrrole receptor, a neutral binding site usually consists of N-H adjacent to an electron withdrawing group (i.e. C=O, C=S, or S=O).⁴⁴ The need of these neutral binding sites arises from the fact that ionic species might

aggregate in non-polar solvents, which limits the ability of investigating their binding to the guests.¹⁶⁷ In addition to this, the reversible binding offered by these neutral receptors allows continuous monitoring of their binding phenomena.^{36,167} Among these neutral receptors, sulfonamide is more acidic than other neutral receptors having similar structures.⁴⁴ Table 5.1 shows the pK_a values of common neutral receptors in DMSO (i.e. polar aprotic solvent). The inclusion of additional electron-withdrawing groups adjacent to the binding site was shown to enhance binding and selectivity towards specific anions.⁴⁴ This is explained by the increased acidity of the N-H making it more available as hydrogen bond donor.^{44,164} Moreover, the increased acidity renders the N-H receptor more vulnerable to deprotonation by basic anions.^{29,168} Therefore the use of these neutral moieties as hosts for anions requires the use of an aprotic solvent²⁹ (i.e. a solvent that cannot act as a hydrogen bond donor and subsequently does not compete with the N-H receptor for the anion).¹⁶⁹ The aprotic solvent can be either polar (i.e. DMSO) or non-polar (i.e. chloroform).²⁹ An increased solvent polarity leads to an increased solvation energy of the anion, and therefore to a less stable receptor-anion H-bond complex.¹⁶⁸ This can favor deprotonation over hydrogen bonding.¹⁶⁸ It might be useful to compare the pK_a of the host receptor with the pK_a of the guest anion.⁴⁴ This comparison may help in interpretation of the binding mechanism, and probably in predicting cases where the deprotonation takes over hydrogen bonding. New anion sensing approaches are still being introduced. The selective deprotection of trialkylsilyl ethers by fluoride was reported as a reaction-based sensing method for fluoride anion, Figure 5.3.¹⁷⁰ However, this method showed limitations due to interference with some other basic anions, such as hydroxide and carboxylate.¹⁷⁰ In 2008, Lee *et al.* reported the reaction-induced fluorescence detection of cyanide, by the mean of nucleophilic

addition of cyanide to a non-fluorescent aromatic aldehyde, leading to a highly fluorescent cyanohydrin.²⁷ The induced fluorescence by nucleophilic addition induced has been shown to occur, selectively, for cyanide anions only.²⁷ Sensors that exhibit a turn-on or turn-off in fluorescence upon recognition of the anion are known as optical sensors (i.e. beside electronic sensors mentioned earlier). In 2011, a novel fluoride-exclusive reaction-based sensing approach was reported by Padie and Zeitler.¹⁷⁰ In which a non-fluorescent monomer reacts selectively with fluoride to produce a fluorescent polymer.¹⁷⁰ In 2012, Dong *et al.* reported for the first time a sequential triple output mode recognition of fluoride (based on the deprotection method shown in Figure 5.3), followed by a subsequent recognition of cyanide, Figure 5.4.¹⁷¹ The ongoing introduction of new sensing approaches indicates that the design of compounds and receptors of particular selectivity towards a single anion exclusively, remains a vague and relatively under-explored research field.

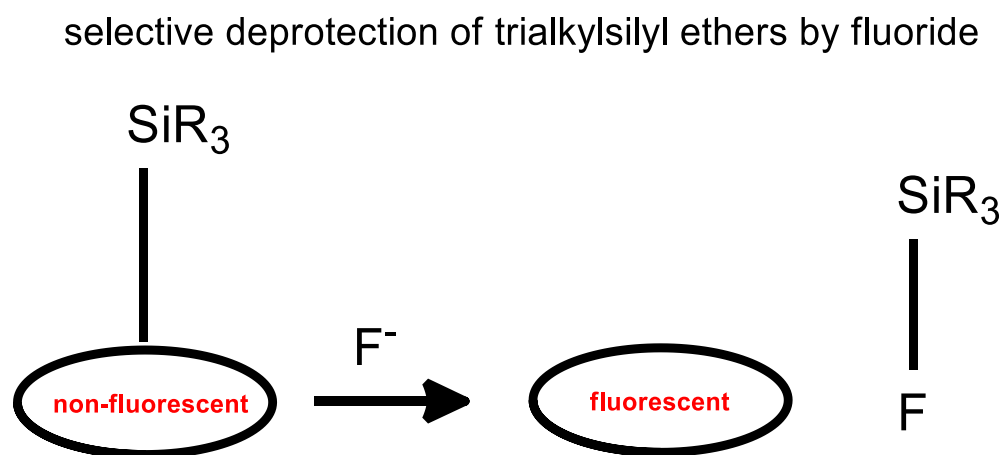


Figure 5.3. Deprotection-induced fluorescence selectively used for fluoride detection.¹⁷⁰

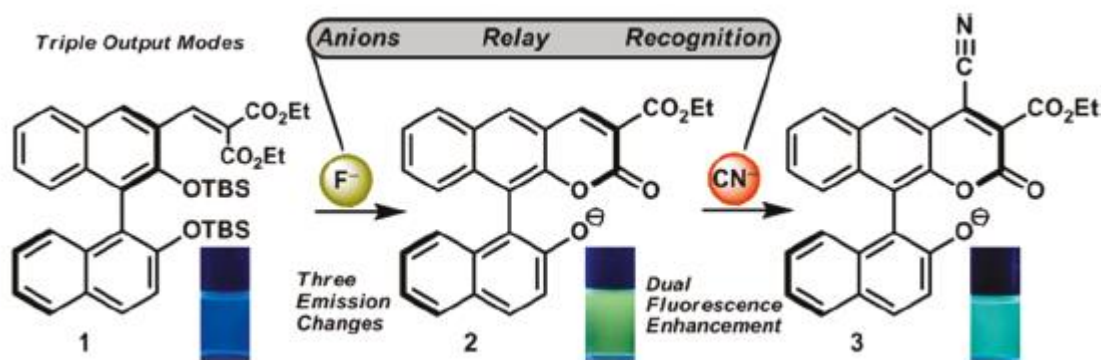


Figure 5.4. Reaction-based sequential relay recognition of fluoride followed by cyanide using a triple output mode.¹⁷¹ Reprinted with permission from (Dong, M.; Peng, Y.; Dong, Y.-M.; Tang, N.; Wang, Y.-W. *Org. Lett.* **2012**, *14*, 130). Copyright (2012) American Chemical Society

5.1.2. Our Contribution to the Field

Our research group has previously reported on the synthesis and binding studies of fluorescent sensors for anions and cations based on different fluorophores and binding sites. Fluorophores investigated were phenanthrophenazine (DPP) as a core in cation sensors,¹⁷²⁻¹⁷⁴ dibenzophenazine as a core in anion sensors,¹⁷⁵ and quinoxalinophenanthrophenazine (TQPP) as a core in both cation^{172,174} and anion³⁶ sensors. While receptors investigated were sulfonamides as binding site for anions,^{36,175} and crown ether as binding site for cations.¹⁷²⁻¹⁷⁴

In this work, we are interested in designing efficient sensors for anions based on a neutral sulfonamide binding site, along with a dithienophenazine as a core, which is being investigated for the first time in our research group in anion sensors.⁴⁹ Unsubstituted dithieno[3,2-*a*:2',3'-*c*]phenazine has been investigated as a fluorophore in anion sensor, for the first time, by Aboubakr *et al.*, in 2013.¹⁷⁶ Thiophene-based fluorophores, such as dithienobenzoimidazole, have been previously investigated in cation sensor by Satapathy *et al.* in 2012.¹⁷⁷

Fluorophores containing two thiophene rings have been previously reported for OFET¹⁷⁸ and OPV¹⁷⁹ applications. However, they are still much less explored as cores in anion sensors. Among neutral receptors for anions, sulfonamides show high sensitivity and selectivity which makes them of particular interest.^{169,176} However, they are still among the least investigated neutral receptors for anions.^{169,180} The actual work can be regarded as a design of new sensors by combining one of the least investigated fluorophores to one of the least investigated neutral receptor.

A competent anion sensor usually satisfies the following conditions:^{34,170,176}

- Selective binding to specific guest (i.e. able to discriminate between different guests).
- Reversible binding to the anions in order to allow continuous monitoring of binding phenomena.
- Good stability in solution. In other words, the sensor's photophysical properties must not change over time unless specific guest anions are added.
- Efficient signaling from the binding site to the fluorescent core upon binding. An efficient signaling must induce clear changes in one of the properties of the fluorophore (i.e. color, redox potential, absorption, emission, proton NMR spectra...).

The anion-induced spectral changes are controlled by the binding affinity of the host (binding site) to its guest, and the signaling from the binding site to the fluorescent core.³⁴ For the binding affinity, it can be monitored through cyclic voltammetry in electronic sensors, and through calorimetric and spectroscopic titrations for optical sensors.³⁴ Based on which the calculation of the binding constant (i.e. affinity) of the sensor to different anions can be done.

For the signaling process, the signal from the receptor to the core induces detectable changes in absorption, emission and proton NMR upon binding to the anion.³⁴ The signaling process can be compared to the way human eyes (i.e. receptor/binding site) signal to the brain (i.e. signaling to the fluorescent core) upon the recognition of something they can see (i.e. specific guest/anion). This signal might trigger or inhibit a certain reaction in the brain (i.e. enhancing or quenching fluorescence of the fluorophore).

Different signaling mechanisms are reported in the literature for fluorescent sensors,³⁶ among which we can list: PET (photoinduced electron transfer),¹⁸¹ ICT (intramolecular charge transfer),¹⁸² FRET (Förster resonance energy transfer),¹⁸³ exciplex (excited sensor-ligand complex) or excimer (excited dimer) formation/dissociation,^{28,184} MLCT (metal to ligand charge transfer),¹⁸⁵ and ESIPT (excited state intramolecular proton transfer).¹⁸⁶ Brief explanations of some signaling mechanisms are provided as examples in Figures 5.5 and 5.6.^{32,149}

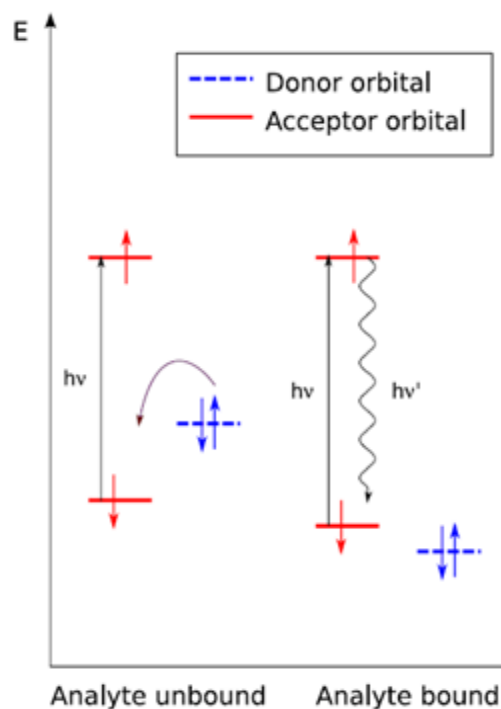


Figure 5.5. PET signaling that induces a “switch-on” of fluorescence.¹⁴⁹ Reprinted with permission from (Kowalczyk, T.; Lin, Z.; Van Voorhis, T. *J. Phys. Chem. A* **2010**, *114*, 10427). Copyright (2010) American Chemical Society.

Examples of PET sensors are donor-acceptor (D-A) systems in which the initial photoexcitation is localized on the acceptor.¹⁴⁹ In the absence of analyte, nonradiative relaxation pathways are present, due to the HOMO of the donor being higher in energy than that of the acceptor, Figure 5.5.¹⁴⁹ Binding of the sensor to its particular analyte “turns on” fluorescence by lowering the energy level of the donor HOMO below that of the acceptor, Figure 5.5.¹⁴⁹ The analyte-free PET quenching (i.e. in the absence of analyte in Figure 5.5) is similar to the one discussed previously in Chapter 4, for compound **4.5**, Figure 4.19.¹⁴⁹

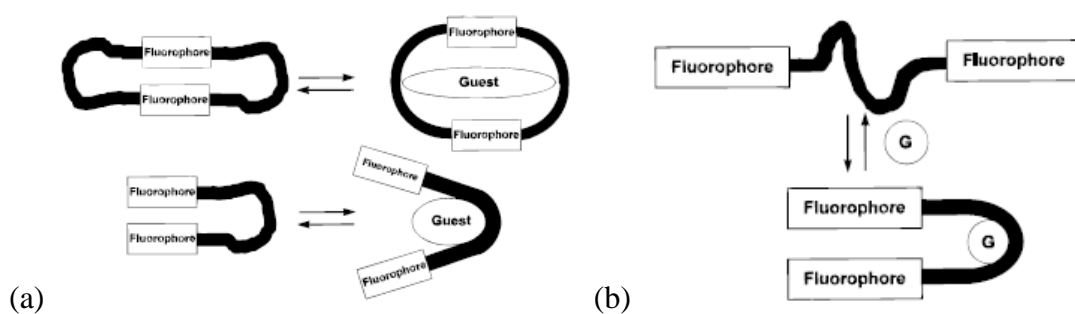


Figure 5.6. (a) excimer to monomer; (b) monomer to excimer.³² Reprinted with permission from (De Silva, A. P.; Gunaratne, H. Q. N.; Gunnlaugsson, T.; Huxley, A. J. M.; McCoy, C. P.; Rademacher, J. T.; Rice, T. E. *Chem. Rev.* **1997**, *97*, 1515). Copyright (1997) American Chemical Society.

The cornerstone of the monomer-excimer signaling mechanism is that the monomer and the excimer have different emission wavelengths.³² Therefore, upon binding, the emission will be quenched at one wavelength and enhanced at another one; depending on either the excimer is being dissociated into separate monomers or it is being formed upon binding of the guest, Figures 5.6a and 5.6b, respectively.³²

Table 5.1. Reported pK_a values in DMSO at 25 °C of some neutral receptors.¹⁸⁷⁻¹⁸⁹

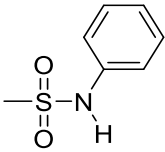
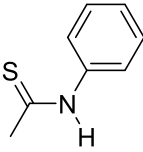
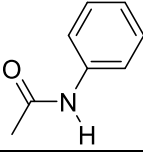
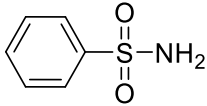
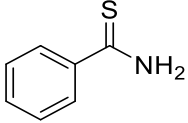
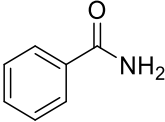
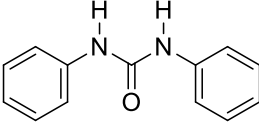
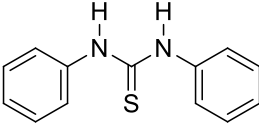
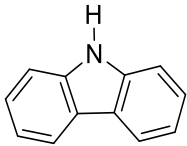
Neutral Receptor	pK _a
	12.9
	14.7
	21.5
	16.1
	16.9
	23.3
	19.5
	13.4
	19.9

Table 5.2. Reported pK_a values in DMSO at 25 °C of some anions.¹⁸⁷

Anion Added of TBA salts	pK _a
Acetate	12.3
Benzoate	11.1
Bromide	0.9
Chloride	1.8
Cyanide	12.9
Fluoride	15.0

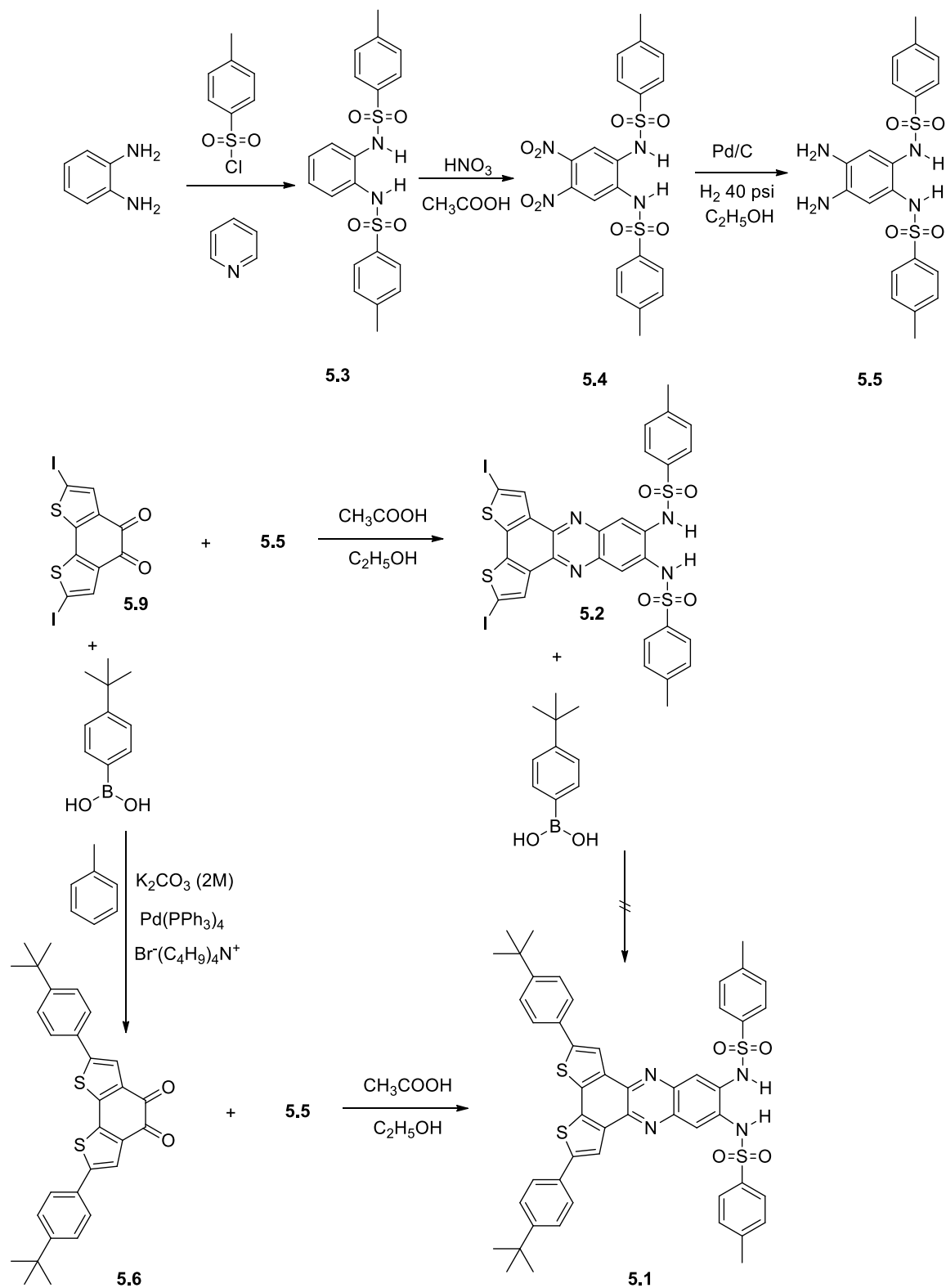
5.2. Results and Discussion

5.2.1. Synthesis and Stability

Sensors **5.1** and **5.2** were synthesized according to scheme 5.1. Synthesis of compound **5.5** was done through a three-reaction pathway (tosylation, nitration and reduction) starting from benzene-1,2-diamine, with an overall yield of 40% according to literature procedures.¹⁹⁰⁻¹⁹² Diketone **5.9** was obtained from Prof. Seth R. Marder's research group. Suzuki coupling reaction was performed using two different literature procedures involving toluene²³ and 1,4-dioxane¹⁹ as solvents, to give diketone **5.6** (with yields of 49% and 85%, respectively); which upon condensation with **5.5** according to a literature procedure,¹⁹³ yielded sensor **5.1** with a 51% yield. The condensation of **5.5** with **5.9** according to the same literature procedure,¹⁹³ yielded sensor **5.2** with 70% yield. Suzuki reaction on sensor **5.2** did not yield sensor **5.1**, probably due to the presence of sulfonamide groups that may interfere with the palladium-catalyzed Suzuki reaction. Therefore, Suzuki reaction is done before the condensation (using the diketone), and not after it (using the sensor). In the following the photophysical properties of two new dithienophenazine-based sensors **5.1** and **5.2** are discussed. Comparison with other sulfonamide-based sensors investigated previously by our research group (sensors **5.7**¹⁷⁵ and **5.8**³⁶ in Figure 5.7), is also discussed, when needed in the discussion. Some properties of these four sensors are summarized in Table 5.3.

Table 5.3. Some properties of the sulfonamide-based anion sensors **5.1**, **5.2**, **5.7** and **5.8**.

Sensor	Fluorophore	Solubility in CHCl ₃	λ_{max}^{em} , nm
5.1	Dithienophenazine	+	620 in CHCl ₃
5.2	Dithienophenazine	-	575 in DMSO/CH ₃ CN
5.7 ¹⁷⁵	Dibenzophenazine	+	440 in CHCl ₃
5.8 ³⁶	TQPP	+	500 in CH ₂ Cl ₂ /CH ₃ CN



Scheme 5.1. Synthetic scheme of sensors **5.1** and **5.2**.

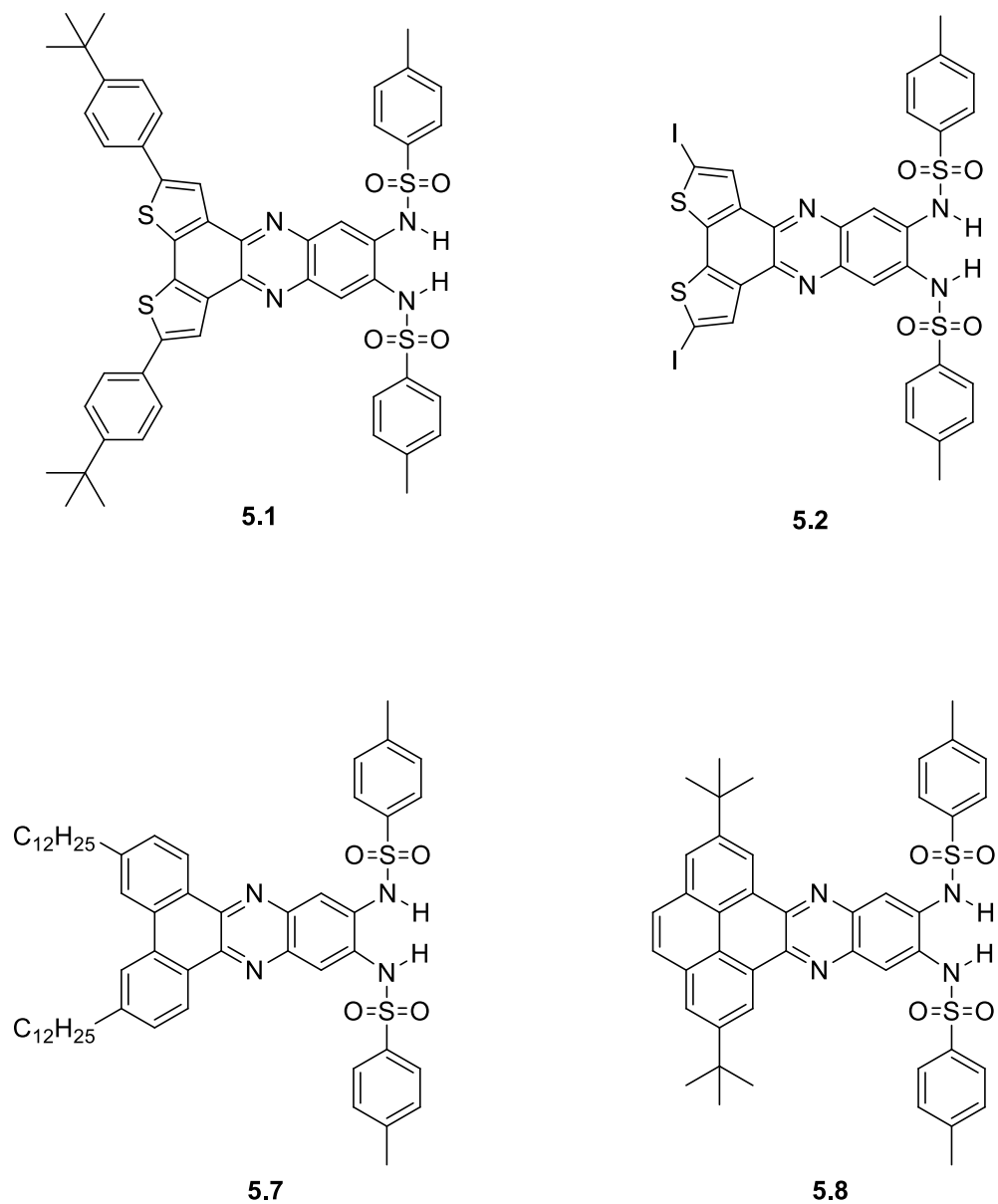


Figure 5.7. Structures of novel dithienophenazine sensors **5.1** and **5.2**; and the previously investigated dibenzophenazine sensor **5.7**¹⁷⁵ and quinoxalinophenanthrophenazine sensor **5.8**³⁶ by our research group.

Sensor **5.1** was fairly soluble in chloroform; however, sensor **5.2** was found to be soluble in DMSO only. This is attributed to the inclusion of the hydrophobic *tert*-butylphenyl substituents instead of the iodines of sensor **5.2** through the Suzuki-Miyaura coupling reaction, Scheme 5.1.

Furthermore, unlike the unstable sensor **5.2** in DMSO, sensor **5.1** showed a decent stability in chloroform solution, Figure 5.8. This is explained by the change in absorption and emission spectra of sensor **5.2** in DMSO, over time, without the addition of anion, despite the storage at low temperature in dark, Figure 5.9. Whereas the spectra of sensor **5.1** in chloroform did not change after a storage of 48 hours, Figure 5.8. This might be attributed to an aggregation of the sensor in DMSO at the molecular level (i.e. the case might be similar to the aggregation of adjacent unsubstituted pyrene cores introduced in Chapter 2 of this thesis, and once aryl substituents are introduced this aggregation is inhibited). This spectral instability limited the possibility of investigating sensor **5.2** in DMSO. Preparing a stock solution of **5.2** in DMSO, and then diluting it with chloroform improved the stability of its spectroscopic properties over time to a certain extent, Figure 5.10, and diluting with acetonitrile seemed to induce further improvement, Figure 5.11. However, the limitation faced in the latter case is a significant decrease in solubility.

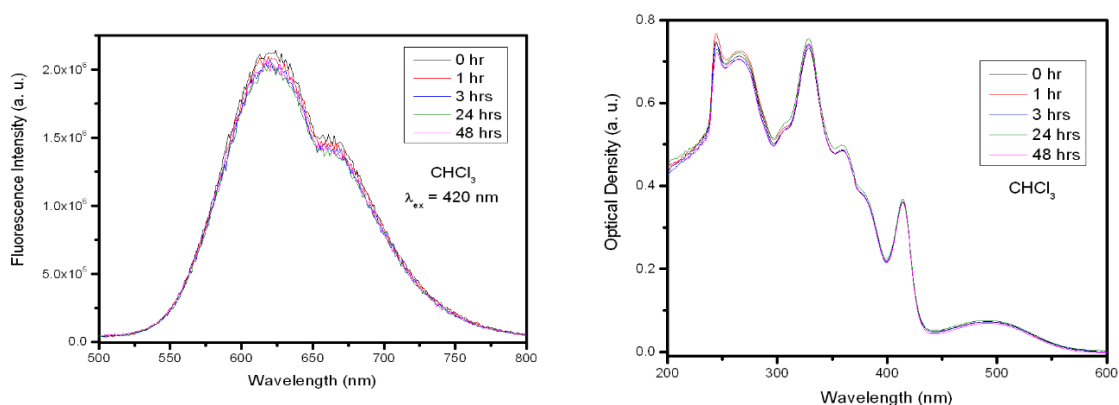


Figure 5.8. Emission (left) and absorption (right) changes of 10 μM solution of sensor **5.1** in chloroform over 48 hours (kept in dark at 0 °C) without the addition of anion.

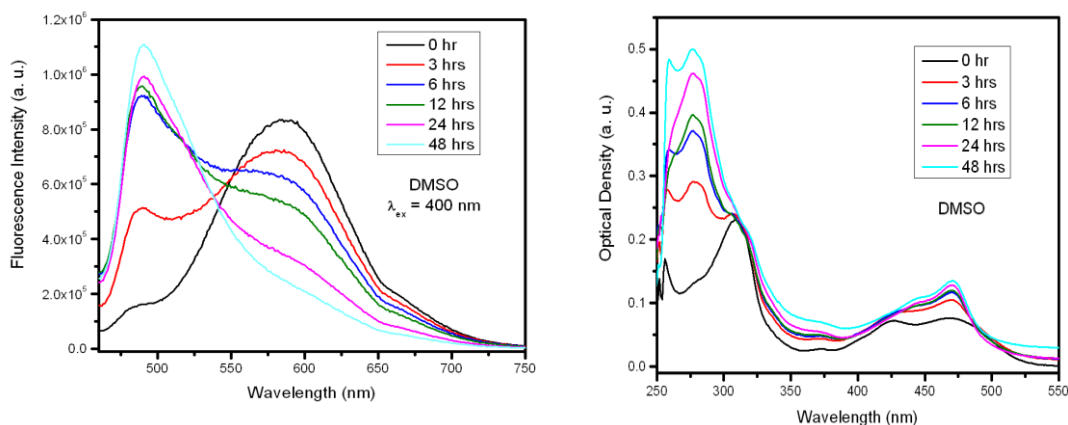


Figure 5.9. Emission (left) and absorption (right) changes of 5 μM solution of sensor 5.2 in DMSO over 48 hours (kept in dark at 0 $^{\circ}\text{C}$) without the addition of anion.

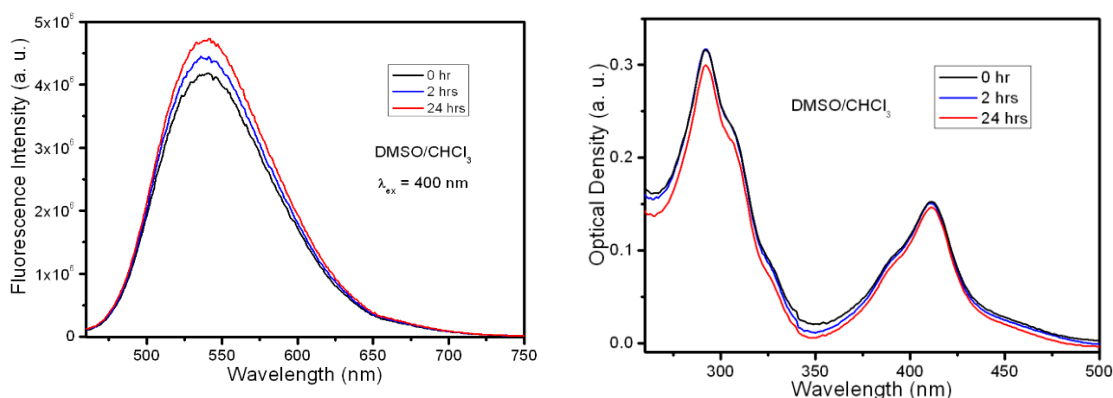


Figure 5.10. Emission (left) and absorption (right) changes of 5 μM solution of sensor 5.2 in 5% DMSO in CHCl₃ over 24 hours (kept in dark at 0 $^{\circ}\text{C}$) without the addition of anion.

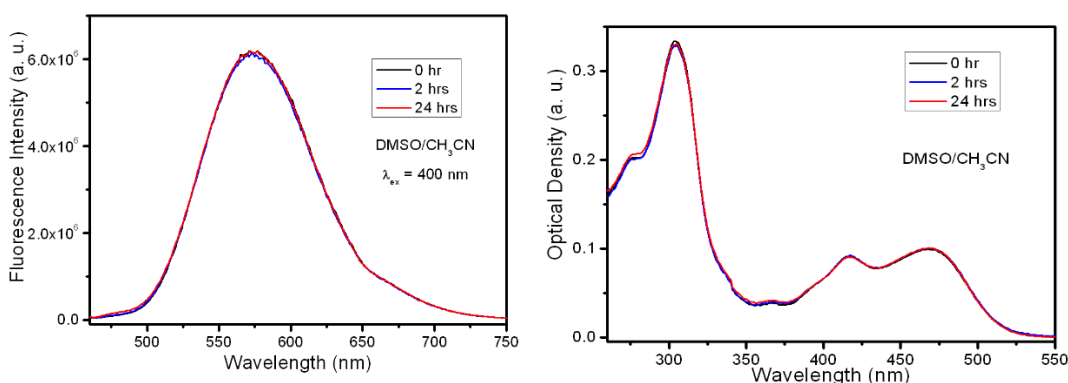


Figure 5.11. Emission (left) and absorption (right) changes of 5 μM solution of sensor 5.2 in 5% DMSO in CH₃CN over 24 hours (kept in dark at 0 $^{\circ}\text{C}$) without the addition of anion.

5.2.2. Spectroscopic Titrations of Sensor 5.1

As previously mentioned, the two main types of anion sensors are electronic and optical sensors. Electronic sensors are usually investigated through cyclic voltammetry experiments.³⁴ However, for optical sensors, as in the case of sensors studied in this Chapter, there are mainly four different types of titration experiments that can be done, as follows:

- Calorimetric titration is a powerful titration method, but it is not affordable everywhere. The technique allows the determination of binding affinity constant, and the estimation of binding stoichiometry by measuring enthalpy changes (ΔH) upon the addition of guest to host in an apparatus called isothermal calorimeter.¹⁹⁴
- Proton NMR titration is usually a very informative method. It consists of adding guest solution to a host and measuring the change in chemical shift values of the protons affected by the host-guest binding. It allows the calculation of binding constant, but is applicable only when $\log(K) < 5$ (i.e. for relatively weak-binding anions).¹⁹⁴
- Absorption and emission titrations can be used for determining binding constants of anions having relatively large binding constants, that cannot be determined based on proton NMR.¹⁹⁴

In this study, the binding of nine anions to sensor **5.1** was studied in chloroform. The anions were used as tetrabutylammonium and/or tetraethylammonium salts (i.e. acetate, benzoate, bromide, chloride, cyanide, fluoride, iodide, nitrate and phosphate monobasic/dihydrogen phosphate). Tetramethylammonium salts did not dissolve in chloroform. Proton NMR titrations were used for the determination of binding constants of bromide, chloride, iodide and nitrate, since these anions showed $\log(K) < 4$, and thus satisfied the main condition for the applicability of proton NMR titrations.

5.2.2.1. Absorption and Emission Studies of Sensor **5.1**

Sensor **5.1** in chloroform displays three characteristic absorption peaks at 327, 414, and 498 nm. Excitation at 420 nm leads to an emission spectrum with a single peak at 620 nm, Figure 5.12. Emission spectra obtained by exciting at different excitation wavelengths were collected for different solutions of different concentrations of **5.1** in chloroform. These spectra showed no change upon variation of excitation wavelengths or/and concentrations, beside the expected change in the intensity of emission, Figure 5.12. Similar results were obtained upon collecting the excitation spectra at different emission wavelengths. This proves that $S_1 \rightarrow S_0$ of the sensor is the only emitting species, and rules out any excimer formation.^{15,32}

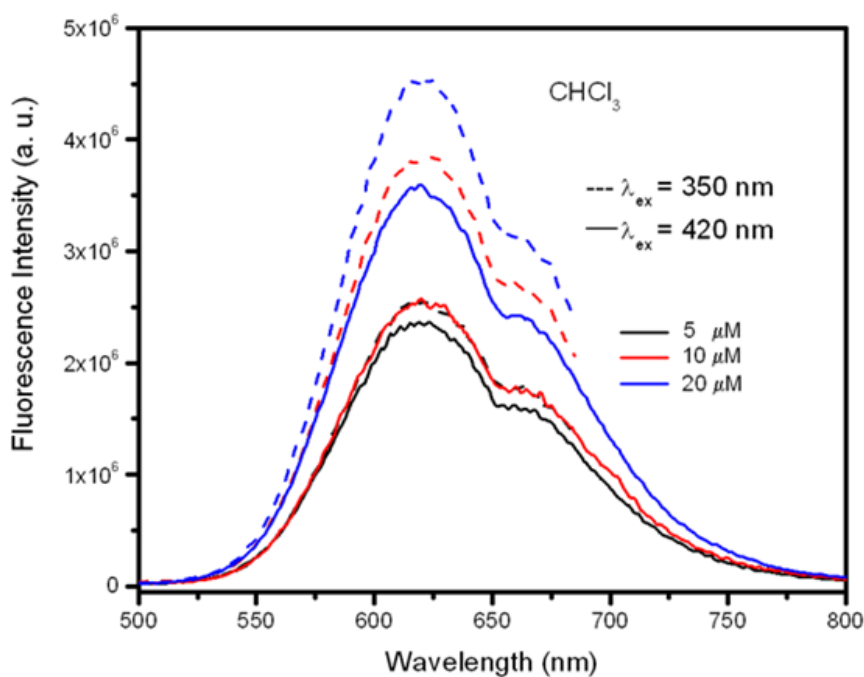


Figure 5.12. Emission spectra of sensor **5.1** at different concentrations in chloroform collected at different excitation wavelengths.

Addition of anions leads to changes in the absorption and emission spectra of the sensor. These changes are more pronounced for acetate, benzoate, cyanide and phosphate (i.e. strong-binding anions). Three isosbestic points appear in the absorption spectra at 420, 388 and 365 nm after the addition of strong-binding anions, indicating a clean transformation from the free sensor state to the bound state with anion (i.e. sensor-anion complex). In parallel to the absorption changes, the emission maximum shifts from 620 gradually towards 560 nm. Less pronounced changes occur upon titration with fluoride, and much smaller for larger-sized halides and nitrate. Spectra of absorption and emission titration experiments with three strong-binding anions are shown in Figure 5.13-5.15. Figure 5.16 shows the relative change in emission at 560 nm upon the addition of the nine selected anions. The plot in Figure 5.16 is generated based on the average of three repetitions for every titration with a specific anion. In case of inconsistent results, a fourth repetition was performed. Figure 5.17 shows the clear change in the sensor properties upon addition of strong-binding anions, where the change in color is detectable by naked eye. Sensors that exhibit a change in color upon binding are known as colorimetric sensors.

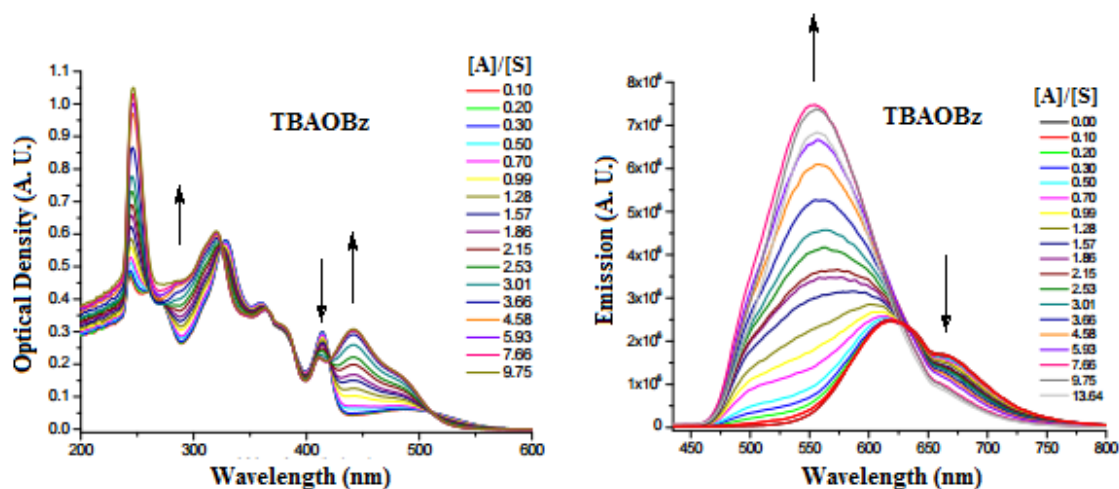


Figure 5.13. Absorption (left) and emission (right) spectra of sensor **5.1** (10 μM) upon titration with tetrabutylammonium benzoate in chloroform at 25 $^{\circ}\text{C}$.

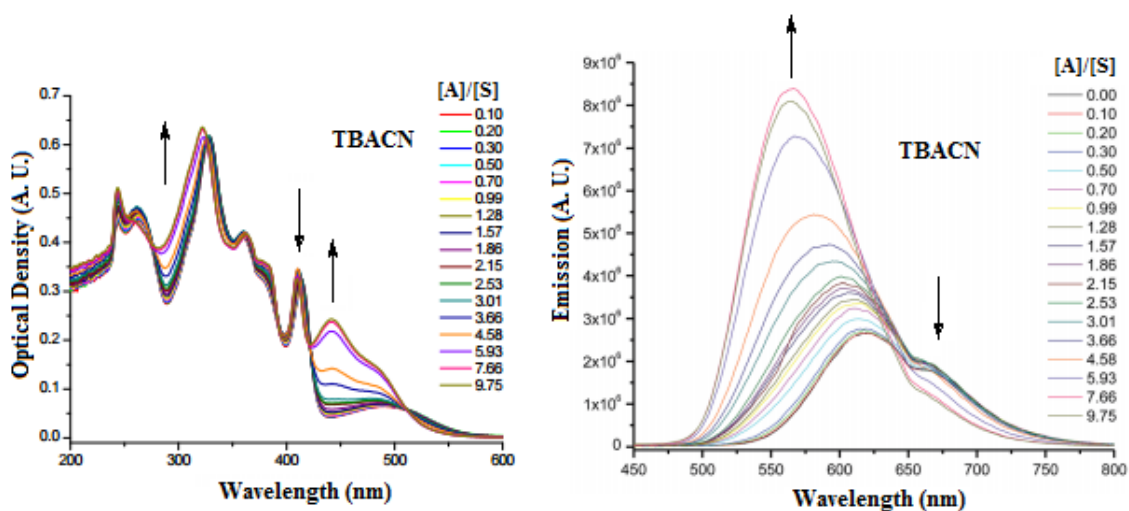


Figure 5.14. Absorption (left) and emission (right) spectra of sensor **5.1** ($10 \mu\text{M}$) upon titration with tetrabutylammonium cyanide in chloroform at 25°C .

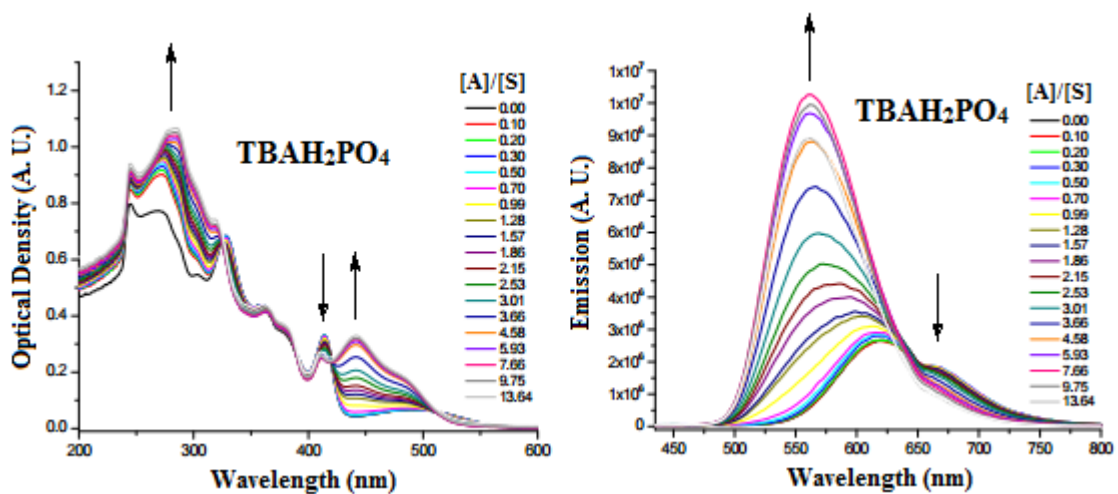


Figure 5.15. Absorption (left) and emission (right) spectra of sensor **5.1** ($10 \mu\text{M}$) upon titration with tetrabutylammonium phosphate monobasic in chloroform at 25°C .

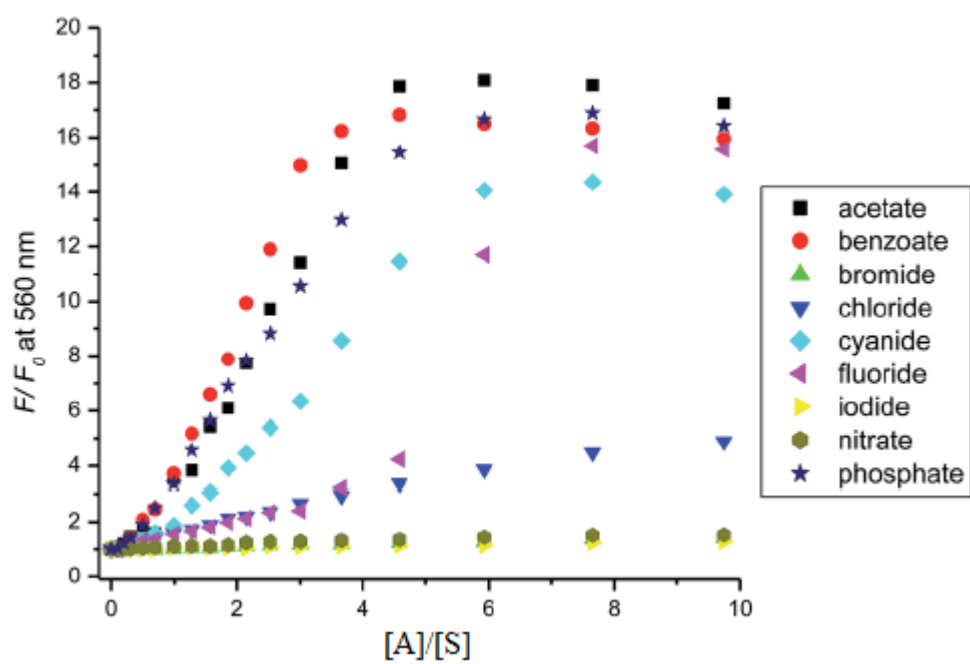


Figure 5.16. Relative change in emission intensity of **5.1** (10 μM) at 560 nm upon titration with different anions in chloroform at 25 $^{\circ}\text{C}$.



Figure 5.17. Solution of **5.1** (10 μM) turning from orange to yellow upon addition of one equivalent of tetrabutylammonium benzoate in chloroform at 25 $^{\circ}\text{C}$.

The main difference observed by comparing sensor **5.1** to similar sensors investigated previously by our group (**5.7** and **5.8**) is the presence of sulfur atoms. The non-bonding electron pairs on sulfur might create a new binding site for the tetrabutylammonium cation. The interaction with the cation affects the absorption and emission spectra and the observed spectral changes upon adding tetrabutylammonium salts of strong binding anions. Dramatic changes in the emission spectra of **5.1** were observed after the addition of these strong binding anions (acetate, benzoate, cyanide and phosphate), and saturation was not reached until exceeding four equivalents of these anion, Figure 5.16. This was not the case for sensors **5.7** and **5.8**, where the changes in spectra were limited to below one equivalent of the strong binding anions. This is explained by the very high binding affinity for these anions, where saturation occurs immediately after the anion is added in the correct stoichiometric ratio (depending on the binding stoichiometry, which is 1:1 for sensors **5.7** and **5.8**). The need of more than four equivalents of salt to reach saturation might be related to an interaction between the tetrabutylammonium cation and the complex (sensor/anion). The affinity of the cation turns out to be stronger than its affinity to the corresponding anion in the tetrabutylammonium salts used. Therefore, after addition of one equivalent of salt, the hydrogen bonding site with anion is saturated (i.e. very strong-binding anions), and the changes occurring in the emission spectra after exceeding one equivalent of added salt might be due to an electrostatic binding between the cation and the four non-bonding electron pairs available on sulfur. This might explain the need of more than four equivalents of salt in order to reach saturation in emission spectra for very strong-binding anions. The most popular way of determining stoichiometry of binding is the method of continuous variations, also called Job's method.¹⁹⁴ This method, as its name

suggests, involves close and continuous monitoring of the variations in spectral properties (i.e. changes in optical density at a specific wavelength) upon changing the molar fractions of both sensor and anion, while the total concentration of both species together is maintained constant.¹⁹⁴ Applying Job's method to determine the stoichiometry of sensor/anion binding might be limited here by the presence of the cation/(sensor-anion complex) interaction. In this case, the stoichiometry of binding is estimated from the spectral changes observed during spectroscopic titrations using strong-binding anions (i.e. having a large binding constant).¹⁹⁴

5.2.2.2. Proton NMR Titrations of Sensor 5.1

Sensor **5.1** showed very strong affinities towards carboxylate (acetate and benzoate), cyanide, and dihydrogen phosphate anions. Excluding dihydrogen phosphate, similar trends in the changes in chemical shifts of aromatic protons in NMR spectra upon titrating **5.1** with the other three anions were observed. Weaker affinity towards fluoride was observed and very weak affinity towards larger-sized halides and nitrate anions. These results look consistent with the ones obtained in the absorption and emission titrations.

As suggested from the absorption and emission titrations with strong-binding anions, the use of a sulfur-containing dithienophenazine core might be changing the mechanism of binding between the sensor and the tetrabutylammonium salts. Interestingly, due to the suspected new binding mechanism, significant and informative changes in chemical shifts of every single aromatic proton were observed upon the addition of tetrabutylammonium salts of strong-binding anions to the sensor solution, which was not the case for sensors **5.7** and **5.8**.

Monitoring the sulfonamide-anion binding can be detected by a significant downfield shift of the N-H peak in case of hydrogen bonding. This has been reported earlier by Al-Sayah and Branda upon titrating sensors having thiourea and squaramide receptors.¹⁶⁶ However, as previously mentioned, deprotonation can take place due to the basicity of the anion (i.e. fluoride, Table 5.2).⁴⁴ In this case, the formation of a very stable HF_2^- complex can be detected in the proton NMR spectrum as a new triplet (due to H-F coupling) appearing around 16 ppm, upon the addition of fluoride anion.¹⁹⁵ Regardless a recognition by hydrogen bonding or by deprotonation, the binding process of the anion to the N-H binding site induces changes in the electron density map at different sites of the fluorophore. This affects the chemical shifts of many protons of the fluorophore, and not only the N-H proton of the binding site. In the case of sensor **5.1**, the binding site N-H proton could not be monitored; since the peak disappeared completely after the first anion addition, probably due to an exchange with residual water in CDCl_3 . This was the case in all titration experiments with all selected anions. Therefore, proton NMR titration experiments are done in this case to analyze the changes in chemical shifts of aromatic protons of the fluorophore (i.e. $\text{H}_a - \text{H}_f$, Figure 5.18) and not the proton of the binding site.

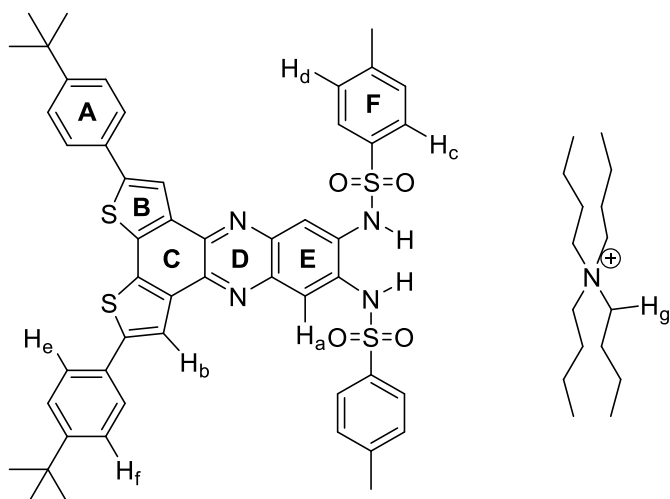


Figure 5.18. Labeling of hydrogens and rings of sensor **5.1**.

Monitoring the electrostatic binding between sulfur and tetrabutylammonium cation was done through tracking the chemical shift of H_g , due to its close proximity from the positively charged nitrogen of the ammonium group. No change in the chemical shift of this proton was observed for sensors **5.7** and **5.8**. This supports the observation of an electrostatic interaction taking place between sulfur and the cation.

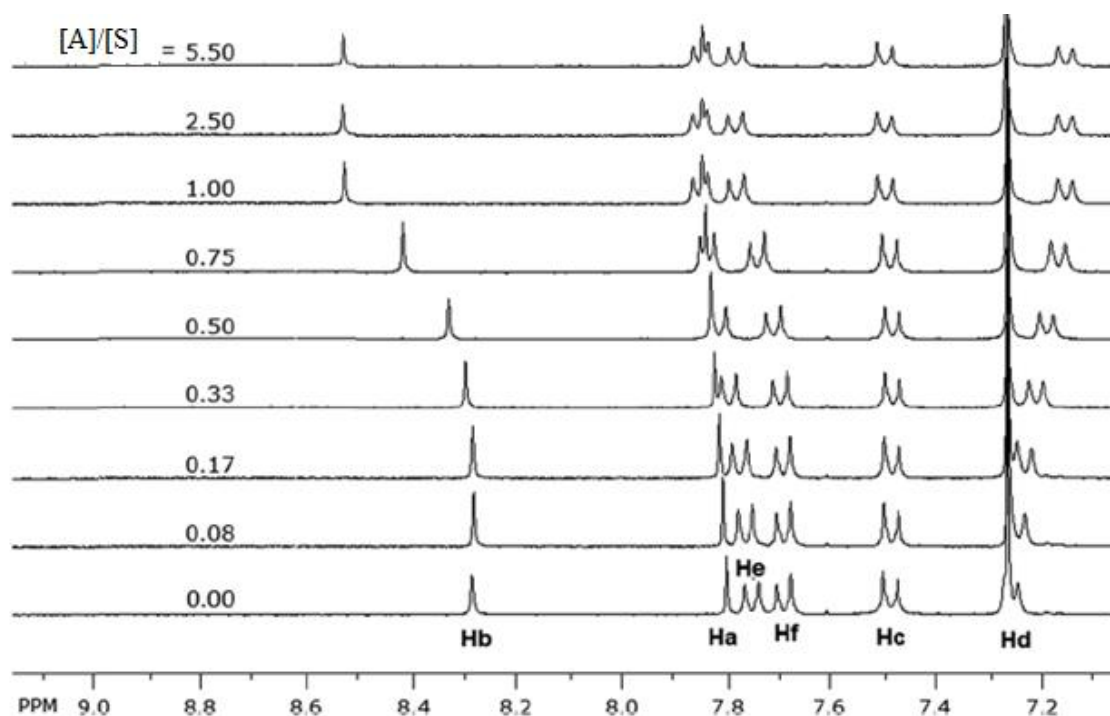


Figure 5.19. Changes in chemical shifts of aromatic protons of sensor **5.1** (2.0 mM) upon titration with tetrabutylammonium acetate in CDCl_3 .

- H_b , H_e , H_f : The interaction of tetrabutylammonium cation with the lone pairs of the sulfur creates a partial positive charge on the sulfur atoms. This is enough to explain the pronounced downfield shift of H_b of the thiophene ring **B**, which showed the largest change in chemical shift among all aromatic protons. Subsequently, moderate downfield shifts of H_e and H_f were consistent with a decrease of electron density in ring **A** because of the same cation-induced partial positive charge on sulfur (i.e. cation-induced electron-withdrawing effect).

- H_c , H_d : As expected, the binding of the anion increases the electron density on the sulfonamide binding site of the sensor, and subsequently on ring **F** because the $\text{S}=\text{O}$ becomes more electron-rich (i.e. less electron-withdrawing) due to increased electron density on the adjacent nitrogen. This explains the upfield shift of H_d .

However, for H_c, a slight downfield shift was observed, despite the increased electron density. This may be due to its close proximity to the binding site of the anion (*ortho*-position) which causes a through-space (hydrogen bond-like) interaction between the anion and H_c. This through-space interaction inhibits the upfield shift (expected due electron density increase in ring **F**), and induces a slight downfield shift instead. This is consistent with previous observations regarding the protons directly adjacent (*ortho*-position) to sulfonamide binding in sensors investigated by our research group in chloroform-d solutions.^{36,175} However, the use of DMSO-d₆, which can itself exhibit hydrogen bonding, has been found to block this through-space interaction, resulting in the expected upfield shift for protons in the *ortho* position to S=O, by the increase of electron density.³⁶

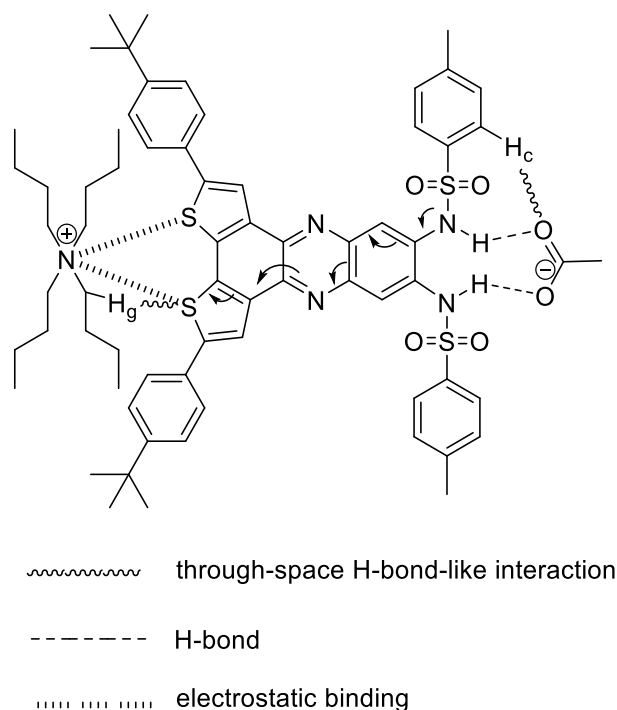


Figure 5.20. Illustration of the suggested binding mechanism of tetrabutylammonium acetate to sensor **5.1** and the interactions of H_c and H_g with the guest ions.

H_a seems to be affected by two effects as follows:

- The anion-induced increase in electron density on the nitrogen of the sulfonamide receptor. This subsequently means an increase in electron density in ring **E** (similarly to the other binding-site-adjacent ring **F**).
- The cation-induced electron withdrawing effect of the sulfur in the thiophene ring **B**. This subsequently leads to a redistribution of the electron density map in all rings of the fluorophore, in a way that ring **B** receives electrons from all adjacent rings.

In sensors **5.7** and **5.8**, a pronounced upfield shift was observed due to the anion-induced effect (since these sensors are not affected by cations). However, the cation-induced effect seems to be dominating in the case of sensor **5.1**. This was observed through a slight downfield shift of this H_a proton during NMR titrations.

Unexpectedly, the downfield shift observed for H_a upon titrating with different anions, was followed by an upfield shift in the case of fluoride and dihydrogen phosphate anion exclusively. The upfield shift took place upon exceeding one equivalent of these two anions, Figure 5.21. This upfield shift (which is stronger for fluoride) is an indicator of an unusual increase in electron density on H_a. This might suggest a deprotonation of the N-H by these anions upon exceeding 1:1 ratio, consistent with their relatively higher basicity, Table 5.2.

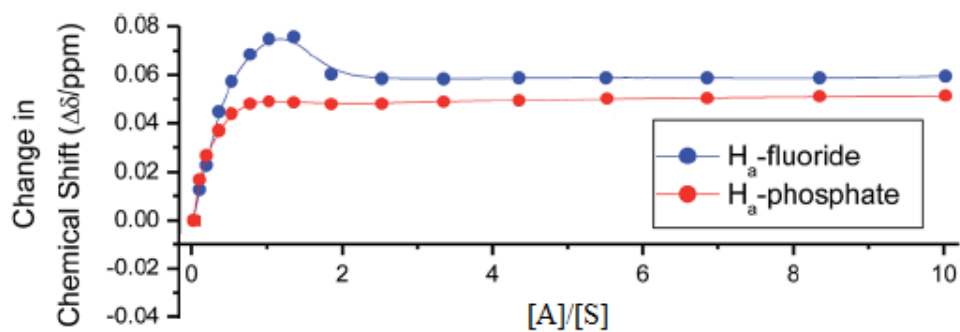


Figure 5.21. Change in chemical shifts of H_a upon titration of sensor **5.1** (2.0 mM) with tetrabutylammonium salts of fluoride (blue) and dihydrogen phosphate (red) in CDCl₃.

The change in chemical shifts of all aromatic protons discussed above was mainly occurring upon addition of one equivalent of a strong-binding anion (i.e. mainly acetate, benzoate and cyanide). This might suggest a 1:1 binding stoichiometry between sensor **5.1** and these anions, and is consistent with previously reported sulfonamide-based sensors.^{36,44,169,175,176} Small changes of aromatic protons of **5.1** were observed upon addition of nitrate, chloride, bromide and iodide. This is consistent with a weak affinity towards these anions previously observed in absorption and emission titrations.

- H_g: Upon titrating sensor **5.1** with strong binding anions, a very small upfield shift for H_g was observed before reaching one equivalent of anion concentration (i.e. before the N-H binding site is saturated). This was followed by a large downfield shift until exceeding four equivalents of added strong-binding anion, Figures 5.22 and 5.23. Such behavior was not reported for sulfonamide-based sensors **5.7** and **5.8**. This might suggest that H_g proton is involved in through-space H-bond-like interaction with the lone pair of sulfur upon exceeding 1:1 ratio of **5.1** to tetrabutylammonium salt. This may be seen similarly to the downfield shift of H_c, adjacent to the anion binding site due to through-space H-bond-like interaction with the anion.

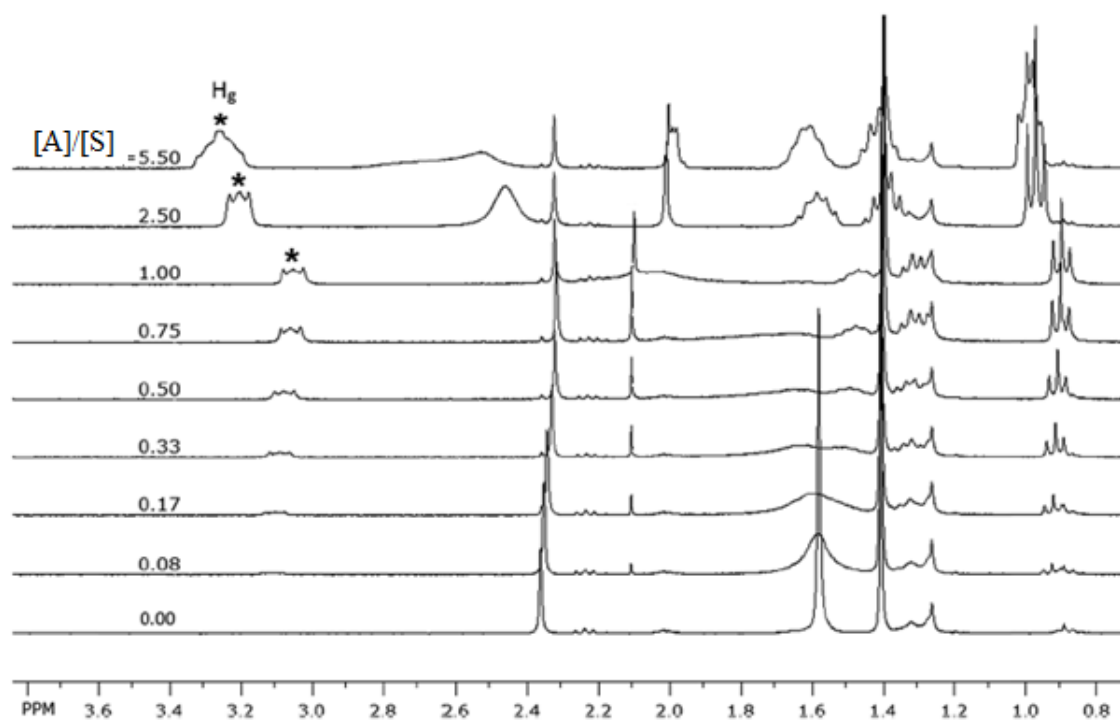


Figure 5.22. Change in chemical shifts of aliphatic protons upon titration of sensor **5.1** (2.0 mM) with tetrabutylammonium acetate in CDCl_3 .

The electrostatic binding between the thiophene and tetrabutylammonium cation was significant only in titrations with strong-binding anions (i.e. might be occurring in parallel to the hydrogen bonding between the corresponding anion and the N-H receptor). Small changes in the chemical shift of H_g was observed upon the addition of weak-binding anions such as halides and nitrate, Figure 5.23. Furthermore, upon the titration with tetraethylammonium salts, the downfield shift of H_g was more pronounced with respect to the corresponding tetrabutylammonium salt of the same anion. This can be explained by the smaller size of tetraethylammonium cations, which decreases the steric interactions between the alkyl chains of the cation and ring **A** bearing a bulky *tert*-butyl substituent.

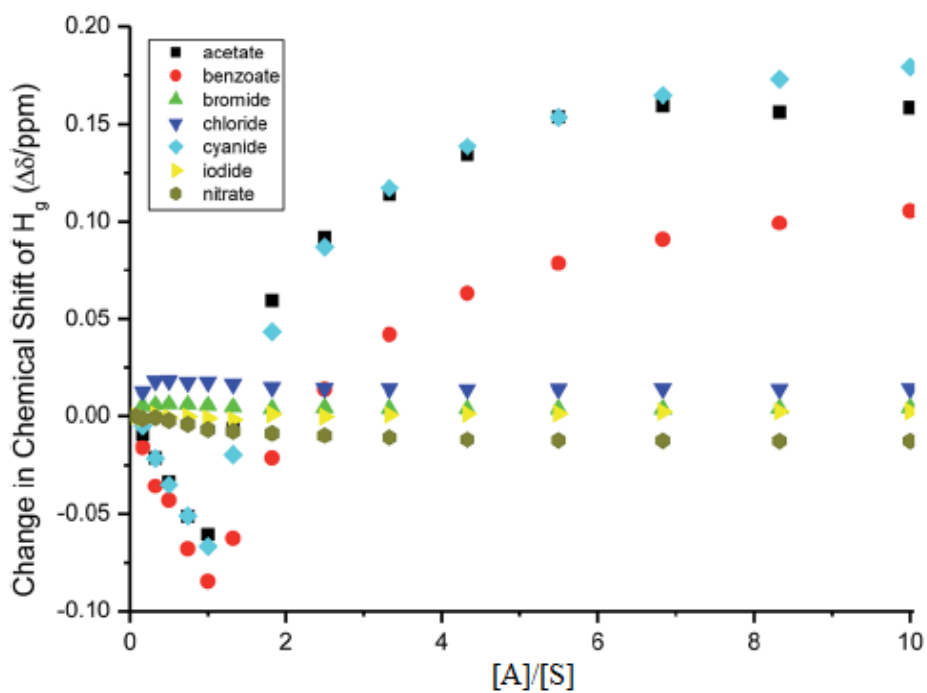


Figure 5.23. Change in chemical shifts of H_g upon titration of sensor **5.1** (2.0 mM) with tetrabutylammonium salts of strong and weak binding anions in $CDCl_3$.

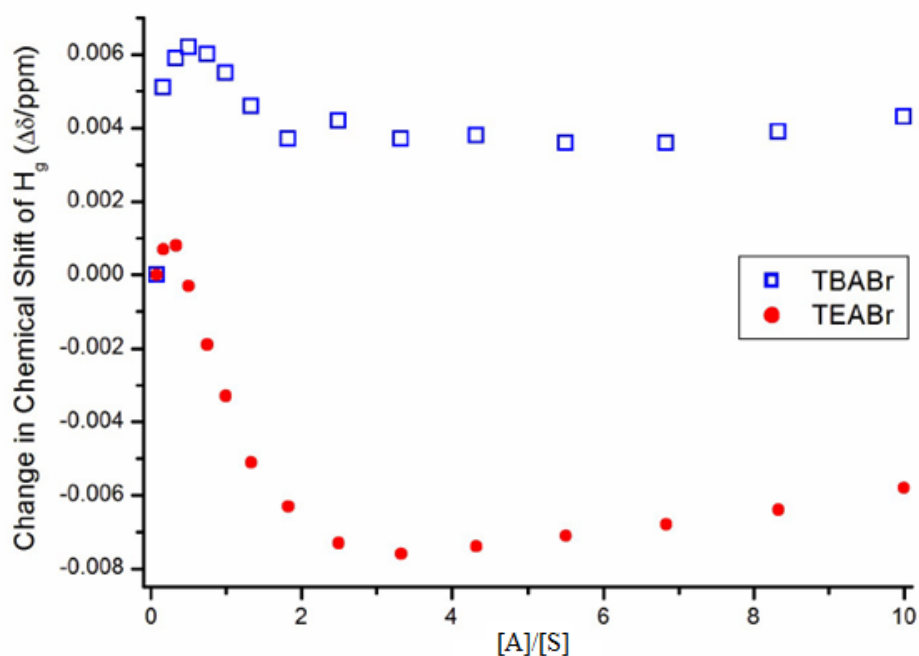


Figure 5.24. Change in chemical shifts of H_g upon titration of sensor **5.1** (2.0 mM) with tetrabutylammonium bromide (TBABr) and tetraethylammonium bromide (TEABr) in $CDCl_3$.

The electrostatic binding between thiophene and tetrabutylammonium cation was not mentioned in the previous study of Aboubakr *et al.*¹⁷⁶ for a very similar dithienophenazine based anion sensor, Figure 5.25. The structural difference is that the thiophene ring of the fluorophore in their sensor is unsubstituted (i.e. ring **A** of sensor **5.1** does not exist), Figure 5.25.¹⁷⁶ In fact, the aliphatic region of the proton NMR titrations and the emission changes occurring upon exceeding 1:1 of strong binding anions to sensor were not shown in that study.¹⁷⁶ Thus, it is not possible to tell if the cation-related interactions observed for sensor **5.1** were occurring in the case of the unsubstituted dithienophenazine or not. Checking if the cation-related interactions occurred or not in the study of Aboubakr *et al.* could reveal the role of ring **A** in these interactions.

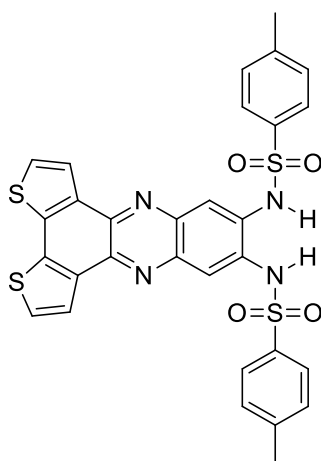
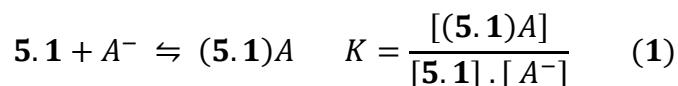


Figure 5.25. Structure of the first reported dithienophenazine anion sensor studied by Aboubakr *et al.*¹⁷⁶

5.2.2.3. Calculation of the Binding Constants

In case the estimations regarding a 1:1 binding stoichiometry of **5.1** to strong binding anions (acetate, benzoate and cyanide), and the subsequent binding of the sensor/anion complex to tetrabutylammonium cation, were both validated, the binding reactions can be written, as follows:



Where TBA^+ stands for tetrabutylammonium cation and A^- stands for the anion. $[]$ denotes the concentration of the species.

The changes in chemical shift for the signal of H_a were fit for all anion according to equation (1), and binding isotherms were generated according to a 1:1 fitting model using hypNMR2008 software, Figure 5.26. The weak binding anions (chloride, iodide and nitrate) did fit that model with binding constants in the range of 10^2 - $10^4 M^{-1}$, Table 5.4. However, the strong binding anions (acetate, benzoate and cyanide) did not due to having a large binding affinity (i.e. above 10^5 - $10^6 M^{-1}$).

Changes in the absorption spectra for strong binding anions were fit to binding equation (2) using hypSPEC2008. Experimental and calculated spectra by the program from binding model (2) were matched, Figures 5.27-5.29, with large binding affinities in the range of 10^8 - $10^{10} M^{-1}$, Table 5.5. Whereas fluoride and dihydrogen phosphate could not fit to any of the two models discussed above (i.e. probably due to the occurrence of deprotonation as suspected from NMR titrations).

HypNMR2008 and HypSpec2008 from Hyperquad2008 by Protonic Software (Leeds LS15 0HD, England) handling general host-guest association equilibria.

The program performs a Gauss–Newton–Marquardt least-squares fitting of the experimental data by minimizing the error square sum. The program performs simultaneous fit of multiple signals to models involving multiple equilibria. The refinement process yields best-fit values for equilibrium constants and individual absorbance on every wavelength for each chemical species.

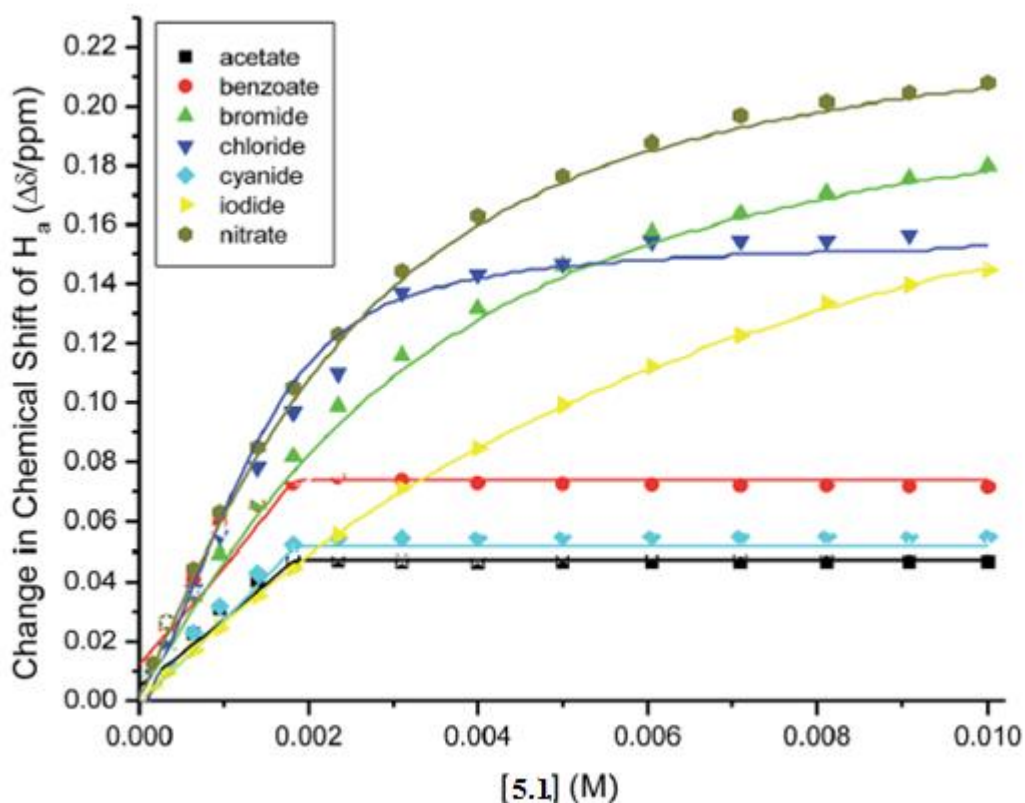


Figure 5.26. Binding isotherms generated from proton NMR titrations of sensor **5.1**.

Table 5.4. Affinity constants to weak binding anions determined from the change in chemical shift of H_a in proton NMR titration experiments of 2 mM **5.1** in $CDCl_3$ at 25 °C.

Anion	Log K	e.s.d.
Bromide	2.65	± 0.03
Chloride	3.62	± 0.07
Iodide	2.17	± 0.02
Nitrate	2.84	± 0.01
Acetate	> 5	---
Benzoate	> 5	---
Cyanide	> 5	---

Table 5.5. Affinity constants to strong binding anions determined from absorption titration experiments of 10 μM **5.1** in chloroform at 25 $^{\circ}\text{C}$.

Anion	Log K	e.s.d.
Acetate	9.252	± 0.002
Benzoate	9.525	± 0.004
Cyanide	8.662	± 0.005

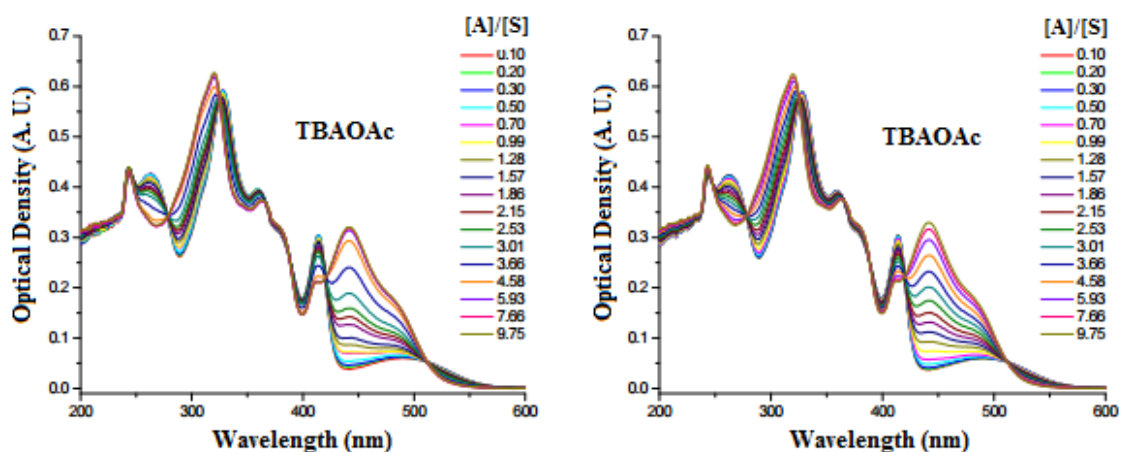


Figure 5.27. Experimental (left) vs. calculated from model (right) absorption spectra of sensor **5.1** (10 μM) upon titration with tetrabutylammonium acetate in chloroform at 25 $^{\circ}\text{C}$.⁴⁹

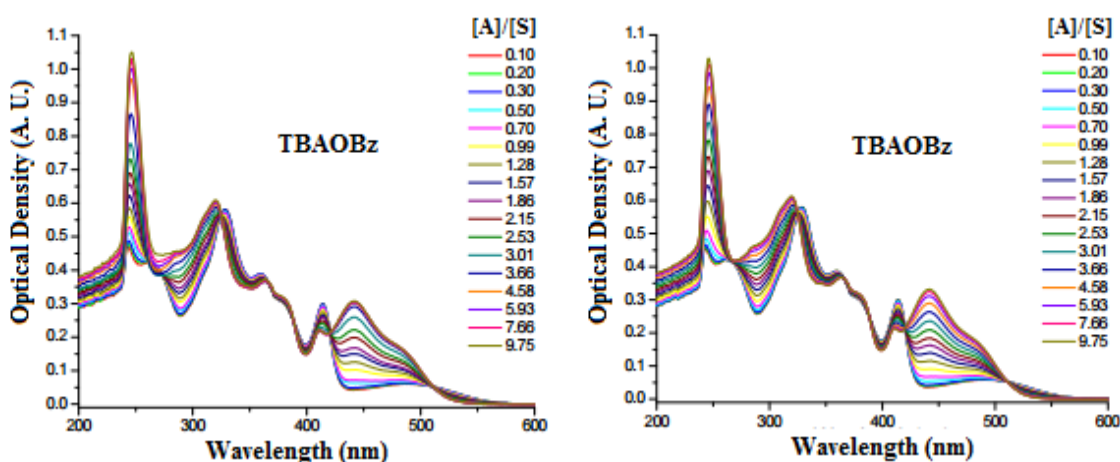


Figure 5.28. Experimental (left) vs. calculated from model (right) absorption spectra of sensor **5.1** (10 μM) upon titration with tetrabutylammonium benzoate in chloroform at 25 $^{\circ}\text{C}$.⁴⁹

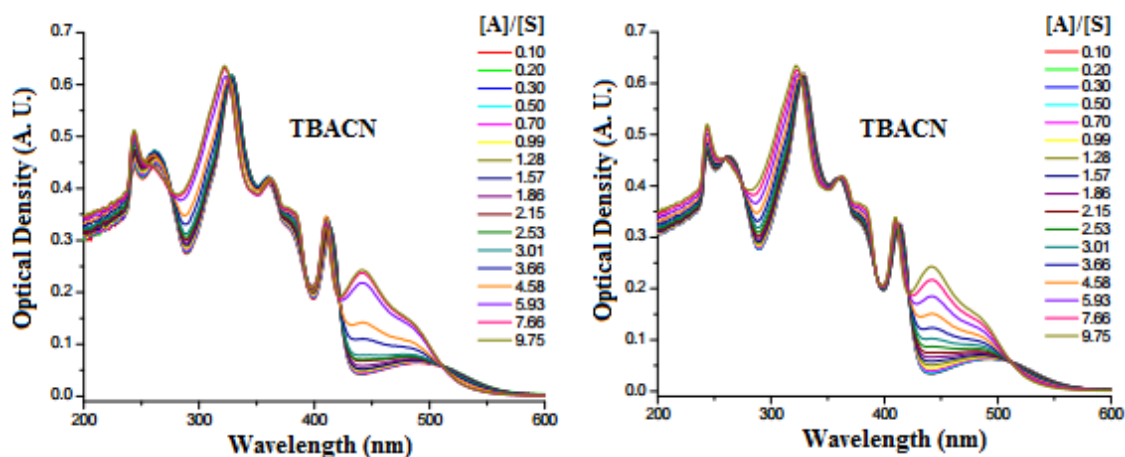


Figure 5.29. Experimental (left) vs. calculated from model (right) absorption spectra of sensor **5.1** (10 μ M) upon titration with tetrabutylammonium cyanide in chloroform at 25 $^{\circ}$ C.⁴⁹

5.2.3. *New Sensor Based on Dibenzophenazine Fluorophore*

The synthesis of sensor **5.11** was achieved using a similar synthetic route to the one followed for the synthesis of sensor **5.2**, previously presented in Scheme 5.1.

However, diketone **5.10**, obtained from Prof. Seth R. Marder research group, was used for the condensation reaction with the diamine **5.5**, Figure 5.30. Sensor **5.11** showed a similar instability problem to that of sensor **5.2**. The fluorescence of sensor **5.11** gets quenched gradually by sitting in solution for 48 hours without the addition of any anion, in both chloroform and DMSO, Figure 5.31. Thus, sensors **5.2** and **5.11** do not meet the criteria of a good fluorescent sensor. Subsequently, the titrations carried on these sensors lead to inconsistent and inconclusive results regarding their affinity to different anions (i.e. it was hard to obtain a consistent result over three repetitions for every single anion, given that the two sensors are unstable and exhibit changes in fluorescence without adding any anion). Hence, the study through titrations is limited to sensor **5.1**, exclusively, out of the three sensors synthesized and investigated in this Chapter (i.e. **5.1**, **5.2** and **5.11**).

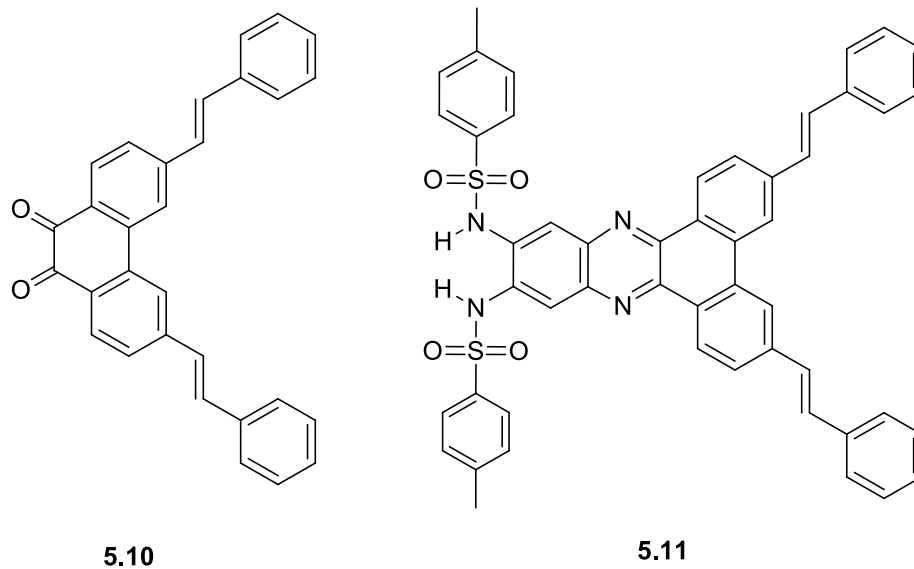


Figure 5.30. Structure of sensor **5.11** synthesized through condensation of diketone **5.10** with intermediate **5.5**.

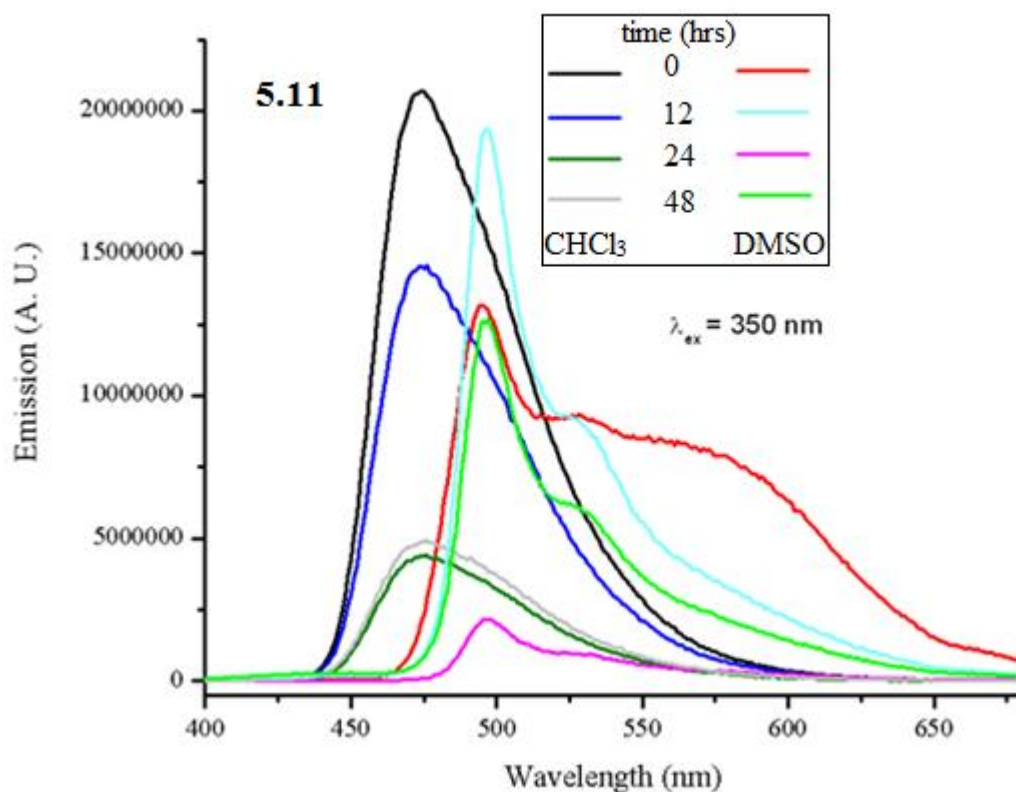


Figure 5.31. Stability of emission over 48 hours for sensor **5.11** in chloroform and DMSO (1 μM solutions stored at 0 °C in dark).

5.3. Conclusions and Future Work

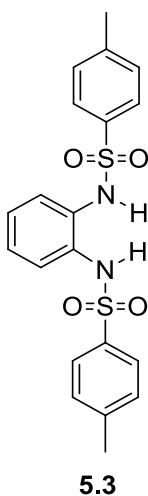
2,5-Disubstituted dithienophenazine was investigated as fluorophore in a sulfonamide-based anion sensor and reported for the first time in the literature. The use of 4-*tert*-butylphenyl as substituent showed to enhance the solubility and stability of the sensor in solution compared to iodine. Similar to most sulfonamide-based sensors, the affinity of the sensor was high towards carboxylates, cyanide and phosphate. However, low affinities towards nitrate and halides. Affinity towards halides was inversely proportional to their atomic radius. A new binding mechanism involving tetrabutylammonium cation was discovered. This might be due to the presence of four non-bonding pair of electrons on the two sulfur atoms of the fluorophore. The binding of tetraethylammonium cation was shown to be easier than tetrabutylammonium cation due to steric factor. Deprotonation of the sulfonamide receptor was suspected upon addition of more than one equivalent of relatively basic anions such as fluoride and dihydrogen phosphate. All the above findings can be further investigated and elaborated in order to open a door on new research involving the sensing of anion and cation simultaneously.

5.4. Experimental

5.4.1. Synthesis

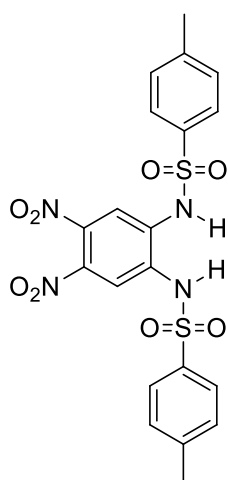
N,N'-(1,2-phenylene)bis(4-methylbenzenesulfonamide) (**5.3**)

The title compound was prepared according to a literature procedure.¹⁹² To 30 mL of pyridine, benzene-1,2-diamine (5.00 g, 46.23 mmol) was added, the mixture was stirred in a round bottom flask until all solid was dissolved. 4-Methylbenzenesulfonyl chloride (19.39 g, 101.71 mmol) was then added in small portions while cooling the flask on ice. The reaction mixture was left to stir overnight at room temperature. The reaction was then quenched with water, extracted with dichloromethane (2 x 50 mL). The combined organic layer was washed with brine (2 x 20 mL), and dried over magnesium sulfate and filtered. Solvent was removed under reduced pressure. The obtained solid was recrystallized twice from ethanol to yield white crystals of *N,N'*-(1,2-phenylene)bis(4-methylbenzenesulfonamide) **5.3** (15.60 g, 81 %), mp 204-205 °C (Lit.¹⁹² 205-206.5 °C). ¹H NMR (500 MHz, DMSO-d₆): δ 9.34 (s, 2H), 7.64 (d, *J* = 8.5 Hz, 4H), 7.33 (d, *J* = 8.5 Hz, 4H), 6.96-7.05 (m, 4H), 2.32 (s, 6H). ¹³C NMR (125 MHz, DMSO-d₆): δ 144.12, 136.55, 130.19, 130.17, 127.41, 126.30, 123.85, 21.45



***N,N'*-(4,5-dinitro-1,2-phenylene)bis(4-methylbenzenesulfonamide) (5.4)**

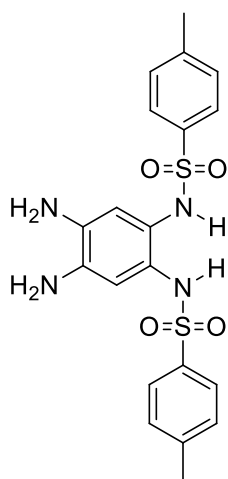
The title compound was synthesized according to a literature procedure.¹⁹⁰ *N,N'*-(1,2-phenylene)bis(4-methylbenzenesulfonamide) (**5.3**) (5.00 g, 12.00 mmol) was dissolved in 80 mL of CH₃COOH while stirring at 55 °C. A mixture of CH₃COOH and HNO₃ (1:1, 6 mL) was then added, and the reaction mixture was left to stir for 30 mins at 55 °C. The mixture was then filtered; the obtained yellowish solid was recrystallized from ethanol to yield *N,N'*-(4,5-dinitro-1,2-phenylene)bis(4-methylbenzenesulfonamide) **5.4** (4.30 g, 71 %) as white yellowish solid, mp 249-250 °C (Lit.¹⁹⁰ 248-250 °C). ¹H NMR (500 MHz, DMSO-d₆): δ 7.81 (s, 2H), 7.72 (d, *J* = 8.5 Hz, 4H), 7.38 (d, *J* = 8.5 Hz, 4H), 2.36 (s, 6H). ¹³C NMR (125 MHz, DMSO-d₆): δ 144.89, 137.71, 136.11, 133.63, 130.49, 127.43, 116.59, 21.48.



***N,N'*-(4,5-diamino-1,2-phenylene)bis(4-methylbenzenesulfonamide) (5.5)**

The title compound was synthesized according to a literature procedure.¹⁹¹ *N,N'*-(4,5-dinitro-1,2-phenylene)bis(4-methylbenzenesulfonamide) (**5.4**) (5.00 g, 9.87

mmols) was dissolved in 250 mL ethanol, 0.50 g of Pd/C was then added, and the mixture was shaken on Parr hydrogenator at 40 psi H₂ for 48 hrs at room temperature. The reaction was then filtered on celite to remove Pd/C. Celite and Pd/C were washed with boiling ethanol (4 x 25 mL), and solvent was removed under reduced pressure. *N,N'*-(4,5-diamino-1,2-phenylene)bis(4-methylbenzenesulfonamide) **5.5** (3.09 g, 70 %) was obtained as dark purple solid, mp 208-209 °C (Lit.¹⁹⁶ 210 °C). The compound was used immediately for the next step without further purification.

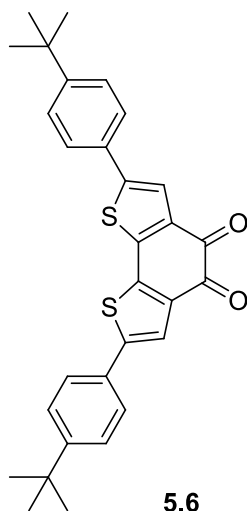


5.5

2,7-Bis(4-(*tert*-butyl)phenyl)benzo[2,1-*b*:3,4-*b'*]dithiophene-4,5-dione (5.6)

The title compound was prepared according to a literature procedure.²³ In 30 mL toluene, 2,7-diiodobenzo[2,1-*b*:3,4-*b'*]dithiophene-4,5-dione (**5.9**) (0.10 g, 0.21 mmol) was dissolved. (4-(*tert*-butyl)phenyl)boronic acid (0.11 g, 0.64 mmol, 3 eq.) was then added, followed by 3 mL of 2M aqueous K₂CO₃ and tetrabutylammonium bromide (10 mg). The mixture was stirred and purged with Argon at room temperature for 30 minutes. Pd(PPh₃)₄ (50 mg, 0.04 mmol) was then added, and the mixture was stirred at 110 °C for 48 hrs under argon and dark atmosphere. The reaction was then quenched

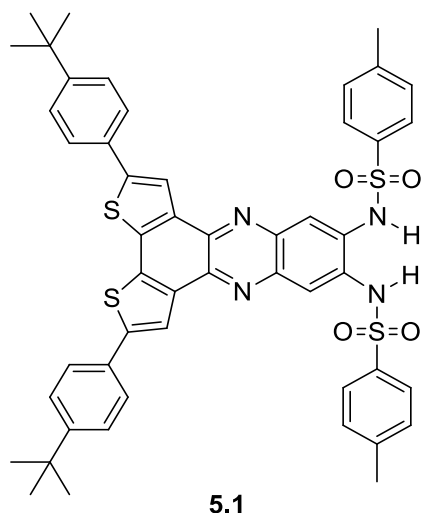
with 50 mL water, and solvents were removed under reduced pressure. Soxhlet extraction of the isolated black solid using chloroform was performed, and the chloroform dark purple extract was washed with 10% K_2CO_3 (2 x 20 mL) and with brine solution (2 x 20 mL), then dried over $MgSO_4$ then filtered. Chloroform was then removed under reduced pressure. An impure dark purple solid was obtained. The solid was purified by column chromatography using hexanes to (hex : DCM (2 : 1)) as mobile phase. Product 2,7-Bis(4-(*tert*-butyl)phenyl)benzo[2,1-*b*:3,4-*b'*]dithiophene-4,5-dione **5.6** (0.05 g, 49 %), mp 314.1 °C, was isolated as pure dark blue needles and were dried under reduced pressure for 48 hrs. 1H NMR (500 MHz, $CDCl_3$): δ 7.58 (s, 2H), 7.48 (d, $J = 8.5$ Hz, 4H), 7.40 (d, $J = 8.5$ Hz, 4H), 1.29 (s, 18H). ^{13}C NMR (125 MHz, $CDCl_3$): δ 174.65, 152.51, 144.88, 142.38, 135.84, 129.35, 126.22, 125.55, 122.11, 34.80, 31.17. HR-MALDI (m/z): $[M]^+$:calcd for $C_{30}H_{28}O_2S_2$, 484.1531; found, 484.1516. Anal. Calcd for $C_{30}H_{28}O_2S_2$: C, 74.34; H, 5.82; S, 13.23. Found: C, 74.25; H, 5.97; S, 13.06.



***N,N'*-(2,5-bis(4-(*tert*-butyl)phenyl)dithieno[3,2-*a*:2',3'-*c*]phenazine-9,10-diyl)bis(4-methylbenzenesulfonamide) (5.1)**

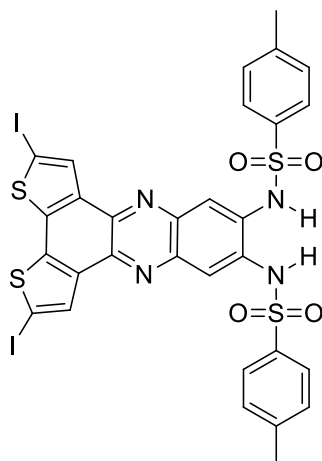
The title compound was prepared according to a literature procedure.¹⁹³

A mixture of ethanol and acetic acid (1:1, 40 mL) was added to a flask containing *N,N'*-(4,5-diamino-1,2-phenylene)bis(4-methylbenzenesulfonamide) (**5.5**) (1.00 g, 2.23 mmol (excess)). This mixture was purged with argon for 15 minutes, then **5.4** (0.16 g, 0.33 mmol) was added, the mixture was purged with argon for additional 15 minutes, and then the reaction was left to stir at 105 °C for 3 days. After three days, the reaction was cooled, vacuum filtered, and an orange solid was obtained. The crude material was recrystallized from toluene, and **5.1** was obtained as orange reddish crystals (0.15 g, 51%), mp 301.1 °C, ¹H NMR (CDCl₃, 500 MHz): δ 8.11 (s, 2H), 7.70 (d, *J* = 8.0 Hz, 4H), 7.67 (s, 2H), 7.59 (d, *J* = 8.0 Hz, 4H), 7.49 (bs, 2H), 7.41 (d, *J* = 8.5 Hz, 4H), 7.19 (d, *J* = 8.5 Hz, 4H), 2.28 (s, 6H), 1.33 (s, 18H). ¹³C NMR (CDCl₃, 125 MHz): δ 151.65, 144.63, 143.38, 139.57, 139.47, 134.92, 134.82, 132.12, 130.79, 129.89, 127.77, 126.03, 125.93, 123.06, 119.40, 34.77, 31.28, 21.62. HR-MALDI (*m/z*): [M]⁺:calcd for C₅₀H₄₆N₄O₄S₄, 894.2395; found, 894.2408. Anal. Calcd for C₅₀H₄₆N₄O₄S₄: C, 67.09; H, 5.18; N, 6.26; S, 14.33. Found: C, 67.38; H, 5.40; N, 6.17; S, 14.03.



***N,N'*-(2,5-diiododithieno[3,2-*a*:2',3'-*c*]phenazine-9,10-diyl)bis(4-methylbenzenesulfonamide) (5.2)**

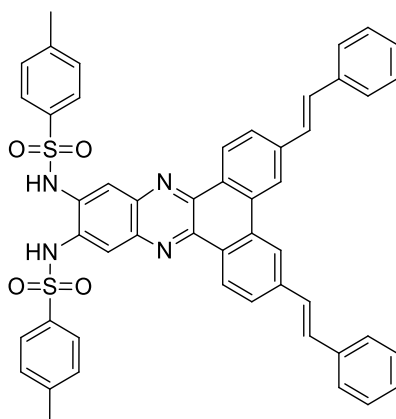
The title compound was synthesized according to a literature procedure. A mixture of ethanol and acetic acid (40 mL: 40 mL) was added to a flask containing **5.5** (1.70 g, 3.78 mmol). This mixture was purged with argon for 15 minutes then **5.9** (0.36 g, 0.76 mmol) was added and the whole mixture was purged with argon for additional 15 minutes and then the reaction was left to stir at 105 °C for 3 days. After three days, the reaction was cooled and filtered, a dark yellow solid was obtained. This solid was triturated with toluene using a soxhlet extraction apparatus. After four days a bright yellow solid was obtained **5.2** (0.48 g, 72%). ¹H NMR (300 MHz, DMSO-*d*₆): δ 8.40 (s, 2H), 7.82 (s, 2H) 7.80 (d, *J* = 8.4 Hz, 4H), 7.40 (d, *J* = 8.4 Hz, 4H), 2.34 (s, 6H). ¹³C NMR (75 MHz, DMSO-*d*₆): δ 144.03, 138.54, 137.75, 136.55, 136.08, 135.03, 133.13, 130.03, 126.99, 79.36, 79.16, 78.92, 78.48, 21.02. Anal. Calcd. For C₃₀H₂₀I₂N₄O₄S₄: C, 40.83; H, 2.28; N, 6.35. Found: C, 41.10; H, 2.20; N, 6.34.



5.2

***N,N'*-(3,6-di(*E*)-styryl)dibenzo[*a,c*]phenazine-11,12-diyl)bis(4-methylbenzenesulfonamide) (5.11)**

The title compound was synthesized according to a modified literature procedure. A 60 mL (1:1) mixture of ethanol and acetic acid was added to a flask containing **5.5** (1.20 g, 2.69 mmol, 3.2 eqv), followed by **5.10** (0.35 g, 0.85 mmol). The reaction mixture was purged with argon for 30 minutes, and then was left to stir at 105 °C for three days. The mixture was cooled in an ice bath, and then filtered. The green solid was washed with ethanol to remove excess **5.5**, and triturated with hot toluene using a soxhlet extraction apparatus, then left for 24 hours to dry under reduced pressure. **5.11** yellowish solid was obtained (0.50 g, 71%), mp 298.9 °C, ¹H NMR (300 MHz, DMSO-*d*₆): δ 9.04 (d, *J* = 8.4 Hz, 2H), 8.95 (s, 2H), 8.00 (d, *J* = 8.7 Hz, 2H), 7.87 (s, 2H), 7.31-7.81 (m, 24H), 2.34 (s, 6H). ¹³C NMR (75 MHz, DMSO-*d*₆): δ 144.03, 141.22, 139.25, 138.83, 136.85, 136.07, 132.50, 131.58, 130.57, 130.01, 128.83, 128.38, 128.06, 126.97, 126.71, 125.91, 121.87, 118.25, 21.00. Anal calcd for: C₅₀H₃₈N₄O₄S₂: C, 72.97; H, 4.65; N, 6.81; S, 7.79. Found: C, 72.75; H, 4.71; N, 6.84; S, 7.94.



5.11

5.4.2. Spectroscopic Titrations

All titration procedures are very sensitive to many sources of experimental errors (mainly dilution, volatility of solvent, balance error, glassware error, human error, and presence of impurities).¹⁹⁴ Therefore the following experimental precautions were taken in order to minimize these errors during titration experiments:¹⁹⁴

- Weighing relatively big amounts of sensor and anions to prepare stock solutions, and then diluting. This will minimize balance error.
- Weighing the solvent rather than just relying on volumetric flasks to minimize visual and glassware errors.
- Performing each titration at least three times and repeating in case of inconsistent results.
- Performing the titrations using a dry batch of sensor that is proven pure by proton and carbon NMR and passed elemental analysis.
- Each titration must include 15-20 measurements and not more. Very long titration experiments increase the error due to solvent volatility.

Performing a 15-measurement titrations with three repetitions to get consistent results is better than performing a 45-measurement single titration experiment.

- The anion solution must be prepared using the same sensor solution used in titrations and not raw solvent; this will prevent the dilution of sensor solution upon addition of anion. In other words, the concentration of the sensor must be maintained constant during the whole experiment.

- Choosing the suitable concentrations of sensor and anion solutions based on the limit of detection and sensitivity of the machine used in each titration technique.

5.4.2.1. Absorption and Emission Titrations

A stock solution **A** of **5.1** (1.0 mM in CHCl_3) was prepared, and diluted to 1/100. The obtained 0.01 mM solution **B** (the titrand solution) was used as a solvent to prepare 1.0 mM anion solution **C** (the titrant solution). 2.0 mL of solution **B** was placed in a 1 x 1 cm quartz cuvette and was titrated by addition of aliquots of solution **C** to the cuvette using a suitable size microsyringe according to the titration chart below, Table 5.6. Following each addition, absorption and emission spectra were collected. All emission spectra were collected with an excitation wavelength of 420 nm, and a slit width of 2 nm. 0.216 mL of solution **C** was added over 17 additions in total which makes almost ten equivalents of corresponding anion.

Stock solution **A** was stored in the freezer and used within a maximum of 24 hours. Solutions **B** and **C** were immediately discarded after each titration.

This procedure was repeated many times for each single anion until consistent results were obtained in at least three runs.

Table 5.6. Absorption and emission titration chart for sensor **5.1**

Addition #	V Added (μL)	Total V(μL)	[Sensor] (S) $\times 10^{-5}$ M	[anion] (A) $\times 10^{-5}$ M	[S]/[A]	[A]/[S]
0	0	2000	1.00	0.00	--	0.00
1	2	2002	1.00	0.10	10.00	0.10
2	2	2004	1.00	0.20	5.00	0.20
3	2	2006	1.00	0.30	3.33	0.30
4	4	2010	1.00	0.50	2.00	0.50
5	4	2014	1.00	0.70	1.43	0.70
6	6	2020	1.00	0.99	1.01	0.99
7	6	2026	1.00	1.28	0.78	1.28
8	6	2032	1.00	1.57	0.64	1.57
9	6	2038	1.00	1.86	0.54	1.86
10	6	2044	1.00	2.15	0.46	2.15
11	8	2052	1.00	2.53	0.39	2.53
12	10	2062	1.00	3.01	0.33	3.01
13	14	2076	1.00	3.66	0.27	3.66
14	20	2096	1.00	4.58	0.22	4.58
15	30	2126	1.00	5.93	0.17	5.93
16	40	2166	1.00	7.66	0.13	7.66
17	50	2216	1.00	9.75	0.10	9.75

5.4.2.2. Proton NMR Titrations

600 μL of a solution of **5.1** (2.0 mM in CDCl_3) was placed into a dry and clean NMR tube, and was titrated by the addition of aliquots of anion solution (20 mM in CDCl_3) to the NMR tube using a suitable sized microsyringe according to the titration chart below, Table 5.7; until a total of 600 μL of anion solution was added over 15 additions. Proton NMR was collected by a 16-scan experiment following each anion addition. Lock and shim steps were repeated at each experiment. All NMR spectra were collected using a 300 MHz Bruker NMR machine. All solutions were immediately discarded after each titration.

Table 5.7. Proton NMR titration chart of sensor **5.1**.

Addition #	V Added (μL)	Total V (μL)	[Sensor] (S) $\times 10^{-3}$ M	[Anion] (A) $\times 10^{-3}$ M	[A]/[S]
0	0	600	2.00	0.00	0.00
1	5	605	1.98	0.17	0.08
2	5	610	1.97	0.33	0.17
3	10	620	1.94	0.65	0.33
4	10	630	1.90	0.95	0.50
5	15	645	1.86	1.40	0.75
6	15	660	1.82	1.82	1.00
7	20	680	1.76	2.35	1.33
8	30	710	1.69	3.10	1.83
9	40	750	1.60	4.00	2.50
10	50	800	1.50	5.00	3.33
11	60	860	1.40	6.05	4.33
12	70	930	1.29	7.10	5.50
13	80	1010	1.19	8.12	6.83
14	90	1100	1.09	9.09	8.33
15	100	1200	1.00	10.00	10.00

CHAPTER 6

SUPPORTING DATA

In this Chapter, we include the spectral data (^1H and ^{13}C NMR) of the compounds reported throughout this thesis, in addition to some important titration overlays for sensor **5.1** that are not presented in Chapter 5. Appendices A, B and C show the absorption, emission and ^1H NMR titration overlays, respectively, for sensor **5.1**. The ^1H NMR titration overlays were generated using the software “SpinWorks 3”. Whereas Appendices D and E show the ^1H -NMR and the ^{13}C -NMR spectra, respectively, of compounds of which the synthesis was described in Chapters 2 (TPPy, **2.21-2.25** and **2.27-2.29**), 3 (**2.15-2.17**, **3.1-3.4** and **3.6**), 4 (**4.1**), and 5 (**5.1-5.4**, **5.6** and **5.11**) of this thesis.

Titration experiments were run following the procedure discussed in Chapter 5. One extra measurement was performed upon leaving sensor **5.1** and the corresponding anion (13.64 eqv), in solution, for a specific period of time after the corresponding titration experiment is over. This was the case for bromide (Figures 6.3 and 6.12), cyanide (Figures 6.5 and 6.14), iodide (Figures 6.7 and 6.16), nitrate (Figure 6.17), and dihydrogen phosphate (Figures 6.9 and 6.18). In each of these Figures, the extra measurement is indicated as $[\text{A}]/[\text{S}] = 13.64$, in addition to the specific duration in which the sensor and the corresponding anion were left in solution before this measurement. The results of these extra measurements did not offer any information that could be used to support the discussion presented in Chapter 5.

APPENDIX A
ABSORPTION TITRATION OVERLAYS

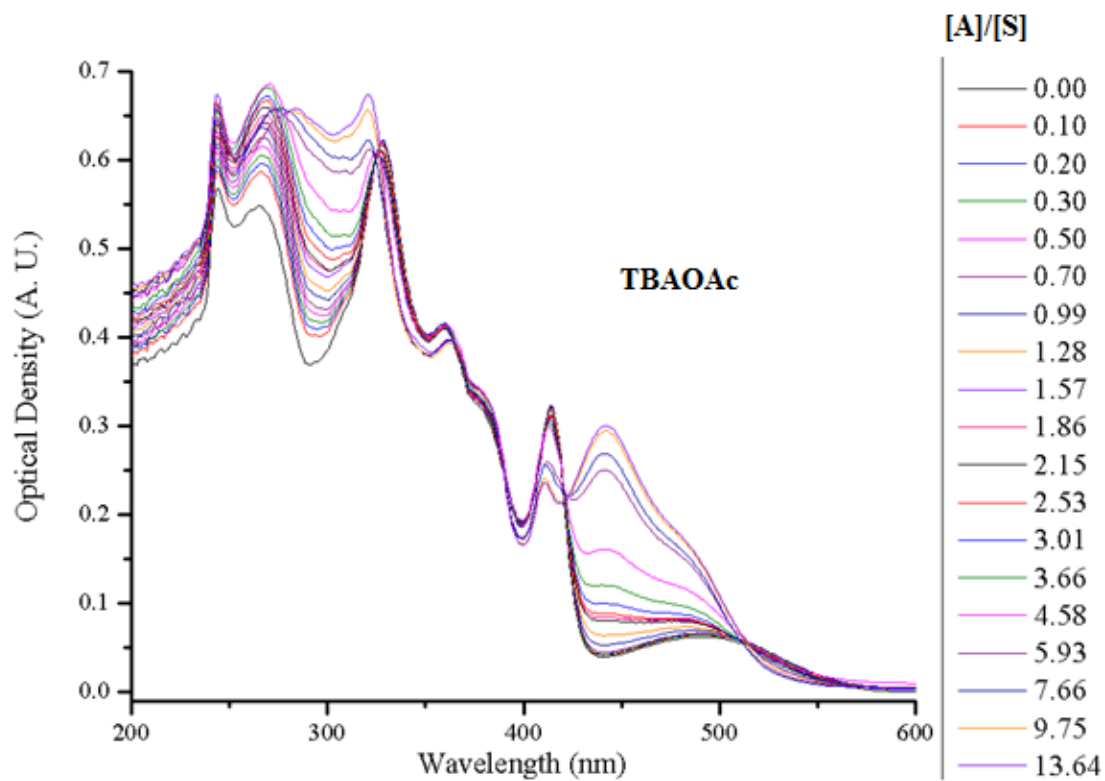


Figure 6.1. Absorption titration overlay of sensor **5.1** with tetrabutylammonium acetate.

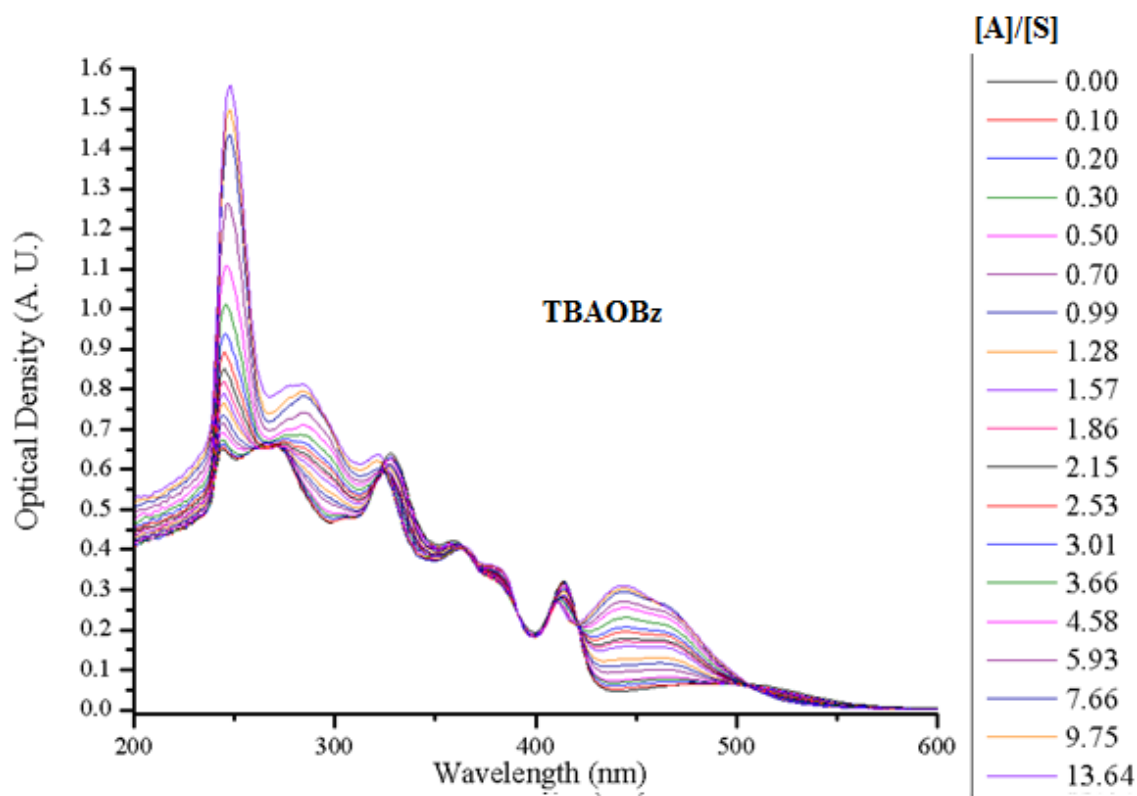


Figure 6.2. Absorption titration overlay of sensor **5.1** with tetrabutylammonium benzoate.

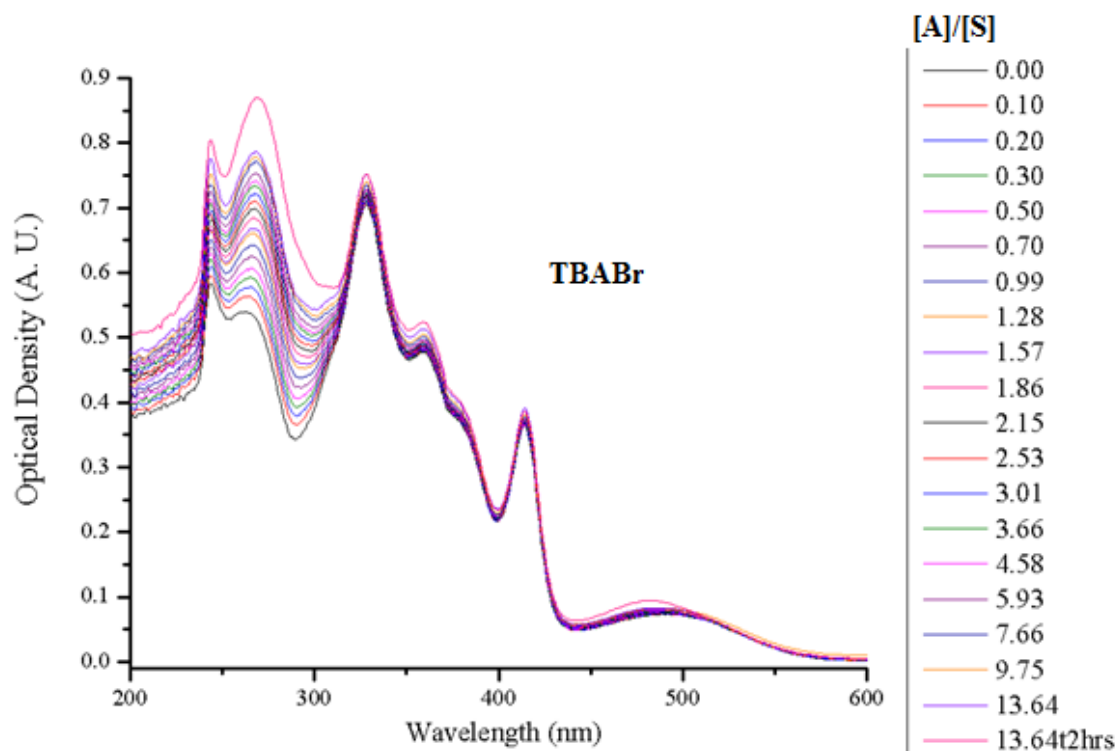


Figure 6.3. Absorption titration overlay of sensor **5.1** with tetrabutylammonium bromide.

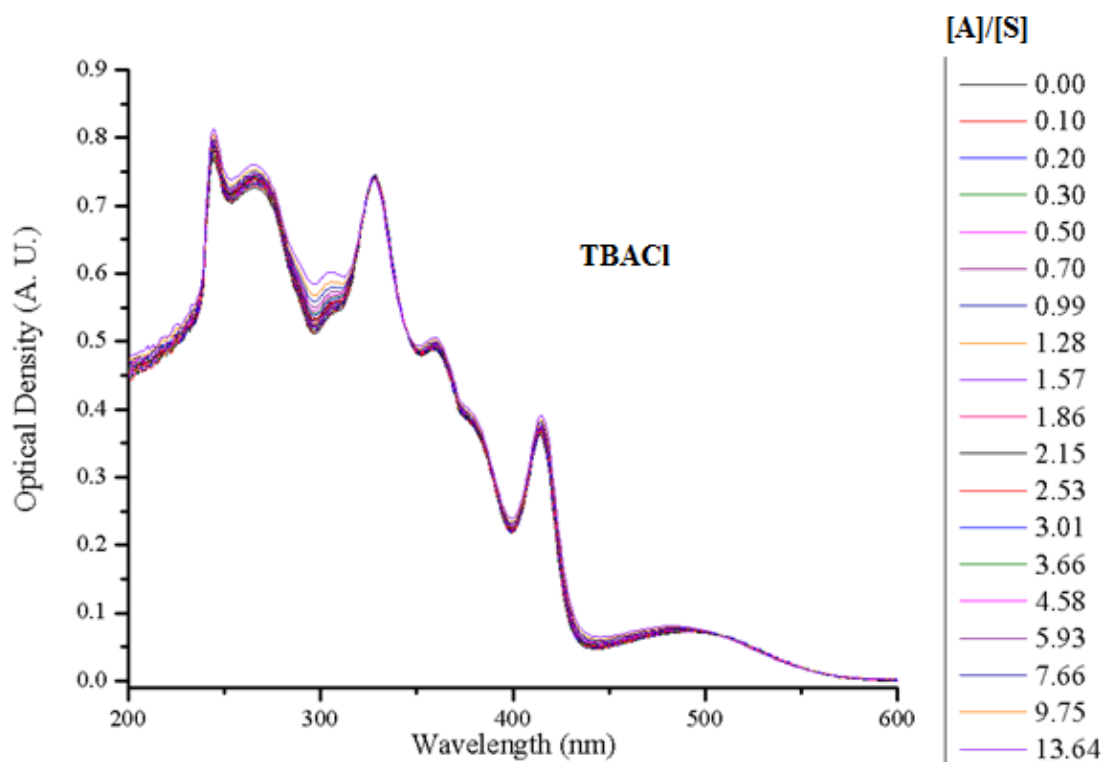


Figure 6.4. Absorption titration overlay of sensor **5.1** with tetrabutylammonium chloride.

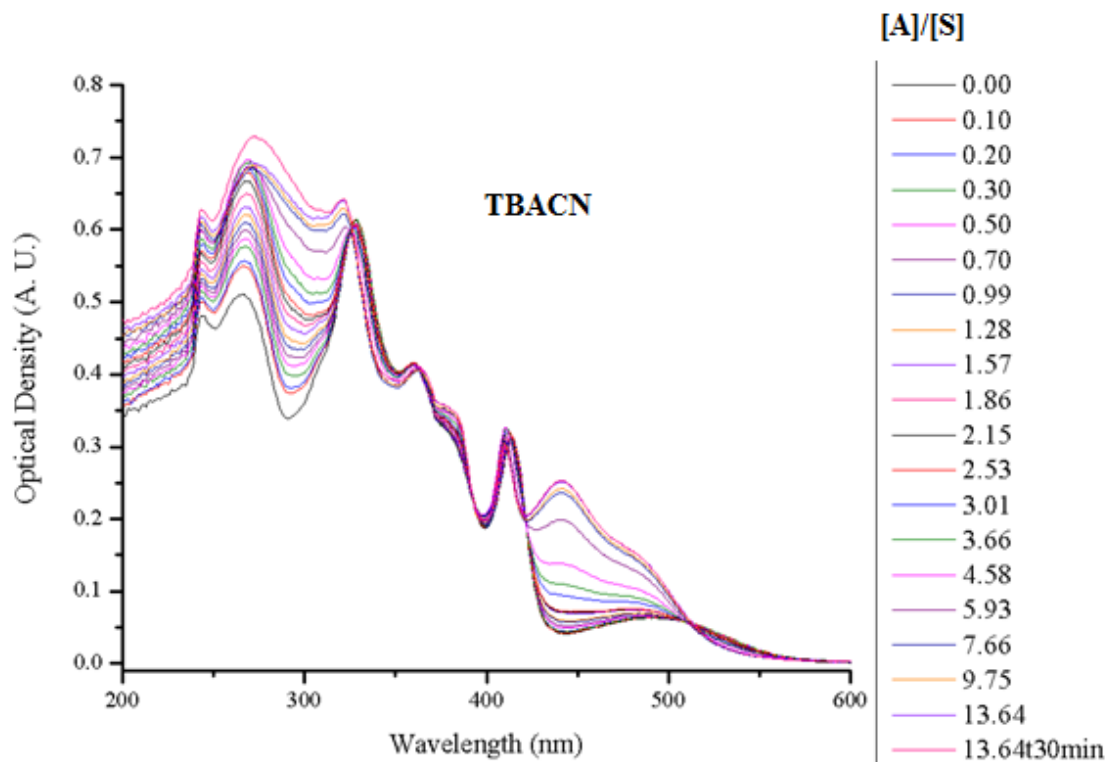


Figure 6.5. Absorption titration overlay of sensor **5.1** with tetrabutylammonium cyanide.

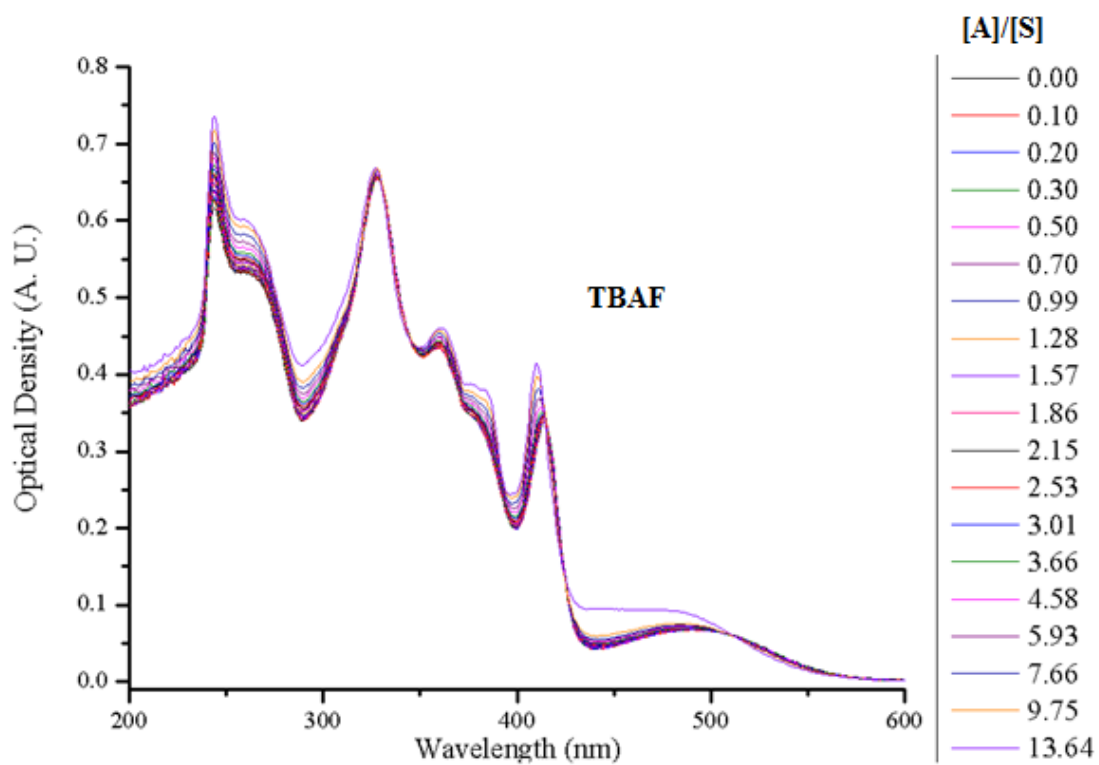


Figure 6.6. Absorption titration overlay of sensor **5.1** with tetrabutylammonium fluoride

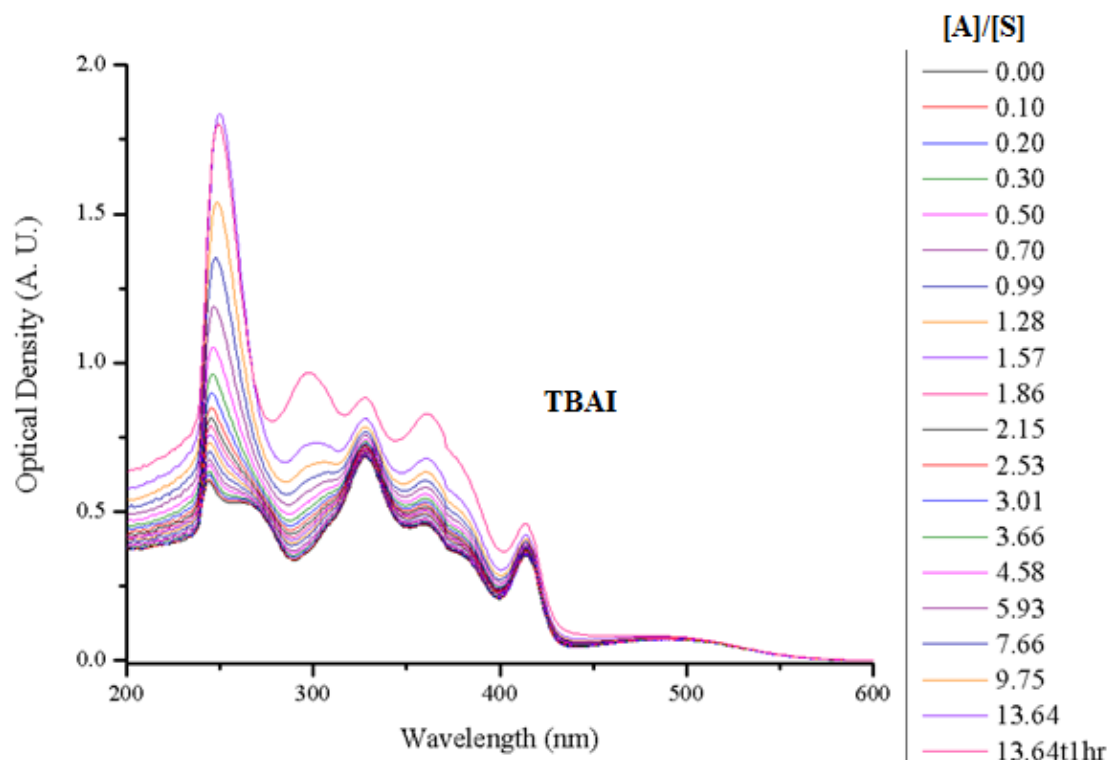


Figure 6.7. Absorption titration overlay of sensor **5.1** with tetrabutylammonium iodide

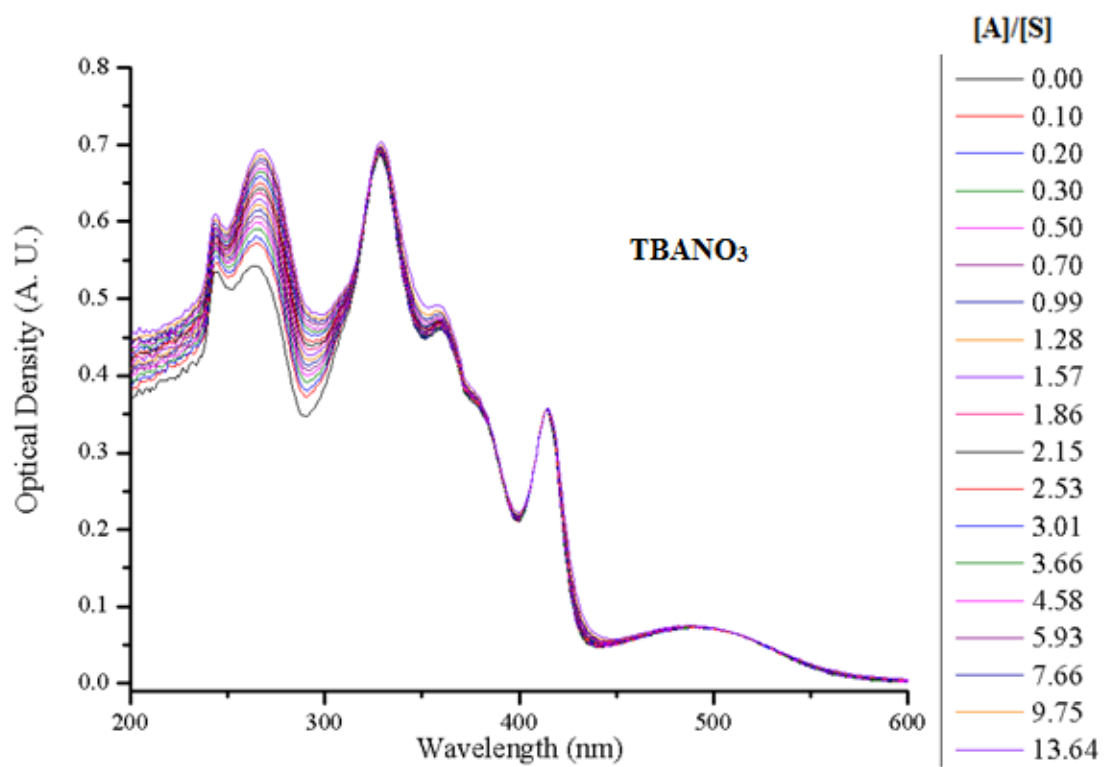


Figure 6.8. Absorption titration overlay of sensor **5.1** with tetrabutylammonium nitrate.

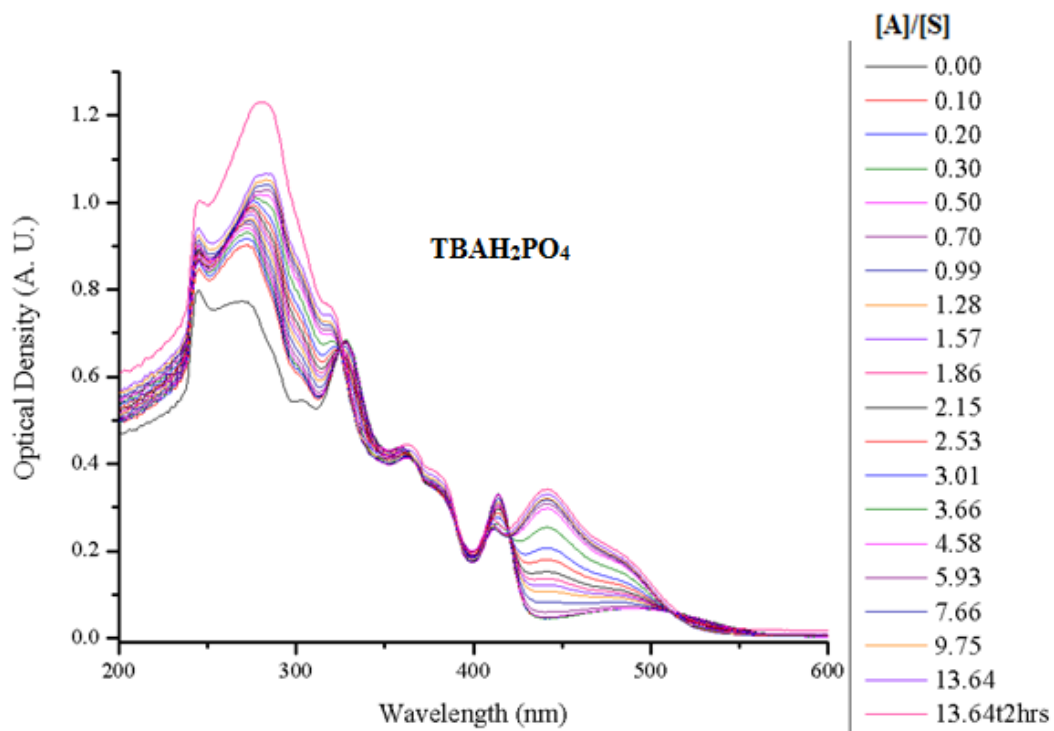


Figure 6.9. Absorption titration overlay of sensor **5.1** with tetrabutylammonium dihydrogen phosphate.

APPENDIX B

EMISSION TITRATION OVERLAYS

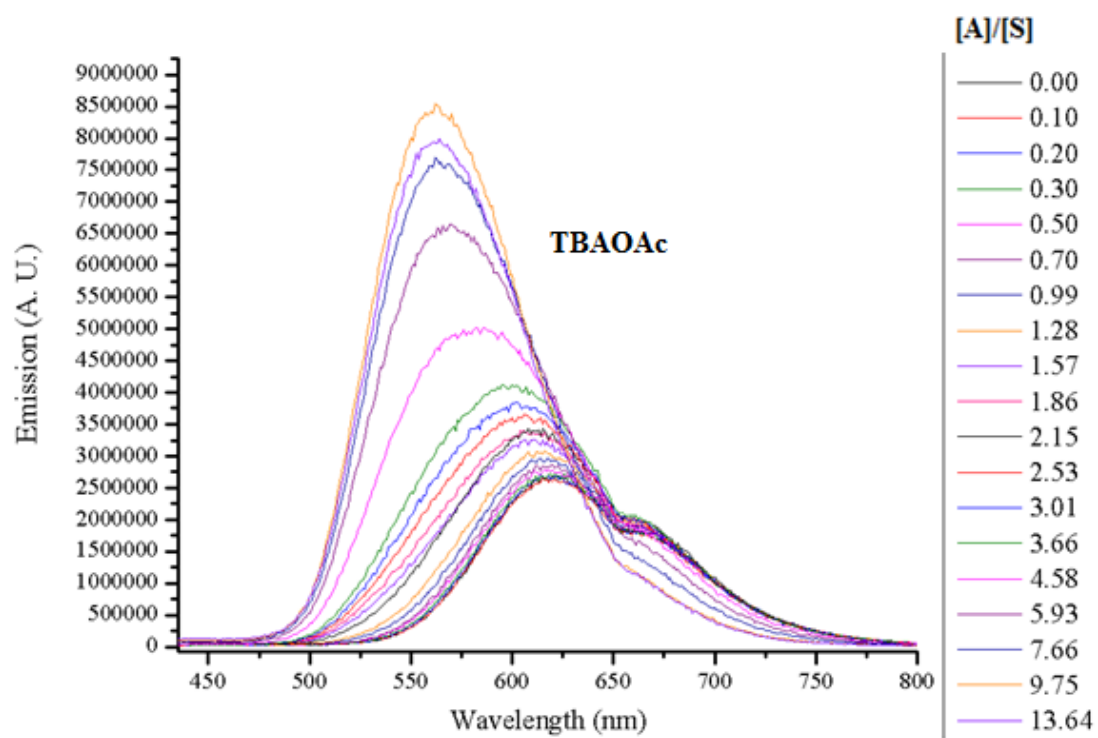


Figure 6.10. Emission titration overlay of sensor **5.1** with tetrabutylammonium acetate.

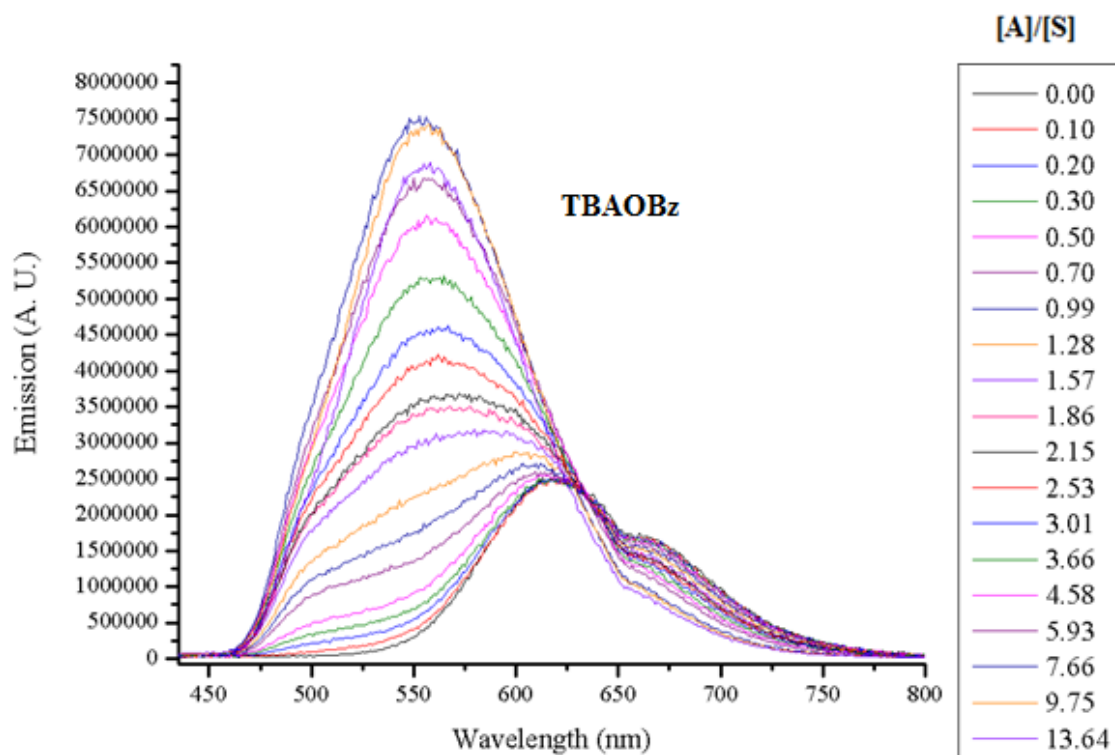


Figure 6.11. Emission titration overlay of sensor **5.1** with tetrabutylammonium benzoate

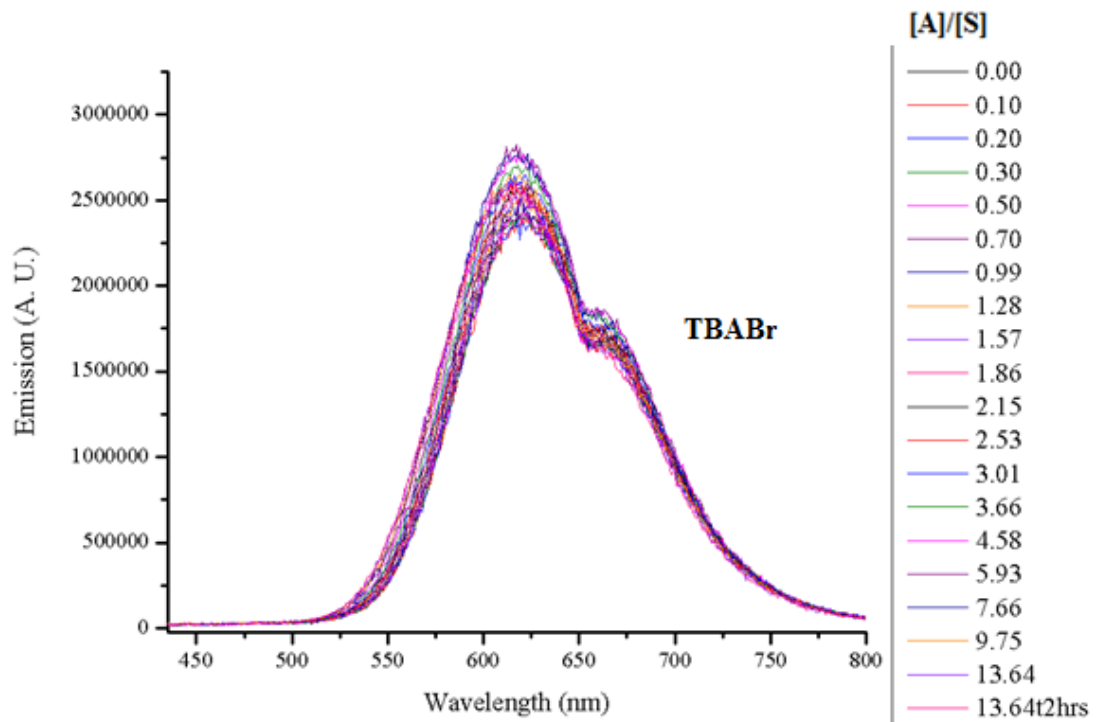


Figure 6.12. Emission titration overlay of sensor **5.1** with tetrabutylammonium bromide.

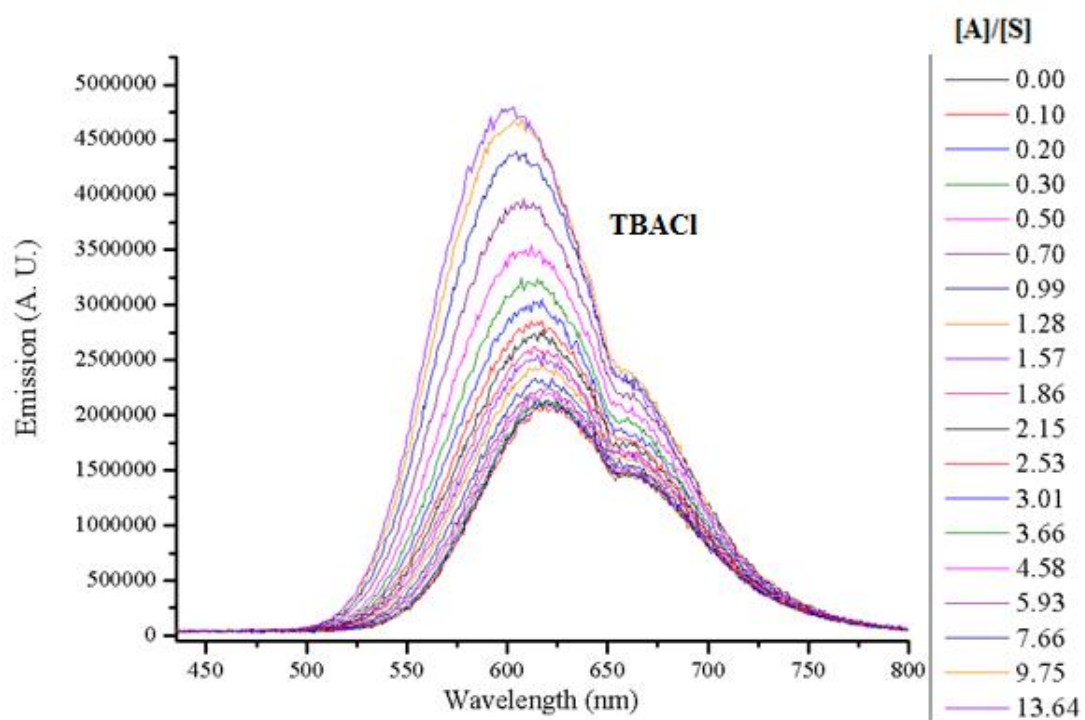


Figure 6.13. Emission titration overlay of sensor **5.1** with tetrabutylammonium chloride.

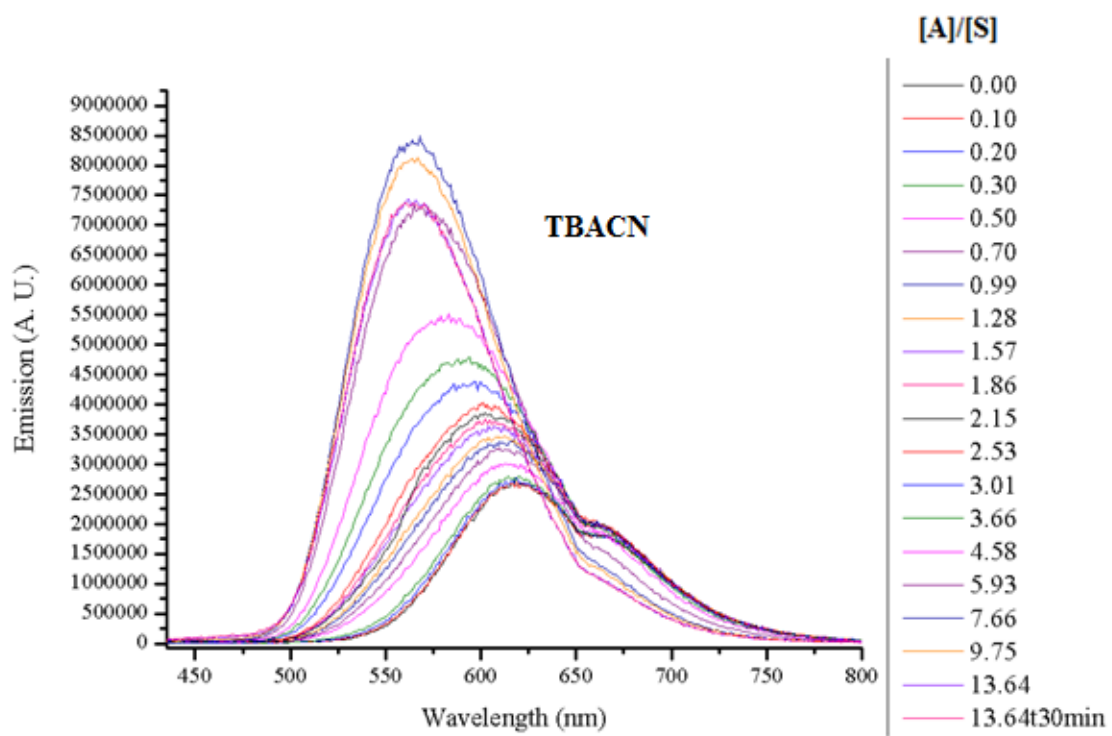


Figure 6.14. Emission titration overlay of sensor **5.1** with tetrabutylammonium cyanide.

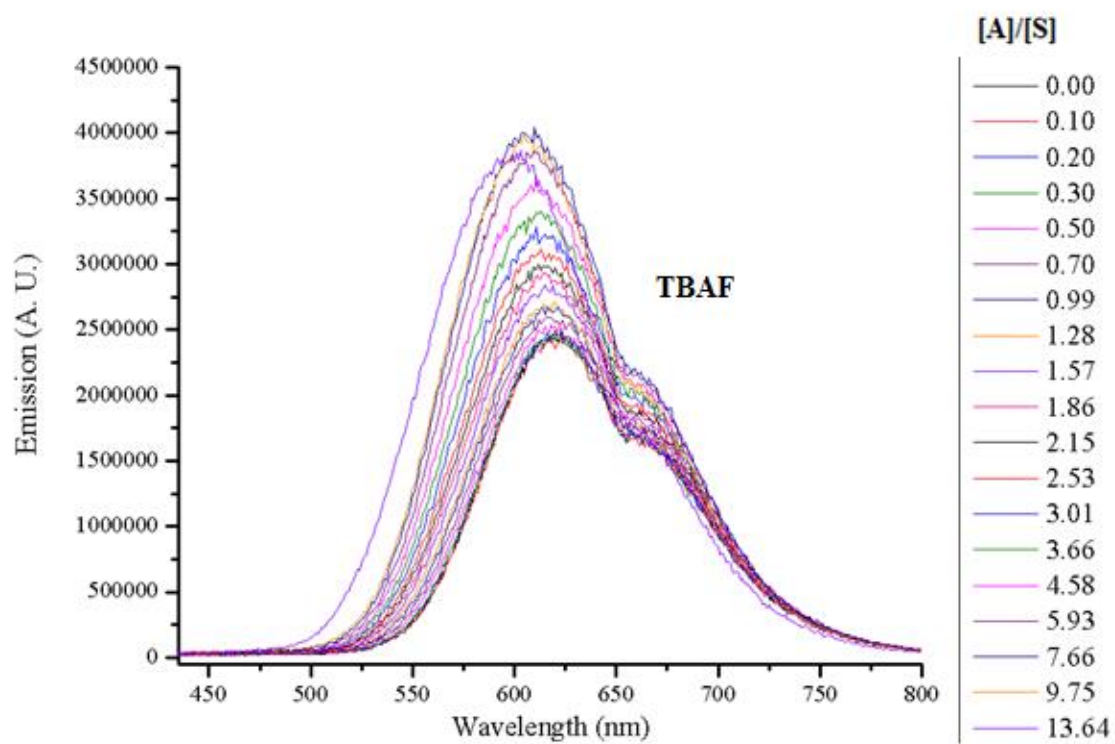


Figure 6.15. Emission titration overlay of sensor 5.1 with tetrabutylammonium fluoride.

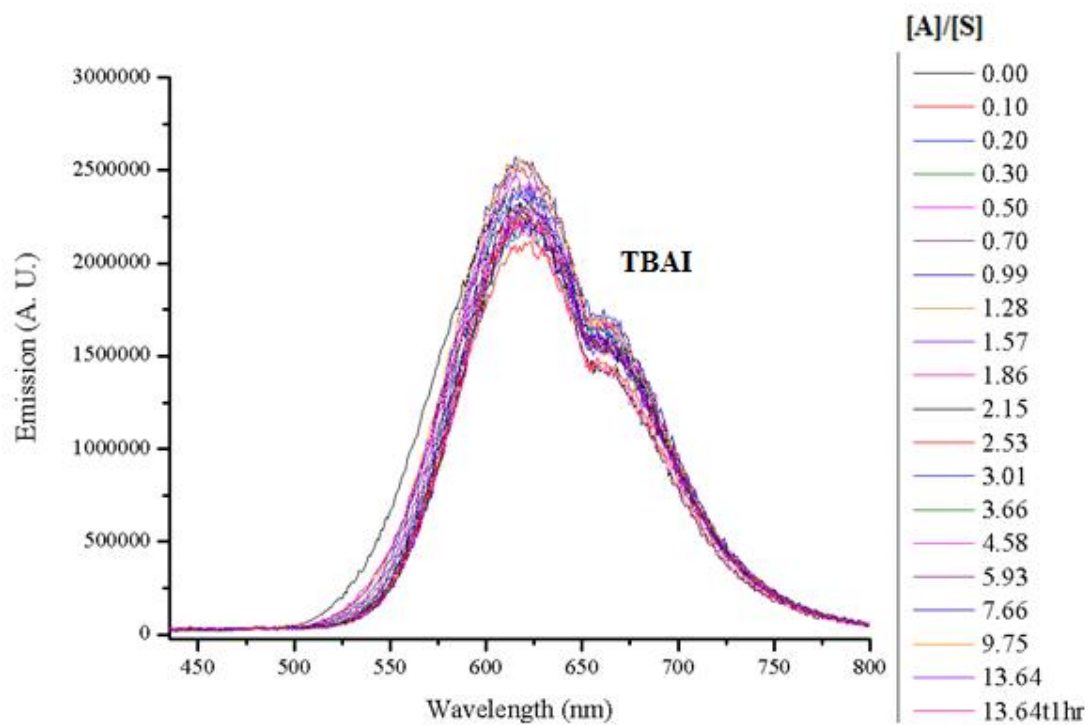


Figure 6.16. Emission titration overlay of sensor **5.1** with tetrabutylammonium iodide.

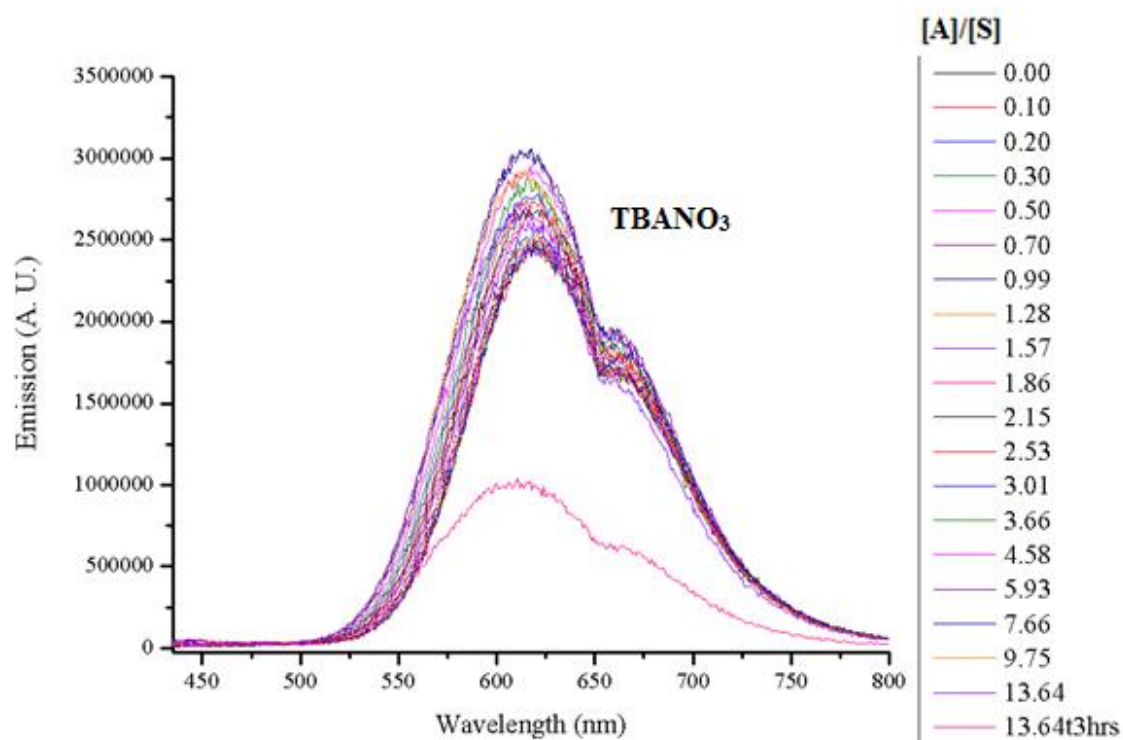


Figure 6.17. Emission titration overlay of sensor 5.1 with tetrabutylammonium nitrate

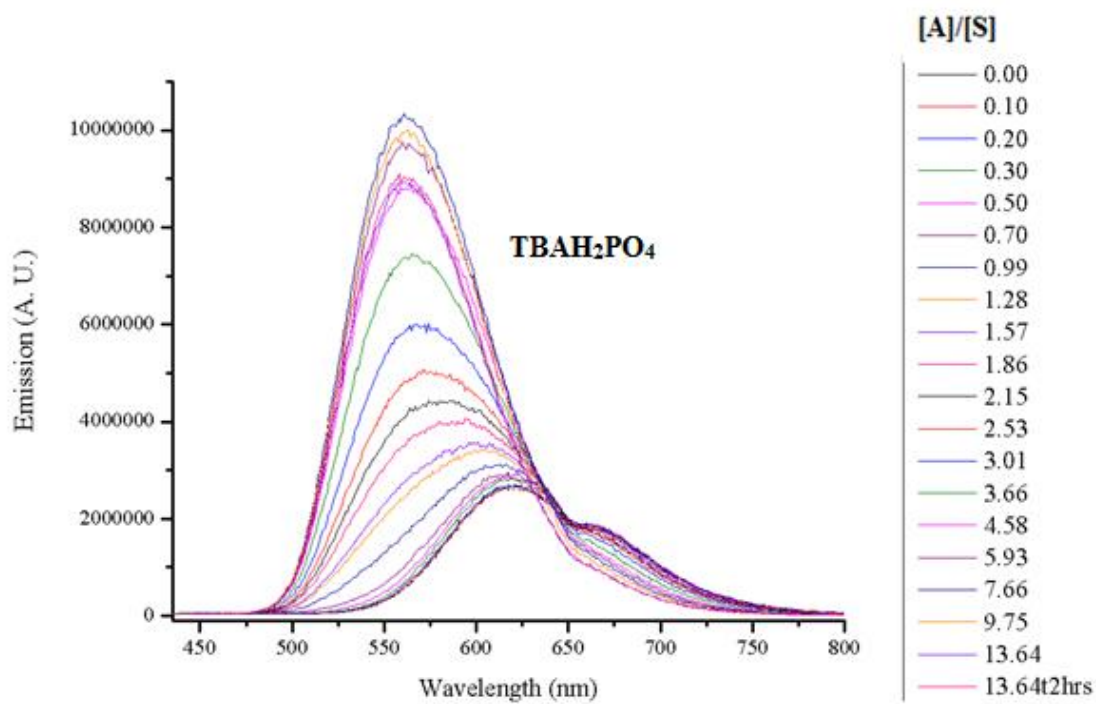


Figure 6.18. Emission titration overlay of sensor **5.1** with tetrabutylammonium dihydrogen phosphate.

APPENDIX C

PROTON NMR TITRATION OVERLAYS

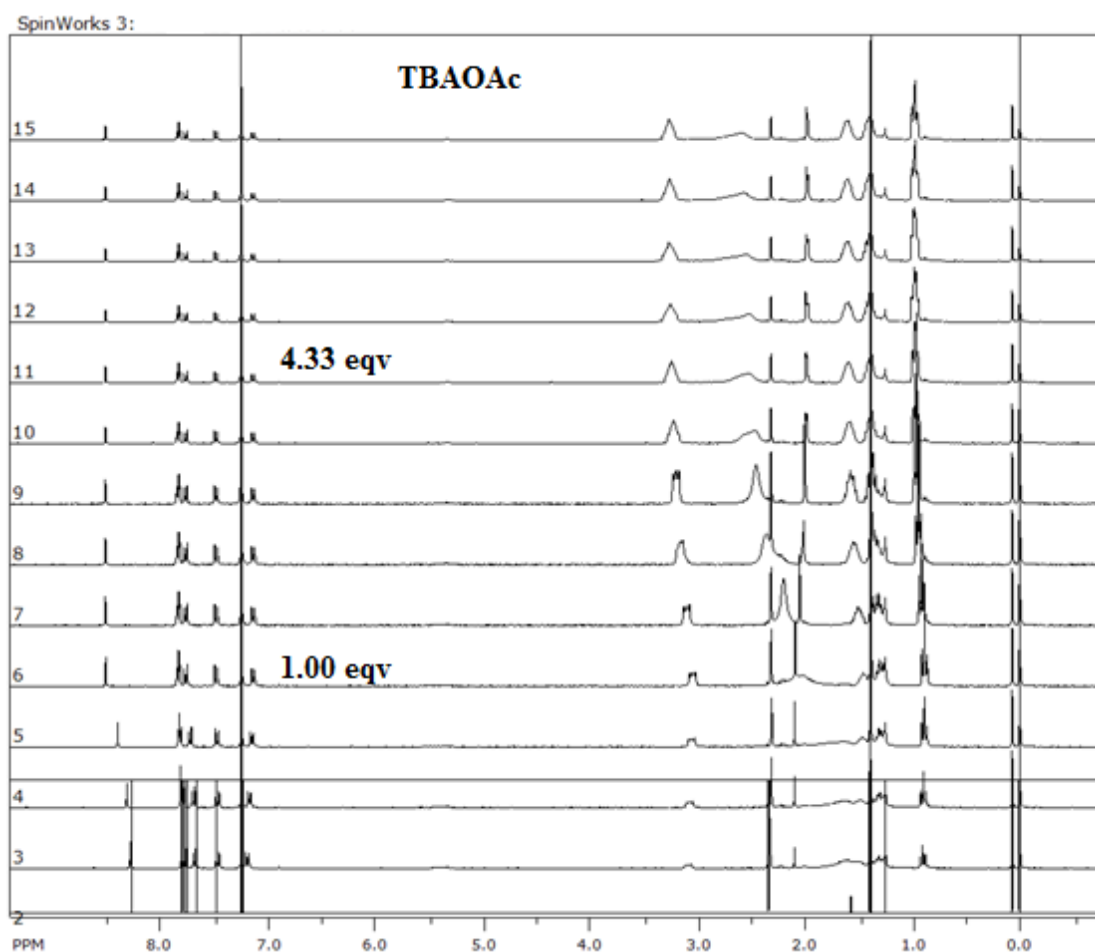


Figure 6.19. ^1H NMR titration overlay of sensor **5.1** with tetrabutylammonium acetate.

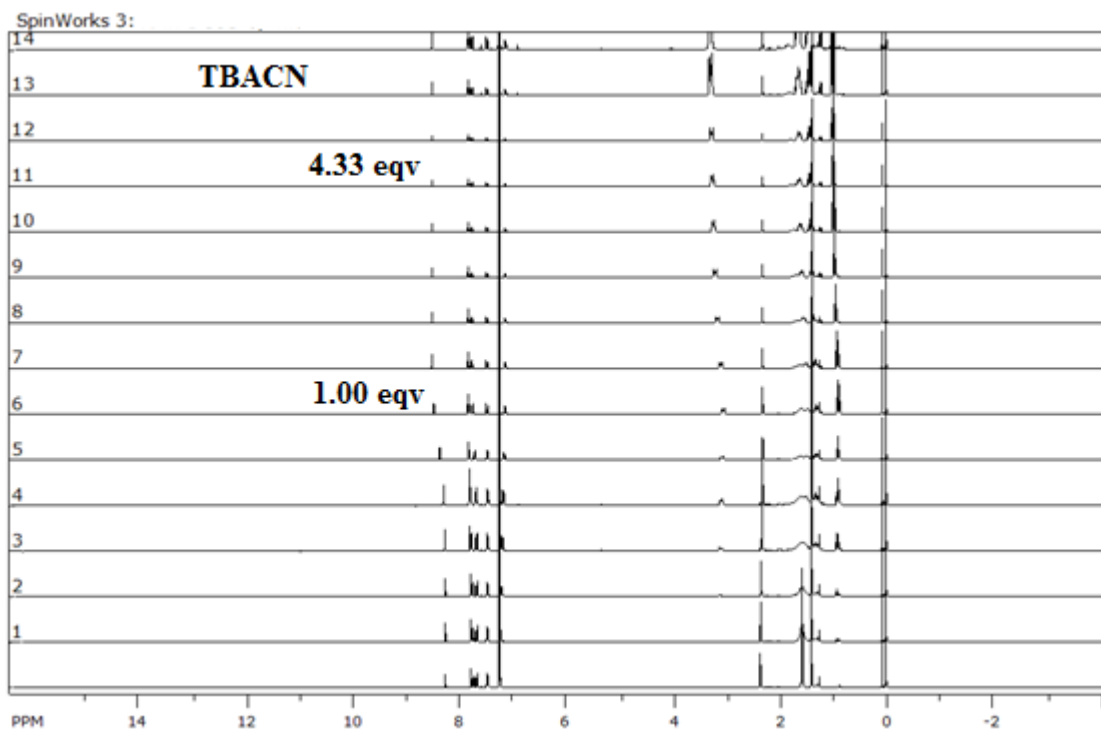


Figure 6.20. ^1H NMR titration overlay of sensor **5.1** with tetrabutylammonium cyanide.

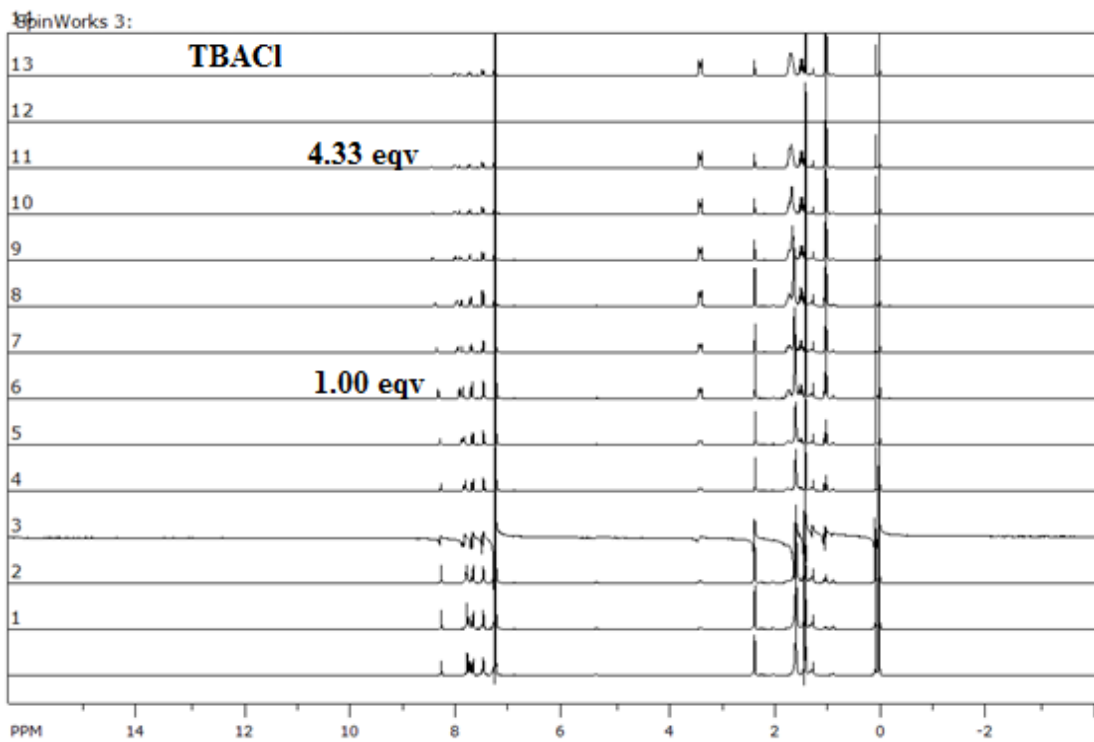


Figure 6.21. ^1H NMR titration overlay of sensor **5.1** with tetrabutylammonium chloride.

APPENDIX D

PROTON NMR SPECTRA

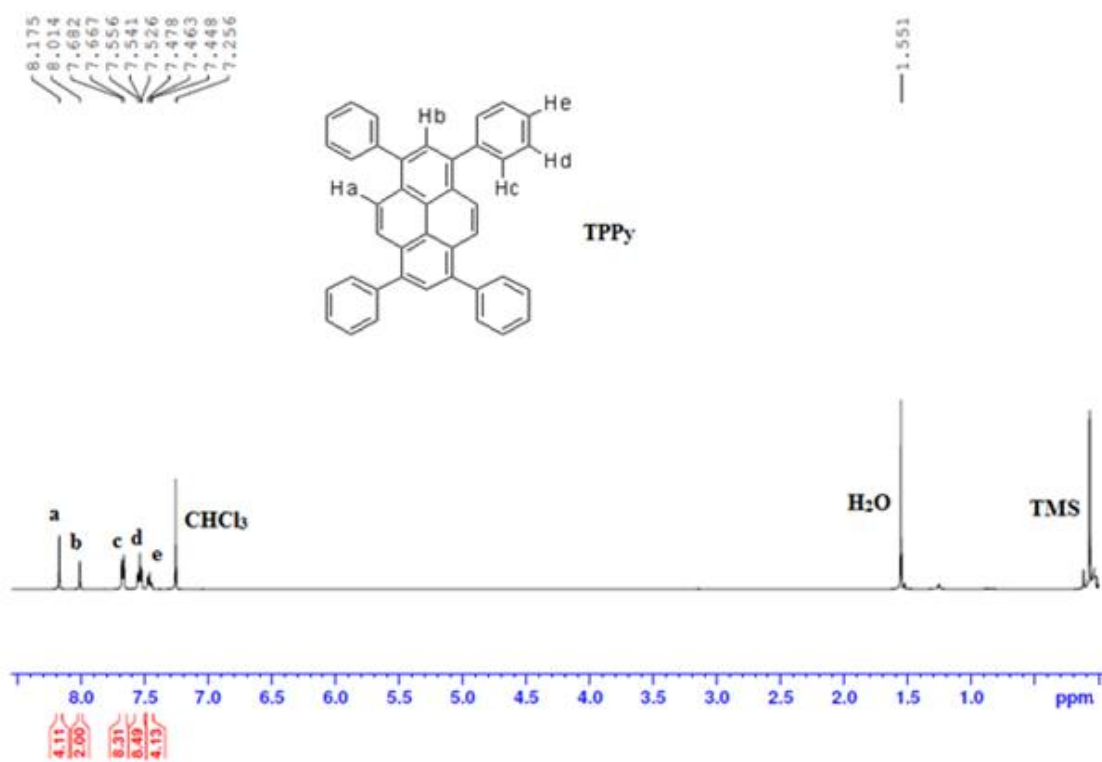


Figure 6.22. ^1H NMR of 1,3,6,8-tetraphenylpyrene in CDCl_3 at 500 MHz.

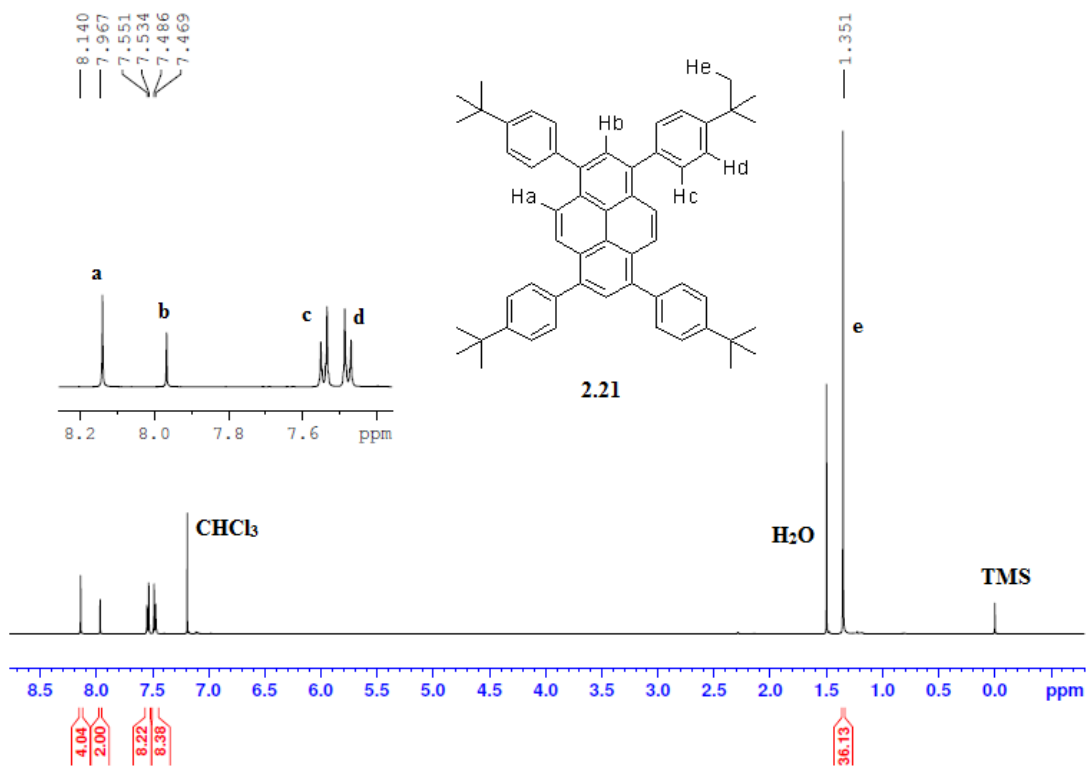


Figure 6.23. ^1H NMR of compound **2.21** in CDCl_3 at 500 MHz.

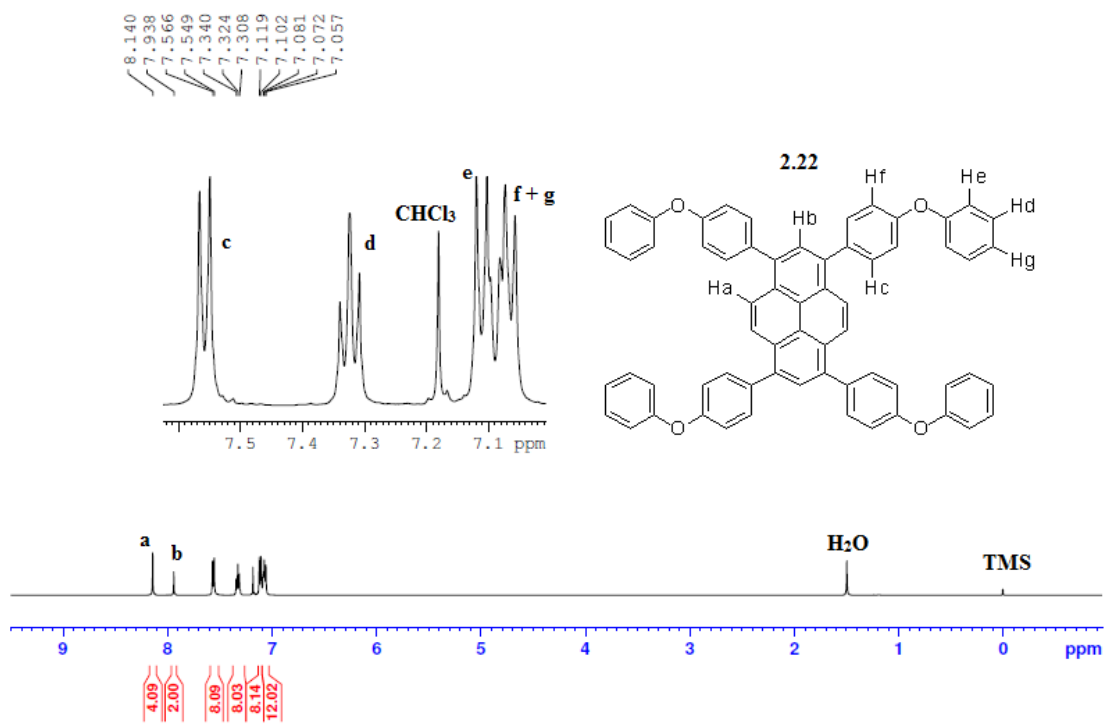


Figure 6.24. ¹H NMR of compound **2.22** in CDCl₃ at 500 MHz.

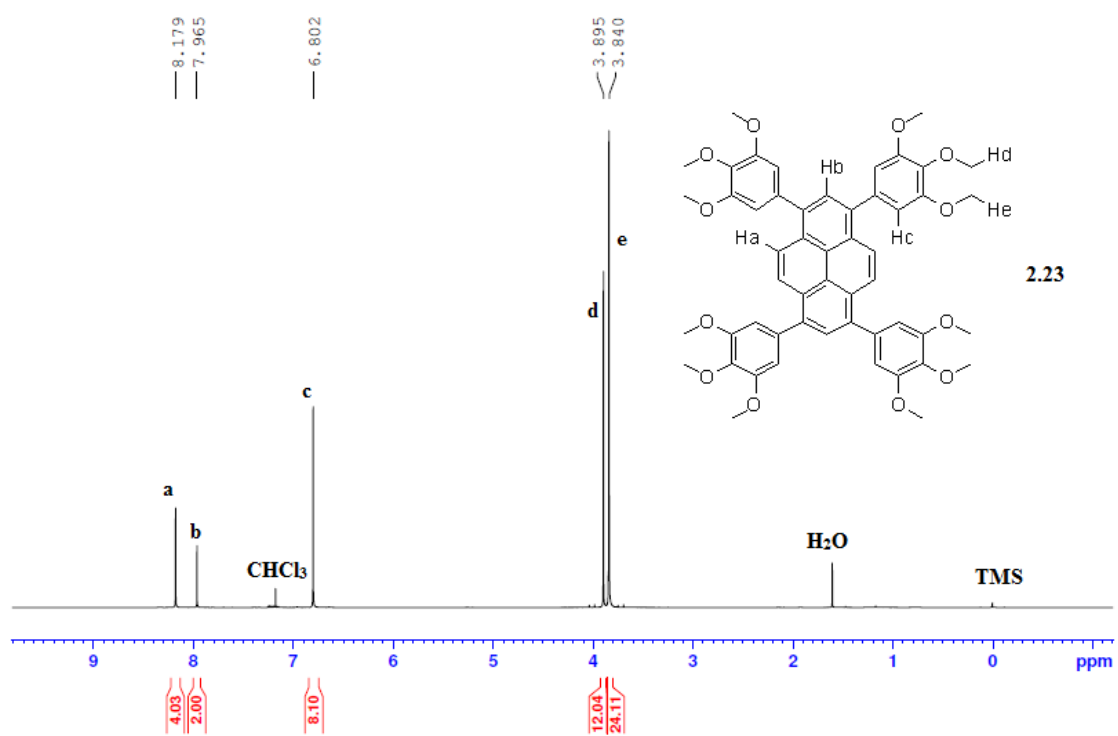


Figure 6.25. ^1H NMR of compound **2.23** in CDCl_3 at 500 MHz.

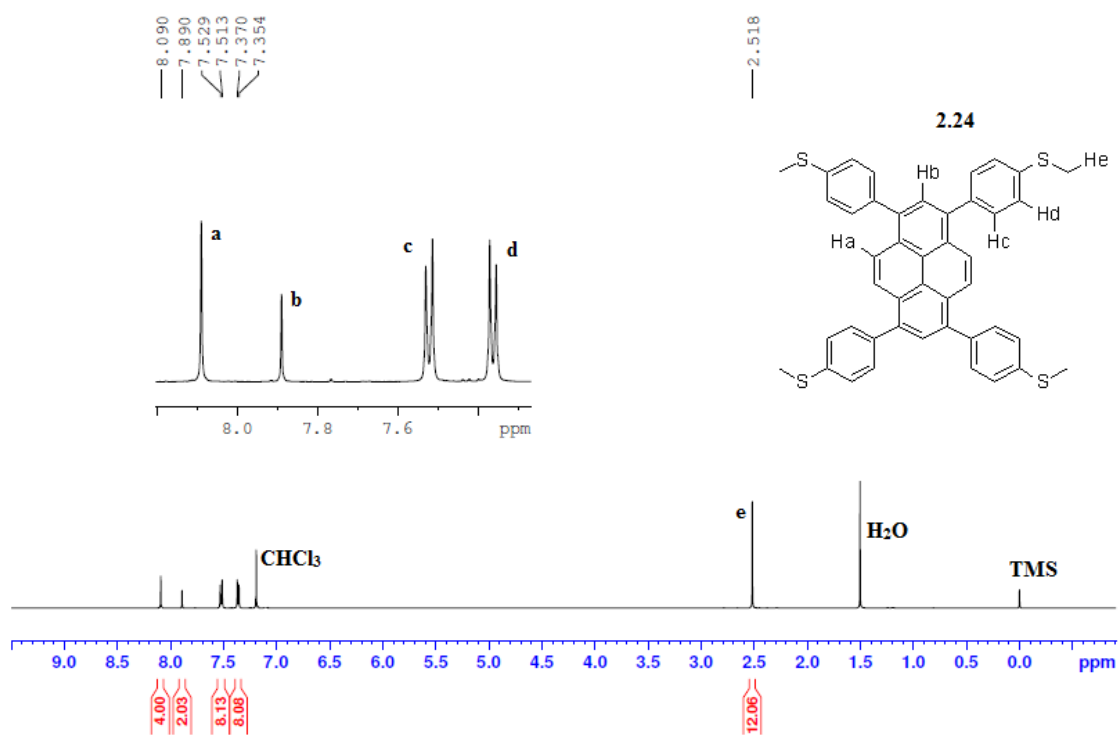


Figure 6.26. ^1H NMR of compound **2.24** in CDCl_3 at 500 MHz.

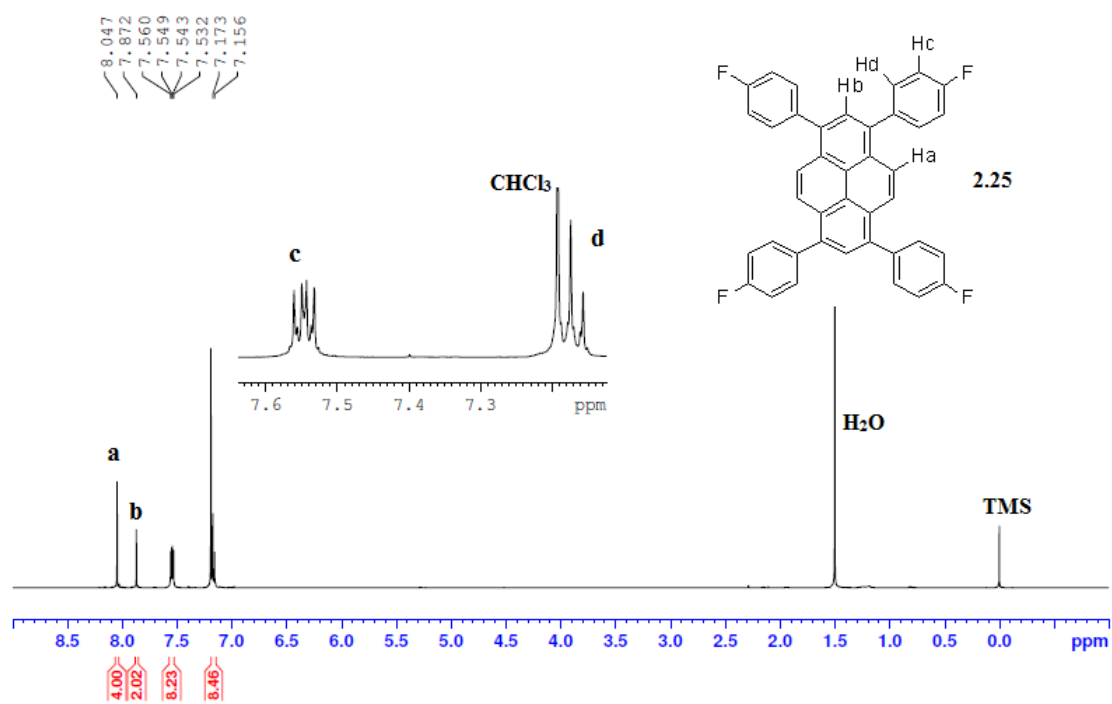


Figure 6.27. ^1H NMR of compound **2.25** in CDCl_3 at 500 MHz.

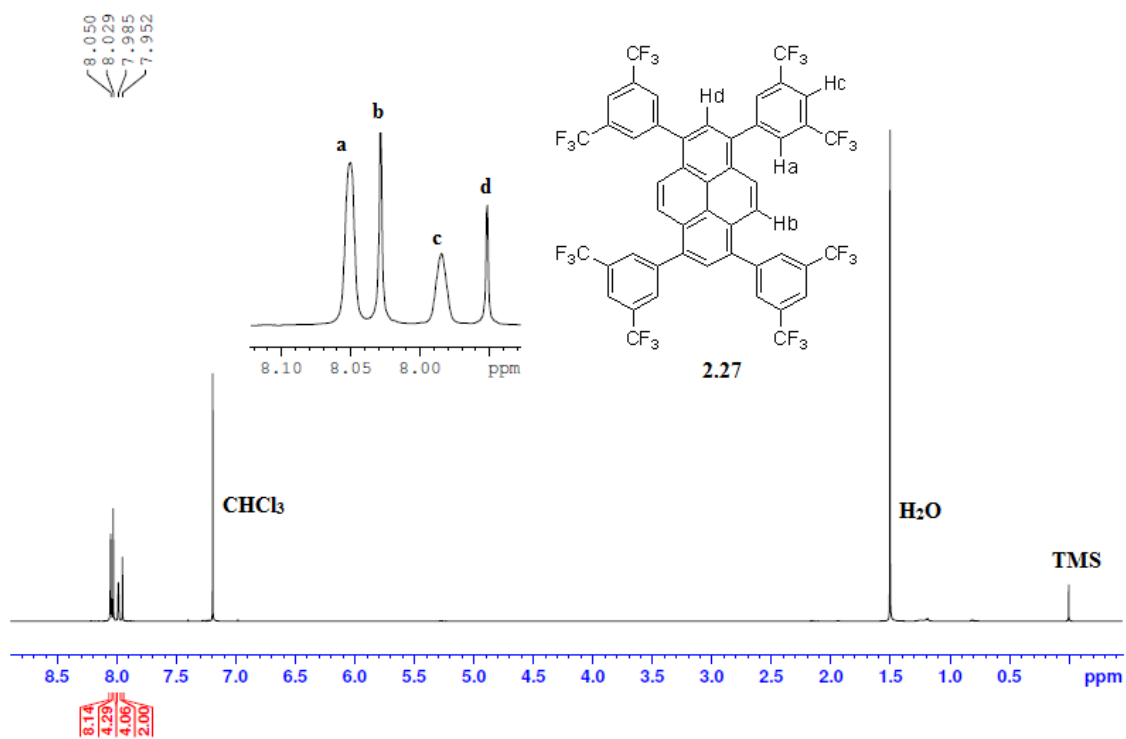


Figure 6.28. ¹H NMR of compound **2.27** in CDCl₃ at 500 MHz.

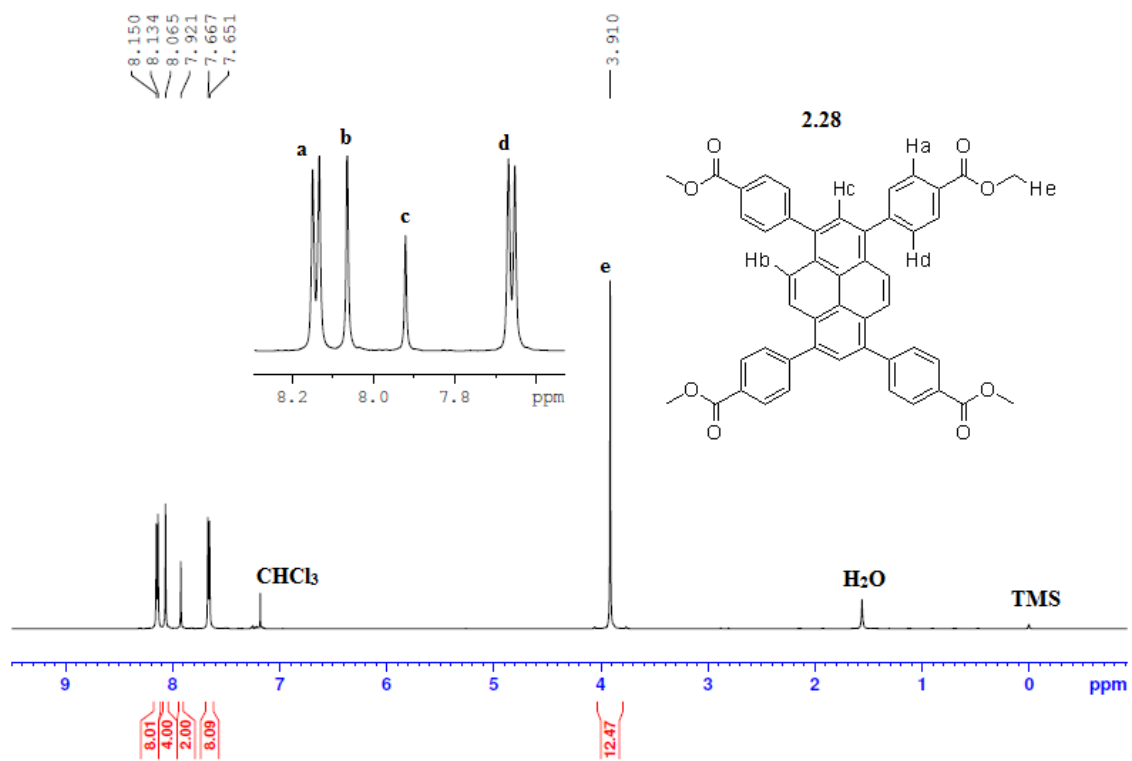


Figure 6.29. ^1H NMR of compound **2.28** in CDCl_3 at 500 MHz.

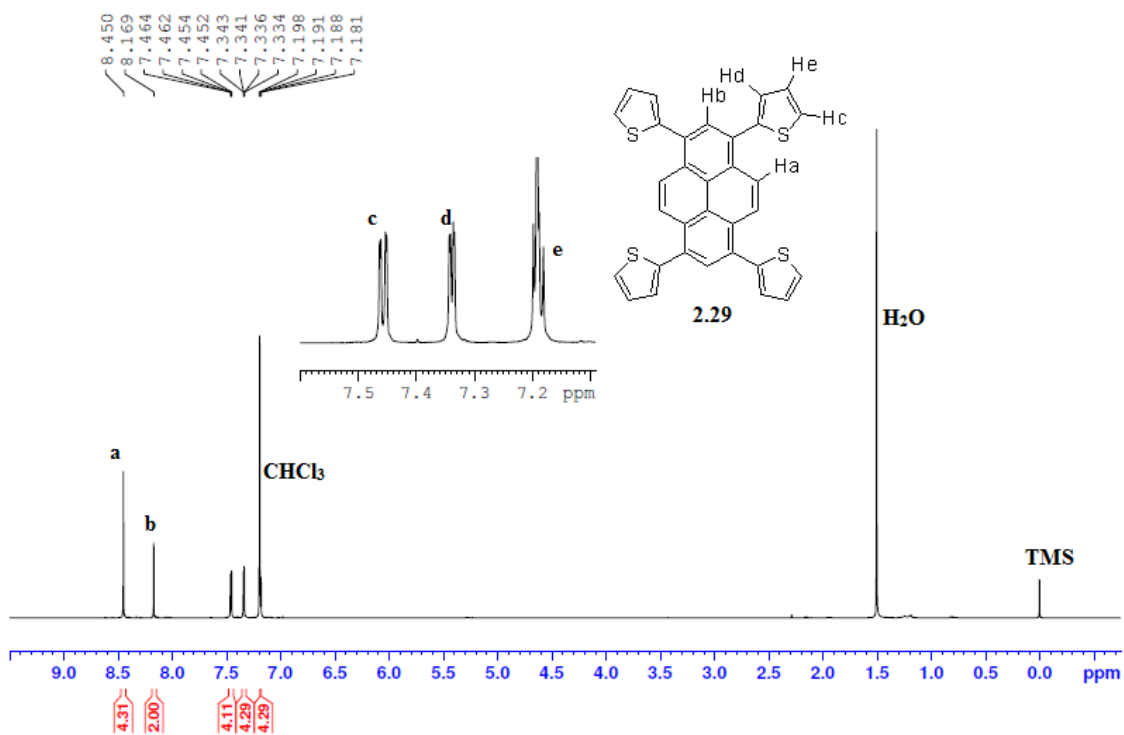


Figure 6.30. ^1H NMR of compound **2.29** in CDCl_3 at 500 MHz.

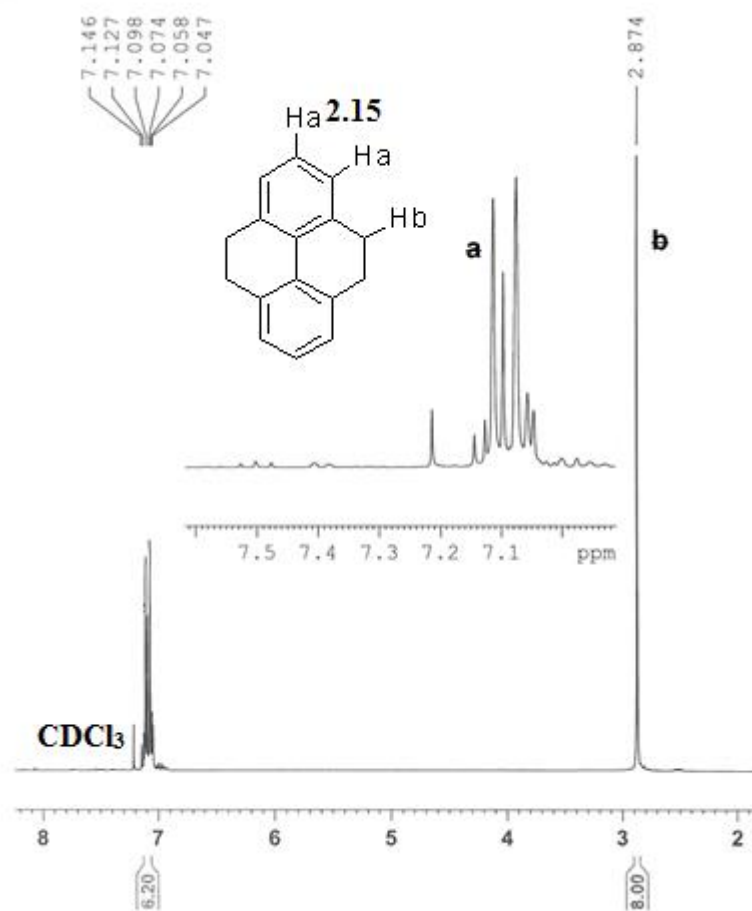


Figure 6.31. ^1H NMR of compound **2.15** in CDCl_3 at 300 MHz.

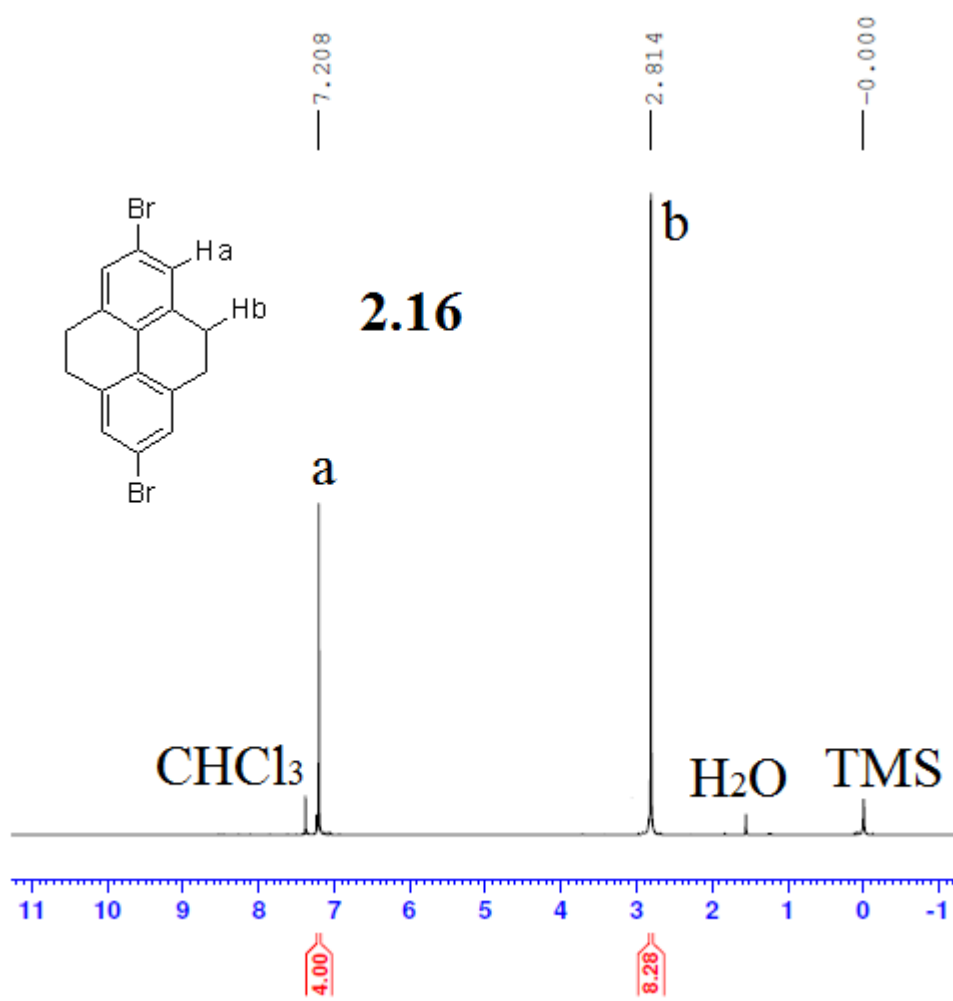


Figure 6.32. ^1H NMR of compound **2.16** in CDCl_3 at 500 MHz.

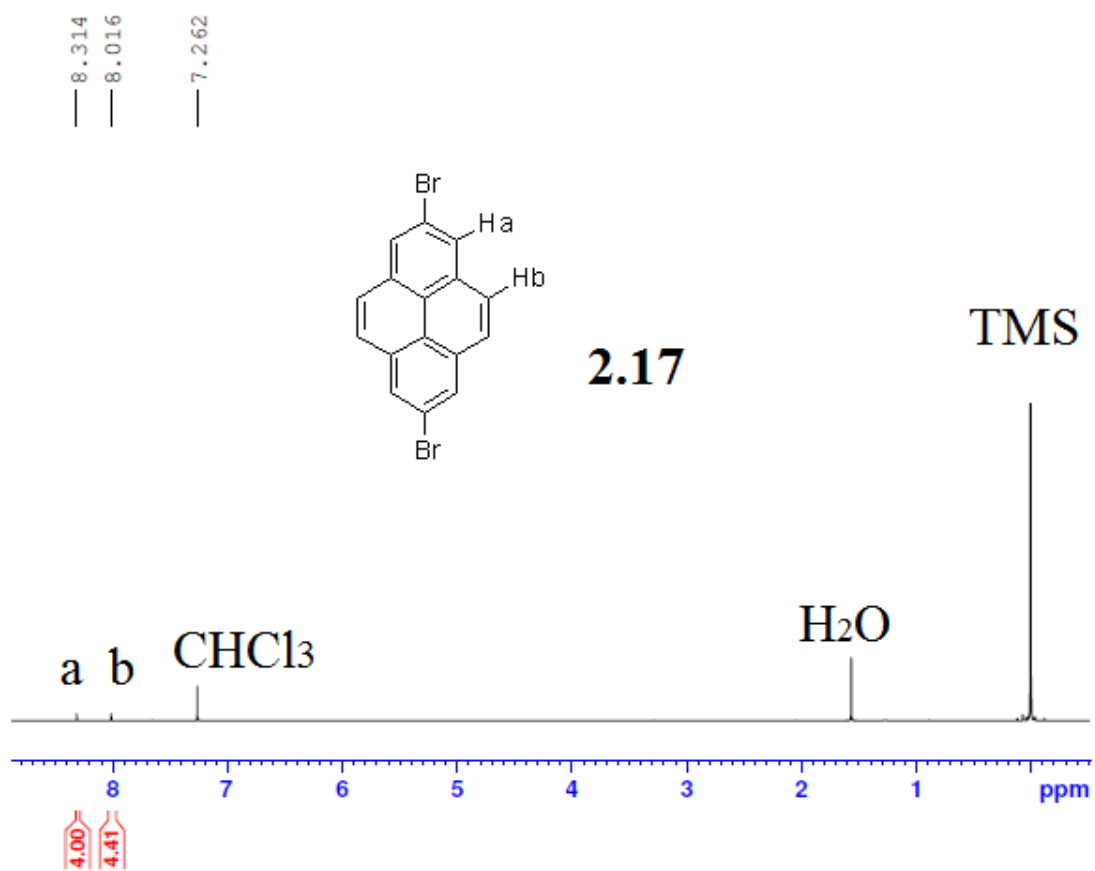


Figure 6.33. ^1H NMR of compound **2.17** in CDCl_3 at 500 MHz.

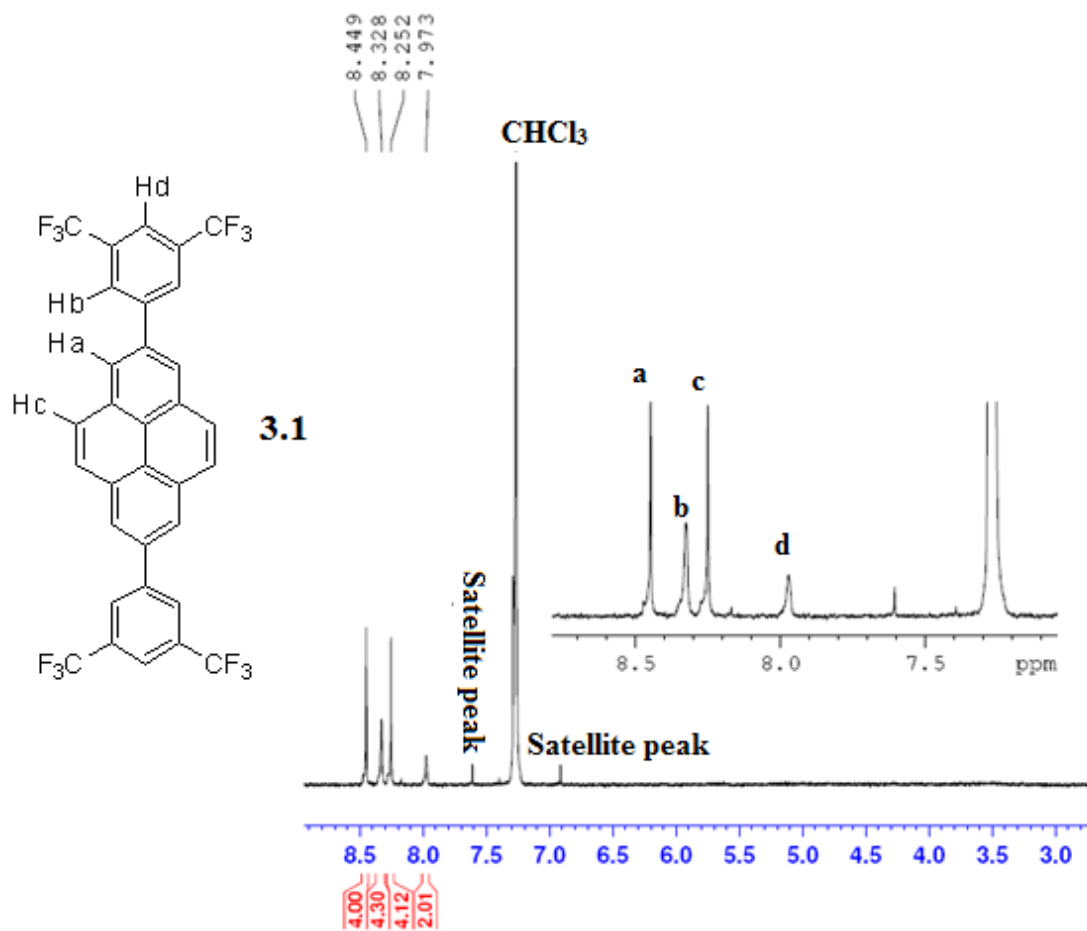


Figure 6.34. ¹H NMR of compound **3.1** in CDCl₃ at 300 MHz.

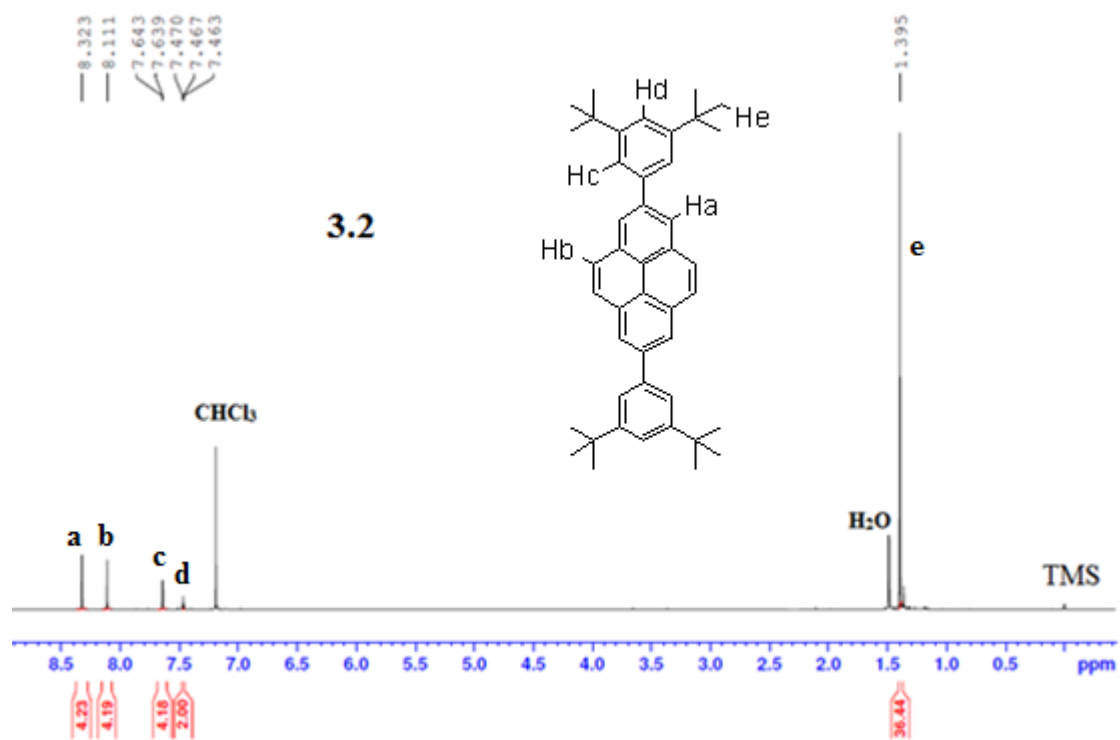


Figure 6.35. ^1H NMR of compound **3.2** in CDCl_3 at 500 MHz.

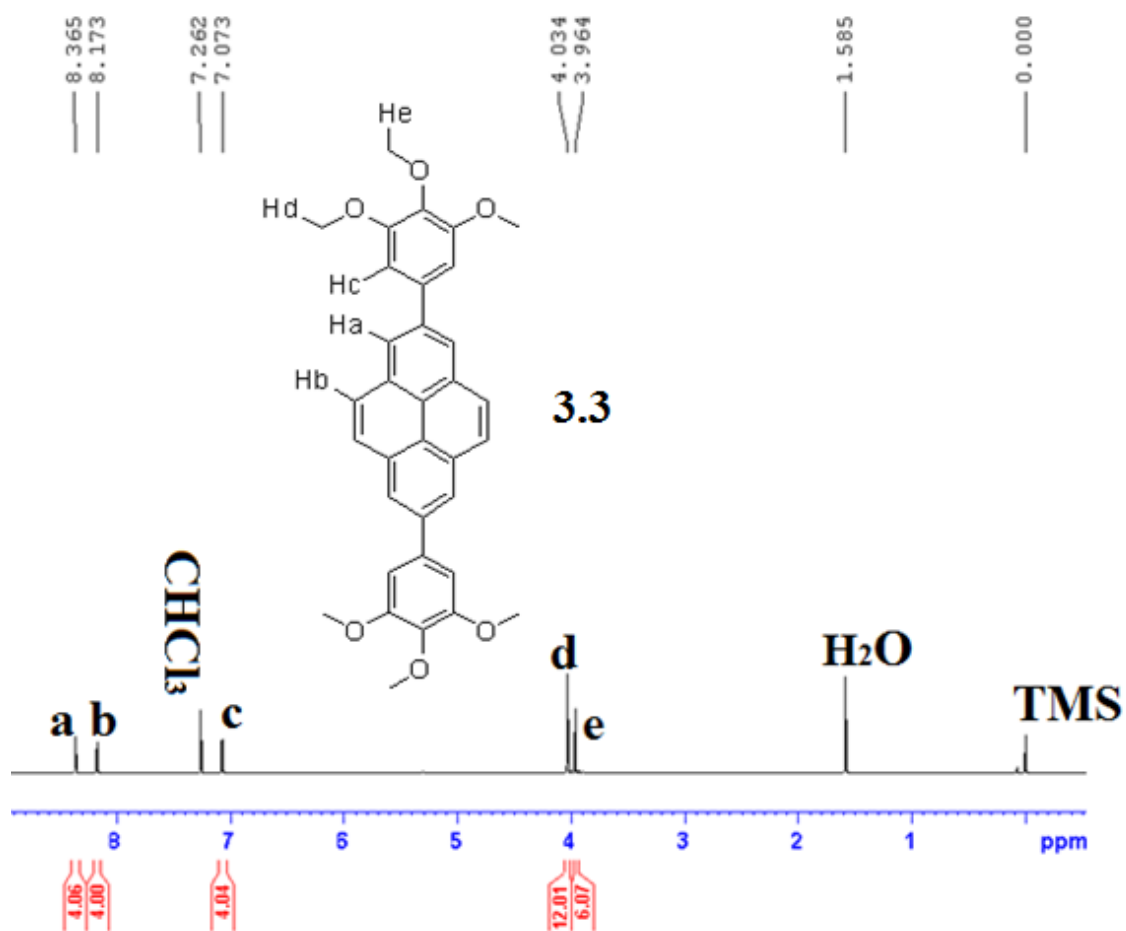


Figure 6.36. ^1H NMR of compound **3.3** in CDCl_3 at 300 MHz.

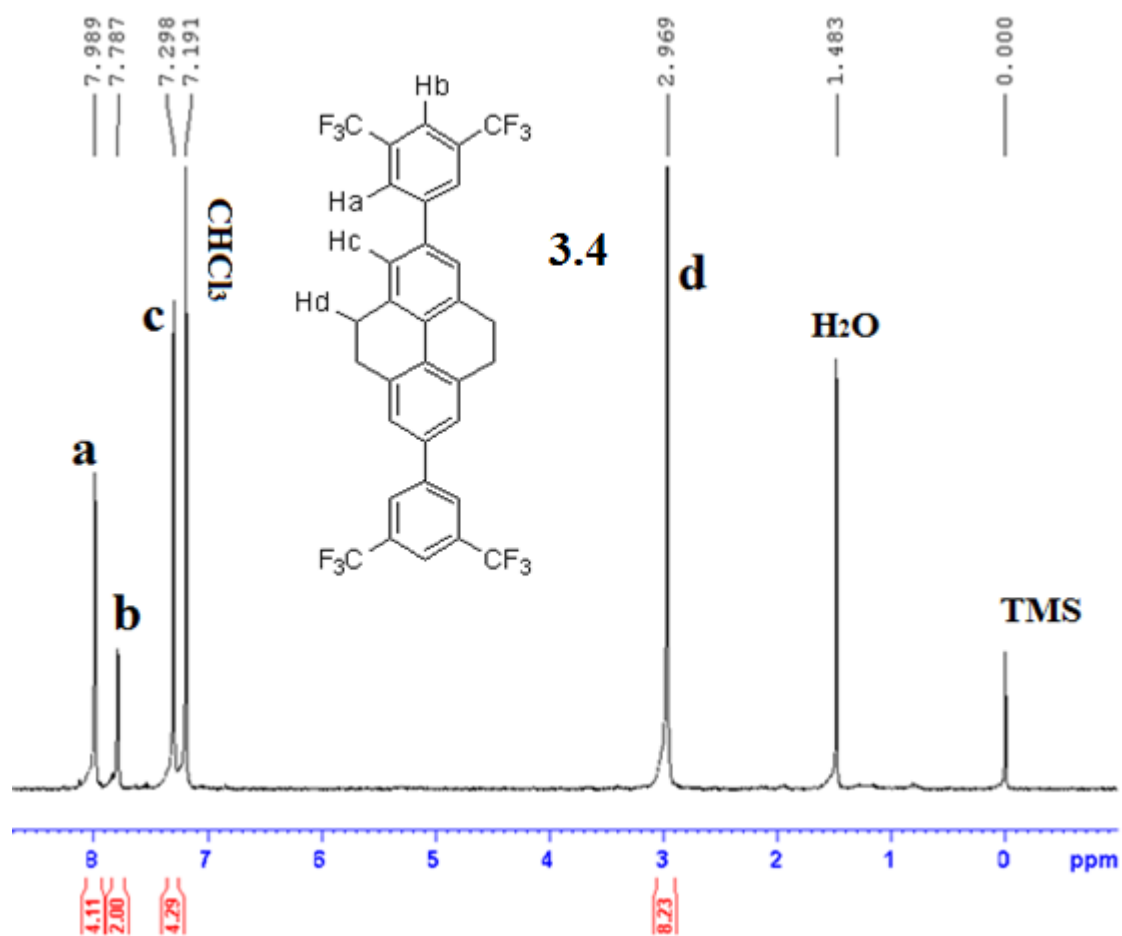


Figure 6.37. ^1H NMR of compound **3.4** in CDCl_3 at 300 MHz.

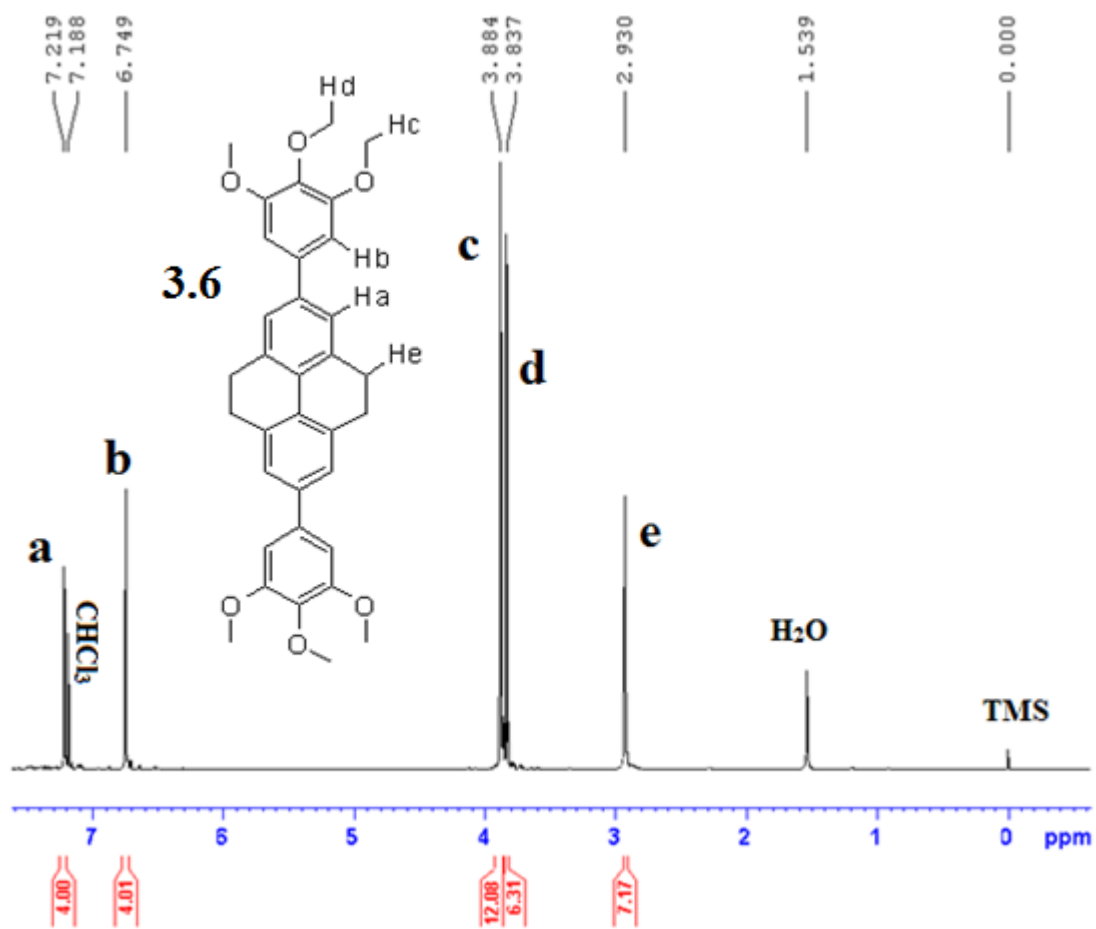


Figure 6.38. ^1H NMR of compound **3.6** in CDCl_3 at 300 MHz.

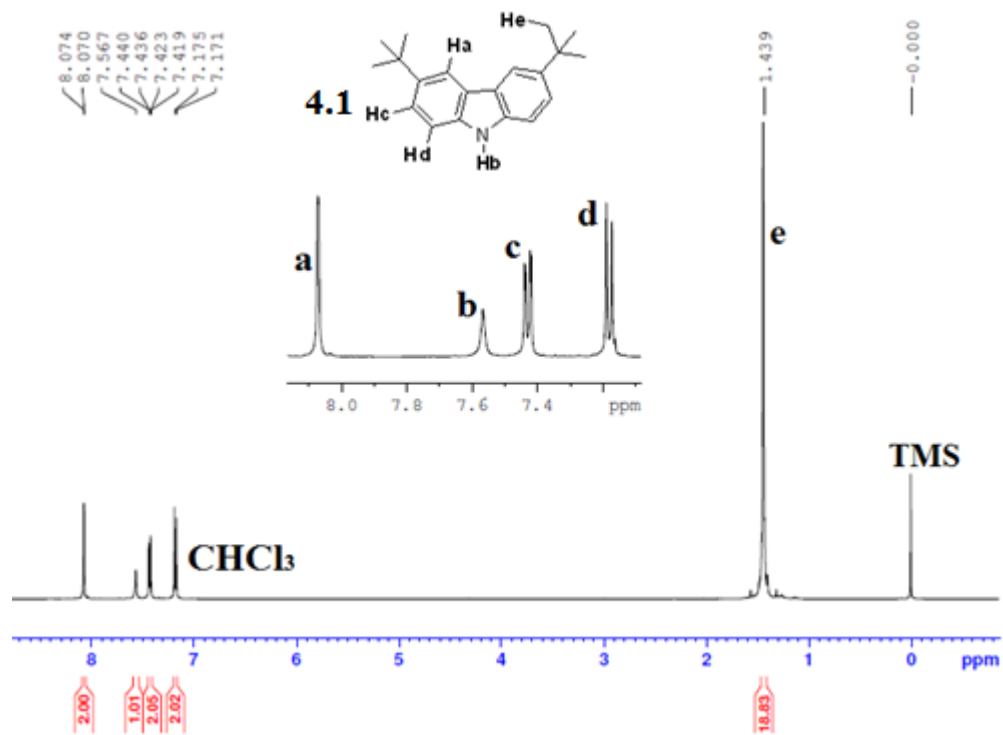


Figure 6.39. ^1H NMR of compound **4.1** in CDCl_3 at 500 MHz.

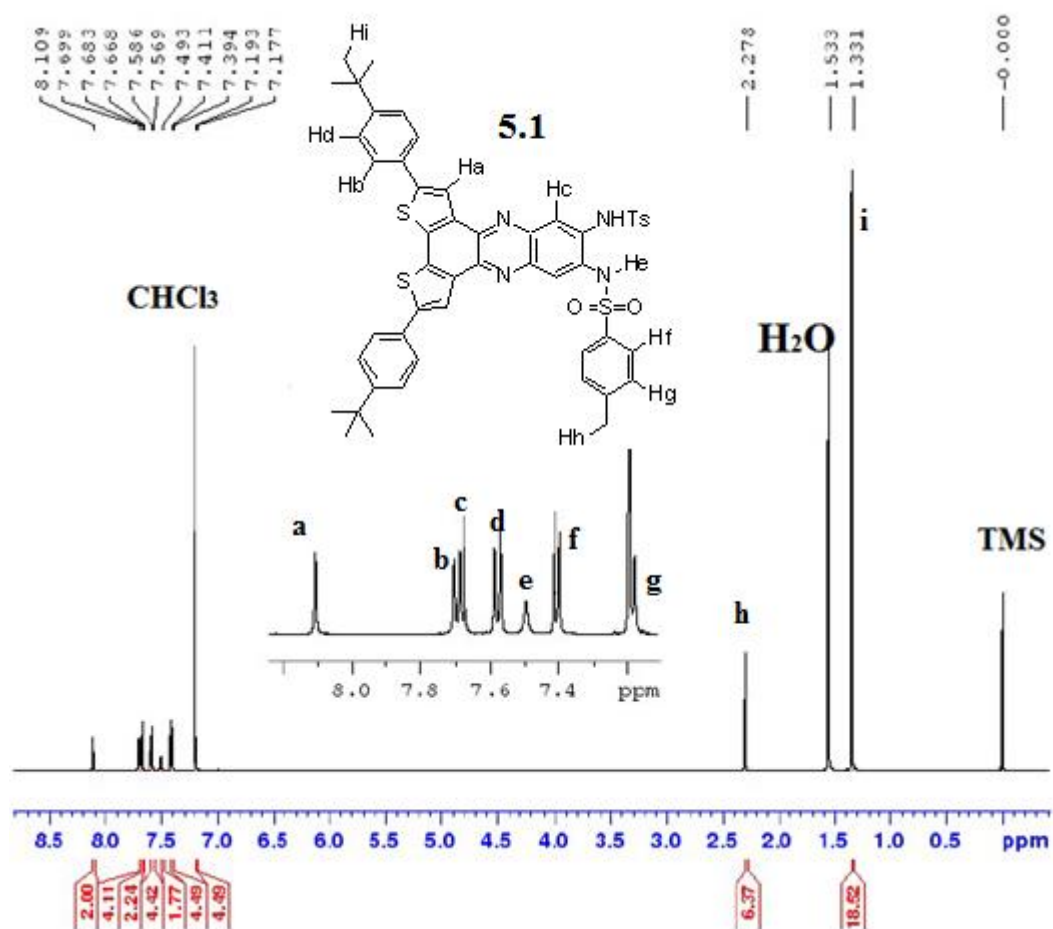


Figure 6.40. ^1H NMR of compound **5.1** in CDCl_3 at 500 MHz.

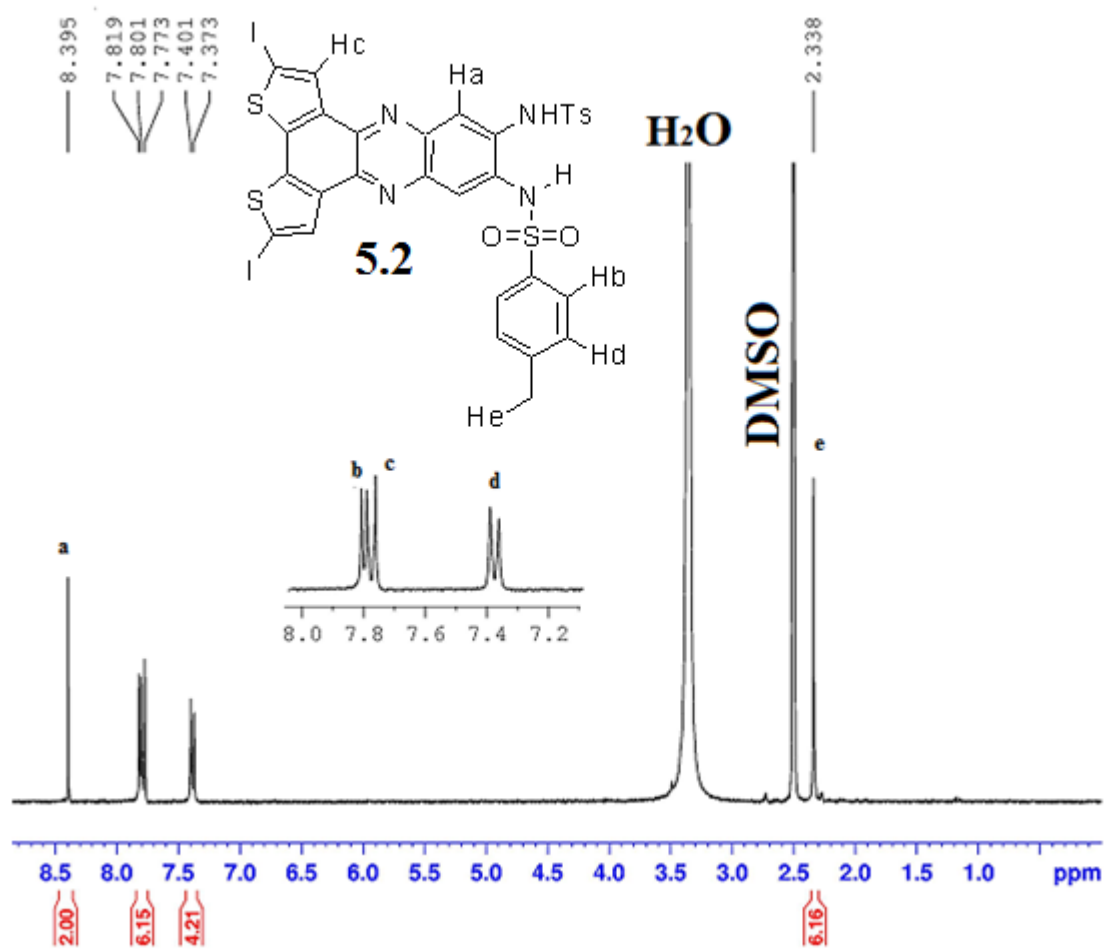


Figure 6.41. ¹H NMR of compound **5.2** in DMSO-d₆ at 300 MHz.

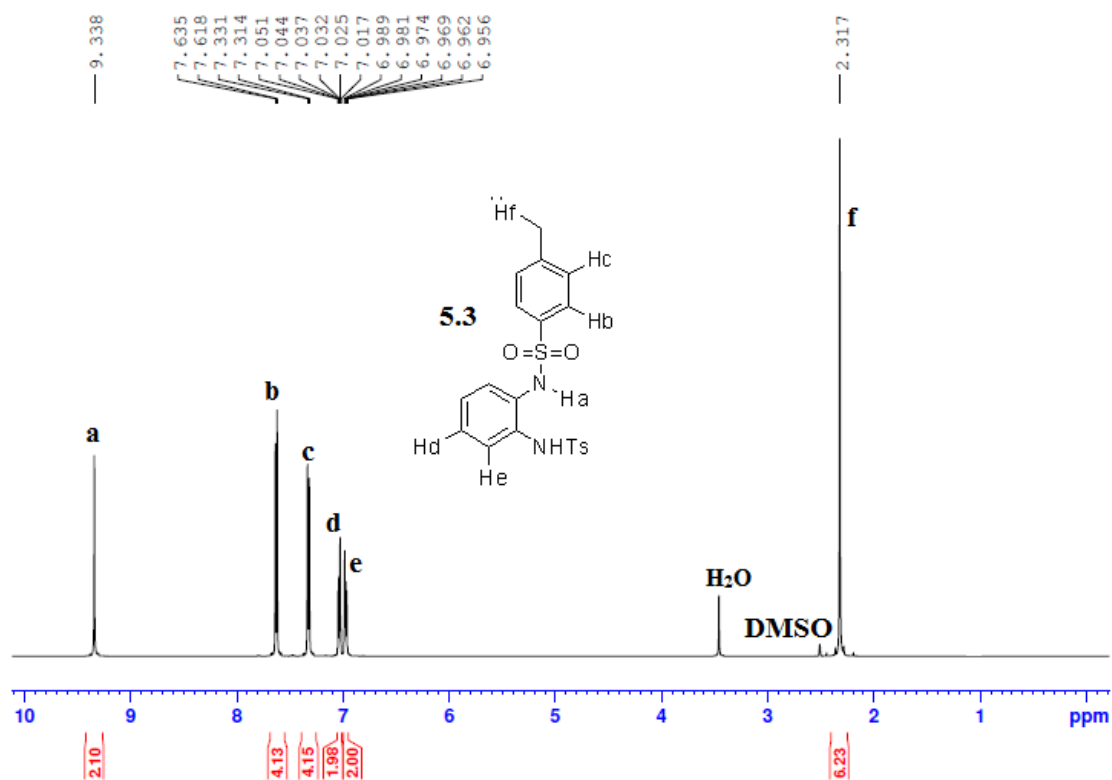


Figure 6.42. ^1H NMR of compound **5.3** in DMSO-d_6 at 500 MHz.

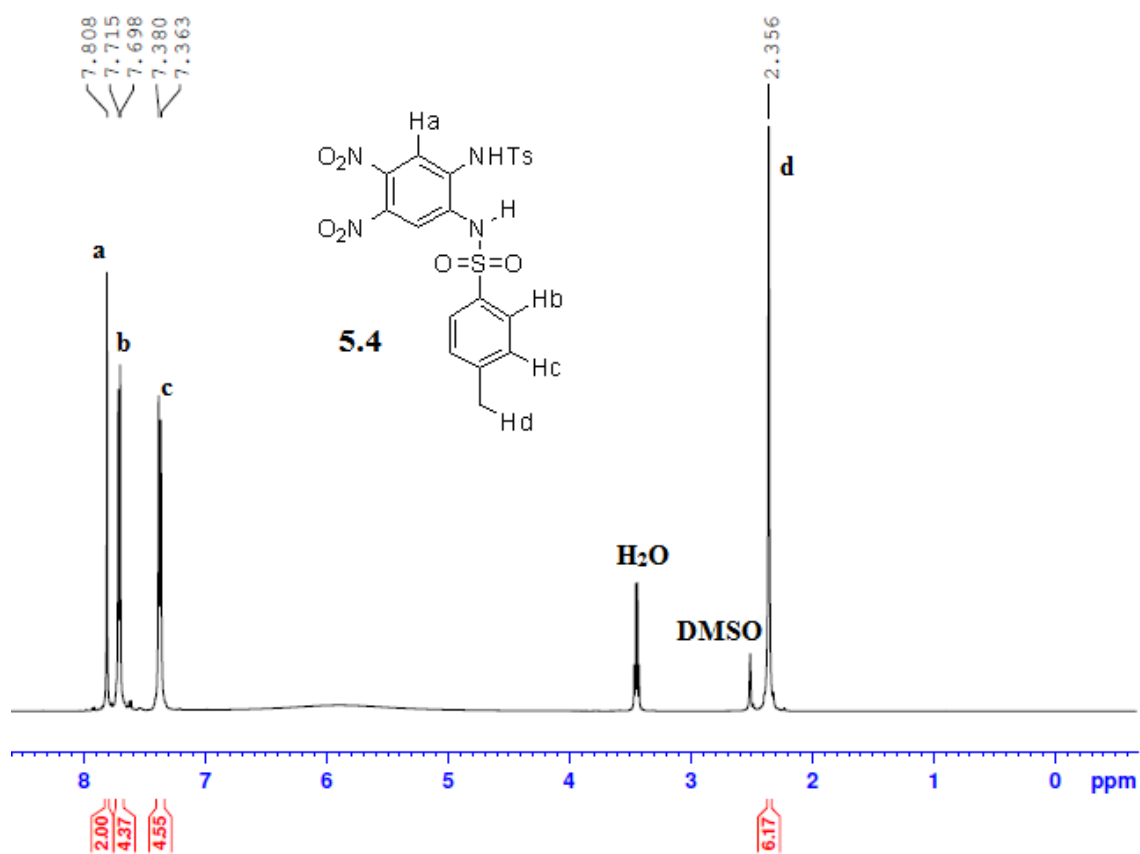


Figure 6.43. ¹H NMR of compound **5.4** in DMSO-d₆ at 500 MHz.

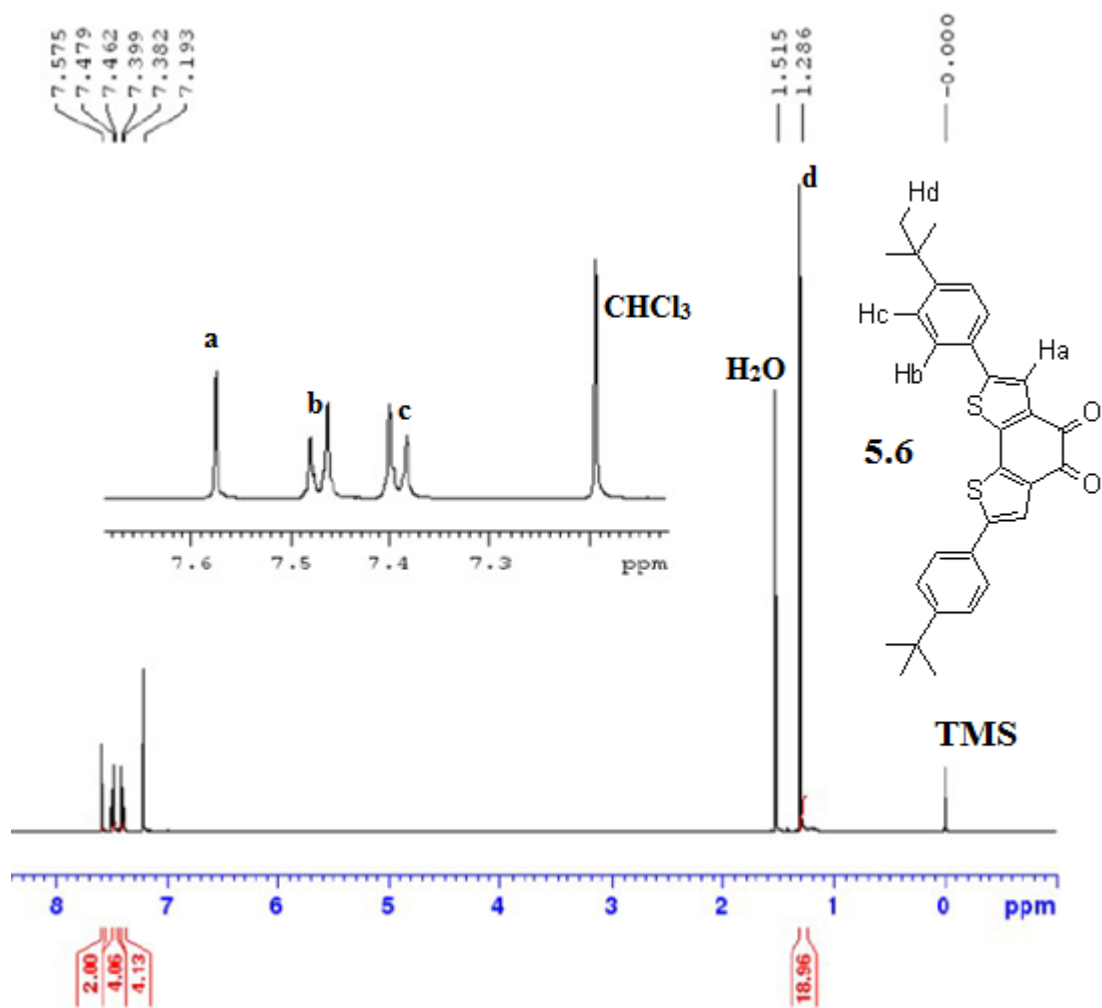


Figure 6.44. ^1H NMR of compound **5.6** in CDCl_3 at 500 MHz.

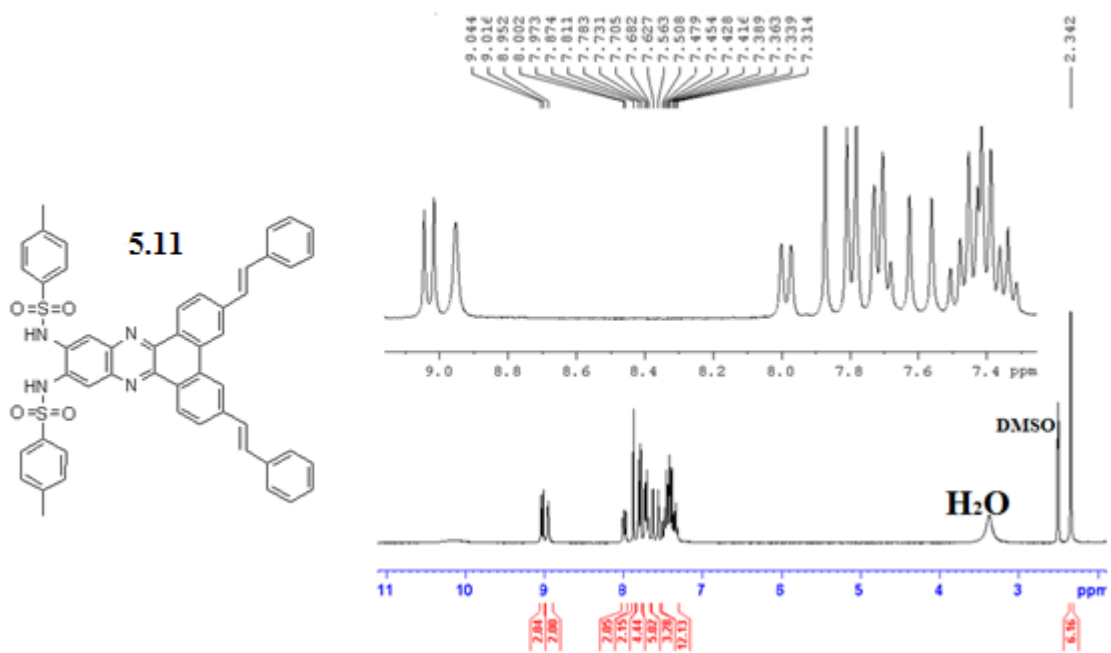


Figure 6.45. ^1H NMR of compound **5.11** in DMSO-d_6 at 300 MHz.

APPENDIX E

CARBON-13 NMR SPECTRA

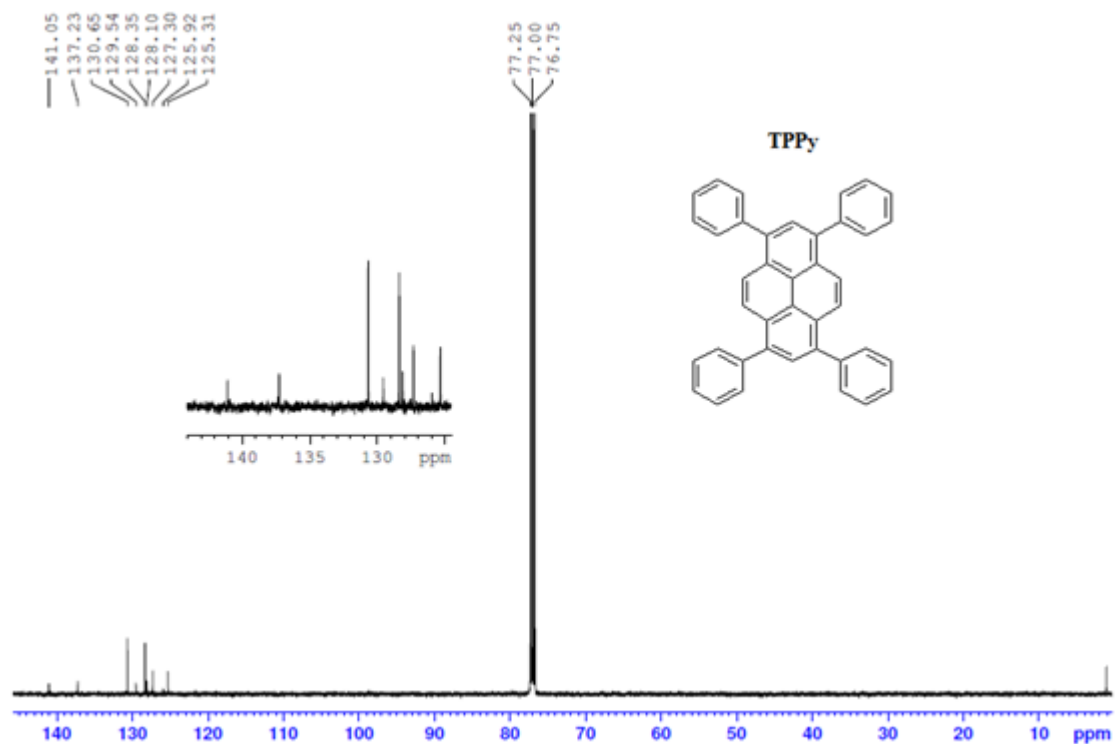


Figure 6.46. ^{13}C NMR of 1,3,6,8-tetraphenylpyrene in CDCl_3 at 125 MHz.

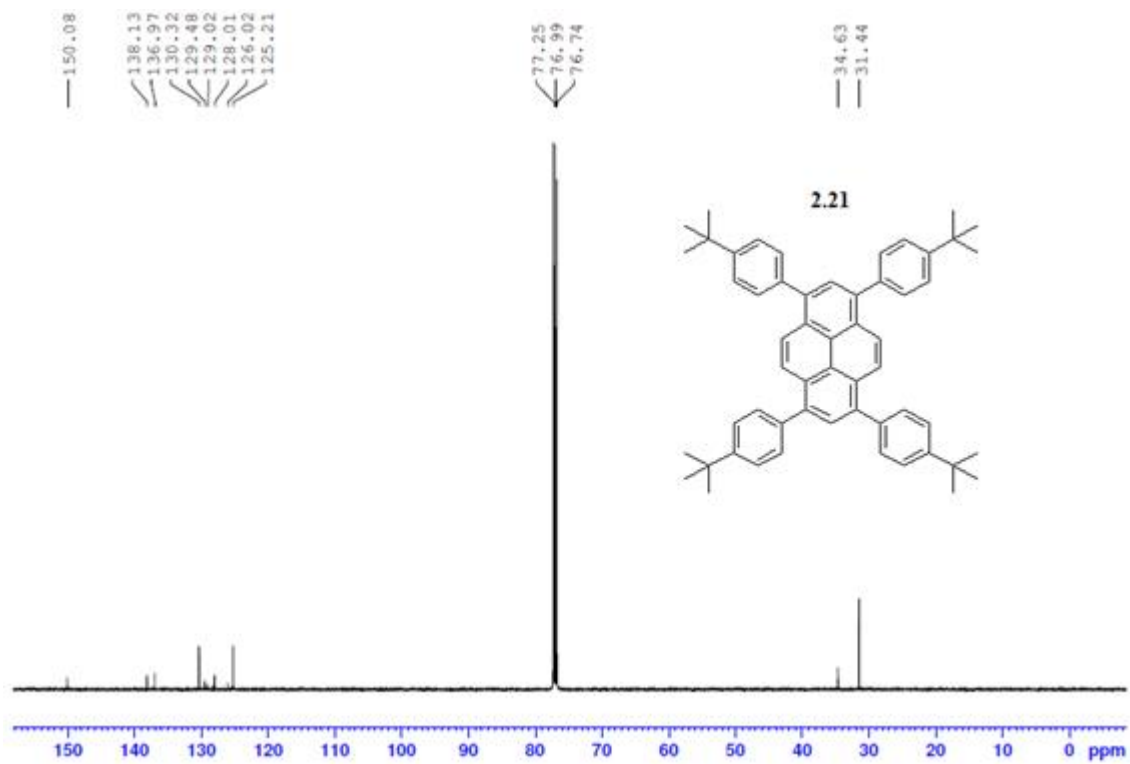


Figure 6.47. ^{13}C NMR of compound **2.21** in CDCl_3 at 125 MHz.

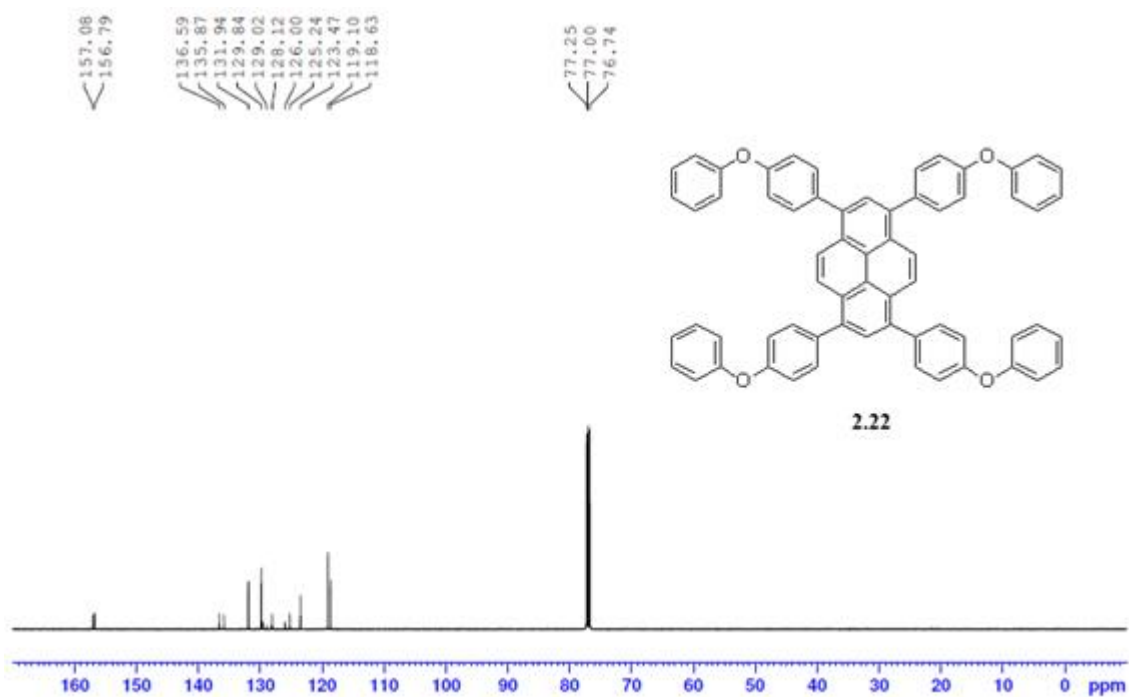


Figure 6.48. ^{13}C NMR of compound **2.22** in CDCl_3 at 125 MHz.

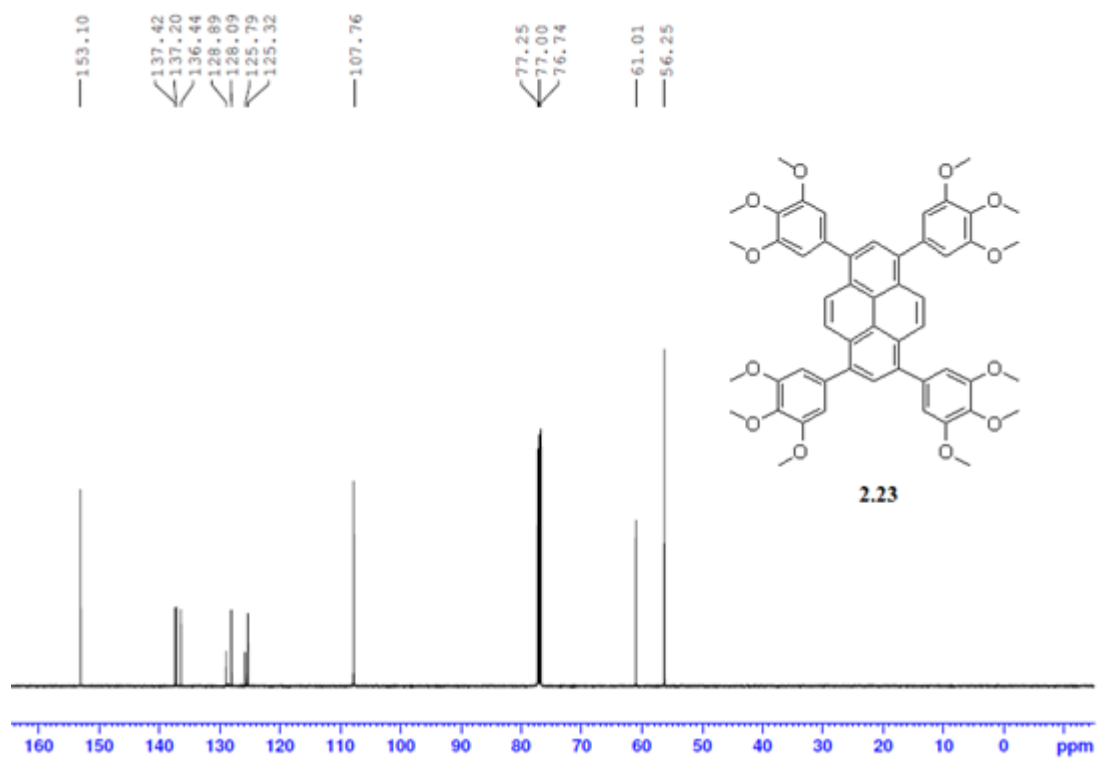


Figure 6.49. ^{13}C NMR of compound **2.23** in CDCl_3 at 125 MHz.

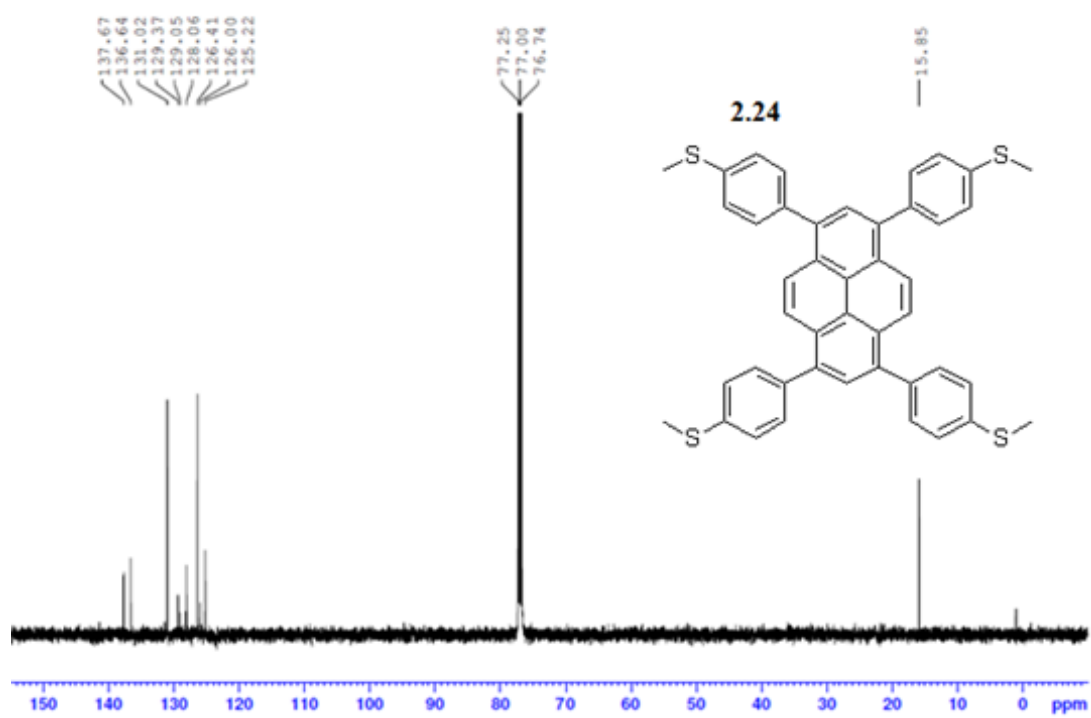


Figure 6.50. ^{13}C NMR of compound **2.24** in CDCl_3 at 125 MHz.

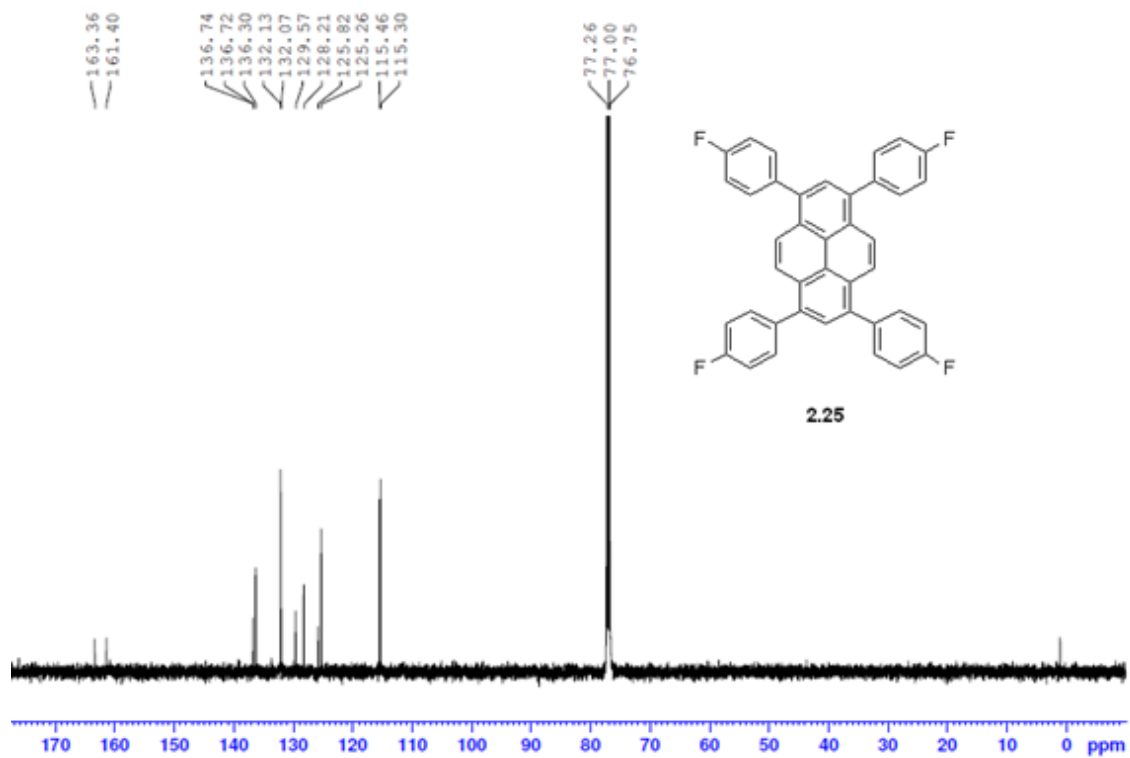


Figure 6.51. ^{13}C NMR of compound **2.25** in CDCl_3 at 125 MHz.

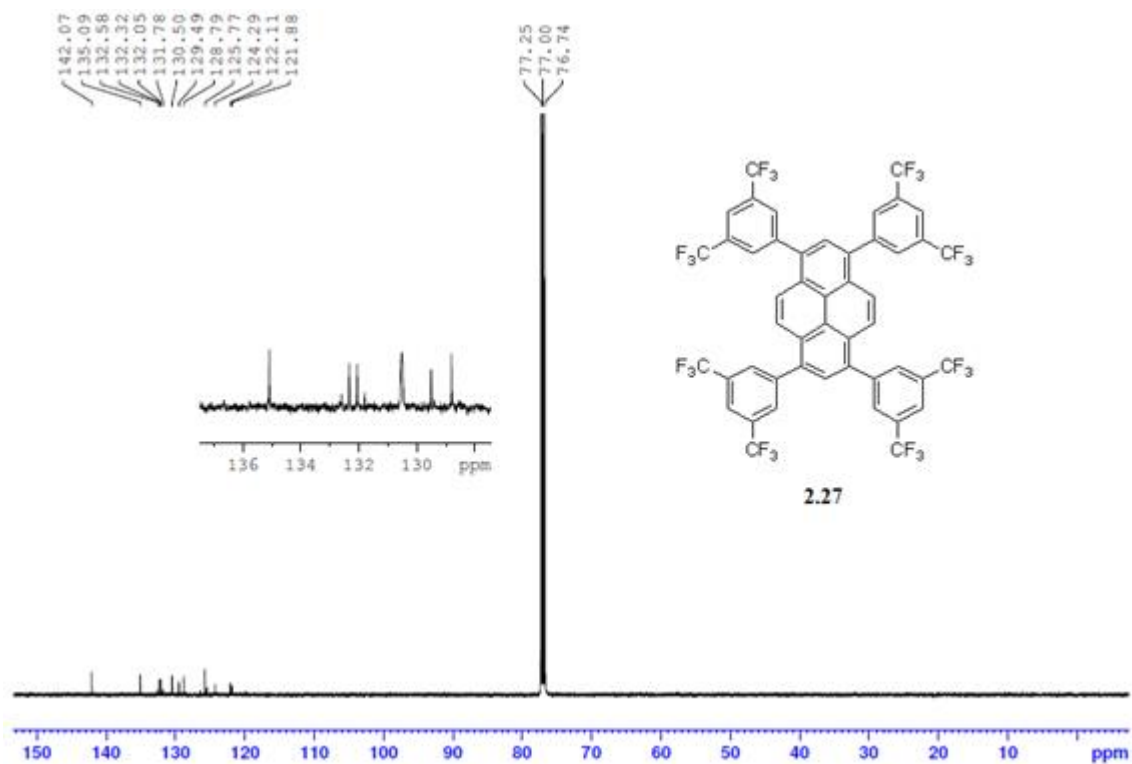


Figure 6.52. ^{13}C NMR of compound **2.27** in CDCl_3 at 125 MHz.

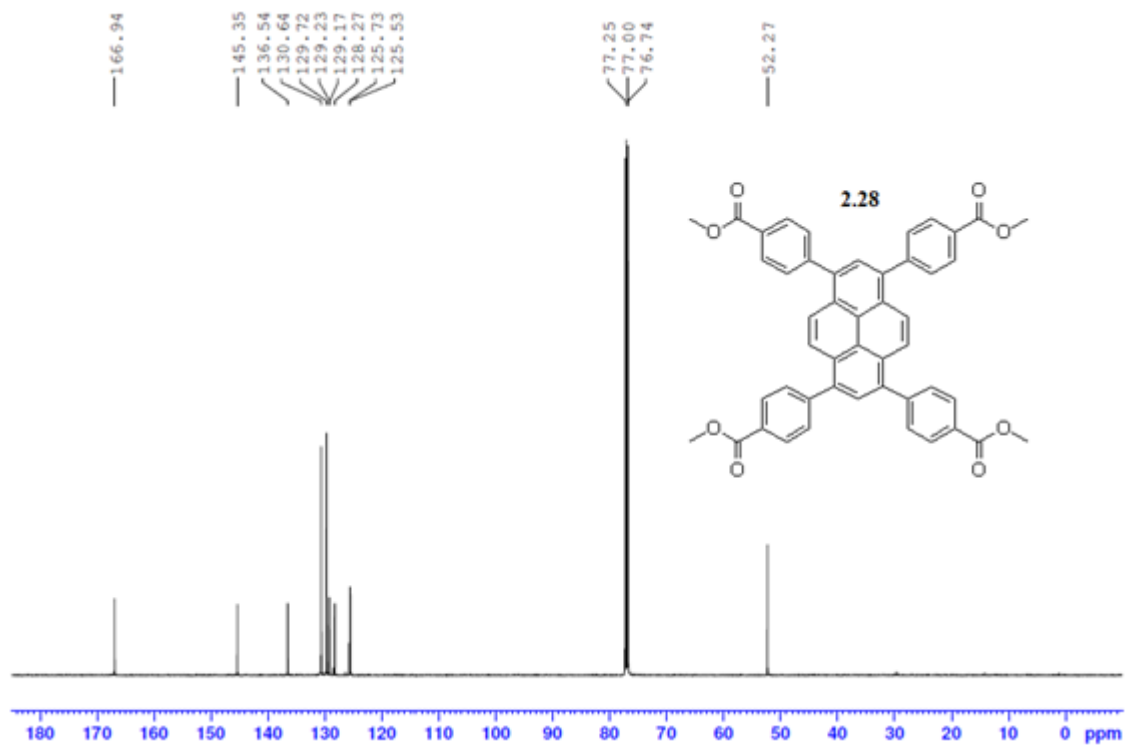


Figure 6.53. ^{13}C NMR of compound **2.28** in CDCl_3 at 125 MHz.

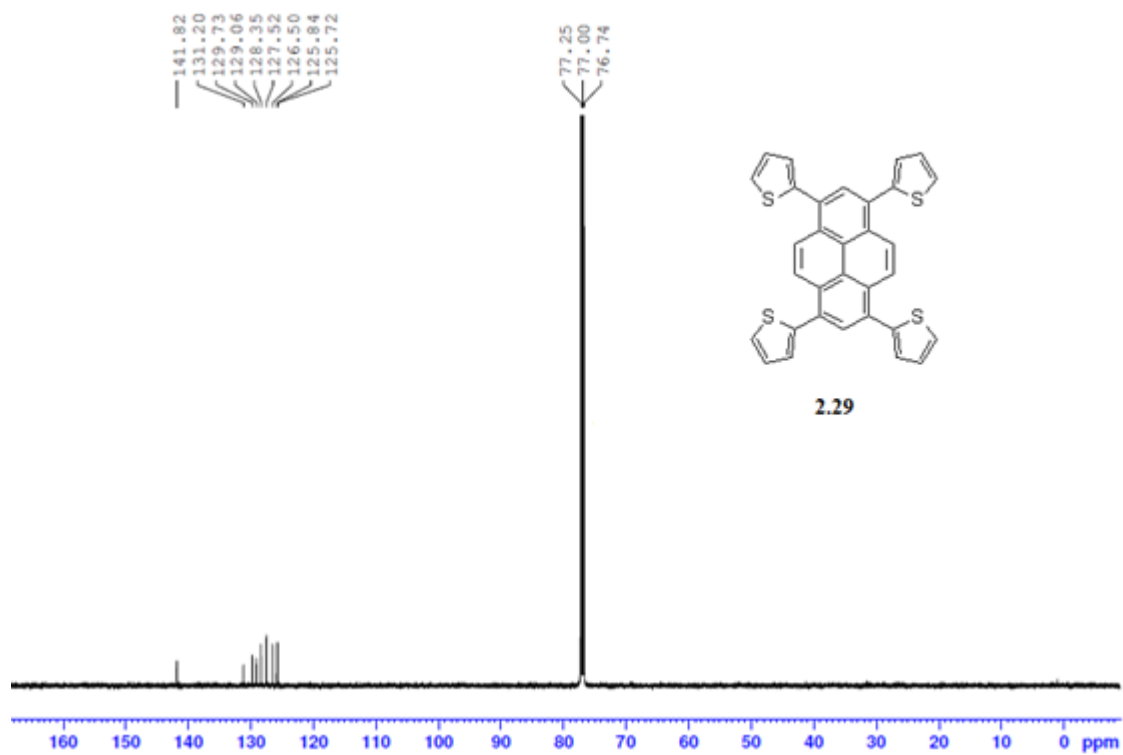


Figure 6.54. ^{13}C NMR of compound **2.29** in CDCl_3 at 125 MHz.

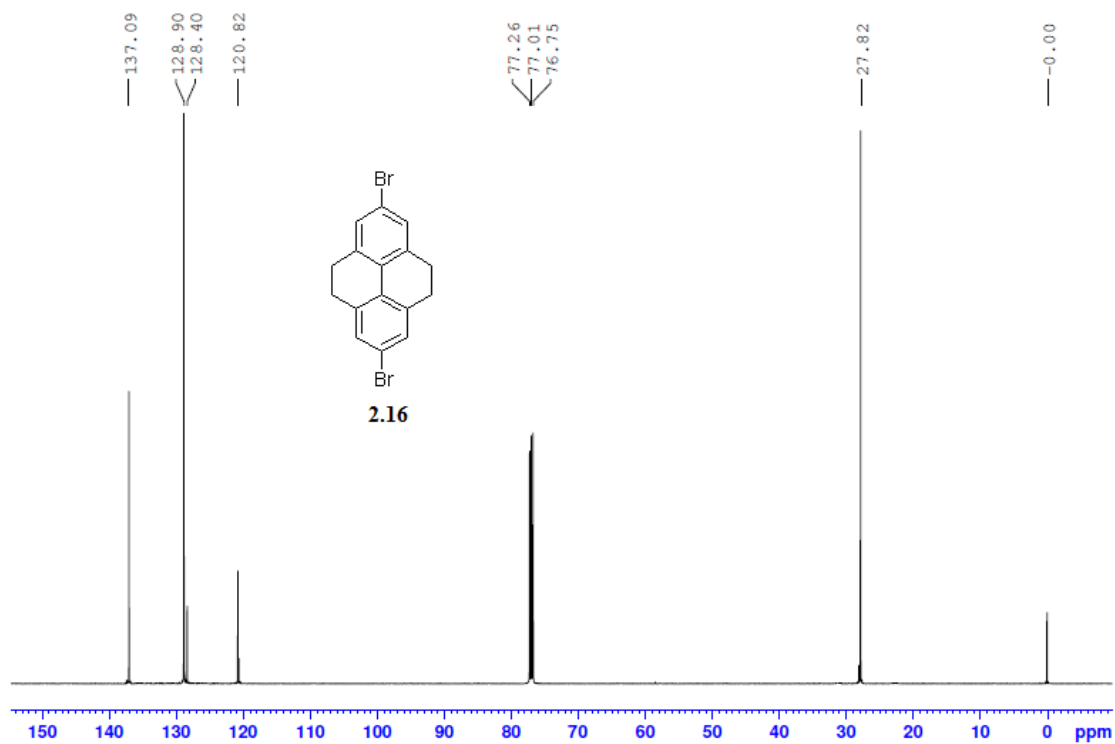


Figure 6.55. ^{13}C NMR of compound **2.16** in CDCl_3 at 125 MHz.

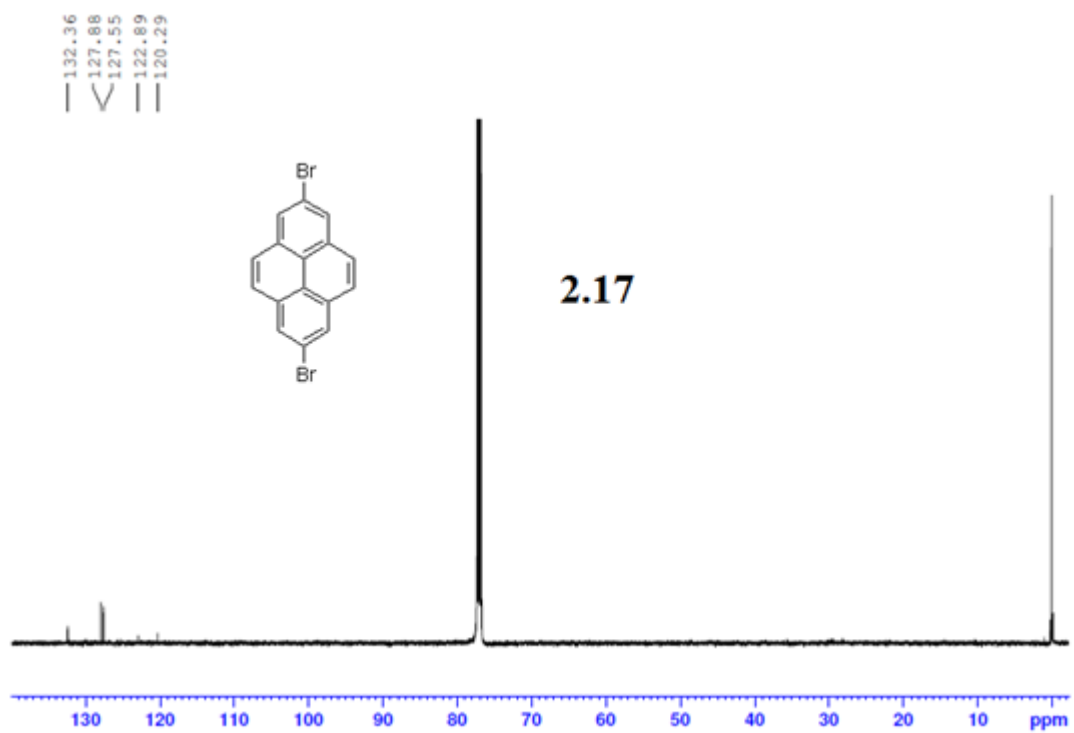


Figure 6.56. ^{13}C NMR of compound **2.17** in CDCl_3 at 125 MHz.

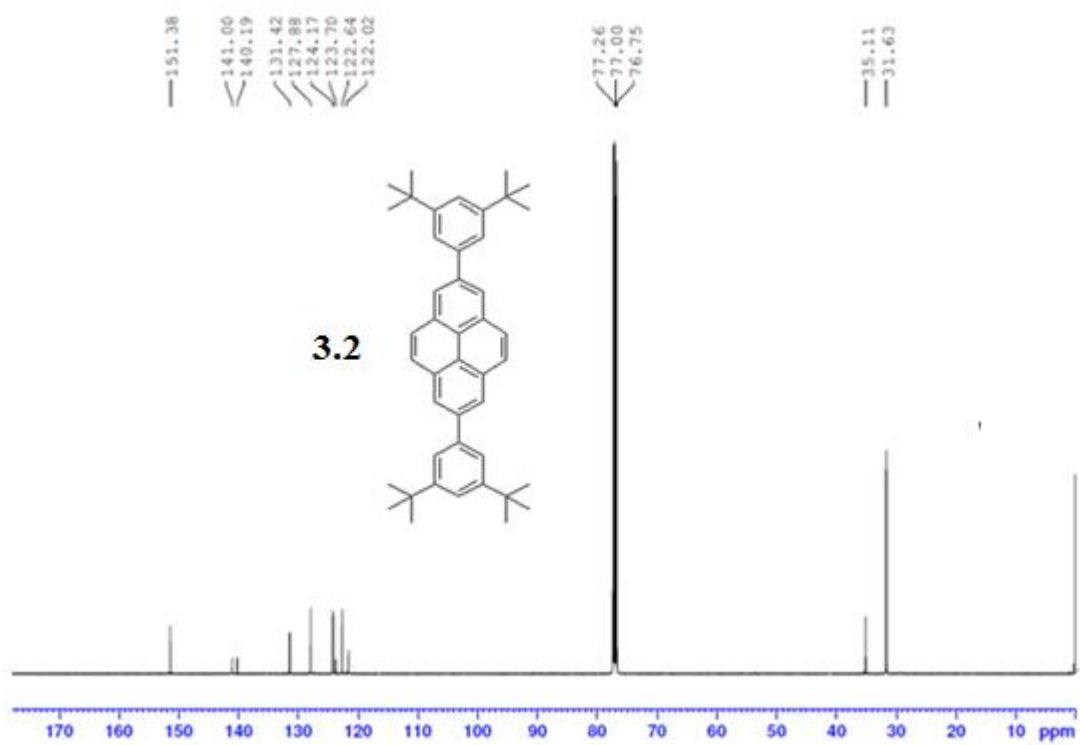


Figure 6.57. ^{13}C NMR of compound **3.2** in CDCl_3 at 125 MHz.

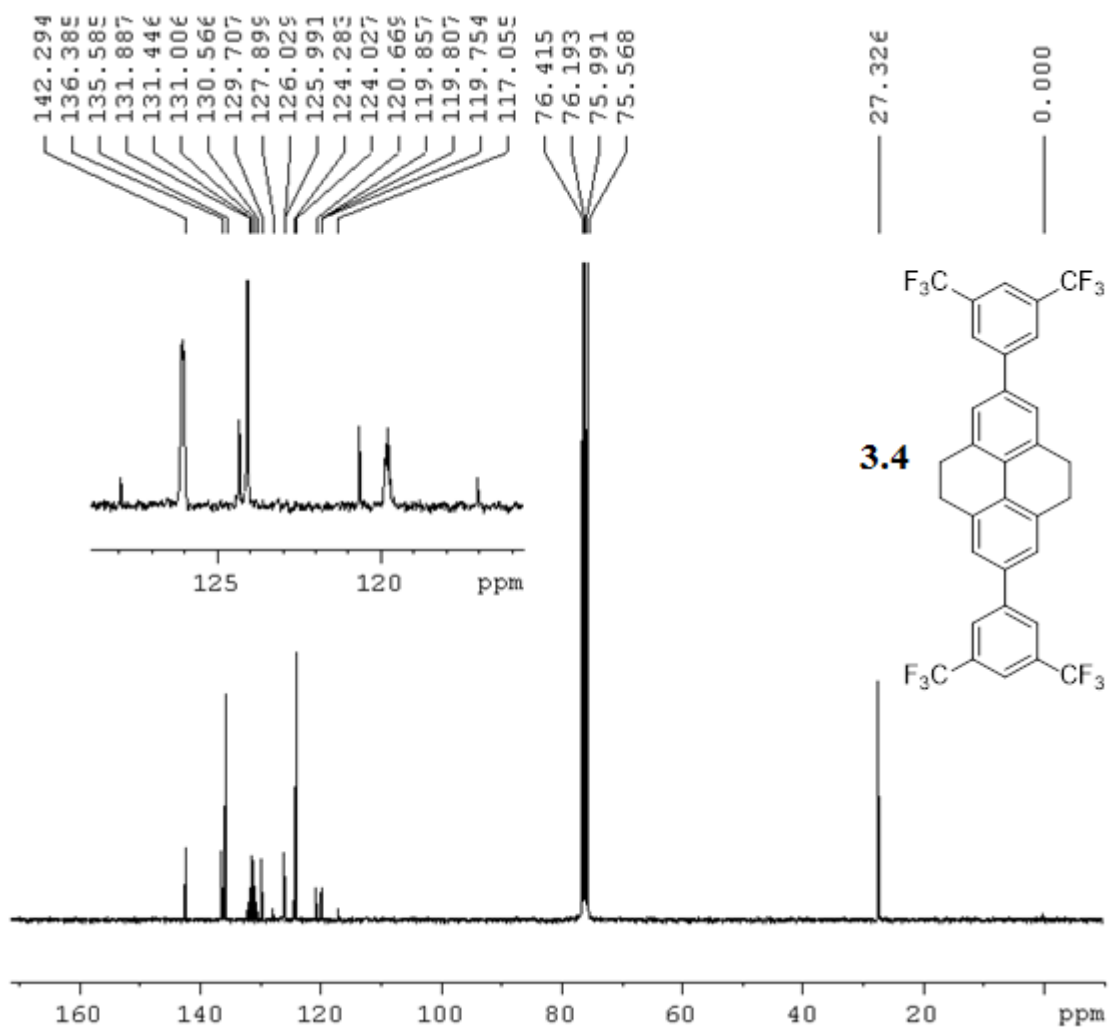


Figure 6.58. ^{13}C NMR of compound **3.4** in CDCl_3 at 75 MHz.

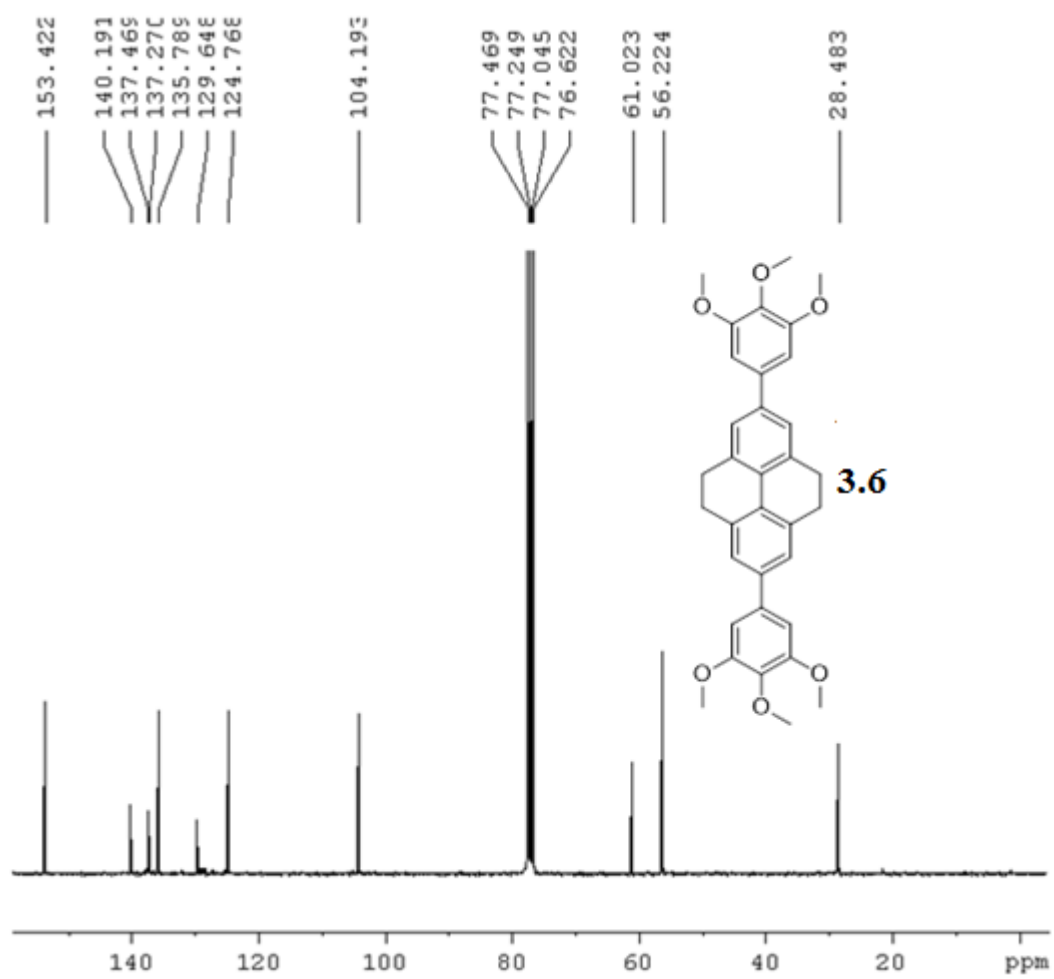


Figure 6.59. ^{13}C NMR of compound **3.6** in CDCl_3 at 75 MHz.

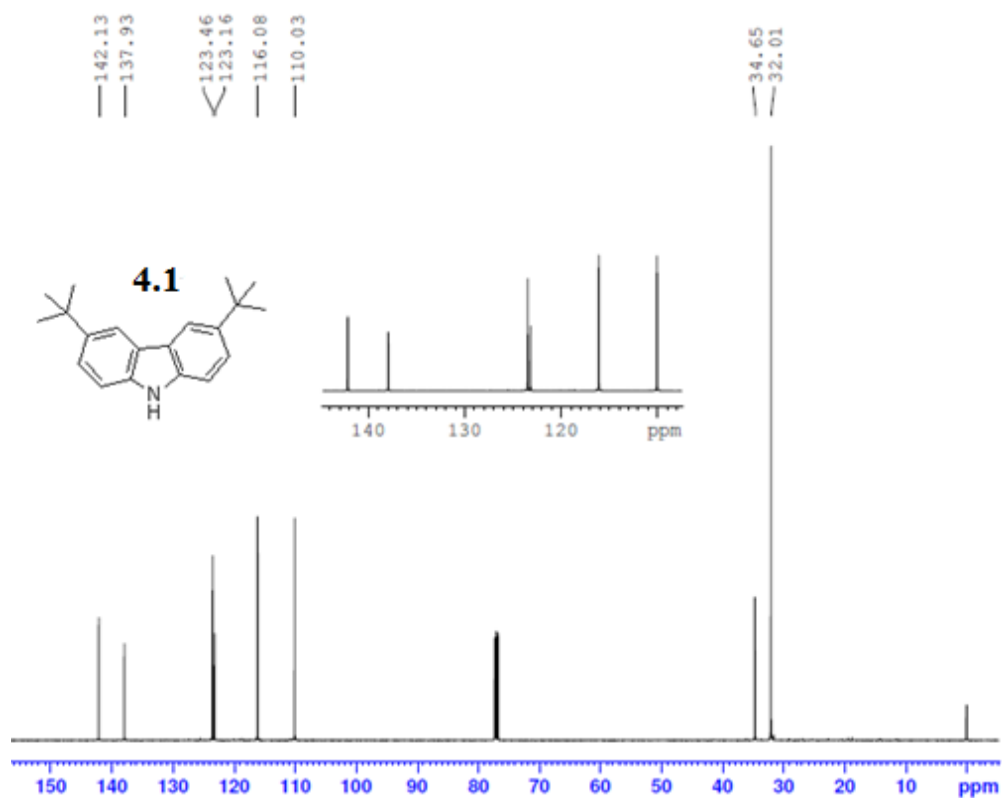


Figure 6.60. ¹³C NMR of compound **4.1** in CDCl₃ at 125 MHz.

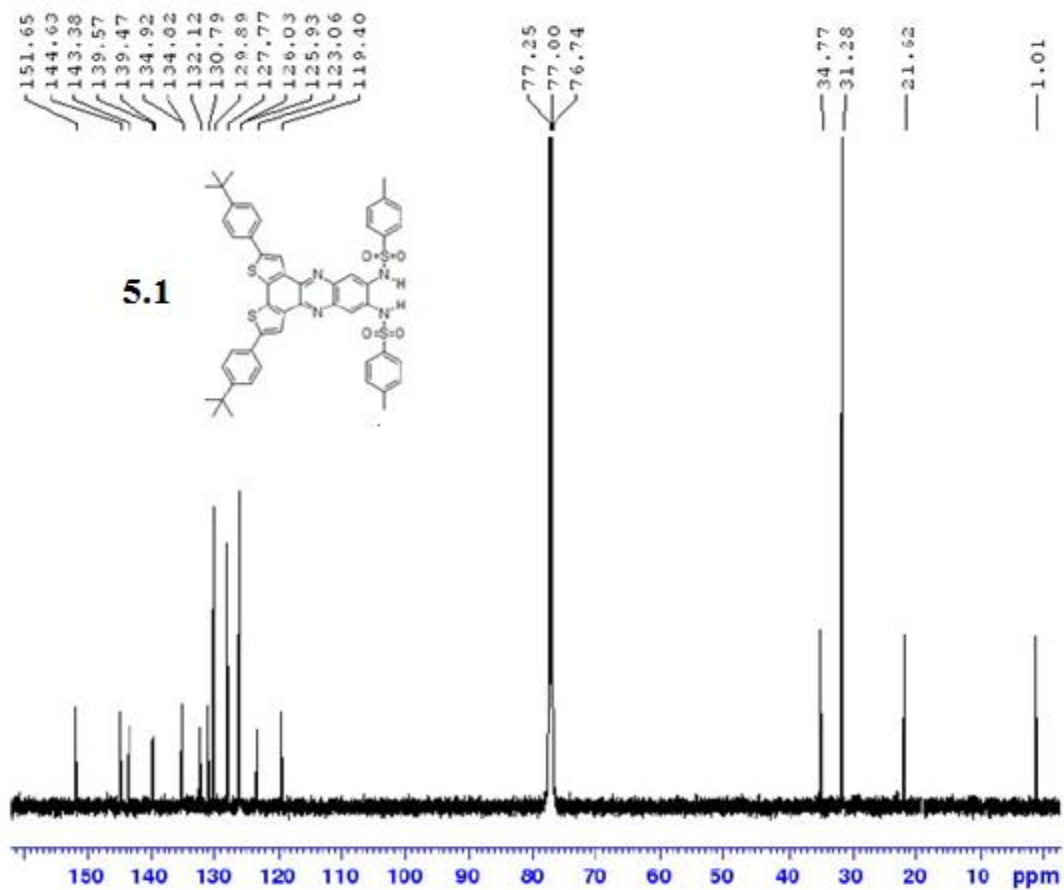


Figure 6.61. ¹³C NMR of compound **5.1** in CDCl₃ at 125 MHz.

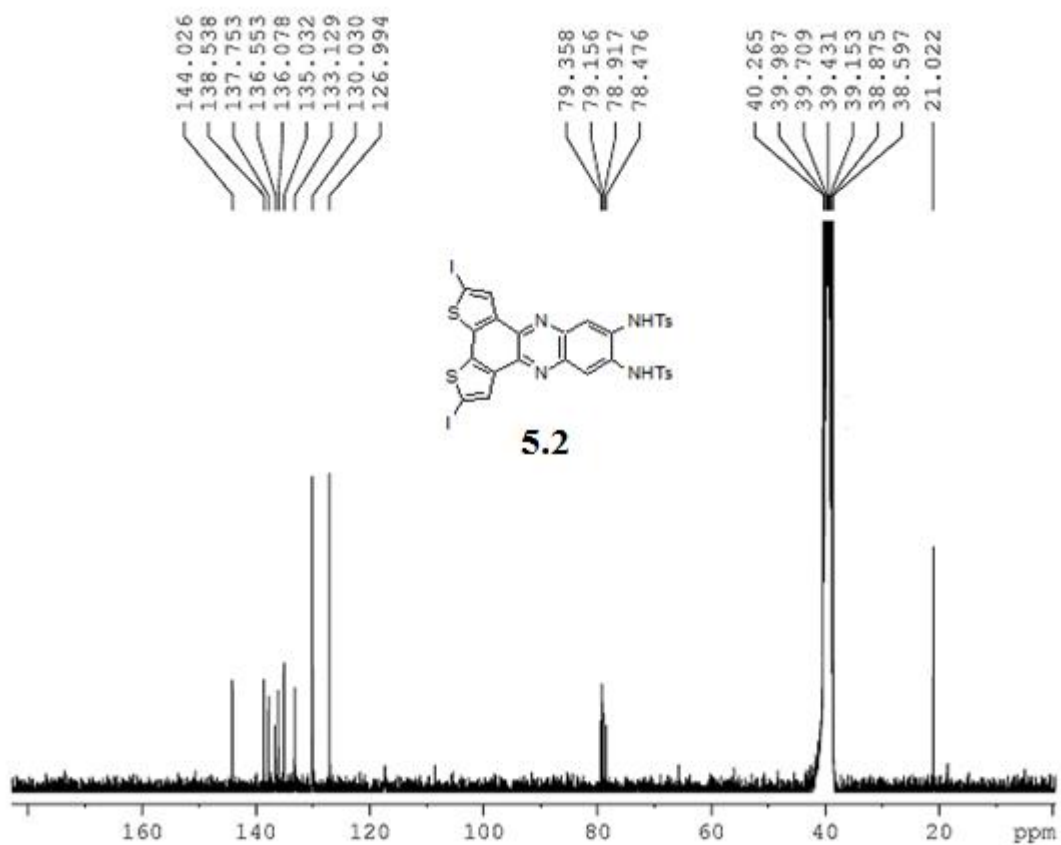


Figure 6.62. ^{13}C NMR of compound **5.2** in DMSO-d_6 at 75 MHz.

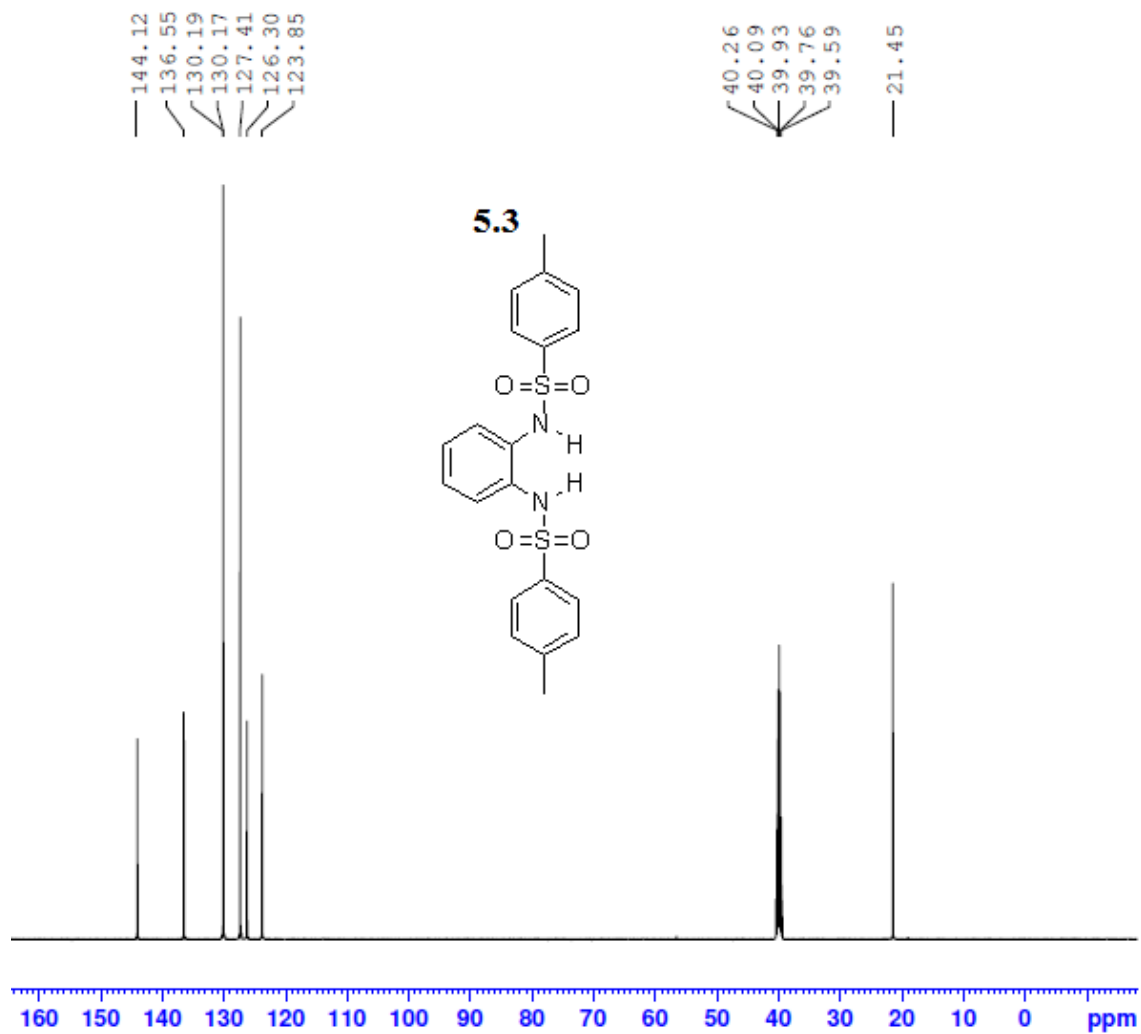


Figure 6.63. ^{13}C NMR of compound **5.3** in DMSO-d_6 at 125 MHz.

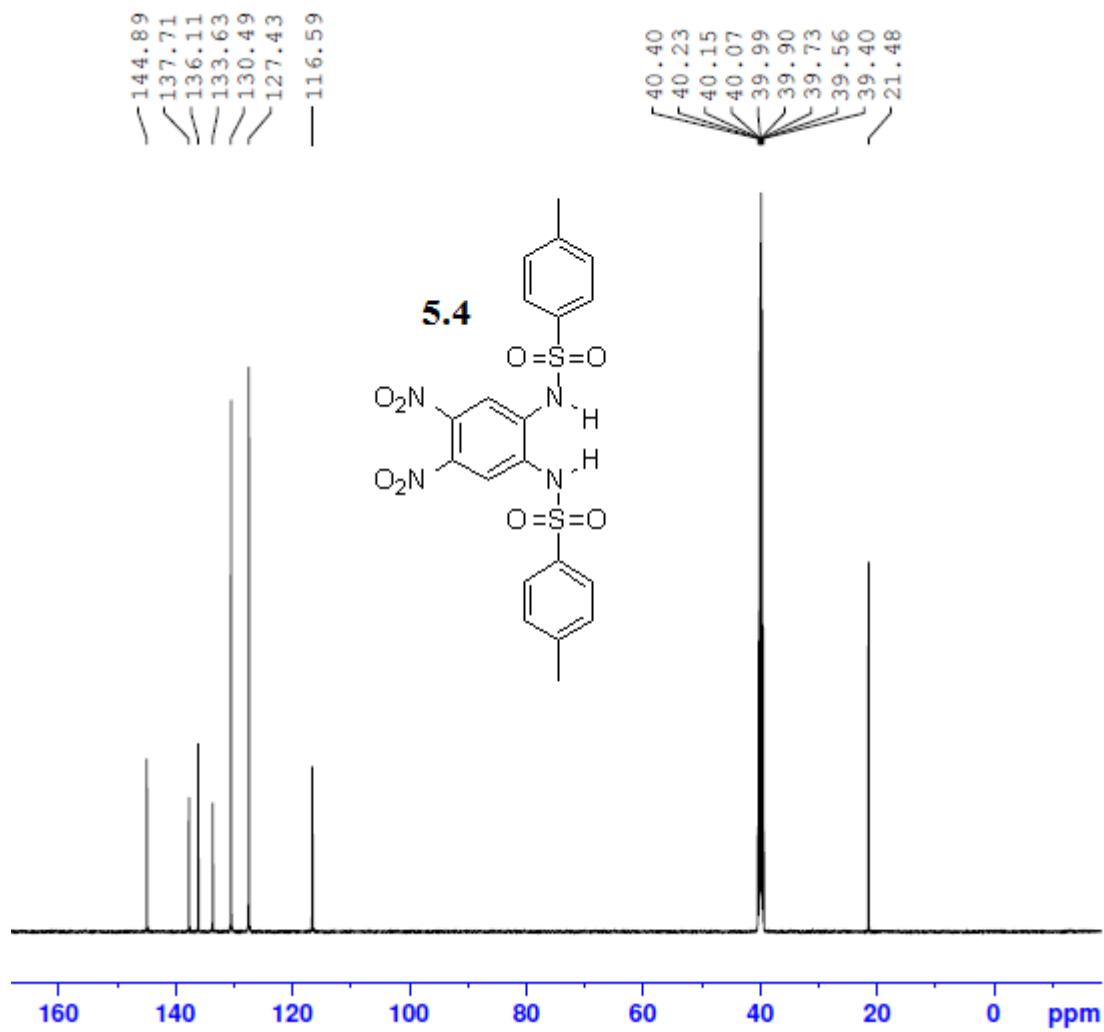


Figure 6.64. ^{13}C NMR of compound **5.4** in DMSO- d_6 at 125 MHz.

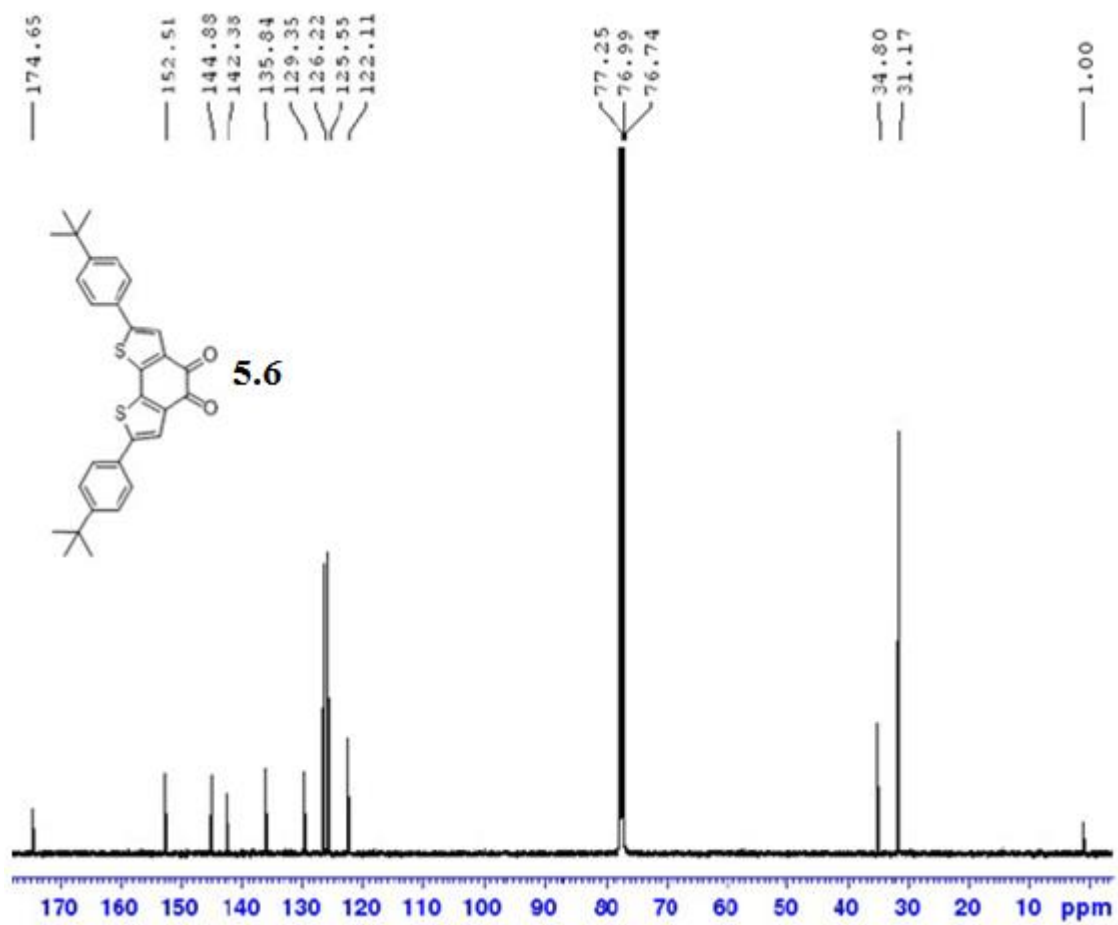


Figure 6.65. ^{13}C NMR of compound **5.6** in CDCl_3 at 125 MHz.

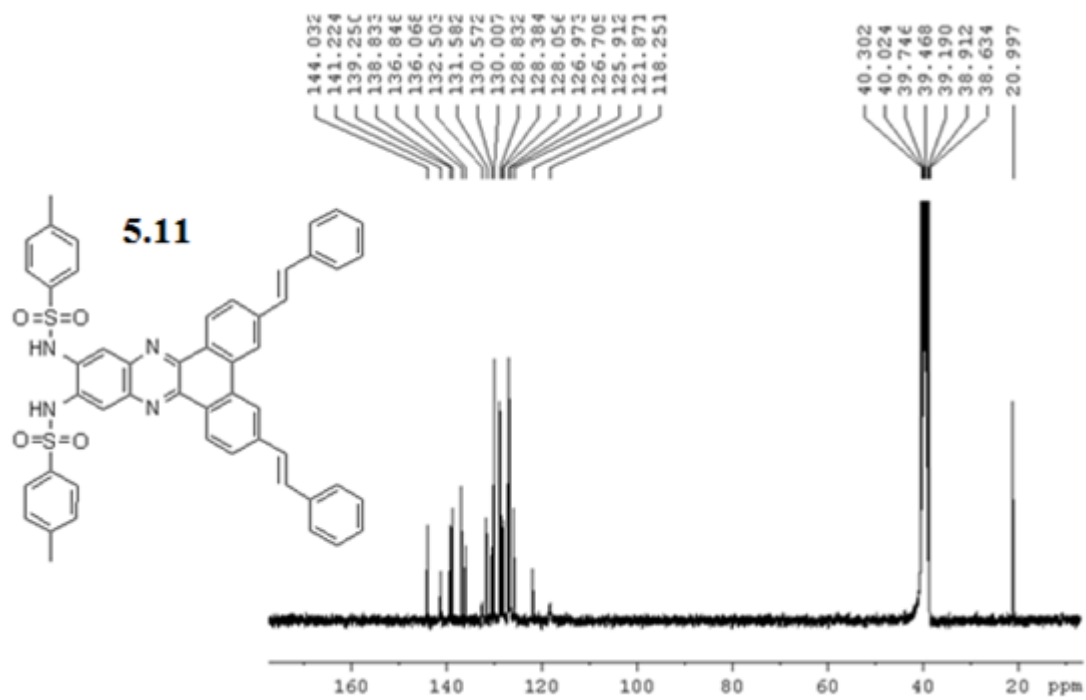


Figure 6.66. ^{13}C NMR of compound **5.11** in DMSO-d_6 at 75 MHz.

REFERENCES

- (1) Kelly, S. M. *Flat panel displays advanced organic materials : Advanced organic materials*; The Royal Society of Chemistry, **2000**.
- (2) Zhong, M.; Shi, C.; Gao, X.; Wu, X.; Chen, F.; Zhang, S.; Zhang, X.; Olsen, J. W. *Chin. Sci. Bull.* **2014**, *59*, 335.
- (3) Kamtekar, K. T.; Monkman, A. P.; Bryce, M. R. *Adv. Mater.* **2010**, *22*, 572.
- (4) Johnson, J. *Chem. Eng. News* **2007**, *85*, 49.
- (5) *Anon Elec. Rev.* **1921**, *79*, 361;1 illus.
- (6) Raju, R. D. *Int. J. Earth Sci. Eng.* **2012**, *5*, 1472.
- (7) Chen, C. H.; Shi, J.; Tang, C. W. *Macromol. Symp.* **1997**, *125*, 1.
- (8) Wilson, J. S.; Dhoot, A. S.; Seeley, A. J. A. B.; Khan, M. S.; Kohler, A.; Friend, R. H. *Nature* **2001**, *413*, 828.
- (9) Widder, E. A.; Falls, B. *IEEE J. Sel. Top. Quantum Electron.* **2014**, *20*, 7100710/1.
- (10) Chandra, B. P.; Chandra, V. K.; Jha, P. *Solid State Phenom.* **2015**, *222*, 1.
- (11) Wei, Y.; Wu, Z.; Jia, Y.; Liu, Y. *J. Alloys Compd.* **2015**, *646*, 86.
- (12) Nakajima, R.; Hayashi, Y.; Choi, P.-K. *Jpn. J. Appl. Phys.* **2015**, *54*, 1.
- (13) Leelachao, S.; Muraishi, S.; Sannomiya, T.; Shi, J.; Nakamura, Y. *J. Lumin.* **2016**, *170*, 24.
- (14) Pope, M.; Kallmann, H. P.; Magnante, P. *J. Chem. Phys.* **1963**, *38*, 2042.
- (15) Lakowicz, J. R. *Principles of fluorescence spectroscopy*; Springer: New York, **2006**.
- (16) D'Andrade, B. W.; Forrest, S. R. *Adv. Mater.* **2004**, *16*, 1585.
- (17) Schubert, E. F. *Light-Emitting Diodes*; **2006**.
- (18) Figueira-Duarte, T. M.; Müllen, K. *Chem. Rev.* **2011**, *111*, 7260.
- (19) De Halleux, V.; Calbert, J.-P.; Brocorens, P.; Cornil, J.; Declercq, J.-P.; Bredas, J.-L.; Geerts, Y. *Adv. Funct. Mater.* **2004**, *14*, 649.

- (20) Wu, C.; Wang, C.; Yan, L.; Yang, C. J. *J. Biomed. Nanotechnol.* **2009**, *5*, 495.
- (21) Sotoyama, W.; Sato, H.; Kinoshita, M.; Takahashi, T.; Matsuura, A.; Kodama, J.; Sawatari, N.; Inoue, H. *Dig. Tech. Pap. - Soc. Inf. Disp. Int. Symp.* **2003**, *34*, 1294.
- (22) Tang, C.; Liu, F.; Xia, Y.-J.; Xie, L.-H.; Wei, A.; Li, S.-B.; Fan, Q.-L.; Huang, W. *J. Mater. Chem.* **2006**, *16*, 4074.
- (23) Anant, P.; Lucas, N. T.; Ball, J. M.; Anthopoulos, T. D.; Jacob, J. *Synth. Met.* **2010**, *160*, 1987.
- (24) El-Ballouli, A. a. O.; Khnayzer, R. S.; Khalife, J. C.; Fonari, A.; Hallal, K. M.; Timofeeva, T. V.; Patra, D.; Castellano, F. N.; Wex, B.; Kaafarani, B. R. *J. Photochem. Photobiol., A* **2013**, *272*, 49.
- (25) Gwon, S.-Y.; Rao, B. A.; Kim, H.-S.; Son, Y.-A.; Kim, S.-H. *Spectrochim. Acta, Part A* **2015**, *144*, 226.
- (26) Yeung, M. C.-L.; Yam, V. W.-W. *Chem. Soc. Rev.* **2015**, *44*, 4192.
- (27) Lee, K.-S.; Kim, H.-J.; Kim, G.-H.; Shin, I.; Hong, J.-I. *Org. Lett.* **2008**, *10*, 49.
- (28) Beyazkılıç, P.; Yildirim, A.; Bayındır, M. *ACS Appl Mater Interfaces* **2014**, *6*, 4997.
- (29) Amendola, V.; Bonizzoni, M.; Esteban-Gomez, D.; Fabbrizzi, L.; Licchelli, M.; Sancenon, F.; Taglietti, A. *Coord. Chem. Rev.* **2006**, *250*, 1451.
- (30) Ma, B.; Xu, M.; Zeng, F.; Huang, L.; Wu, S. *Nanotechnology* **2011**, *22*, 065501/1.
- (31) Gunnlaugsson, T.; Kruger, P. E.; Lee, T. C.; Parkesh, R.; Pfeffer, F. M.; Hussey, G. M. *Tetrahedron Lett.* **2003**, *44*, 6575.
- (32) De Silva, A. P.; Gunaratne, H. Q. N.; Gunnlaugsson, T.; Huxley, A. J. M.; McCoy, C. P.; Rademacher, J. T.; Rice, T. E. *Chem. Rev.* **1997**, *97*, 1515.
- (33) Fabbrizzi, L.; Licchelli, M.; Rabaioli, G.; Taglietti, A. *Coord. Chem. Rev.* **2000**, *205*, 85.
- (34) Davis, F.; Collyer, S. D.; Higson, S. P. J. *Top. Curr. Chem.* **2005**, *255*, 97.
- (35) Schmidtchen, F. P.; Berger, M. *Chem. Rev.* **1997**, *97*, 1609.
- (36) Raad, F. S.; El-Ballouli, A. a. O.; Moustafa, R. M.; Al-Sayah, M. H.; Kaafarani, B. R. *Tetrahedron* **2010**, *66*, 2944.
- (37) Black, C. B.; Andrioletti, B.; Try, A. C.; Ruiperez, C.; Sessler, J. L. *J. Am. Chem. Soc.* **1999**, *121*, 10438.

- (38) Katsu, T.; Furuno, K.; Yamashita, S.; Kawasaki, H.; Gomita, Y.; Ohtsuka, Y.; Ohtahara, S. *Clin. Chim. Acta* **1995**, *234*, 157.
- (39) Liu, D.; Lin, X.; Yu, F.; Zhang, M.; Chen, H.; Bao, W.; Wang, X. *Biol. Trace Elem. Res.* **2015**, *168*, 447.
- (40) Rathikrishnan, K. R.; Indirapriyadharshini, V. K.; Ramakrishna, S.; Murugan, R. *Tetrahedron* **2011**, *67*, 4025.
- (41) Reiners, C.; Schneider, R. *Radiat. Environ. Biophys.* **2013**, *52*, 189.
- (42) Chandra, S.; Raizada, S.; Sharma, S. *J. Chem. Pharm. Res.* **2012**, *4*, 3769.
- (43) Sessler, J. L.; Davis, J. M.; Kral, V.; Kimbrough, T.; Lynch, V. *Org. Biomol. Chem.* **2003**, *1*, 4113.
- (44) Amendola, V.; Fabbrizzi, L.; Mosca, L.; Schmidtchen, F.-P. *Chem. - Eur. J.* **2011**, *17*, 5972.
- (45) Goswami, S.; Chakrabarty, R. *Tetrahedron Lett.* **2009**, *50*, 5994.
- (46) Morozumi, M.; Hossain, R. Z.; Yamakawa, K.-i.; Hokama, S.; Nishijima, S.; Oshiro, Y.; Uchida, A.; Sugaya, K.; Ogawa, Y. *Urol. Res.* **2006**, *34*, 168.
- (47) Lin, Y.-C.; Chen, C.-T. *Org. Lett.* **2009**, *11*, 4858.
- (48) El-Assaad, T. H.; Auer, M.; Castaneda, R.; Hallal, K. M.; Jradi, F. M.; Mosca, L.; Khnayzer, R. S.; Patra, D.; Timofeeva, T. V.; Bredas, J.-L.; List-Kratochvil, E. J. W.; Wex, B.; Kaafarani, B. R. *J. Mater. Chem. C* **2015**, DOI: 10.1039/c5tc02849c.
- (49) El-Assaad, T. H.; Shiring, S. B.; Getmanenko, Y. A.; Hallal, K. M.; Bredas, J.-L.; Marder, S. R.; Al-Sayah, M. H.; Kaafarani, B. R. *RSC Adv.* **2015**, *5*, 43303.
- (50) Kalinowski, J. *Mater. Sci.* **1981**, *7*, 43.
- (51) Kwon, S. M.; Lee, K. H.; Lee, S. J.; Kim, Y. K.; Yoon, S. S. *Mol. Cryst. Liq. Cryst.* **2013**, *584*, 103.
- (52) Turker, L.; Tapan, A.; Gumus, S. *Polycyclic Aromat. Compd.* **2009**, *29*, 139.
- (53) Liu, F.; Lai, W.-Y.; Tang, C.; Wu, H.-B.; Chen, Q.-Q.; Peng, B.; Wei, W.; Huang, W.; Cao, Y. *Macromol. Rapid Commun.* **2008**, *29*, 659.
- (54) Zhang, G.; Baumgarten, M.; Auer, M.; Trattnig, R.; List-Kratochvil, E. J. W.; Müllen, K. *Macromol. Rapid Commun.* **2014**, *35*, 1931.
- (55) Sasson, R.; Braitbart, O.; Weinreb, A. *J. Lumin.* **1988**, *39*, 223.

- (56) Yao, C.; Yu, Y.; Yang, X.; Zhang, H.; Huang, Z.; Xu, X.; Zhou, G.; Yue, L.; Wu, Z. *J. Mater. Chem. C* **2015**, *3*, 5783.
- (57) Wisniak, J. *Educ. Quim.* **2009**, *20*, 166.
- (58) Leroy, S.; Soujanya, T.; Sohna, J. E. S.; Fages, F. *Int. J. Photoenergy* **2001**, *3*, 49.
- (59) Karpovich, D. S.; Blanchard, G. J. *J. Phys. Chem.* **1995**, *99*, 3951.
- (60) Dong, D. C.; Winnik, M. A. *Photochem. Photobiol.* **1982**, *35*, 17.
- (61) Delouis, J. F.; Delaire, J. A.; Ivanoff, N. *Chem. Phys. Lett.* **1979**, *61*, 343.
- (62) Bohne, C.; Abuin, E. B.; Scaiano, J. C. *J. Am. Chem. Soc.* **1990**, *112*, 4226.
- (63) Herndon, W. C. *Int. J. Quantum Chem., Quantum Biol. Symp.* **1974**, *1*, 123.
- (64) Moss, G. P. *Pure Appl. Chem.* **1998**, *70*, 143.
- (65) Cyvin, S. J. *J. Mol. Struct.* **1983**, *100*, 75.
- (66) Crawford, A. G.; Dwyer, A. D.; Liu, Z.; Steffen, A.; Beeby, A.; Palsson, L.-O.; Tozer, D. J.; Marder, T. B. *J. Am. Chem. Soc.* **2011**, *133*, 13349.
- (67) Ham, N. S.; Ruedenberg, K. *J. Chem. Phys.* **1956**, *25*, 13.
- (68) Yoshinaga, T.; Hiratsuka, H.; Tanizaki, Y. *Bull. Chem. Soc. Jpn.* **1977**, *50*, 3096.
- (69) Steehler, J. K. *J. Chem. Educ.* **2010**, *87*, 1298.
- (70) Cornil, J.; Beljonne, D.; Calbert, J.-P.; Bredas, J.-L. *Adv. Mater.* **2001**, *13*, 1053.
- (71) Bernhardt, S.; Kastler, M.; Enkelmann, V.; Baumgarten, M.; Müllen, K. *Chem. - Eur. J.* **2006**, *12*, 6117.
- (72) Crawford, A. G.; Liu, Z.; Mkhaliid, I. A. I.; Thibault, M.-H.; Schwarz, N.; Alcaraz, G.; Steffen, A.; Collings, J. C.; Batsanov, A. S.; Howard, J. A. K.; Marder, T. B. *Chem. - Eur. J.* **2012**, *18*, 5022.
- (73) Miura, Y.; Yamano, E.; Tanaka, A.; Yamauchi, J. *J. Org. Chem.* **1994**, *59*, 3294.
- (74) Feng, X.; Hu, J.-Y.; Iwanaga, F.; Seto, N.; Redshaw, C.; Elsegood, M. R. J.; Yamato, T. *Org. Lett.* **2013**, *15*, 1318.
- (75) Hu, J.-Y.; Ni, X.-L.; Feng, X.; Era, M.; Elsegood, M. R. J.; Teat, S. J.; Yamato, T. *Org. Biomol. Chem.* **2012**, *10*, 2255.

- (76) Yamato, T.; Fujimoto, M.; Miyazawa, A.; Matsuo, K. *J. Chem. Soc., Perkin Trans. 1* **1997**, 1201.
- (77) Connor, D. M.; Allen, S. D.; Collard, D. M.; Liotta, C. L.; Schiraldi, D. A. *J. Org. Chem.* **1999**, *64*, 6888.
- (78) Rausch, D.; Lambert, C. *Org. Lett.* **2006**, *8*, 5037.
- (79) Lee, H.; Harvey, R. G. *J. Org. Chem.* **1986**, *51*, 2847.
- (80) Mkhaliid, I. A. I.; Barnard, J. H.; Marder, T. B.; Murphy, J. M.; Hartwig, J. F. *Chem. Rev.* **2010**, *110*, 890.
- (81) Niamnont, N.; Kimpitak, N.; Wongravee, K.; Rashatasakhon, P.; Baldrige, K. K.; Siegel, J. S.; Sukwattanasinitt, M. *Chem. Commun.* **2013**, *49*, 780.
- (82) He, C.; Zhu, D.; He, Q.; Shi, L.; Fu, Y.; Wen, D.; Cao, H.; Cheng, J. *Chem. Commun.* **2012**, *48*, 5739.
- (83) Figueira-Duarte, T. M.; Simon, S. C.; Wagner, M.; Druzhinin, S. I.; Zachariasse, K. A.; Müllen, K. *Angew. Chem., Int. Ed.* **2008**, *47*, 10175.
- (84) Yamato, T.; Miyazawa, A.; Tashiro, M. *Chem. Ber.* **1993**, *126*, 2505.
- (85) Cherney, A. H.; Kadunce, N. T.; Reisman, S. E. *Chem. Rev.* **2015**, *115*, 9587.
- (86) Wagner, F. F.; Comins, D. L. *J. Org. Chem.* **2006**, *71*, 8673.
- (87) Machuy, M. M.; Wuertele, C.; Schreiner, P. R. *Synthesis* **2012**, *44*, 1405.
- (88) Callam, C. S.; Lowary, T. L. *J. Chem. Educ.* **2001**, *78*, 947.
- (89) Coulson, D. R. *Inorg. Synth.* **1990**, *28*, 107.
- (90) Mason, S. F. *J. Chem. Soc.* **1959**, 1263.
- (91) Oh, M. H. J.; Salvador, M. R.; Wong, C. Y.; Scholes, G. D. *ChemPhysChem* **2011**, *12*, 88.
- (92) Dimroth, K.; Reichardt, C.; Siepmann, T.; Bohlmann, F. *Ann.* **1963**, *661*, 1.
- (93) Iwunze, M. O. *Phys. Chem. Liq.* **2005**, *43*, 195.
- (94) Reichardt, C.; Schaefer, G. *Liebigs Ann.* **1995**, 1579.
- (95) Kamlet, M. J.; Abboud, J. L.; Taft, R. W. *J. Am. Chem. Soc.* **1977**, *99*, 6027.
- (96) Laurence, C.; Nicolet, P.; Dalati, M. T.; Abboud, J.-L. M.; Notario, R. *J. Phys. Chem.* **1994**, *98*, 5807.

- (97) Jou, J.-H.; Kumar, S.; Agrawal, A.; Li, T.-H.; Sahoo, S. *J. Mater. Chem. C* **2015**, *3*, 2974.
- (98) Periasamy, A. *Methods in cellular imaging*; Springer, **2013**.
- (99) Berlman, I. *Press, New York & London* **1965**.
- (100) Nijegorodov, N.; Zvolinsky, V.; Luhanga, P. V. C. *J. Photochem. Photobiol., A* **2008**, *196*, 219.
- (101) Shyamala, T.; Sankararaman, S.; Mishra, A. K. *Chem. Phys.* **2006**, *330*, 469.
- (102) Niko, Y.; Kawauchi, S.; Otsu, S.; Tokumaru, K.; Konishi, G.-i. *J. Org. Chem.* **2013**, *78*, 3196.
- (103) Moorthy, J. N.; Natarajan, P.; Venkatakrisnan, P.; Huang, D.-F.; Chow, T. J. *Org. Lett.* **2007**, *9*, 5215.
- (104) Qiao, Y.; Zhang, J.; Xu, W.; Zhu, D. *Tetrahedron* **2011**, *67*, 3395.
- (105) Henssler, J. T.; Zhang, X.; Matzger, A. J. *J. Org. Chem.* **2009**, *74*, 9112.
- (106) Oyamada, T.; Akiyama, S.; Yahiro, M.; Saigou, M.; Shiro, M.; Sasabe, H.; Adachi, C. *Chem. Phys. Lett.* **2006**, *421*, 295.
- (107) Pakpahan, E. N.; Isa, M. H.; Kutty, S. R. M.; Malakahmad, A. **2009**.
- (108) Johns, I. B.; McElhill, E. A.; Smith, J. O. *J. Chem. Eng. Data* **1962**, *7*, 277.
- (109) Yoon, J.; Lesser, A. J.; McCarthy, T. J. *PMSE Prepr.* **2007**, *97*, 742.
- (110) Zhang, H.; Wang, Y.; Shao, K.; Liu, Y.; Chen, S.; Qiu, W.; Sun, X.; Qi, T.; Ma, Y.; Yu, G.; Su, Z.; Zhu, D. *Chem. Commun.* **2006**, 755.
- (111) Bernanose, A.; Comte, M.; Vouaux, P. *J. Chim. Phys. Phys.-Chim. Biol.* **1953**, *50*, 64.
- (112) Meerheim, R.; Luessem, B.; Leo, K. *Proc. IEEE* **2009**, *97*, 1606.
- (113) Sun, C.-Y.; Wang, X.-L.; Zhang, X.; Qin, C.; Li, P.; Su, Z.-M.; Zhu, D.-X.; Shan, G.-G.; Shao, K.-Z.; Wu, H.; Li, J. *Nat Commun* **2013**, *4*, 2717.
- (114) Kulkarni, A. P.; Tonzola, C. J.; Babel, A.; Jenekhe, S. A. *Chem. Mater.* **2004**, *16*, 4556.
- (115) Hughes, G.; Bryce, M. R. *J. Mater. Chem.* **2005**, *15*, 94.
- (116) Tang, C. W.; VanSlyke, S. A. *Appl. Phys. Lett.* **1987**, *51*, 913.
- (117) Michaelson, H. B. *J. Appl. Phys.* **1977**, *48*, 4729.

- (118) Zhang, X.; Jenekhe, S. A. *Macromolecules* **2000**, *33*, 2069.
- (119) Akasaki, I. *Ann. Phys.* **2015**, *527*, 311.
- (120) Girtan, M.; Rusu, M. *Sol. Energy Mater. Sol. Cells* **2010**, *94*, 446.
- (121) Roberts, J. D.; Weigert, F. J. *J. Amer. Chem. Soc.* **1971**, *93*, 2361.
- (122) Reilly, C. A. *Analytical Chemistry* **1958**, *30*, 839.
- (123) Solomatin, G. G.; Filippov, M. P.; Shchigalevskii, V. A.; Gerasimenko, Y. E. *Zh. Prikl. Khim.* **1985**, *58*, 621.
- (124) SAINT, P. Inc., *Madison, WI, USA* **2001**.
- (125) Sheldrick, G. *University of Göttingen, Germany* **2003**.
- (126) Dolomanov, O. V.; Bourhis, L. J.; Gildea, R. J.; Howard, J. A. K.; Puschmann, H. *J. Appl. Crystallogr.* **2009**, *42*, 339.
- (127) Sheldrick, G. *Göttingen, Germany* **1997**.
- (128) Hwang, F.-M.; Chen, H.-Y.; Chen, P.-S.; Liu, C.-S.; Chi, Y.; Shu, C.-F.; Wu, F.-I.; Chou, P.-T.; Peng, S.-M.; Lee, G.-H. *Inorg. Chem.* **2005**, *44*, 1344.
- (129) Yang, C.-H.; Chen, C.-H.; Sun, I. W. *Polyhedron* **2006**, *25*, 2407.
- (130) Tanaka, K.; Yamane, H.; Yoshii, R.; Chujo, Y. *Bioorg. Med. Chem.* **2013**, *21*, 2715.
- (131) Chemla, D. S. *Nonlinear optical properties of organic molecules and crystals*; Elsevier, **2012**; Vol. 1.
- (132) Panigrahi, M.; Dash, S.; Patel, S.; Behera, P. K.; Mishra, B. K. *Spectrochim. Acta, Part A* **2007**, *68A*, 757.
- (133) Turro, N. J. *Modern molecular photochemistry*; University Science Books, **1991**.
- (134) Wang, Y.; Herron, N.; Grushin, V. V.; LeCloux, D.; Petrov, V. *Appl. Phys. Lett.* **2001**, *79*, 449.
- (135) Wang, J.; Xu, X.; Tian, Y.; Yao, C.; Li, L. *J. Mater. Chem. C* **2014**, *2*, 5036.
- (136) Connor, D. M.; Allen, S. D.; Collard, D. M.; Liotta, C. L.; Schiraldi, D. A. *J. Org. Chem.* **1999**, *64*, 6888.
- (137) Kaafarani, B. R.; El-Ballouli, A. a. O.; Trattnig, R.; Fonari, A.; Sax, S.; Wex, B.; Risko, C.; Khnayzer, R. S.; Barlow, S.; Patra, D.; Timofeeva, T. V.; List, E. J. W.; Bredas, J.-L.; Marder, S. R. *J. Mater. Chem. C* **2013**, *1*, 1638.

- (138) Jeon, Y. P.; Kim, K. S.; Lee, K. K.; Moon, I. K.; Choo, D. C.; Lee, J. Y.; Kim, T. W. *J. Mater. Chem. C* **2015**, *3*, 6192.
- (139) Uoyama, H.; Goushi, K.; Shizu, K.; Nomura, H.; Adachi, C. *Nature* **2012**, *492*, 234.
- (140) Ahmed, N.; Geronimo, I.; Hwang, I.-C.; Singh, N. J.; Kim, K. S. *Chem. - Eur. J.* **2011**, *17*, 8542.
- (141) Rettig, W.; Zander, M. *Chem. Phys. Lett.* **1982**, *87*, 229.
- (142) McClenaghan, N. D.; Passalacqua, R.; Loiseau, F.; Campagna, S.; Verheyde, B.; Hameurlaine, A.; Dehaen, W. *J. Am. Chem. Soc.* **2003**, *125*, 5356.
- (143) Zhao, Z.; Xing, Y.; Wang, Z.; Lu, P. *Org. Lett.* **2007**, *9*, 547.
- (144) Zaion, S. M.; Hashim, R.; Taylor, A. G.; Phillips, D. *J. Mol. Struct.: THEOCHEM* **1997**, *401*, 287.
- (145) Ho, M.-H.; Balaganesan, B.; Chu, T.-Y.; Chen, T.-M.; Chen, C. H. *Thin Solid Films* **2008**, *517*, 943.
- (146) Ambrose, J. F.; Carpenter, L. L.; Nelson, R. F. *J. Electrochem. Soc.* **1975**, *122*, 876.
- (147) Grabowski, Z. R.; Rotkiewicz, K.; Rettig, W. *Chem. Rev.* **2003**, *103*, 3899.
- (148) Galievsky, V. A.; Druzhinin, S. I.; Demeter, A.; Mayer, P.; Kovalenko, S. A.; Senyushkina, T. A.; Zachariasse, K. A. *J. Phys. Chem. A* **2010**, *114*, 12622.
- (149) Kowalczyk, T.; Lin, Z.; Van Voorhis, T. *J. Phys. Chem. A* **2010**, *114*, 10427.
- (150) Johnson, G. E. *J. Phys. Chem.* **1980**, *84*, 2940.
- (151) Neugebauer, F. A.; Fischer, H. *Chem. Ber.* **1972**, *105*, 2686.
- (152) Liu, Y.; Nishiura, M.; Wang, Y.; Hou, Z. *J. Am. Chem. Soc.* **2006**, *128*, 5592.
- (153) Bruckner, R. **2007**.
- (154) Böhmer, V.; Rathay, D.; Kämmerer, H. *Organic Preparations and Procedures International* **1978**, *10*, 113.
- (155) Seeboth, H. *Angewandte Chemie International Edition in English* **1967**, *6*, 307.
- (156) Ding, J.; Lu, J.; Cheng, Y.; Xie, Z.; Wang, L.; Jing, X.; Wang, F. *Adv. Funct. Mater.* **2008**, *18*, 2754.
- (157) El-Khouly, M. E.; Lee, S.-H.; Kay, K.-Y.; Fukuzumi, S. *New J. Chem.* **2013**, *37*, 3252.

- (158) Prachumrak, N.; Pansay, S.; Namuangruk, S.; Kaewin, T.; Jungsuttiwong, S.; Sudyoadsuk, T.; Promarak, V. *Eur. J. Org. Chem.* **2013**, 2013, 6619.
- (159) Morra, N. A.; Pagenkopf, B. L. *Org. Synth.* **2008**, 85, 53.
- (160) Ishow, E.; Camacho-Aguilera, R.; Guerin, J.; Brosseau, A.; Nakatani, K. *Adv. Funct. Mater.* **2009**, 19, 796.
- (161) Frant, M. S.; Ross, J. W., Jr. *Science* **1966**, 154, 1553.
- (162) Park, C. H.; Simmons, H. E. *J. Amer. Chem. Soc.* **1968**, 90, 2431.
- (163) Bowman-James, K. *Acc. Chem. Res.* **2005**, 38, 671.
- (164) Smith, P. J.; Reddington, M. V.; Wilcox, C. S. *Tetrahedron Lett.* **1992**, 33, 6085.
- (165) Zielinski, T.; Jurczak, J. *Tetrahedron* **2005**, 61, 4081.
- (166) Al-Sayah, M. H.; Branda, N. R. *Thermochim. Acta* **2010**, 503-504, 28.
- (167) Smith, P. J.; Wilcox, C. S. *J. Org. Chem.* **1990**, 55, 5675.
- (168) Amendola, V.; Esteban-Gomez, D.; Fabbrizzi, L.; Licchelli, M. *Acc. Chem. Res.* **2006**, 39, 343.
- (169) Qiao, Y.-H.; Lin, H.; Lin, H.-K. *Chin. J. Chem.* **2007**, 25, 683.
- (170) Padie, C.; Zeitler, K. *New J. Chem.* **2011**, 35, 994.
- (171) Dong, M.; Peng, Y.; Dong, Y.-M.; Tang, N.; Wang, Y.-W. *Org. Lett.* **2012**, 14, 130.
- (172) Jradi, F. M.; El-Ballouli, A. a. O.; Al-Sayah, M. H.; Kaafarani, B. R. *Supramol. Chem.* **2014**, 26, 15.
- (173) Jradi, F. M.; Fonari, A.; Timofeeva, T. V.; Al-Sayah, M. H.; Kaafarani, B. R.; American Chemical Society: **2009**, 65th Southwest Regional Meeting.
- (174) Jradi, F. M.; Al-Sayah, M. H.; Kaafarani, B. R. *Tetrahedron Lett.* **2008**, 49, 238.
- (175) El-Ballouli, A. a. O.; Zhang, Y.; Barlow, S.; Marder, S. R.; Al-Sayah, M. H.; Kaafarani, B. R. *Tetrahedron Lett.* **2012**, 53, 661.
- (176) Aboubakr, H.; Brisset, H.; Siri, O.; Raimundo, J.-M. *Anal. Chem.* **2013**, 85, 9968.
- (177) Satapathy, R.; Wu, Y.-H.; Lin, H.-C. *Chem. Commun.* **2012**, 48, 5668.

- (178) Getmanenko, Y. A.; Fonari, M.; Risko, C.; Sandhu, B.; Galan, E.; Zhu, L.; Tongwa, P.; Hwang, D. K.; Singh, S.; Wang, H.; Tiwari, S. P.; Loo, Y.-L.; Bredas, J.-L.; Kippelen, B.; Timofeeva, T.; Marder, S. R. *J. Mater. Chem. C* **2013**, *1*, 1467.
- (179) Ye, L.; Zhang, S.; Huo, L.; Zhang, M.; Hou, J. *Acc. Chem. Res.* **2014**, *47*, 1595.
- (180) Lin, T.-P.; Chen, C.-Y.; Wen, Y.-S.; Sun, S.-S. *Inorg. Chem.* **2007**, *46*, 9201.
- (181) Doose, S.; Neuweiler, H.; Sauer, M. *ChemPhysChem* **2009**, *10*, 1389.
- (182) Serrano-Andres, L.; Merchan, M.; Roos, B. O.; Lindh, R. *J. Am. Chem. Soc.* **1995**, *117*, 3189.
- (183) Clapp, A. R.; Medintz, I. L.; Mattoussi, H. *ChemPhysChem* **2006**, *7*, 47.
- (184) Jin, T.; Ichikawa, K.; Koyama, T. *J. Chem. Soc., Chem. Commun.* **1992**, 499.
- (185) Atkinson, P.; Bretonniere, Y.; Parker, D. *Chem. Commun.* **2004**, 438.
- (186) Cukier, R. I.; Nocera, D. G. *Annu. Rev. Phys. Chem.* **1998**, *49*, 337.
- (187) Bordwell, F. G. *Acc. Chem. Res.* **1988**, *21*, 456.
- (188) Bordwell, F. G.; Drucker, G. E.; Fried, H. E. *J. Org. Chem.* **1981**, *46*, 632.
- (189) Bordwell, F. G.; Ji, G. Z. *J. Am. Chem. Soc.* **1991**, *113*, 8398.
- (190) Shang, X.-F.; Lin, H.; Lin, H.-K. *J. Fluorine Chem.* **2007**, *128*, 530.
- (191) Kleineweischede, A.; Mattay, J. *Eur. J. Org. Chem.* **2006**, 947.
- (192) Moerkved, E. H.; Neset, S. M.; Bjoerlo, O.; Kjoesen, H.; Hvistendahl, G.; Mo, F. *Acta Chem. Scand.* **1995**, *49*, 658.
- (193) Kestemont, G.; de Halleux, V.; Lehmann, M.; Ivanov, D. A.; Watson, M.; Geerts, Y. H. *Chem. Commun.* **2001**, 2074.
- (194) Thordarson, P. *Chem. Soc. Rev.* **2011**, *40*, 1305.
- (195) Su, Z.-M.; Ye, H.-M.; Zhu, X.-X.; Xie, L.-L.; Bai, S.; Yuan, Y.-F. *J. Organomet. Chem.* **2014**, *750*, 162.
- (196) Bhosale, S. V.; Bhosale, S. V.; Kalyankar, M. B.; Langford, S. J. *Org. Lett.* **2009**, *11*, 5418.

